AD NUMBER

AD881796

NEW LIMITATION CHANGE

TO

Approved for public release, distribution unlimited

FROM

Distribution authorized to U.S. Gov't. agencies and their contractors; Administrative/Operational Use; Jan 1971. Other requests shall be referred to Air Force Rocket Propulsion Lab, Attn: DOG/STINFO, Edwards AFB, CA 93523.

AUTHORITY

Air Force Rocket Propulsion Lab ltr dtd 29 Sep 1971

AIR FORCE REUSABLE ROCKET ENGINE PROGRAM

XLR129-P-1
FINAL REPORT
AFRPL-TR-71-1 VOL III
JANUARY 1971

Prepared Under
Contract F04611-68-C-0002 for
Air Force Rocket Propulsion Laboratory
Edwards Air Force Base, California 93523

Printed in the United States of America

NOTICES

1. "When US Government drawings, specifications, or other data are used for any purpose other than a definitely related Government procurement operation, the Government thereby incurs no responsibility nor any obligation whatsoever, and the fact that the Government may have formulated, furnished, or in any way supplied the said drawings, specifications, or other data, is not to be regarded by implication or otherwise, or in any manner licensing the holder or any other person or corporation, or conveying any rights or permission to manufacture, use or sell any patented invention that may in any way be related thereto."

2. "This document is subject to special export controls and each transmittal to foreign governments or foreign nationals may be made only with prior approval of AFRPL (DOZ), Edwards, California 93523."

AIR FORCE REUSABLE ROCKET ENGINE PROGRAM

XLR129-P-1
FINAL REPORT
AFRPL-TR-71-1 VOL III
JANUARY 1971

STATEMENT #2 UNCLASSIFIED

This document is subject to special export controls and each transmittal to foreign government or foreign nationals may be made only with prior approval of Air Force Rocket Propulsion Laboratory, attn: DOG/STINFO Edwards AFB Calif 93523

Prepared Under
Contract F04611-68-C-0002 for
Air Force Rocket Propulsion Laboratory
Edwards Air Force Base, California 93523

Printed in the United States of America

FOREWORD

This final report describes the Air Force XLR129-P-1 Reusable Rocket Engine Program conducted during the period 6 November 1967 to 15 August 1970, and is submitted in accordance with the requirement of Contract F04611-68-C-0002.

This effort was the second phase of the Air Force Cryogenic Rocket Engine Advanced Development Program, Project 2 of the Program Element 63408F.

This publication was prepared by the Pratt & Whitney Aircraft Florida Research and Development Center as report PWA FR-3832.

This Technical Report has been reviewed and is approved.

Robert E. Probst
Captain, USAF
Program Manager
Air Force Rocket Propulsion Laboratory

SECTION VI
CONTROL SYSTEM

A. SYSTEM DESCRIPTION

1. Introduction

The high-pressure rocket engine uses a staged combustion cycle in which most of the fuel is burned with a portion of the oxygen in a preburner, to provide turbopump power, before combustion with the remainder of the oxygen in the mainburner chamber. A complete propellant flow schematic illustrating the principal flowpaths and functional component arrangement of this engine is shown in figure 783.

Hydrogen enters at the engine driven fuel low-speed inducer where sufficient pressure rise is produced to satisfy the main fuel pump net positive suction head (NPSH) requirements. The low-speed inducer is used to minimize vehicle NPSH (tank pressure) requirements and allows high-speed main propellant pump operation at high turbopump efficiency. Hydrogen is pumped to the system operating pressure by the main fuel pump. The principal hydrogen flowpath from the pump is through the preburner supply heat exchanger, and then into the preburner chamber through the preburner injector. The remainder of the hydrogen flows through the transpiration supply heat exchanger and then through low-speed fuel inducer drive turbine before being passed into the main chamber as transpiration coolant. A small amount of hydrogen is bled off at the main fuel pump interstage to provide coolant for the two-position nozzle. This coolant flows to the nozzle through a regulating orifice and a shutoff valve that is provided to stop the flow when the two-position nozzle is in the retracted position.

Oxygen enters at the oxidizer low-speed inducer where enough pressure rise is produced to satisfy the main oxidizer pump NPSH requirements. The oxygen is then pumped to system operating pressure levels by the main oxidizer pump. Pump discharge flow is split between the preburner and the main combustion chamber. The principal oxidizer flow passes through and becomes the working fluid for the oxidizer low-speed inducer turbine before being injected into the mainburner chamber. The remainder of the oxygen is ducted to the preburner where it is burned with the hydrogen. The resulting combustion products split through parallel ducts passing through the two main pump turbines, arranged in parallel. The energy required to drive the main pumps is extracted from these combustion products, which then exhaust from the turbines and mix in a common passage of the transition case. These gases then pass through the mainburner injector and into the mainburner chamber where they mix and burn with the principal oxidizer flow. The combustion gases are then expanded through the bell nozzle to provide thrust.

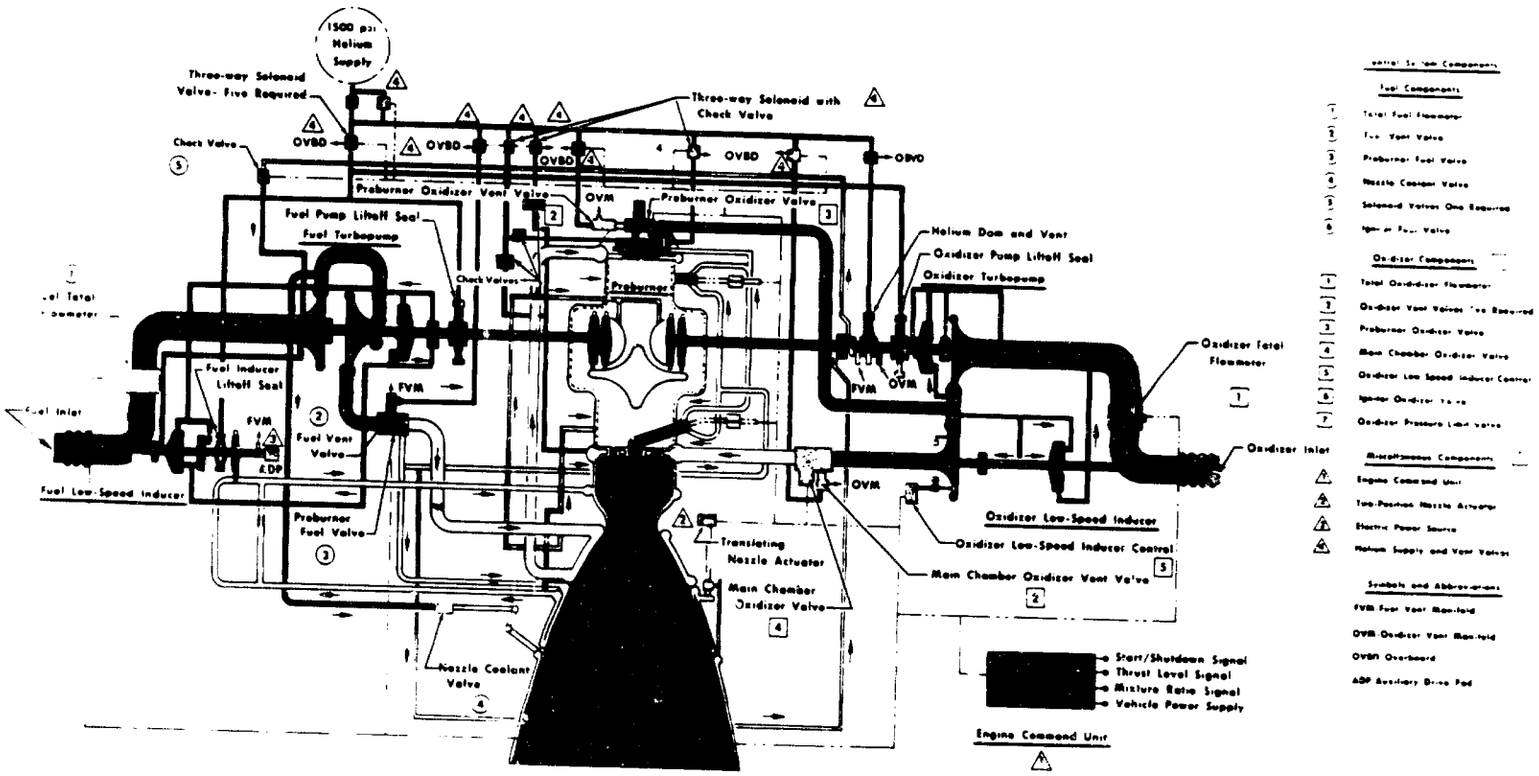

Figure 783. Demonstrator Engine Control System

FD 44916

2. Main Control Valves

Analysis of the engine cycle has established that the following control points are required for satisfactory steady-state operation:

1. Preburner oxidizer valve

2. Preburner fuel valve

3. Main chamber oxidizer valve

4. Oxidizer low-speed inducer variable turbine actuator.

The preburner oxidizer valve is a translating sleeve valve that regulates the total flow and flow split to the primary and secondary oxidizer elements of the preburner injector during engine operation. The resultant variation in primary and secondary flow split controls the velocity of the oxidizer entering the preburner and ensures stable and efficient preburner combustion. This valve has a major influence on the available main turbine power and engine thrust, but only a minor influence on the overall engine mixture ratio. The preburner oxidizer valve also shuts off the oxidizer flow to the preburner when the engine is not operating.

The preburner fuel valve is a straight-shaft butterfly valve located downstream of the fuel pump in the line to the preburner heat exchanger. This valve regulates the hydrogen flow to the preburner, and splits off the transpiration coolant flow for the main chamber. Because this valve regulates hydrogen flow, it has a major influence on pump discharge pressure, chamber mixture ratio, and available turbine power. It has only a minor influence on thrust, because fuel flow is a small part of the total propellant weight flow. Because the fuel valve influences pump discharge pressure, it affects the low-speed inducer drive power (i.e., main fuel pump NPSH) as well as transpiration cooling flow. Further, the fuel valve provides pressure loss to aid fuel system stability and provides the main fuel flow shutoff function.

The main chamber oxidizer valve is a canted-shaft butterfly valve, which is located in the oxidizer supply line to the main chamber. Because this control regulates the main burner flow, which is a major portion of the total propellant flow, it has a strong influence on both engine mixture ratio and thrust.

The oxidizer low-speed inducer control actuator schedules the nozzle (admission) area of the oxidizer low-speed inducer turbine. Modulation of this control affects available main oxidizer pump NPSH because the turbine nozzle velocity determines turbine power and, therefore, oxidizer low-speed inducer pressure rise. Because this control is in series with the main chamber oxidizer valve, it also has a strong effect on engine mixture ratio and thrust.

Each of the above control points is monitored and controlled by an electronic Engine Command Unit (ECU). Schedules that are programed into the ECU will be those of known engine and valve operating characteristics. This

will allow the use of an open loop primary control system with its inherent reliability. The addition of sensors, for several operating parameters, will provide closed loop trim and critical limit protection operation.

B. PREBURNER OXIDIZER VALVE

1. Introduction

The preburner oxidizer valve is a translating sleeve valve that divides the oxidizer supply into two separate flows as required by the preburner injector. The translating sleeve valve was chosen during the Phase I valve selection study as the optimum configuration to meet the requirements for preburner oxidizer flow division, modulation, and shutoff. The valve is designed with fixed primary passages and variable area secondary ports. Control of the preburner oxidizer flow over the engine operating range is accomplished by modulating the area of the secondary ports. The valve will allow primary flow without secondary flow for engine ignition during the start transient. The preburner oxidizer valve also provides a positive shutoff for the total preburner oxidizer supply.

2. Summary, Conclusions and Recommendations

The design of the preburner oxidizer valve evolved from the Phase I flow divider valve. Particular emphasis was directed toward reducing valve size and weight. Complete design details are presented in the Demonstrator Engine Design Report, AFRPL-TR-70-6.

Parts were fabricated for two complete valve assemblies. Additional piston rings, seals, and other expendables were provided for use during testing.

The preburner oxidizer valve was flow calibrated with water, and the test results agreed closely with the predicted values for effective area versus valve stroke.

The valve was endurance tested in LN_2 and demonstrated less than the allowable 10 standard cubic centimeters per second (sccs) GN_2 leakage for the shutoff and actuator shaft seals. Actuation forces remained below 600 lb throughout endurance testing.

The preburner oxidizer valve operated successfully in LO_2 during testing of the preburner, hot gas system, and hot gas turbopump test rigs.

It was concluded that the preburner oxidizer valve met all requirements for use with the XLR129 demonstrator engine.

3. Hardware Description

The preburner oxidizer valve, shown disassembled in figure 784 and in cross section in figure 785, consists of a translating sleeve and a fixed housing that incorporates six contoured ports as shown in figure 786 for secondary flow and six equally spaced radial holes for distribution of the primary flow. Operating characteristics are shown in figure 787. The valve assembly is bolted to the lower flange of the preburner dome.

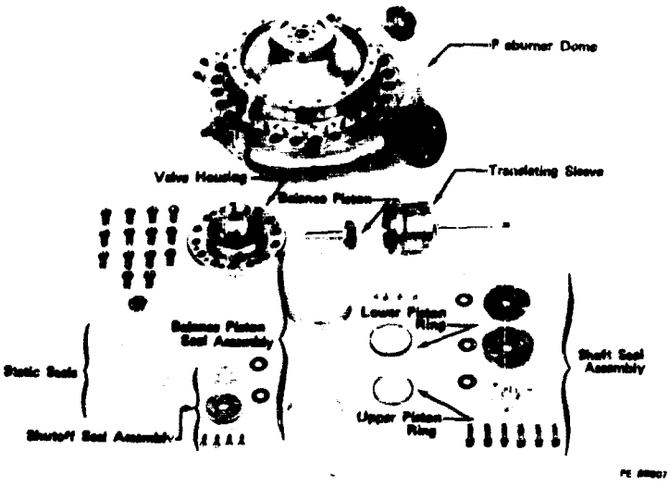

Figure 784. Preburner Oxidizer Valve FD 35633A

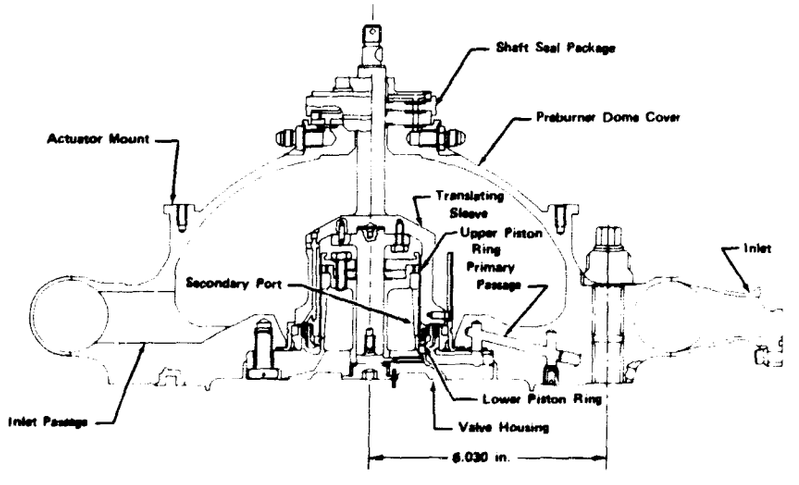

Figure 785. Preburner Oxidizer Valve Layout FD 25595C

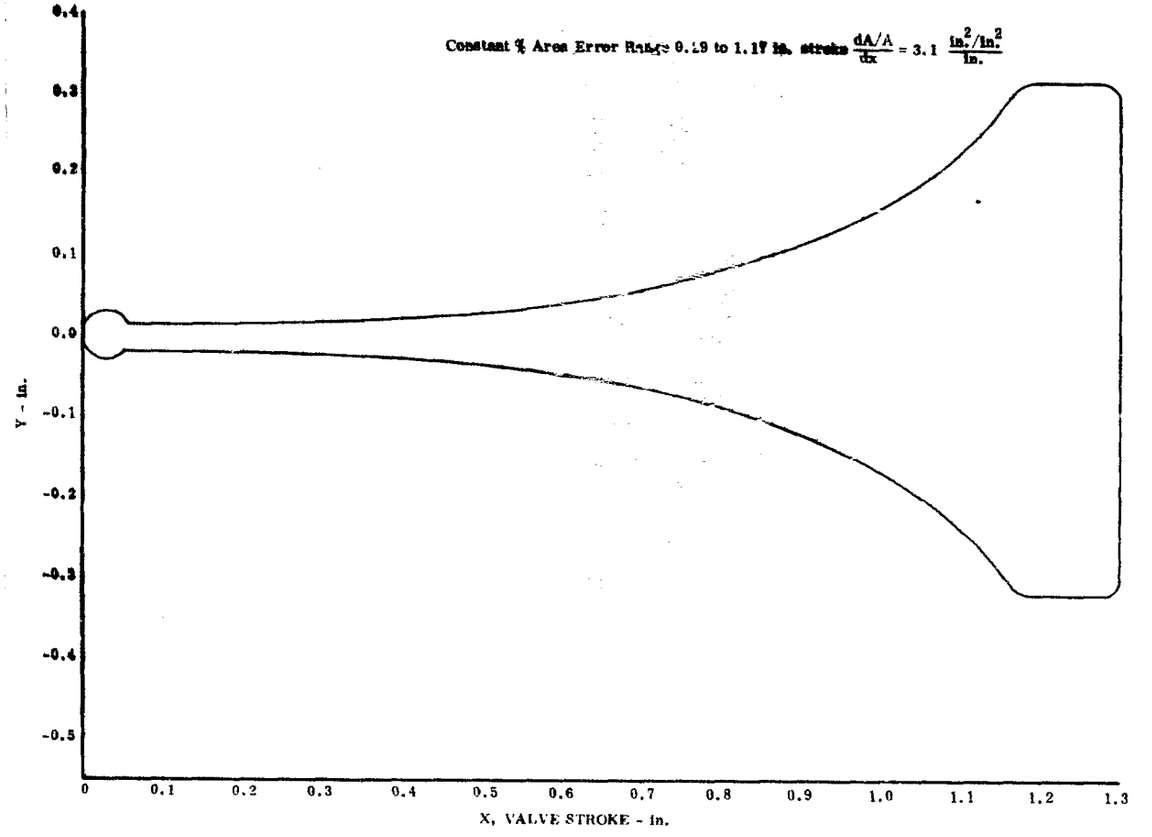

X	Y
0 - in.	0 - in.
0.03	0.03
0.06	0.0175
0.29	0.0175
0.33	0.020
0.38	0.023
0.48	0.0316
0.58	0.0425
0.68	0.0587
0.78	0.0797
0.88	0.1086
0.98	0.1480
1.07	0.1750
1.08	0.210
1.13	0.252
1.17	0.300
1.19	0.310
1.29	0.310
1.30	0.300

Figure 786. Preburner Oxidizer Valve Port, Contour

DF 69952

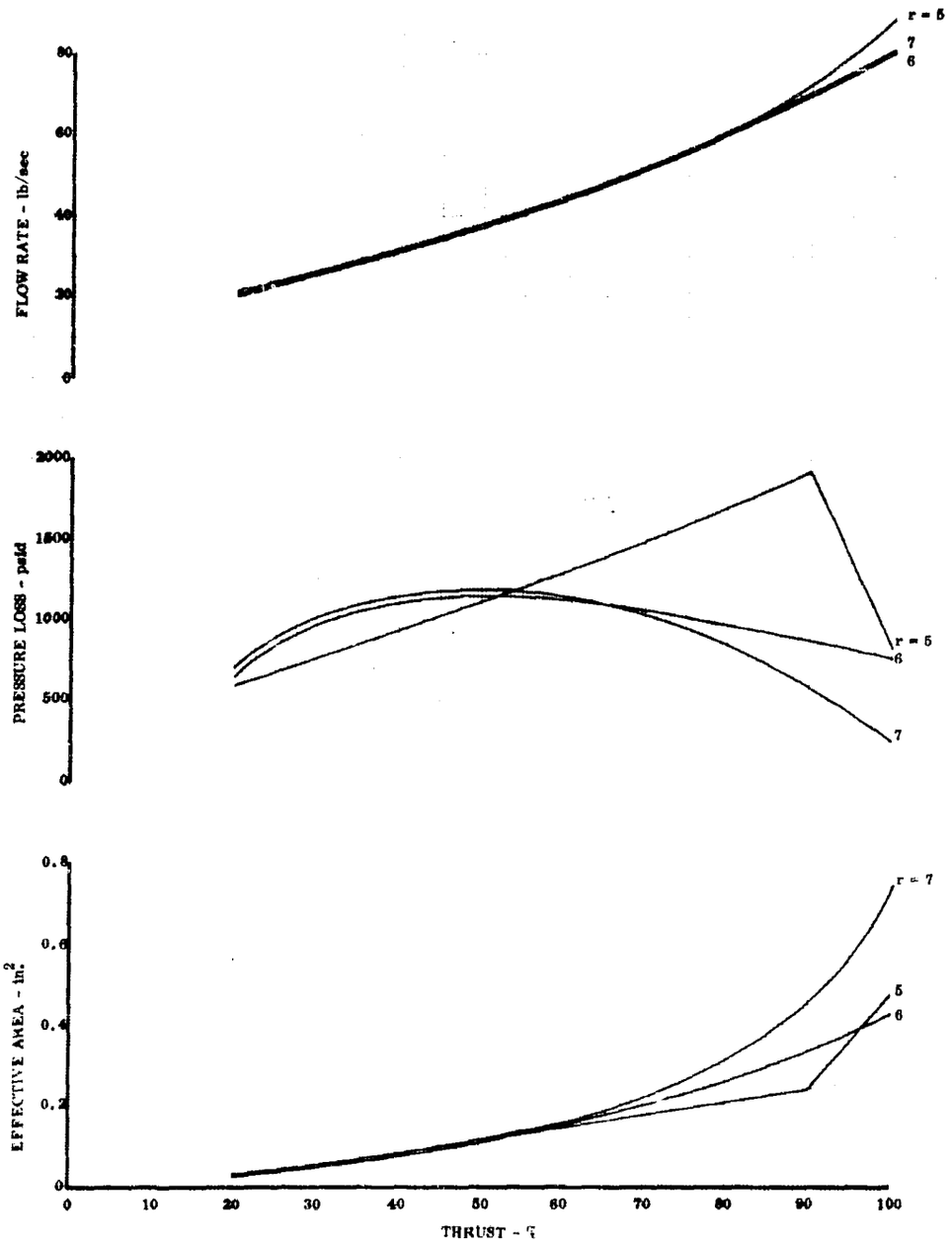

Figure 787. Preburner Oxidizer Valve Operating Characteristics DF 69951

The preburner dome, illustrated in figure 788, has a 180-deg ring manifold with a flanged inlet located centrally relative to the manifold. The ring manifold also has a mounting flange at one end for the vent valve. The manifold is divided by a baffle plate that separates the oxidizer inlet flow from the vent flow. After entering the ring manifold, the oxidizer flows into the dome cavity through 12 radial ports located between studs. There are three additional radial ports for oxidizer to flow from the dome through the vent valve prior to engine starting. The 12 oxidizer inlet ports permit the oxidizer to be well distributed as it enters the dome cavity so that hydraulic side force on the translating sleeve is minimized. The dome housing contains drilled passages for the primary oxidizer supply to the injector, provisions for temperature and pressure instrumentation, purges, and seal leakage connections. A precision surface for mounting the actuation system is low on the dome for minimum deflection. Tapered shims are available during assembly to align the actuation system and dome valve housing assembly.

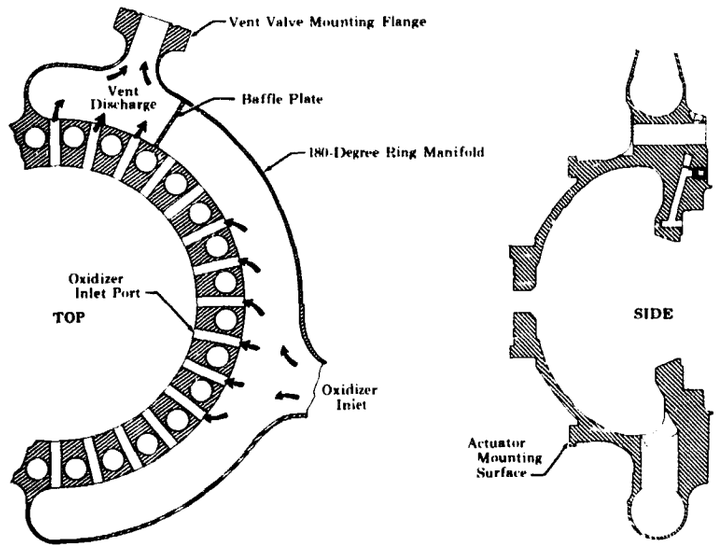

Figure 788. Preburner Dome Cross Sections FD 25979A

Engine thrust modulation requires variation of the preburner oxidizer flow by modulating the secondary port effective area. The desired preburner injector performance is maintained by the fixed area of the primary passages which increase the ratio of primary to secondary flow as thrust level is decreased. The primary oxidizer flow is provided to the preburner injector through six equally spaced radially located holes. The primary flow passages are designed to flow at 10% of preburner oxidizer flow at a mixture ratio of 7 and 100% thrust. The primary flow orifices are 0.120 in. diameter; however, the orifice is provided as a removable plug to permit experimental adjustment of the flow split at design point. The secondary oxidizer flow is metered by the six contoured ports and flows through the valve housing to the preburner injector as shown in figure 789. The valve is designed with 25% excess secondary area, accomplished with 0.070 in. of additional valve stroke. The volumes and the effective areas of the primary and secondary flowpaths at the valve and injector passages are shown in figure 790.

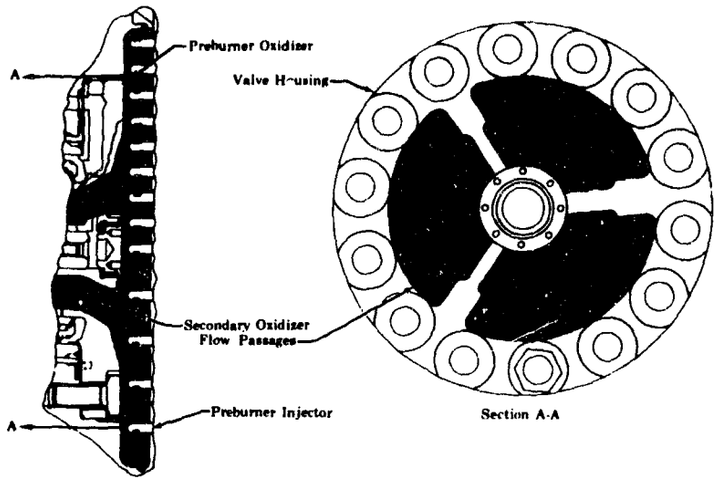

Figure 789. Secondary Oxidizer Flow Passages FD 25388

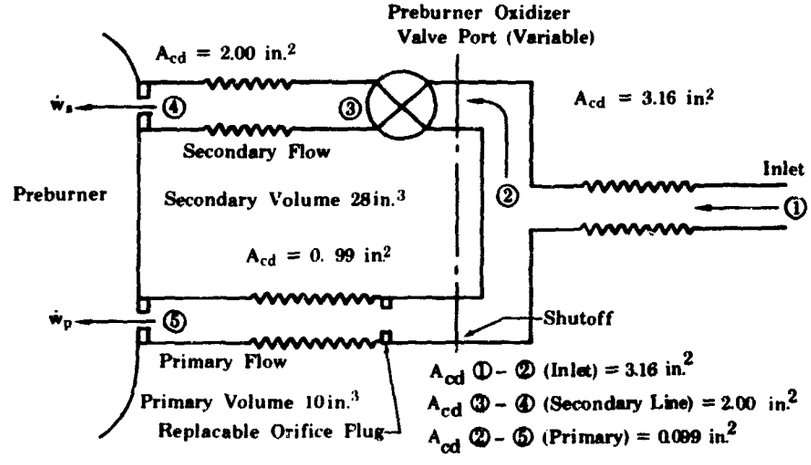

Figure 790. Preburner Oxidizer Valve Flow Schematic FD 27528A

The valve's contoured secondary metering ports provide constant percent area error. The predicted 3.1% flow area error will remain constant over 87% of the operating range (a valve stroke of 0.29 to 1.17 in.), with the error increasing at the low area end and diminishing near the full-open end as shown in figure 791. The width of the secondary metering port is constant (0.62 inch) from 1.14 in. to the maximum stroke of 1.3 in.

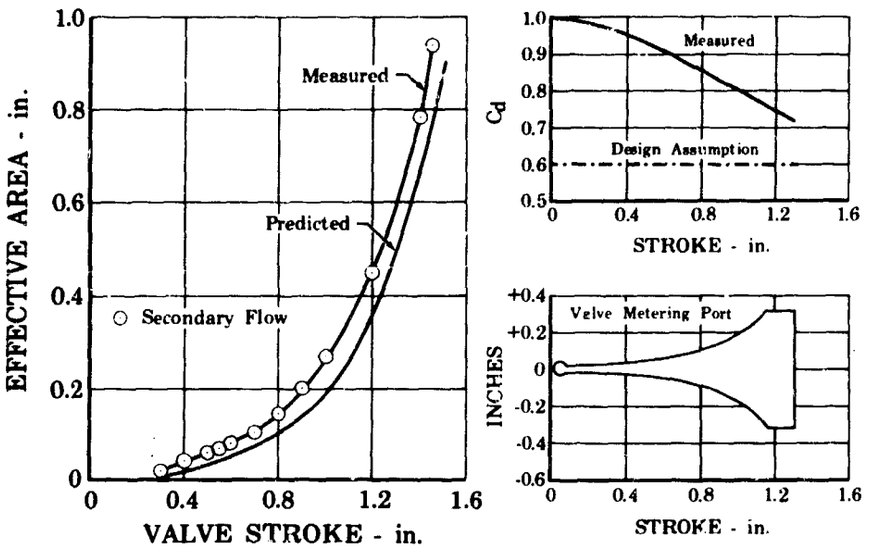

Figure 791 Oxidizer Valve Effective Flow Area vs Valve Stroke FD 33007

The lip seal package fastens to the top of the dome to prevent leakage where the shaft of the translating sleeve protrudes from the dome as previously shown in figure 785. The shaft seals were designed for less than 10 sccs external leakage and were based on Phase I translating seal rig and flow divider valve test results. Another lip seal group on the secondary sleeve balance piston prevents excessive oxidizer leakage overboard where the balance piston passes through the core of the valve housing. The translating shaft lip seal package is illustrated in figure 792 and the balance piston lip seal package is illustrated in figure 793. The lip seals are a 5-ply laminate of TFE Teflon and Kapton. The translating shaft seal package can be shifted laterally approximately 0.025 in. to accommodate overall misalignment between the sleeve and the main housing.

The preburner oxidizer valve has two pressure-balanced piston rings, an upper ring attached to the valve housing as shown in figure 793, and a lower ring attached to the sleeve by a dowel pin as shown in figure 794. Both rings are made of Berylco 25 (AMS 4650 or 4532). The preburner oxidizer valve piston rings have a nominal sealing diameter of 2.50 inches. The balanced piston rings were designed for minimum actuation force and were based on test results from the supporting data and analysis task where prototype piston ring designs were evaluated using Phase I flow divider valve hardware.

The balancing grooves on the lower ring were designed so that a minimum amount of leakage would occur through the grooves and into the metering port of the valve. This leakage is kept below 5% of the total flow.

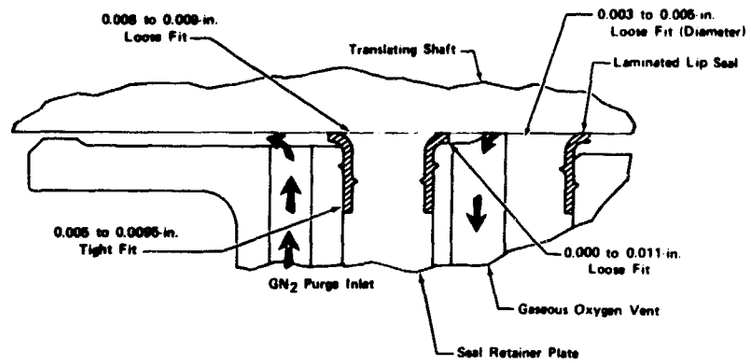

Figure 792. Translating Shaft Lip Seal Package FD 27525A

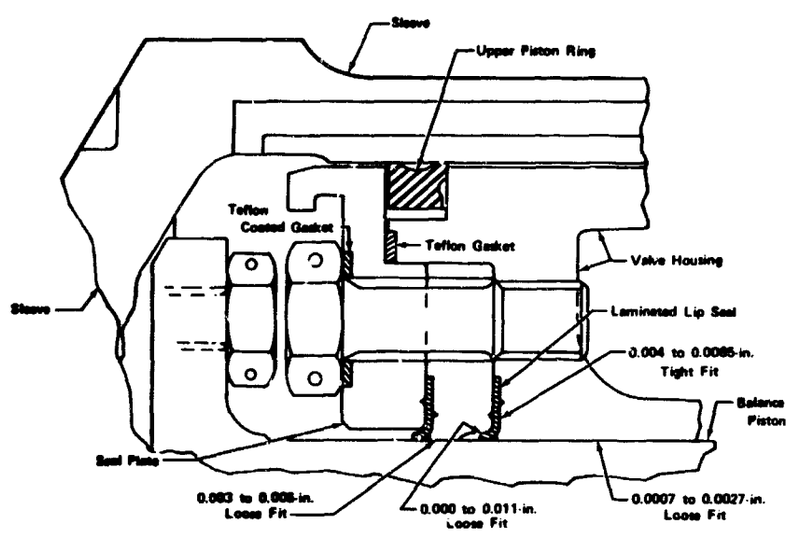

Figure 793. Balance Piston Lip Seal Package and Upper Piston Ring FD 27526A

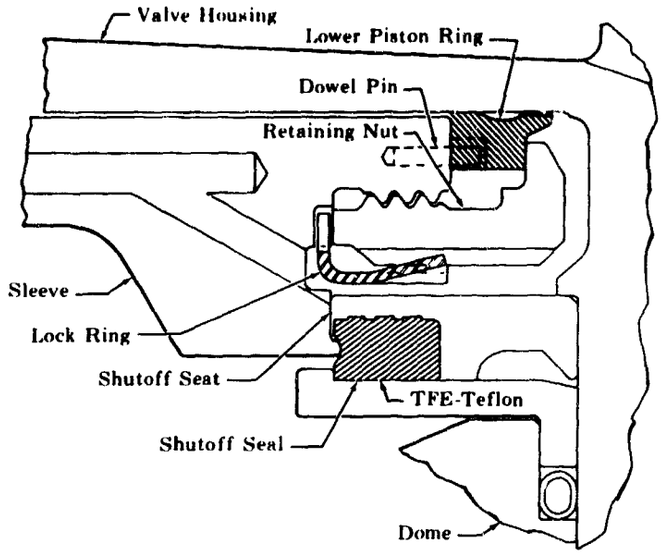

Figure 794. Lower Piston Ring Installation FD 27527

The sleeve and balance piston were established as a matched set to achieve the necessary precision between the shaft sections that must be parallel to avoid adverse bearing conditions relative to the translation movement. The lower piston ring, retained at the end of this sleeve set, is maintained in a fixed angular relationship to the ports in the valve housing with a dowel pin. Study of the tolerances involved for the pins, holes, slots, and port location errors shows a possible misalignment, however, +0.033 in between the balance groove cuts of the piston ring and their related ports.

The sleeve incorporates eleven 0.110-in. diameter holes to vent the cavity between the sleeve and valve housing.

Teflon coated metallic O-rings are used for static seal, and Teflon and Teflon-coated flat gaskets are used for external fitting seals. Both ID and OD vented rings are used, as required, where pressure difference is expected to exceed 100 psi. A Parker 8814 Series Inconel X750 Teflon-coated V-seal is used for the valve housing-to-injector overboard static seal.

A trapped TFE Teflon shutoff seal is used as previously shown in figure 794. Deflection of the Teflon seal by the shutoff sealing lip is limited to 0.020 in. by metal-to-metal contact of the secondary sleeve and seal retainer. The shutoff seal was designed for less than 10 sccs leakage and was based on the Phase I flow divider valve test results.

4. Fabrication

No major fabrication problems were encountered during the POV parts procurement phase. The Inconel 718 preburner dome was the long lead time item and required weld repair of cracks in the vent flange after receipt from the vendor. Repairs were made at P&WA.

The preburner dome was machined from an Inconel 718 pancake forging using conventional machining methods. The bolt holes were then drilled and the radial flow distribution ports were bored. The manifold closures were machined from bar stock and hand welded to the dome. The dome was then solution and precipitation heat treated and the pilot diameters were finished machined.

The preburner valve sleeve was machined from Inconel 718 bar stock using the conventional machining methods, and tablock slots were eloxed. Chrome coating for the sleeve was applied to a thickness of 0.0001 to 0.0002 in. 0.0001 to 0.0002 in.

The balance piston was machined from AMS 4650 CuBe bar stock using conventional machining methods. The piston was precipitation heat treated prior to final machining.

The valve housing was machined from Inconel 718 bar stock using conventional machining methods. The flow ports were cut by EDM and the housing was chrome coated to a thickness of 0.0001 to 0.0002 in.

The piston rings for the preburner valve were conventionally machined from AMS 4650 CuBe bar stock. Prior to final machining the rings were precipitation heat treated.

The shutoff seal was machined from an extrusion of AMS 3656 Teflon using conventional machining methods.

The lip seals were fabricated by bonding two 0.005-in. thick layers of Dupont 500F-131 Kapton with three 0.005-in. thick layers of AMS 3647 FEP Teflon, and then cutting the required seals from the resultant laminated sheet.

Bonding is accomplished by baking the material in an oven at 550° ± 25° F, with a 20 psi load, for 30 minutes.

Table XCIV indicates the lead times required for the aforementioned parts.

Table XCIV. Preburner Oxidizer Valve Parts Lead Times

Part Name	Lead Time (weeks)	
	Raw Material	Machining
Dome	13	32
Valve Sleeve	4	12
Balance Piston	5	12
Valve Housing	4	28
Piston Rings	7	17
Shutoff Seal	3	9
Lip Seals	8	1

The valve assembly was proof tested to 1.2 times maximum operating pressure at cryogenic temperature. Zyglo after pressure test showed no evidence of structural cracks.

Chrome thickness for the valve housing and sleeves was originally specified to be 0.001 to 0.0015 in. but was changed to a thickness of 0.0001 to 0.0002 in. because of uneven buildup with the original thickness requirement.

The upper and lower piston rings were lapped to the housing and sleeve assemblies to provide an optimum fit.

All detail moving parts were glass bead peened to give a smooth clean surface.

As a result of testing, the ID of the shutoff seal was reduced from 3.636 in. diameter to 3.617 in. diameter and the seal thickness increased from 0.275 in. to 0.283 in. to improve the static sealing characteristics at the ID by providing a tighter radial fit when the seal is installed. The assembled valve and actuator is shown in figure 795.

Assembly of the valve and actuator was accomplished with no major problems.

5. Testing

a. Water Flow Tests

Water flow calibrations of the preburner oxidizer valve were conducted on B-21 stand and the results are shown on figure 796. The measured valve effective area was greater than the predicted value since a 0.6 C_d was originally assumed for the entire range of valve travel.

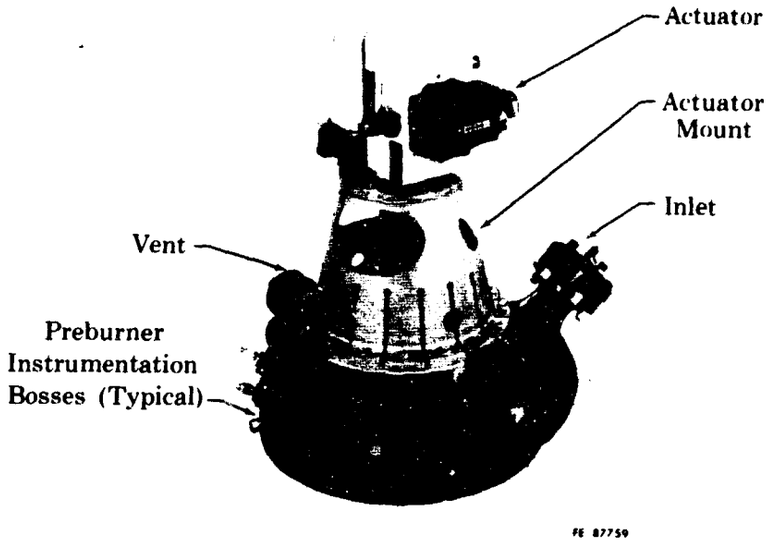

Figure 795. Preburner Oxidizer Valve FD 31516

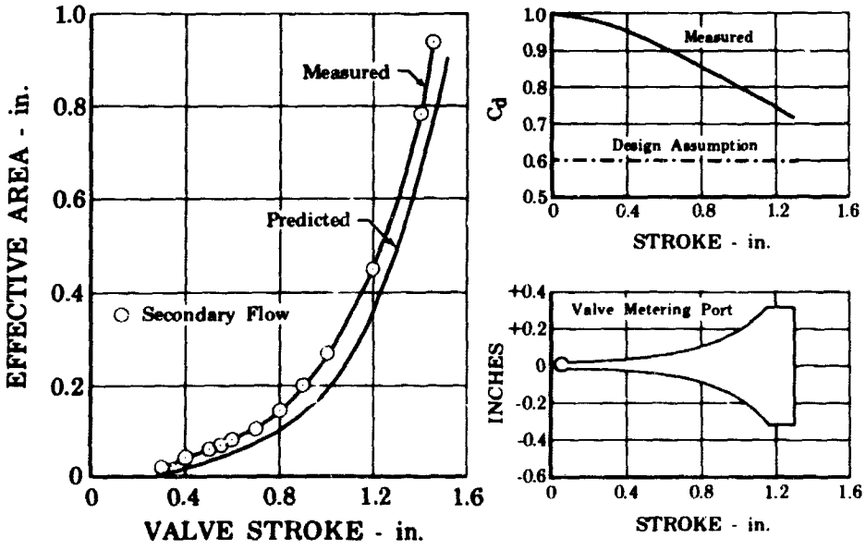

Figure 796. Preburner Oxidizer Valve Test Results FD 33007

Test results showed that the average C_d ranged from 1.0 at the minimum valve areas to an average of 0.7 at the maximum valve area. The nozzle-like characteristic C_d of 1.0 occurs at the minimum valve areas where the ratio of valve port width to port length is less than one and rounded endurance effects are more pronounced. At the maximum valve opening conditions, the ports approach a sharp-edges orifice with a characteristic C_d of 0.6.

b. Actuator Calibration

The interim test stand hydraulic actuator with linear potentiometer position feedback instrumentation was calibrated to determine linearity and frequency response characteristics. The actuation system linearity is shown in figure 797 and the frequency response characteristics are shown in figure 798. The linear potentiometers were replaced by linear variable differential transformers. This change provides a position feedback system less susceptible to contamination. This actuation system linearity is shown in figure 799 and the frequency response characteristics are shown in figure 800.

A series of qualification and endurance tests were performed on the preburner oxidizer valve to determine wear characteristics, seal and piston ring leakage tolerances, and force loads on the actuator. The preburner oxidizer valve was instrumented and interconnected as illustrated in figure 801.

The preburner oxidizer valve was endurance tested in an ambient environment and a liquid nitrogen environment, at a pressure variation from 50 psi to 6000 psi. The valve was tested to determine operational characteristics and upon qualification was subjected to a series of cycling tests. The first test was 10,000 cycles to determine piston ring leakage; the second was a 10,000 cycle test to determine shaft seal leakage; and the third test was a 10,000 cycle test to determine shutoff seal leakage. Throughout the testing and cycling, actuator forces were recorded to determine the forces acting on the valve.

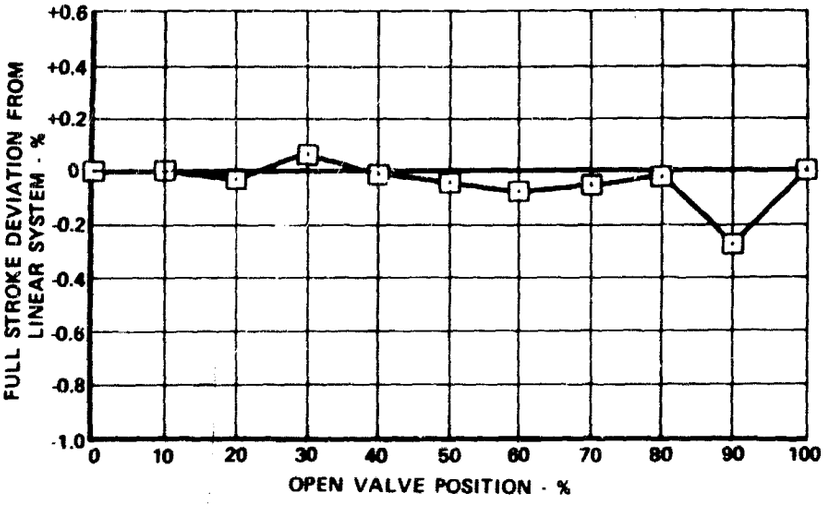

Figure 797. Actuation System Linearity FD 44480

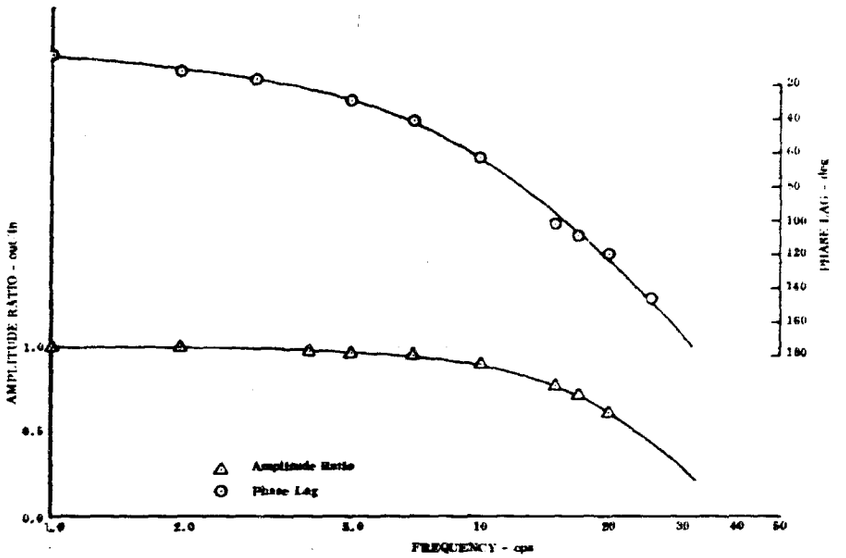

Figure 798. Frequency Response Characteristics DF 71895

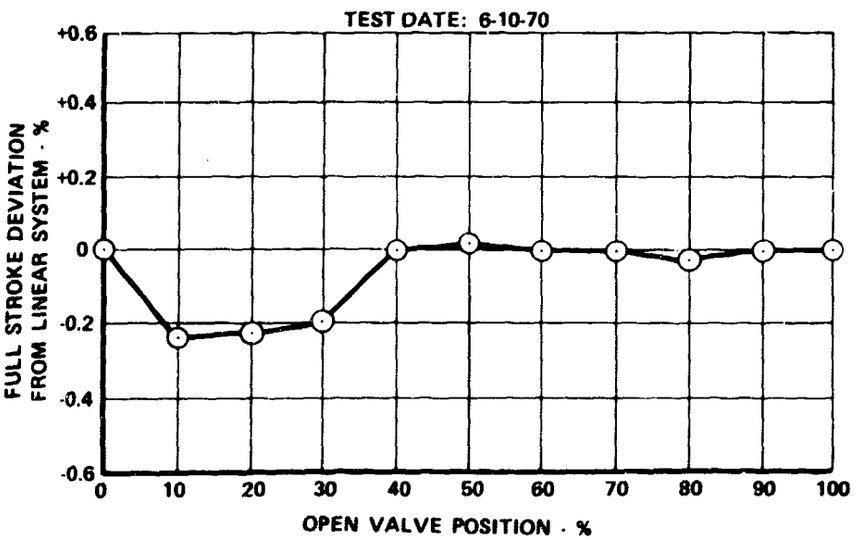

Figure 799. Actuation System Linearity FD 43077

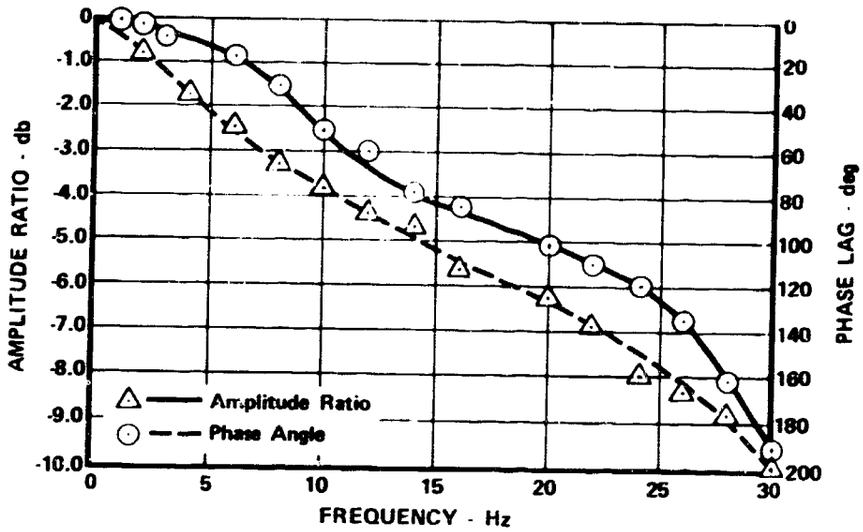

Figure 800. Frequency Response Characteristics FD 44481

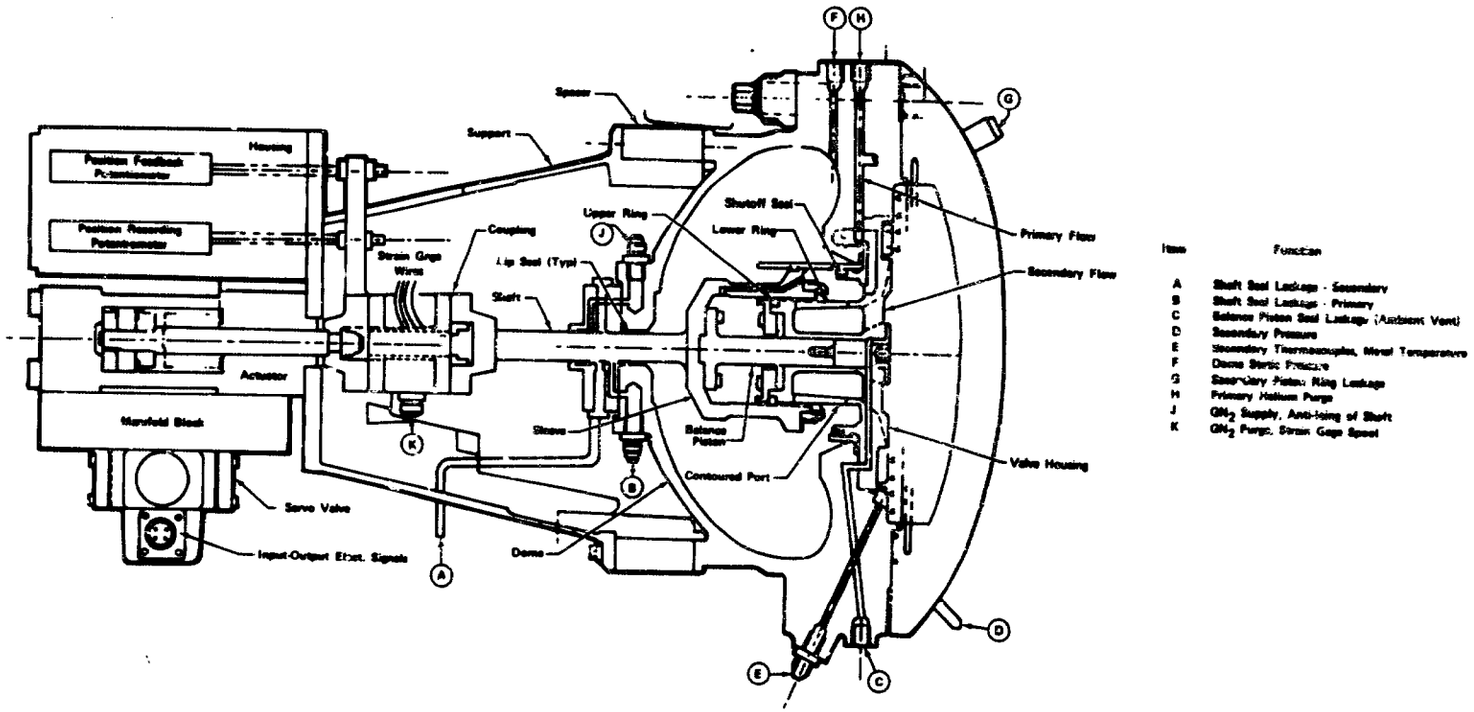

Figure 801. Preburner Oxidizer Valve Instrumentation

FD 38219B

The changes to the valve assembly to facilitate testing are as follows:

1. The upper seal package positioning plate was reworked to provide an adapter which was mounted on the exterior of the plate. This adapter was used to record shaft seal leakage past the secondary shaft seal.

2. In order to correctly measure the forces on the actuator shaft and the valve, a spool was inserted between the mount flanges of the actuator and the valve. The spool piece was strain gaged with three gages which could record forces in compression and tension as shown in figure 802. An additional spacer was added between the actuator mount and the valve dome to accommodate the installation spool piece. The spool piece was initially calibrated to establish the force versus strain relationship.

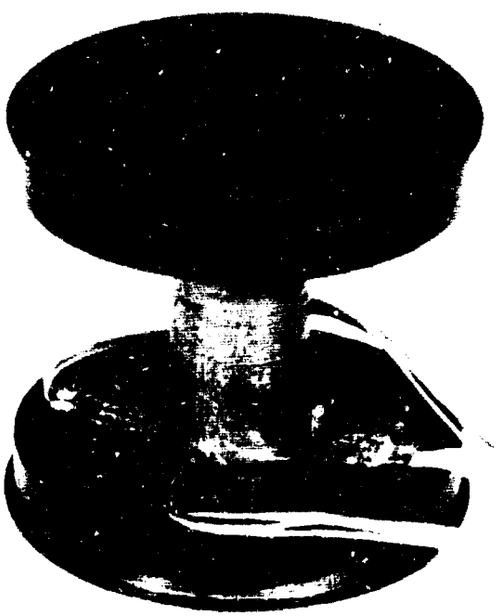

Figure 802. Strain Gaged Spool Piece FE 96344

c. Cryogenic Tests

A cryogenic endurance test was performed on the valve. The valve was positioned at a stroke of 0.100 in. with a secondary differential pressure of 0 psig. The valve was then cycled with a sinusoidal input at 2 to 3 cps sine frequency at an amplitude of 0.50 in. for 500 cycles. The secondary differential pressure was then increased to 500 psig and an additional 500 cycles were run. Following this, the stroke position was changed to 0.450 in., and a secondary differential pressure of 1000 psig was maintained for an additional 4500 cycles.

The final stroke position was 0.250 in., with a secondary differential pressure of 1500 psig. The valve was then cycled for 4500 cycles to complete the 10,000 cycle endurance run.

At 0, 3500, 6500, 9500, and 10,000 cycles, the positions were held for varying secondary differential pressures of 500, 1000, and 1500 psig while strain gage data for actuator shaft force measurements were recorded on an oscillograph. Piston ring, shaft seal, and shutoff seal leakage were also manually recorded at this time.

Piston ring load effects are plotted in figure 803. Test results agree favorably with the empirical data that were obtained from the Phase I flow divider valve data.

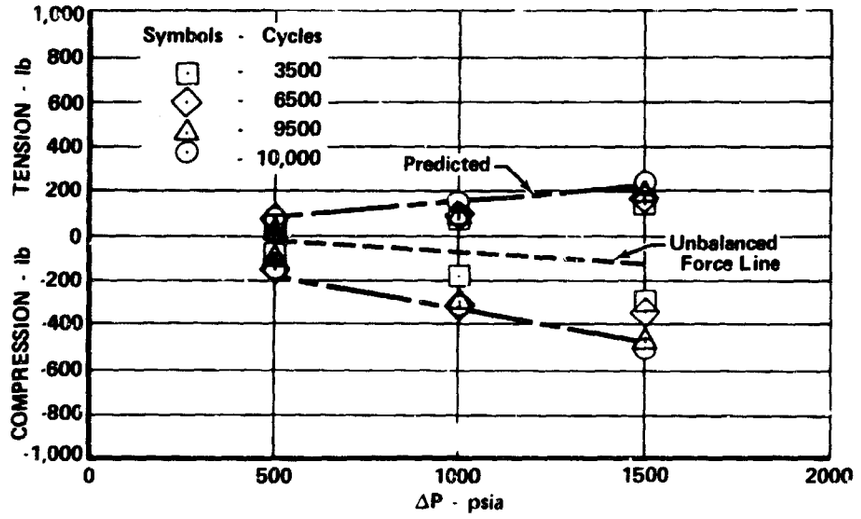

Figure 803. Piston Ring Load FD 39116

The piston ring leakage versus endurance cycles was also measured and is shown in figure 804 for data taken during cycling, and in figure 805 for static test data. Leakage at 1500 psid ranged from 40,000 sccs at 0 cycles to 29,000 sccs at 10,000 cycles. The leakage from the Phase I flow-divider valve, balanced piston ring endurance tests, scaled to the smaller valve diameter, was 18,600 sccs at 0 cycles and 26,700 sccs at 10,000 cycles at 1500 psid. These data compared favorably, considering that the piston rings tested were pressure balanced to a greater extent than the Phase I configuration and the sealing land was 62.5% of the Phase I ring.

The valve was repositioned at a stroke of 0.768 in. with zero differential pressure and cycled for a total of 10,000 cycles with a sinusoidal input at 2 to 3 cps at an amplitude of 0.100 in., at various dome pressures. The strain gage data were recorded on an oscillograph to define shaft seal forces. Shaft seal force measurement results are plotted in figure 806. In no instance did the forces exceed 90 lb and the average is approximately 50 lb. The average force load of the shaft seals decreased as a function of cycle time.

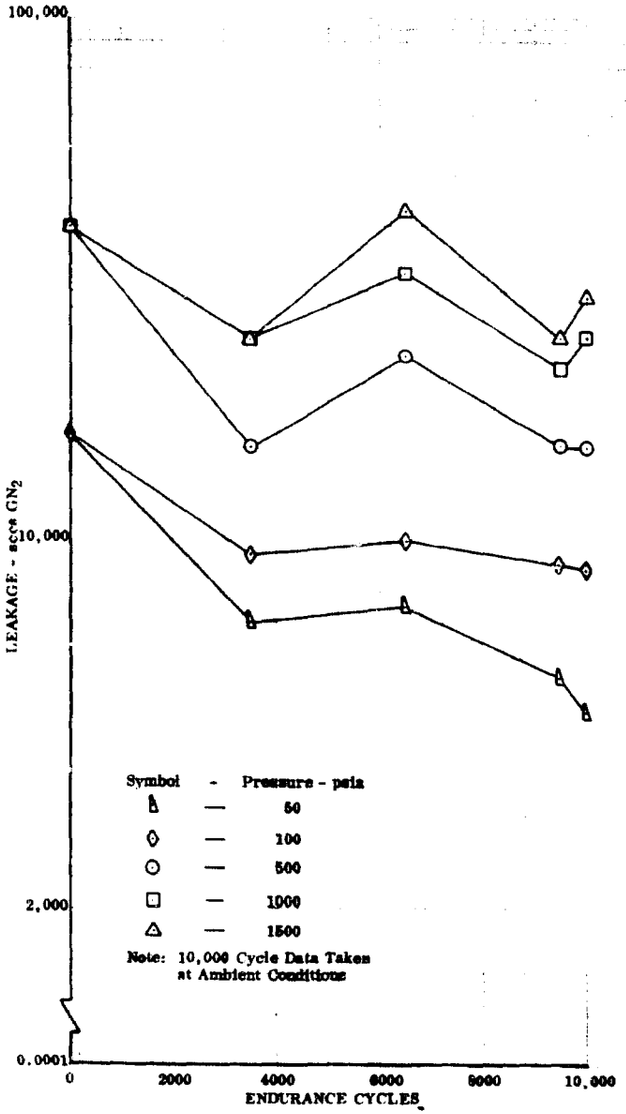

Figure 804. Piston Ring Leakage - Cycling DF 77788

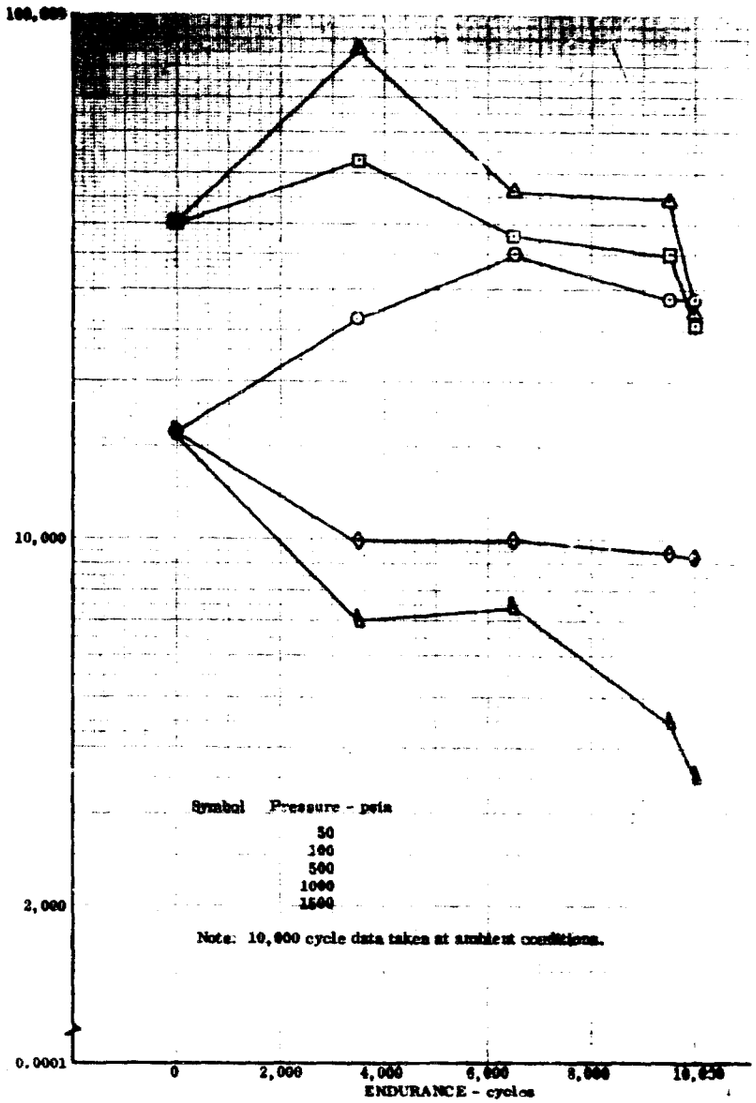

Figure 805. Piston Ring Static Test Leakage Data DF 77789

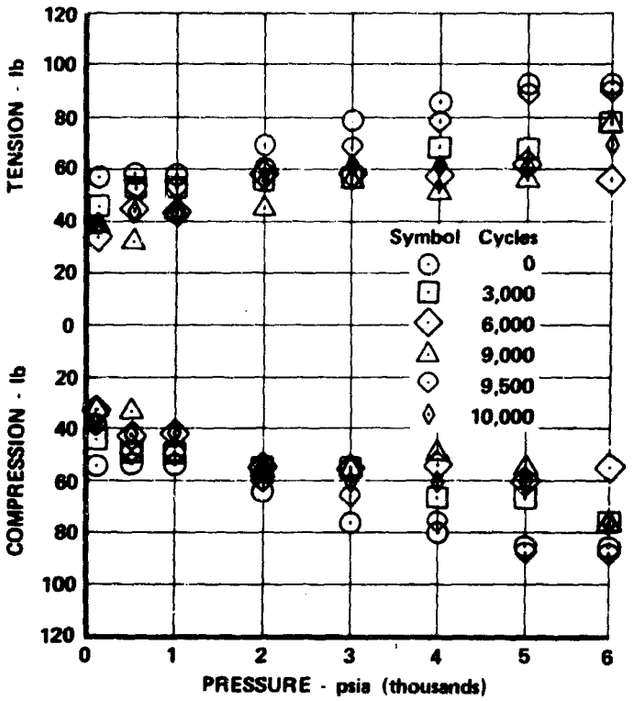

Figure 806. Shaft Seal Force FD 44470

Figure 807 shows a curve of primary shaft seal leakage versus pressure under cycling conditions, and figure 808 shows primary shaft seal leakage versus pressure under static conditions. The leakage rates remain consistent up to a pressure of 4000 psi. Figures 809 and 810, respectively, illustrate the secondary shaft seal leakage versus pressure for cycling and static tests. Measurements for secondary shaft seal leakage are taken past the second shaft seal, and all indicate leakage well within the 10 sccs limit. Primary and secondary shaft seals are shown respectively as taken in post-test condition in figures 811 and 812. Shaft seal typical condition is illustrated in figure 813.

Balance piston seal leakage vs endurance cycles is shown in figure 814 as a plotted curve for the test. Leakage averaged between 200 and 300 sccs for the complete 10,000 cycle endurance test. Leakage was substantially reduced at the 10,000-cycle data point showing improved sealing characteristics at ambient conditions. Previous endurance tests run during Phase I, using reversed configuration seals where the seal was attached to the balance piston and sealed on the OD, showed leakage rates averaging 2000 sccs and degrading with cycle time.

The shutoff seal leakage test consisted of positioning the valve in the closed position, and opening it to the 0.050-in. position under the 3 to 6 cps cycling condition.

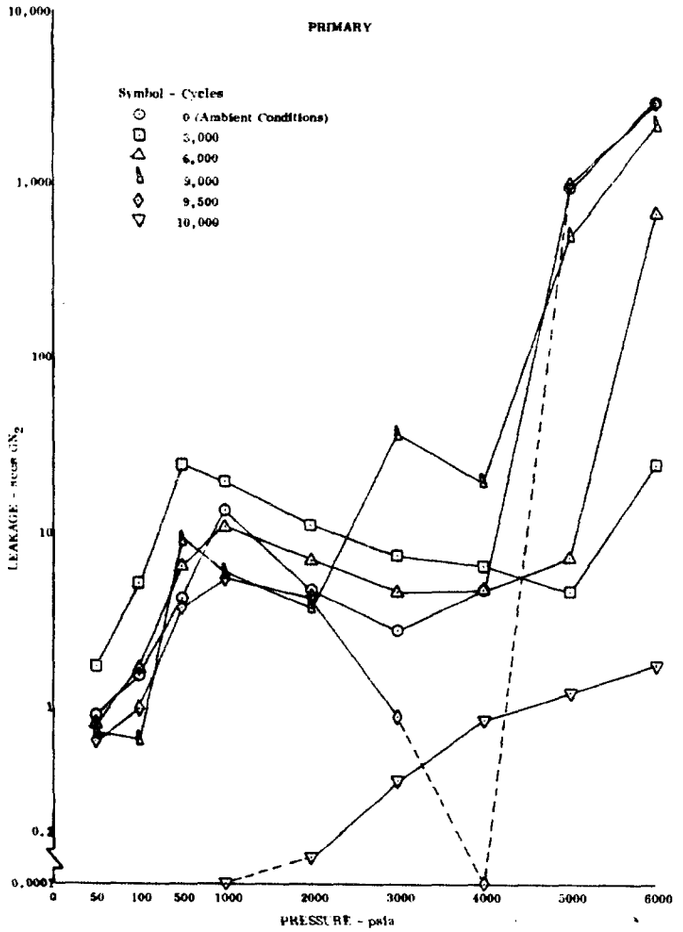

Figure 807. Shaft Seal Leakage - Cycling (Primary) DF 77784

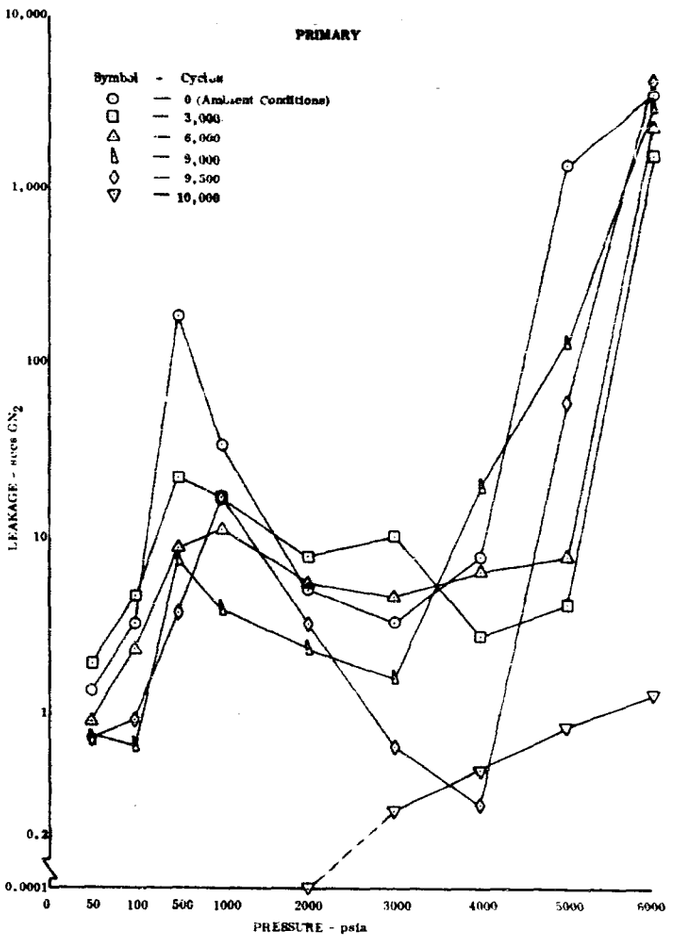

Figure 808. Shaft Seal Leakage - Static (Primary) DF 77783

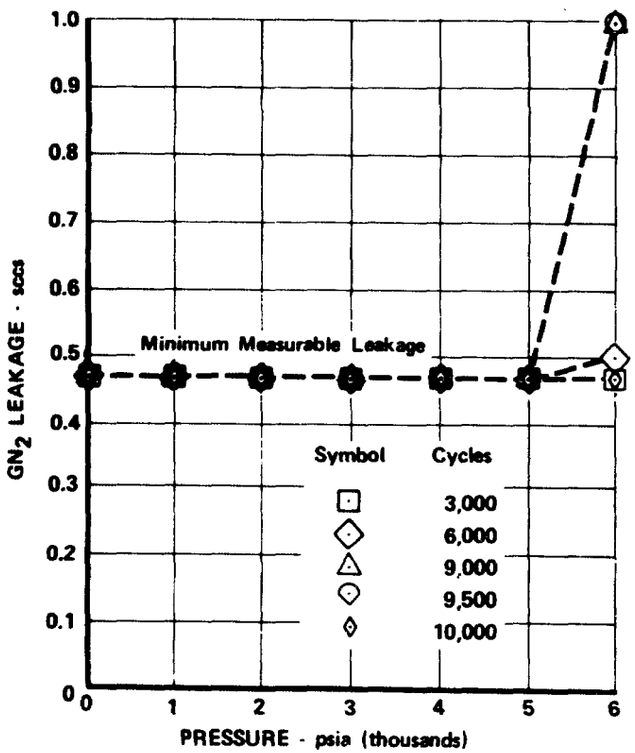

Figure 809. Shaft Seal Leakage - Cycling (Secondary) FD 44482

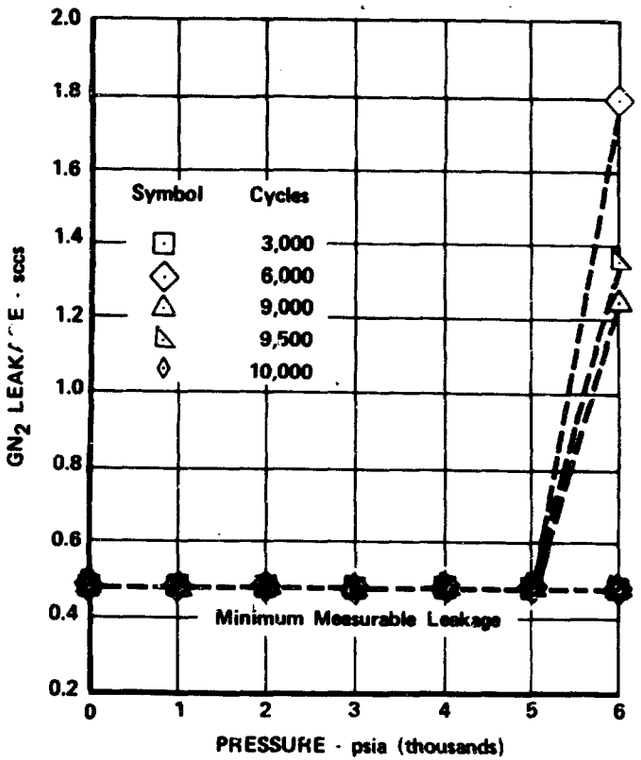

Figure 810. Shaft Seal Leakage - Static (Secondary) FD 44483

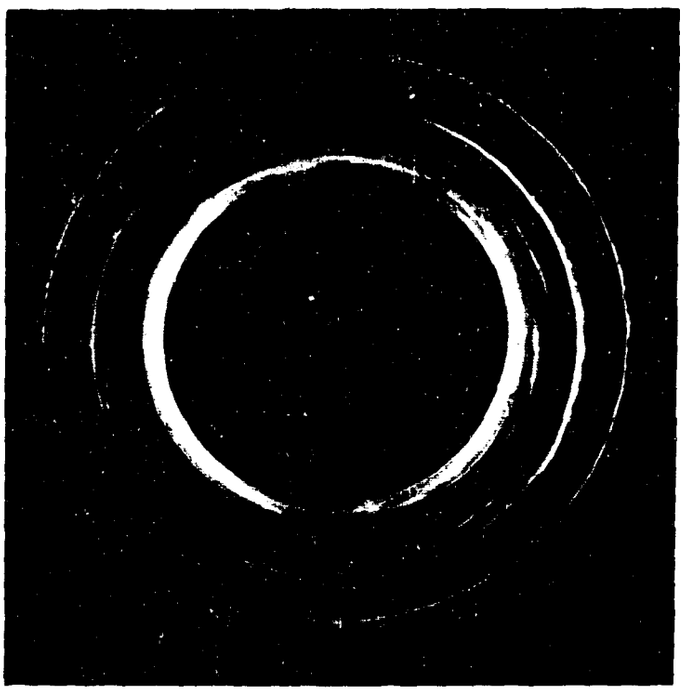

Figure 811. Shaft Seal Post-Test Condition (Primary) FE 92376

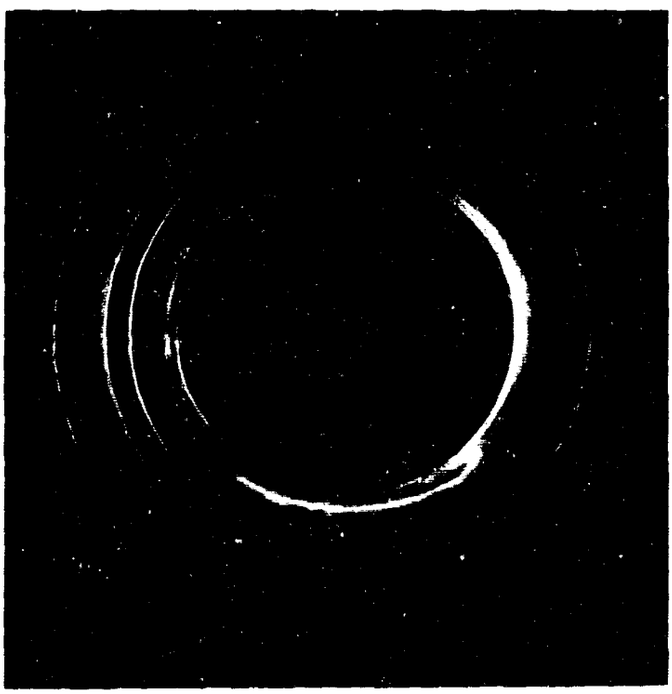

Figure 812. Shaft Seal Post-Test Condition (Secondary) FE 92377

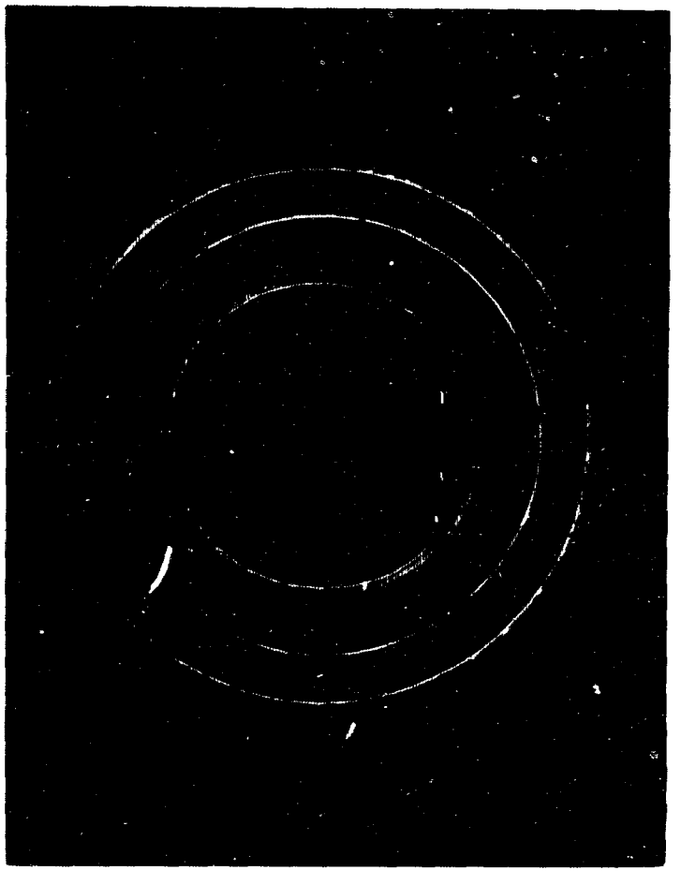

Figure 813. Shaft Seal in Typical Condition FE 95855

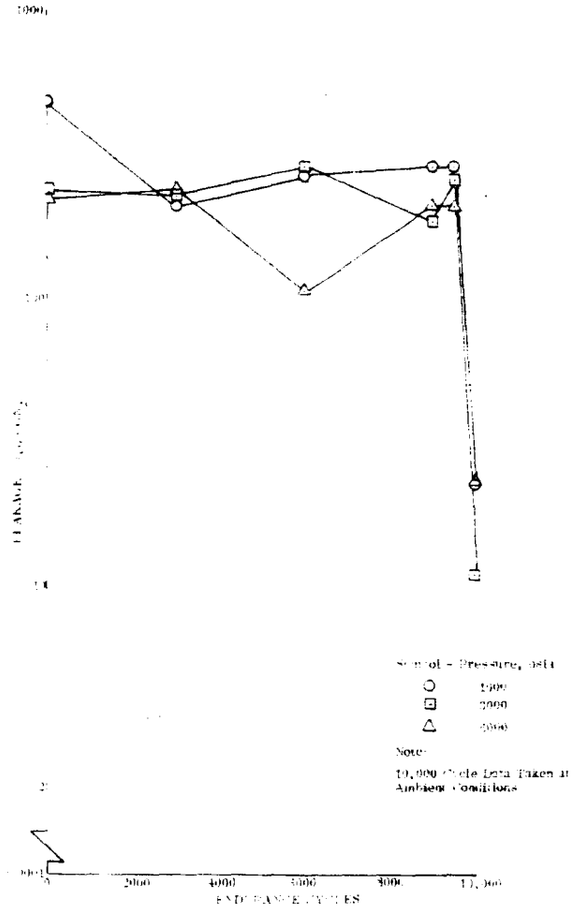

Figure 814. Balance Piston Seal Leakage - Static DF 77787

The shutoff seal leakages versus endurance cycles are shown in figure 815. The leakages are within the 10-sccs maximum limit throughout the 10,000 cycle endurance test. At each endurance cycle point, the valve was opened and closed five times and leakage recorded. This measurement was repeated three times at each endurance point. Figure 816 shows the shutoff seal before the test was run, and figure 817 shows the resultant post-test effect on the seal.

d. Deflection Tests

During the qualification and endurance testing of the preburner oxidizer valve at cryogenic temperatures, a sharp increase in primary seal leakage was encountered above 4000 psig. As dome pressure was increased above 6500 psig, an overboard leak was observed. To determine if the leakage was caused by the seal package separation from the dome, a series of deflection tests was performed. Dial indicators were spaced at various locations across the dome and it was then pressurized to 6600 psig. Readings of the dial indicators were recorded. Test data indicated that the dome top (where the seal package mounts) did have a concave deflection under pressurized conditions (shown in figure 818) as predicted from stress analysis using the finite element deck. The seal package that is bolted to the dome was also deflected, but because of its internal rigidity, did not deflect as much as the upper dome surface. The result was that the seal package pivoted about the outside diameter, and the inner diameter of the seal package was lifted away from the dome surface. (See figure 819.) Because this was the location of the primary static seal, an overboard leak path resulted between the dome and seal package radially to the seal package OD.

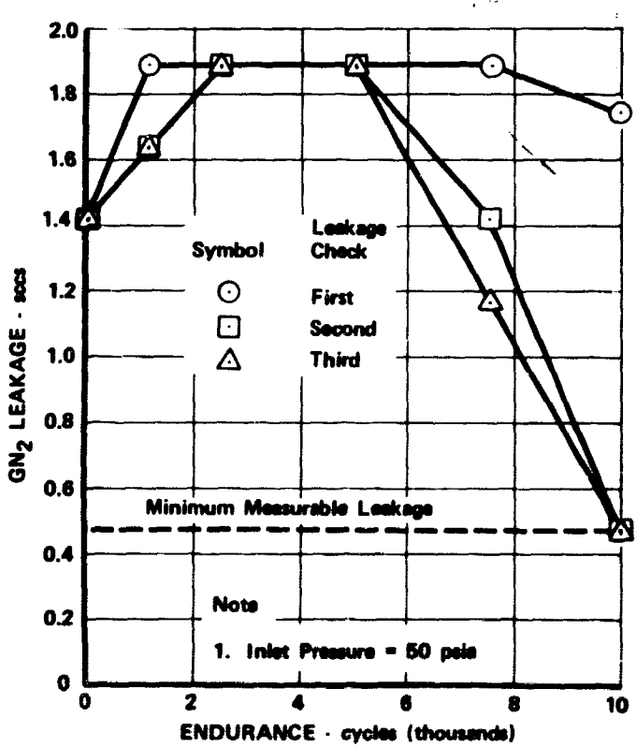

Figure 815. Shutoff Seal Leakage FD 44484

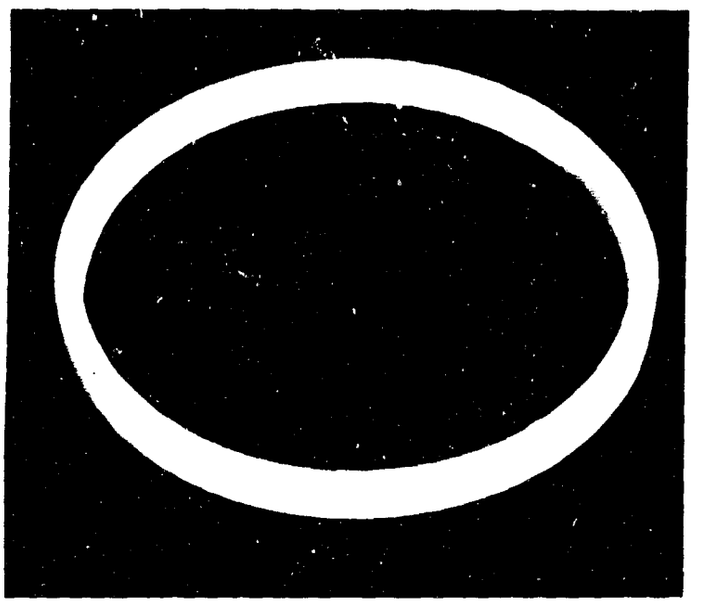

Figure 816. Shutoff Seal Before Test Run FE 90464

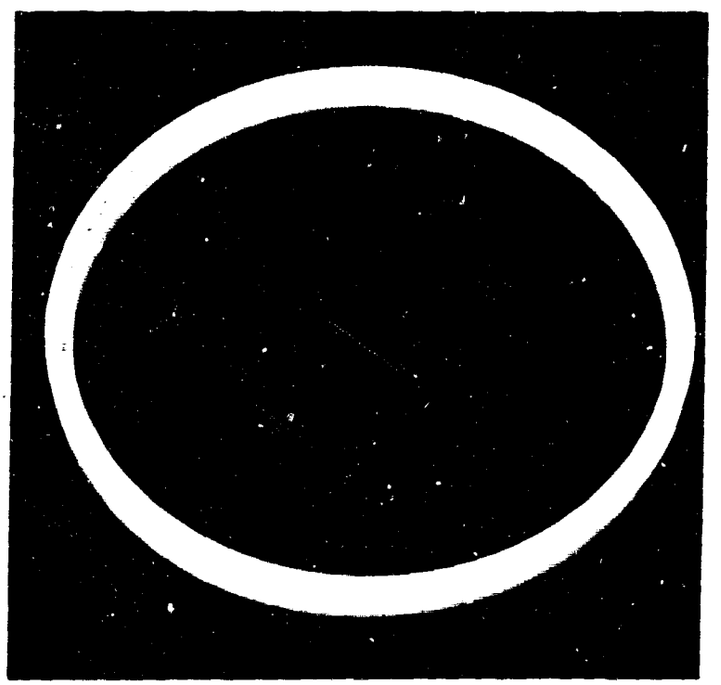

Figure 817. Shutoff Seal, Post-Test Condition FE 94076

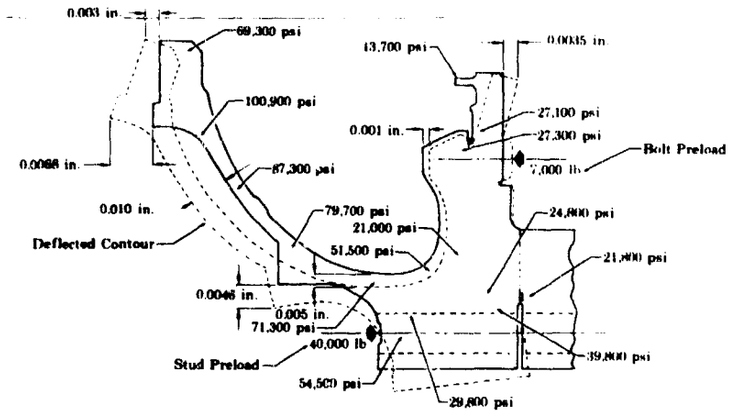

Figure 818. Preburner Dome Structural Analysis FD 27523

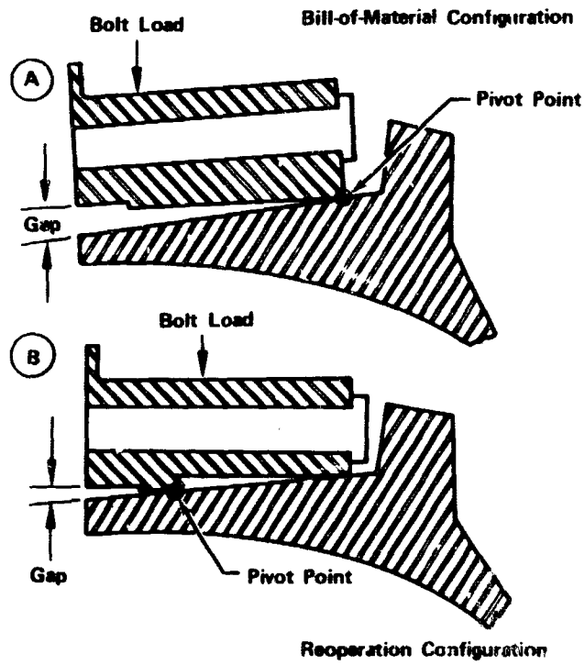

Figure 819. Effect of Seal Package Reoperation FD 38221

To reduce the separation at the static sealing surface, the lower seal plate was reoperated. The reoperation consisted of removing material to create a 0.007-in. raised ID on the bottom of the plate 1.340 to 1.345 inches in diameter. Figure 820 is a schematic of the bill-of-material and reoperated configuration. Preliminary evaluation of the reoperation indicated that deflection in the vicinity of the static seal was reduced. Final evaluation of the reoperated seal will require high-pressure cryogenic testing.

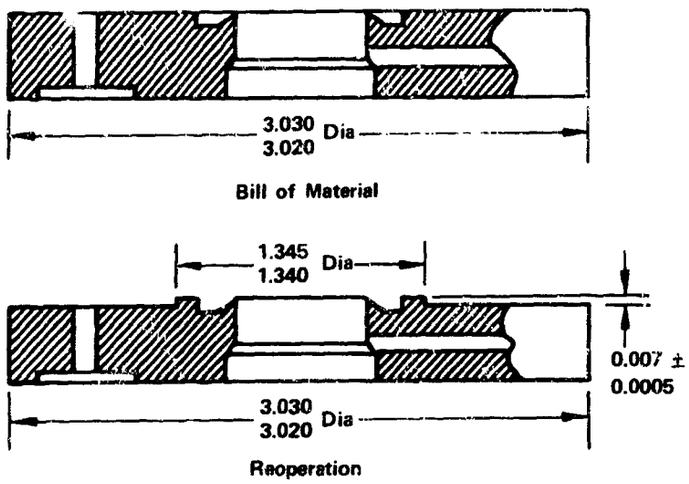

Figure 820. Reoperated Lower Seal Plate FD 38220

C. PREBURNER FUEL VALVE

1. Introduction

The preburner fuel valve is located downstream of the fuel pump in the line to the preburner supply heat exchanger. The function of this valve is to regulate the hydrogen flow to the preburner, and provide a tapoff port for the transpiration coolant flow for the main chamber. This control regulates hydrogen flow; therefore it has a major influence on fuel pump discharge pressure, chamber mixture ratio, and available turbine power. It has only a minor influence on thrust, because fuel flow is a small part of total propellant weight flow. Because the fuel valve influences pump discharge pressure, it affects fuel low-speed inducer drive power (i.e., main fuel pump NPSH) as well as transpiration cooling flow. The fuel valve provides pressure loss to aid fuel system stability and provides the main fuel flow shutoff function.

2. Summary, Conclusions and Recommendations

The design of the preburner fuel valve evolved from a study conducted to find a lightweight and compact fuel flow regulating and shutoff valve. Complete design details are presented in the Demonstrator Engine Design Report, AFRPL-TR-70-6.

Parts were fabricated for two complete valve assemblies. Additional seals and other expendable parts were provided for use during testing.

The preburner fuel valve was flow calibrated with water, and the test results agreed closely with the predicted values for effective area vs shaft angular movement.

The valve was endurance tested in LN_2 but failed to meet design requirements due to an incorrectly installed shim, and poor quality lip seals.

The errors found during testing of the preburner fuel valve have been corrected to prevent recurrence of the problems, and it is recommended that additional testing be performed to substantiate the design of the valve.

3. Hardware Description

The preburner fuel valve is a truncated ball valve with a straight shaft as shown in figure 821. The valve has a regulating range of 0.42 to 3.42 sq in. effective area with a maximum design effective area of 5.3 sq in. A tapoff port for the transpiration coolant flow required by the main burner is also provided. When viewed from the spline end of the valve shaft, the valve disk opens counterclockwise as shown in figure 821. As the valve is opened, the transpiration coolant port exposure starts at 4 deg and is fully uncovered at 28 deg.

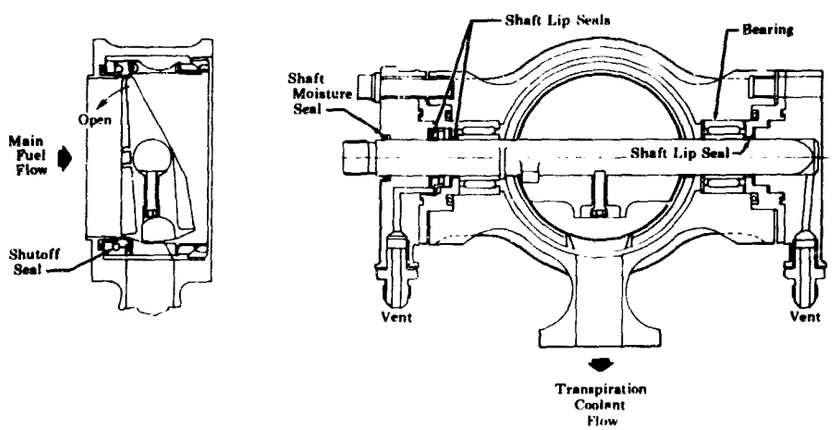

Figure 821. Preburner Fuel Valve FD 27536A

Positive fuel shutoff is provided when the spherical surface of the valve disk is sealed against a pressure-energized, hoop-type shutoff seal. Figure 822 shows a cross section of the hoop seal. The shutoff seal consists of a thin, silver-plated, hydroformed Inconel X-750 (AMS 5542) seal element welded in a seal housing.

Shaft lip seals of Kapton/TFE Teflon laminate are located between the roller bearings and the outer load-bearing surfaces. As illustrated in figure 823, a double lip seal is used at the spline end of the shaft, and a single lip seal is used at the blind end of the shaft. At the spline end of the shaft, the double lip seals are separated by a seal plate with radial vent passages. Leakage past the primary lip seal passes through the seal plate and is vented to a safe location. A single lip seal is used at the blind end of the shaft because the cover collects all of the leakage and vents it to a safe location. The use of a shaft seal and vent

at the blind end of the shaft prevents unbalanced shaft loads caused by internal pressure and eliminates the need for a thrust bearing.

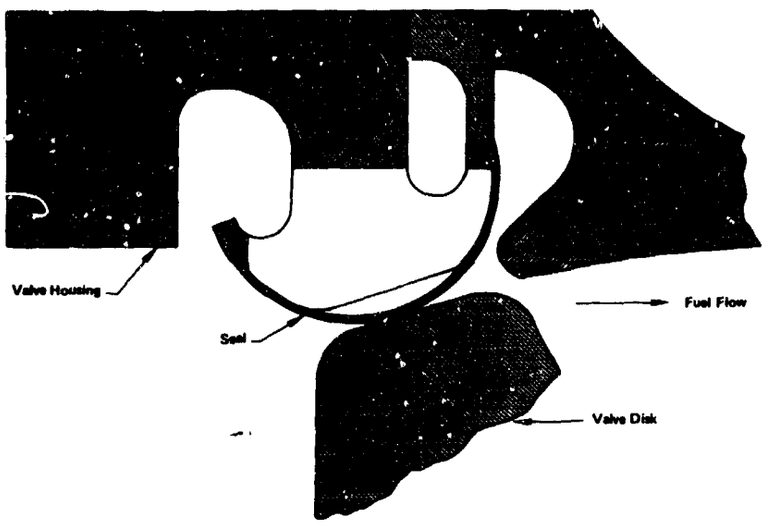

Figure 822. Hoop Seal Cross Section FD 27537A

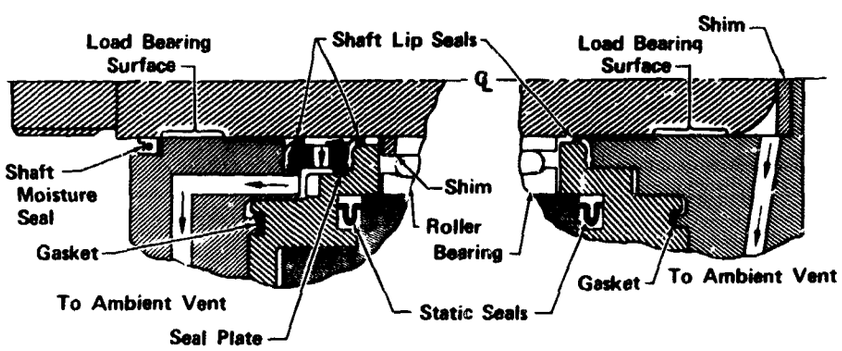

Figure 823. Shaft Lip Seals FD 27538B

The high-pressure static seals are silver plated Inconel 718 (AMS 5596) metal V-rings, and the low-pressure static seals are fluorocarbon gaskets of TFE Teflon film.

The preburner fuel valve housing shaft, disk, covers, and bolts are made of Inconel 718 (PWA 1010). Each end cover is bolted to the valve housing by six 0.375 in. x 24 bolts. The bearings are 440C corrosion resistant iron base alloy (AMS 5630). Silver plating is used on rubbing surfaces (outer bushings, the shutoff seal, thrust faces, and bolts) to prevent galling. Devices that require material deformation for locking are constructed of soft stainless steel (300 series) because of its ductility.

4. Fabrication

Procurement of two complete sets of detail parts was completed. The major difficulty encountered was the fabrication of the 0.005 in. thick Inconel X-750 seal element. Previously, seals of this type had been machined from bar stock but attempts to machine this seal were not successful. A search of other fabrication methods indicated that hydroforming a 0.005 in. sheet around a machined die would provide a suitable seal element. Development of the hydroforming process resulted in production of a uniform seal element. The procedure developed for the seal forming process is shown in figure 824. The formed hoop seal is then EB welded to the seal carrier, solution and precipitation heat treated in a hydrogen atmosphere, and the sealing surface is plated with 0.003 in. of silver.

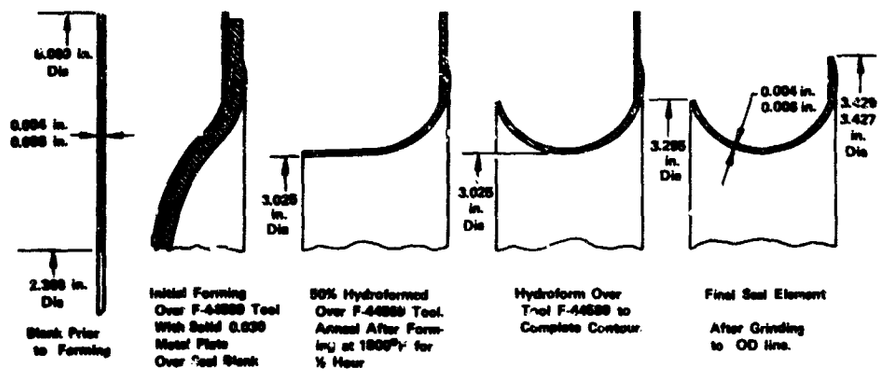

Figure 824. Fabrication of Preburner Fuel Valve Seal Element FD 39146

The preburner fuel valve disk was machined from Inconel 718 bar stock using conventional machining methods. Once machined, the spherical sealing surface was chrome coated to a thickness of 0.0001 to 0.0002 in.

The shaft for the valve was machined from Inconel 718 bar stock using conventional machining methods. The disk drive tab was silver plated per specification AMS 2470.

The valve housing was also machined from Inconel 718 bar stock using conventional machining methods.

The lip seals for the preburner fuel valve were fabricated as shown in figure 825. These seals consisted of three 0.005 in. thick layers of Dupont 500F-131 and one 0.005 in. thick layer of AMS 3647.

Table XCV indicates the lead times for the aforementioned parts.

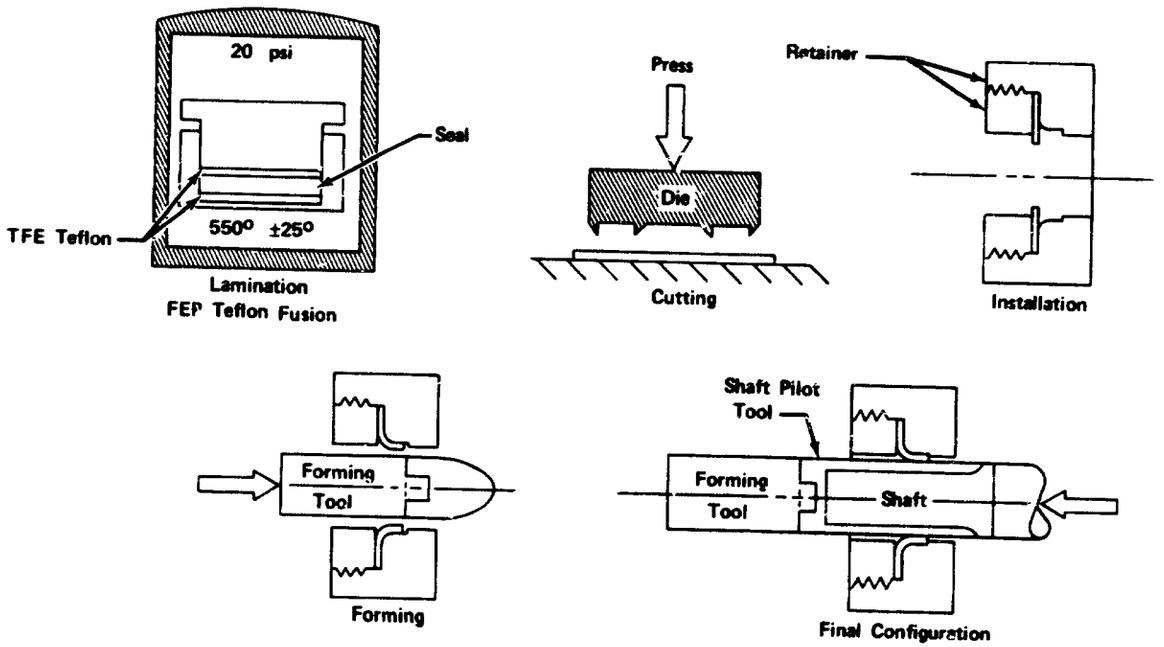

Figure 825. Lip Seal Fabrication

FD 47709

Table XCV. Preburner Fuel Valve Part Lead Times

Part Name	Lead Time (weeks)	
	Raw Material	Machining
Shutoff Seal	4	5
Disk	4	1
Shaft	4	1
Valve Housing	6	12
Lip Seals	8	0.2

Three builds of the preburner fuel valve were completed. The installation of the shutoff seal on the disk was accomplished by heating the seal element to 760°R and cooling the disk and shaft in liquid nitrogen. The parts were then mated centering the disk in the housing with tool F462436 as shown in figure 826. A shim was added to the shaft drive inner bearing race stackup to reduce the shaft end play to 0.001 in. The assembled valve weight was 15.02 lb.

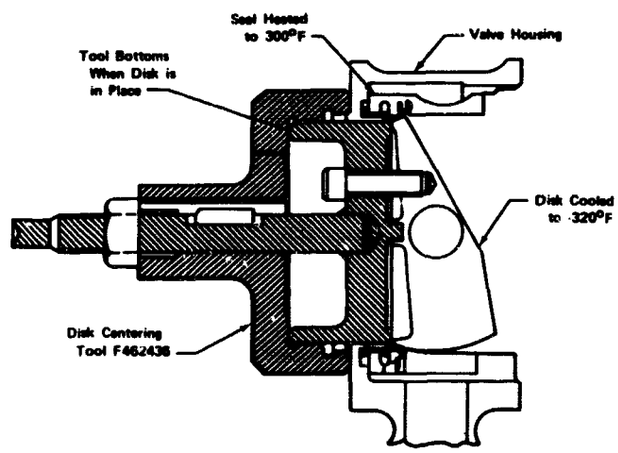

Figure 826. Assembly of Preburner Fuel Valve Shutoff Seal and Disk FD 39147

A commercial hydraulic servoactuator was used to provide valve rotation. The actuator support was custom machined to provide precise alignment with the valve in the closed position. The splines of the shaft coupling were silver plated for a shear silver fit to prevent looseness between the valve and the actuator.

Build 2 assembly of the preburner fuel valve was completed in essentially the same manner as build 1 assembly.

It was found, after build 1, that radial self alignment clearance between the shutoff seal assembly and valve housing was undesirable because the seal

tended to follow the disk as it opened and closed resulting in damage to the seal. For build 2, the seal assembly was nickel plated and remachined to pilot in the housing. In addition, the housing was machined to ensure concentricity of the seal assembly with the valve disk.

Build 3 of the preburner fuel valve was completed in essentially the same manner as build 2 assembly.

To prevent the locking of the spacers that occurred in build 2, an additional spacer with tangs to hole it in place was added. Also, the build 2 disk seal was reused. The valve assembly was stored without testing.

5. Testing

a. Water Flow Test

The water flow test was accomplished during build 1. Before cycling the valve, ambient shutoff seal leakage at 50 psid GN_2 across the seal was 0.785 sccs. The shaft seals did not leak at 50 psig valve pressure.

The valve was mounted on the B-21 water flow test stand. Flows were conducted to determine the effective area characteristics of the valve and the results are shown compared to the design prediction on figure 827. At several points during the flows, the valve torque requirements were measured by oscillating the valve approximately plus and minus two degrees and recording the actuator differential pressure required to move the valve. A comparison of the torque measured during test to the post test torque is shown on figure 828. The valve dynamic torque is shown on figure 829. The effective area determined by flow calibration of the transpiration coolant port compared to the actual area is shown on figure 830. Inspection of the valve during the water calibration testing after the points previously shown in figure 827 was completed showed the valve to be in generally good condition with some rubbing noted on the seal housing ID as shown in figure 831. Shutoff seal leakage was 25 sccs water at 50 psid. The stand plumbing was reinstalled and additional flow testing was performed. A shift in effective area was noted and another valve inspection indicated the seal loading nut lock ring had collapsed in one section as shown in figure 832. The ring was determined to have collapsed due to a low pressure area caused by the high flow velocity at the small valve area when the valve was near the closed position.

To prevent the collapse of the seal loading nut lock ring that occurred in build 1, the lock ring was modified to the configuration shown in figure 833. The modifications to the lock ring consisted of pressure equalization holes at base of the lip, and a shorter lip.

Prior to valve disassembly, the valve housing was stress coated and hydrostatically proof-pressure tested at 7300 psig. The results of this pressure check indicated no yielding of the valve housing. The stress patterns are shown in figure 834 and 835.

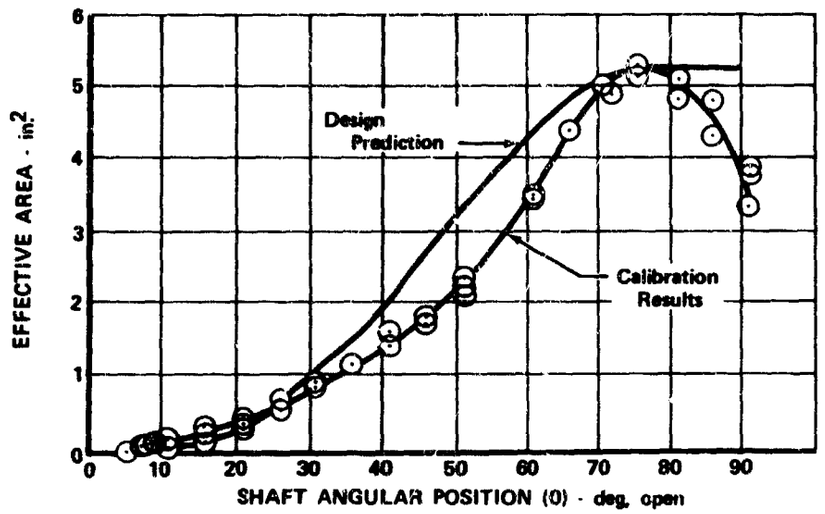

Figure 827. Results Compared to Design Prediction FD 44485

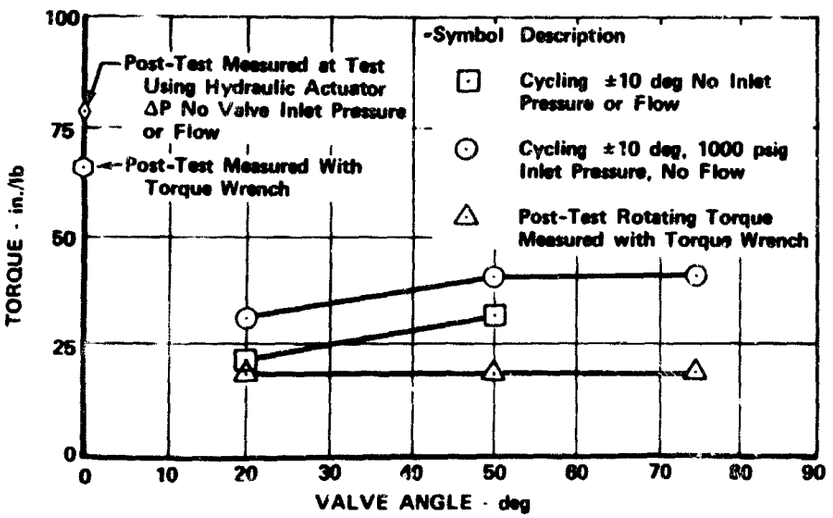

Figure 828. Post-Test Torque FD 44486

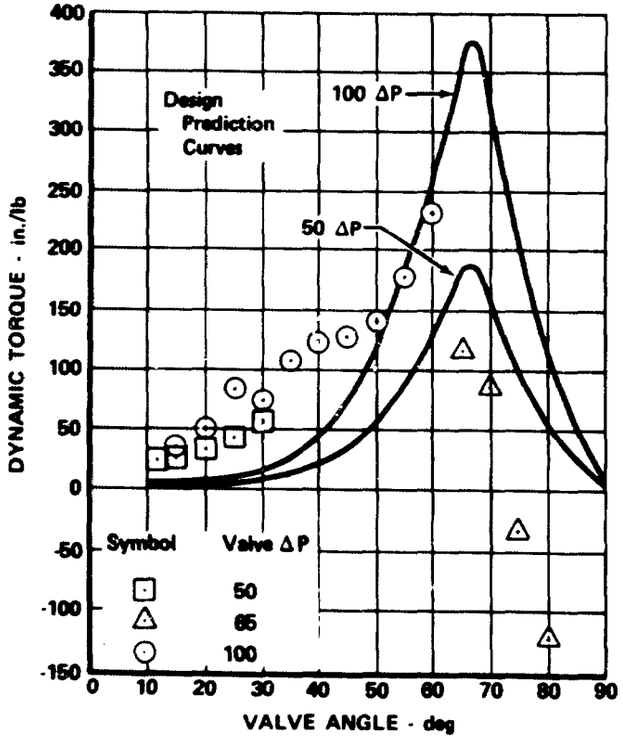

Figure 829. Valve Dynamic Torque FD 44487

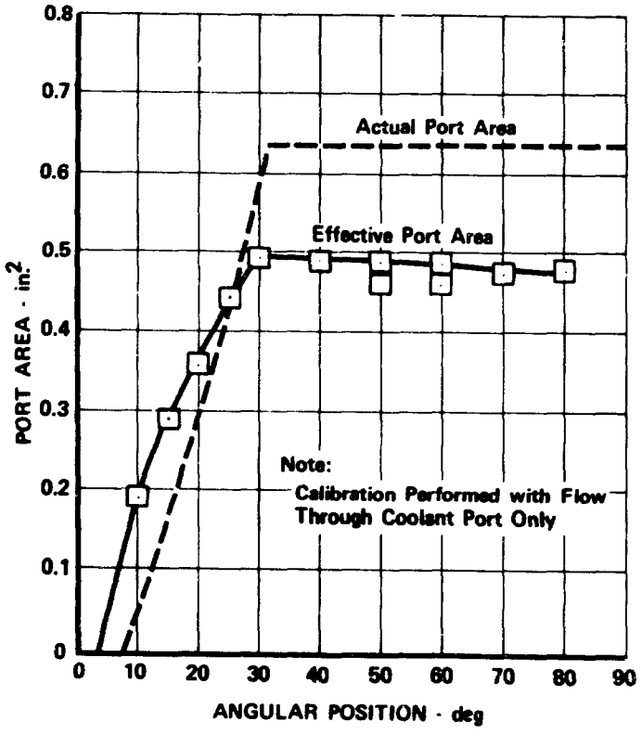

Figure 830. Transpiration Coolant Port Compared to the Actual Area FD 44488

Figure 831. Seal Rubbing On Seal Housing Inside Diameter FE 93460

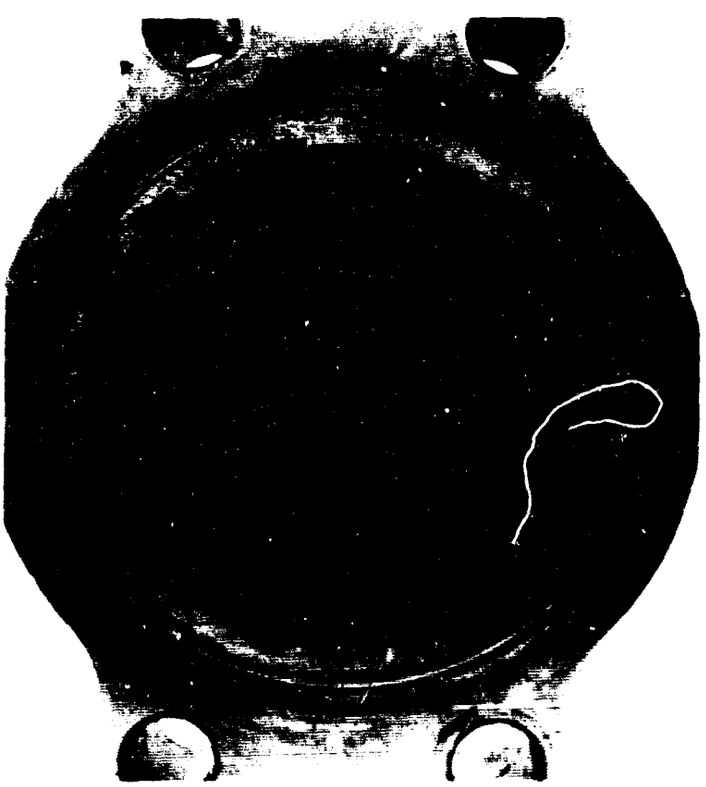

Figure 832. Collapsed Seal Loading Nut Lock Ring FE 95607

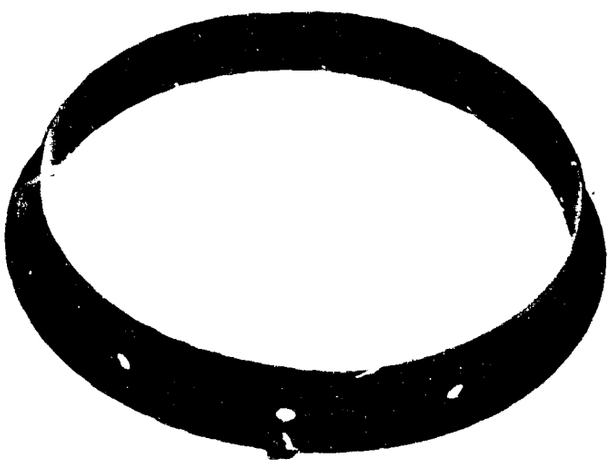

Figure 833. Modified Seal Loading Nut Lock Ring FE 99411

Figure 834. Preburner Fuel Valve Housing Stress Patterns FE 95526

Figure 835. Preburner Fuel Valve Housing Stress Patterns FE 95513

Post-test shutoff seal leakage was excessive. Valve disassembly showed the seal housing had been moving during disk actuation. Rub marks partially shown in figure 836 were noted 360 deg around the seal housing ID. The circular rub mark on the face of the seal housing as shown in figure 837, the radial marks on seal retaining ring as shown in figure 838, and rub marks on the shaft and the disk all indicated relative movement between the seal housing and the valve housing. The static seal support ring, as shown in figure 839 also indicated a relative motion between the valve housing and the seal housing. The seal element was scored and marred as previously shown in figure 838 and 836. Pressure check of the 0.005 in. thick seal element indicated the seal element to be intact in spite of the heavy seal wear.

The location of the collapsed retaining ring as previously shown in figure 832 indicates the valve was near the closed position when the failure occurred. The ring apparently collapsed because of external pressure differential caused by the high local flow velocity. The remaining parts were in excellent condition.

Figure 836. Rub Marks On Seal Housing ID FE 96719

Figure 837. Circular Rub Mark On Face Of Seal Housing FE 96331

Figure 838. Radial Marks On Seal Retaining Ring FE 96331

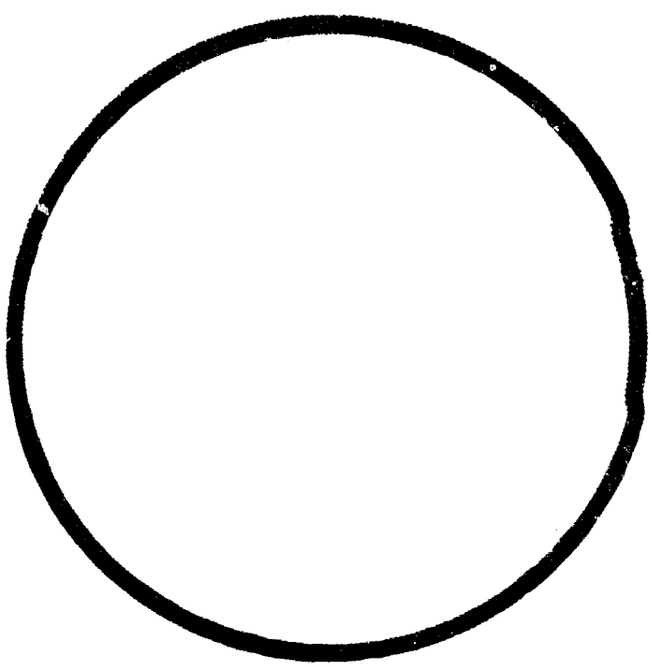

Figure 839. Static Seal Support Ring Indicated Relative Motion Between Valve Housing and Seal Housing FE 95659

b. Endurance Test

The endurance test was accomplished with build 2 assembly.

Before test, ambient temperature shutoff seal leakage at 50 psid was 0.108 sccs. The shaft seals did not leak at 50 psig valve pressure.

The valve was mounted on B-22 test stand, with object being to perform a cycle endurance test at cryogenic and ambient temperatures. Of primary interest was the performance of the disk shutoff seal and shaft lip seals in terms of leakage. Also, torque and valve/actuator frequency response and time constant (τ) were to be determined.

The testing consisted of shutoff cycle endurance, torque measurement cycling, frequency response cycling and time constant checks.

A total of 10,000 shutoff cycles between 0 deg and 35 deg were performed - the first 2500 at cryogenic (liquid argon) temperature and the remainder at ambient temperature. During the endurance test, leakage measurements were made at 1, 19, 50, 100, 500, and each succeeding 500 cycles. The shutoff seal leakage is shown in figure 840. The drive end shaft lip seal leakage and blind end shaft lip seal leakage are presented in figures 841 and figure 842, respectively. After the ambient temperature endurance cycles were completed, cryogenic temperature post-test leakage measurements were made.

At the end of each 500 shutoff cycles, the valve was cycled at 1/2 cps between 5 deg and 40 deg with 50 psig inlet pressure applied. The valve actuator differential pressure was read at 40 deg from oscillograph traces to determine the torque required to move the valve, i.e., total torque. This data is presented in figure 843.

After the completion of the endurance cycles, the valve was cycled between 40 deg and 45 deg and between 60 deg and 65 deg at varying frequencies from 1 cps to 20 cps. From oscillograph traces, amplitude ratio and phase lag was calculated. These data are shown in figures 844, 845, 846, and 847. The frequency response is down 2.5 to 3.0 db at 10 cps. No significant difference is noted between ambient and cryogenic valve temperatures. However, the valve lags the request signal by 100 deg at 10 cps.

Step change requests for 5-deg valve rotation were made from the 5 deg, 30 deg, and 60 deg positions at both cryogenic and ambient temperatures. No detectable difference in the time constant (τ) was apparent at the different positions. Plots at the 5-deg position are presented in figures 848 and 849.

At teardown all static seals in the pressure covers were in excellent condition, as expected, since post-test external leak check at 50 psig revealed no leaks.

All of the three shaft lip seals were cracked and frayed, with the TFE Teflon layer showing significant wear, delamination, and pressure rupture. The blind end shaft lip seal in the end cover is shown in figure 850. The seal is shown after end cover disassembly, in figure 851. The drive end cover assembly showing the crack in the primary lip seal and frayed secondary lip seal is seen in figure 852. The seals are shown after cover disassembly in figure 853.

A

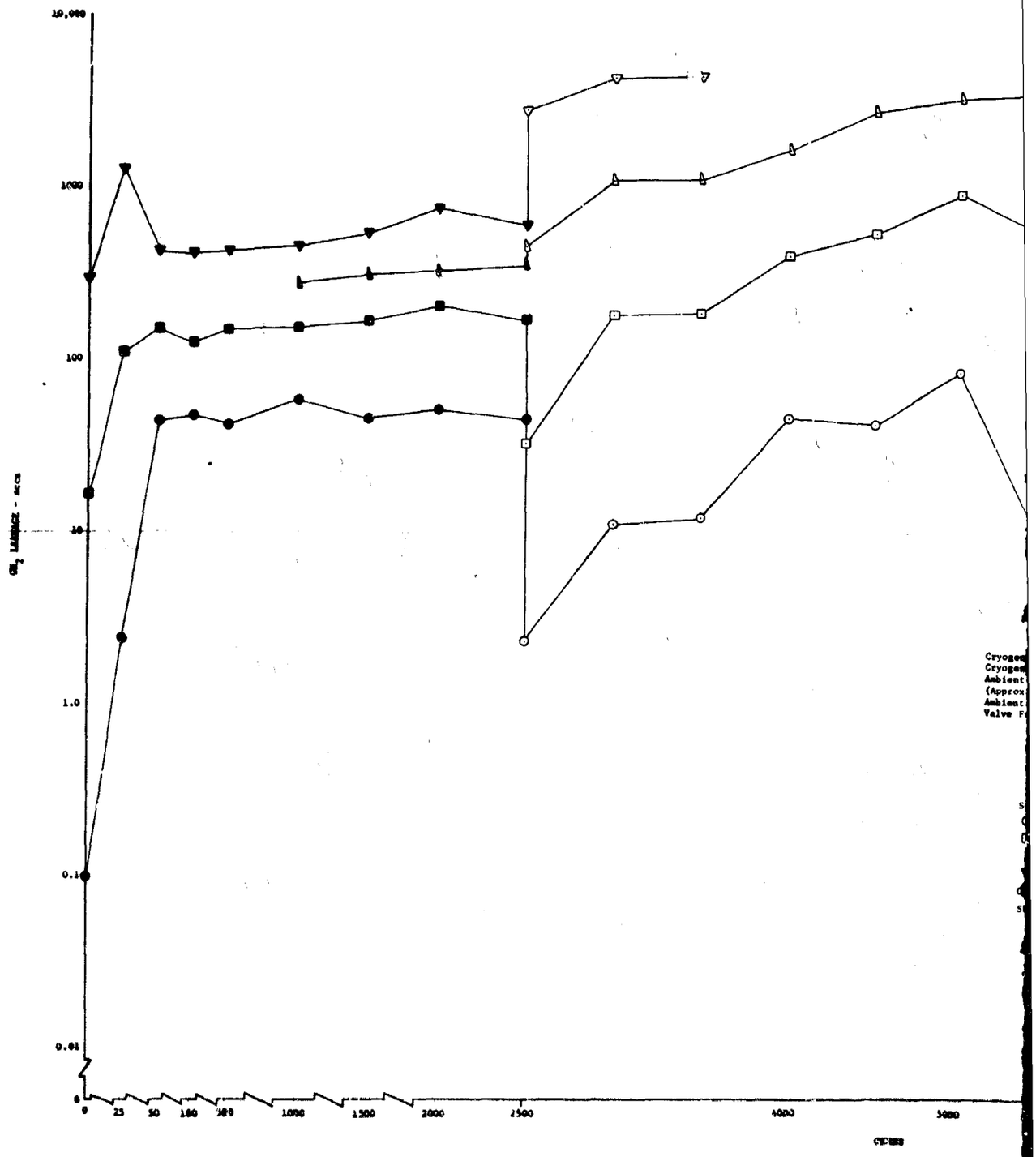

Figure 840. Shutoff Seal Leakage

1 B

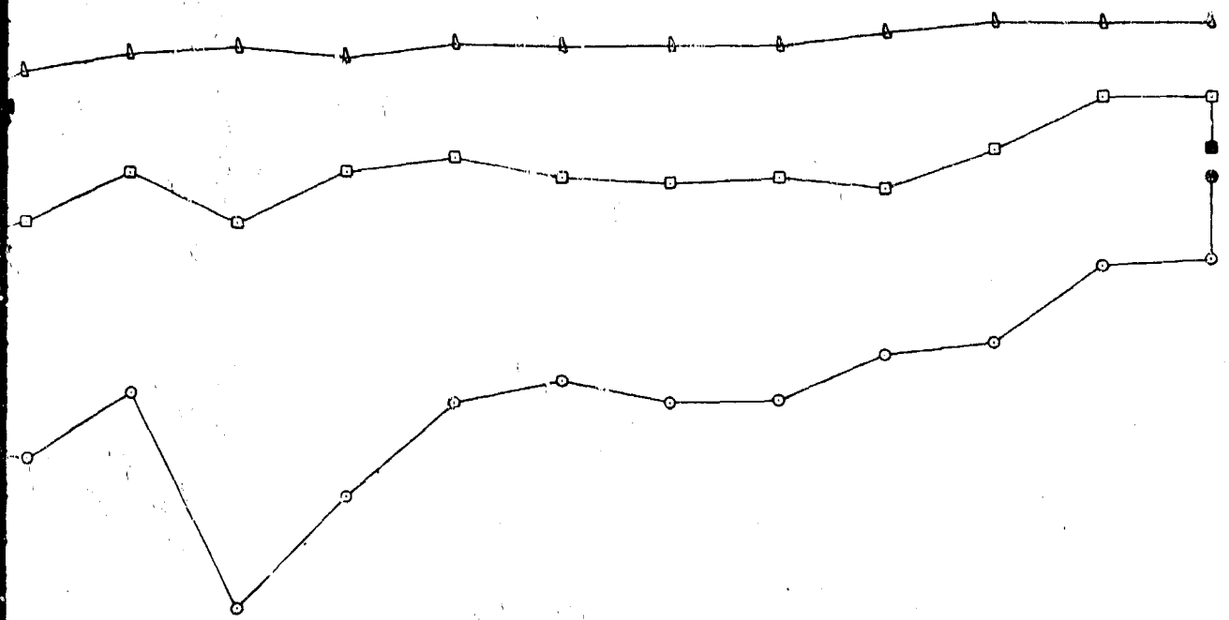

Cryogenic Valve Inlet Temperature = 150°
Cryogenic Bath Temperature = 158°
Ambient Valve Inlet Temperature
(Approximately 80°F)
Ambient Bath Temperature Approximately 80°F
Valve Fully Closed at 0°

Symbol	P
⊙ ●	50
⊡ ■	150
▲ ▲	300
▽ ▼	500

Open Symbol - Ambient Conditions

Shaded Symbol - Cryogenic Conditions

CYCLES

A

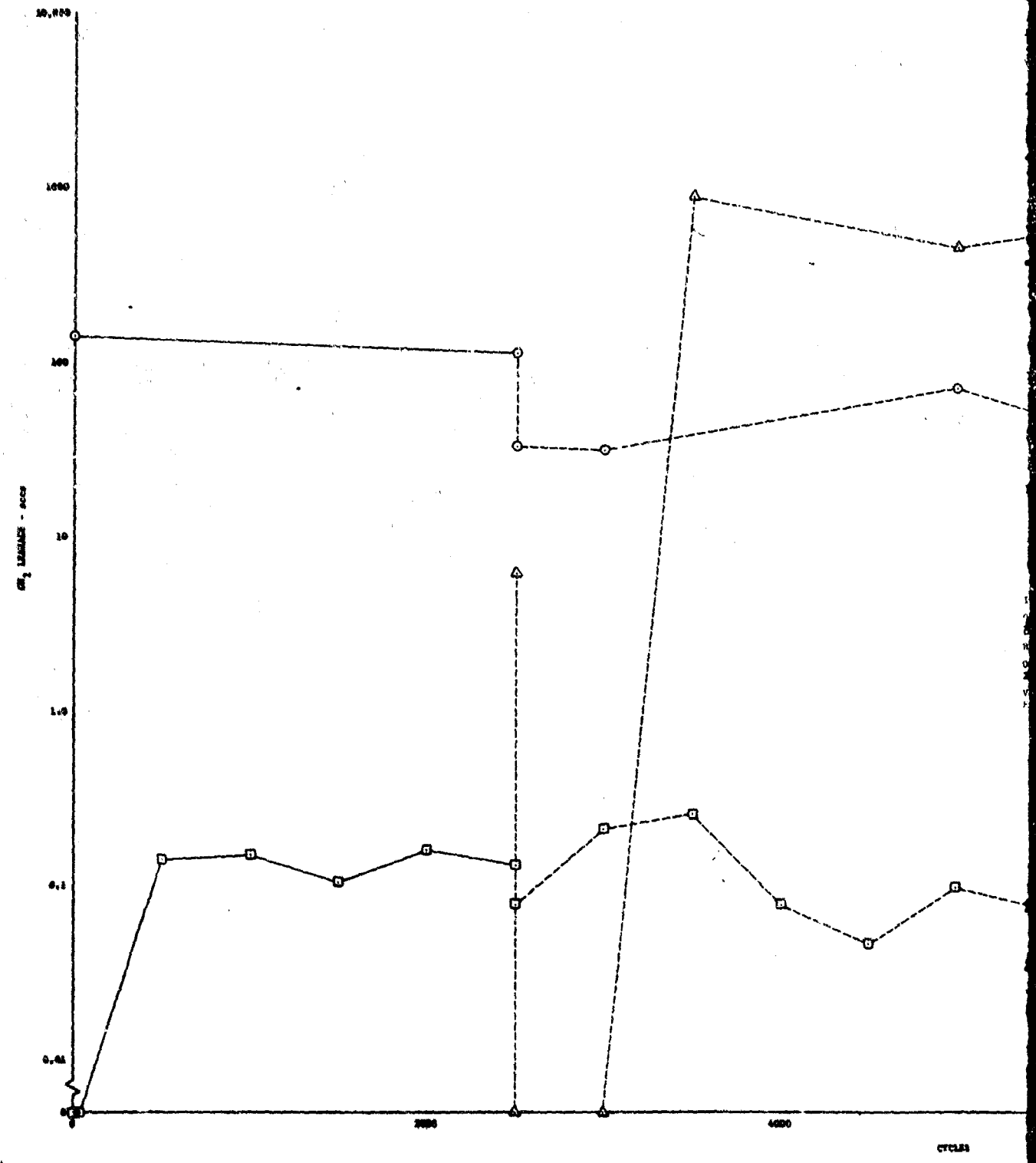

Figure 841. Drive End Lip Seal Leakage - (Primary)

B

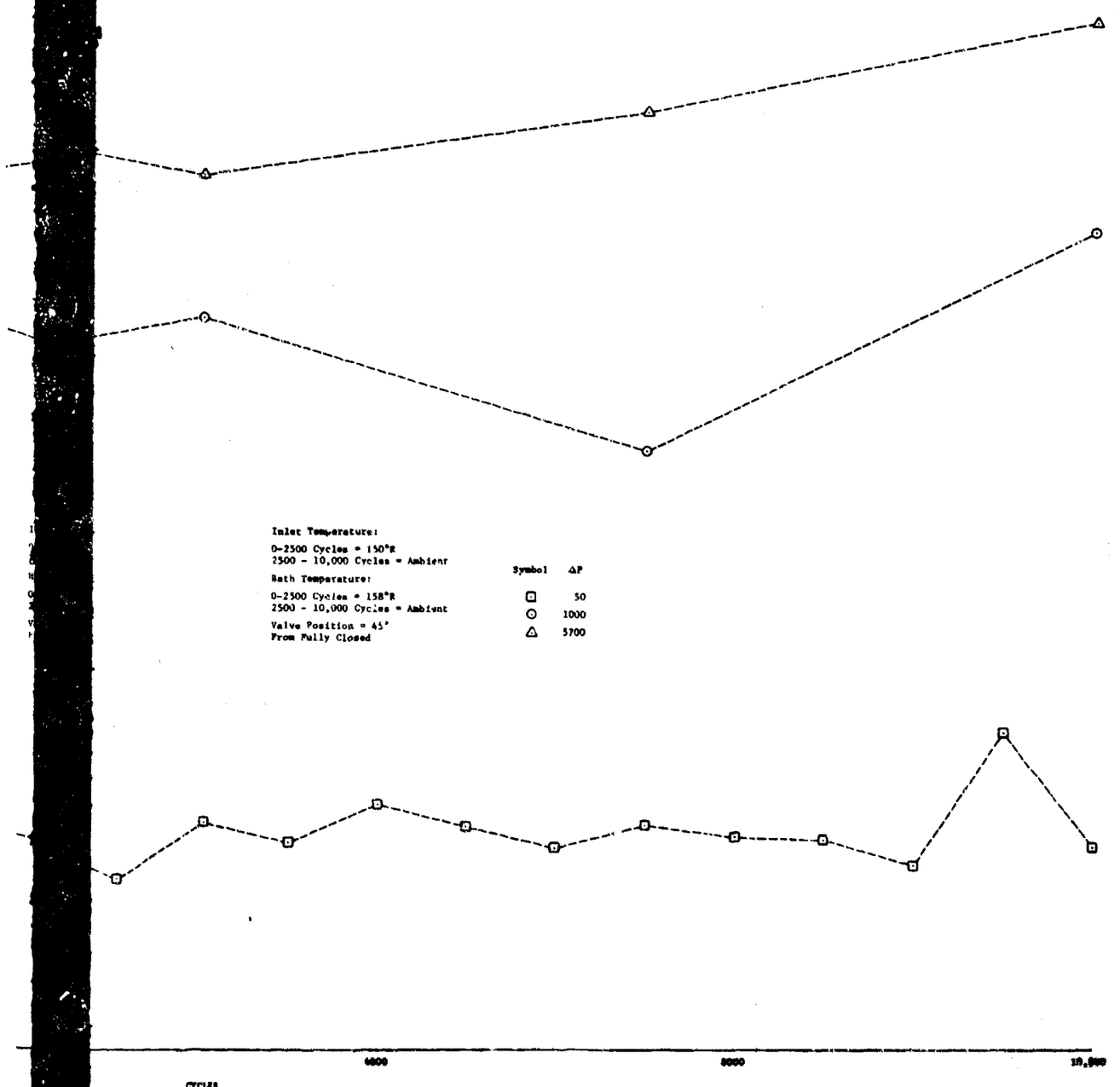

DF 80279

883/884

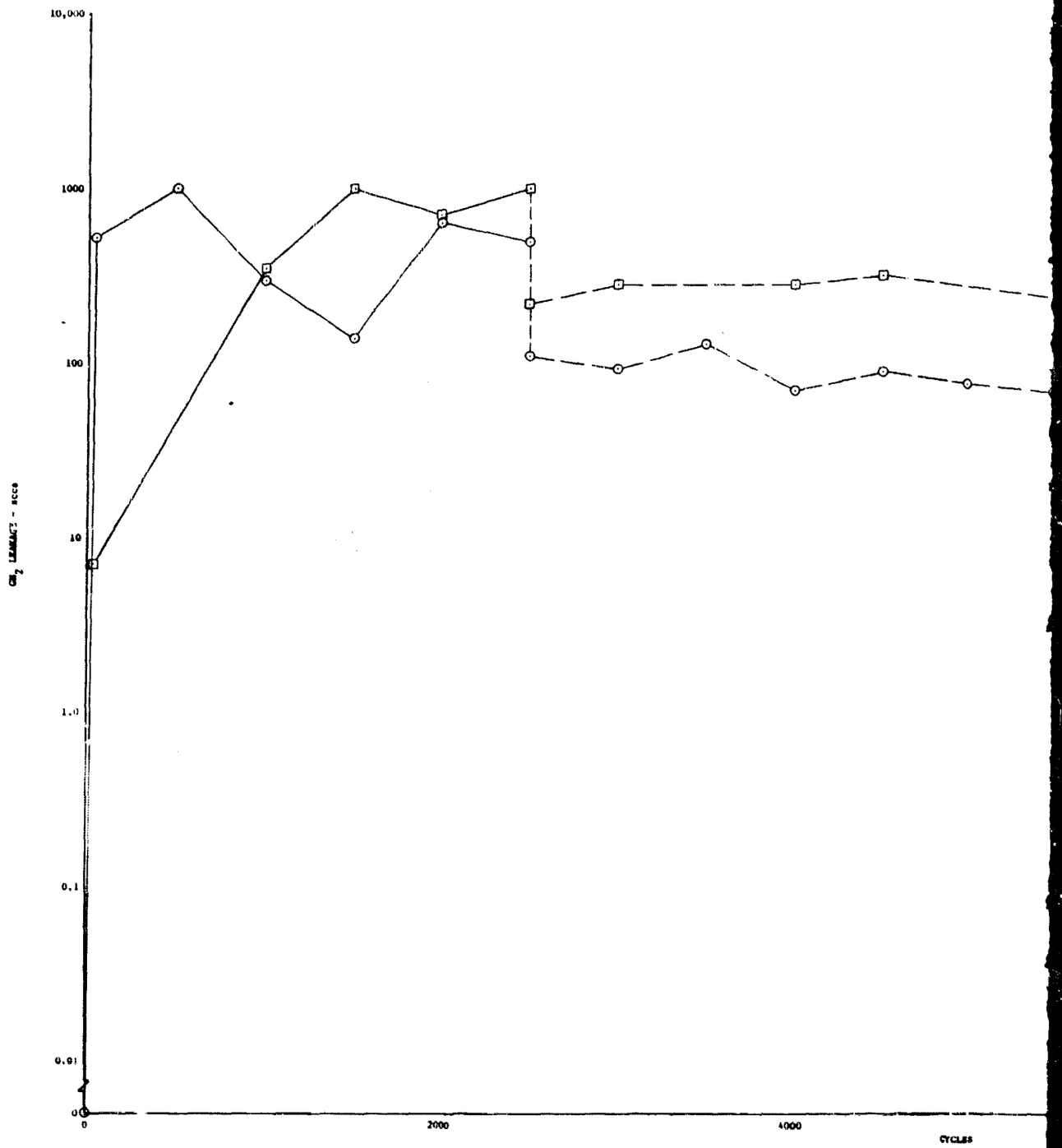

Figure 842. Blind End Shaft Lip Seal Leakage

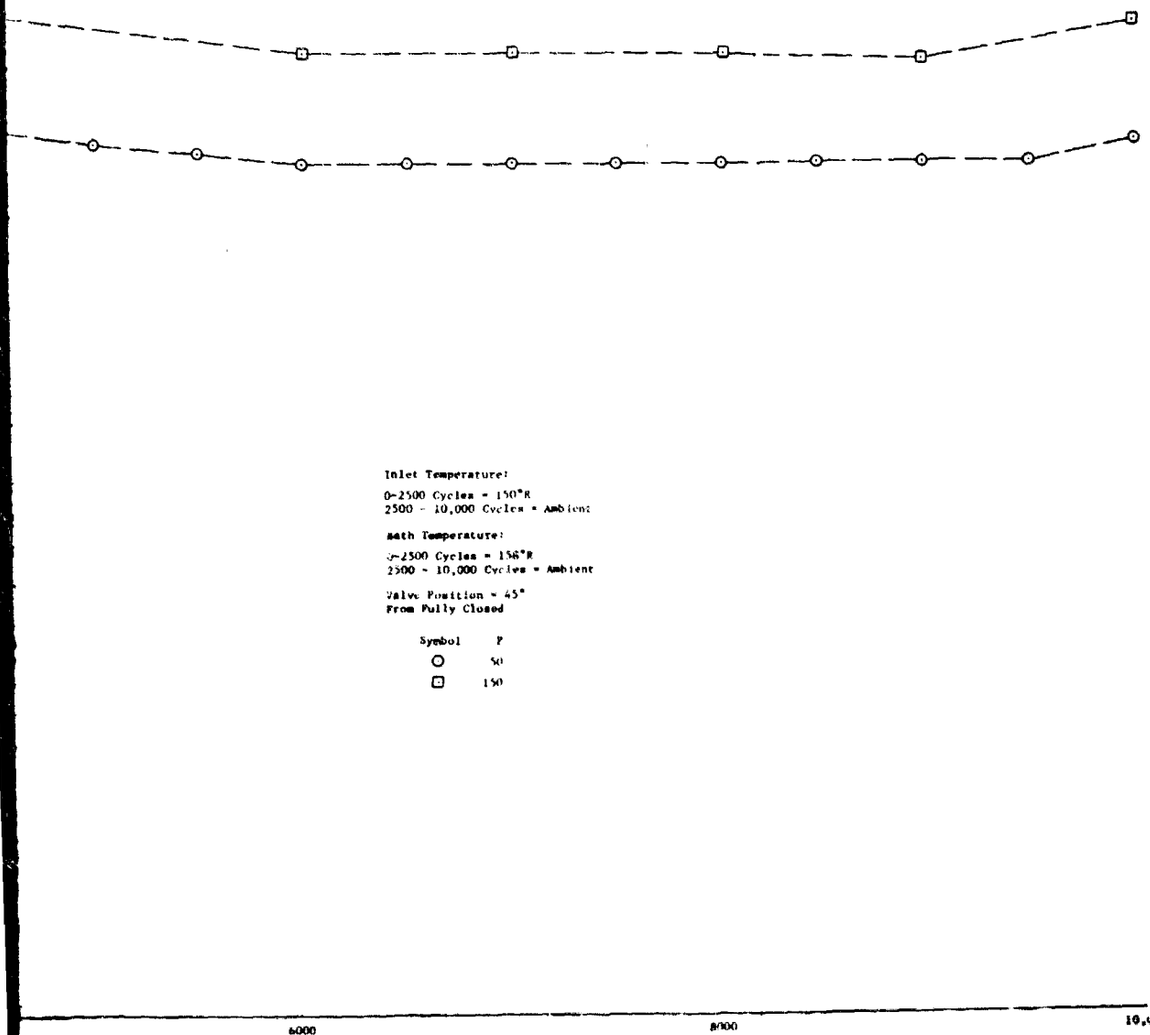
Inlet Temperature:
0-2500 Cycles = 150°R
2500 - 10,000 Cycles = Ambient
Bath Temperature:
0-2500 Cycles = 156°R
2500 - 10,000 Cycles = Ambient
Valve Position = 45°
From Fully Closed
Symbol P
50
150
6000
8000
10,000
CYCLES

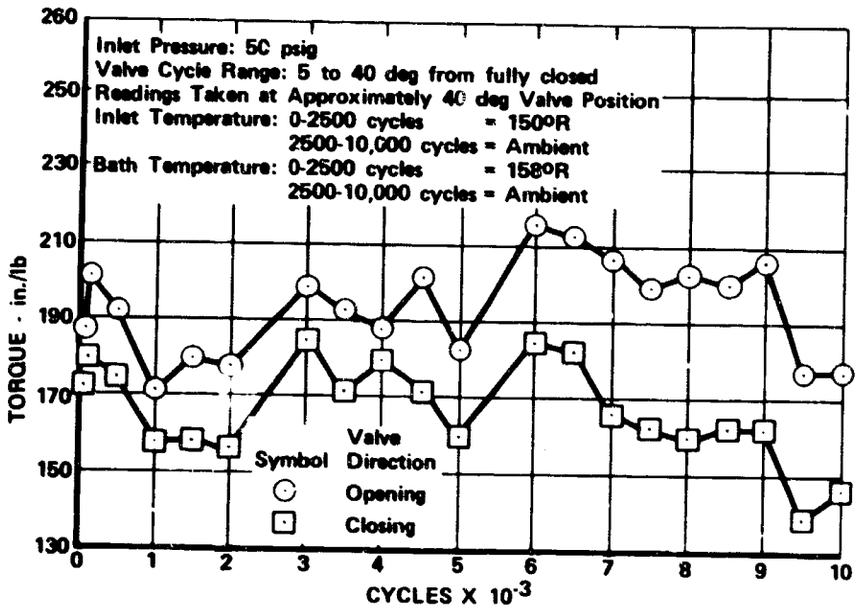

Figure 843. Total Torque Data FD 44489

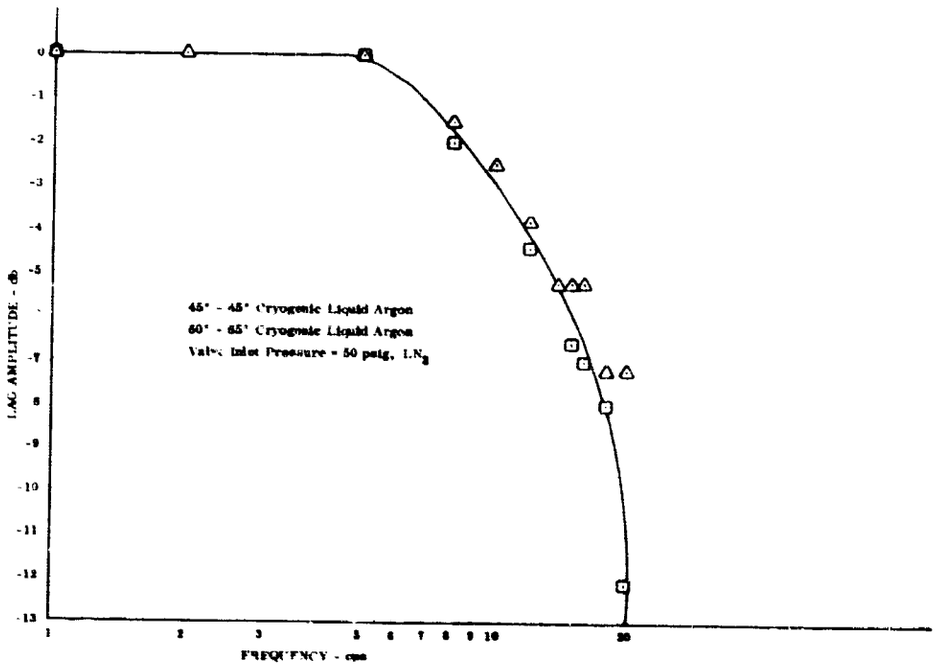

Figure 844. Amplitude Ratio and Phase Lag DF 80281

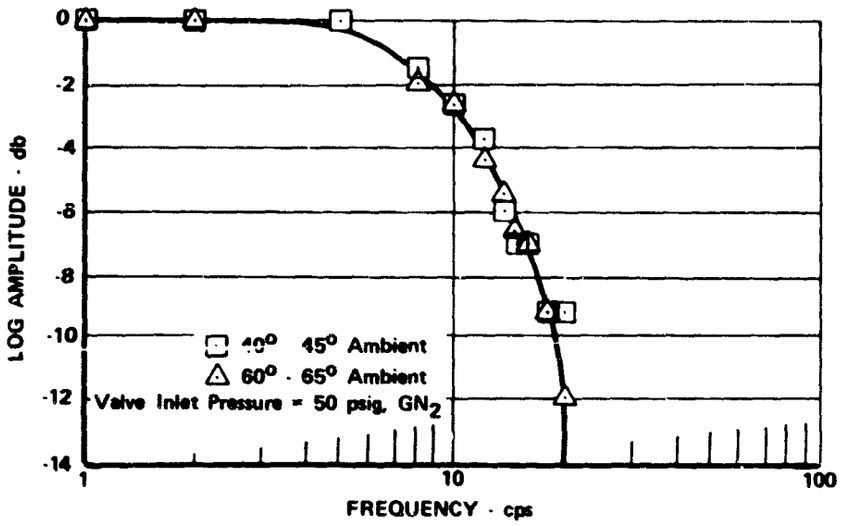

Figure 845. Amplitude Ratio and Phase Lag FD 44465

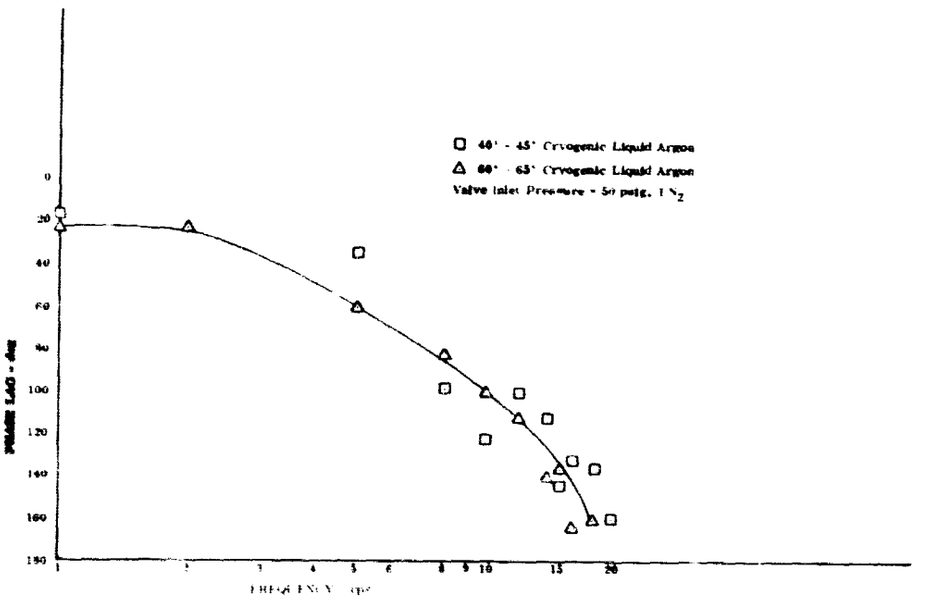

Figure 846. Amplitude Ratio and Phase Lag DF 80283

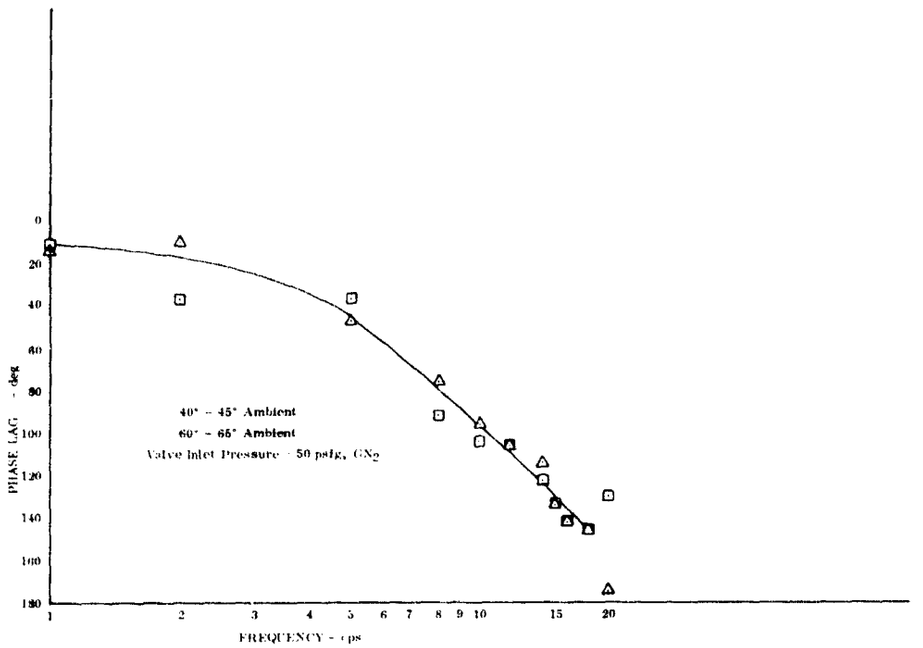

Figure 847. Amplitude Ratio and Phase Lag DF 80284

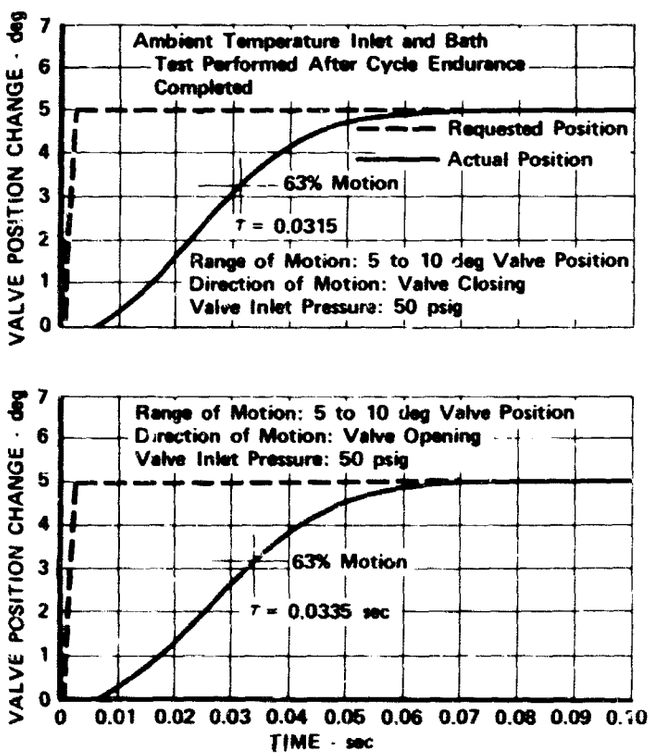

Figure 848. Plots At the 5-degree Position FD 44467

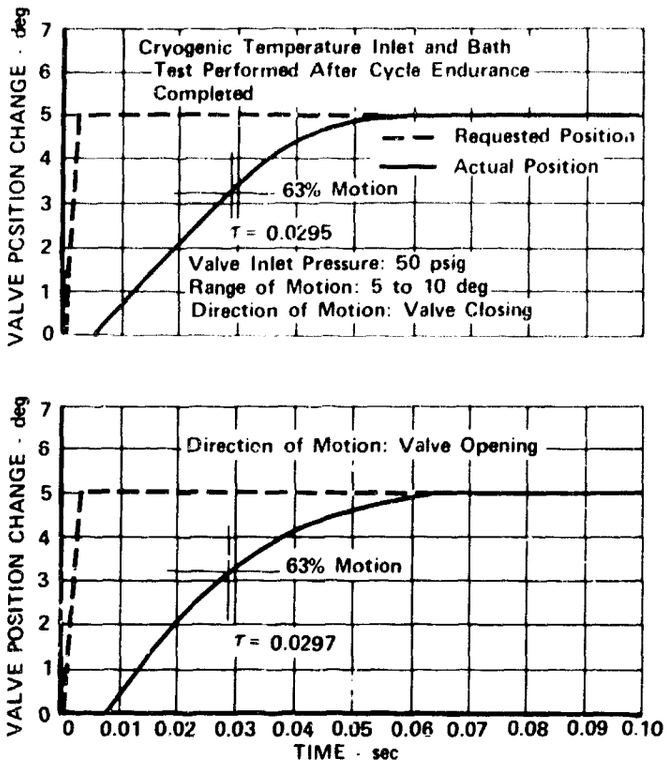

Figure 849. Plot At the 5-degree Position FD 44463

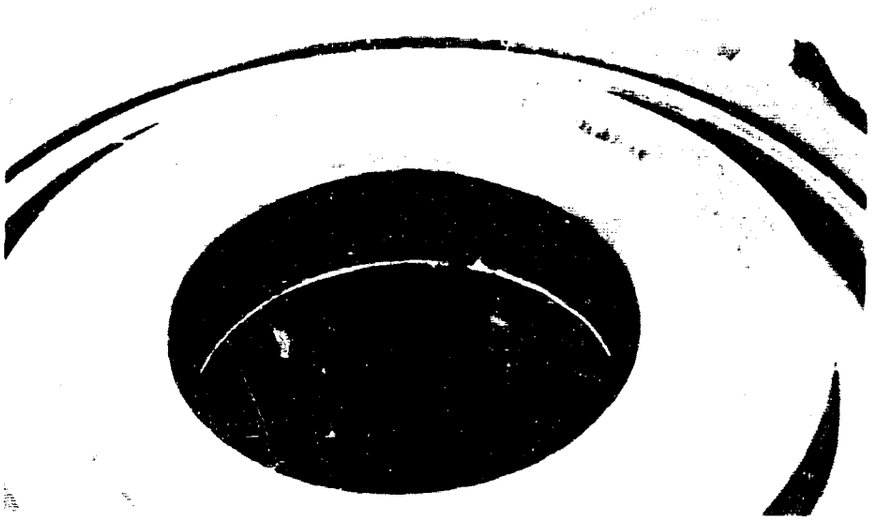

Figure 850. Blind End Shaft Lip Seal In the End Cover FE 97709

Figure 851. Seal Shown After End Cover Disassembly FE 97793

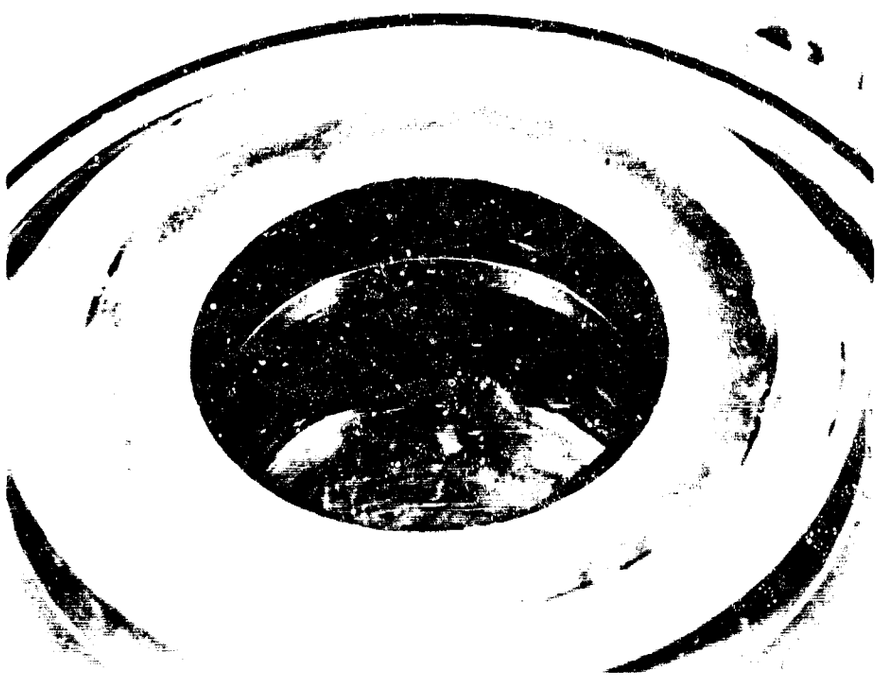

Figure 852. Drive End Cover Assembly Showing Crack In Primary Lip Seal and Frayed Secondary Lip Seal FE 97710

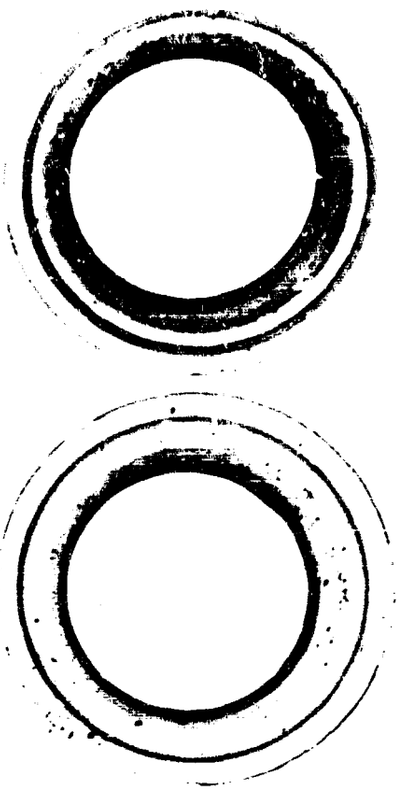

Figure 853. Seals Viewed After Cover Disassembly FE 97794

Severe wear occurred in the silver plating at the blind end of the valve shaft. The reason for this is seen in figure 854, showing the shaft end cover with end play shim and spacer installed, and in figure 855, showing the condition of the shim after removal. It appears that the spacer became canted during assembly and partially rolled under the end of the shaft. The amount of axial load applied to the shaft was considerable as evidenced by the amount of spacer and shim deformation. The end wear on the shaft is shown in figure 856. However, the disk position relative to the shutoff seal was reasonably stable, judging by the seal wear pattern.

The shutoff seal was in very good condition considering the number of cycles performed. It is shown in figure 857. As expected, the hoop seal element silver plating was worn, but the wear area was nearly symmetrical. The 0.005 in. thick Inconel 750-X element was not ruptured, but the shutoff seal assembly liner showed wear marks indicating that the disk had moved toward the drive end of the shaft. As the silver plate on spacer became worn, the disk and shaft were allowed to move until the disk rubbed the liner. Based on pre-build measurements and parts tolerances, this indicated disk movement was approximately 0.005 in.

Figure 354. Severe Wear In Silver Plating At Blind End of Valve Shaft FE 97706

Figure 855. Condition of Shim After Removal FE 97792

Figure 856. End Wear On Valve Shaft FE 97705

Figure 857. Shutoff Seal Showing Good Condition After Cycle Test FE 97712

Profilometer measurements of the disk seal show an approximate overall deformation of the seal from design specifications of 0.005 of an inch. The area 60 deg from the centerline of the blind end shaft opening show a deformation of approximately 0.016 in. from design specifications. Figure 858 shows an overlay of the deformations mentioned. The overall 0.005 in. deformation is a result of shutoff wear of the seal while the 0.016 in. wear stems from the cocked shim and ovalizing of the 0.005 in. disk seal.

The valve disk is shown in figure 859. The photo points up both rotational and circumferential wear marks in the chrome coating. These marks are similar to those of build I and are considered normal except for some very small scratches apparently caused by particulate contamination imbedded in the hoop seal plating.

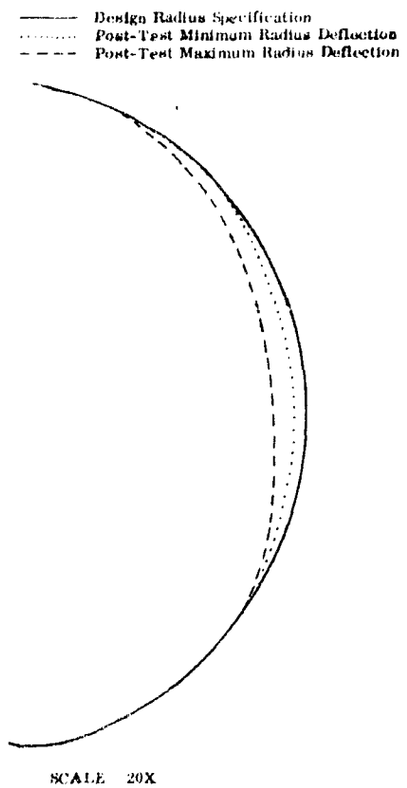

Figure 858. Shutoff Seal Deformations DF 80354

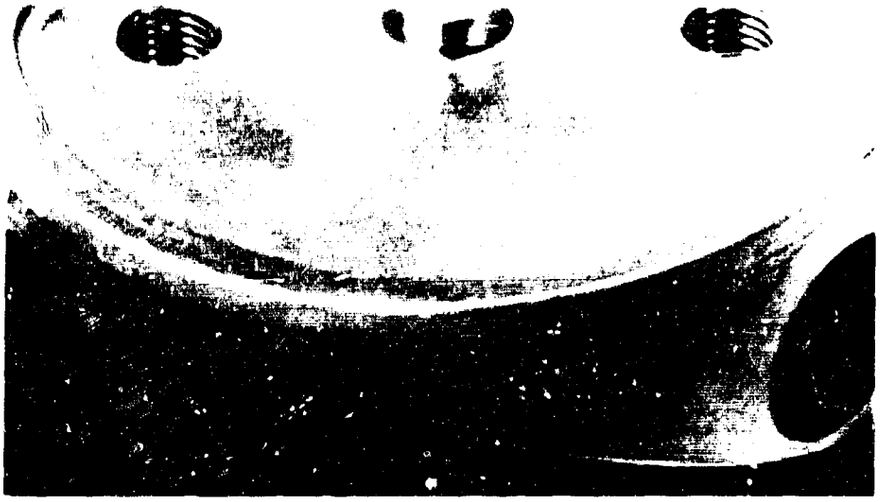

Figure 859. Disk Showing Wear Pattern FE 97713

The shaft had a wear mark on the blind end. In addition, burnishing occurred on the shaft at the bearing locations. The shaft and bearings are shown in figure 860. The bearings show no evidence of wear other than that caused by end load wear with the positioning spacer. They had become contaminated, however. At disassembly, 3 lb-in. of torque were required to turn the blind end shaft bearing.

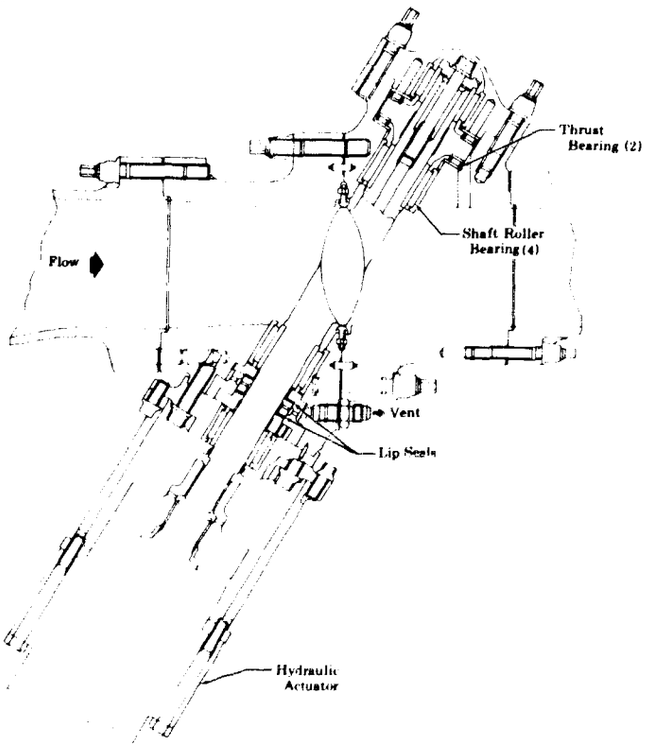

Figure 860. Main Chamber Oxidizer Valve FD 29151

The shutoff seal leakage exceeded limits (10 sccs GN_2 at 50 psid) between the 19th and 50th cycles.

The lip seal leakage was high out of limits from the beginning at pressures above 150 psig for the blind end shaft seal. The drive end seal seated at high pressures until the 4000 cycle data point.

D. MAIN CHAMBER OXIDIZER VALVE

1. Introduction

The main chamber oxidizer valve is located in the oxidizer supply line to the main chamber. Because this control regulates the mainburner flow, which is a major portion of the total propellant flow, it has a strong influence on both engine mixture ratio and thrust. The main chamber oxidizer valve was designed during this report period to obtain a small, lightweight valve.

The valve is a butterfly type and incorporates a shutoff seal for the oxidizer flow to the mainburner injector. To accommodate this shutoff feature, a canted shaft with an integral design is used so that an uninterrupted disk sealing surface is provided.

2. Summary, Conclusions, and Recommendations

The design of the main chamber oxidizer valve evolved from the Phase I mixture ratio valve. Particular emphasis was directed toward reducing valve size and weight. Complete design details are presented in the Demonstrator Engine Design Report, AFRPL-TR-70-6.

Parts were fabricated for two complete valve assemblies. Additional seals and other expendable parts were provided for use during testing.

It is recommended that assembly and testing of this valve be conducted.

3. Hardware Description

The main chamber oxidizer valve is a canted-shaft butterfly valve as previously shown in figure 860.

The maximum effective area of 4.65 square inches is approximately 38% greater than required. The maximum pressure drop across the valve is 1580 psid.

The canted-shaft, integral disk arrangement allows an unbroken shutoff sealing surface, but results in a higher ratio of shaft diameter to throat diameter than would occur in a 90-degree design. It also requires a two-piece main housing so that the valve can be assembled. The angle shaft results in shaft thrust that varies in direction and magnitude with engine operating conditions. The shaft is supported by four roller bearings and is positioned by two roller thrust bearings that ensure low operating friction and minimum wear. Oxidizer leakage at the actuator end of the shaft is held to the minimum by laminated lip seals. Leakage at the blind end of the shaft is prevented by the thrust cover and a static seal.

Positive oxidizer shutoff is provided by the pressure assisted, hoop-type shutoff seal. The valve disk and shaft material is Inconel 718 (AMS 5663), and the seal element is a hydroformed, silver plated, Inconel X-750 (AMS 5598) hoop. Figure 861 shows a cross section of the hoop seal.

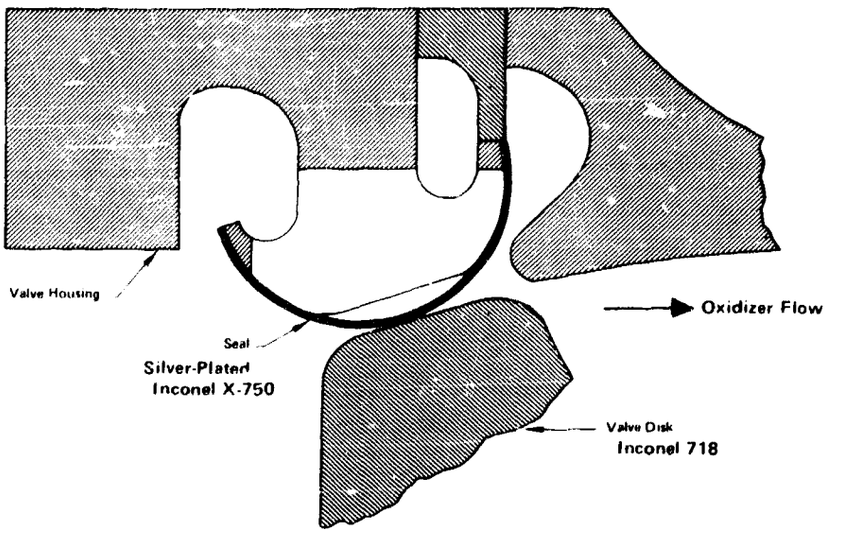

Figure 861. Hoop Seal Cross Section FD 27537A

The shaft size was established by the minimum acceptable size of radial roller bearings required to withstand the maximum pressure loading on the butterfly disk. This condition occurs at 100% thrust and a mixture ratio of 5.0. The resulting disk force and bearing reaction loads as well as a stress analysis summary are presented in figure 862.

The maximum deflection at the disk centerline is about 0.006 in., and the corresponding disk bending stress is 50,000 psi. The maximum reaction load on the inboard bearings is 6500 lb, or about 40% of the quoted capacity.

The corresponding value for the outboard bearings is approximately 10%. The calculated shear stress at the splined neck diameter is 43,000 psi at an assumed torque of 2400 lb-in. This torque consists of 1400 lb-in. of hydraulic unbalance and a conservative estimate of 100 lb-in. caused by seal and bearing friction loads. The maximum thrust load expected for the outboarding thrust bearing is 2300 lb at 100% thrust and a mixture ratio of 5. The maximum thrust load expected for the inboard thrust bearing is 700 lb at 100% thrust and mixture of 7. The bearing loads expected for the outboard thrust bearing during the engine shutdown transient are 2000 pounds at 20% thrust and mixture ratio of 7 and 2150 lb at 20% thrust and a mixture ratio of 5. The bearing load capacity quoted by the vendor is 11,900 lb.

Double lip seals, consisting of an inner layer of FEP Teflon and three layers of Kapton F, are used at the actuator end of the valve shaft between the inboard and outboard roller bearings. The nominal thickness of the seals is 0.0195 inch. As shown in figure 863, a fitting is provided to vent leakage past the primary lip seal overboard.

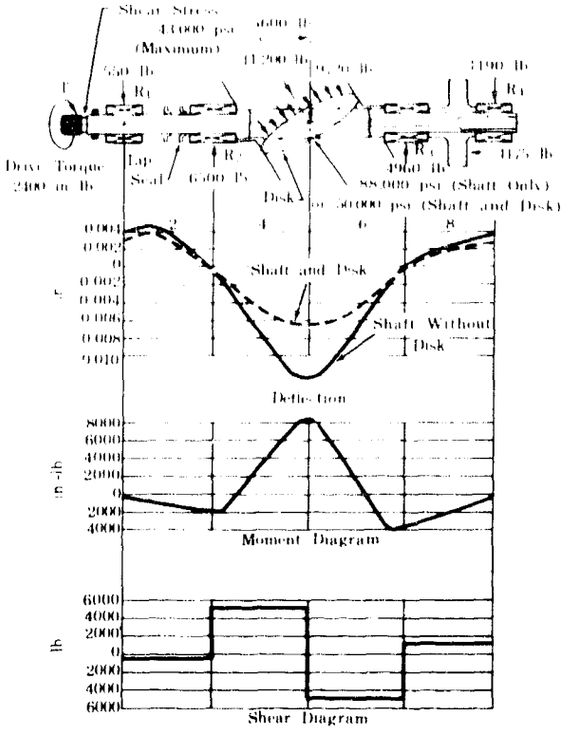

Figure 862. Shaft Stress Analysis Summary FD 29177

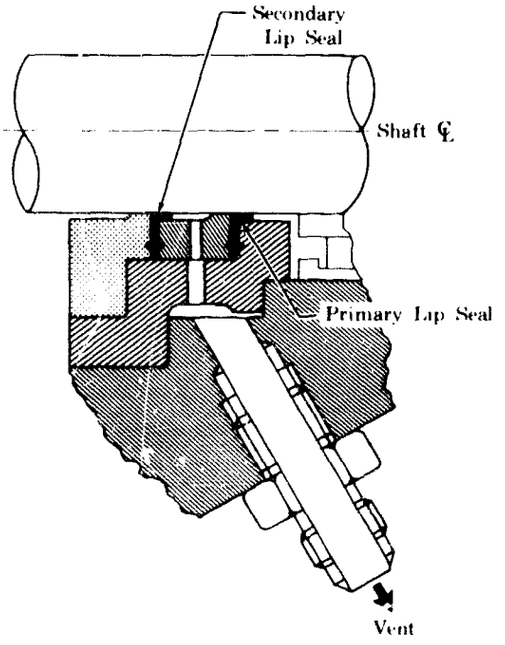

Figure 863. Main Chamber Oxidizer Valve Shaft Lip Seals FD 29153

E. Secondary Control Valves And Systems

1. Helium System
2. Vent Valves
3. Nozzle Coolant System

A helium purge fitting is in the split flange just downstream of the butterfly disk. This location will provide injector purge capability at engine shutdown.

The main housing components are designed as a matched set to achieve the required dimensional precision for bearing and shutoff seal alignment. Bolts and flanges are designed for a proof pressure factor of 1.5 times the maximum local operating pressures. Studs are used where necessary to minimize the torsional stresses inherent in bolt torquing. Flange thicknesses are designed for 0.002-in. maximum deflection at the seal mean diameter. Results of a complete analysis of the flange configuration assumptions are summarized in figure 864. Simplified geometry was employed in the analysis as shown to overcome the complications of the actual housing design shapes. The results of the inlet and outlet flanges are also valid for the mating flanges.

The split-flange bolt circle has two pairs of holes located 0.5 in. outside the remainder of the circle to avoid the bearing cavities. As appropriate ridge is left to increase wall thickness locally to keep flange deflection within the established limits. The overall length of the housing is minimized and external contouring is employed to save weight.

4. Fabrication

Fabrication of parts for two assemblies of the main chamber oxidizer valve was completed without major difficulty. Parts layout is shown in figure 865.

The inlet and discharge housings were machined from Inconel 718 bar forgings. Material microstructure checks were made prior to machining to ensure material conformance with specification requirements. The valve shaft bearing bores were line bored after final heat treatment.

The shaft and disk were machined from Inconel 718 bar stock using conventional machining methods. The spherical sealing surface was chrome coated per specification PWA 48.

The shutoff seal was fabricated in the same manner using essentially the same material as the preburner fuel valve shutoff seal except for the use of different detail parts for the assembly.

The lip seals for the main chamber oxidizer valve were fabricated in the same manner as described for the preburner fuel valve.

Table XCVI indicates the lead times for the aforementioned parts.

5. Testing

Main chamber oxidizer valve testing was not conducted because of the program redirection.

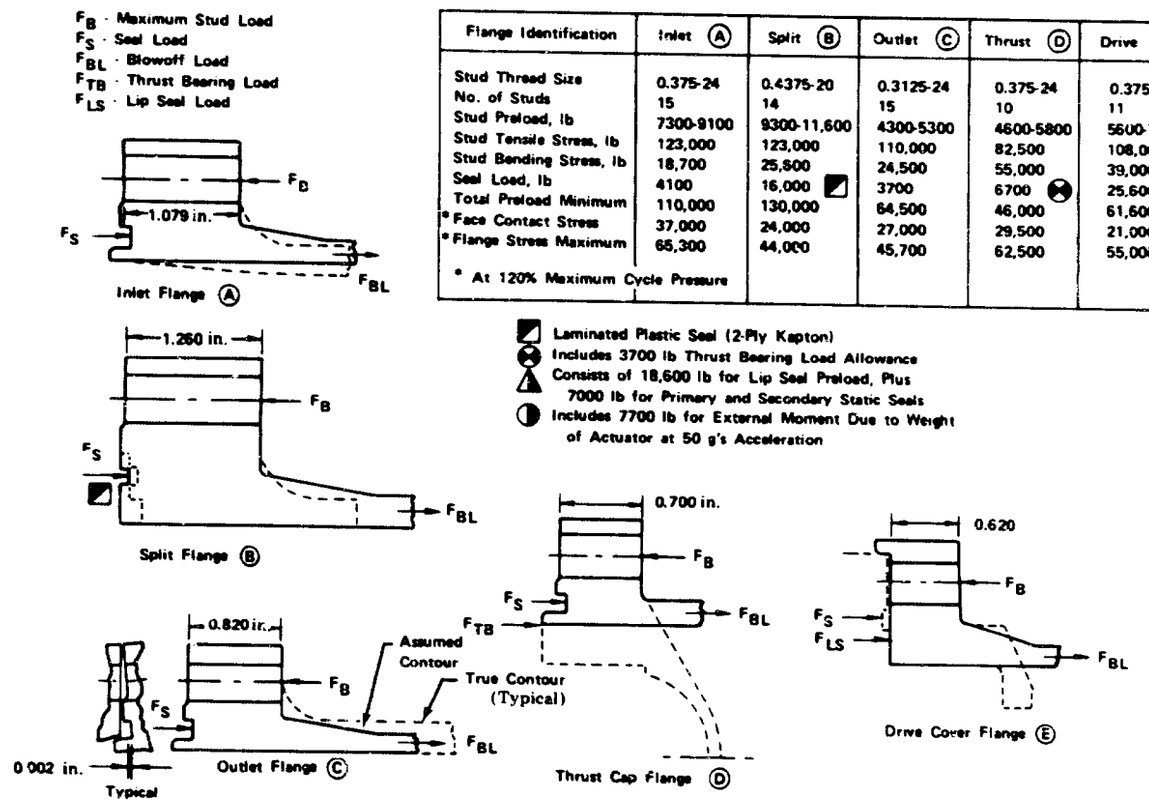

Flange Identification	Inlet (A)	Split (B)	Outlet (C)	Thrust (D)	Drive (E)
Stud Thread Size	0.375-24	0.4375-20	0.3125-24	0.375-24	0.375-24
No. of Studs	15	14	15	10	11
Stud Preload, lb	7300-9100	9300-11,600	4300-5300	4600-5800	5600-7000
Stud Tensile Stress, lb	123,000	123,000	110,000	82,500	108,000
Stud Bending Stress, lb	18,700	25,500	24,500	55,000	39,000
Seal Load, lb	4100	16,000 ◪	3700	6700 ⊗	25,600 △
Total Preload Minimum	110,000	130,000	64,500	46,000	61,600 ◑
* Face Contact Stress	37,000	24,000	27,000	29,500	21,000
* Flange Stress Maximum	65,300	44,000	45,700	62,500	55,000

* At 120% Maximum Cycle Pressure

◪ Laminated Plastic Seal (2-Ply Kapton)
⊗ Includes 3700 lb Thrust Bearing Load Allowance
△ Consists of 18,600 lb for Lip Seal Preload, Plus 7000 lb for Primary and Secondary Static Seals
◑ Includes 7700 lb for External Moment Due to Weight of Actuator at 50 g's Acceleration

Figure 864. Flange Stress Analysis Summary

FD 29178

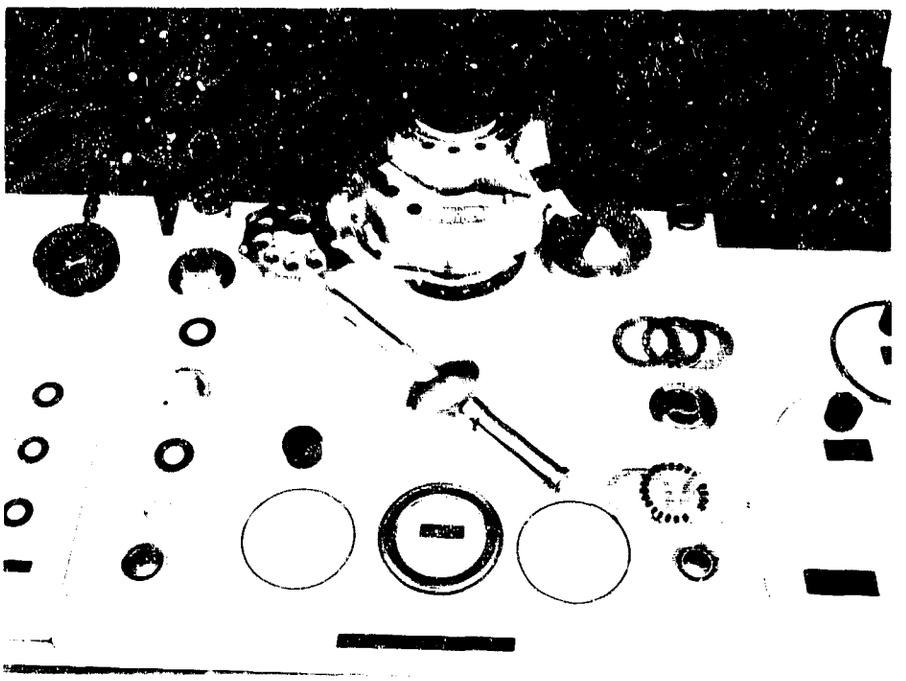

Figure 865. Oxidizer Valve Parts Display FE 96266

Table XCVI. Main Chamber Oxidizer Valve Parts Lead Times

Part Name	Lead Time (weeks)	
	Raw Material	Machining
Inlet Housing	6	8
Discharge Housing	6	8
Shaft and Disk	6	12
Shutoff Seal	4	3
Lip Seals	8	0.15

E. SECONDARY CONTROL VALVES AND SYSTEMS

1. Helium System

a. Mechanical Description

The helium system supplies helium to the engine at 1500 psia and 500° R for valve actuation, seal actuation, and engine purges. The system consists of solenoid actuated valves, check valves, a relief valve and the flow control orifices required for helium management. Figure 866 schematically depicts the helium system.

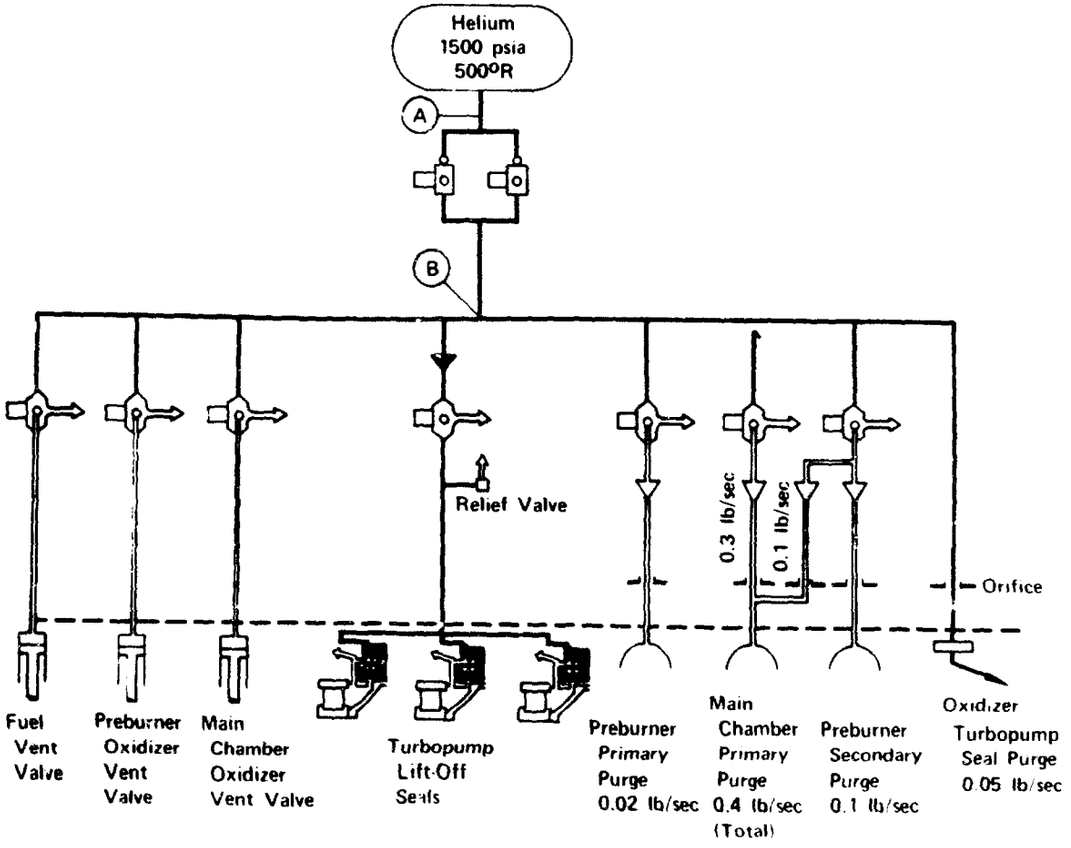

Figure 866. Helium System Schematic

FD 27849C

Helium is used to actuate the three engine vent valves and the three turbopump liftoff seals. Helium purges are provided for the preburner primary and secondary injector manifolds and for the main chamber oxidizer manifold. A purge is also provided for the oxidizer turbopump shaft seal package.

The helium system will consist of a modular package that will include the required solenoids, check valves and flow control orifices. The package will be attached to the transition case flange and located between the fuel and oxidizer turbopumps.

Nine solenoid-operated valves are required for the engine system. Two types are used, direct-lift operated and pilot-piston, pressure-actuated. Of these two types, both two-way and three-way valves are used.

In the direct-lift type, the magnetic pull of the solenoid coil opens the valve port directly by lifting the plunger and stem assembly off the valve seat. These valves depend solely on the power of the solenoid for operation.

Pilot-operated solenoid valves are used for the valves requiring higher flow and higher operating pressure drops. In these valves, the plunger and stem assembly does not open the main port directly, but opens a pilot orifice and the source pressure forces the piston off the seat, opening the valve and keeping it open.

Valve solenoids are energized with 28 (±1) vdc and have response times of 50 milliseconds. Maximum current drain for each energized solenoid is 1.0 ampere.

A description of the valves selected for this system is provided in table XCVII.

Table XCVII. Solenoid Valve Description

Valve Description	Number Required	Valve Type	Energized Position
Fuel and oxidizer vent solenoid valves	3	Three-way direct-operated	Open
Preburner primary injector purge solenoid valve	1	Three-way direct-operated	Closed
Turbopump liftoff seal solenoid valve	1	Three-way direct-operated	Open
Main supply shutoff solenoid valves	2	Two-way pilot operated	Open
Main burner injector purge solenoid valve	1	Three-way pilot-operated	Closed
Preburner secondary purge solenoid valve	1	Three-way pilot-operated	Closed

A total of five check valves are required to prevent backflow and contamination of the helium system. They are utilized as follows: Four valves to isolate the engine purge system, and one valve to isolate the turbopump shaft seal actuation system.

A relief valve is required for turbopump shaft seal actuation system. This valve is included as a fail-safe feature in the event of a liftoff seal bellows failure.

Replaceable orifices are required to establish the required helium flowrates. Four orifices are in the engine purge flow lines and one orifice is included in the turbopump damseal purge line.

The helium system allowable envelope is shown on figure 867.

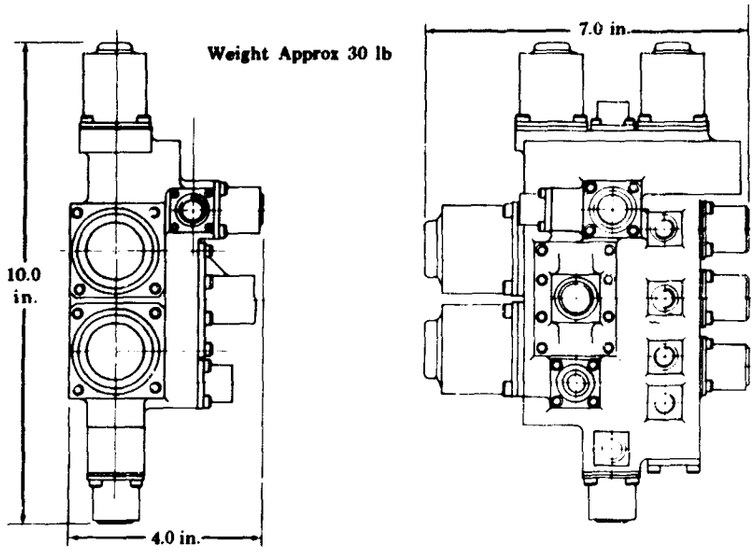

Figure 867. Helium System, Typical Packaging FD 32000

b. Fabrication

A purchase specification was written, vendor proposals were submitted, and Scherer Engineering and Manufacturing Company was selected as the system vendor; however, procurement has been held. Drawings of the proposed system are shown in figures 866 and 867. Fabrication was not pursued because of the program redirection.

2. Vent Valves

Vent valves for engine cooldown are located in the preburner fuel and oxidizer lines and in the main chamber oxidizer line. The main chamber oxidizer vent valve is also opened at shutdown to aid in decelerating the oxidizer turbopump.

The vent valves are two-position ball valves. Helium pressure actuation through a rack and pinion mechanism moves the valve to the open position. The rack is spring loaded to return to the shutoff position, when helium pressure is removed.

a. Hardware Description

The propellant vent valve, shown in figure 868, incorporates an integral ball and shaft opened by helium pressure and closed by spring force. The valve is sized to provide a maximum effective area of 0.75 in^2, including entrance losses. Provision for installing a flow restriction orifice is incorporated in the inlet seal housing so that the valve effective area may be varied as required for particular applications. A metal-to-metal shutoff seal is incorporated at the valve inlet.

The shutoff seal design figure 869 uses a thin metal cylinder to allow the silver-plated metal seal lip to center on the spherical surface of the ball, and to provide support when the lip is deflected by contact with the ball surface. The seal carrier radially supports the thin cylinder at high pressures. Propellant leakage is minimized by limiting the valve assembly high-pressure sealing requirements to the shutoff seal. The shutoff seal material is Inconel 718, silver-plated to a thickness of 0.00075 in.

One high-pressure static seal will be required in the flange to which the valve is mounted. All other seals in the valve are required to seal only when the valve is open and are, therefore, exposed to static pressures of less than 900 psia. The valve internal static seals are compressed, trapped TFE Teflon. The seal recesses are double-piloted with a maximum loose fit of 0.0015 inch to prevent Teflon extrusion.

The ball shaft is supported by two caged needle roller bearings. The maximum bearing static load per bearing is 1815 pounds, which is 47% of the bearing capacity. The maximum dynamic load is 570 lb per bearings. A full complement ball bearing is used to support the pinion. This bearing is lightly loaded and serves also to axially position the pinion and ball shaft. The rollers, balls, and races of these bearings are made of AISI 440C stainless steel (AMS 5630).

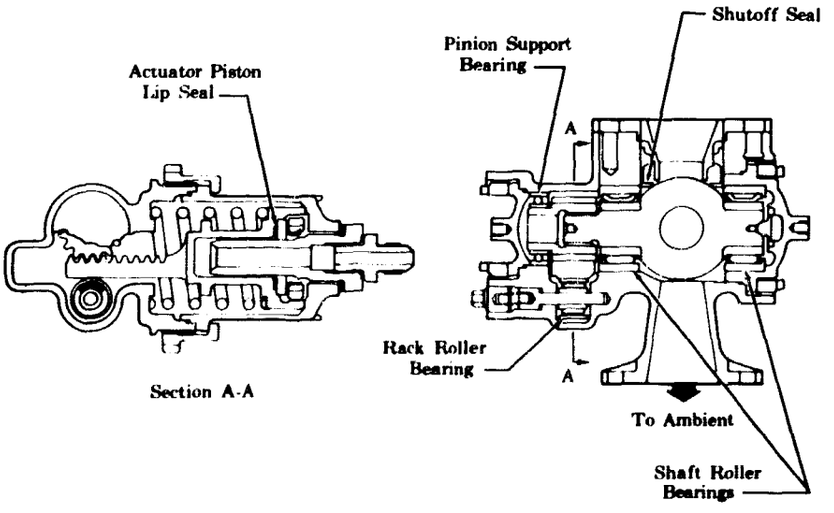

Figure 868. Propellant Vent Valve FD 29201

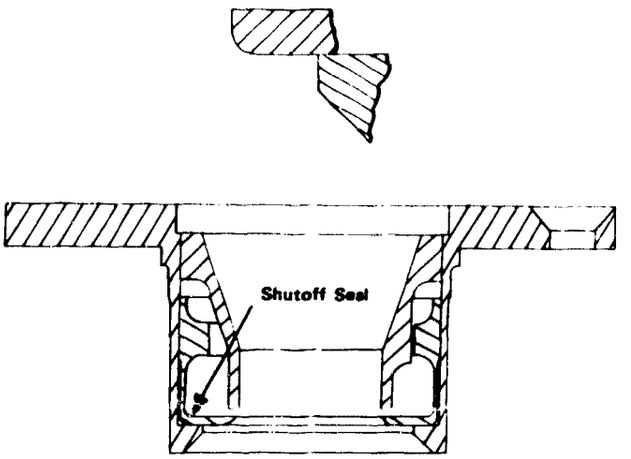

Figure 869. Propellant Vent Valve Shutoff Seal FD 47711

The valve is actuated to the open position by a pneumatically operated rack acting on the pinion, which is splined to the valve shaft. The rack is supported by a lightly loaded roller bearing that was selected for its compactness and availability. The backlash between the rack and pinion is adjusted by selecting the appropriate rack support bearing sleeve. The sleeves are size classified to obtain the required backlash control with reasonable tolerances on the related parts. The maximum contact stress between the rack and pinion involute surfaces is 100,000 psi. A-286 stainless steel (AMS 5737) was selected for the rack and pinion because of its good tensile strength and excellent impact strength at cryogenic temperatures. The involute surfaces of the rack and pinion are coated with MOS_2 dry film lubrication to minimize wear. A combination of 17 gear teeth and 18 splines was selected for the pinion to facilitate alignment of the valve ball. Included in the actuator design is the provision for incorporating a helium flow control orifice to adjust valve response time by limiting the rate of actuator pressure rise.

A 17-7PH stainless steel (AMS 5673) spring is used to retain the valve in the normally closed position when helium pressure is not applied. This material was selected because of its high strength and has a spring fatigue life five times greater than required. The calculated weight of the valve assembly is 5.6 lb.

b. Fabrication

The fabrication of five vent valve assemblies was completed without major difficulty.

The ball and shaft was conventionally machined from Inconel 718 bar stock. The ball was chrome coated to a thickness of 0.0001 to 0.0002 in. following final machining and the small neck section of the shaft below the spline was peened per specification AMS 2430.

The cover assembly containing the shutoff seal was fabricated from Inconel 718 bar stock and sheet using conventional fabrication methods. The detail parts were hand welded to form the assembly. The assembly was then precipitation heat treated and final machined. The seal area was then silver plated.

The housing was conventionally machined to final dimensions from Inconel 718 bar stock; then, precipitation heat treated and final machined.

The actuator rack was conventionally machined from AMS 5737 stainless steel bar stock. The teeth of the spline were coated with dry film lubricating compound 0.0001 to 0.0003 in. thick, following final machining.

The trapped Teflon static seals were fabricated by conventional machining methods from AMS 3662 film.

The actuator lip seals were fabricated in the same manner as the preburner fuel valve lip seals except for the use of two layers of Dupont No. 500-131 and one layer of AMS 3647.

Table XCVIII indicates the lead times for the preceding parts.

Table XCVIII. Propellant Vent Valve Parts Lead Time

Part Name	Lead Time (weeks)	
	Raw Material	Machining
Ball and Shaft	6	24
Cover Assembly	6	8
Valve Housing	12	12
Actuator Rack	5	12
Static Teflon Seals	4	0.15
Lip Seals	8	0.15

c. Testing

No vent valve testing was conducted because of program redirection. It is recommended that valve testing be conducted to verify this vent valve concept.

3. Nozzle Coolant System

The two-position nozzle coolant supply system provides liquid hydrogen coolant to the two-position nozzle from a fixed coolant source. This system provides the flowrate necessary to cool the nozzle throughout the engine operating regime, and also provide shutoff of the coolant flow when the nozzle is retracted.

a. Hardware Description

The two-position nozzle coolant supply system consists of three basic components: (1) a venturi to establish the required coolant flowrate, (2) a solenoid-operated valve providing coolant shutoff, and (3) a two-part tubular linkage with ball joints that incorporates dynamic lip seals and provides a coolant flowpath to the translating nozzle.

Liquid hydrogen enters the coolant supply system, and immediately passes through a venturi, which establishes the coolant flowrate and dynamically decouples the fuel pump flow system from the nozzle coolant supply system. The venturi is sonic choked at the higher thrust levels and acts as a cavitating venturi at the lower thrust levels. Before the two-position nozzle is extended, the solenoid operated valve opens allowing coolant to flow through the two-piece tubular linkage shown in figure 870 into the nozzle manifold inlet. The nozzle manifold distributes the coolant to 360 nozzle coolant passages, and the coolant exits into the exhaust stream. The two-position nozzle is extended 52.61 in. to place the inlet in the same plane as the primary nozzle exhaust plane. During translation of the two-piece tubular linkage, the triangular segment of the two-part linkage system swings through a 16-in. radius arc.

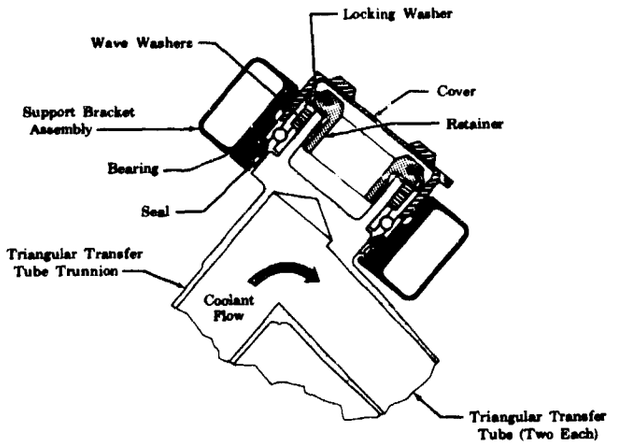

Figure 870. Triangular Transfer Tube Assembly Closed-End Trunnion FD 31012A

The venturi insert is mounted and held between the fuel pump interstage supply flange and the mating flange on the shutoff valve shown previously in figure 869. The venturi geometry is shown in figure 871.

The cooling system shutoff valve is solenoid-operated, with a minimum design effective area (A_{cd}) of 0.074 in^2. The valve will be a vendor supplied item. Valve specifications include a response of 50 milliseconds, fully open to fully closed, and a maximum shutoff leakage of 10 sccs gaseous nitrogen at the maximum steady-state operating pressure of 2048 psia. Voltage of 28 vdc with maximum current of 1.0 amp defines the electrical characteristics. The maximum allowable vane envelope is a box 4-1/2 x 4 x 6 inches. A weight limit of 4.0 lb for the solenoid valve is imposed. The ambient exterior environment for the valve is 395° R to 625° R and 14.7 psia to space vacuum.

A 1-in. OD tube with a 0.035-in. wall transfers coolant flow from the valve to the first arm of the translating linkage. The tube is the smallest that can be used consistent with the remaining system pressure drop without causing the system back pressure to exceed 80% of the venturi inlet pressure and unchoke the venturi, thereby reducing the coolant flowrate from its desired level.

Venturi Classes	
Coolant Flow At r = 7.0, 100%	Throat Diameter
2.8 lb/sec	0.282 in.
2.5	0.266
2.23	0.252
2.1	0.244

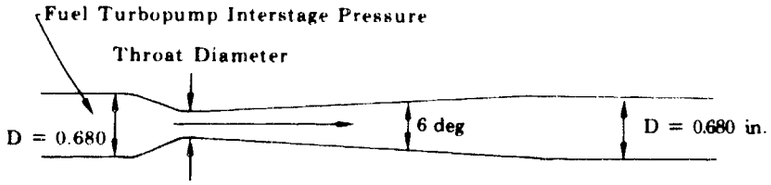

Figure 871. Two-Position Nozzle Choked Venturi Configuration FD 31018A

The flow proceeds from the 1-in. OD tube to the movable nozzle via a two-part tubular linkage. The first bar is a triangular shaped tubular assembly. Extensions on the base of the triangle attach through two ball bearings, shown in figures 870 and 872, to a bracket, allowing movement in a fixed plane about its base. The structure has sufficient wheel base along the line of rotation to hold itself rigidly in the rotation plane, despite vibrational or dynamic loading normal to this plane. A second bar is fixed to the apex of the triangular assembly and to the movable nozzle by ball joints at each end, shown in figures 873 and 874. During nozzle translation, this arm articulates in a vertical plane producing rotary motion at each joint. The ball joint feature allows the arm to readily "rock" out of its articulating plane to accommodate motion of the nozzle attachment joint or the apex joint of the first arm from this plane. Each ball joint is sealed by double Kapton-Teflon laminated lip seals bearing on the spherical ball surface, shown in figure 873. An interstage vent passage is supplied between seals to reduce overboard leakage at each joint to acceptable levels. A series of passages in each joint ducts the leakage back to a fuel vent manifold fixed on the engine. The vent leakage path is integrally fabricated with the two-position nozzle manifold, thus completing the flow passage.

The mounting bracket that retains the triangular shaped tubular arm is attached to lugs provided on the upper segment of the primary nozzle, shown in figure 875. Ball bearings are used to attach each end of the rotating arm to sealed housings at each end of the bracket. The housing contains a bearing, a rotary seal that prevents water vapor from entering the housing and freezing on the bearing, and two lip seals to seal the rotating joint. A vent passage is supplied between the lip seals. The opposite housing, previously shown in figure 870, contains an identical ball bearing and rotary seal plus a stack of wave washers which axially preload the bearing races within the housing and allow the tubular arm to thermally contract independently of the support bracket.

b. Fabrication

Proposals were submitted for the solenoid operated two-way valve in response to P&WA purchase specification. Valcor Engineering was selected as the vendor. Procurement of the solenoid valve was not accomplished because of the program redirection.

The fabrication of two sets of feed system linkages was completed. Component parts for one assembly are shown in figure 876.

The linkage tubing was conventionally fabricated from AISI 347 stainless steel sheet, bar stock, and tubing. Upon completion of required machining of tube ends they were hand welded to the tubing then the vent tube was furnace brazed to complete the assembly.

The ball joints were fabricated from AMS 5735 stainless steel bar stock using conventional machining methods. The vent holes for overboard leakage were eloxed in the ball joint and a plug was hand welded in the tower end of one vent hole to direct the flow. The ball was then heat treated to relieve the stresses and a chrome coat was applied per specification PWA 48.

The lower ball seats were conventionally machined from AMS 5646. The balls and seats were then lapped to form matching pairs then a 0.00075 in. thick silver plate was applied to the seats.

The upper ball seats consisted of a conventionally machined AMS 5645 ring and Dupont Vespel SP-3 insert.

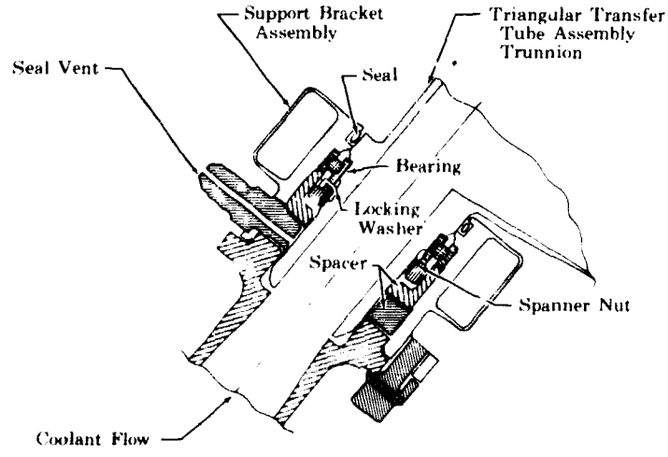

Figure 872. Triangular Transfer Tube Assembly Cooled Inlet Trunnion FD 31011A

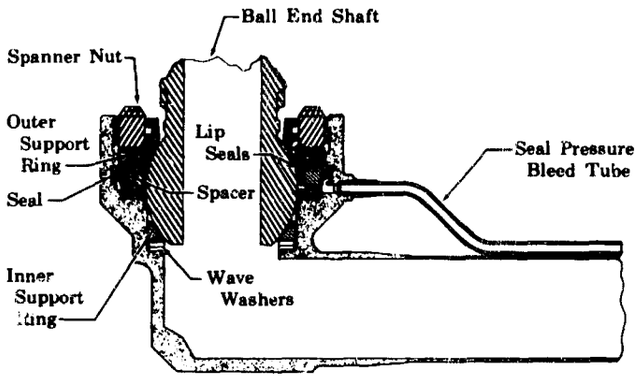

Figure 873. Single Transfer Tube Assembly FD 31016A

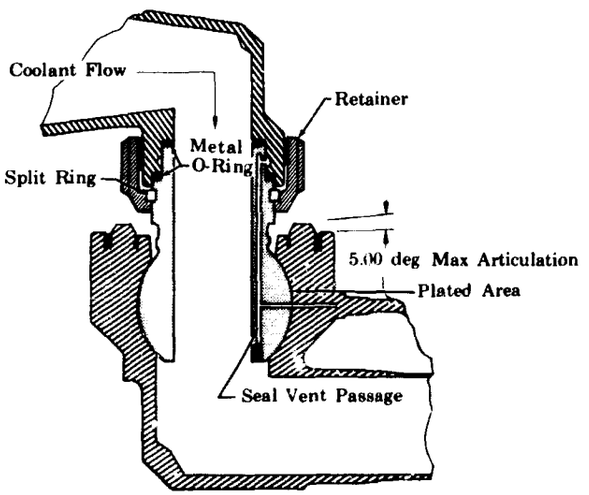

Figure 874. Single Transfer Tube Assembly Ball Joint Passages and Shaft Retention FD 31017A

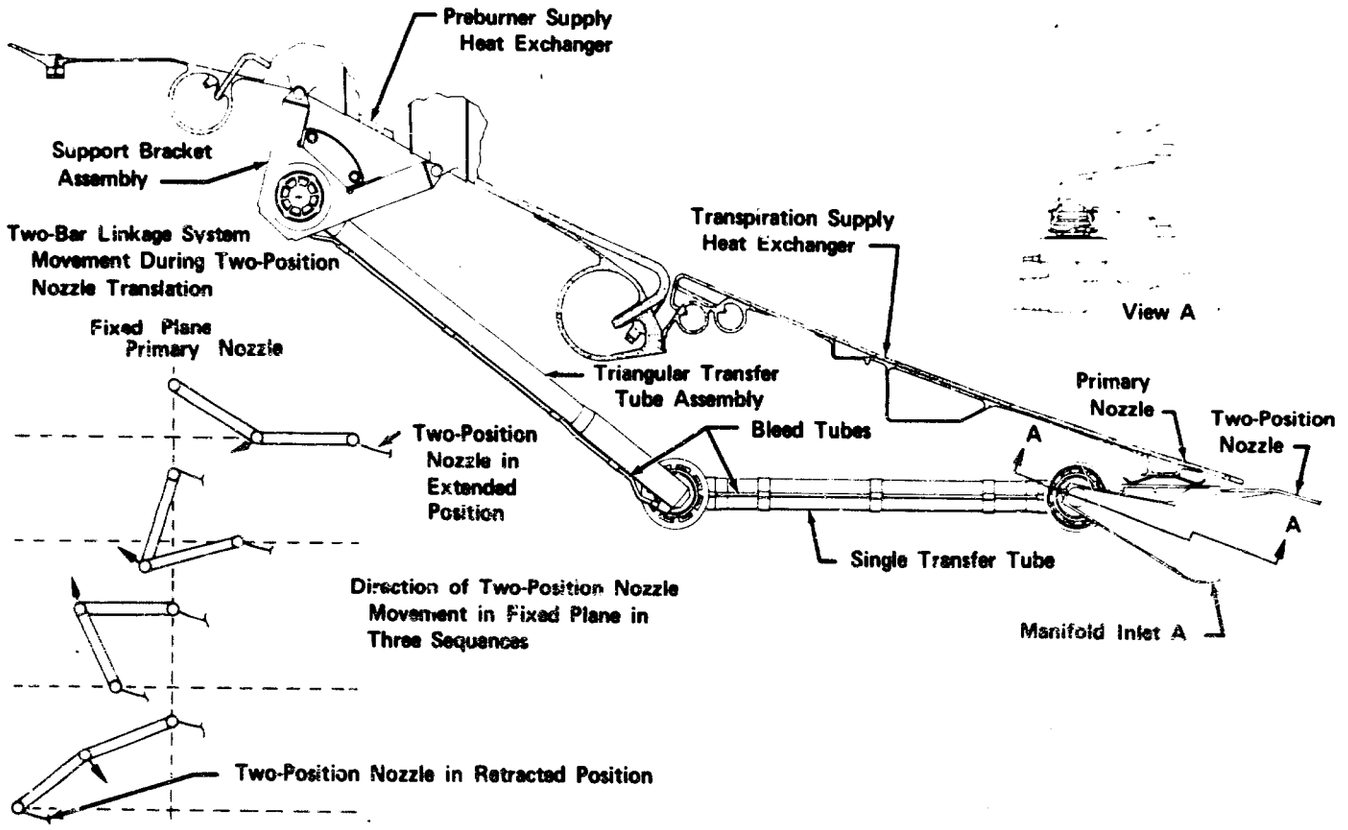

Figure 875. Two-Position Nozzle Coolant Supply System, Extended Position

FD 31008B

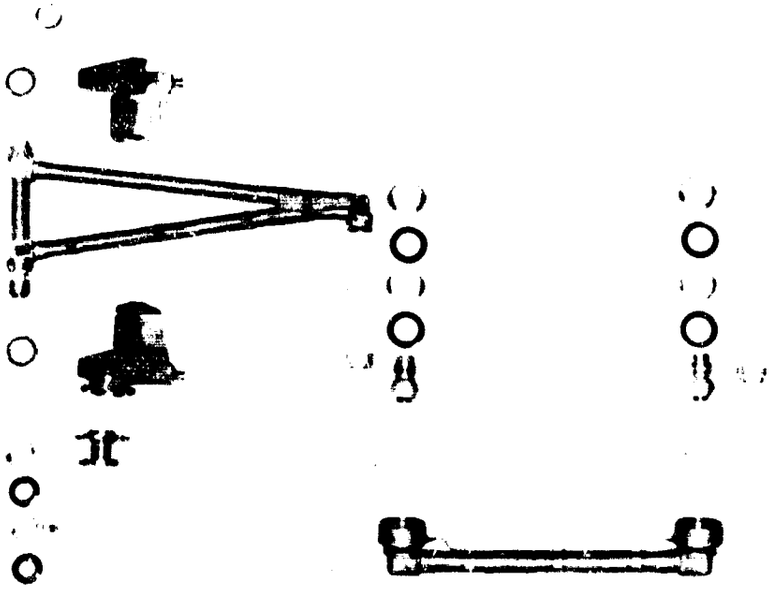

Figure 876. Nozzle Detail Parts KFE 95824

The lip seals were fabricated in the same manner as those for the preburner fuel valve.

Table XCIX indicates the lead times for the preceding parts.

Table XCIX. Solenoid Valve Parts Lead Times

Part Name	Lead Times (weeks)	
	Raw Material	Machining
Linkage	3	12
Ball Joints	4	10
Lower Ball Seats	3	8
Upper Ball Seat	3	10
Lip Seals	8	0.15

An initial build of one assembly was completed with no major problem areas and is shown in figure 877.

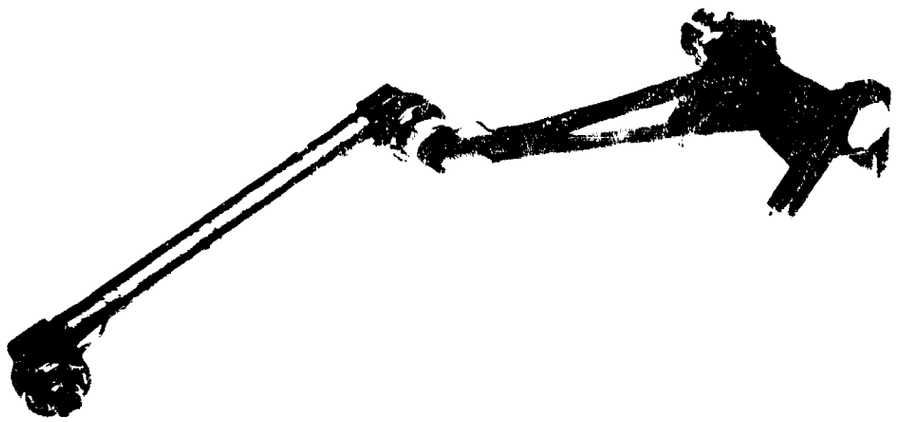

Figure 877. Assembled Feed System Linkage FE 96345

c. Testing

The nozzle coolant system was not tested because of the program redirection. It is recommended that testing be conducted to verify the design concept.

4. Electrical Ignition System

The electrical ignition systems are integral spark igniter exciter units that are mounted on the preburner and main chamber torch igniters. Two systems are provided for the preburner igniter and two for the main chamber igniter to provide total spark redundancy. These units ignite oxygen/hydrogen torches, which in turn ignite the preburner and mainburner chamber. The torch igniters are of the same basic design that demonstrated vacuum ignition without failure in the RL10 program.

A purchase specification was written and quotes for the ignition system were received. The Benton Corporation was chosen to supply units for evaluation and development testing.

Two units were received from the Benton Corporation and initial testing was completed. The first unit failed to meet the weight, spark rate, and tip pressure requirements. The second unit met all these requirements and was used during tests of the hot gas system and hot turbopump test rigs.

a. Hardware Design

The design effort by P&WA was limited to an envelope definition, which is shown in figure 878. Solid state circuit design was conducted by the Benton Corporation.

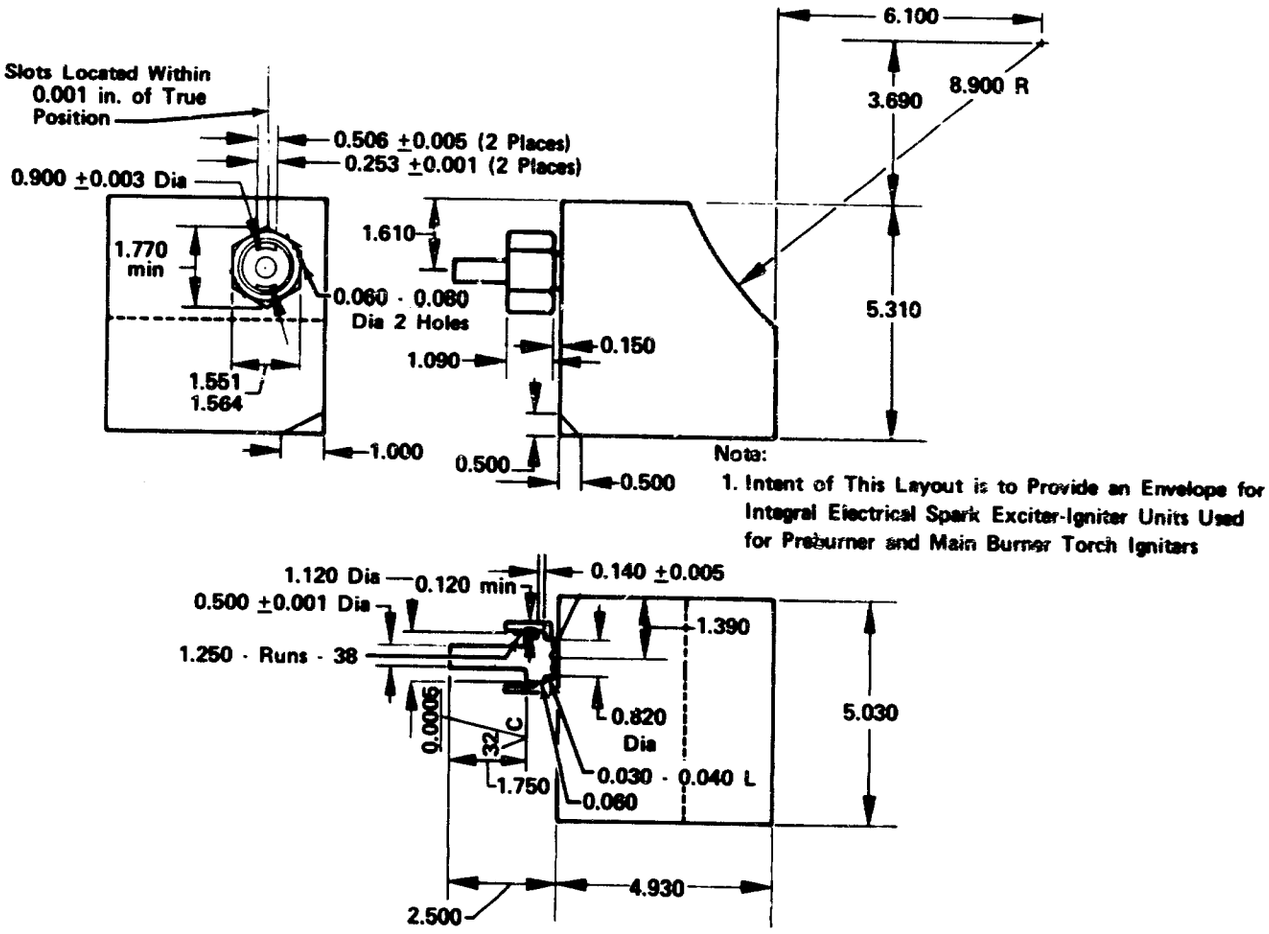

Figure 878. Electrical System Definition Envelope

FD 49504

b. Fabrication

The selected ignition systems are solid-state high tension units that are vacuum potted with polyurethane after assembly and fire through an integral spark plug supplied by Champion. A breadboard version of the exciter was assembled and tested with acceptable results by Benton during the circuit design effort.

In addition, it was decided to use RL10 exciter boxes with Phase I plugs, connected with a flexible high tension lead as a backup to the Benton system.

c. Testing

Two reworked Phase I ignition systems were bench checked satisfactorily under atmospheric and 30 psig tip pressures.

The first Benton exciter, figure 879, FE95269, was calibrated and sent to B-7 stand for qualification tests on the preburner injector torch igniter. The unit performed satisfactorily for 25 one-second spark times. Following the qualification testing, the exciter was recalibrated, on the counter. There was no appreciable deviation between pre- and post-test calibrations.

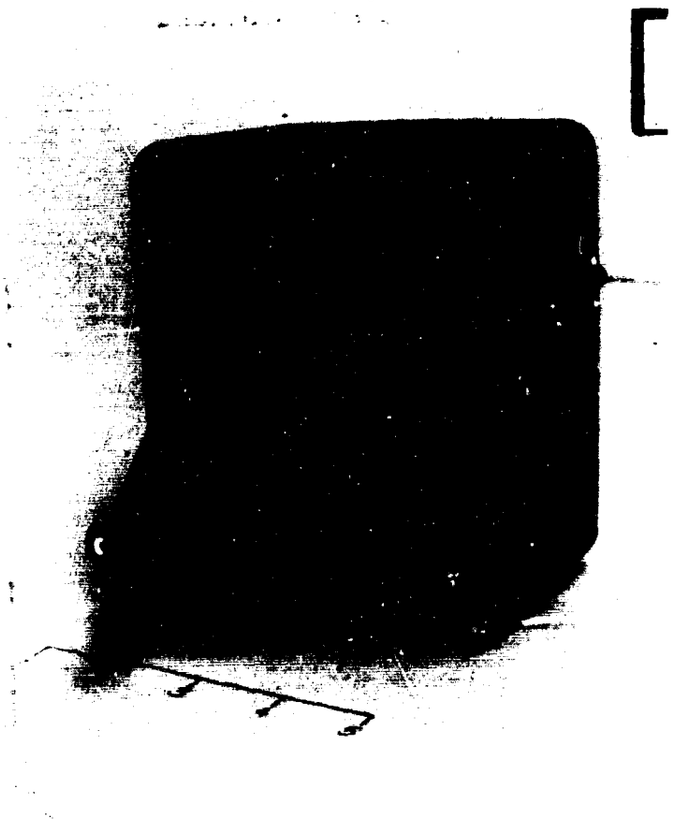

Figure 879. First Benton Exciter FE 95269

The exciter was then subjected to a pressure test of the exciter plug. The pressure test was performed on B-22 stand, the object was to increase the pressure on the tip of the exciter plug to 7500 psig and determine if the seal between the tip and electrical components box would prevent leakage into the box.

The seal failed at 1300 psig tip pressure with a subsequent deformation of the electrical components box (figures 880 and 881). A post-test calibration of the exciter showed no appreciable deviation from the pretest calibration.

Output voltage from the tip of the exciter plug was determined to be 60,000 volts and the amount of pressure required to quench the spark was 65 psig. Once the 60,000 volts level was obtained, the exciter began to spark internally.

The second Benton exciter, figure 882, was calibrated and found to operate within prescribed limits of the Purchase Performance Specification.

This unit was also pressure tested to 7500 psig without a failure of the seal between the tip and the electrical components box. The pre- and post-calibrations agreed without significant deviation.

The second exciter was used during tests of the hot gas system and hot turbopump test rigs.

Figure 880. Electrical Components Deformed Because of Seal Failure At 1300 psig FE 98507

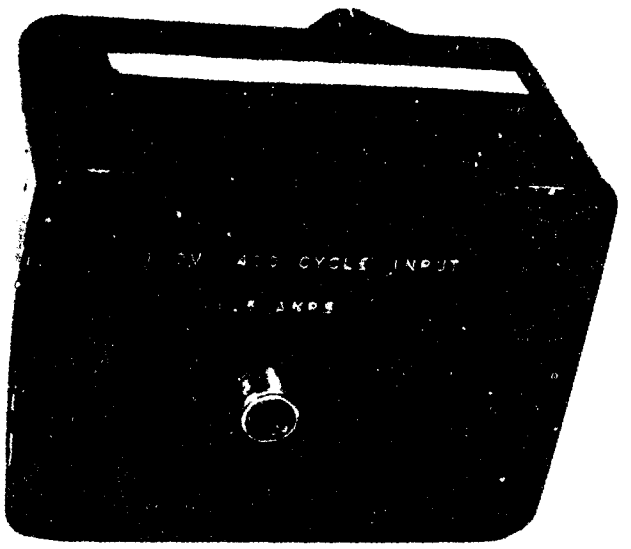

Figure 881. Deformation of Electrical Components Box After Seal Failure

FE 98508

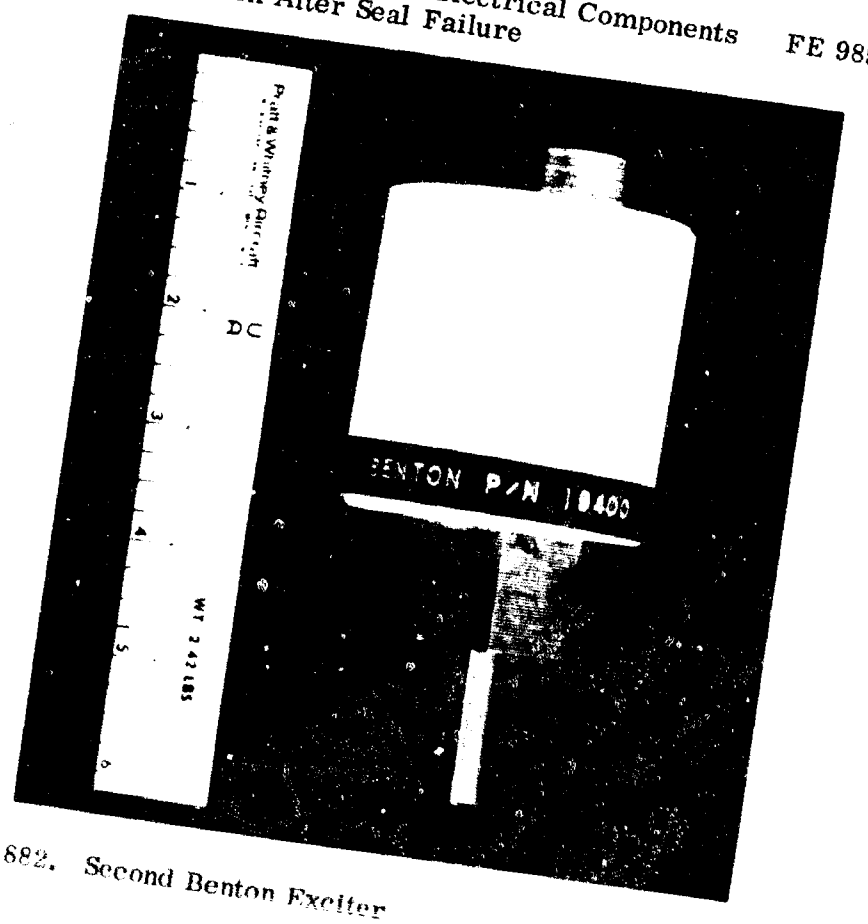

Figure 882. Second Benton Exciter

FE 98172

F. ENGINE COMMAND UNIT

1. Introduction

The Engine Command Unit (ECU) consists of digital computer, input-output networks, and signal conditioning equipment, and it forms the basis for the engines' full-time control system. The primary function of the ECU is to receive and analyze sensor data pertinent to engine operation, to receive and interpret discrete signals from the vehicle guidance equipment or a pilots' control console, and to generate control signals which modify engine operation (figure 883).

The ECU responds to four different discrete signals: prestart and start, shutdown, modulate thrust, and modify mixture ratio. It also responds to sensor data which reflect engine conformance to scheduled operating conditions (fuel pump speed and propellant flow) or potentially hazardous conditions (cavitation, overspeed, and overtemperature).

Design of the ECU and computer simulation of its operational capabilities were subcontracted to the Navigation and Control Division of the Bendix Corporation, Teterboro, New Jersey.

2. Summary, Conclusions, and Recommendations

Development of an ECU to operate the control system for the XLR129 engine is feasible within the present state-of-the-art. The principal conclusions and recommendations resulted from the ECU design and simulation program are listed below. Other recommendations are listed in table C, including recommendations for control system sensors and actuators to enhance the effectiveness of the ECU, and are substantiated in the Appendix.

1. The ECU should be based on a specially designed, engine-mounted digital computer with an 8196-word memory capacity and a computation rate of 1 megahertz. This computer could be readily implemented using current state-of-the-art components.

2. A commercially available digital computer such as the Bendix BDX-800 could be adapted to the requirements of the central processing unit of the ECU to reduce cost and improve reliability.

3. The recommended engine control logic is a time-based, gross mode, open loop system which actuates four primary control valves according to predetermined schedules for basic steady-state and transient operation. This logic should incorporate three full-time, limited authority, closed feedback loop for accurate trim of engine operation and six part-time closed limiter loops for engine protection.

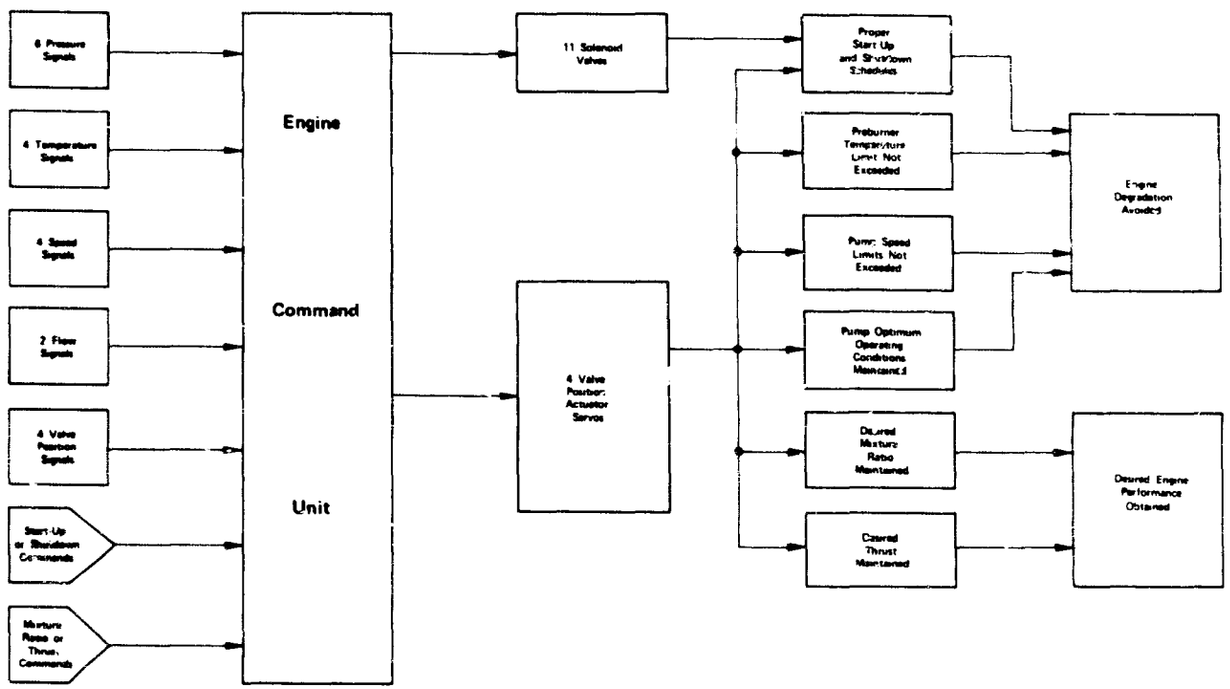

Figure 883. Block Diagram Defining Engine Control Task

FD 45054

Table C. Design Recommendations

	Recommended Method	Reason
Input System Multiplexer	Junction Field Effect Transistor Switches	High Accuracy and Temperature Stability
Analog-to-Digital Converter	Successive Approximation Technique	Rapid Access to Data, High Accuracy, and Small Hardware Requirements
Output System Analog Conversion	Incorporate Digital Multiplexer with Digital-to-Analog Converters	Improve Accuracy, Temperature Stability, and Conversion Rate
Actuator Servos	Brushless DC Torquer Servos with DC Compensation	Increase Reliability and Reduce Cost
Speed Signal Conversion	Variable Time Method	Increase Reliability and Reduce Cost
Propellant Flow Sensor	Force Screen Type	Fast Response and High Accuracy
Valve Actuators	Pneumatic	See Appendix A
Pump Speed Measurement	Proximity Probe, Eddy Current Type	See Appendix A
High Temperature Sensor	Dual Junction Chromel Alumel Thermocouple	See Appendix A
Low Temperature Sensor	Platinum Resistance Type of Immersion Probe	See Appendix A
Pressure	Thin Film Strain Gage Pressure Transducer Package for Quick Thermal Equilibrium	See Appendix A

3. Logic Description and Operational Characteristics

The ECU modes of logic in the full-time control system consist of a basic gross mode, open-loop scheduling system, three closed-loop monitoring systems to supply current feedback information to the gross mode system, and six protective loops to monitor critical engine parameters. The three full-time systems monitor main fuel pump speed, total fuel flow, and total oxidizer flow. The six protective loops monitor critical pressures, temperatures, and pump speeds and become active only when a parameter approaches its limit.

a. Primary Control System Logic

The primary control system logic is a time-based gross mode system which positions four primary control valves for basic steady-state and transient operation. Computer simulations have established that the engine can be decelerated and its oxidizer-to-fuel ratio regulated by the open-loop, gross mode system. However, the engine cannot be accelerated rapidly using only a timed sequence of events along steady-state schedules because of the normal tendency for fuel pump speed and pressure to lag behind the rest of the system due to slower pump dynamics. The resulting low fuel pressure could result in inadequate cooling flow and fuel supply to the engine unless an acceleration biasing scheme is built into the engine.

A unique acceleration scheme was conceived which permits rapid accelerations by keeping the fuel and oxidizer turbopumps dynamically balanced during the transient. The compensation consists of biasing the oxidizer-to-fuel ratio of each control valve's steady-state schedule differently so that the engine will always accelerate along a known, safe path between any thrust levels. This unique acceleration path is traveled for every acceleration regardless of the initial state of the engine. The specific bias values keep the main turbopumps matched and near their steady-state speed schedules during the transient by loading the oxidizer pump and unloading the fuel pump so that they accelerate together. The net effect of biasing is that the engine accelerates in the middle of the oxidizer-to-fuel ratio range with the turbopumps balanced and near the middle of the oxidizer-to-fuel ratio schedule.

(1) Fuel Pump Speed Control

The fuel pump speed is the primary closed-loop control because it contributes to turbopump matching by modifying the acceleration mode with feedback information on the state of the fuel turbopump. Secondary closed-loop controls are total fuel flow and total oxidizer flow to assist in maintaining the proper pump loads during transients and to trim thrust and oxidizer-to-fuel ratio during steady-state operation. These closed-loop controls, combined with acceleration biasing, permit the inherent simplicity and reliability of open-loop gross mode control to be retained without sacrificing safety or efficiency.

The closed-loop fuel pump speed control assists the gross mode in reducing the fuel pump lag during transients for an additional improvement in acceleration performance. A reference steady-state fuel pump speed is computed as a function of requested thrust and oxidizer-to-fuel ratio. This is compared to the actual speed to form a speed error signal. The error signal proportionally changes the scheduled preburner oxidizer valve position which

results in a change in available pump power, thereby changing the pump speed to hold it within the droop of the proportional closed loop. Computer studies of this system have shown:

1. It is extremely effective in producing safe accelerations.
2. It maintains proper power to the fuel pump during all transients.
3. It provides ample transpiration cooling flow.
4. Proper fuel flow is delivered for every scheduled area.
5. The oxidizer pump is kept near its scheduled path.

(2) Propellant Flow Control

Controlled thrust level is a basic requirement for engine operation. Precise thrust level is provided by accurately trimming total engine oxidizer flow to the scheduled value. A reference total oxidizer flow is scheduled as a function of velocity limited vehicle oxidizer-to-fuel ratio and velocity limited thrust level requests. The actual total oxidizer flow is either a direct measurement or, in the event of a flow sensor failure, a synthesized signal computed as a function of the oxidizer low speed inducer (LSI) turbopump speed, inlet and exit pressures generate an error signal. The error signal acts through a proportional plus integral controller to trim the thrust level request to all control valve schedules. The thrust level request to the total oxidizer flow schedule is taken directly from the thrust servo and does not contain the oxidizer flow trim value. The authority limits around the integrator fix the amount of thrust trim available at all engine thrust levels by zeroing the input to the integrator. The error to the oxidizer flow trimmer is also limited to restrict the rate of thrust level correction. The resultant rate of thrust request to the schedules is the rate of the velocity servo plus the trimmed rate. During starting and shutdown cycles, the thrust trim loop is opened and the integrator zeroed.

Accurate mixture ratio balance must be maintained at steady-state for proper propellant management. During a transient it is important that a coordination of oxidizer and fuel pump loads be made to keep the pumps balanced and moving along known schedules. A fuel flow reference value is calculated by dividing the measured total oxidizer flow by either the velocity limited oxidizer-to-fuel ratio or, during an acceleration, the constant acceleration bias value. The actual total fuel flow is measured directly or, in the case of flow sensor failure, computed as a function of fuel LSI turbopump speed, inlet and exit pressures. The reference fuel flow is compared with the actual total fuel flow to generate an error signal. This error signal acts through a dynamically compensated integrator to trim the gross mode scheduled preburner fuel valve position. The trimming of the fuel valve drives the actual fuel flow, and therefore the pump load and engine oxidizer-to-fuel ratio, to the desired value. Integrator authority limits are provided in the trim loop to prevent excessive fuel valve excursions. During start and shutdown cycles, the fuel trim is opened and the integrator zeroed.

b. Engine Protection Control System Logic

The engine protection system continuously monitors six basic engine parameters during engine operation; however, the system remains inactive unless one of the parameters approaches a limit. The six protective closed-loop controls monitor:

1.	Main oxidizer pump NPSP	Pressure
2.	Main fuel pump NPSP	
3.	Preburner temperature	Temperature
4.	Transpiration cooling	
5.	Main oxidizer pump speed	Speed
6.	Main fuel pump speed	

These controls protect the engine by restoring the critical parameter to a safe condition, either directly if there is a control point which directly affects the parameter or indirectly by slowing the transient to bring the engine closer to steady-state equilibrium.

(1) Pressure Protection

Oxidizer flow cavitation occurring in the main turbopump causes a sudden reduction in the total oxidizer flow delivered to the engine. This disturbance in oxidizer flow will change the engine thrust and unbalance the oxidizer-to-fuel ratio. The oxidizer low speed inducer (LSI) valve provides direct control of the main oxidizer pump inlet pressure and can be trimmed by a closed loop to prevent cavitation in the main pump. A minimum safe main oxidizer turbopump inlet pressure is calculated as the sum of actual main oxidizer pump Net Positive Suction Pressure (NPSP) plus the vaporization pressure of the oxidizer at the inlet to the main pump. The main pump NPSP is computed as a function of the turbopump speed and the actual total oxidizer flow. The vaporization pressure is calculated as a function of the main turbopump oxidizer inlet temperature plus an additional safety margin. This minimum inlet pressure is compared with the actual pressure to generate an error signal. When the actual pressure drops below the minimum operating pressure, the error signal acts through a dynamically compensated network to close the LSI area and open the main chamber area in proportion to the cubic ratio of valve areas. This double area reset results in a larger pressure drop existing across the LSI turbine without disturbing the scheduled oxidizer flow into the main chamber. As a result, more power is supplied to the LSI pump which raises the inlet pressure of the main pump above the value where cavitation occurs.

Cavitation at the main fuel pump inlet can be the cause of a sudden reduction in fuel flow through the pump to the engine. This disturbance in fuel flow will unbalance the oxidizer to fuel ratio and cause serious overtemperature in the engine. The pressure supplied by the fuel boost pump gives the NPSP margin needed by the main fuel pump to prevent cavitation. The power to drive the

inducer pump is delivered by the low speed inducer turbine placed in the transpiration cooling flow circuit. As described for transpiration cooling flow protection, the high pressure delivered by the main fuel pump provides the pressure drop across the circuit to maintain cooling flow and also power to the boost pump.

During an acceleration transient, the lagged response of the fuel boost turbopump causes the pressure delivered to the main pump to be lowered. The lowered pressure reduces the NPSP margin. The NPSP margin is improved in two ways: first, by decreasing thrust and acceleration rate, and second, by augmenting the speed schedule to maintain pump speed, i.e., fuel pressure. The total action improves the NPSP margin by:

1. Increasing the power to the low speed inducer by increasing the pressure drop across the cooling flow circuit

2. Increasing boost pump output pressure by unloading the boost pump with a reduction in total fuel flow

3. Preventing the required NPSP from increasing and allowing the slower boost pump to catch up by holding the main fuel pump speed constant.

The NPSP of the main fuel pump is given by a map or an equation which has inputs of main fuel pump speed and total fuel flow passing through the pump. The saturation pressure is a function of the fuel temperature entering the main pump. The sum of NPSP and the saturation pressure is the required minimum main pump inlet pressure needed to prevent cavitation. Comparing the required pressure with the measured pressure forms an error signal which is dynamically conditioned and acts to improve the cavitation margin as described above.

(2) Temperature Protection

The preburner temperature or turbine inlet temperature is influenced directly by the preburner oxidizer-to-fuel ratio. If an abnormal condition occurs to cause a high preburner temperature at any time, the preburner temperature limiter loop will act to reduce the preburner oxidizer-to-fuel ratio and consequently the preburner temperature by increasing the fuel flow into the preburner. When a temperature correction is necessary, the preburner temperature loop acts to lower the oxidizer-to-fuel ratio reference value to the preburner fuel valve schedule and the oxidizer-to-fuel ratio reference to the fuel flow trim loop. With a lower oxidizer-to-fuel ratio reference value, the schedule and the loop increase the fuel flow to the engine and the preburner temperature is lowered to a safe value. The maximum reference temperature limit is scheduled as a function of the main fuel pump speed to allow maximum operating temperatures. The preburner temperature is indirectly sensed by four probes located at the exit of each turbine. Trim occurs only if the highest temperature sensed exceeds the scheduled limit. Compensation is provided in the loop to overcome the effects of thermocouple dynamics.

The walls of the main chamber must be cooled to prevent overheating by the hot combustion gases. A portion of total fuel flow is supplied to the main chamber through the transpiration cooling circuit which contains a fixed-area restriction in parallel with the fuel low speed inducer turbine. Since the flowpath

effectively consists of a constant-area restriction, the proper transpiration cooling flow must be supplied by the pressure drop maintained from the output pressure of the fuel pump to the pressure in the main chamber. The proper pressure drop is assumed to exist normally at steady-state by controlling the main fuel pump speed with a closed-loop.

The required transpiration cooling flow is strongly affected by and increases nearly linearly with the thrust level of the engine. Also, if the fuel pump speed is held to its scheduled value with thrust level, adequate cooling flow will be supplied for the reasons mentioned above. If, during an acceleration transient, cooling flow becomes marginal due to a lagged response by the fuel pump, the cooling flow limiter will slow the request thrust rate to allow the main fuel pump speed to catch up to its scheduled value. In addition, the limiter will improve the cooling flow margin by reducing the required cooling flow with respect to the actual cooling flow. This improvement in margin is accomplished by reducing thrust without changing fuel pump speed. The limiter proportionally reduces the requested thrust level to all the schedules and simultaneously biases the scheduled fuel pump speed so that there is no change in requested speed.

The transpiration supply regenerative heat exchanger exit temperature provides a good indication of the cooling conditions in the main chamber. By sensing this exit temperature and comparing it to a scheduled value a temperature error is formed which indicates the cooling flow margin. Correction will be made only if the actual temperature rises above the scheduled value. Dynamic compensation is provided to allow optimization of the response of the transpiration cooling protection loop.

(3) Speed Protection

The overspeed protection for both main fuel and main oxidizer turbopumps gives positive corrective action without upsetting the power and flow balance within the engine. By trimming the thrust request during overspeed conditions, corrective action will be taken while keeping all of the system schedules coordinated.

Both main pump speeds are compared to their maximum limits to form two speed errors. Each error is conditioned to remove the dynamic characteristics of each pump speed loop. Thrust level trim occurs only when an overspeed condition exists. If an overspeed condition exists simultaneously for both pumps, the largest error is selected for corrective action by a select high function.

The error from the select high function acts to slow or to reduce the thrust level set by the thrust request servo. A speed error will act in a proportional plus integral manner to reduce thrust level to correct for the turbopump overspeed problem.

c. Start and Shutdown Sequence Control Logic

During prestart, start, and shutdown sequences, the closed-loops are opened, the trim integrators are zeroed, and the gross mode assumes complete control of the sequence. The velocity limited thrust servo incorporates the logic for start and shutdown. It also provides the time base for sequencing all of the control valves and solenoids. The four control valves are scheduled by extending their normal steady-state schedules into thrust levels below idle.

The prestart logic prevents engine startup unless the prestart request is cycled on and off. When the prestart cycle is complete, the engine starting sequence begins immediately if the thrust level requested is sufficiently high (at least to idle). The gross mode control system then schedules the four control valves until the engine is operating at the requested level. In the event of ignition failure, the system is held at a safe starting level.

The shutdown sequence similarly uses only scheduled sequences, all closed-loop control systems being opened.

4. Components

The ECU receives data from the pressure, temperature, speed and flowmeter sensors, monitors the positions of the actuators, and supplies output commands to the actuators and solenoids. In addition, the ECU is given operational commands by the ship's central computer, provides test signals to the ECU subsystems, observes the effect of the test signals, and outputs data to the ship's central computer, which judges the validity of the ECU performance.

The ECU is divided into four sections:

1. Input Subsystem
2. Output Subsystem
3. CPU Interface
4. Central Processing Unit

The input subsystem includes the analog multiplexer, analog-to-digital (A/D) converter, speed measurement circuits and sensor failure input circuits. The output subsystem is composed of the digital-to-analog (D/A) converters, the actuator servo amplifiers, and the solenoid drivers. The CPU interface permits communication between the central processing unit and the input subsystem, output subsystem, and ship's central computer. The central processing unit executes all required computations, and stores the XLR129 operational and test programs.

a. Input Subsystem

The input subsystem contains the following components:

1. Analog Multiplexer
2. Analog-to-Digital Converter
3. Speed Measurement Circuits
4. Sensor Failure Input Circuits

The preconditioned input sensor signals (up to 40 channels) are multiplexed by an analog multiplexer (J-FET type) in accordance with central computer control signals. The J-FET switch was selected because of its low ON resistance, zero offset voltage, good temperature stability, and adequate speed.

In order to process the various input sensor signals by a single A/D converter, a multiplexer is required in the input section. The basic theory of analog multiplexing is relatively simple. A multiplexer accepts several signal sources and switches them sequentially, or as required, to a single output line. Thus, an analog multiplexer performs the same function as a rotary switch in which the wiper arm is rotated electrically instead of mechanically. However, a solid-state multiplexer can switch channels much faster than its mechanical counterpart.

The output of the multiplexer is then converted to 12-bit digital words by means of A/D converter. The successive-approximation converter is recommended since it has a faster data access time and requires less hardware than the range-comparison method.

The speed inputs will be measured continuously to provide a maximum number of samples. This feature is particularly important for low speeds, which consume the most time for each measurement. At 1800 rpm, each revolution and measurement requires 33-1/3 milliseconds, and 30 measurements per second are possible.

The circuits for each input will be designed for a specific speed range. However, the speed input may lie outside this range. This condition may arise during engine start-up or shutdown, and from engine, sensor, or circuit failures. The computer program can detect such occurrences.

Comparison of the fixed time interval and variable time interval methods of speed measurement indicates that the variable time interval technique is smaller, lighter and less costly to implement with hardware, and requires fewer program instructions to input data. Also, higher solution rates are possible for low speeds with this approach. This technique employs a higher operating speed (3.28 MHz versus 1 MHz) than the fixed time interval measurement method, but this increase does not appear to be significant. Consequently, the variable time interval measurement method will be applied to all the speed inputs.

The fault detection task is divided into two areas -- sensor fault detection and circuit fault detection. The sensor fault detection plan employs constant sensor monitoring. When a sensor malfunction is observed, this information is sent to the computer, which uses this data to select the good sensor (if one exists) as a source of blade pulses. The computer also can clear a sensor fault, either when the system begins operation or later if desired, provided the sensor is operable. Of course, the monitoring and measurement circuits may also fail. The detection of these faults depends upon the computer test program, which is executed periodically. This program involves blocking the sensor inputs, inserting simulated sensor faults into the sensor monitoring circuits, and observing the monitor circuits' outputs. In addition, if these circuits pass these tests, a simulated sensor signal is inserted, and the measuring circuits process this input. The computer then observes the measuring circuits' output and determines the validity of the measurement circuits.

b. Output System

The output subsystem is composed of the following elements:

1. Digital-To-Analog Converters

2. Servo Amplifiers

3. Solenoid Drivers

The digital output of the CPU is converted to an analog signal by one of four parallel resistor ladder type of D/A converters. This converter method is recommended because of its high accuracy, fast operation, and good temperature stability.

The servos controlling the actuator valves utilize brushless DC torque motors. The major advantage of these servos are the elimination of gear trains, a wide servo bandwidth, and low power dissipation at null.

The servo electronics utilize op-amp microcircuits, DC lead-lag compensation, and miniature components throughout. This approach results in efficient servo compensation, minimum heat generation, and a small packaging size.

Eleven solenoid drivers in the output system are actuated by the CPU. A standard solenoid driver and a pull-hold solenoid drive circuit were evaluated for this application. The standard solenoid driver typically requires approximately 0.5 ampere to actuate the solenoid and a continuous application of this power to keep it energized. The pull-hold circuit requires approximately 0.5 ampere to actuate the solenoid; however, the holding function can be satisfied with about 0.2 ampere. While the pull-hold circuit can conserve system power, the standard solenoid driver is much simpler and cheaper. On that basis, the standard solenoid driver was selected.

c. Central Processing Unit

The central processing unit is a conventional Bendix BDX 800 general purpose digital computer. The memory stores the system operational and test programs. The CPU accepts and supplies data from and to the device controllers (CPU interface) and performs computations as directed by the system programs.

The BDX 800 CPU is a 16 bit, parallel, general purpose processor designed for aerospace application. The salient features of the computer are summarized below:

Type:	General purpose, full parallel organization, single address
Arithmetic:	Binary, fixed point, negative numbers in 2's complement form 16-bit data word
Operation Registers:	A register - most significant half of accumulator - 16 bits

Q register - least significant half of accumulator - 16 bits

X register - Index register

P register - Program counter

Status Register - 3-bit condition register
5-bit N register

Instruction Repertoire: Arithmetic: add, subtract, multiply, divide, load, store, shifts, rotations, and normalize.

Jumps: unconditional jump, variable skips, two subroutine jumps.

The central processor unit of the BDX 800 is a programable digital processor which executes sequences of instructions stored in memory. The CPU performs arithmetic and logical operations on data; it decides what and how operations are to be performed, where the necessary information is to be obtained, and where the results are to be stored.

The memory unit provides storage capabilities for both instructions and data. The storage requirements are met with a 8192 word metal oxide semiconductor (MOS) memory, and these words are each 16 bits in length. The destructive readout (DRO) core memory will permit computer program modifications and changes in system constants to be made rapidly and conveniently via software during the development phase of the program. Production units will use a MOS read only memory to provide the program, and a MOS random access memory to store data and command information. Each storage location has a unique address used to specify that location. The memory unit interfaces with the CPU via two buses: a data bus and an address bus. The 16-bit bidirectional data bus is used for the transmission of a data word to and from the memory unit, while the 16-bit unidirectional address bus is used for selecting a unique location in memory.

d. Central Processing Unit Interface

Communications between the BDX 800 central processing unit and the input/output subsystem are defined in terms of computer instruction repertoire, instruction timing and logical implementation. An exchange of information is initiated by a BDX 800 input/output instruction in the computer program. Each instruction triggers the start of a series of steps subdivided to function in the computer timing intervals. In addition, the CPU and input/output units generate, initiate and acknowledge signals to control the flow of the data transmitted and received.

e. Preliminary Requirements for Input and Output Systems

The preliminary requirements which have been defined for the input and output systems are as follows:

1. Input Isolation

The input signal lines shall be buffered to prevent a failure in one channel from propagating into another channel.

2. Updating Rate

The input and output systems shall be capable of processing a minimum of 40 channels within each computer cycle time of 10 milliseconds.

3. Shielded Wires

When required, signal lines may be shielded to prevent EMI pickup.

4. A/D Converter

Data input: 0 to + 10 volts DC
Conversion time: less than 100 μs
Data access time: less than 120 μs
Source resistance: less than 500 ohms
Output code: 12 bit resolution, natural binary code
Output register: parallel output, 0 to + 5 volts TTL compatible
Accuracy: ± 1-1/2 LSB (least significant bit) (common reference supply voltage for A/D converter and input sensors)

5. Input Analog Multiplexer

Number of input channels = 40
Input voltage range = 0 to + 10 volts
Address logic levels = 0 and + 5 volts
On Resistance = less than 250 ohms
Off Resistance = greater than 100 megohms
Switching time = less than 2 μs

6. D/A Converter

Data input: 12 bit natural binary, parallel
Conversion Time: less than 5 μs
Input logic levels: 0 and + 5 volts, TTL compatible
Output signals = 0 to + 10 volts DC
Accuracy = ± 1 LSB (Common reference supply voltage for D/A Converters and servo feedback device)

7. Speed Sensor Converter

Range of input pulses per revolution = 4095 to 20,475
Clock frequency: 3MHz
Output code: 15 bit resolution, natural binary
Output buffer register: parallel output, 0 to + 5 volts TTL compatible

8. Controllers

Input address: 4 bits
Control inputs: 5 channels

Output control: 2 channels
Transfer gating: Bidirectional Control for 16 lines
Storage register: 16 bits
Clock frequency: 1 MHz
I/O instruction time: 6 μs

9. Discrete Outputs

Solenoid drivers: Seven drivers for 0.5 to 1.0A capacity
Gating control for drivers: 0 or + 5 volts logic
Actuator Changeover switches: Four Switches with 0 or + 5 volts gating logic control

10. Discrete Inputs

Sensor faults: Detect 35 sensor inputs
Selector control: Divide inputs into 3 groups of 12 each

11. Operational Temperature Range

-55° C to +125° C

12. Warm-Up Time

The time required for the equipment to warm-up prior to operation shall not exceed five minutes.

13. Power Consumption

The total power consumption of the input and output systems shall be less than 45 VA.

Multiplexer	0.40
A/D Converter	1.50
Reference Supply (I/O + Sensors)	4.00
Speed Circuits	3.00
4 D/A Converters	2.40
11 Solenoid Drivers	2.20
4 Servo Amplifiers	8.00
Logic Gating	3.60
5 Volt Power Supply	7.00
Misc. Power Supplies	6.00
	38.10 Watts

14. Accuracy Estimate

Multiplexer	±0.012%
A/D Converter	±0.034%
D/A Converter	±0.025%
	±0.071%
(Approx. =	±3 LSB)

SECTION VII
INTEGRATED COMPONENTS

A. HOT GAS SYSTEM RIG

1. Introduction

The hot gas system allowed the integration of the preburner injector and transition case components that were previously designed, fabricated, structurally proof tested to be integrated and tested as integrated components. The hot gas system rig permitted testing of the integrated components under engine conditions.

The hot gas system rig was made up of a bill-of-material preburner oxidizer valve, preburner injector and transition case assembly with rig hardware to simulate the fuel and oxidizer turbopumps.

The hot gas system rig allowed the preburner injector to be check fired into the hot gas flow path used in the engine system before driving the fuel turbopump turbine with the preburner. In addition, the transition case assembly operation could be evaluated under actual hot gas firing conditions before a fuel turbopump was mounted in the transition case.

2. Summary, Conclusions and Recommendations

The No. 2 preburner injector and No. 1 transition case assembly were integrated with the fuel and oxidizer pump simulators as a hot gas system rig. The hot gas system was mounted on E-8 test stand and six hot firings were made.

During the six hot firings, it was demonstrated that the preburner and transition case could be satisfactorily run together as integrated components. The turbine inlet temperature profile on the fuel pump simulator of 103° R maximum to average at an average temperature of 1452° R is satisfactory for operation of the fuel turbopump.

3. Hardware Description

Hardware used in the assembly of the hot gas system rig F-35139 included the main case, transition case, outer case cooling liner, centerbody, preburner injector flow duct, preburner injector, oxidizer control valve, oxidizer and fuel turbine simulators, main burner injector simulator, preburner igniter, and gimbal ball. The transition case is the spherical mounting structure for the remaining hardware described.

After fabrication of the transition case was completed, skin thermocouples for monitoring case temperature were installed on the inside diameter of the outer case (figure 884). Following instrumentation installations, the outer case cooling liner was assembled into the outer case by welding together preformed spherical segments (figure 885) fabricated from sintered L-605 (AMS 5759) wire mesh. This liner shields the outer case structure from the high-temperature turbine exhaust gases as they are discharged to the main burner injector. The liner is hydrogen cooled, and prevents the case external skin from exceeding 540° R.

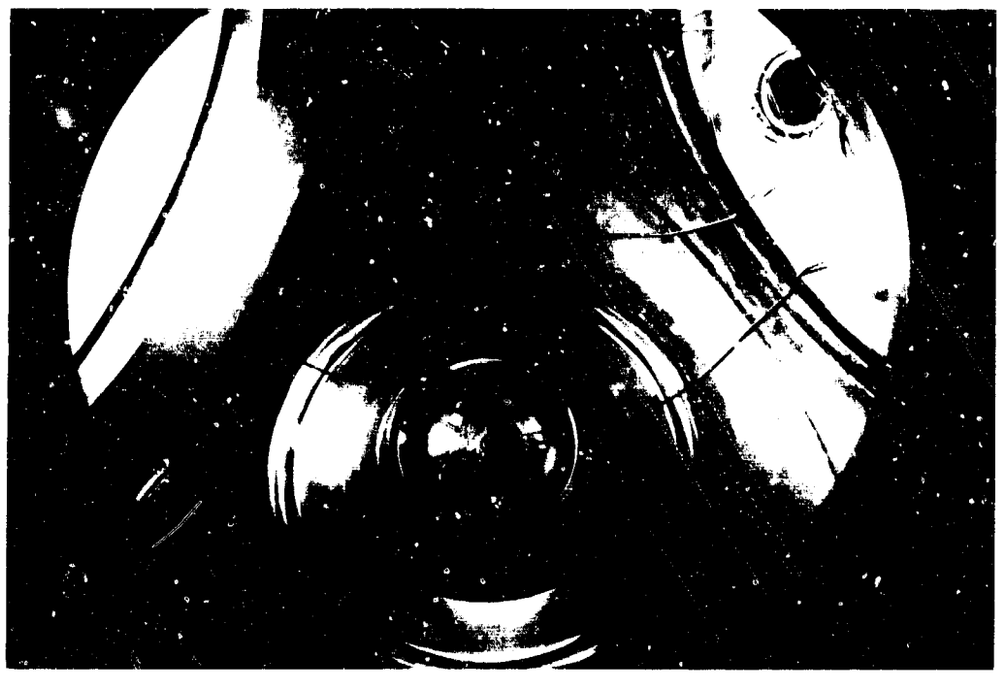

Figure 884. Skin Thermocouples Installed on Inside Diameter of Transition Case FE 97307

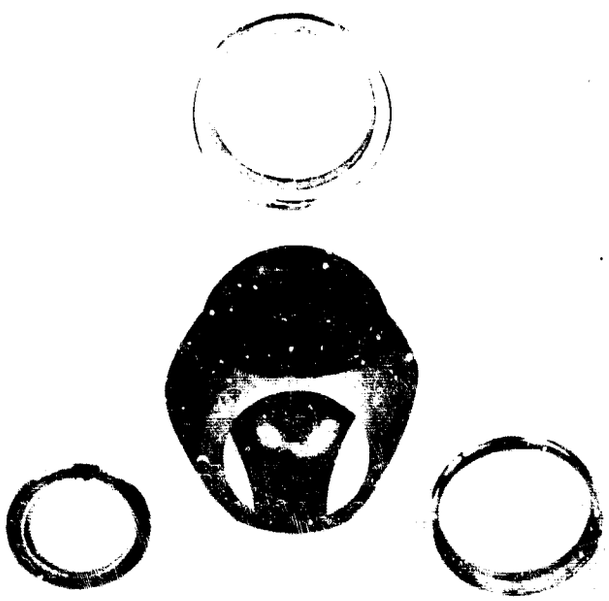

Figure 885. Preformed, Welded, Spherical Segments FE 97226

Before starting the assembly of the rig, backflush adapters were installed on the transition case so the cooling liner and transition case could be flushed with trichlorethylene to remove all contaminants. After completion of a bake cycle that follows the back flush operation, static and dynamic strain gages were installed on the outer skin for measuring outer skin stresses during testing. To start the rig assembly, the outer case was placed on the mounting fixture with the main burner centerline in a horizontal position. The mounting fixture was designed so that the transition case rotated about the main burner centerline. This permitted rotation of the transition case and positioned the sphere flanges so that each component could be lowered into the transition case.

The centerbody was installed in the interior of the transition case (figure 886), by threading it into the gimbal cone of the transition case. To properly locate the centerbody both angularly and axially, a locating fixture was fabricated for installation on the fuel flange of the transition case. The centerbody, illustrated in figure 887 consists of the structural body, the outer porous cooling liner, and the inner liner assemblies. The structural body is a sphere intersected by three cylindrical rings equally spaced around the equator of the sphere.

With the centerbody installed, the transition case was readied for the installation of the preburner injector flow duct. The transition case was rotated with the preburner flange on top with the face of the flange in a horizontal position.

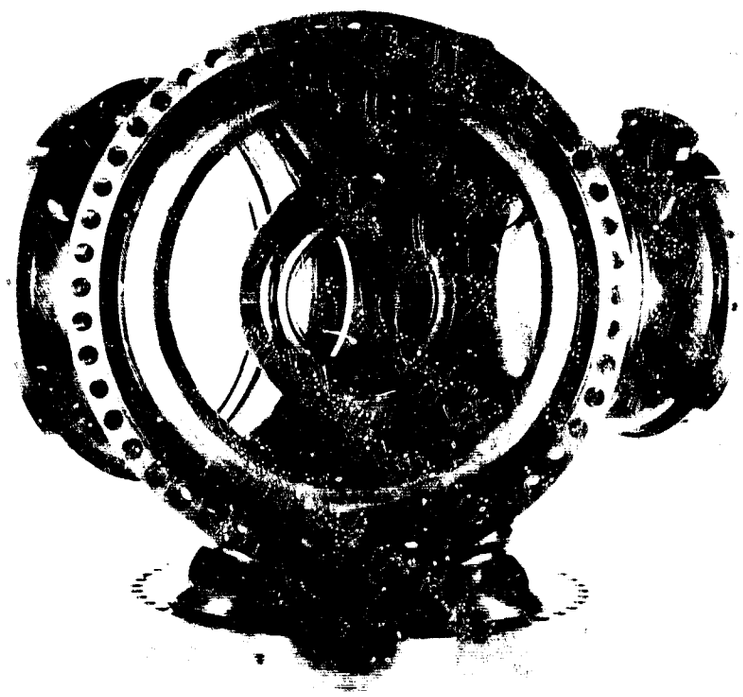

Figure 886. Centerbody Installed in Interior of Transition Case FE 97596

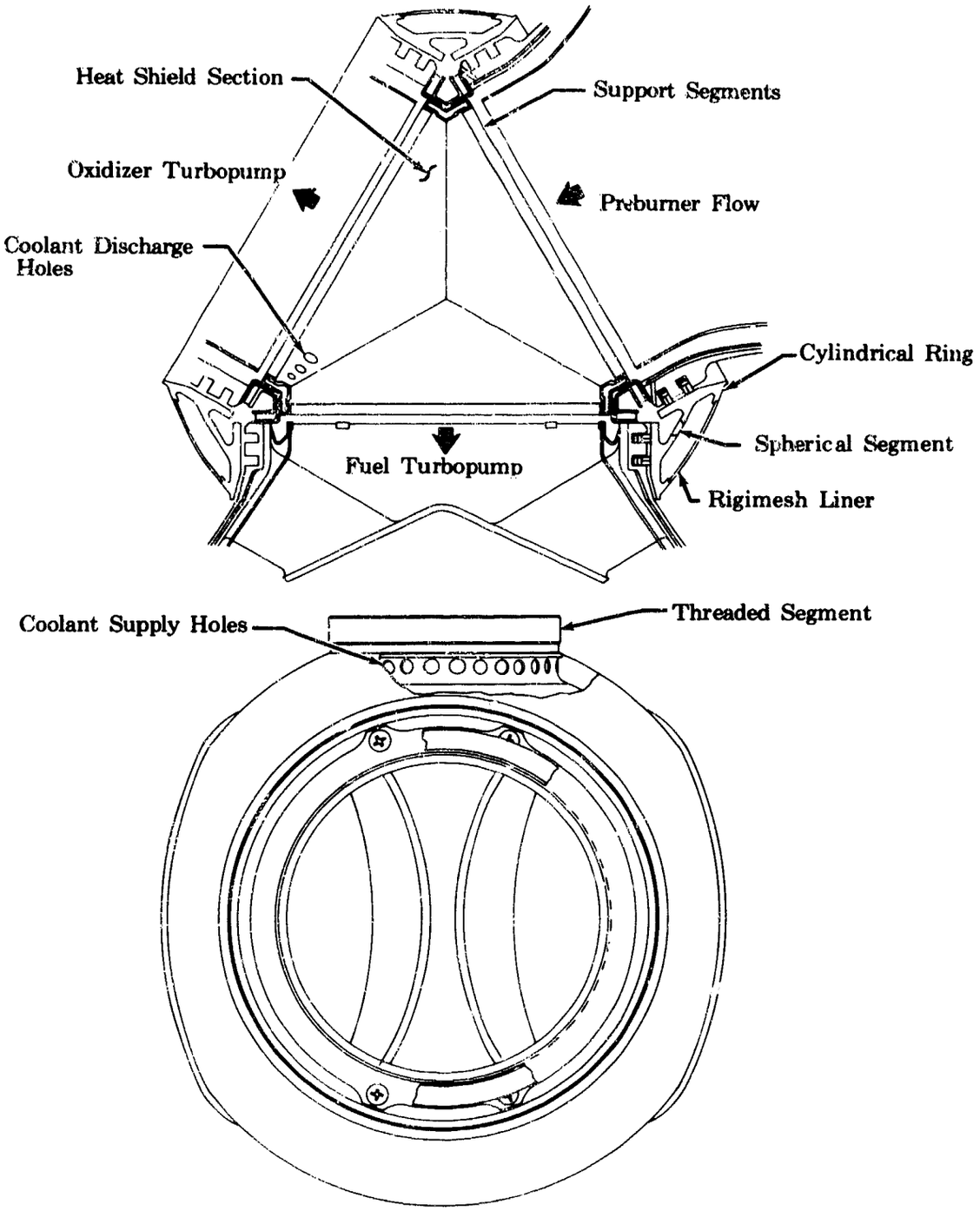

Figure 887. Centerbody Consisting of Cooling Liner and Outer Liner FD 29179

The preburner flow duct is a contoured duct (figure 888) in which combustion takes place, and through which the gas flows from the preburner injector to the centerbody. The duct is composed of a cooled structural duct (figure 889), a hot gas scrub liner, an outer heat shield, and a transpiration cooled liner (figure 890).

Figure 888. Preburner Flow Duct FE 95742

The upstream end of the preburner flow duct is supported by the transition case preburner flange as shown in figure 891.

A teflon coated aluminum ring is used to seal the preburner coolant cavity from the transition case. At assembly, a measurement from the front face of the duct to the preburner injector was taken. A preburner injector catcher-ring was machined on a line-to-line fit considering thermal conditions to ensure the preburner injector faceplate blowoff load was balanced. The downstream end of the preburner duct outer structural wall contains a ring into which two grooves are machined. These grooves form the seats of a three piece piston ring seal design, shown in figure 892. The piston ring seals against the wall of the cylindrical ring in the centerbody. The duct outer heat shield has a knife edge seal (figure 893) that rests on a seal ring portion of the main case cooling liner. This seal separates the hot combustion gases from the ambient hydrogen coolant. A spacer ring was required to obtain the correct crush of the seal which allows for thermal growth of elements and faceplate. When the preburner duct prebuild had been completed, the preburner flow duct was held in a vertical position and lowered into the main case. After installation, stack up dimensions were again taken to ensure the proper crush against the injector faceplate.

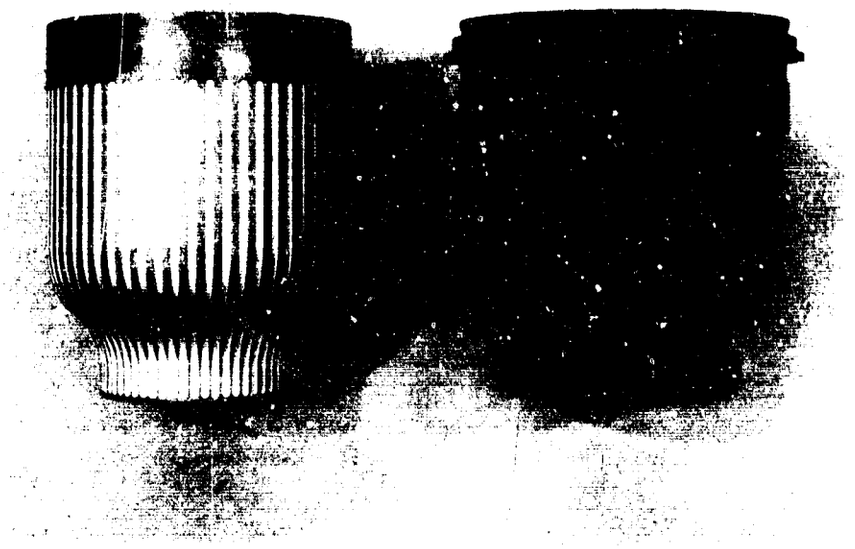

Figure 889. Cooled Structural Duct FE 95743

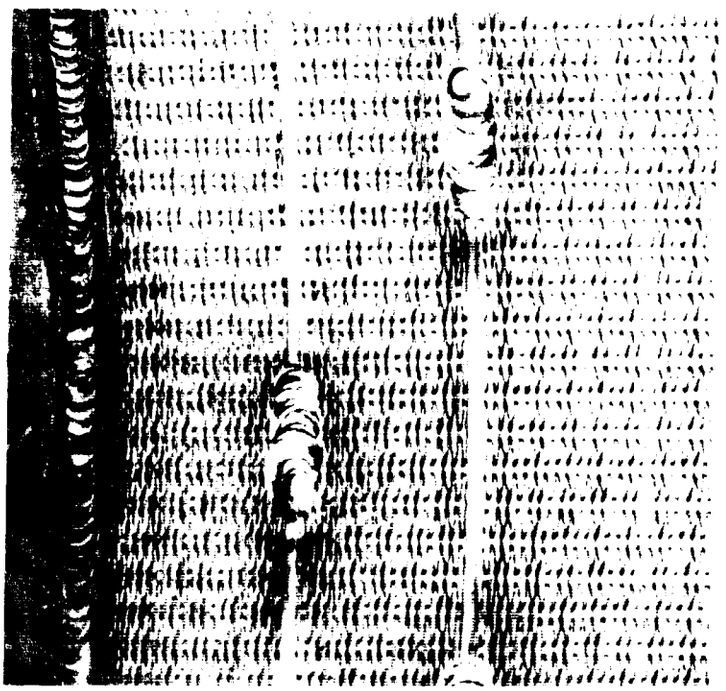

Figure 890. Transpiration Cooled Liner FE 99393

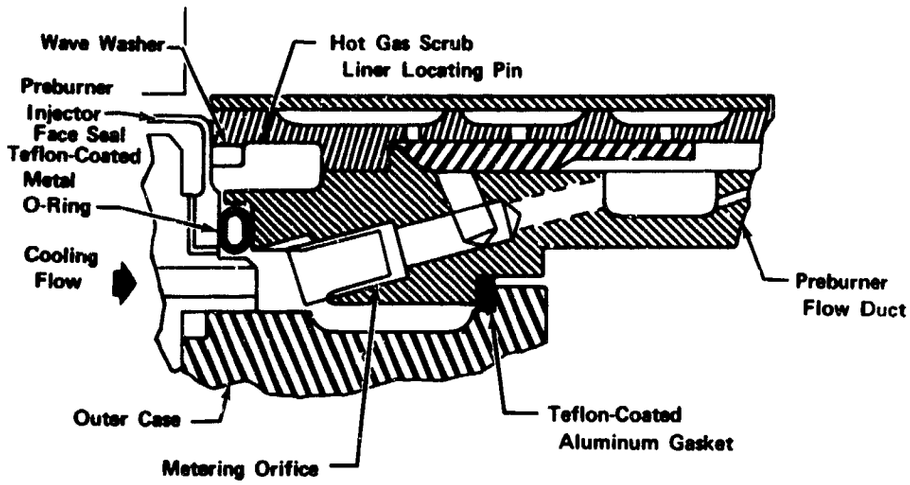

Figure 891. Preburner Flow Duct Front Support FD 29145A

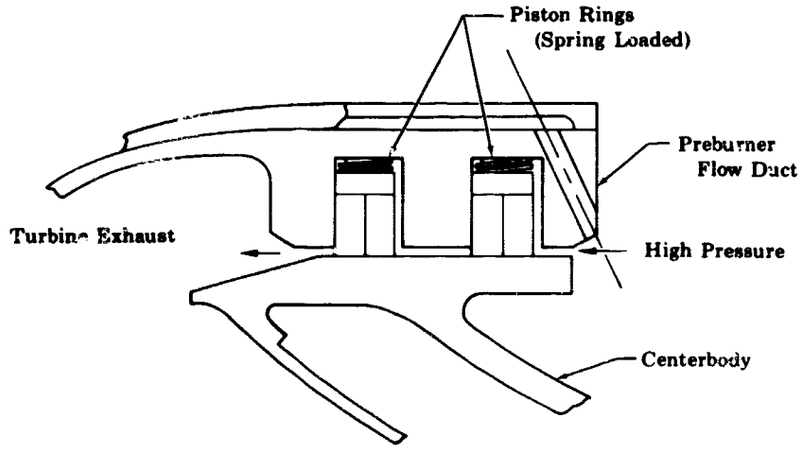

Figure 892. Preburner Flow Duct to Centerbody Piston Ring Connection FD 29139

Figure 893. Knife Edge Seal of Duct Outer Heat Shield FE 99392

With the assurance of the necessary fit to the preburner injector faceplate, the injector assembly was installed on the preburner flange of the transition case. Building a preburner injector into a subassembly involved various operations, oxidizer elements were individually flowed with water and categorized on the basis of total flow and primary only flow. The fuel injector faceplate was calibrated by flowing each fuel orifice with water and GN_2. The injector faceplate fuel orifices were machined with 253 oxidizer elements to give a constant mixture ratio over the entire faceplate. With the matching complete, four braze cycles were required for full assembly. They are:

1. Au-Ni braze of 253 elements into injector housing.

2. Au-Ni braze of primary/secondary divider plate to housing and elements.

3. Au-Ni fillet braze of elements to injector housing on fuel cavity side.

4. Ag braze of each element to adjacent 3 tangs on fuel faceplate.

With the injector assembly resting on the preburner flange of the transition case, the oxidizer control valve was placed on top of the injector and bolted to the transition case. The oxidizer control valve regulates the liquid oxygen supply to the primary and secondary cavities of the injector housing.

The fuel turbine (figure 894) and oxidizer turbine (figure 895) simulators consist of the inlet, turnaround, and diffuser sections of the respective pumps. Orifice plates were used in place of the pump rotors and 2nd-stage stators to provide the proper turbine pressure differential. Backpressure plates were used to complete the simulation assembly. These plates are bolted to the transition case. Both backpressure plates have removable plugs which provide access to the inlet, stator and orifice plate regions of the ducts. Much of the instrumentation (temperature and pressure rakes) can be replaced or repaired by use of these access ports. Diaphragms on the pump simulators form crush seals with knife edge rings on the outer case cooling liner. The seals separate the hot combustion gases from the outer case coolant. After prebuild had been completed, the pump simulators were held in a vertical position and lowered into the outer case. The main burner simulator (figure 896) is a water cooled plate that simulates the back pressure to the transition case and is assembled to the main burner flange of the transition case.

Since the igniter port provides the only opening to the preburner flow duct and pump inlet sections, it was left open to permit final checks of the rig assembly. The igniter is a mixing chamber for gaseous hydrogen and oxygen with an exciter to provide the ignition spark. The igniter assembly was installed in the igniter port and bolted to the igniter boss flange on the preburner sphere of the transition case.

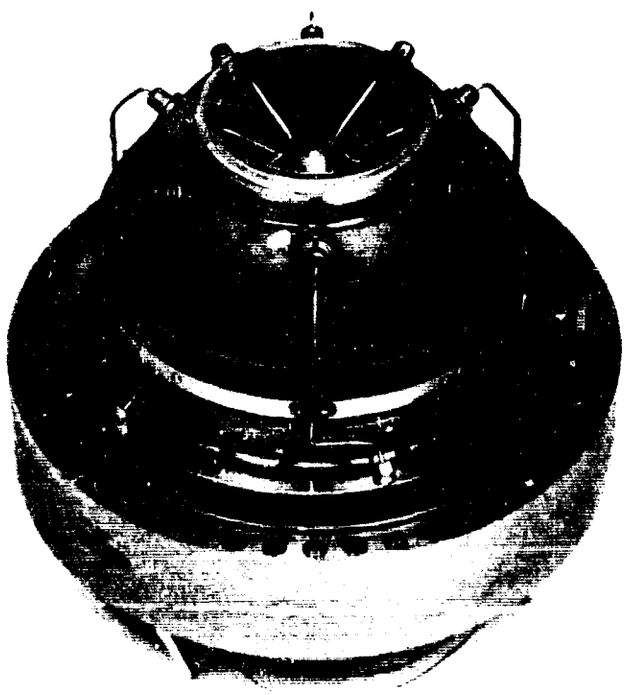

Figure 894. Fuel Pump, Turbine Simulator FE 97980

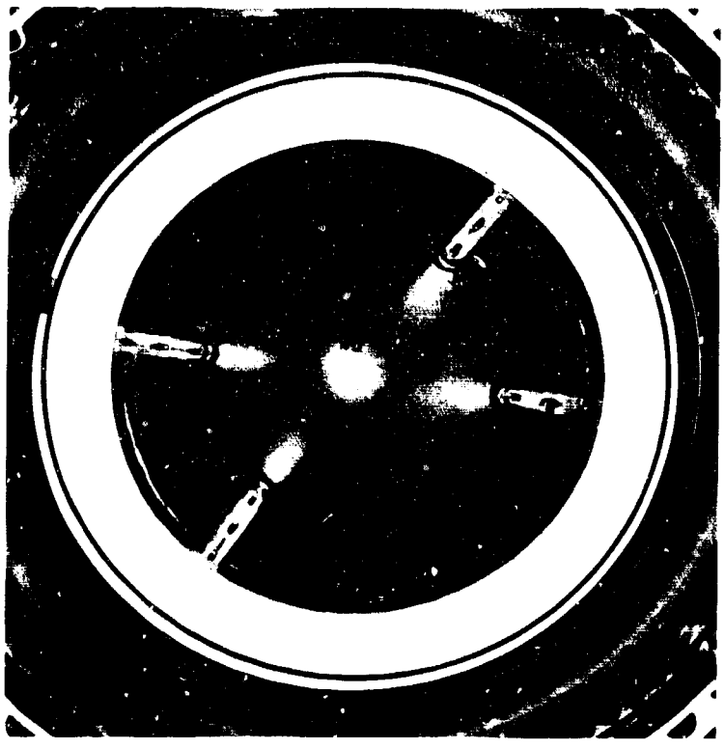

Figure 895. Oxidizer Pump Turbine Simulator FE 97984

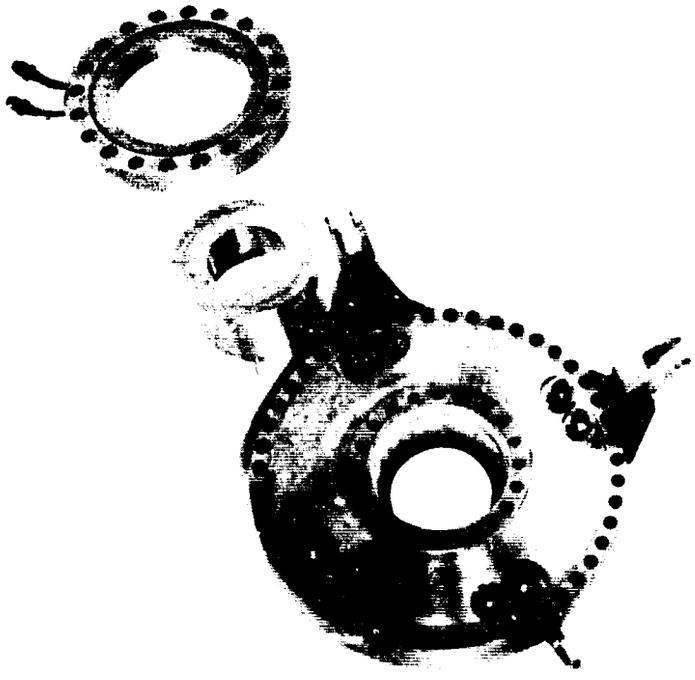

Figure 896. Main Burner Simulator FE 98013

The assembly was removed from the mount stand by a lifting arm and was held by the main burner flange while the gimbal (figure 897) was attached by means of a split retainer ring. The gimbal was then bolted to a test transport stand and was shipped to E-8 test stand.

Figure 897. Gimbal Thrust Ball Attached to Outer Case Gimbal Cone FE 96107

4. Testing

a. Instrumentation

Instrumentation of the hot gas system rig, F-35139, is as shown in sketch AKS 8252. The instrumentation serves to provide rig performance data and provides (figure 898) protection against abnormal temperatures, pressures, and flows.

Instrumentation to monitor conditions in the transition case cavity between the outer case and porous cooling liner was applied to the case as shown in figure 899 and 900. Skin temperatures on the inside of the case shell and the static pressure of the coolant between the case and case cooling liner were monitored.

A

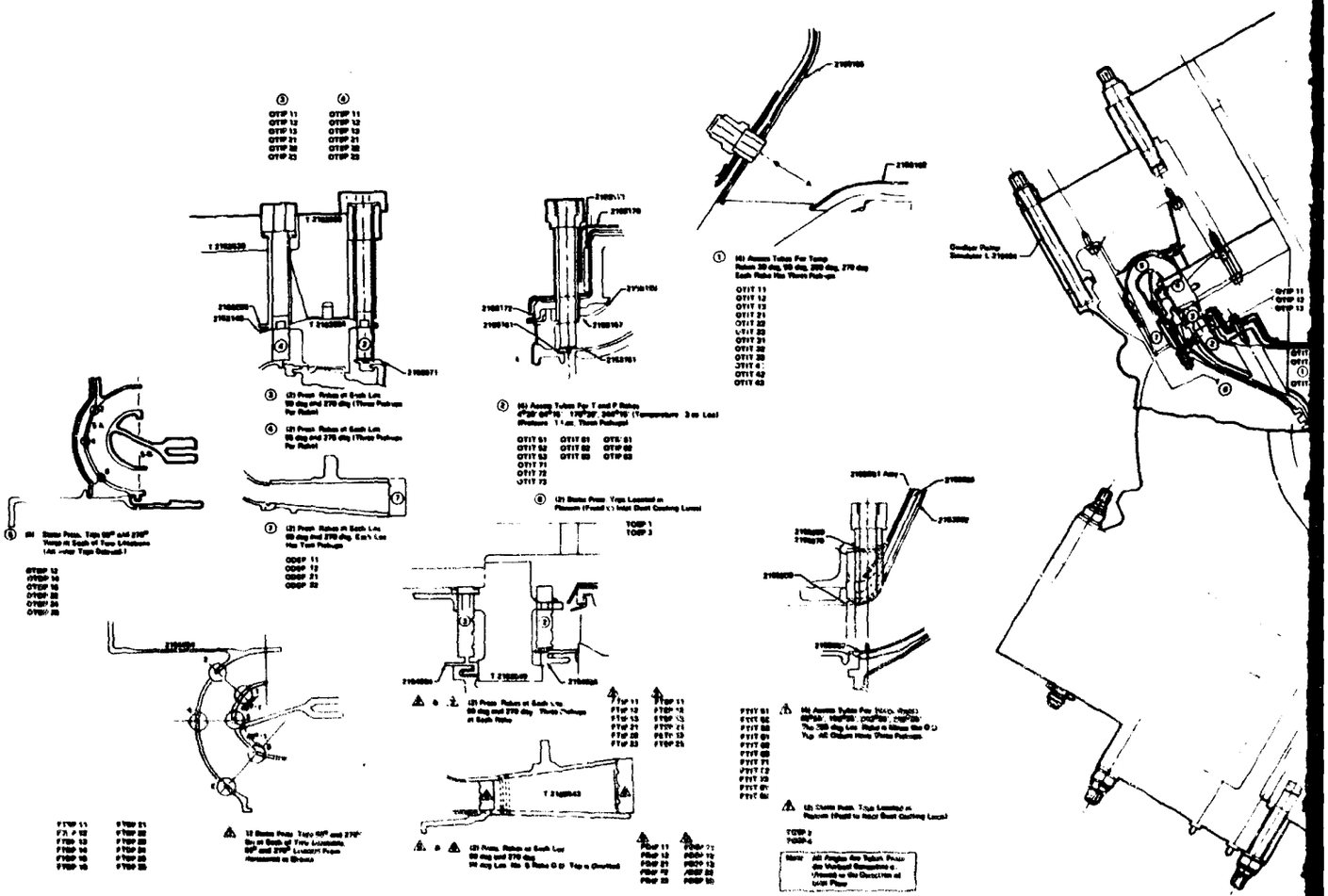

Figure 898. Hot Gas System Rig Instrumentation

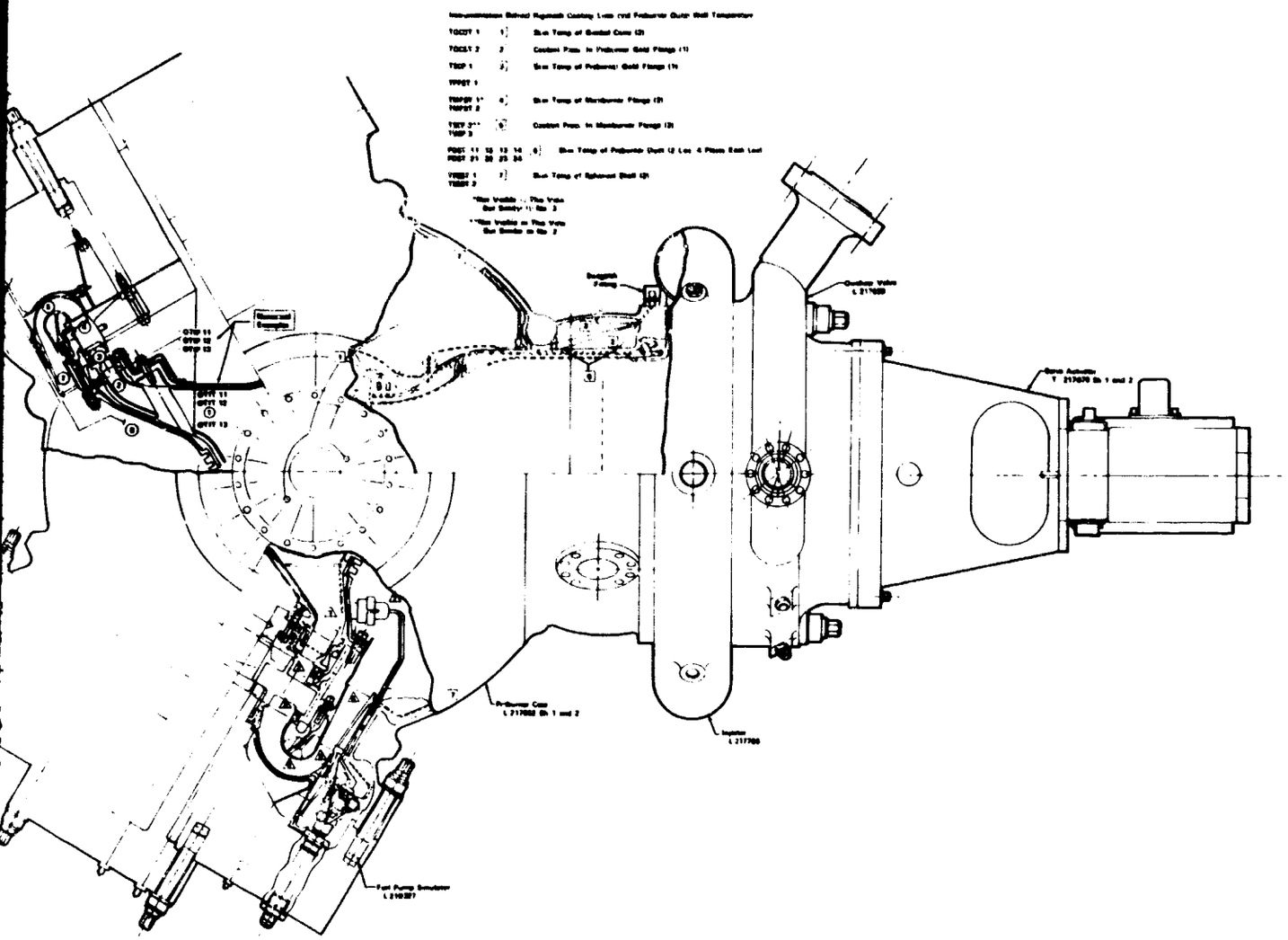

FD 44019

947 / 948

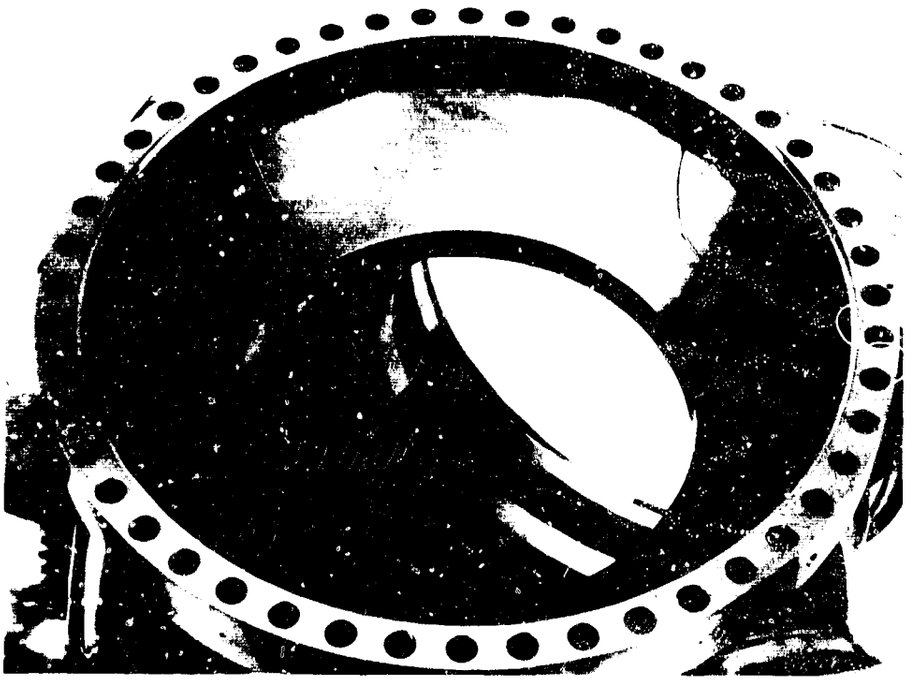

Figure 899. Instrumentation to Monitor Transition Case Cavity Conditions FE 97306

Figure 900. Instrumentation to Monitor Transition Case Cavity Conditions FE 97307

The locations of the temperature instrumentation leads were: the gimbal pad innerskin (TGCST-1 and 2), the spherical shell between the preburner and oxidizer pump spheres (TSSST-2), the spherical shell between the preburner and fuel pump spheres (TSSST-1), the preburner sphere (TPFST-1) and main burner sphere (TMFST 1 and 2). Because only the preburner remained accessible after the transpiration liner was installed, redundant leads were installed at the other three locations before the liner installation. Access to these leads was provided through No. 1 Swagelok fittings installed between bolt holes on the preburner and main burner flanges. Additional Swagelok fittings were provided to monitor preburner injector combustion temperature, and to provide temperature and pressure data through each turbine.

The shape and size of the oxidizer pump inlet bullet allowed an extra plane of instrumentation compared to the fuel pump inlet turbine. This made it possible to place probes directly ahead of the inlet struts of the oxidizer pump (loc. ①). Each of these rakes had three exposed platinum/platinum-rhodium thermocouples to monitor temperature variations across the flowpath. These four temperature rakes provided the data closest to the preburner injector hot combustion gas temperature.

Both turbine simulators had four probes equally spaced radially directly ahead of their respective 1st stage stators. These locations enabled monitoring of temperature and pressure conditions at the turbine inlets (loc. ②and④). Pressure drop through the turbines was monitored by total pressure rakes at the entrance (loc. ③and⑫ and exit (loc. ④and⑬ of the orifice plates, static pressure taps along the wall of the turnaround ducts (loc. 5 and 4) and total pressure rakes at entrance (loc. 5) and exit (loc. 7 and 6) of the diffusers.

Each pump simulator also had static pressure taps located along two of the inlet ducts coolant tubes (loc. 8 and 7). These taps monitored the static pressure in the transition case chamber. The data from these taps and the tap behind the case liner provided the effective pressure drop across the transpiration liner.

The preburner injector external instrumentation monitored fuel and oxidizer parameters; specifically, flow, temperature, pressure and pressure variations (Kistler data). Thermocouples behind the Rigimesh faceplate were monitored for excessive heating in that area to signify possible backflowing of the combustion gases. The outer shell of the cooled preburner duct was instrumented at eight locations to detect possible heating of the scrub liner.

b. Hot Gas System Rig Firings

The hot gas rig was mounted on E-8 test stand and six hot firing tests were made. The following were the test objectives:

1. Determine the temperature profile in the turbine inlet ducts.

2. Determine the pressure profile in the turbine inlet ducts.

3. Calibrate the hot gas internal ducting.

4. Demonstrate hardware durability.

Run 1.01 was programed for 50% thrust, r = 5. The 50% thrust, r = 5 data point was chosen because the preburner transpiration cooled Rigimesh liner was not damaged during previous tests at this data point; thus, the temperature profile could be evaluated prior to committing the rig to higher combustion temperatures. The start sequence for the run was to divert 7% flowrates to the rig and immediately start the ramp to 50% thrust while pressurizing the propellant liquid run tanks to the required pressure level. The flow divider valve is opened to the primary only, with a combined GHe and GN_2 purge entering the injector secondary downstream of the oxidizer valve. As the propellant flowrates accelerate past the 20% thrust level, the oxidizer valve is opened to the secondary cavity and the combined purge is turned off. This start procedure is much shorter than the procedure used in preburner rig testing, thus accounting for the short duration runs.

Run 1.01 was advanced due to a faulty high transition case liner differential pressure at 8.92 seconds which is prior to reaching the 50% data point. Subsequent runs showed that the low side pressure source for the transition case liner differential pressure was not responding properly, thus causing an erroneous high differential pressure reading. Inspection of the rig through the nozzle after run 1.01 showed no problems.

Data from run 1.01 showed a 280 to 150 cps combustion oscillation of 50 to 110 psi peak-to-peak during the transient to 50%. Due to the reduced timing in the start and acceleration sequence the combustion oscillations are short lived. The shutdown temperature spike was not as high (under 2700°R) as it was in preburner rig testing. A summary of runs 1.01 through 6.01 are shown in table CI.

Run 2.01 was a repeat attempt at the run 1.01 program. The run was automatically advanced at 0.51 seconds due to high combustion temperature. The rig remained in good condition after the run.

Analysis of the data from run 2.01 showed that fuel delivery to the rig was not properly maintained after rig ignition thus causing a high combustion temperature that advanced the rig. A 50 second timing change on the fuel valves was expected to cure the fuel delivery problem.

Run 3.01 was programed the same as run 1.01 with the exception of the 50 millisecond timing changes to the fuel valves. Run 3.01 was a full duration run of 13.73 seconds.

The rig was inspected through the nozzle throat as well as through the igniter mount port. No problems were found through the nozzle throat as illustrated in figure 901. Inspection through the igniter port revealed approximately 14 discolored areas in the preburner liner transpiration cooled section with some discoloration extending down onto the uncooled section of the liner as shown in figure 902 which is a typical photo taken through a borescope. In the majority of the cases the discolored areas appear to line up with the ends of the hexagonal pattern of the outer row of injector elements although two of the 14 discolored areas are approximately in the center of the row of the hexagonal pattern. Two of the discolored areas at a row end appear to have some slight metal erosion.

Table CI. Test Data Summary, Hot Firings Using Fuel Pump Simulator

Run	Preburner Chamber Pressure psia	Pump Simulator Discharge Pressure psia	Percent Thrust %	Engine Mixture Ratio	Average Combustion Temperature °R	Maximum Minus Average Temperature °R	Comments
1.01							False high transition case differential pressure advance at 8.9 sec.
2.01							High combustion temperature advance at 0.5 sec due to slow fuel delivery
3.01	2071	1555	50	5	1452	122	Full duration run of 13.7 sec. P/B liner locally discolored.
4.01							False high transition case differential pressure at 6.7 sec. Centerball liner and P/B heatshield buckled during hard ignition caused by facility valve dragging.
5.01							False low combustion temperature at 2.8 sec.
6.01	679	501	20	5	1330	221	Full duration run of 10.1 sec.

Figure 901. Rig Inspected Through Nozzle Throat FE 98487

Figure 902. Discoloration Extending Into Uncooled Section of the Liner FE 98799-1

The conditions that were predicted and obtained for Run 3.01 are shown in table CII. The temperature profile in the fuel and/or pump simulator is shown on figure 903. Figures 904 and 905 show the total pressure profile and static pressures at various locations in the fuel and oxidizer pump simulators ducting. In general, the program set points were attained. The maximum-to-average temperature profile of 122° R at 1452° R average temperature was satisfactory. The 50 millisecond fuel valve timing change corrected the high temperature spike at ignition that was experienced during Run 2.01.

Run 4.01 was programed for 75% thrust, r = 5 and 100% thrust, r = 5.5. The start sequence was the same as used previously in test 3.01. An oxidizer lead of 280 milliseconds in advance of the opening of the main fuel shutoff valve was used. The outer case liner coolant supply valve is sequenced to open 150 milliseconds after the preburner fuel valve allowing the preburner to ignite before coolant is introduced into the transition case.

Run 4.01 was automatically advanced after 6.695 seconds because of a faulty high outer case liner differential pressure. The advance occurred before the first data point was recorded.

The ignition of the rig during test run 4.01 was audibly louder than previous ignitions of this rig. Analysis of the actual timing of rig ignition, as opposed to the sequenced events, shows that the rig ignited approximately 70 milliseconds later in test 4.01 than in tests 1.01, 2.01, or 3.01. The delay in rig ignition was caused by slow opening of the main fuel shutoff valve (ROV 38). The delay in actuation of ROV 38 was approximately 85 milliseconds later than normal, which allowed the main case coolant liner supply valve (CV12) to open and admit GH_2 into the main case before fuel reached the preburner. Rig ignition first occurred inside the main case approximately 15 milliseconds before preburner ignition.

Inspection of the rig after test 4.01 revealed some buckling of the Rigimesh liner surrounding the transition case center ball, and some buckling of the heat shield around the preburner duct. The preburner injector, preburner liner and center ball inside were viewed by borescope and appeared basically the same as shown by post-test 3.01 borescope inspection, except the most downstream weld that forms the lower side of zone 3 in the preburner transpiration liner appeared broken over approximately 1.5 in. of circumference, as evidenced by a slight inward protrusion of the liner at that location. The segments of the liner in the vicinity of the zone 3 broken welds were not in distress after run 4.01.

In general the rig appeared in acceptable condition for continued low-thrust level, low combustion temperature testing.

Inspection of the instrumentation tube to the low side of the main case liner differential pressure showed the tube to be plugged with braze material at a braze connector, thus causing the low side to always read ambient.

Table CII. Preburner-Transition Case Test Results Rig No. 35139-1, Run No. 3.01, Engine Thrust Level 50% Mixture Ratio 5

Preburner	Predicted Engine Cycle 6 *(Cycle 8)	Predicted Rig Cycle	Test Results
Oxidizer Primary Flow - lb/sec	7.856**	7.856	6.63
Oxidizer Secondary Flow - lb/sec	20.38**	20.38	21.8
Oxidizer Primary/Total Flow Split	0.2782**	0.2782	0.233
Injector Face Fuel Flow - lb/sec	36.97	36.91	37.48
Rigimesh Liner Flow - lb/sec	NAV	NAV	0.104
Coolant Liner Flow - lb/sec	0.2286*	NAV	0.064
Injector Mixture Ratio	0.763**	0.763	0.756
Chamber Discharge Mixture Ratio	0.760*	0.7415	0.754
Chamber Pressure - psia	2010.	2056.	2071.
Oxidizer Injector Temperature - °R	208.2**	208.2	193.
Fuel Injector Temperature - °R	142.0**	142.0	143.
Primary Effective Area - in^2	0.063**	0.063	0.0491
Secondary Effective Area - in^2	0.5897**	0.5897	0.667
Fuel Injector Plate Effective Area - in^2	3.7	3.0	3.33
Oxidizer Turbine Simulator			
Turbine Inlet Flow - lb/sec	19.04	NAV	19.58
Turbine Coolant Flow - lb/sec	0.66*	0.6302	0.332
Outer Case Coolant Flow - lb/sec	0.33***	0.33	0.38
Discharge Static Pressure - psia	1439.	1474.	1566.
Turbine Inlet Total Pressure - psia	1995.	NAV	2004.
Turbine Exit Total Pressure - psia	1474.	NAV	1416.
Diffuser Inlet Total Pressure - psia	NAV	NAV	NAV
Diffuser Exit Total Pressure - psia	NAV	NAV	1577.
Turbine Inlet Temperature - °R	1465.	1488.	1406.
Fuel Turbine Simulator			
Turbine Inlet Flow - lb/sec	46.86	NAV	46.50
Turbine Coolant Flow - lb/sec	0.55*	0.5766	0.223
Outer Case Coolant Flow - lb/sec	0.33*	0.87	0.99
Discharge Static Pressure - psia	1460.	1474.	1550.
Turbine Inlet Total Pressure - psia	1989.	NAV	1995.
Turbine Exit Total Pressure - psia	1513.	NAV	1521.
Diffuser Inlet Total Pressure - psia	NAV	NAV	1591.
Diffuser Exit Total Pressure - psia	NAV	NAV	1561.
Turbine Inlet Temperature - °R	1465.	1488.	1471.
Overall Performance			
Total Oxidizer Flow - lb/sec	28.23**	28.23	28.43
Total Fuel Flow - lb/sec	39.07*	39.32	39.41
Total GH_2 Over Case Coolant Flow - lb/sec	0.66*	1.2*	1.37
Overall Mixture Ratio	0.723*	0.718	0.721
Transition Case Plenum Pressure - psia	1462.	1474.	1555.
Temperature Profile - °R	0°	0°	122°
Average Combustion Temperature - °R	1485.**	1488.	1452.
C* Efficiency (Based on Pressure and Flow) - %	100.	100.	(Need errata calc)

**Predicted rig conditions

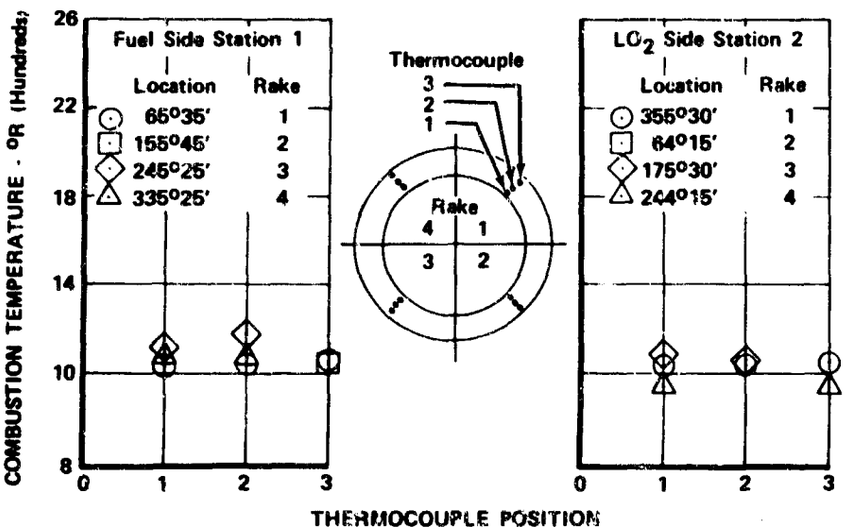

Figure 903. Temperature Profile In Fuel Pump Simulator, Run 3.01 FD 43360

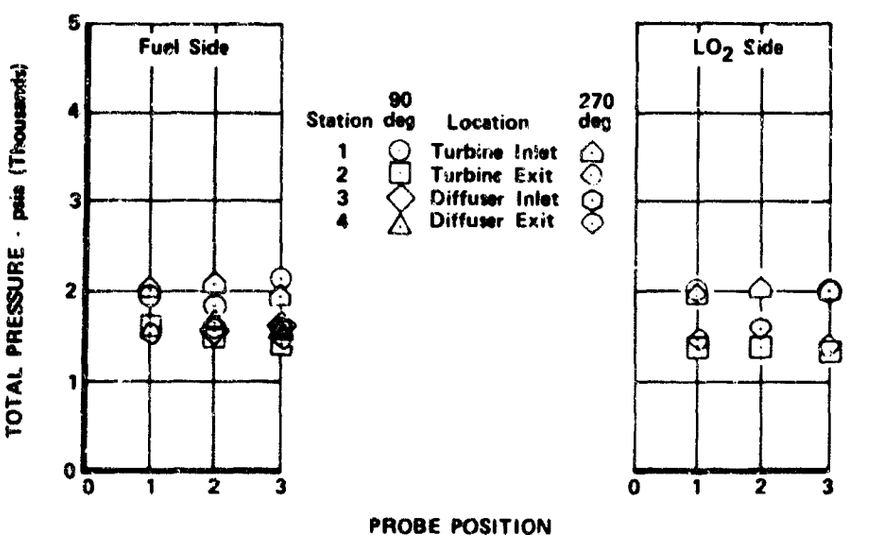

Figure 904. Total Pressure Profile In Fuel Pump Simulator Ducting, Run 3.01 FD 43361

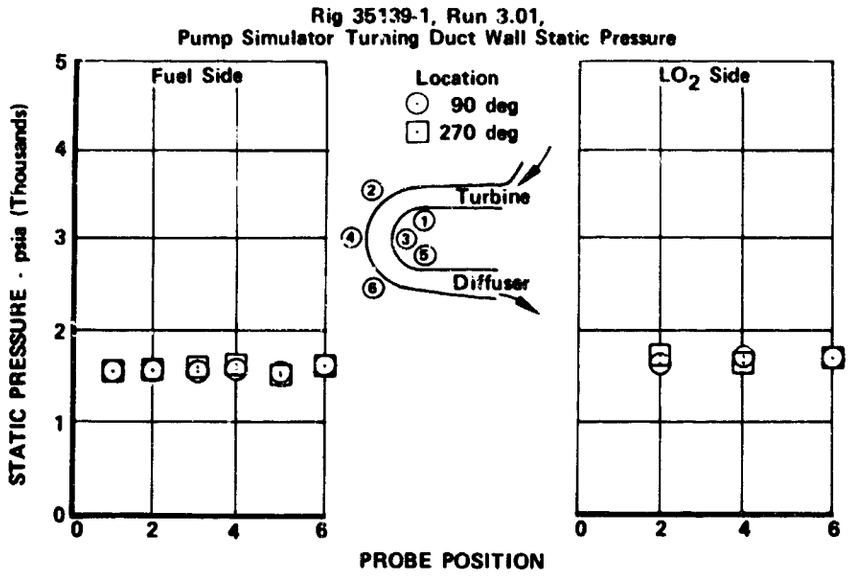

Figure 905. Static Pressure In Oxidizer Pump Simulator Ducting, Run 3.01 FD 43362

The hard start of test 4.01 could have yielded the pump simulator and preburner diaphragm seals, allowing the outer case liner flow to bypass the liner by leaking through the seals. A cold flow was made through the outer case liner in order to determine the liner effective area. The cold flow showed that the liner effective area was 3.7 times greater in previously run test 1.01.

Inspection of ROV 38 revealed sludge accumulation inside the pilot valve porting the hydraulic pressure to the actuator. Another pilot valve was installed on ROV 38 and volve timing returned to normal.

Run 5.01 was programed for demonstration of normal ignition through stand valve repair and sequencing changes, and a data point at 20% thrust, r = 5. The outer case coolant supply valve opening was set 370 milliseconds after ROV 38 was open, sequencing from adding margin to ensure ignition in the preburner rather than the transition case.

Test 5.01 was automatically advanced after 2.798 seconds because of a faulty low combustion temperature. A review of the data from oscillographs showed that the rig was igniting in the preburner instead of in the transition case.

Test 6.01 was a repeat of the program for test 5.01. Test 6.01 was a full duration run of 10.144 seconds.

Visual inspection of the rig after run 6.01 revealed no additional damage to the center ball liner. Borescope inspection of the preburner chamber showed that the weld at the lower side of zone 3 in the preburner transpiration liner had broken over approximately 3/4 of the liner circumference. Also, one additional area of slight metal erosion had occurred on the transpiration liner.

A review of the data showed the outer case coolant liner effective area was approximately 2.3 times greater than cold flows before test 1.01. The conditions that were predicted and attained on run 6.01 are shown in table CIII. The temperature profile in the fuel and oxidizer pump simulators is shown on figure 906. Figures 907 and 908 show the total pressure profile and static pressures at various locations in the fuel and oxidizer pump simulators ducting. In lieu of the above visual inspection, the rig was pulled from the test stand and delivered to the assembly floor for teardown.

The hot gas system rig was disassembled for review of hardware damage caused by the hard light of test 4.01 and for inspection of the preburner duct cooling liner. Inspection showed buckling of the porous liner surrounding the centerbody and buckling of the heat shield around the preburner duct. Buckling was also present between each strut of the oxidizer simulator inlet bullet on the cooling liner. This buckling was not severe and the coolant passages behind the bullet liner were not closed.

Other discrepancies attributed to the hard start was the yielding of the pump simulator diaphragm seals, and partly the yielding of the preburner diaphragm seal. A post-test inspection of the simulator seals showed the oxidizer seal out of flatness by 0.060 in. maximum. Prebuild measurements showed the part 0.009 in. out of flatness.

The knife edge that mates against the diaphragm seals, located on the outer case cooling liner, was also affected. The oxidizer simulator knife edge seal deflected axially a maximum of 0.043 in. and went out of flatness 0.026 in. maximu. The fuel simulator knife edge seal deflected 0.070 in. and was out of flatness 0.047 in.

A gap noted between the outer case main burner flange and the cooling liner measured 0.042 in. (design specification is 0.004 in.). Too large a gap in this area would mean a loss of coolant.

The outer case cooling liner showed no major areas of concern as evidenced by dimensional X-ray visual inspection. The cooling liner was not in contact with the outer shell and the porous liner has not been deformed although there were some indications that the liner moved locally. The preburner duct diaghragm seal to the outer case cooling liner was found in a flattened condition. This seal normally has a radius that provides a metal-to-metal interference fit with the outer case cooling liner. The actual interference fit of the buildup may have been greater than blueprint because a teflon coated aluminum crush washer that provides a seal between the preburner duct and outer case was found partially out of seat at disassembly. Approximately one-quarter of the seal was severely deformed and was broken away from the larger piece. The remaining section of the seal showed no compression marks. If the crush washer had been moved completely out of its seat, the preburner duct could move an additional 0.038 in. The entire load would have been taken by the preburner duct diaphragm seal.

Table CIII. Preburner-Transition Case Test Results Rig No. 35139-1, Run No. 6.01, Engine Thrust Level 20%, Mixture Ratio 5

Preburner	Predicted Engine Cycle 6 *(Cycle 8)	Test Results
Oxidizer Primary Flow - lb/sec	5.782**	6.34
Oxidizer Secondary Flow - lb/sec	3.808**	2.78
Primary/Total Oxidizer Flow Split	0.6029**	0.696
Injector Face Plate Fuel Flow - lb/sec	13.33**	13.52
Rigimesh Liner Flow - lb/sec	NAV	0.71
Coolant Liner Flow - lb/sec	0.833*	0.0486
Injector Mixture Ratio	0.716	0.672
Chamber Discharge Mixture Ratio	0.713*	0.669
Chamber Pressure - psia	732.4	679.
Oxidizer Temperature - °R	200.**	185.7
Fuel Temperature - °R	125.4	128.7
Primary Effective Area - in^2	0.063**	0.0733
Secondary Effective Area - in^2	0.2526**	0.179
Fuel Injector Plate Effective Area - in^2	3.7	3.3
Oxidizer Turbine Simulator		
Turbine Inlet Flow - lb/sec	6.76	6.89
Turbine Coolant Flow - lb/sec	0.43*	0.078
Outer Case Coolant Flow - lb/sec	0.16	0.158
Turbine Discharge Static Pressure - psia	566.3	509.0
Turbine Inlet Total Pressure - psia	NAV	685.3
First Stator Discharge Total Pressure - psia	727.4	654.4
Turbine Discharge Total Pressure - psia	582.8	501.6
Diffuser Inlet Total Pressure - psia	NAV	NAV
Diffuser Discharge Total Pressure - psia	NAV	507.3
Turbine Inlet Temperature - °R	1367.	1235.
Fuel Turbine Simulator		
Turbine Inlet Flow - lb/sec	16.52	15.87
Turbine Coolant Flow - lb/sec	0.27*	0.0602
Outer Case Coolant Flow - lb/sec	0.16	0.417
Turbine Discharge Static Pressure - psia	577.1	505.3
First Stator Discharge Total Pressure - psia	725.6	644.3
Turbine Discharge Total Pressure - psia	595.6	485.6
Diffuser Inlet Total Pressure - psia	NAV	483.8
Diffuser Discharge Total Pressure - psia	NAV	540.3
Turbine Inlet Temperature - °R	1367.	1372.
Overall Performance		
Total Oxidizer Flow - lb/sec	9.59**	9.12
Main Run Line Fuel Flow - lb/sec	14.16	13.78
Total Fuel Flow - lb/sec	14.48	14.56
Overall Mixture Ratio	0.622	0.627
Temperature Profile - °R	0°	221
Average Combustion Temperature - °R	1394.**	1330.
Transition Case Plenum Pressure - psia	557.7	500.6
C* Efficiency (Based on Pressure and Flow) - %	100	97.2

**Predicted rig conditions

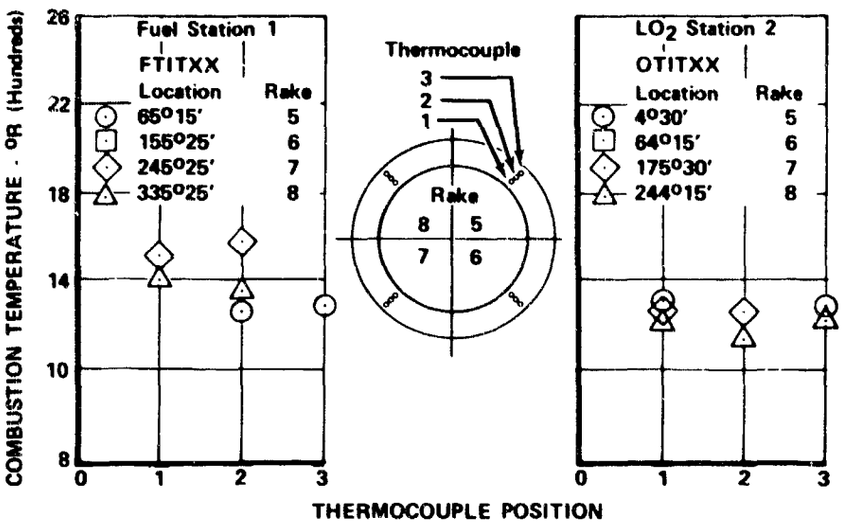

Figure 906. Temperature Profile In Fuel and Oxidizer Pump Simulators, Run 6.01

FD 44074A

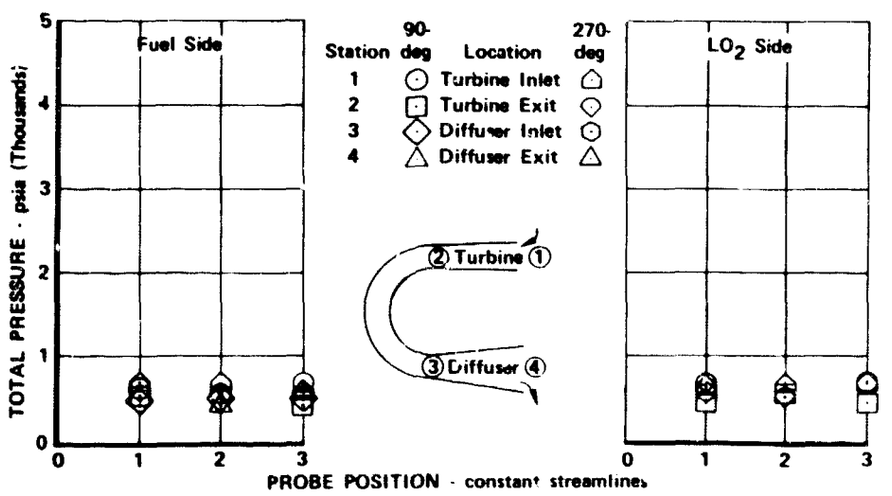

Figure 907. Total Pressure Profile In Fuel Pump Simulator Ducting, Run 6.01

FD 44075

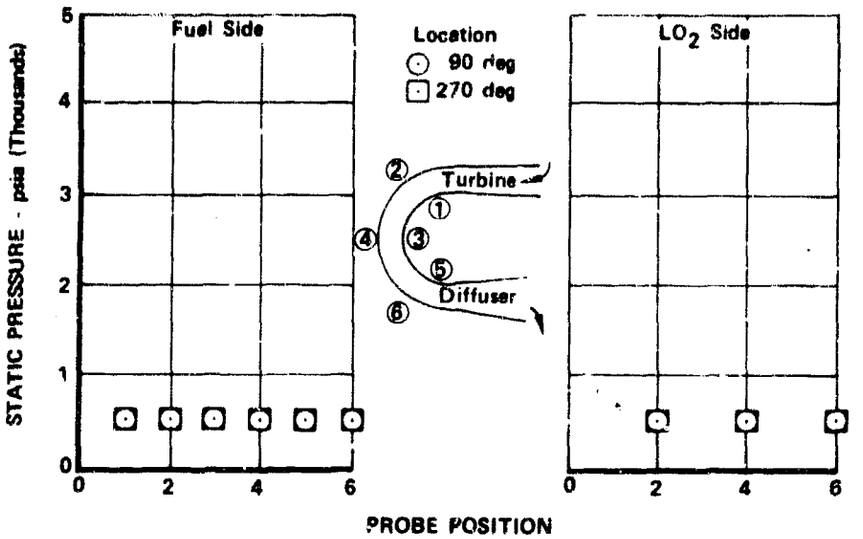

Figure 908. Static Pressure in Fuel Pump Simulator Ducting, Run 6.01 FD 43359

The disassembly also revealed that the preburner duct transpiration liner separated from its carrier downstream of zone 3 for a 180 deg segment. One quadrant of the liner had separated from the carrier over its entire axial distance. X-ray inspection showed the electron beam weld between the liner and carrier to be defective. Sectioning of the part showed that the electron beam welding operation used to join the transpiration liner to its carrier was only partially effective. The weld showed penetration in some areas only, with some of these being shallow penetrations. This condition carried downstream to the uncooled scrub liner as shown in figure 909. These two hardware details contained the only cracks found on any of the hardware inspected.

Figure 909. Partial Effectiveness of Electron Beam Weld In Uncooled Scrub Liner FE 99017

Disassembly of the fuel simulator showed the following:

1. The first stator showed discoloration from heat on the leading and trailing edges. A small crack was present at one of the stator vanes between the two vane flow recirculation holes. Several of the recirculation holes indicated heat discoloration and slight metal erosion.

2. The orifice plate (simulator for the 2nd-stage stator and rotor) showed heat discoloration on the upstream side. This plate also showed a crack at a hole that was drilled for additional instrumentation.

3. One turbine inlet duct seal attachment lug was broken off, allowing the seal to twist slightly.

At this point it was concluded that the hot gas system had performed properly and was sufficiently checked out to allow its use to drive the turbine of a fuel turbopump assembly. Therefore, the rig was reassembled with a fuel turbopump replacing the fuel pump simulator.

B. HOT TURBINE RIG

1. Introduction

A series of six tests were conducted with the fuel turbopump mounted on the hot gas system rig to demonstrate the capability of this integrated unit to operate at engine operating levels of speed, flow, pressure and temperature. During these tests, preburner chamber pressure to 4200 psia was achieved and the fuel turbine operated at temperature levels 86°R in excess of the maximum engine cycle requirement (2325°R). The peak pump flow and discharge pressure demonstrated on these tests was 9,956 gpm and 5,554 psia, respectively.

2. Summary, Conclusion and Recommendations

Six hot firing tests accumulating 95.8 sec of hot turbine testing were completed that demonstrated the capability of the integrated fuel turbopump, transition case, preburner injector and preburner oxidizer valve to operate at conditions equivalent to 50%, 75% and 1000% engine thrust conditions. Successful operation was demonstrated at the 1000% level at conditions equivalent to engine mixture ratios of 5, 6 and 7.

From these hot turbine tests the following conclusions were made:

- The integrated components are capable of operation over a range of mixture ratios and thrust that satisfy engine operational requirements.

- The feasibility of the spherical transition case concept and cooling scheme has been demonstrated. Some modification is required to the centerbody to eliminate ovalization that occurred at the three intersecting holes where the preburner, oxidizer turbopump turbine inlet, and fuel turbopump inlet plug into the centerbody.

- The adequacy of the mixed flow cooling scheme used in the turbine static structures has been demonstrated. Some minor design modifications in this area would make it possible to optimize the configuration to reduce the amount of cooling flow required, and to eliminate the cracking that occurred on the oxidizer turnaround inner flow duct.

- A suitable preburner temperature profile for operation with the turbopump turbines has been demonstrated.

- Fuel pump and turbine performance exceeded the design goals and the axial thrust balance capability was adequate for engine operation over the range of thrust and mixture ratio.

It is recommended that these basic integrated component concepts be used in the design of future high-pressure staged combustion engines.

3. Hardware Design

The hot turbine test rig configuration was identical to that of hot gas system test rig F35139, as described in Section VII, paragraph A, except that the fuel turbine simulator was replaced with fuel turbopump F35147-1A. The fuel turbopump hardware design is described in detail in Section V, paragraph F.

4. Assembly

The fuel turbopump assembly is installed in the transition case and attached with 48 tie bolts. As the fuel turbopump is inserted, the fuel turbine inlet duct piston ring seals engage the center ball access port ring structure to provide a hot gas seal. The fuel turbopump diaphragm seal engages the outer case cooling liner and is preloaded 0.060 in. to seal outer case coolant from the hot turbine discharge gas.

5. Testing

The fuel turbopump turbine was tested at temperature and pressure levels experienced during engine operation. Gaseous hydrogen and liquid oxygen were pressure fed to the preburner injector from the facility high-pressure propellant tanks and liquid hydrogen was supplied to the fuel turbopump at pressure and temperatures equivalent to engine operating levels. The hot fuel-rich preburner combustion gases were ducted to the fuel turbopump turbine and the oxidizer turbopump turbine simulator by the internal ducting of the transition case. The nozzle backpressure plate simulated the main combustion chamber. The fuel turbopump discharge flow was discharged through a throttle control valve to a burn stack disposal. Figure 910 is a schematic of this test setup.

Before initiating the hot firing tests, a cold flow test was conducted on the low pressure hydrogen system and fuel turbopump to establish the pump inlet conditions and system operational characteristics. The initial hot firing test, test No. 1.02, conducted on 15 July 1970 was programed for 13.7 sec duration with 3 sec of operation at 50%, r = 5 preburner cycle conditions. After 1 sec of steady-state operation at 50%, a 2 sec fuel pump flow excursion was scheduled. The test was a full duration run of 13.7 sec, during which pump operation at 29,360 rpm was achieved, and all program objectives were accomplished.

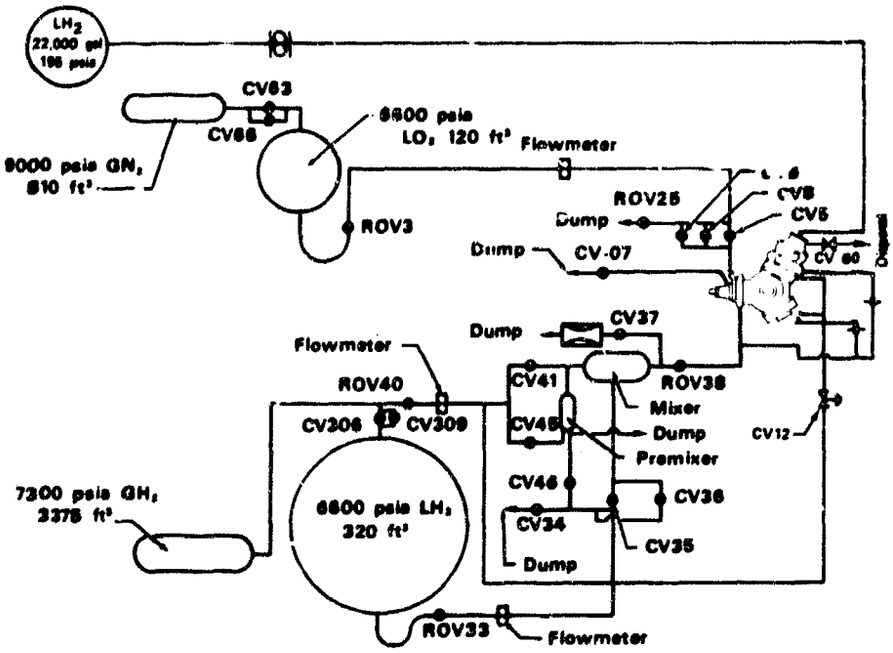

Figure 910. Hot Turbine Test Rig Schematic FD 33032B

Data analysis revealed that the test rig operated as predicted and that the overall pump performance exceeded design goals as were experienced during the calibration tests of the fuel turbopump in the B-6 test facility. The pump discharge pressure vs flow map recorded by x-y plotter during the test is shown in figure 911. Plots of significant fuel turbopump parameters vs time for test No. 1.02 are shown in figures 912 through 915. Table CIV presents a tabulation of data recorded in the combustion system. Figures 916 and 917 describe significant combustion system temperature and pressure profile data recorded for this test. Post-test visual inspection through the backpressure simulator throat and the preburner igniter port using a fiber optic scope revealed the rig was in excellent condition.

Test No. 2.01 was programed for 21.74 sec duration with a 2 sec steady-state operation at 75% thrust, r = 5, 75% thrust, r - 6, and 100% thrust, r = 6 preburner cycle conditions, in that order. The test was manually advanced to shutdown after 6.4 sec because of indication of a high outer case coolant liner differential pressure. A review of the pressure sensor on the low side of the liner differential pressure transducer showed that the low side pressure tap was slow in responding to the power ramp, thus creating a false high differential pressure reading. Visual inspection of the rig through the backpressure simulator throat showed no hardware distress. No steady-state data were recorded on this test.

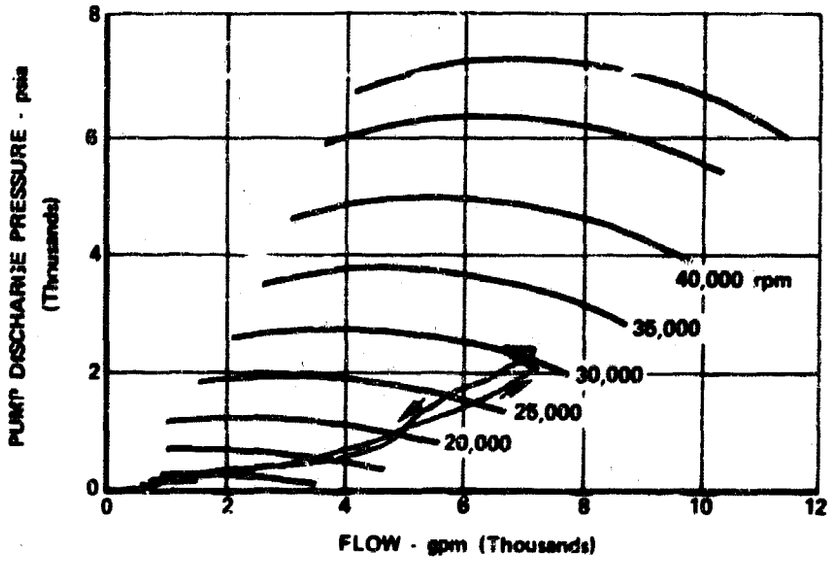

Figure 911. Pump Discharge Pressure vs Flow Test 1.02, Rig 35155-1 FD 42876

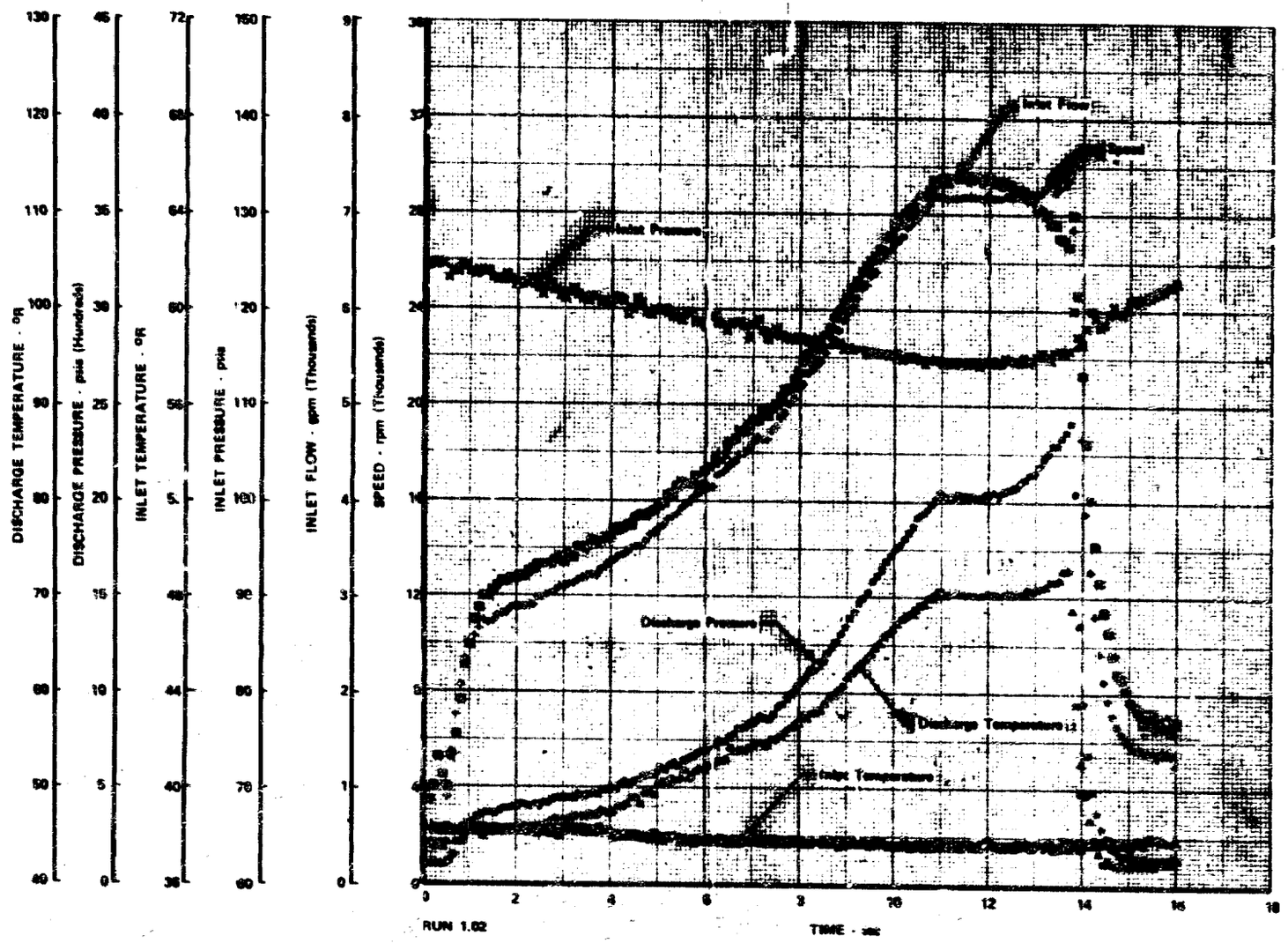

Figure 912. Significant Turbopump Parameters vs Time, Test 1.02, Rig F35155-1, Sheet 1

FD 42839

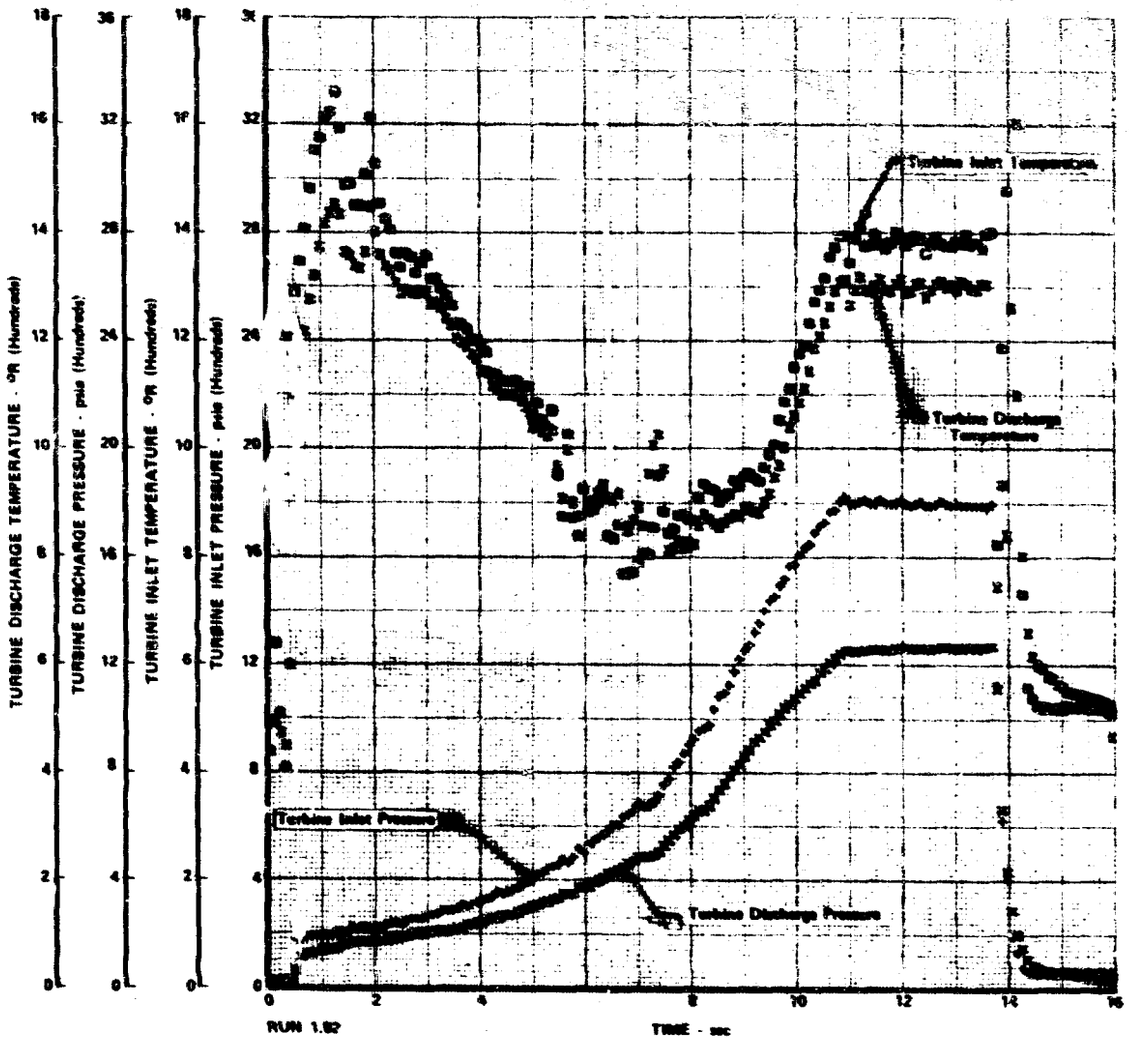

Figure 913. Significant Turbopump Parameters vs Time, Test 1.02, Rig F35155-1, Sheet 2

FD 42840

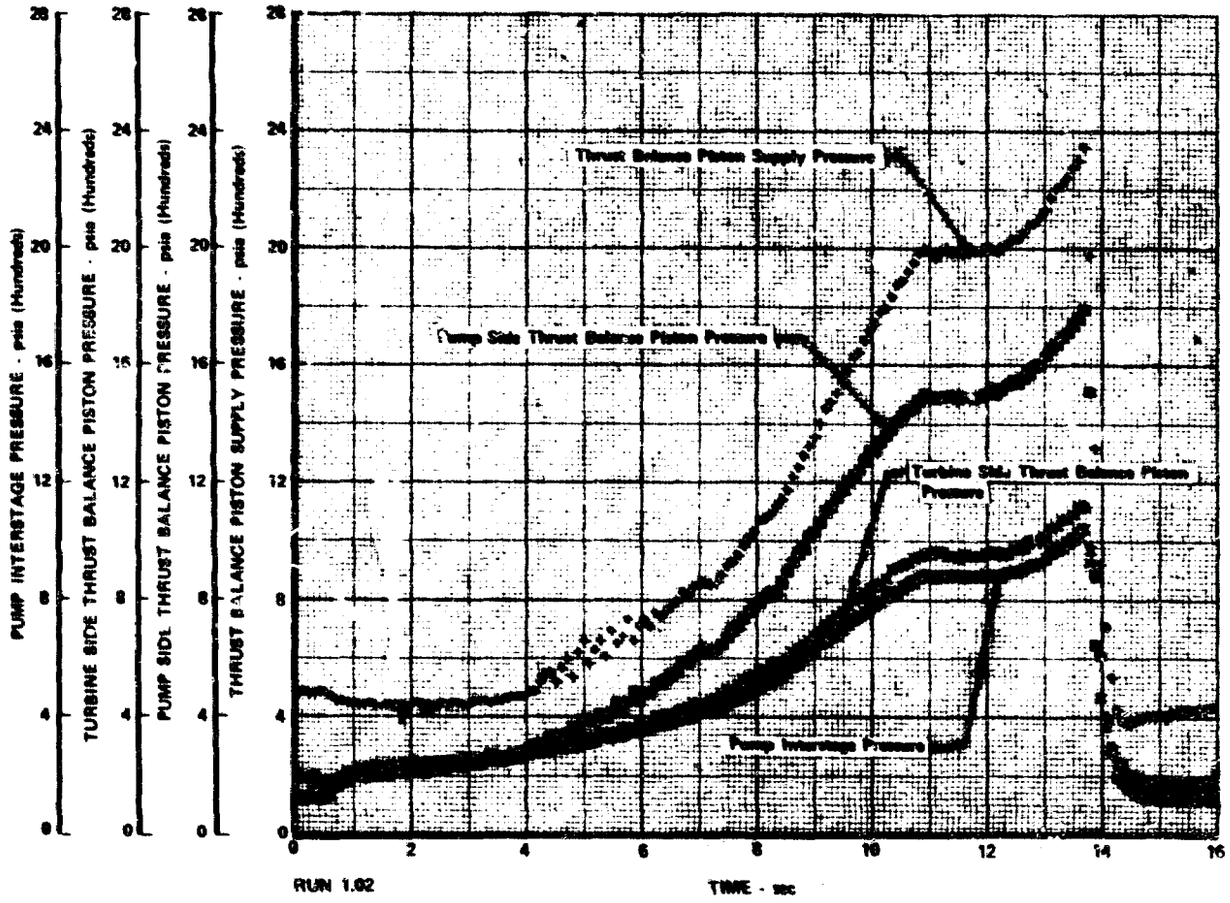

Figure 914. Significant Turbopump Parameters vs Time, Test 1.02, Rig F35155-1, Sheet 3

FD 42841

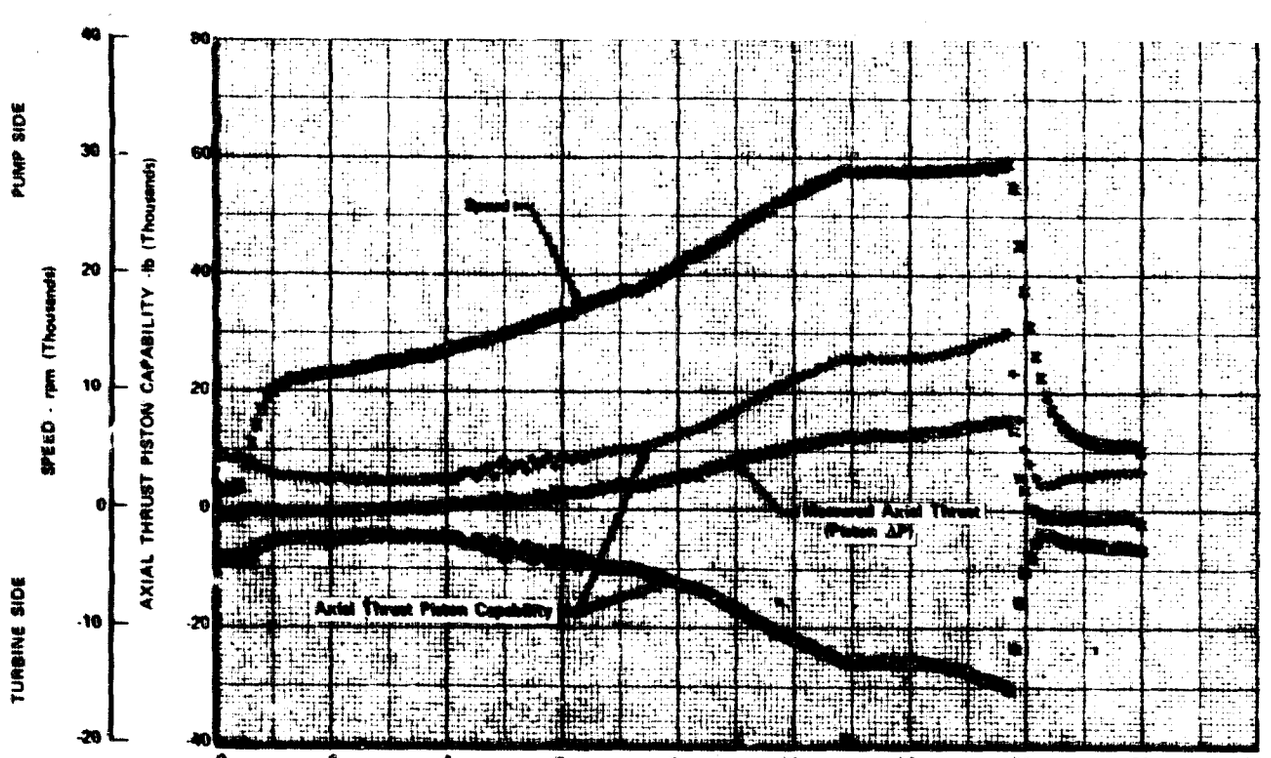

Figure 915. Significant Turbopump Parameters vs Time, Test 1.02, Rig F35155-1, Sheet 4

FD 42842

Table CIV. Hot Turbine Test Run, Rig No. 35155-1, Run No. 1.02, Engine Thrust Level 50%, Mixture Ratio 5.0

Preburner	Predicted Engine Cycle 6	Test Results
Total Fuel Flow - lb_m/sec	40.51	39.81 - 39.82
Total Oxidizer Flow - lb_m/sec	28.24	28.49 - 28.47
Oxidizer Primary - lb_m/sec	7.856	8.03 - 8.05
Oxidizer Secondary - lb_m/sec	20.38	20.46 - 20.42
Primary/Total Flow Split	0.2782	0.282 - 0.283
Injector Fuel Flow - lb_m/sec	36.97	37.23 - 37.31
Rigimesh Coolant Flow - lb_m/sec	NAV	0.591 - 0.520
Coolant Liner Flow - lb_m/sec	0.2286*	0.177 - 0.156
Injector Mixture Ratio	0.763	0.753 - 0.753
Chamber Pressure - psia	2010.	1866. - 1868.
Average Combustion Temperature - °R	1488	1480 - 1480**
Oxidizer Temperature - °R	208.2	175.5 - 177
Fuel Temperature - °R	142.	143.2 - 142.
Oxidizer Turbine Simulator		
Turbine Inlet Flow - lb_m/sec	19.04	20.47 - 20.47
Turbine Coolant - lb_m/sec	0.66*	0.367 - 0.377
Outer Case Coolant - lb_m/sec	0.33*	0.383 - 0.386
Turbine Inlet Total Pressure - psia	1995.	1886. - 1887.
Diffuser Discharge Total Pressure - psia	NAV	1275. - 1333.
Turbine Inlet Temperature (Avg) - °R	1465.	1345. - 1344.
Turbine Discharge Temperature - °R	1386.	NAV
Temperature Profile - (Max - Avg) - °R	0.0	40.1 - 44.2
Fuel Turbine		
Turbine Inlet Flow - lb_m/sec	46.86	46.03 - 45.99
Turbine Coolant Flow - lb_m/sec	0.55*	0.587 - 0.605
Outer Case Coolant - lb_m/sec	0.33	0.467 - 0.469
Turbine Inlet Total Pressure - psia	1989.	1825. - 1827
Diffuser Discharge Total Pressure - psia	NAV	1262. - 1274
Turbine Inlet Temperature - °R	1465.	1382. - 1386.***
Turbine Discharge Temperature - °R	1381.	1298. - 1299.
Fuel Pump		
Fuel Discharge Valve A_{cd} - in^2	NAV	1.4 - 1.1
Volumetric Inlet Flow - gpm	5038.	7386.3 - 6780.3
Inlet Mass Flow - lb_m/sec	45.87	72.8 - 66.81
Inlet Pressure - psia	97.62	112.4 - 114.1
Inlet Temperature - °R	46.6	37.8
Discharge Pressure - psia	2406.5	2030.8 - 2344.7
Discharge Temperature - °R	89.2	70.4 - 72.3
Total Pump Pressure Rise - psia	2309	2003.1 - 2299.4
Pump Speed - rpm	30207	28828 - 29378
Horse Power - hp	11180.	14516 - 14498
Transition Case		
Transition Case Pressure - psia	1462.	1249 - 1257
Transition Case Temperature - °R	1283.	1285 - 1285
Transition Case Total Flow - lb_m/sec	67.3	68.3 - 68.3
Transition Case Total Coolant - lb_m/sec	0.66*	0.850 - 0.855
Injector Effective Areas		
Oxidizer		
Primary A_{cd} - in^2	0.063	0.0705 - 0.0707
Secondary A_{cd} - in^2	0.5897	0.621 - 0.633
Fuel		
Overall - in^2	3.48	2.89 - 3.25
Plate - in^2	3.70	3.41 - 3.40

*Cycle 8 Prediction
**Based On Single Temperature Probe
***Based On Average Mixture Ratio

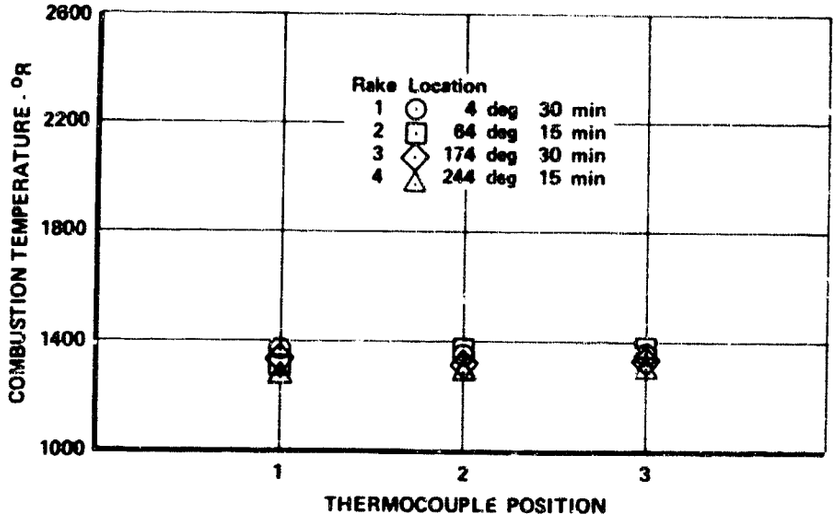

Figure 916. Temperature Profile Data, Test 1.02 FD 44469

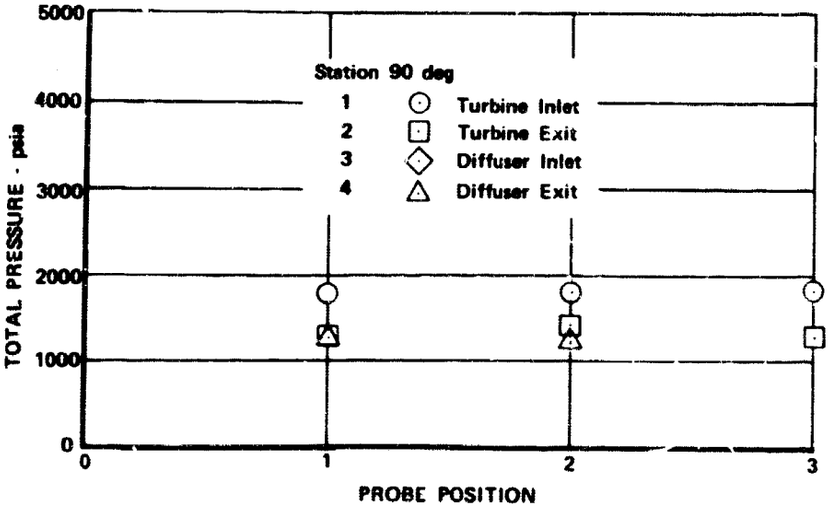

Figure 917. Pressure Profile Data, Test 1.02 FD 44504

The program for test No. 3.01 was a repeat of test No. 2.01. The faulty liner differential pressure low side source was corrected. Test No. 3.01 was automatically advanced to shutdown at 14.5 sec, after achieving the 75% thrust, r = 5 data point because of an indication of high transition case wall temperature. During operation at the 75% thrust level the turbine inlet temperature was 1506°R and the pump speed had stabilized at 35,623 rpm. Except for the excessive transition case wall temperature indication on one of the four case sensors, all other parameters were within the predicted range of operation. Visual inspection of the rig through the backpressure simulator throat revealed no hardware distress. A post-test review of the high speed movies taken of the run showed minor leaks at various points on the test rig adapter plumbing that resulted in a fire external to the test rig. In addition, it was found that the electrical cable to the transition case thermocouple (TSSST2) that triggered the shutdown had damaged insulation that could have allowed the two leads of the cable to short together forming an external thermocouple (secondary junction). The damaged cable was noted to have been in the area of the external fire seen in the movies. Because the measured transition case cooling flow was as predicted and no other case thermocouple indicated high temperatures, it was concluded that the high transition case temperature that caused the shutdown was the result of the secondary thermocouple junction sensing the external fire. The pump discharge pressure vs flow map recorded for this test is shown in figure 918. Plots of significant fuel turbopump parameters vs time for test No. 3.01 are shown in figures 919 through 922. Table CV is a tabulation of data recorded in the combustion system. Figures 923 and 924 describe significant combustion system temperature and pressure profile data recorded for this test.

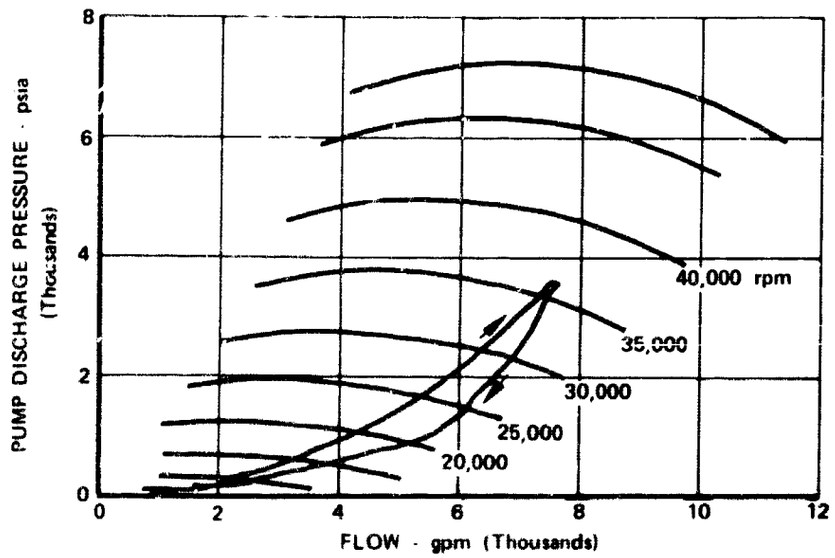

Figure 918. Pump Discharge Pressure vs Flow, Test 3.01, Rig F35155-1 FD 42877

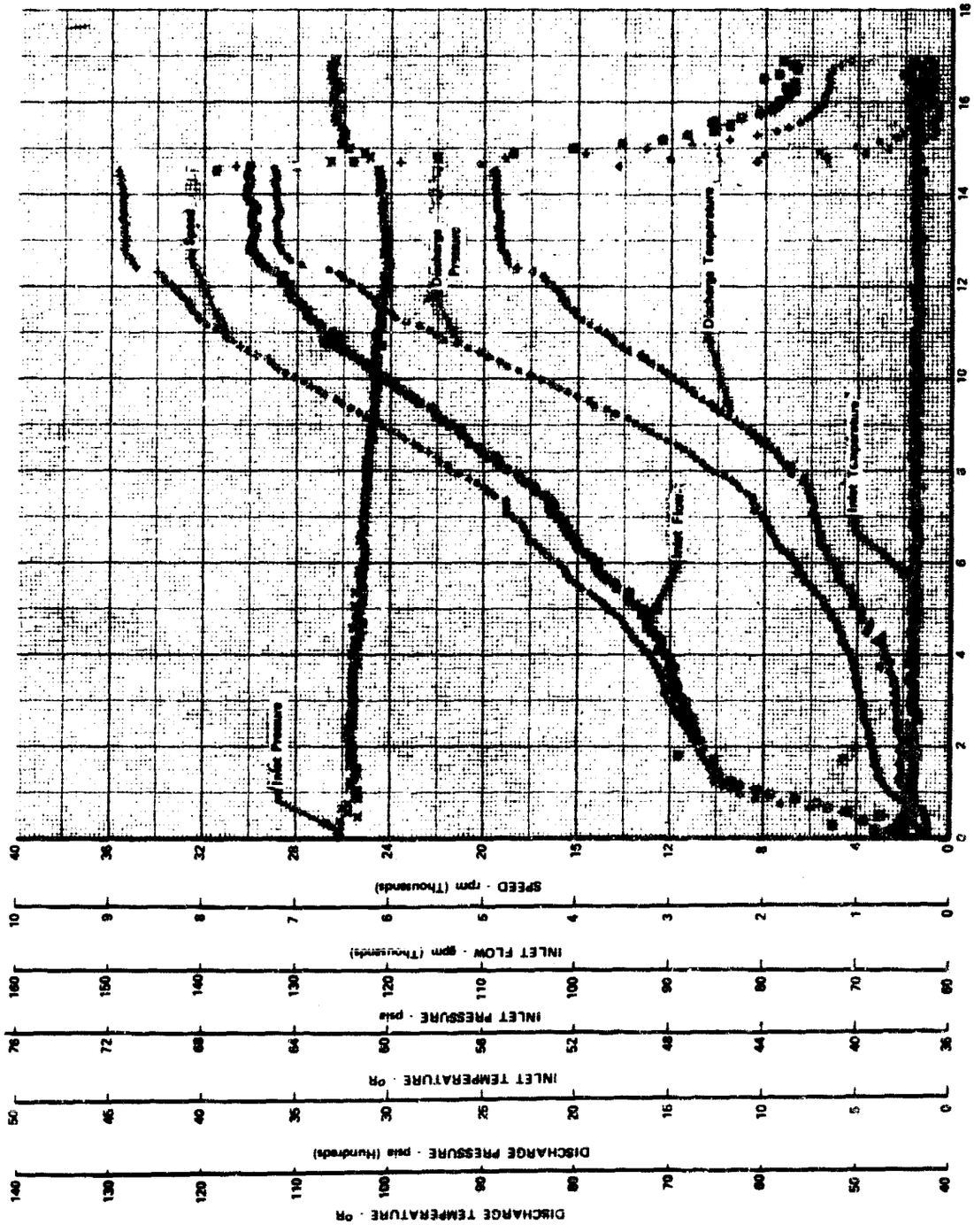

Figure 919. Significant Turbopump Parameters vs Time, Test 3.01, Rig F35155-1, Sheet 1.

FD 42843

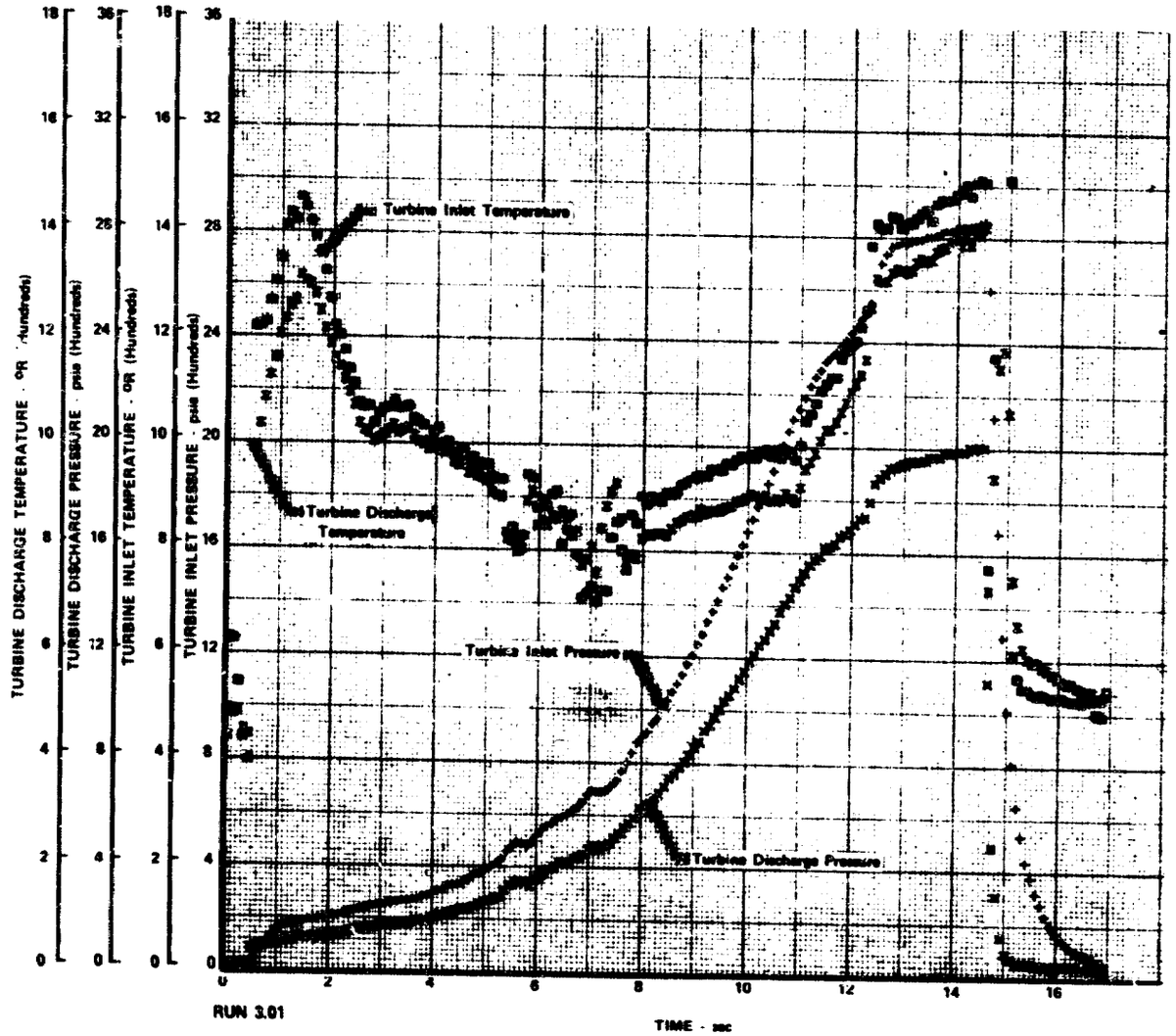

Figure 920. Significant Turbopump Parameters vs Time, Test 3.01, Rig F35155-1, Sheet 2

FD 42844

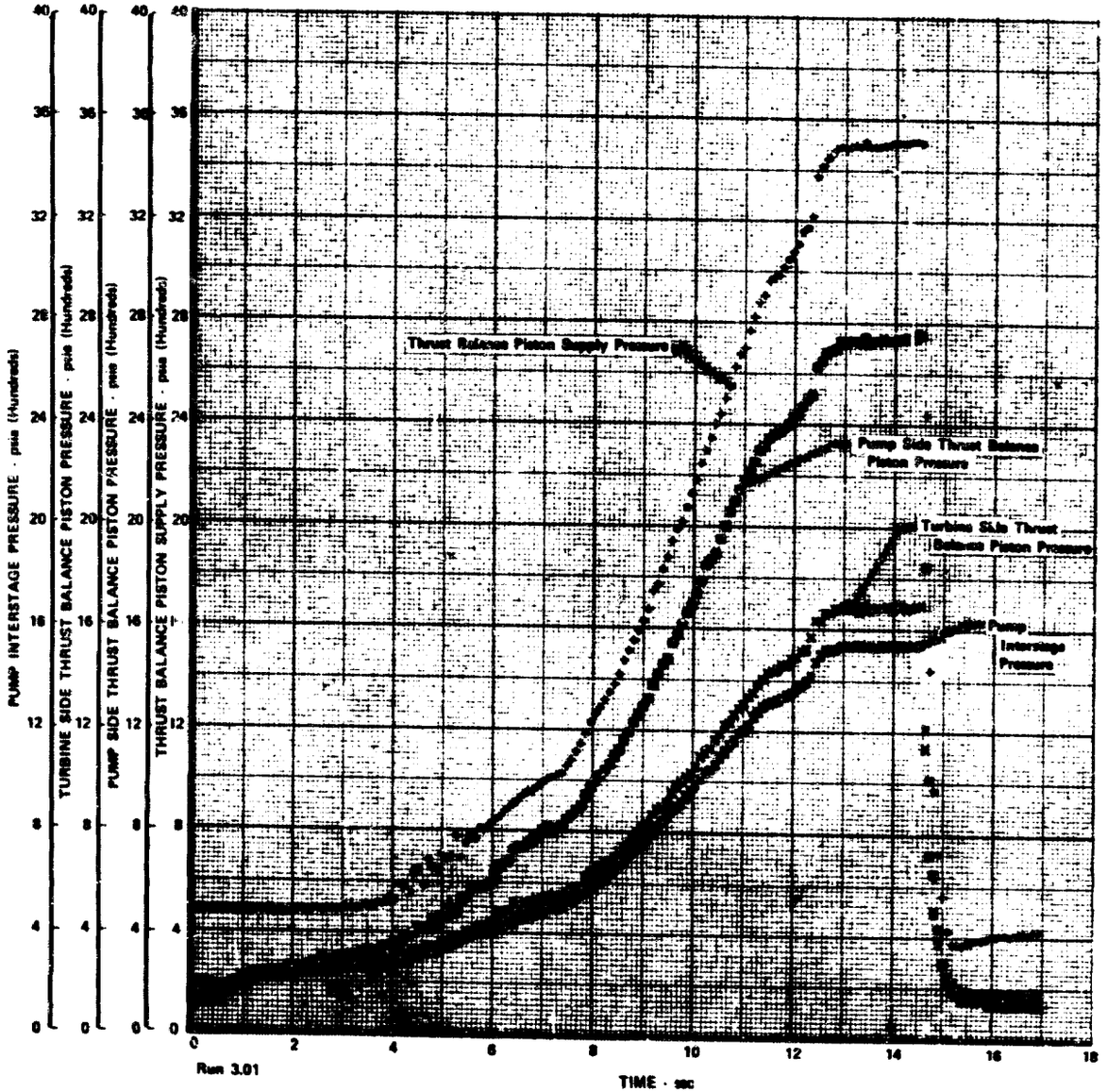

Figure 921. Significant Turbopump Paramters vs Time, Test 3.01, Rig F35155-1, Sheet 3

FD 42845

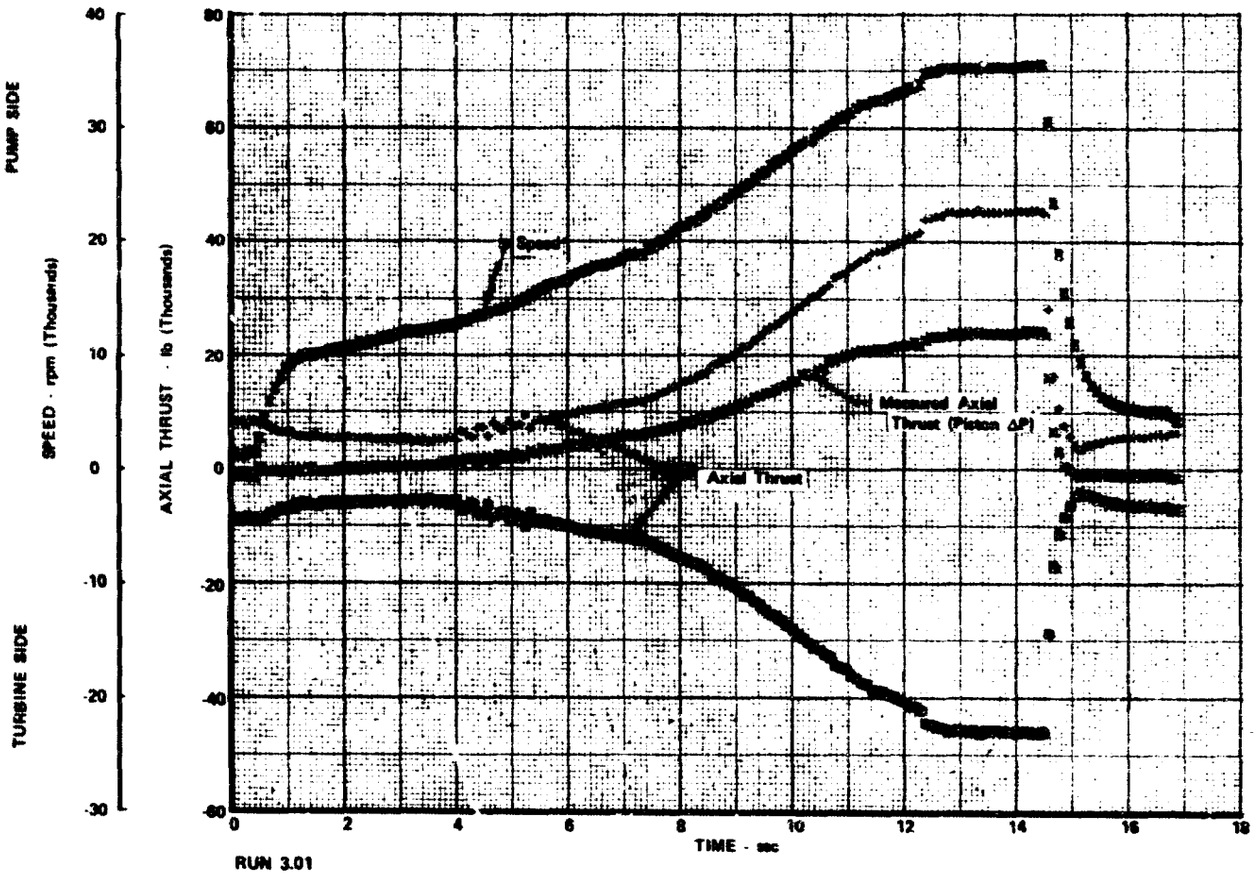

Figure 922. Significant Turbopump Parameters vs Time, Test 3.01, Rig F35155-1, Sheet 4

FD 42846

Table CV. Hot Turbine Test Run
Rig No. 35155-1, Run No. 3.01
Engine Thrust Level 75% Mixture Ratio 5.0

Preburner	Predicted Engine Cycle 6	Test Results
Total Fuel Flow - lb_m/sec	61.14	60.82
Total Oxidizer Flow - lb_m/sec	50.20	47.13
Oxidizer Primary - lb_m/sec	9.82	9.61
Oxidizer Secondary - lb_m/sec	40.38	37.52
Primary/Total Flow Split	0.192	0.208
Injector Fuel Flow - lb_m/sec	56.36	56.07
Rigimesh Coolant Flow - lb_m/sec	NAV	0.350
Coolant Liner Flow - lb_m/sec	0.351	0.255
Injector Mixture Ratio	0.891	0.327
Chamber Pressure - psia	3281.	2969.
Average Combustion Temp - °R	1717.	1600.**
Oxidizer Temp - °R	221.	179.
Fuel Temp	160.	162.
Oxidizer Turbine Simulator		
Turbine Inlet Flow - lb_m/sec	31.01	31.42
Turbine Coolant - lb_m/sec	0.86*	0.627
Outer Case Coolant - lb_m/sec	0.48*	0.821
Turbine Inlet Total Pressure - psia	3254.	3011.
Diffuser Discharge Total Pressure - psia	NAV	2041.
Turbine Inlet Temp (avg) - °R	1687	1490.
Turbine Discharge Temp - °R	1572	NAV
Temp Profile (max-avg) - °R	0.	26.4
Fuel Turbine		
Turbine Inlet Flow - lb_m/sec	75.57	72.88
Turbine Coolant Flow - lb_m/sec	0.78*	1.005
Outer Case Coolant - lb_m/sec	0.48*	0.990
Turbine Inlet Total Pres - psia	3244	2901.9
Diffuser Discharge Total Pressure - psia	NAV	2037
Turbine Inlet Temp - °R	1687	1507.***
Turbine Discharge Temp - °R	1566	1409.
Fuel Pump		
Fuel Discharge Valve A_{cd} - in^2		1.1
Volumetric Inlet Flow - gpm	7526	7552.1
Inlet Mass Flow - lb_m/sec	68.55	74.68
Inlet Pressure - psia	115.8	118.7
Inlet Temperature - °R	47.1	37.5
Discharge Pressure - psia	3786	3614.
Discharge Temperature - °R	112.	89.
Total Pump Pressure Rise - psia	3670.	3581.
Pump Speed - rpm	38733.	35623
Horse Power	25311.	23645.
Transition Case		
Transition Case Pressure - psia	2210.	2006
Transition Case Temperature - °R	1472.	1407.
Transition Case Total Flow - lb_m/sec	111.3	107.75
Transition Case Total Coolant - lb_m/sec	0.9b	1.820
Injector Effective Areas		
Oxidizer		
Primary A_{cd} - in^2	0.063	0.070
Secondary A_{cd} - in^2	0.658	0.679
Fuel		
Overall - in^2	3.48	3.03
Plate - in^2	3.70	3.47

*Cycle 8 Prediction
**Based on Average Mixture Ratio
***Based on Single Temperature Probe

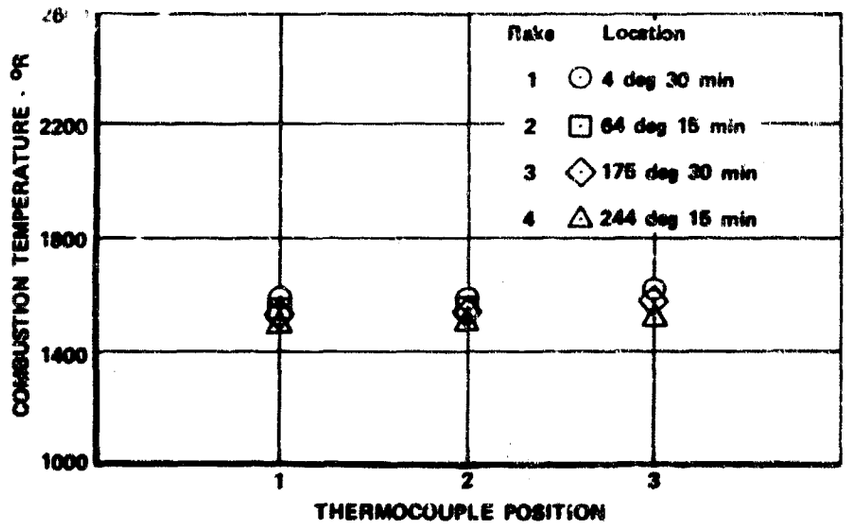

Figure 923. Temperature Profile Data, Test 3.01 FD 44505

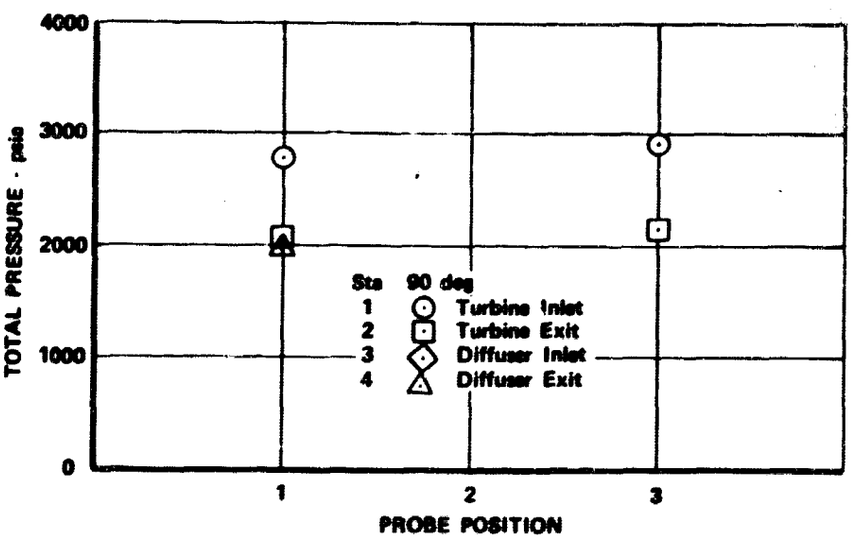

Figure 924. Pressure Profile Data, Test 3.01 FD 44506

The planned program for test No. 4.01 was the same as for the two previous tests. The test was automatically advanced to shutdown after 17.2 sec because of an indication of excessive transition case well temperature (T8SST2). Before the test was terminated, steady-state operation at 75% thrust, r = 5 and 75% thrust, r = 6 preburner cycle conditions was achieved. At the 75% thrust, r = 6 operating point the pump speed was 34,610 rpm and the turbine inlet temperature stabilized at 1869°R. The pump discharge pressure vs flow map recorded for test No. 4.01 shown in figure 925. Plots of significant fuel turbopump parameters vs time for test No. 4.01 are shown in figures 926 through 929. Table CVI tabulates the combustion system data for test No. 4.01. Figures 930 and 931 describe significant combustion system temperature and pressure profile data recorded during the test. Visual inspection of the rig through the backpressure simulator throat and through the igniter port with a fiber optics scope revealed no distress. Minor external damage to the rig instrumentation caused by a test stand fire was observed.

Figure 932 shows a plot of two transition case inner wall thermocouples (T8SST1 and T8SST2) vs time for test No. 4.01. It can be noted that thermocouple T8SST2, the main case thermocouple that caused the premature shutdown, exhibits a characteristic similar to the other comparable parameter until approximately 14 sec. At this time a review of the run movies showed a small fire in the area of the T8SST2 lead which continued through shutdown. Post-test instrumentation checks revealed that the T8SST2 thermocouple lead contained a secondary junction external to the rig as was suspected during test No. 3.01. The location of the secondary junction was established using an external heat source. The faulty lead was removed from the test rig and examined in the Instrument Laboratory. The secondary junction was confirmed with heat and resistance checks. The Inconel sheath was opened at the area of the secondary junction and the thermocouple conductors were found to be shorted together at this point. The magnesium oxide insulation was found to have disintegrated and was the cause of the malfunction.

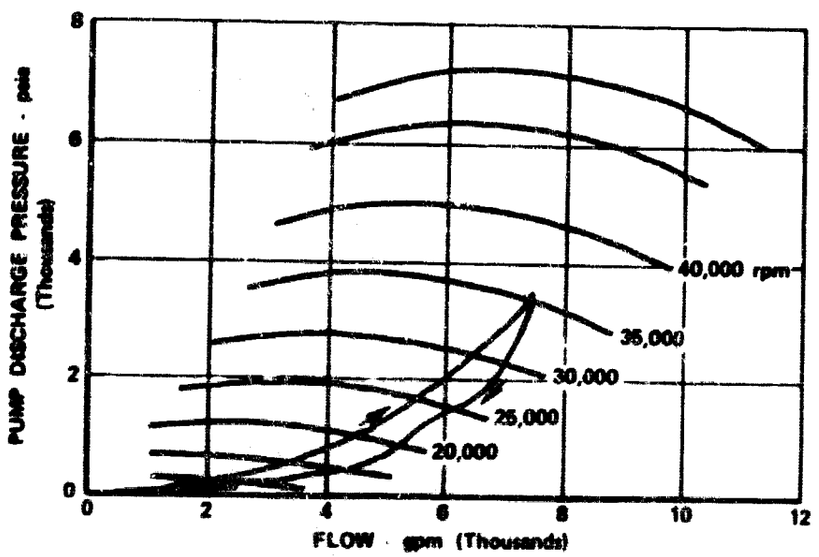

Figure 925. Pump Discharge Pressure vs Flow, Test 4.01, Rig F35155-1 FD 42878A

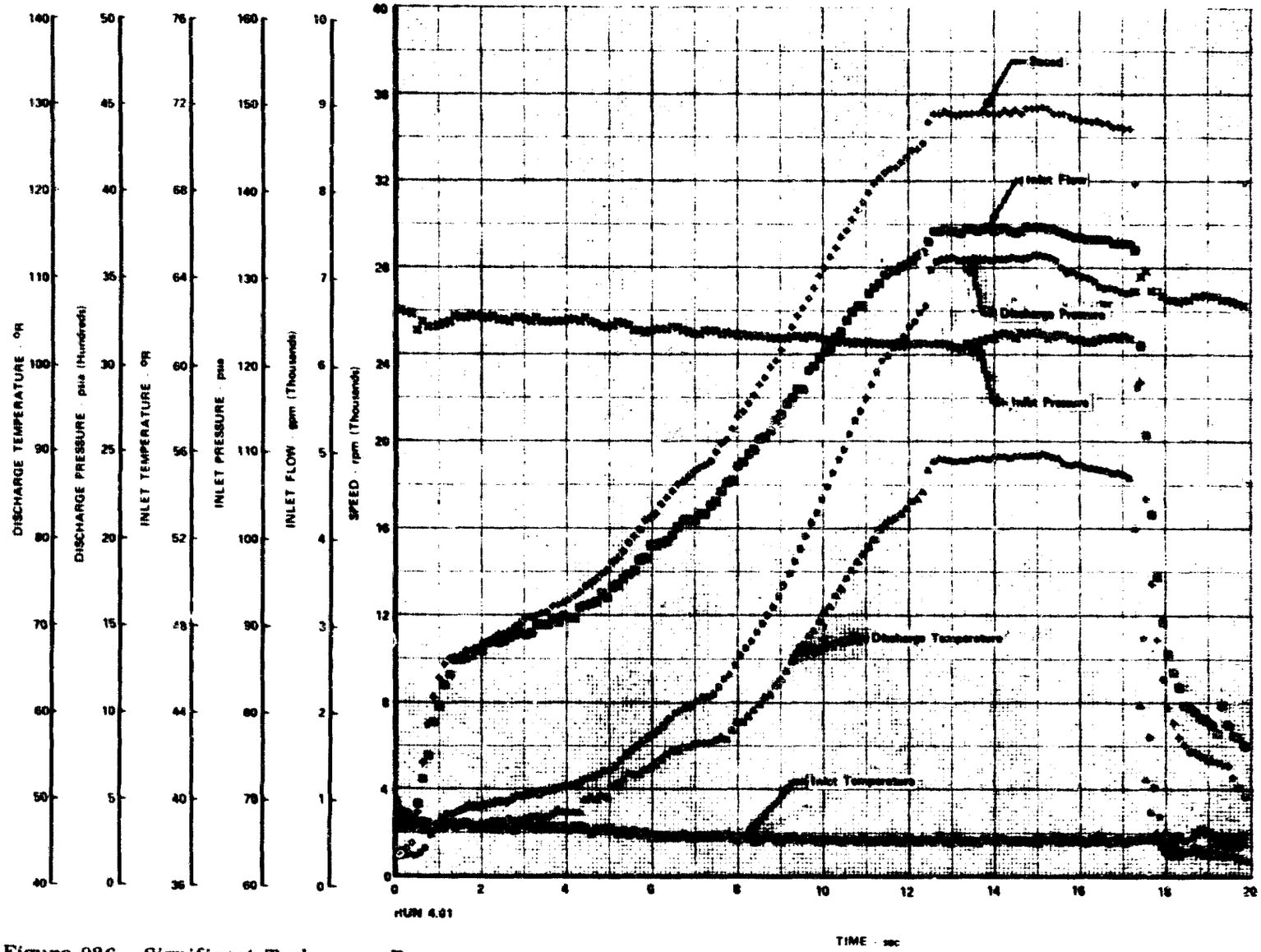

Figure 926. Significant Turbopump Parameters vs Time, Test 4.01, Rig F35155-1, Sheet 1

FD 42847

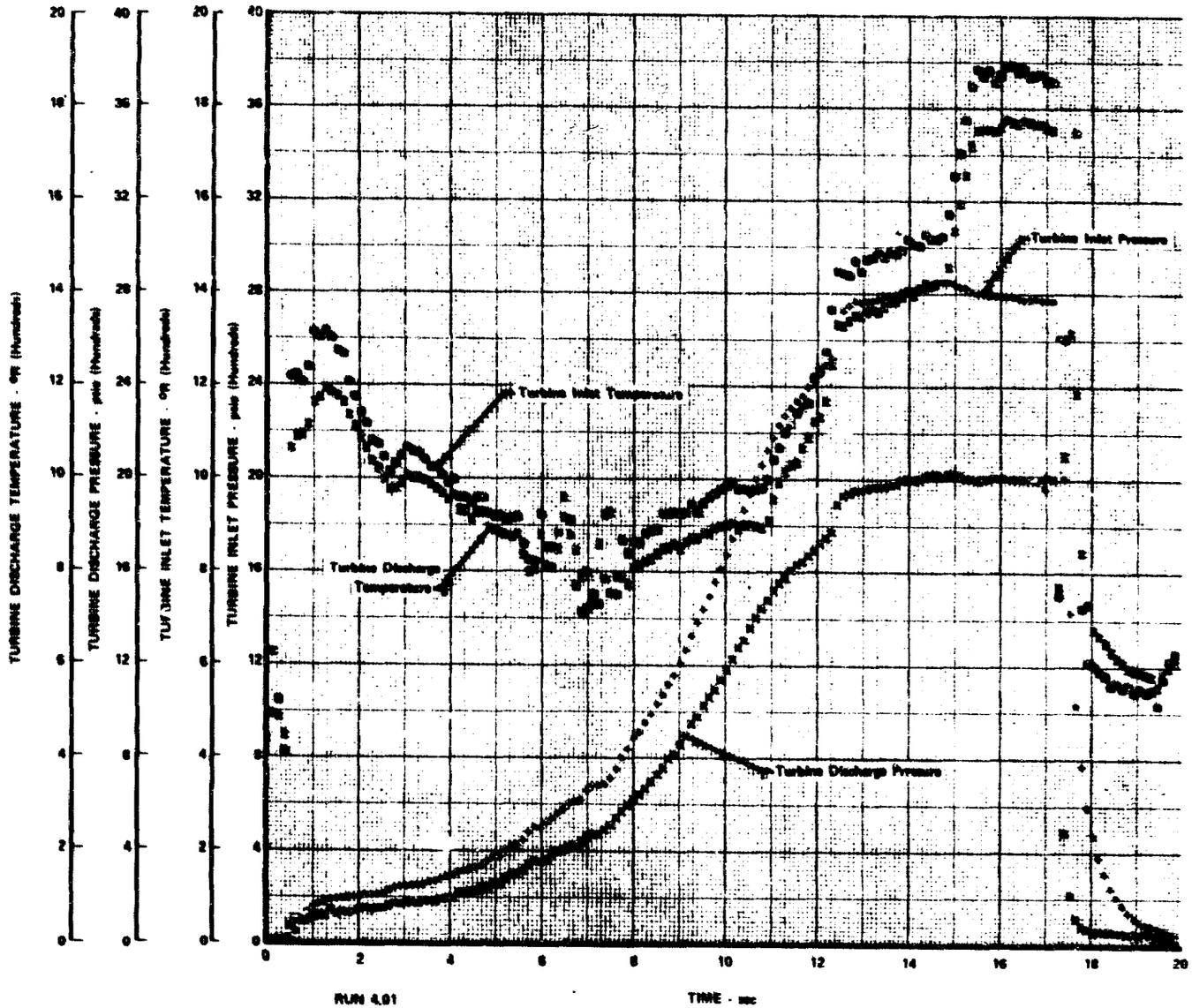

Figure 927. Significant Turbopump Parameters vs Time, Test 4.01, Rig F35155-1, Sheet 2 FD 42848

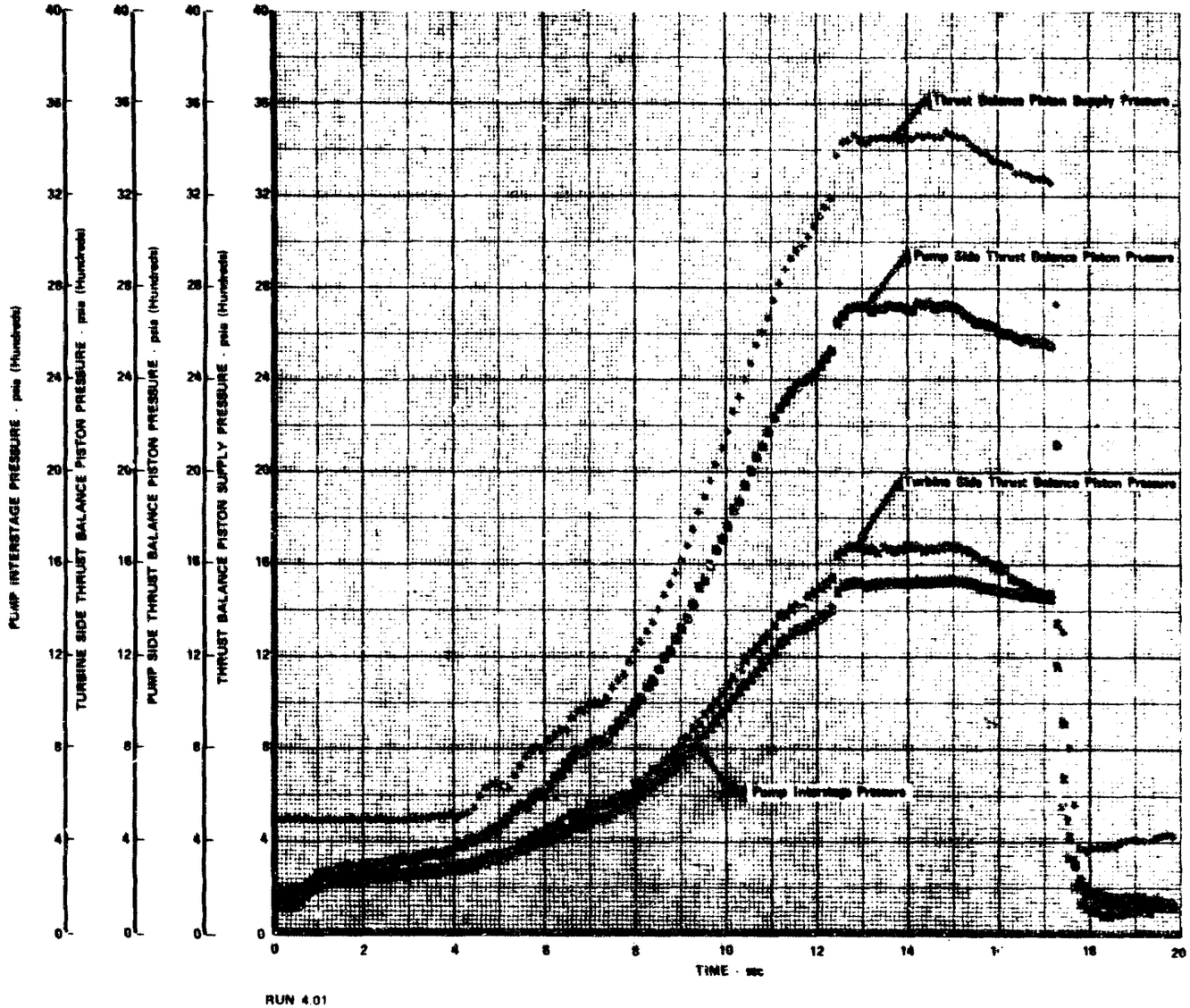

Figure 928. Significant Turbopump Parameters vs Time, Test 4.01, Rig F36155-1, Sheet 3

FD 42849

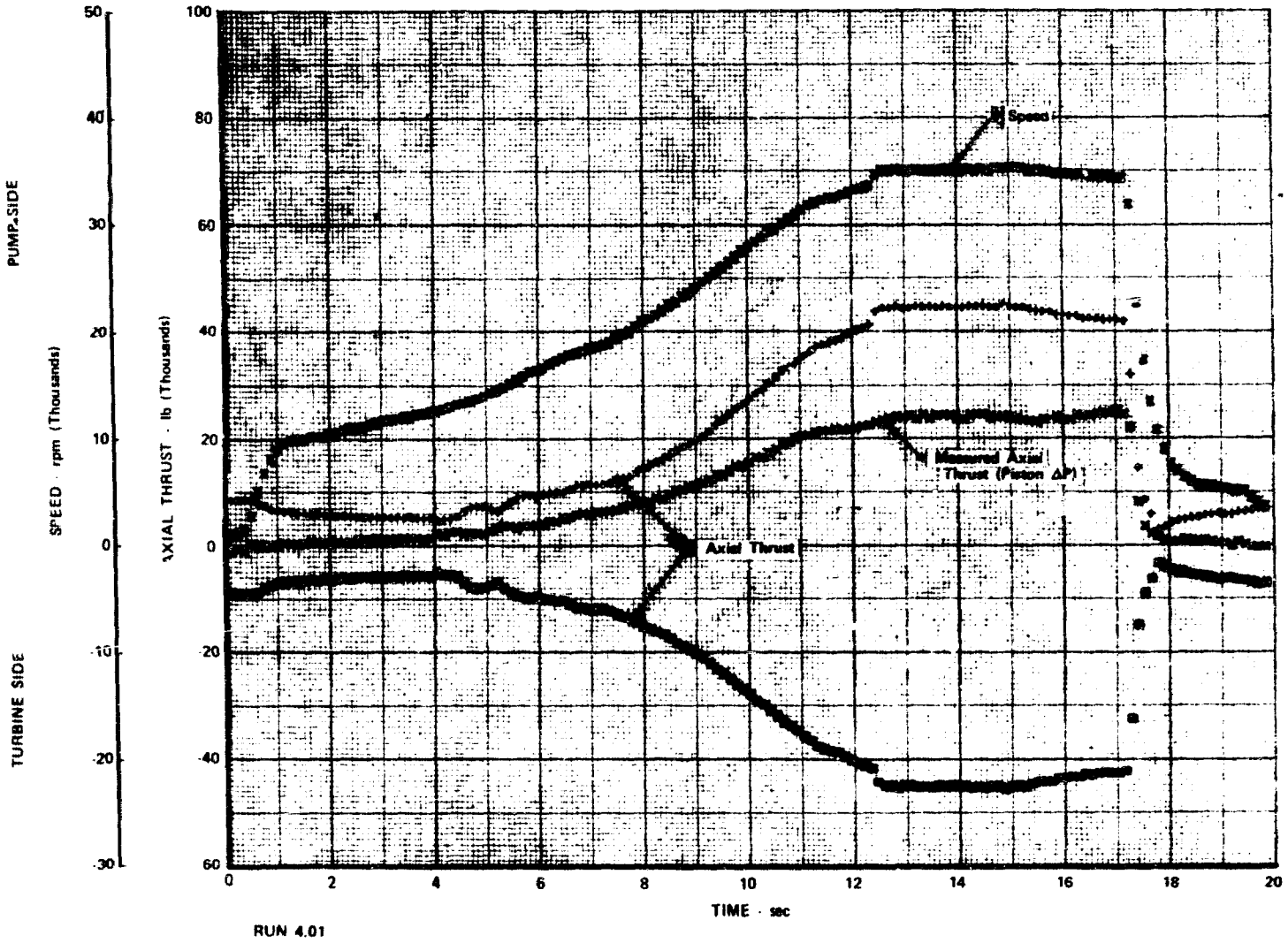

Figure 929. Significant Turbopump Parameters vs Time, Test 4.01, Rig F35155-1, Sheet 4 FD 42850

Table CVI. Hot Turbine Test Run, Rig No. 35155-1, Run No. 4.01, Engine Thrust Level 75%

	Mixture Ratio 5.0		Mixture Ratio 6.0	
Preburner	Predicted Engine Cycle 6	Test Results	Predicted Engine Cycle 6	Test Results
Total Fuel Flow - lb_m/sec	61.14	60.784	51.88	49.6
Total Oxidizer Flow - lb_m/sec	50.20	47.630	48.52	50.432
Oxidizer Primary - lb_m/sec	9.82	10.127	8.075	9.528
Oxidizer Secondary - lb_m/sec	40.38	37.503	40.44	40.904
Primary/Total Flow Split	0.1956	0.213	0.1665	0.189
Injector Fuel Flow - lb_m/sec	56.36	55.924	47.53	47.234
Rigimesh Coolant Flow - lb_m/sec	NAV	0.844	NAV	0.672
Coolant Liner Flow - lb_m/sec	0.351*	0.253	0.293*	0.202
Injector Mixture Ratio	0.891	0.839	1.021	1.053
Chamber Pressure - psia	3281	2965.8	3097.	2882.4
Average Combustion Temperature - °R	1713.	1625**	1934	1980**
Oxidizer Temperature - °R	221.	179.0	213.	177.
Fuel Temperature - °R	160.	162.1	173.	172.
Oxidizer Turbine Simulators				
Turbine Inlet Flow - lb_m/sec	31.01	31.23	28.08	28.22
Turbine Coolant - lb_m/sec	0.86*	0.627	0.798*	0.561
Outer Case Coolant - lb_m/sec	0.48*	0.957	0.49*	0.960
Turbine Inlet Total Pressure - psia	3254.	2990.0	3073	2902
Diffuser Discharge				
Total Pressure - psia	NAV	2039.1	NAV	2030.
Turbine Inlet Temperature (Average) - °R	1687.	1502.	1904.	1854.
Turbine Discharge Temperature - °R	1572	NAV	1789.	NAV
Temperature Profile (Maximum-Average) - °R	0	28.0	0	56.
Fuel Turbine				
Turbine Inlet Flow - lb_m/sec	76.57	73.42	68.87	70.32
Turbine Coolant Flow - lb_m/sec	0.78*	1.015	0.711*	0.919
Outer Case Coolant - lb_m/sec	0.48*	1.164	0.49*	1.167
Turbine Inlet Total Pressure - psia	3244	2886.6	3064	2823.
Diffuser Discharge				
Total Pressure - psia	NAV	2053.3	NAV	2035.
Turbine Inlet Temperature - °R	1687	1519.4***	1904.	1868.***
Turbine Discharge Temperature - °R	1566.	1420.1	1780	1765.
Fuel Pump				
Fuel Discharge Valve A_{cd} - in^2	NAV	1.1	NAV	1.1
Volumetric Inlet Flow - gpm	7526.	7459.	6483.	7309
Inlet Mass Flow - lb_m/sec	68.55	73.7	59.13	72.19
Inlet Pressure - psia	115.8	120.5	128.7	120.3
Inlet Temperature - °R	47.1	37.7	47.4	37.7
Discharge Pressure - psia	3786.	3561.0	3752.9	3368.6
Discharge Temperature - °R	112	88.2	115.	86.2
Total Pump Pressure Rise - psi	3670.	3523.8	3424.	3328.7
Pump Speed - rpm	38733.	35372	38021.	34582.
Horsepower - hp	25311.	23429	23381.	21939.
Transition Case				
Transition Case Pressure - psia	2210	2022.8	2146.	2010.
Transition Case Temperature - °R	1472.	1402.	1666.	1728.
Transition Case Total Flow - lb_m/sec	113.	108.414	100.4	102.15
Transition Case Total Coolant - lb_m/sec	0.96	2.121	0.98*	2.127
Injector Effective Areas				
Oxidizer				
Primary A_{cd} - in^2	0.063	0.0721	0.063	0.0754
Secondary A_{cd} - in^2	0.658	0.676	0.677	0.677
Fuel				
Overall - in^2	3.48	3.04	3.48	3.18
Plate - in^2	3.70	3.46	3.70	3.44

*Cycle 8 Prediction
**Based on Average Mixture Ratio
***Based on Single Temperature Probe

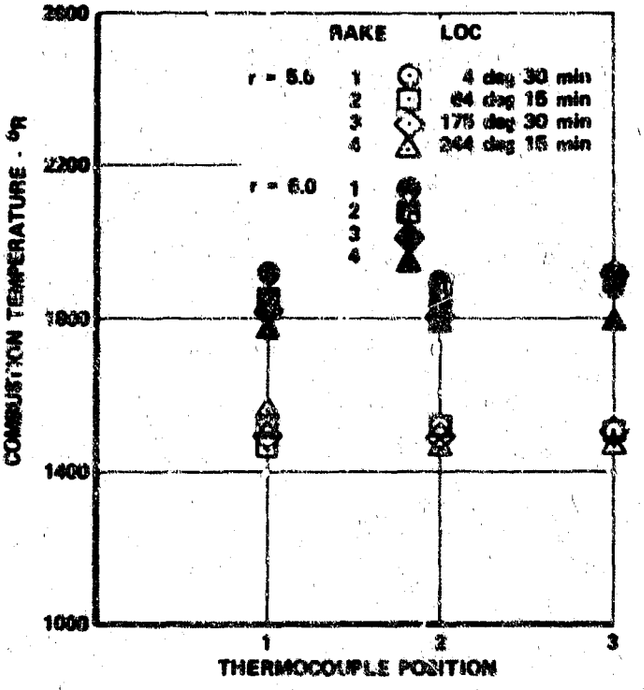

Figure 930. Temperature Profile Data, Test 4.01 FD 44503

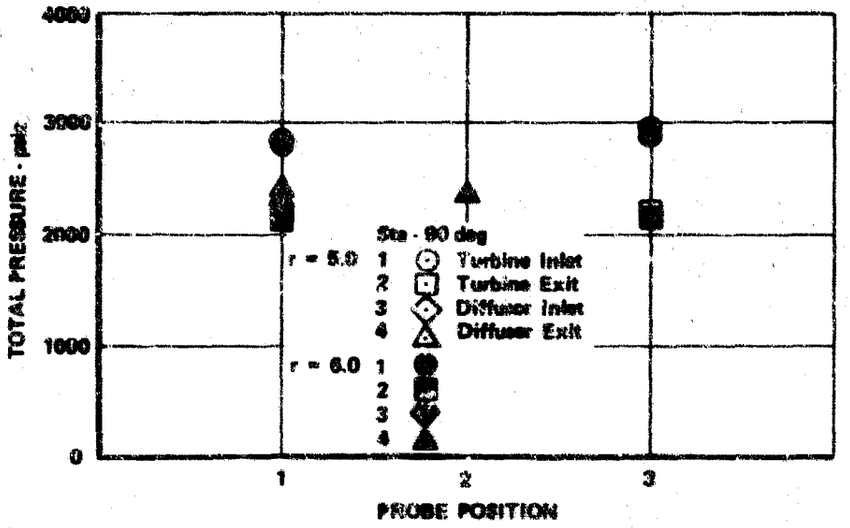

Figure 931. Pressure Profile Data, Test 4.01 FD 44507

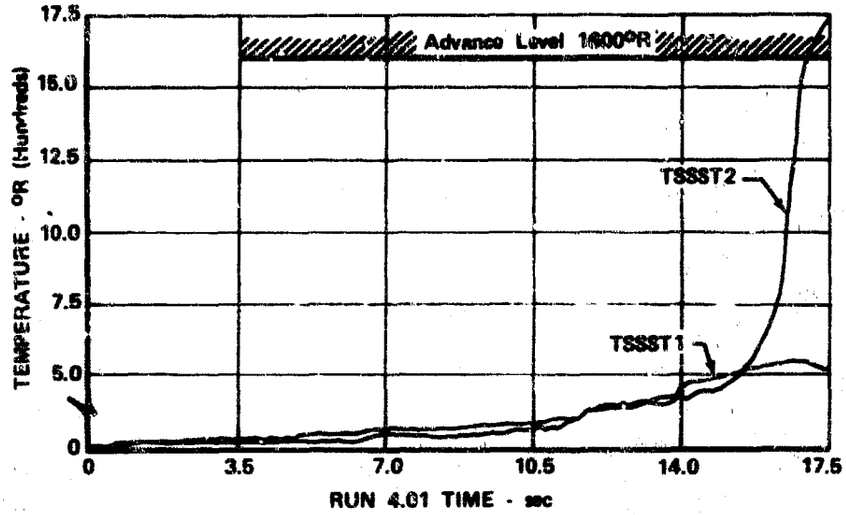

Figure 932. Transition Case Inner Wall Temperature vs Time, Test 4.01, Rig F35155-1 FD 42879A

Data analysis of test No. 4.01 revealed that except for a high-temperature indication in the fuel turbine stationary parts coolant system all systems performed as predicted. Because post-test instrumentation checks revealed that the coolant system thermocouples were operating normally, the rig was removed from the test stand on 29 July 1970 to permit inspection of the fuel turbine coolant system.

Disassembly of the hot turbine test rig was limited to removing the fuel turbopump from the transition case. Inspection revealed all parts were in excellent condition as shown in figures 933 through 938. The turbine inlet duct and the 1st-stage stator were removed from the fuel turbopump. Heat discoloration indications were observed on the 1st-stage stator outer shroud segments, the 1st-stage blade tip shroud ring, and the stationary parts support rings, confirming the excessive coolant temperature to the turbine stationary parts. Indications of excessive hot gas flow into the turbine outer coolant mixing chamber around the 1st-stage stator outer shroud slot seals were also observed. The condition of the turbine parts is shown in figures 939 through 942. Nondestructive tests on the heat discolored parts showed no defects and all these parts were reused in the next turbopump build.

It could not be positively concluded from data analysis that the total measured cold hydrogen coolant flow directed to the fuel turbine reached the coolant mixing chambers. Leak checks had been performed on the coolant distribution system with the exception of the cover-to-turbine inlet duct interface connections. A coolant leak could have occurred at these two areas. It was, therefore, concluded that the excessive coolant mix temperature could have been caused by both excessive hot gas flow and diminished coolant supply.

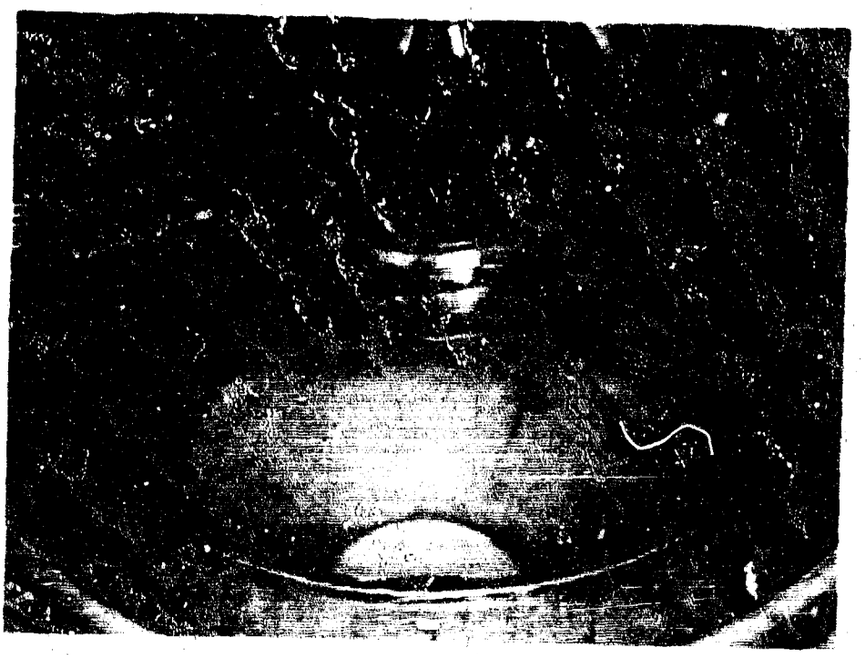

Figure 933. Post-Test 4.01 View Into Transition Case Through Fuel Turbopump Port Showing Good Condition of the Part, (View 1)

FE 100368

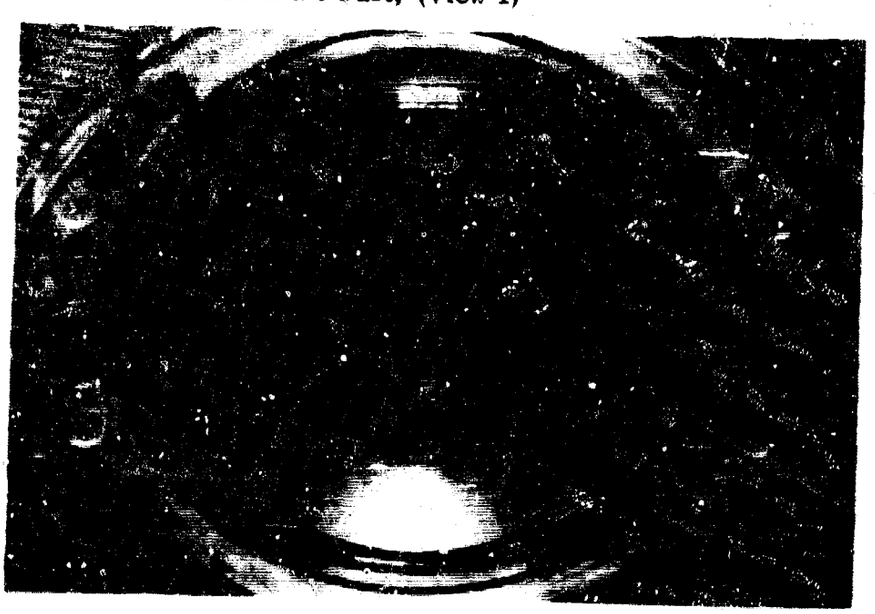

Figure 934. Post-Test 4.01 View Into Transition Case Through Fuel Turbopump Port Showing Good Condition of the Parts (View 2)

FE 100367

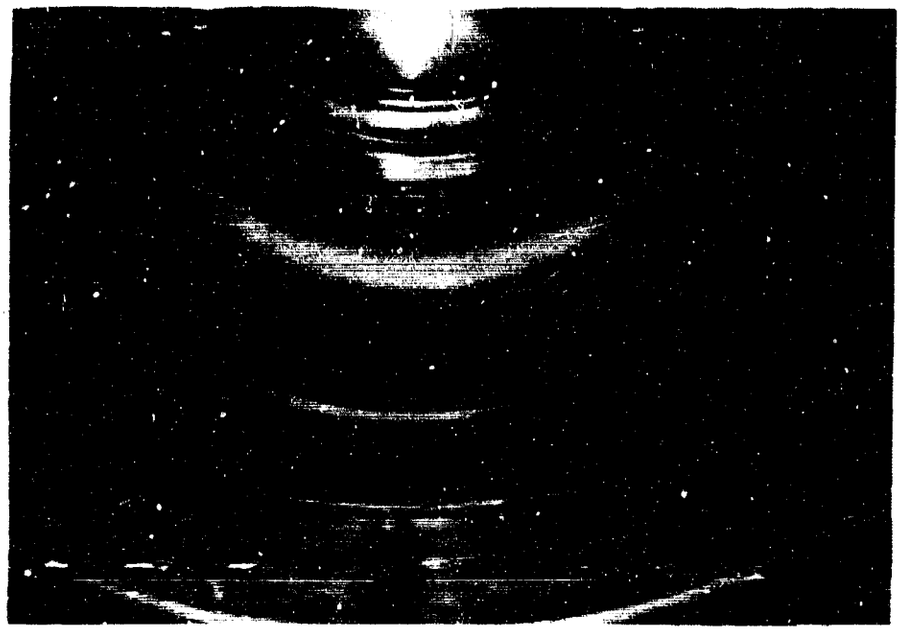

Figure 935. Post-Test 4.01 View Into Transition Case Through Fuel Turbopump Port Showing Good Condition of the Parts (View 3) FE 100366

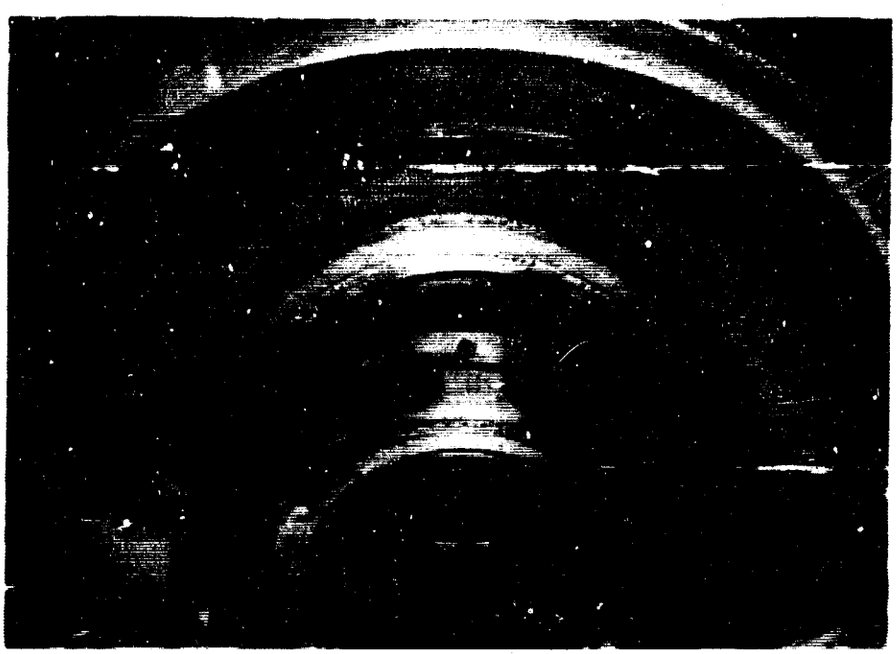

Figure 936. Post-Test 4.01 View Into Transition Case Through Fuel Turbopump Port Showing Good Condition of the Part (View 4) KFE 100359

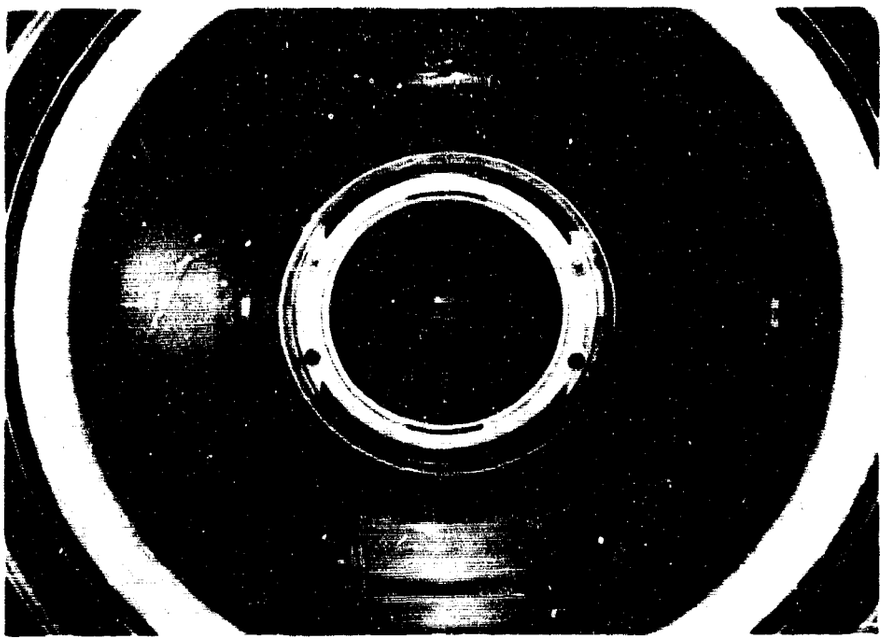

Figure 937. Post-Test 4.01 View Into Transition Case Through Fuel Turbopump Port Showing Good Condition of the Parts (View 5)

FE 100357

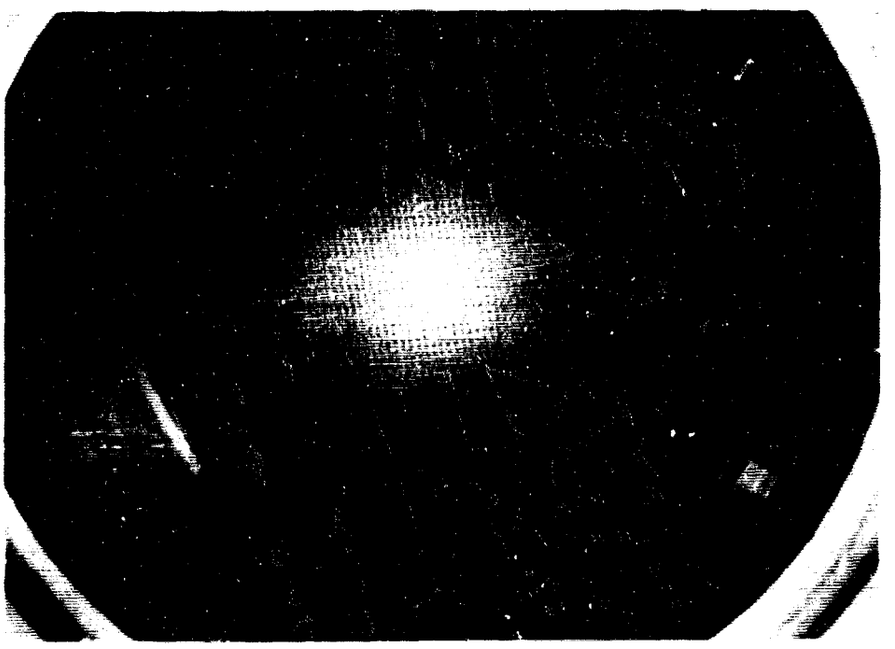

Figure 938. Post-Test 4.01 View Into Transition Case Through Fuel Turbopump Port Showing Good Condition of the Parts (View 6)

FE 100356

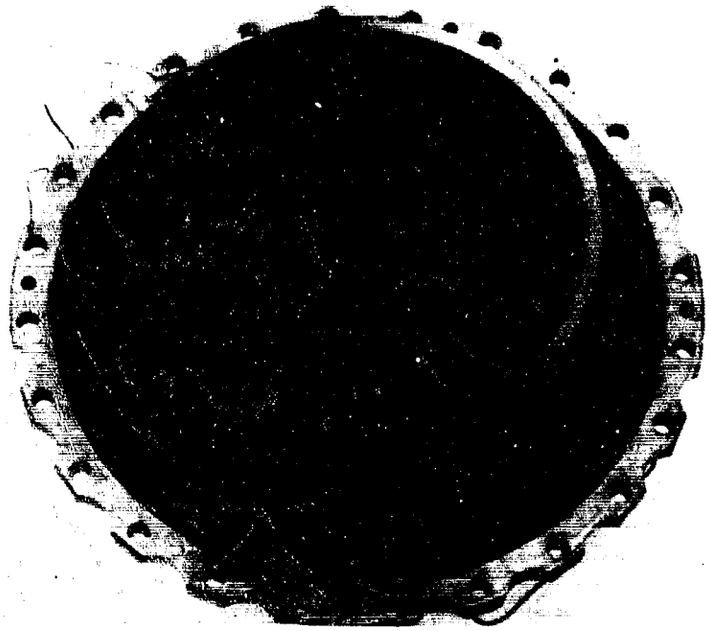

Figure 939. Post-Test 4.01 View of Turbine Inlet Duct Assembly FE 100344

Figure 940. Post-Test 4.01 View of Turbine Inlet Duct Assembly and 1st-Stage Stator (View 1) FE 100346

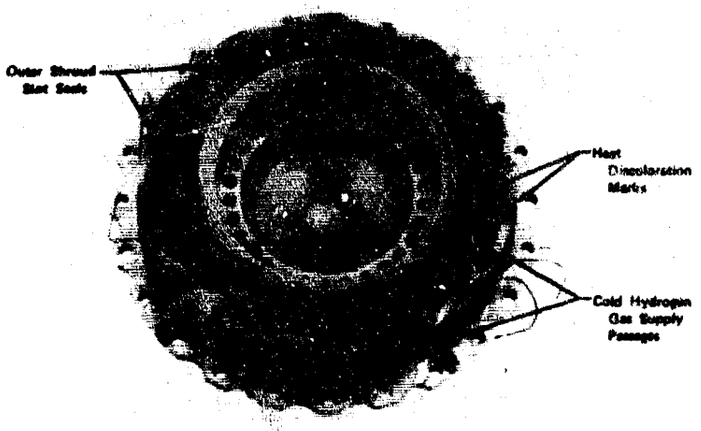

Figure 941. Post-Test 4.01 View of Turbine Inlet Duct Assembly and 1st-Stage Stator (View 2) FD 42880A

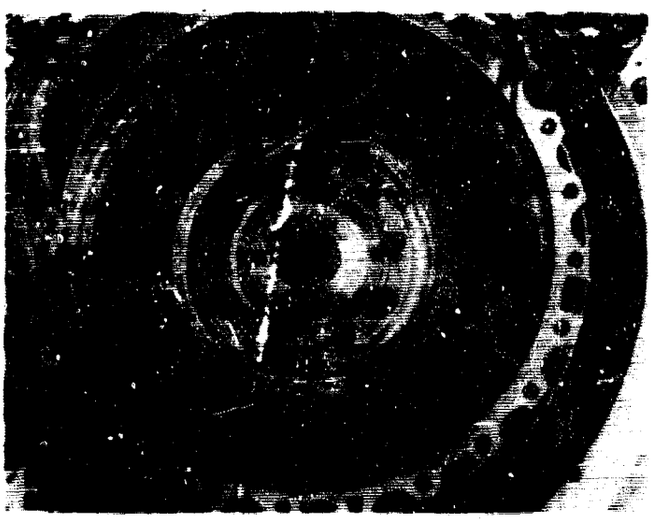

Figure 942. Post-Test 4.01 View of Fuel Turbine Showing Good Condition of the Parts FD 42881

During reassembly of the fuel turbopump turbine, the outer coolant mix was rebalanced by changes to the contributing systems. The hot gas flow was reduced by incorporating new 1st-stage stator outer shroud slot seals that had the hot gas passages omitted. Eleven additional cold hydrogen gas supply passages to the outer mixing chamber were incorporated in the turbine inlet duct supply annulus. In addition, the suspected cold hydrogen gas leak paths at the interface connections between the cover and turbine inlet duct were sealed by electron beam welding.

The movies of the test rig had revealed that, in addition to the stand fires observed during tests No. 3.01 and 4.01, the exhaust discharging from the backpressure simulator was impinging on the heat shields of the preburner fuel inlet and fuel pump discharge lines causing some hot gas recirculation around the test rig. An uncooled sheet metal exhaust nozzle was incorporated on the rebuild of the test rig to prevent facility damage and to eliminate the recirculation effects.

The hot fuel turbine test rig, F35155-2, was returned to the E-8 test facility on 4 August 1970. A system cold flow test (test No. 5.01) was performed before proceeding to the hot tests. The fifth hot firing test, test No. 5.02, was conducted on 10 August and was programed for 22 sec duration with 2 sec of operation at 75%, r = 5, 100%, r = 6 and 100%, r = 7 preburner cycle conditions. The test was a full duration run of 22 sec, during which fuel turbine operation at an inlet temperature of 2405°R with a rotor speed of 39,500 rpm was achieved, and all program objectives were accomplished. Data analysis indicated that the test rig operated as predicted and that the fuel turbine coolant system successfully maintained the desired coolant temperatures to the disks and stationary support structure. Maximum fuel pump speed attained during this test was 40,800 rpm with a corresponding turbine inlet temperature of 2088°R. Visual inspection of the test rig indicated all parts were in good condition and heat discoloration was noted only on the uncooled heat shields as shown in figure 943. Movies of the test rig showed no fires external to the test rig and that the exhaust nozzle, shown in figure 944, successfully prevented exhaust gas recirculation and impingement with the facility plumbing. The pump discharge pressure versus flow map recorded by the x-y plotter during the test is shown in figure 945. Plots of significant fuel turbopump parameters vs time are shown in figures 946 through 949. Table CVII is a tabulation of combustion system data for test 5.02. Figures 950 and 951 are significant combustion system temperature and pressure profile data recorded during this test.

The final hot firing test, test No. 6.01, was conducted on 13 August 1970 and was programed for 22.3 sec with 2 sec of operation at 50%, r = 7 and 3 sec of operation at 100%, r = 5 preburner cycle conditions. After 1 sec of steady-state operation at the 100% level, a 2 sec fuel pump flow excursion was scheduled. The test was automatically advanced to shutdown at 20 sec because of a loss of pump speed indication. At the time of the premature shutdown the pump speed was 44,500 rpm and the preburner had stabilized at the 100%, r = 5 set point. Visual inspection of the test rig revealed no apparent change in the parts condition from the previous test, and also showed that the facility adaptor cable to the pump speed indicator, that caused the erroneous shutdown, had become disconnected. The other two speed indicators recorded the normal pump operating speed level before the shutdown. The pump discharge pressure vs flow map recorded by the x-y plotter during the test is shown in figure 952. Plots of significant fuel turbopump parameters vs time are shown in figures 953 through 956. Table CVIII

presents a tabulation of combustion system data for test 6.01. Figures 957 and 958 describe significant combustion system temperature and pressure profile data recorded during this test. Figure 959 shows the test rig operating at 100%, r = 5 preburner conditions.

Figure 943. Post-Test 5.02 View Into Transition Case Through Exhaust Nozzle Showing Good Condition of the Parts FE100270

Figure 944. Hot Turbine Test Rig Operating at the 100% r = 6 Level, Test 5.02 FE 100607-8

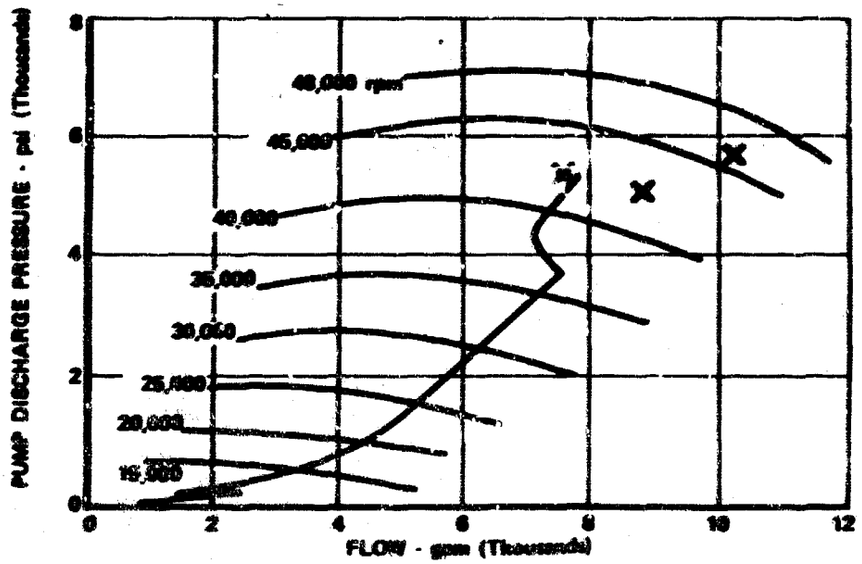

Figure 945. Pump Discharge Pressure vs Flow Test 5.02, Rig F35155-2

FD 38750G

A

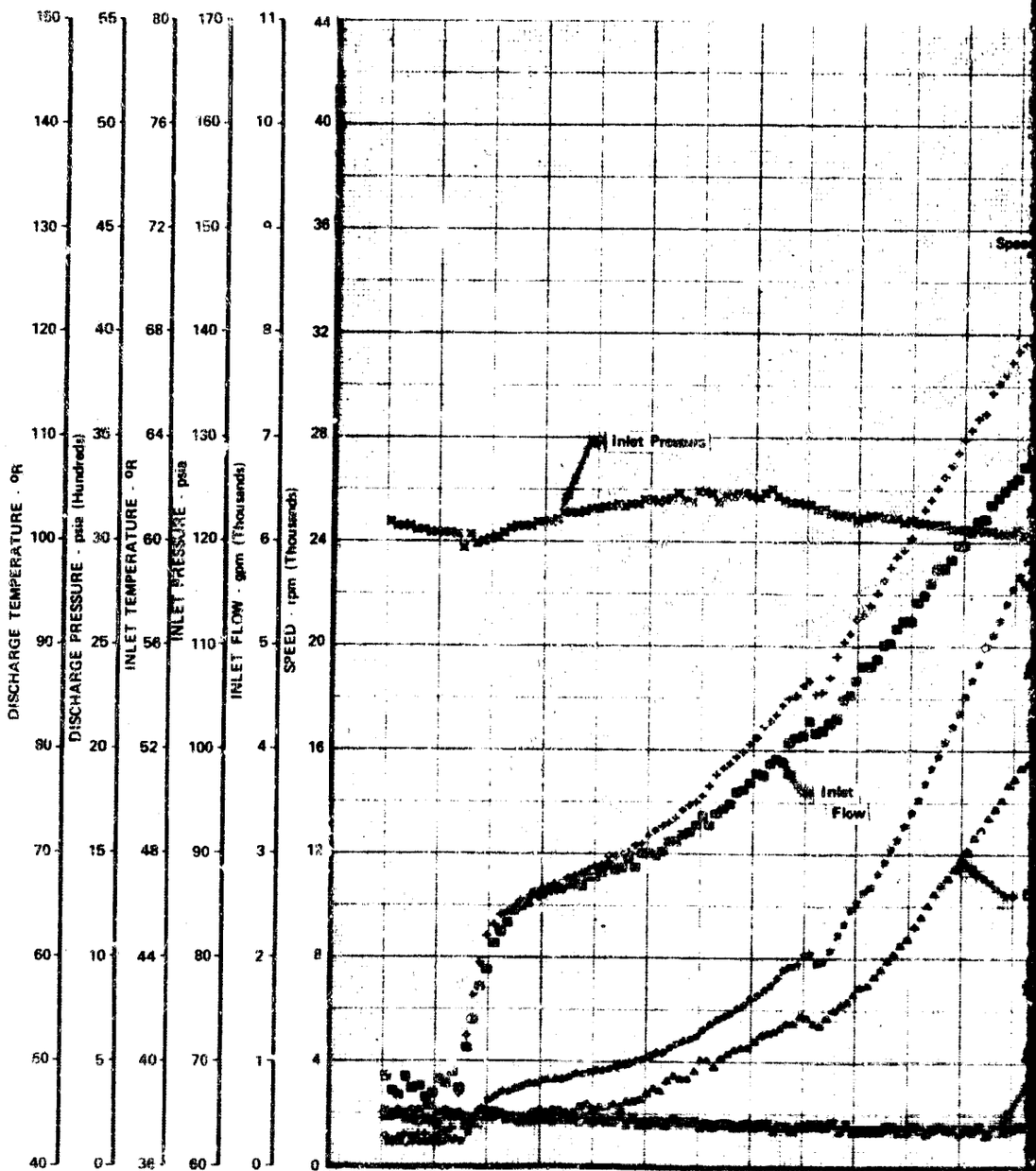

Figure 946. Significant Turbopump Parameters vs Time, Test 5.02, Rig F35155-2, Sheet 1

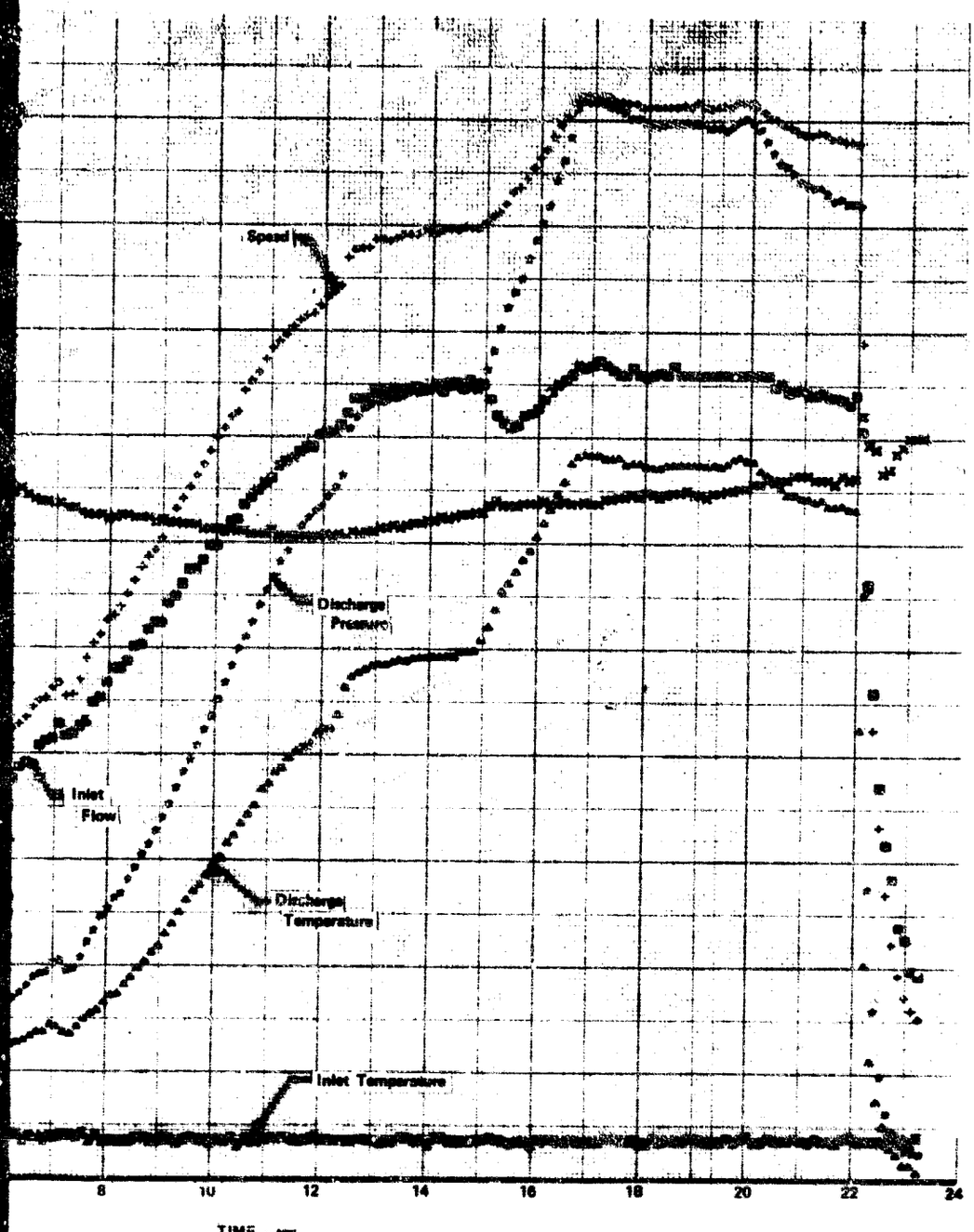

FD 43340

997/ 998

A

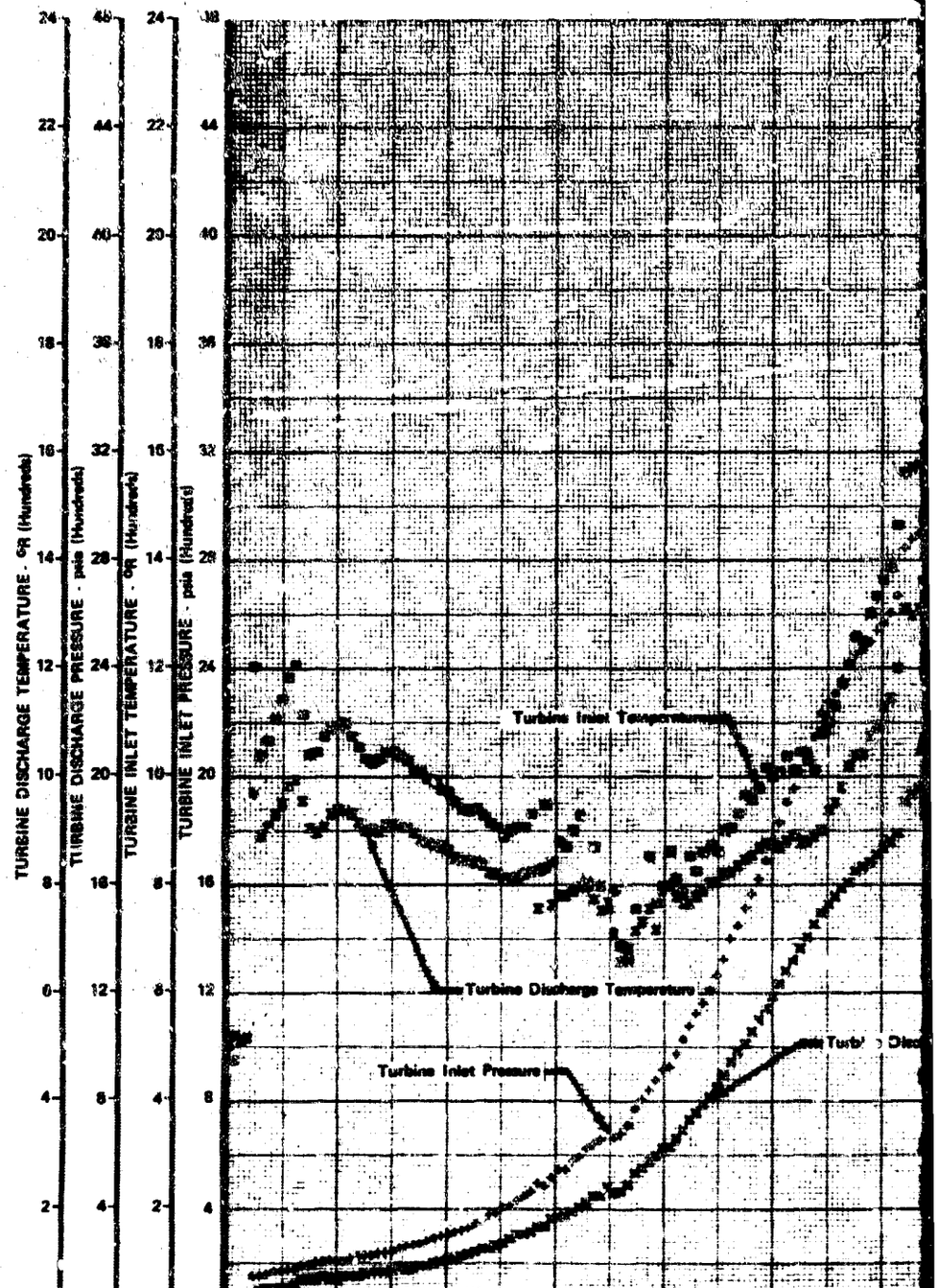

Figure 947. Significant Turbopump Parameters vs Time, Test 5.02, Rig F35155-2, Sheet 2

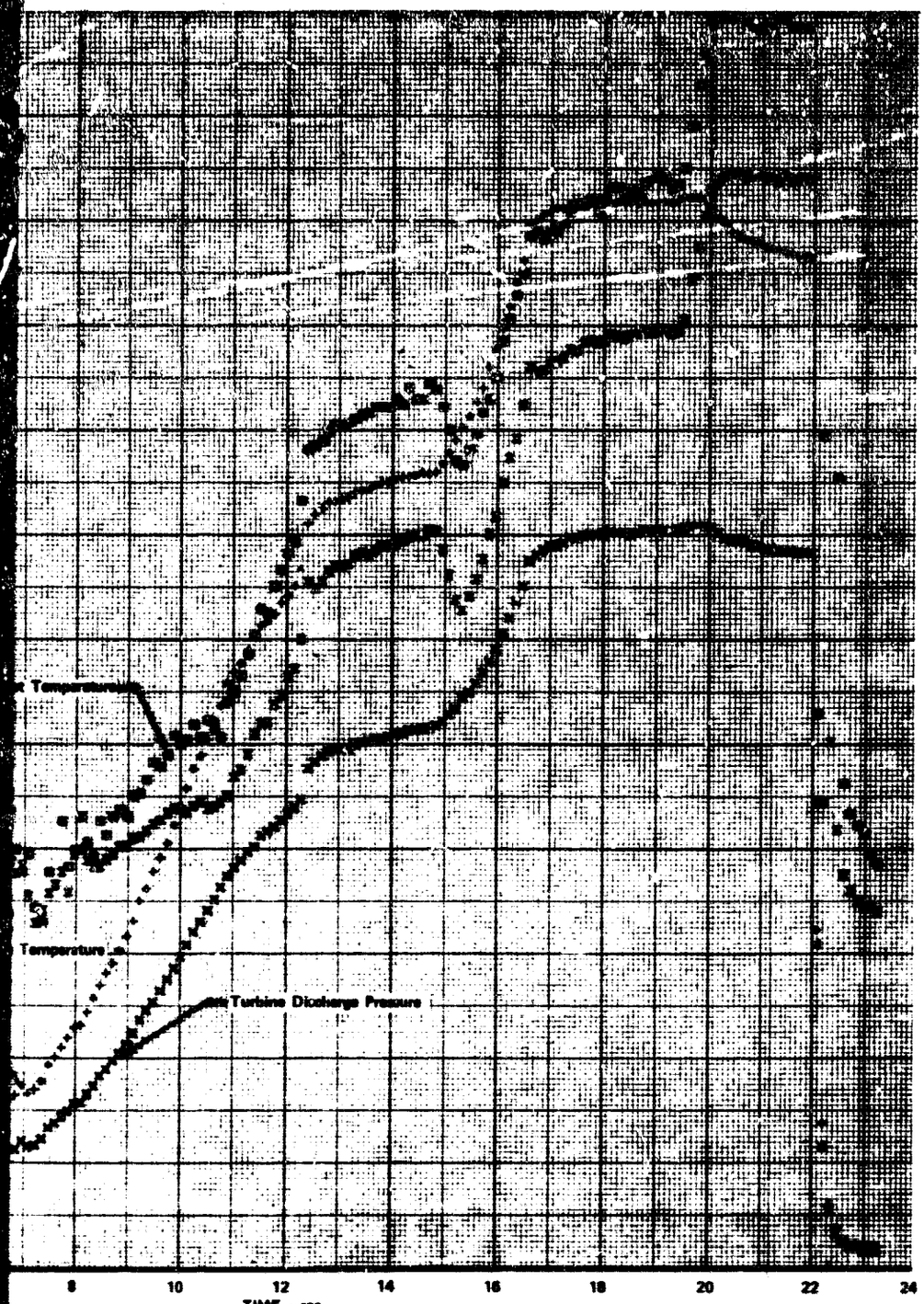
Temperature
Temperature
Turbine Discharge Pressure
8
10
12
14
16
18
20
22
24
TIME - sec

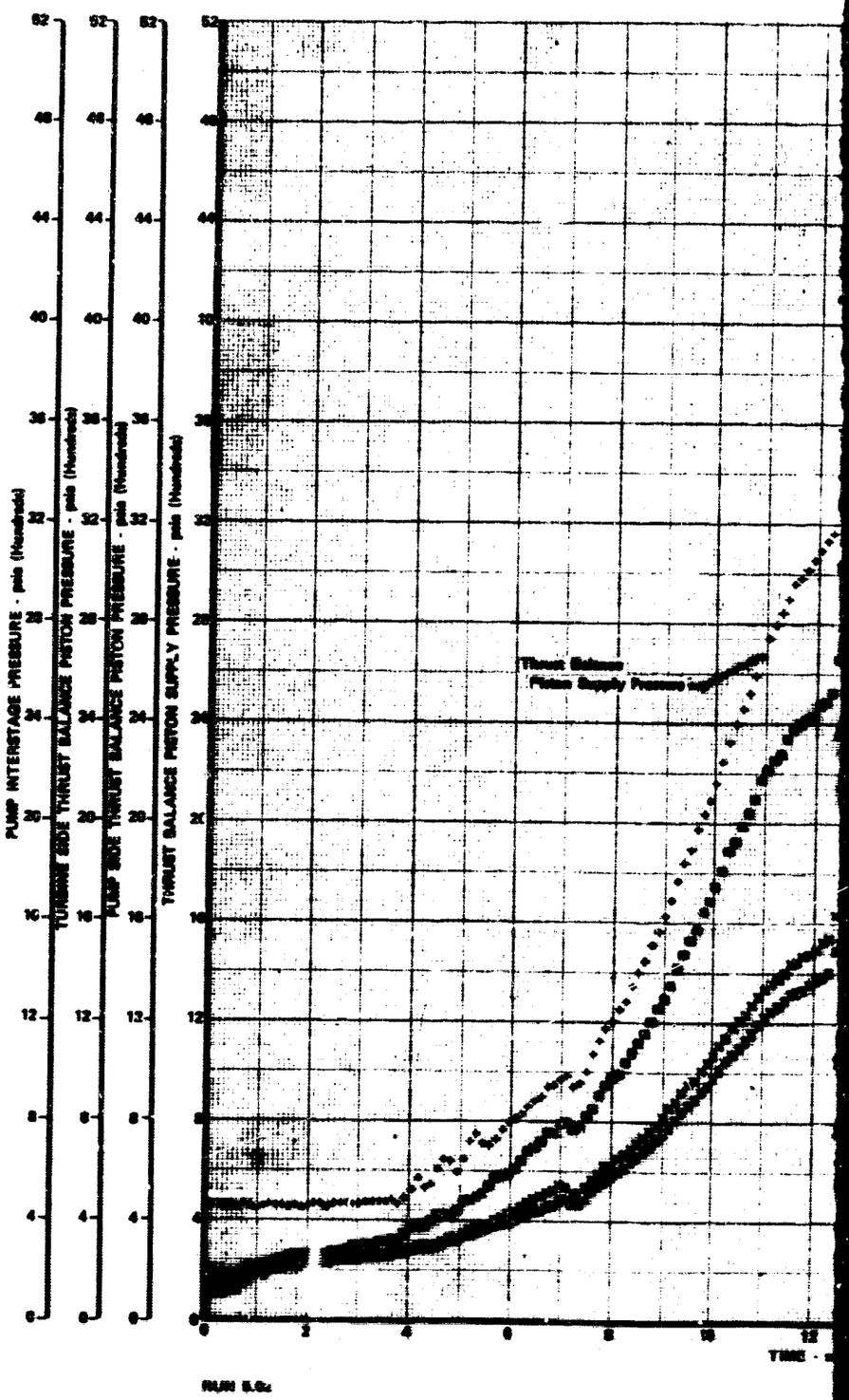

Figure 948. Significant Turbopump Parameters vs Time, Test 5.02, Rig F35155-2, Sheet 3

B

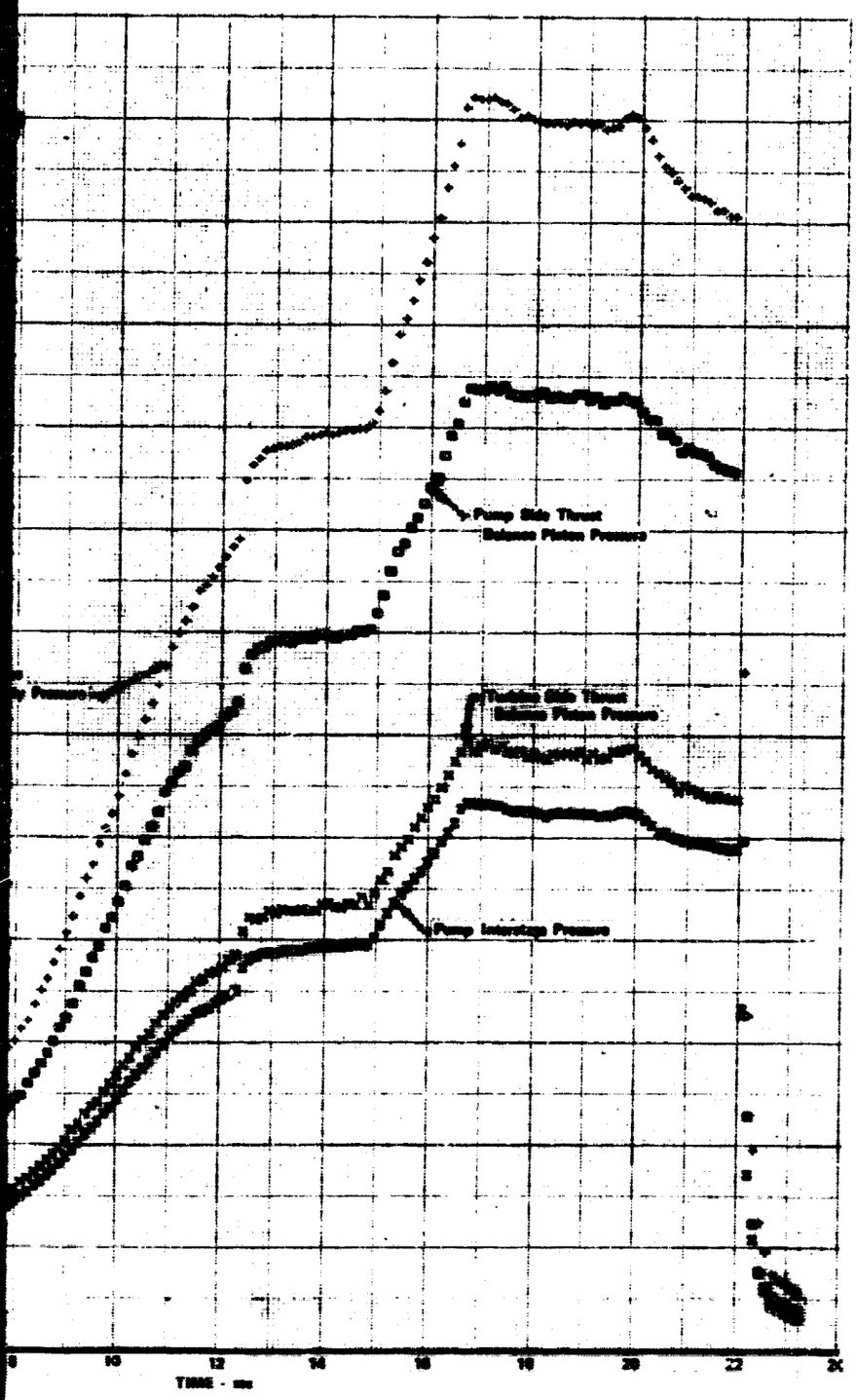

FD 43338

1001 / 1002

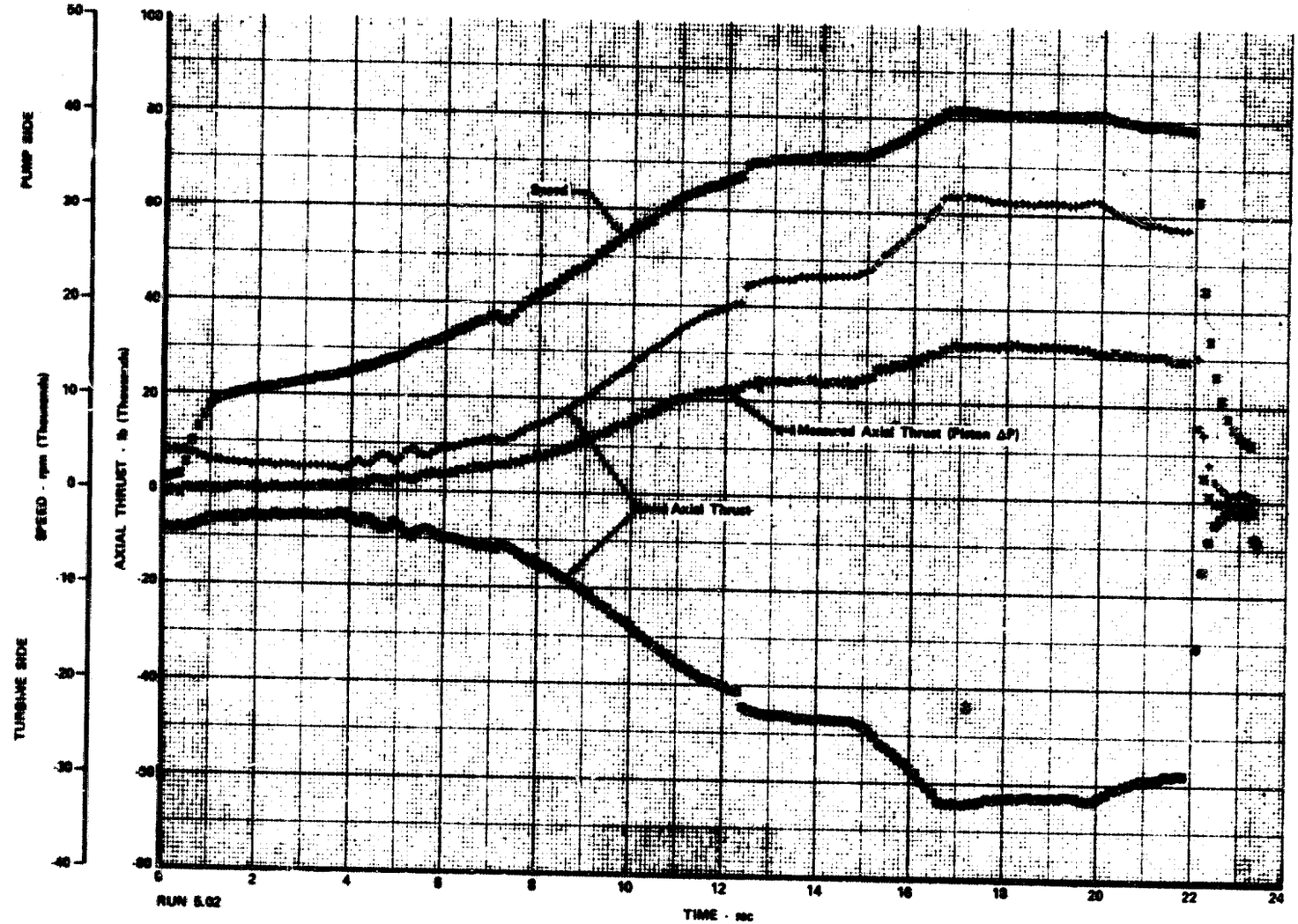

Figure 949. Significant Turbopump Parameters vs Time, Test 5.02, Rig F35155-2, Sheet 4

FD 43337

Table CVII. Hot Turbine Run, Rig No. 35155-2, Run No. 5.02, Engine Thrust Level 75% and 100%, Mixture Ratio 5.0, 6.0, and 7.0

Preburner	Predicted Engine Cycle 6	Test Results	Predicted Engine Cycle 6	Test Results	Predicted Engine Cycle 6	Test Results
Total Fuel Flow - lb_m/sec***	56.71	56.83	64.63	64.12	55.86	55.25
Total Oxidizer Flow - lb_m/sec	50.20	47.73	71.45	70.71	70.02	71.54
Oxidizer Primary - lb_m/sec	9.82	9.70	8.15	8.45	6.08	6.24
Oxidizer Secondary - lb_m/sec	40.38	38.03	63.31	62.26	63.94	65.31
Primary/Total Flow Split - lb_m/sec	0.196	0.203	0.114	0.120	0.086	0.087
Injector Fuel Flow - lb_m/sec	56.36	55.67	64.23	62.85	55.52	54.20
Rigimesh Coolant Flow - lb_m/sec	NAV	0.888	NAV	0.976	NAV	0.806
Coolant Liner Flow - lb_m/sec	0.351*	0.267	0.398*	0.293	0.338*	0.242
Injector Mixture Ratio	0.891	0.844	1.112	1.108	1.261	1.301
Chamber Pressure - psia	3281	3045.	4367.	4086.	4175.	3889.
Average Combustion Temperature - °R	1713.	1634.**	2086.	2090.**	2326.	2405.**
Oxidizer Temperature - °R	221.	178.	220.	177.	215.	178.
Fuel Temperature - °R	160.	159.	183.	178.	197.	199.
Oxidizer Turbine Simulator						
Turbine Inlet Flow - lb_m/sec	31.01	31.45	39.53	39.35	36.55	36.27
Turbine Coolant - lb_m/sec	0.860*	0.642	0.980*	0.824	0.915*	0.726
Outer Case Coolant - lb_m/sec	0.480*	0.947	0.620*	0.913	0.630*	0.914
Turbine Inlet Total Pressure - psia	3234.	3079.	4332	4126	4141.	3921.
Diffuser Discharge Total Pressure - psia	NAV	2076.	2892.	2837.	NAV	2772.
Turbine Inlet Temperature (Average) - °R	1687.	1658.	2055.	2085.	2292.	2398
Turbine Discharge Temperature - °R	1572.	NAV	1911.	NAV	2144.	NAV
Temperature Profile (max - avg) - °R	0.0	45.0	0.0	94.0	0.0	126.0
Fuel Turbine						
Turbine Inlet Flow - lb_m/sec	76.37	73.11	97.31	95.48	89.99	90.52
Turbine Coolant Flow - lb_m/sec	0.780*	1.948	0.920*	2.390	0.848*	2.062
Outer Case Coolant - lb_m/sec	0.680*	1.130	0.620*	1.105	0.630*	1.105
Turbine Inlet Total Pressure - psia	3244.	2990	4318.	4001.	4129.	3820.
Diffuser Discharge Total Pressure - psia	NAV	2071.	NAV	2843.	NAV	2918.
Turbine Inlet Temperature - °R	1687	NAV	2055.	NAV	2292	NAV
Turbine Discharge Temperature - °R	1566.	1404.	1901.	1786.	2132	2086.
Fuel Pump						
Fuel Discharge Valve A_{cd} - in^2	NAV	1.06	NAV	0.94	NAV	0.96
Volumetric Inlet Flow - gpm	7526.	7540.	8608.	7651.	7631	7422.
Inlet Mass Flow - lb_m/sec	68.55	74.58	78.50	75.72	69.69	73.42
Inlet Pressure - psia	116.0	121.0	127.0	127.0	145.0	129.0
Inlet Temperature - °R	47.0	38.0	48.0	38.0	48.0	38.0
Discharge Pressure - psia	3786.	3829.	5002.	5070.	5056.	4706.
Discharge Temperature - °R	112.0	90.0	130.0	107.0	135.0	104.0.
Total Pump Pressure Rise - psi	3670.	3708.	4875.	4943.	4911.	4577.
Pump Speed - rpm	38733.	36085	44477.	40782.	44220.	39498
Horse Power - hp	25311.		38179.	32441.	35335.	30368.
Transition Case						
Transition Case Pressure - psia	2210.	2062.	2872.	2817.	2794.	2738
Transition Case Temperature - °R	1472.	1426.	1792	1808.	1993.	2096
Transition Case Total Flow - lb_m/sec	113.0	109.3	139.2	140.1	130.9	131.6
Transition Case Total Coolant - lb_m/sec	0.960	2.097	1.240*	2.018	1.240*	2.019
Injector Effective Areas						
Oxidizer						
Primary A_{cd} - in^2	0.063	0.067	0.063	0.065	0.063	0.059
Secondary A_{cd} - in^2	0.658	0.679	0.710	0.724	0.723	0.734
Fuel						
Overall - in^2	3.48	2.79	3.48	2.82	3.48	2.97
Plate - in^2	3.70	3.27	3.70	3.19	3.70	3.29

*Cycle 8 Values
**Based Upon Average Mixture Ratio
***For Rig 35155-2 This is Injector Total Fuel Flow (Includes P/B Coolant And Rigimesh Flows)

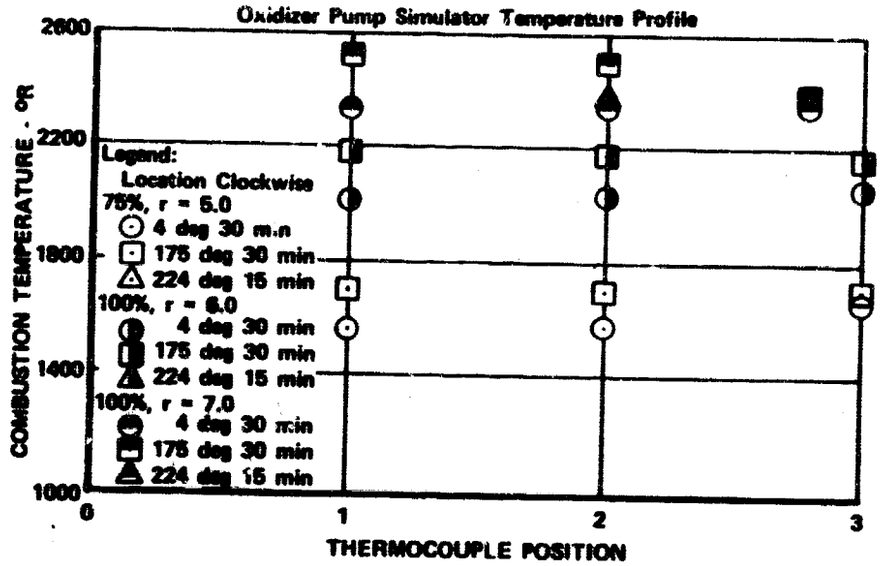

Figure 950. Temperature Profile Data, Test 5.02

FD 45328

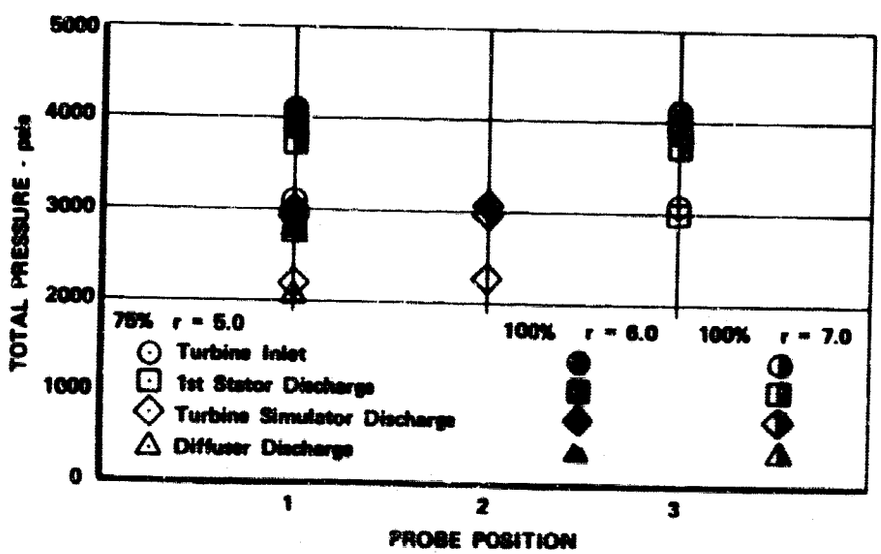

Figure 951. Pressure Profile Data, Test 5.02

FD 44510

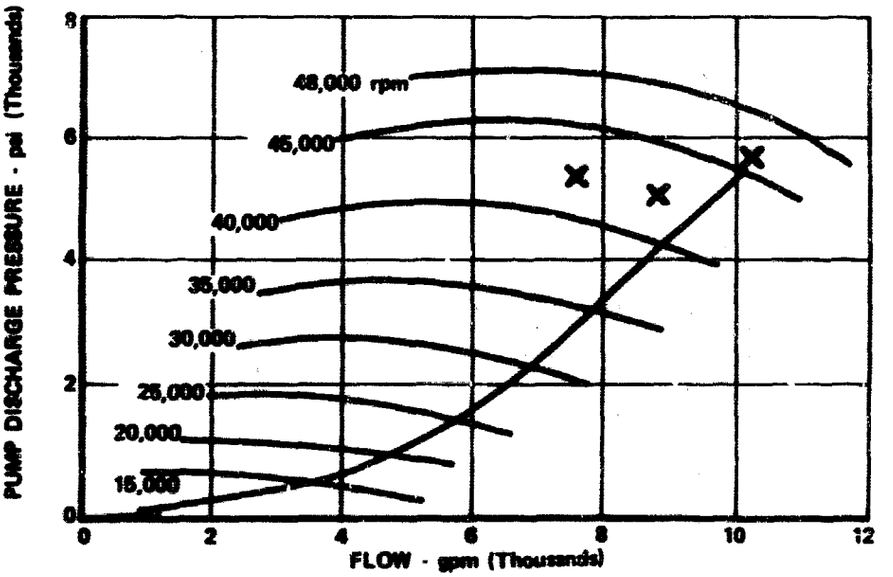

Figure 952. Pump Discharge Pressure vs Flow, Test 6.01, Rig F35155-2

FD 38750H

A

Figure 953. Significant Turbopump Parameters vs Time, Test 6.01, Rig F35155-2, Sheet 1

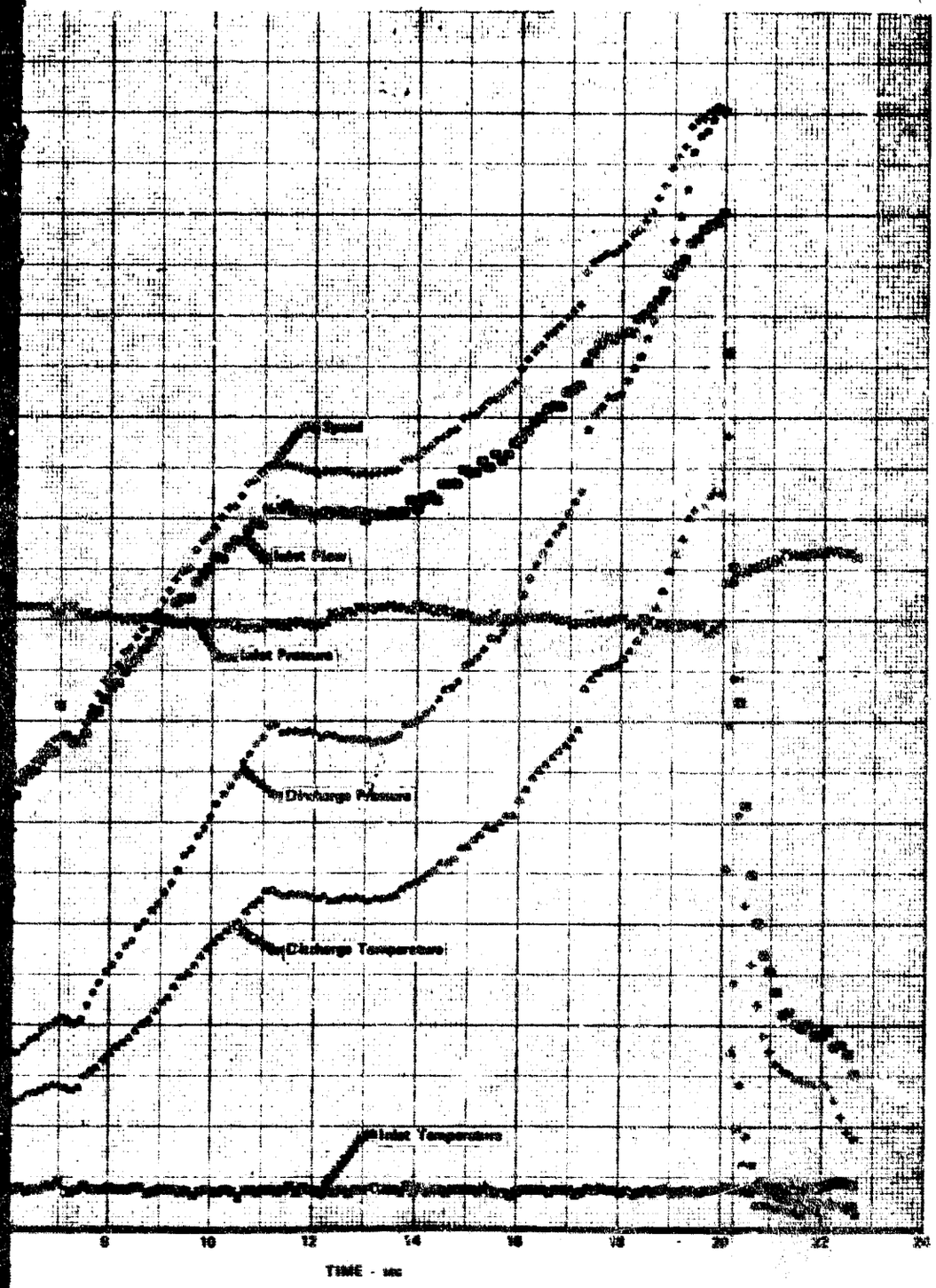

FD 43344

1007 / 1008

A

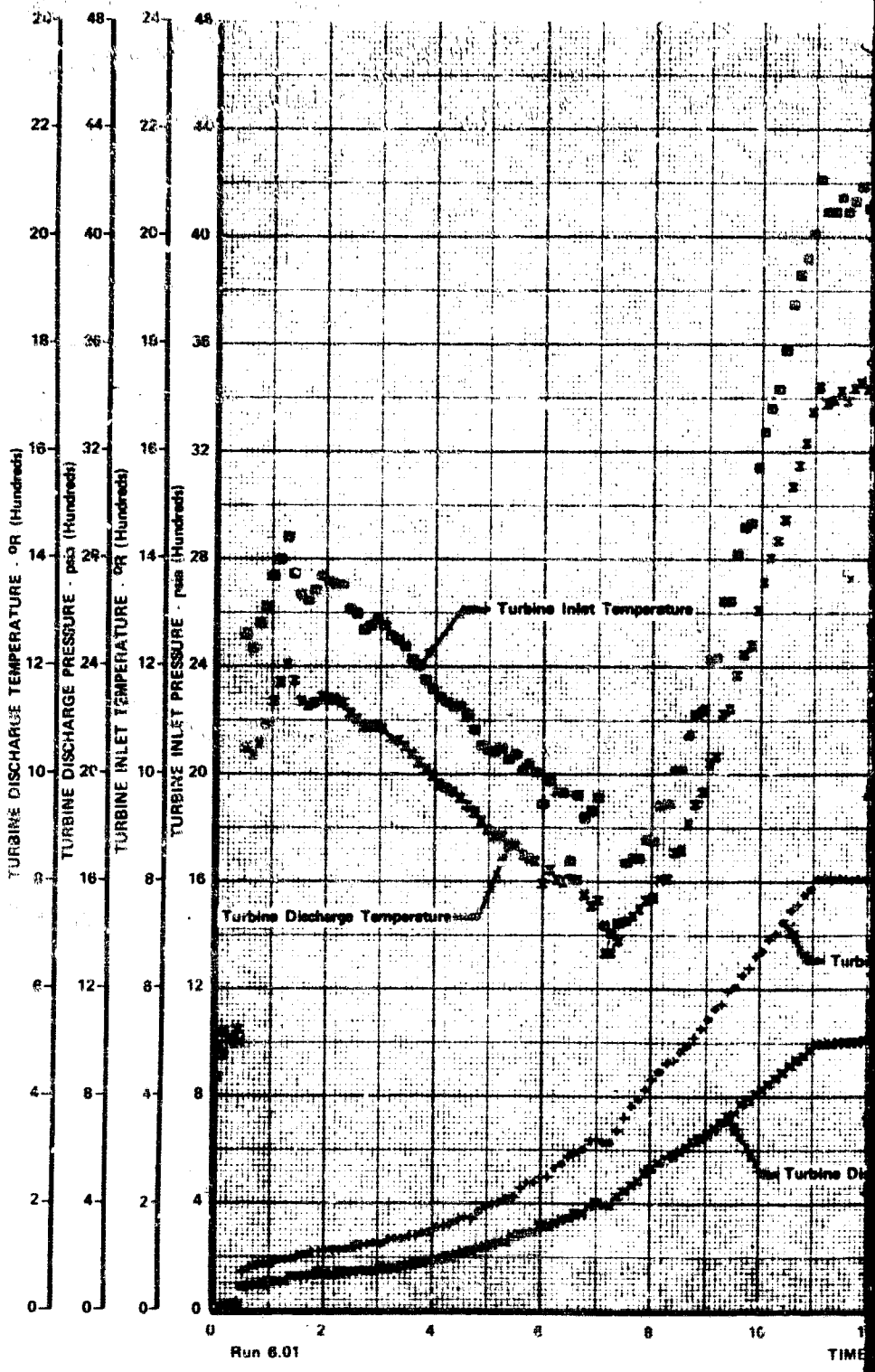

Figure 954. Significant Turbopump Parameters vs Time, Test 6.01, Rig 35155-2, Sheet 2

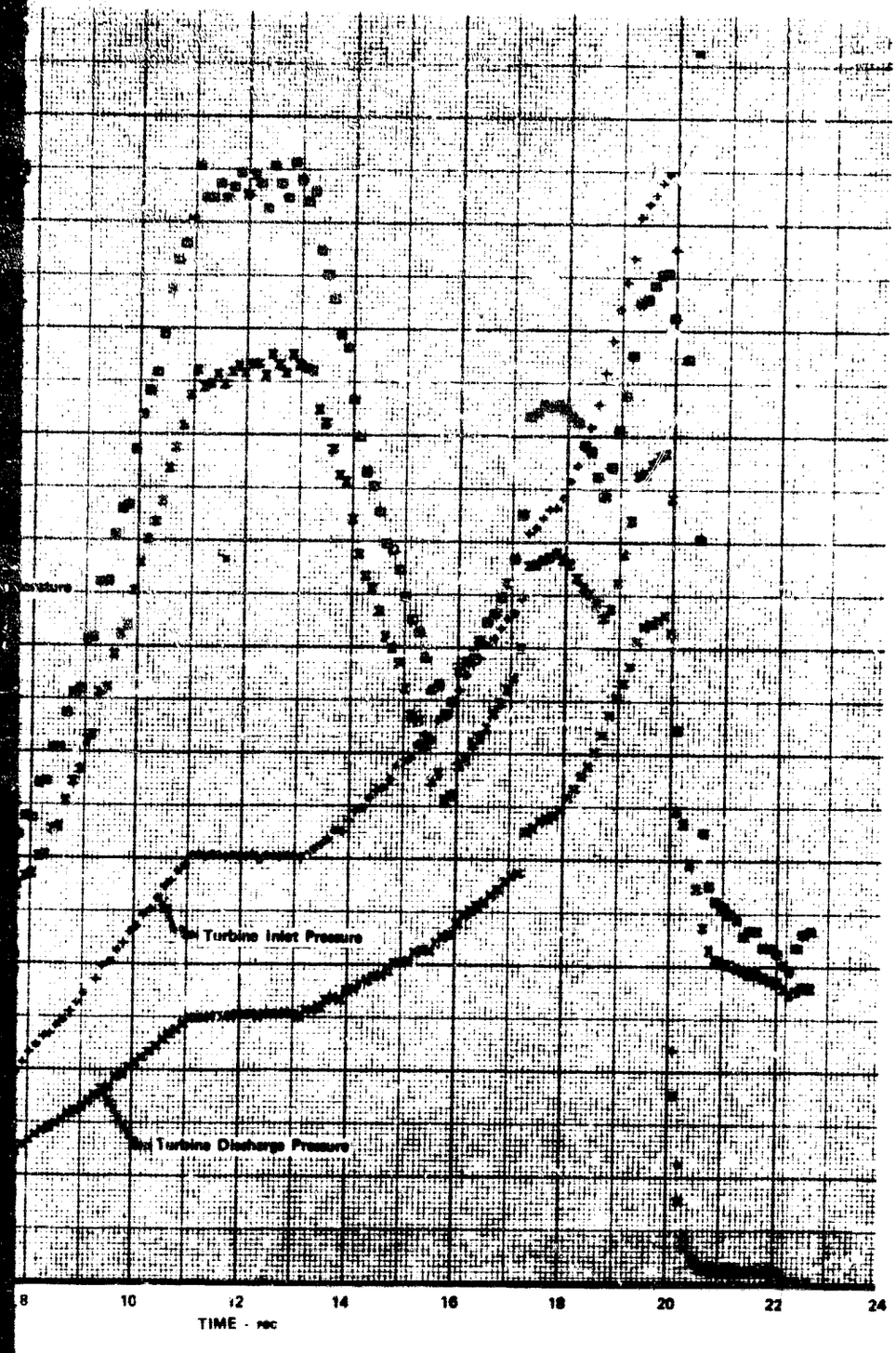

FD 43343

1009 / 1010

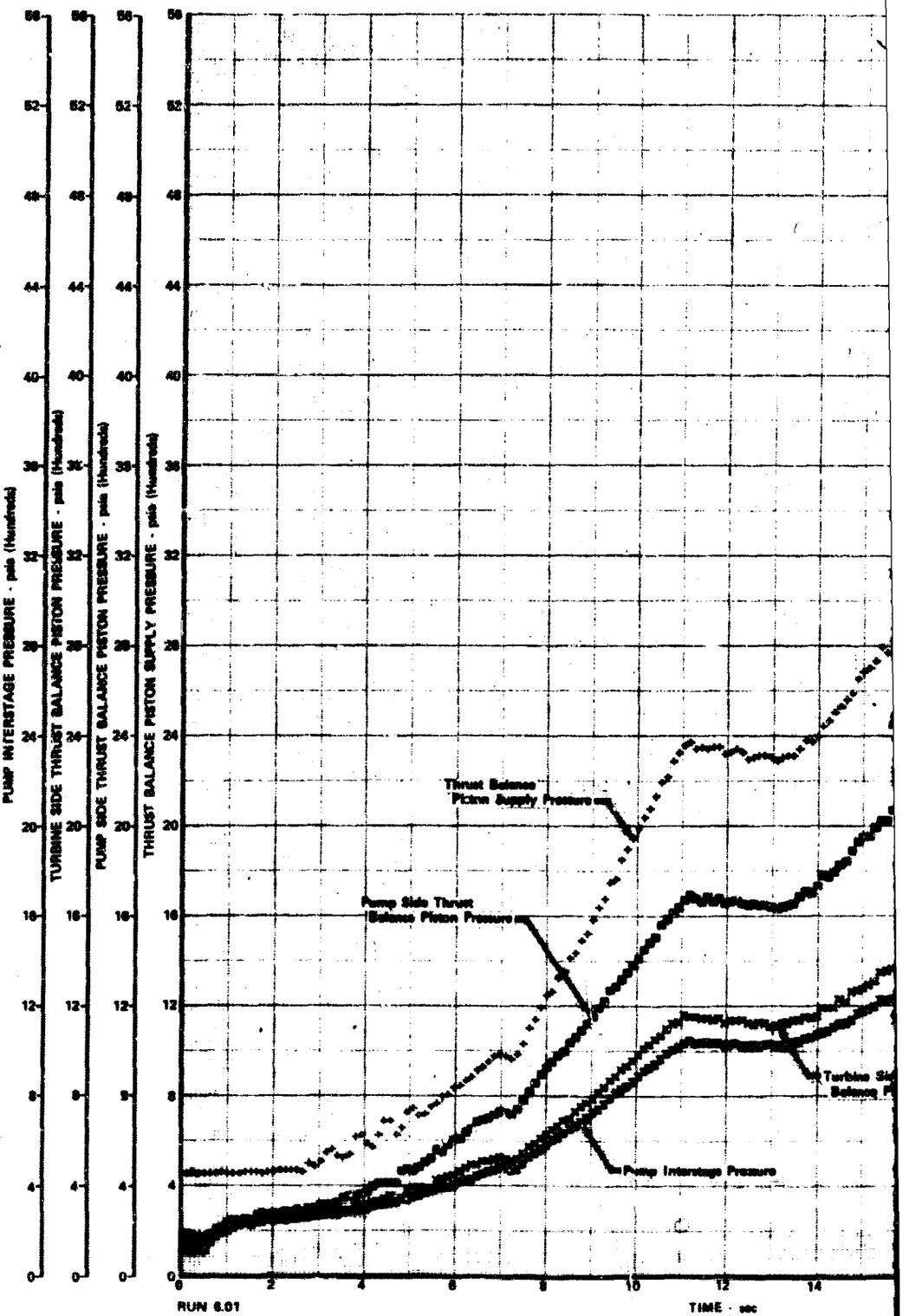

Figure 955. Significant Turbopump Parameters vs Time, Test 6.01, Rig F35155-2, Sheet 3

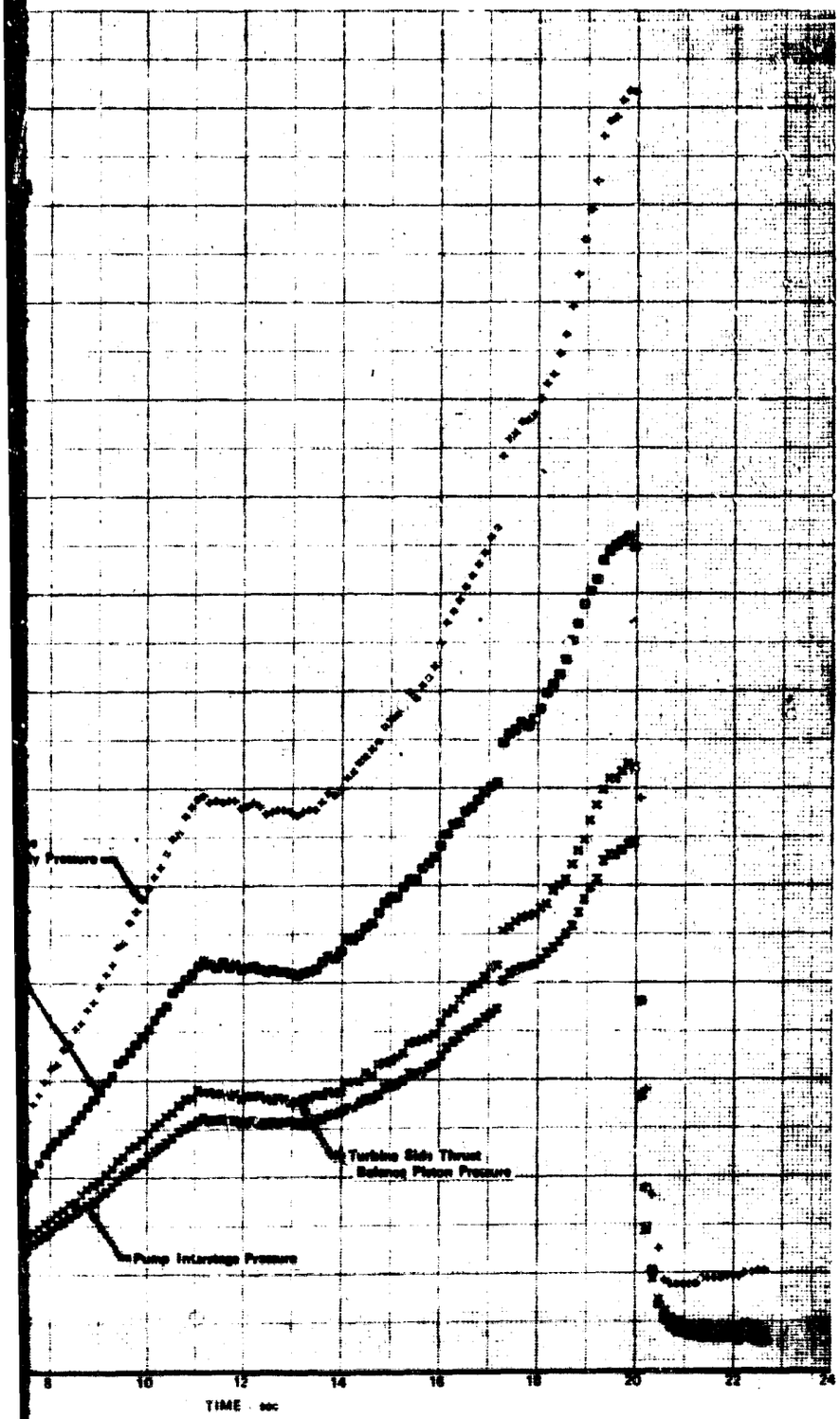

FD 43342

1011 / 1012

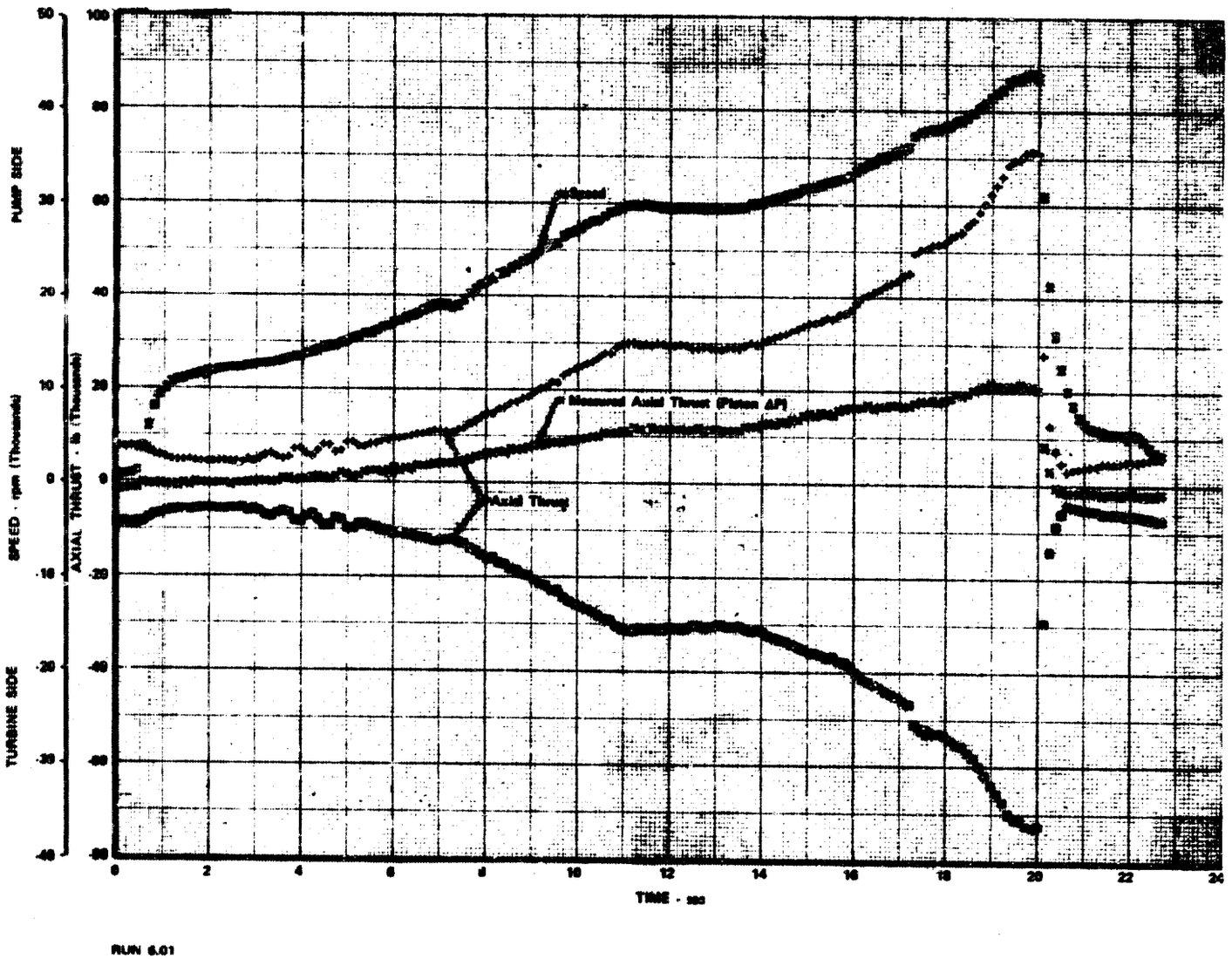

Figure 956. Significant Turbopump Parameters vs Time, Test 6.01, Rig F35155-2, Sheet 4

FD 43341

Table CVIII. Hot Turbine Test Run No. 35155, Run No. 6.01, Engine Thrust Level 50% and 100%, Mixture Ratio 7.0 and 5.0

	Mixture Ratio 7.0		Mixture Ratio 5.0	
Preburner	Predicted Engine Cycle 6	Test Results	Predicted Engine Cycle 6	Test Results
Total Fuel Flow -lb_m/sec	26.56	27.25	75.70	75.74
Total Oxidizer Flow -lb_m/sec	30.59	30.74	79.99	76.43
Oxidizer Primary -lb_m/sec	8.16	8.50	13.43	7.81
Oxidizer Secondary -lb_m/sec	22.44	22.24	66.56	68.62
Primary/Total Flow Split	0.267	0.276	0.168	0.102
Injector Fuel Flow -lb_m/sec	26.40	26.69	75.23	74.18
Rigimesh Coolant Flow -lb_m/sec	NAV	0.427	NAV	1.202
Coolant Liner Flow -lb_m/sec	0.163*	0.128	0.465*	0.361
Injector Mixture Ratio	1.159	1.134	1.063	1.033
Chamber Pressure -psia	1915.	1620.	4817.	4212.
AVG Combustion Temp. -°R	2157.	2125.**	2009.	1920**
Oxidizer Temp. -°R	207.	176.	234.	177.
Fuel Temp. -°R	183.	183.	183.	171.
Oxidizer Turbine Simulator				
Turbine Inlet Flow - lb_m/sec	16.75	15.85	45.27	43.80
Turbine Coolant - lb_m/sec	0.600*	0.299	1.030*	0.949
Outer Case Coolant - lb_m/sec	0.360*	0.721	1.148	0.893
Turbine Inlet Total Pres. - psia	1900.	1638.	4782.	4254.
Diffuser Discharge Total Pressure - psia	NAV	1032.	NAV	2562.
Turbine Inlet Temp (AVG)- °R	2122.	2137.	1986.	1872.
Turbine Discharge Temp - °R	2019.	NAV	1823.	NAV
Temp Profile (max-avg) - °R	0.0	65.0	0.0	65.0
Fuel Turbine				
Turbine Inlet Flow - lb_m/sec	40.78	42.14	111.50	108.4
Turbine Coolant Flow - lb_m/sec	0.470*	0.828	1.070*	2.873
Outer Case Coolant - lb_m/sec	0.360*	0.877	1.392	1.088
Turbine Inlet Total Pres. - psia	1895.	1590.	4766.	4125.
Diffuser Discharge Total Pressure - psia	NAV	1033.	NAV	2556.
Turbine Inlet Temp.- °R	2122.	NAV	1986.	NAV
Turbine Discharge Temp - °R	2008.	1783.	1813.	1582.
Fuel Pump				
Fuel Discharge Valve ACD -in^2	NAV	1.18	NAV	1.15
Volumetric Inlet Flow - GPM	3888.	7075.	10024	9975.
Inlet Mass Flow - lb_m/sec	35.40	69.90	91.32	98.60
Inlet Pressure - psia	122.0	118.0	117.0	116.0
Inlet Temperature - °R	48.0	38.0	48.0	38.0
Discharge Pressure - psia	2750.	2498.	5654.	5694.
Discharge Temperature - °R	110.0	73.0	139.	113.
Total Pump Pressure Rise - psi	2628.	2380.	5537.	5578.
Pump Speed - rpm	32553.	30025.	48025.	44445.
Horsepower - hp	11710.	15540.		
Transition Case				
Transition Case Pressure - psia	1389.	1014.	2967.	2543.
Transition Case Temperature - °R	1834.	1790.	1709.	1516.
Transition Case Total Flow - lb_m/sec	60.3	60.7	161.3	158.0
Transition Case Total Coolant - lb_m/sec	1.280*	1.598	2.540	1.981
Injector Effective Areas				
Oxidizer				
Primary ACD - in^2	0.063	0.068	0.063	0.061
Secondary ACD - in^2	0.620	0.617	0.690	0.731
Fuel				
Overall - in^2	3.48	2.85	3.48	2.86
Plate - in^2	3.70	3.29	3.70	3.37

* Cycle 8 values
**Based on average mixture ratio

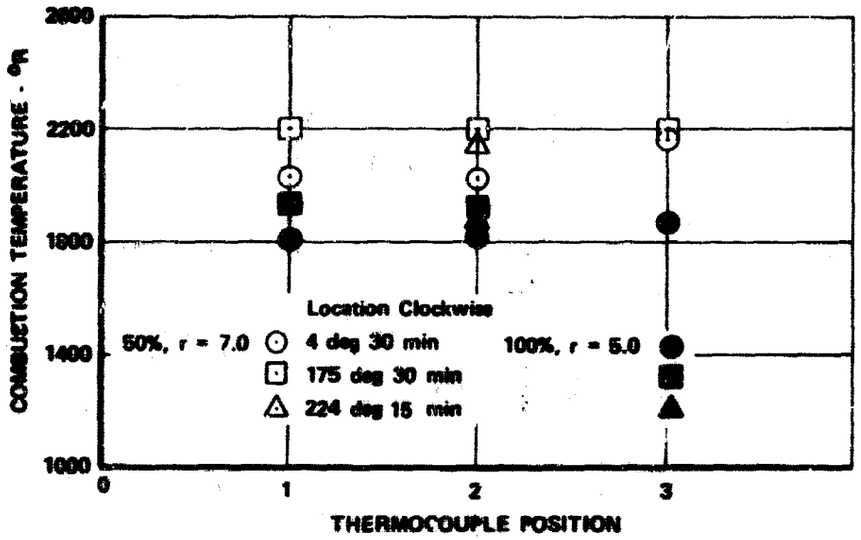

Figure 957. Temperature Profile Data, Test 6.01 FD 44512

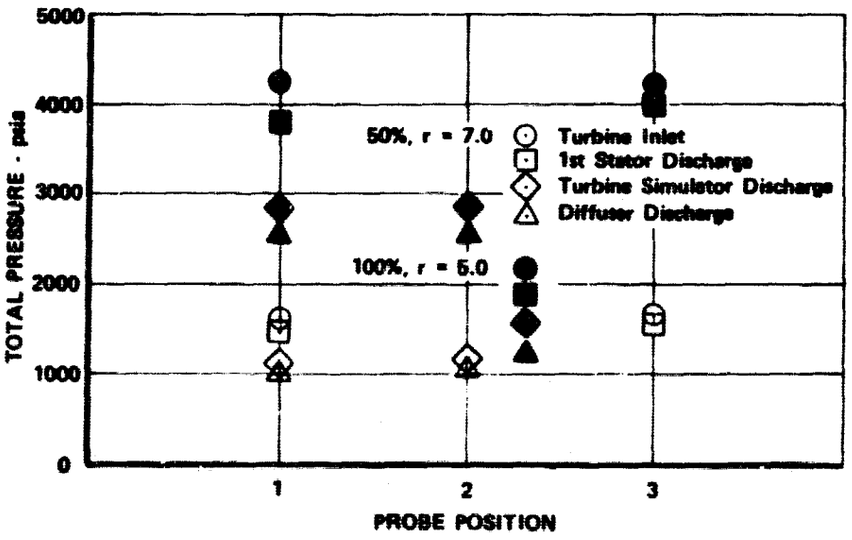

Figure 958. Pressure Profile Data, Test 6.01 FD 44511

Figure 959. Hot Turbine Test Rig Operating at the 100% r = 5 Level, Test 6.01 FE 100685-2

With the completion of test No. 6.01 the program objectives of hot turbine testing at 100%, and equivalent engine r = 5, 6 and 7 had been accomplished. The rig was removed from test stand on 13 August 1970 to permit teardown inspection for parts evaluation and documentation.

Teardown inspection revealed that the fuel turbopump and preburner parts were in good condition. Figures 960 through 964 show the condition of the major subassemblies after removal from the transition case. The major discrepancy detected was an ovalized condition of the transition case center ball structure in the gimbal plane which permitted the piston ring seals of the fuel turbopump, preburner and oxidizer pump simulator to expand out of their retaining grooves and hot extrude as a result of the pressure loading. Figure 965 shows this condition on the fuel turbopump turbine inlet duct and figure 966 shows the ovalized condition of the transition case center ball structure. Teardown inspection of the fuel turbopump turbine showed no significant discrepancy except for thermal distortion of the 1st-stage turbine rotor tip shroud and minor dents on the 1st-stage turbine blade leading edges resulting from ingestion of small fragments of instrumentation hypotubing as shown in figure 967. Subsequent fluorescent penetrant inspection of the turbine blades indicated that no cracks had developed. The post-test condition of the major fuel turbopump turbine components is shown in figures 968 and 969. A detailed inspection of the fuel pump details revealed no significant problem areas and all parts were in excellent condition. Minor indications of rub or wear were noted on the bearings and thrust piston rub faces as shown in figures 970 through 973. Roller end wear was minor with an average wear of 0.0005 in. on the front bearing and 0.0003 in. on the rear bearing. The outer races were loose in their restraining

carriers and showed scoring on the load faces, but were otherwise in good condition. Thrust piston rub face wear was minor as shown in figure 974 and was caused only by shutdown contact when the actuation pressure shut off. No impeller or inducer rub was experienced, as shown in figures 975 through 977.

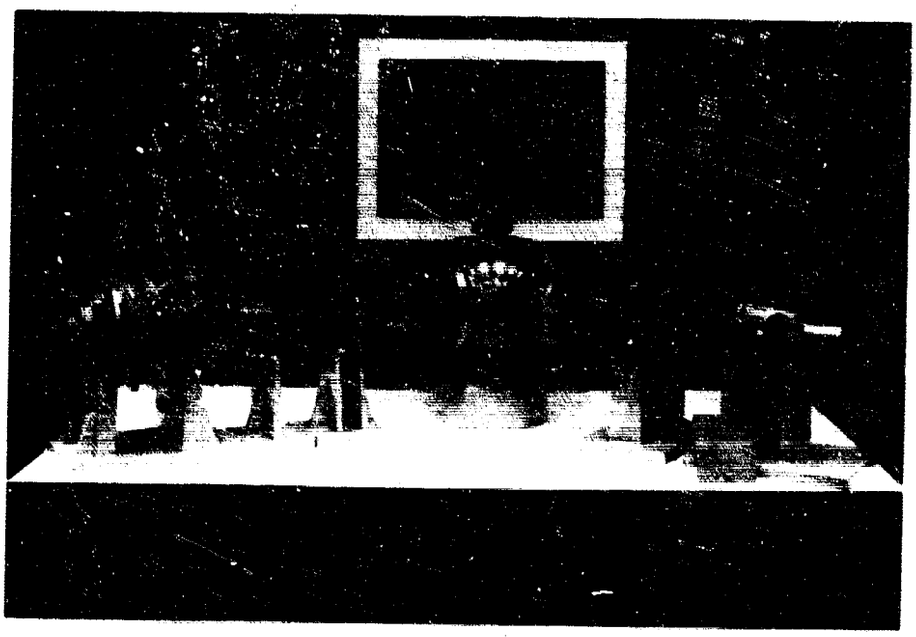

Figure 960. Hot Turbine Test Rig Major Components, Post-Test 6.01, Rig F35155-2 (View 1) KFE 100858

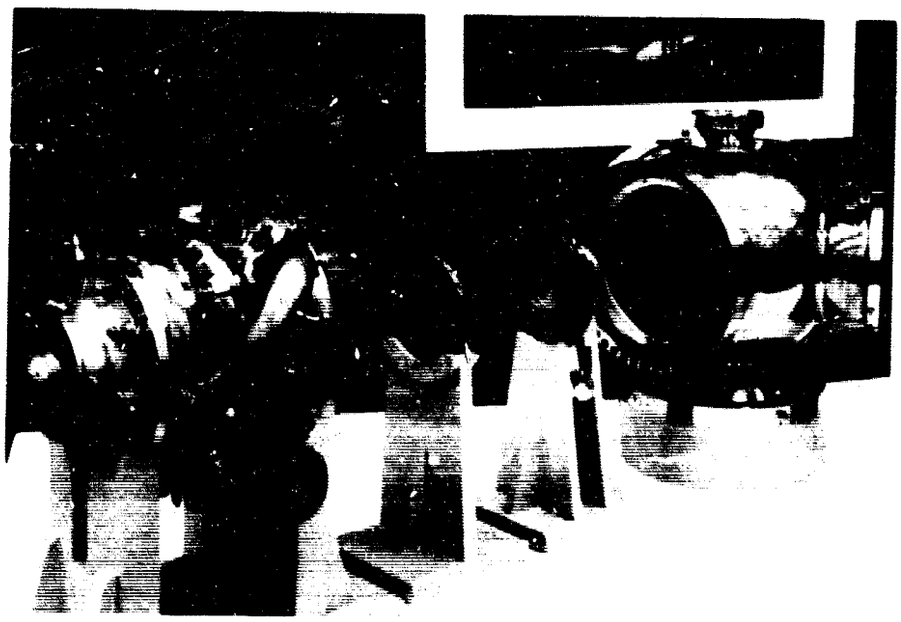

Figure 961. Hot Turbine Test Rig Major Components, Post-Test 6.01, Rig F35155-2 (View 2) KFE 100854

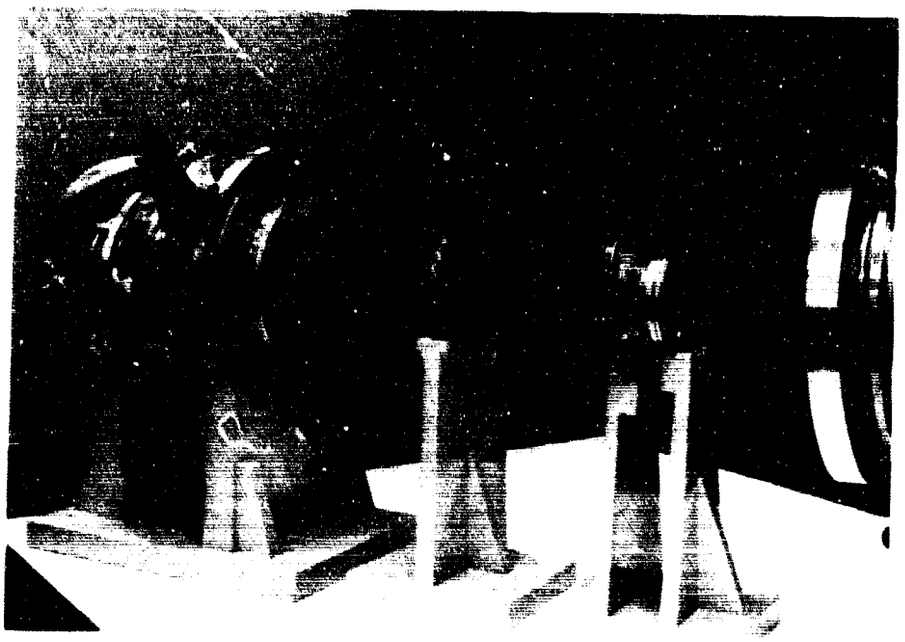

Figure 962. Hot Turbine Test Rig Major Components, Post-Test 6.01, Rig F35155-2 (View 3)

KFE 100856

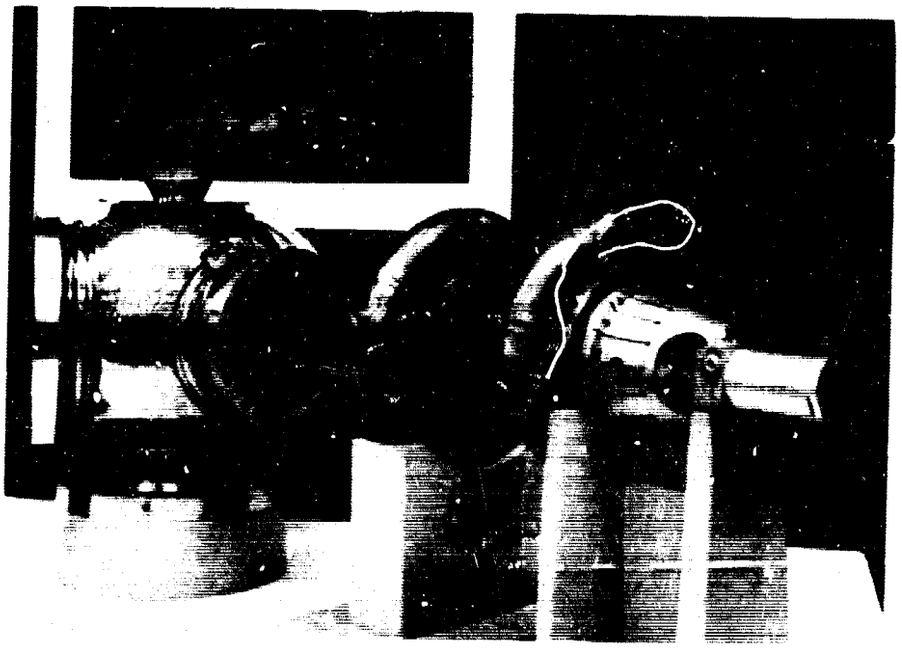

Figure 963. Hot Turbine Test Rig Major Components, Post-Test 6.01, Rig F35155-2 (View 4)

KFE 100855

Figure 964. Hot Turbine Test Rig Major Components, Post-Test 6.01, Rig F35155-2 (View 5) KFE 100857

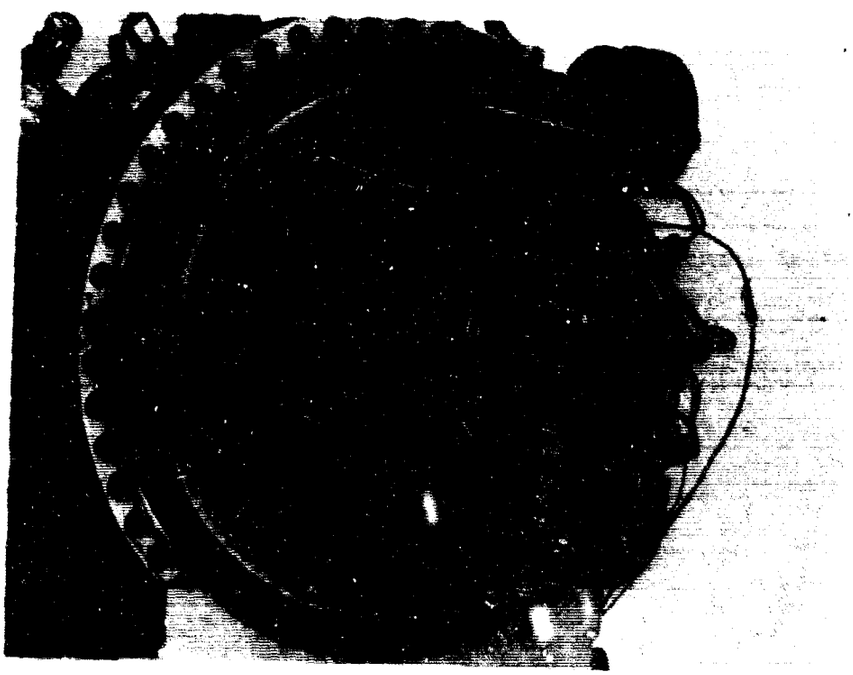

Figure 965. Disassembly View of Fuel Turbopump Turbine Section Showing Deformed Centerball Seal Rings KFE 100695

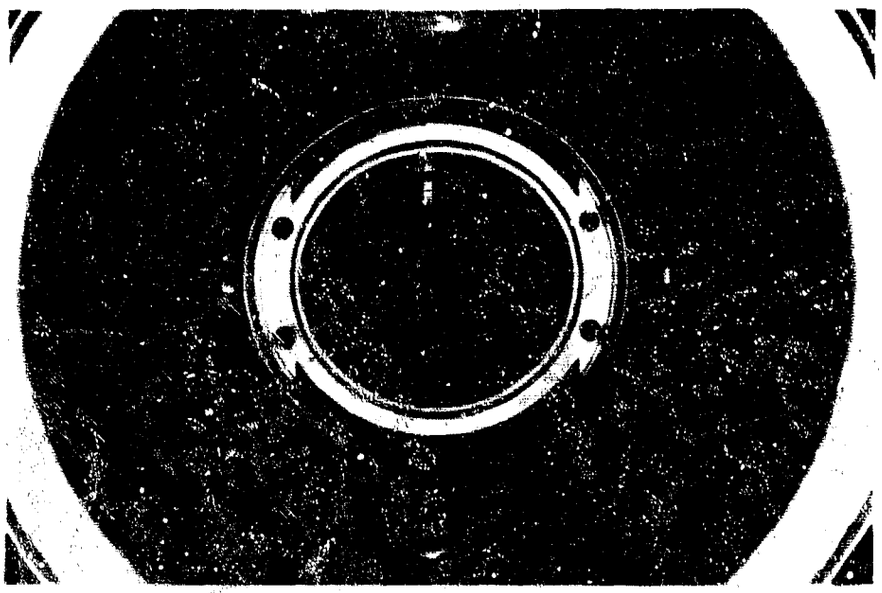

Figure 966. Disassembly View Into Transition Case Through Fuel Turbopump Port Showing Slight Ovalized Centerball FE 100893

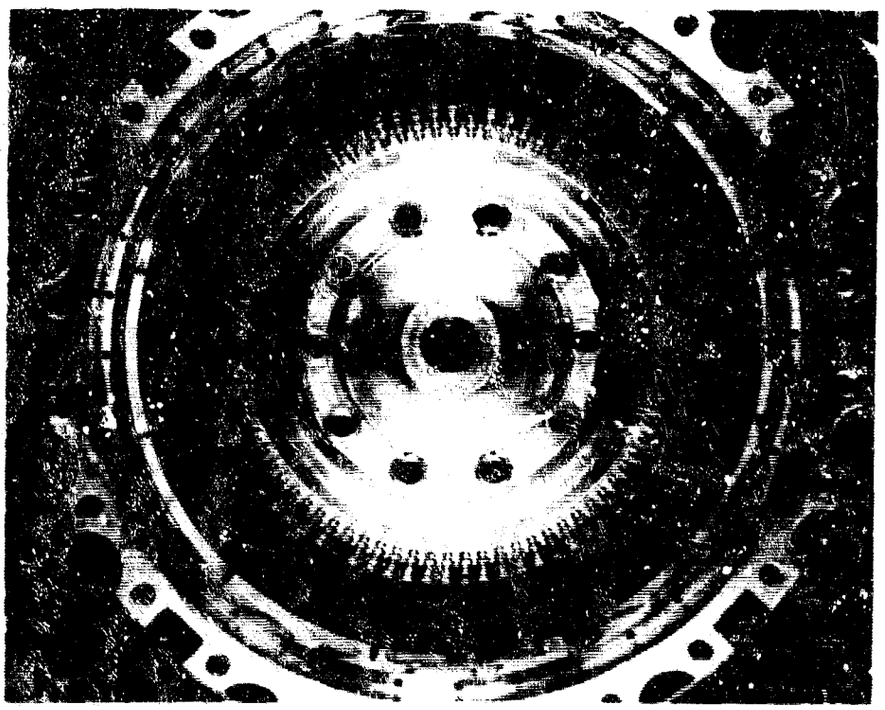

Figure 967. Disassembly View of Fuel Turbine Showing Distorted Tip Shroud and Turbine Blade Dents FE 100710

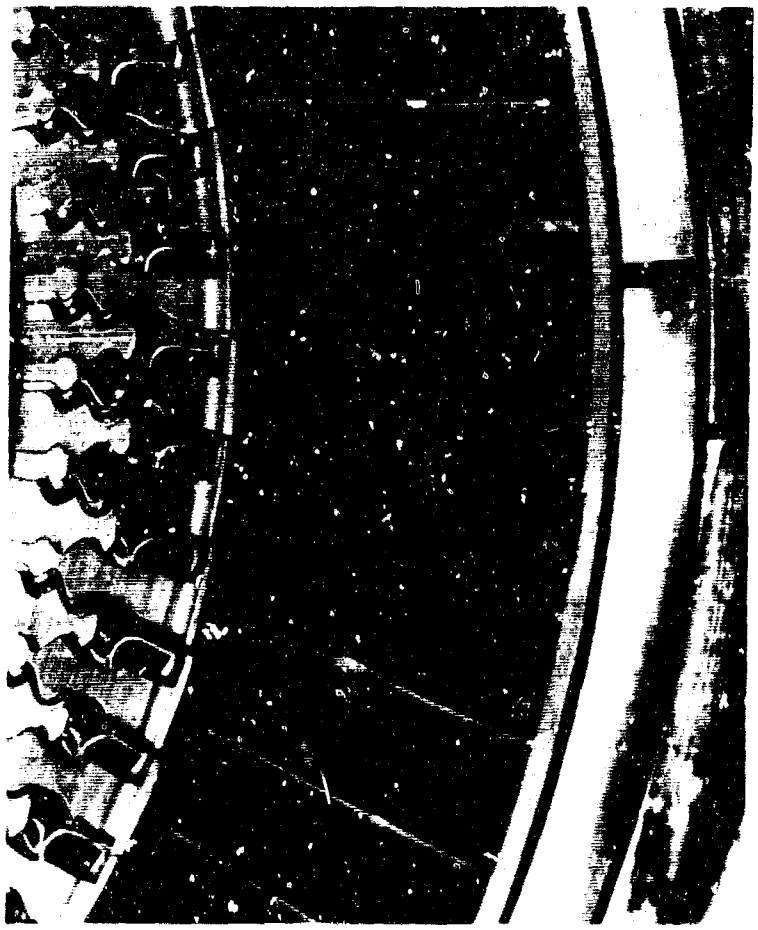

Figure 968. Disassembly View of Fuel Turbine Showing Blade Dents and Distorted Tip Shroud

FE 100711

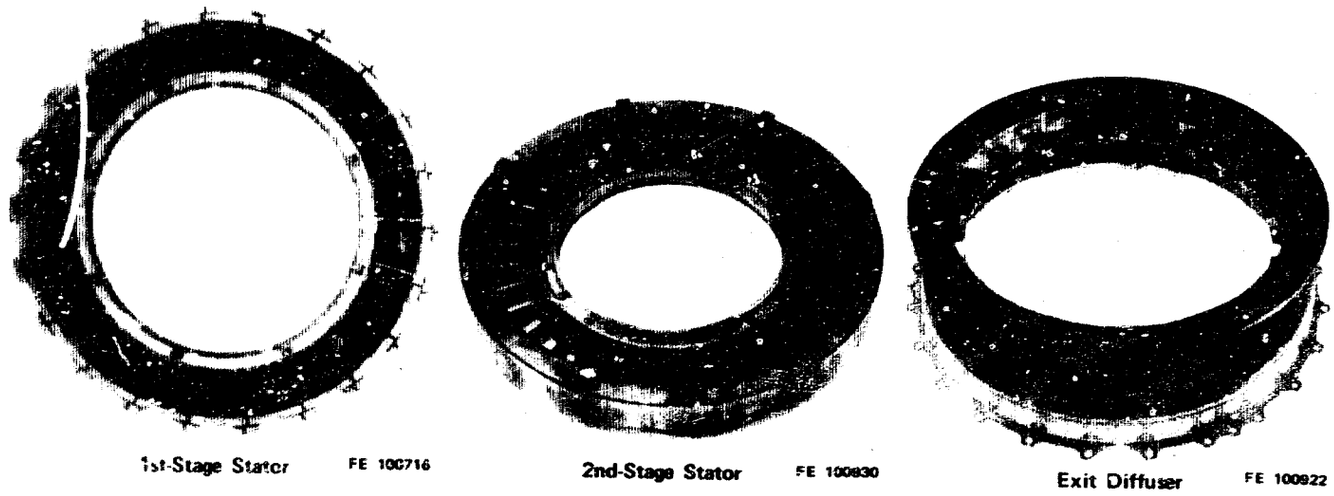

Figure 969. Disassembly View of Fuel Turbine Stators and Exit Diffuser Showing the Excellent Condition

FD 43356

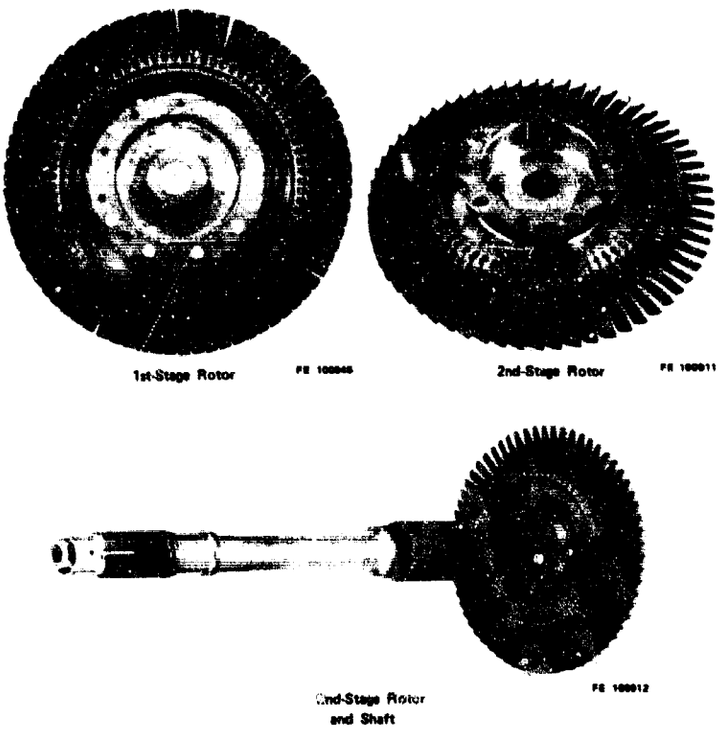

Figure 970. Disassembly View of Fuel Turbine Rotors Showing Good Condition FD 43357

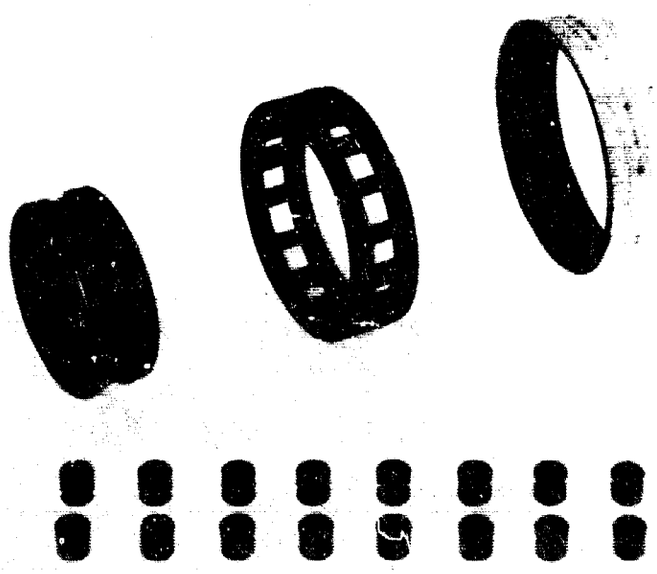

Figure 971. Disassembly View of Fuel Pump Front Bearing Showing Good Condition FE 100939

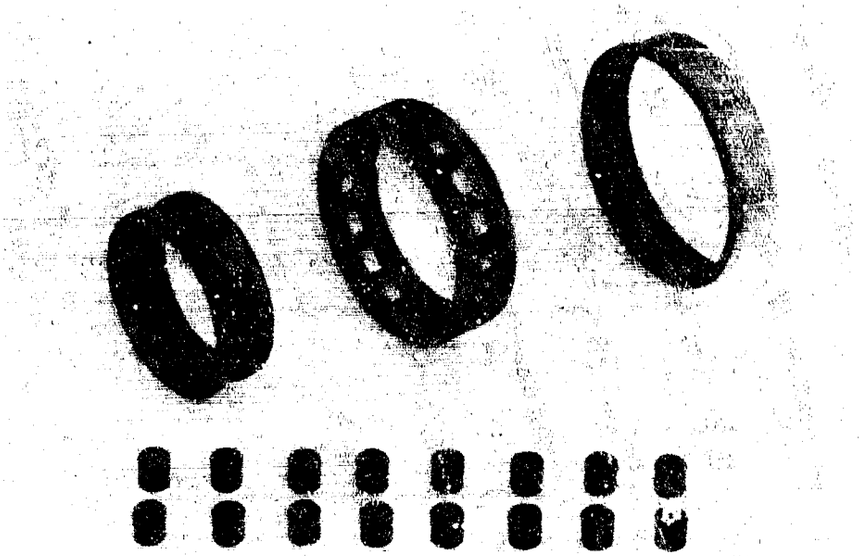

Figure 972. Disassembly View of Fuel Pumps Rear Bearing Showing Good Condition FE 100941

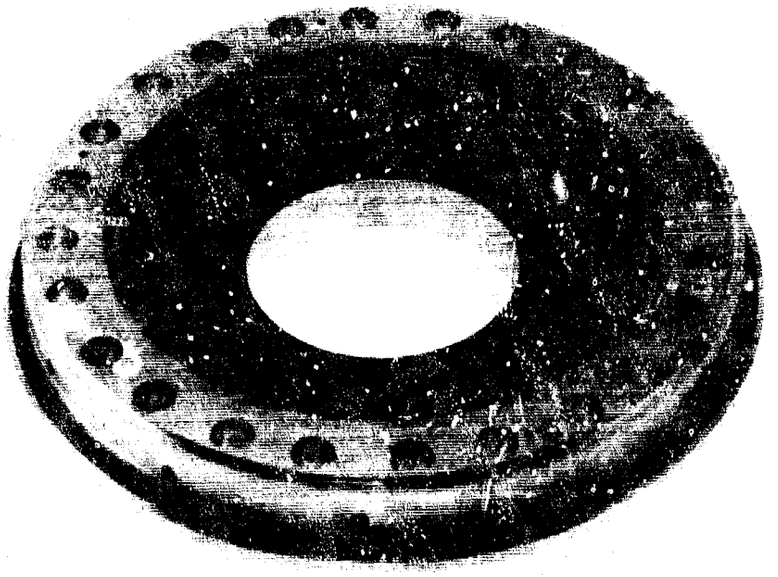

Figure 973. Disassembly View of Fuel Pumps Front Thrust Piston Rub Face Showing Good Condition FE 100914

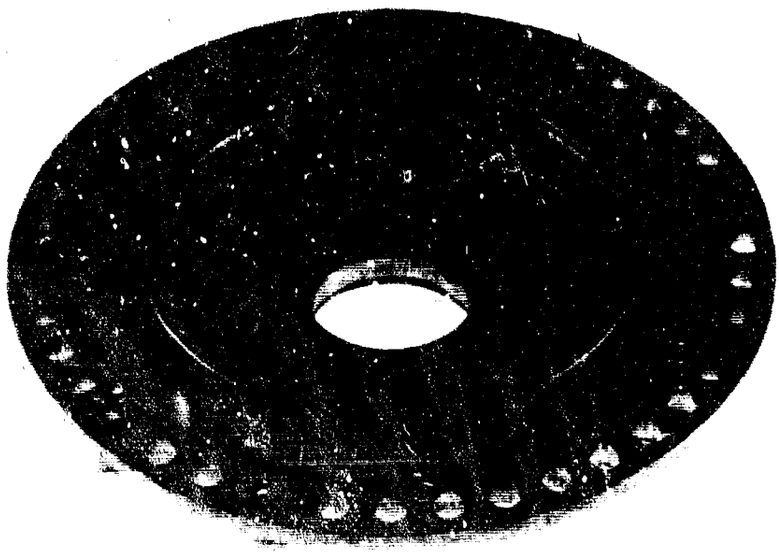

Figure 974. Disassembly View of Fuel Pump Rear Thrust Piston Rub Face Showing Good Condition FE 100913

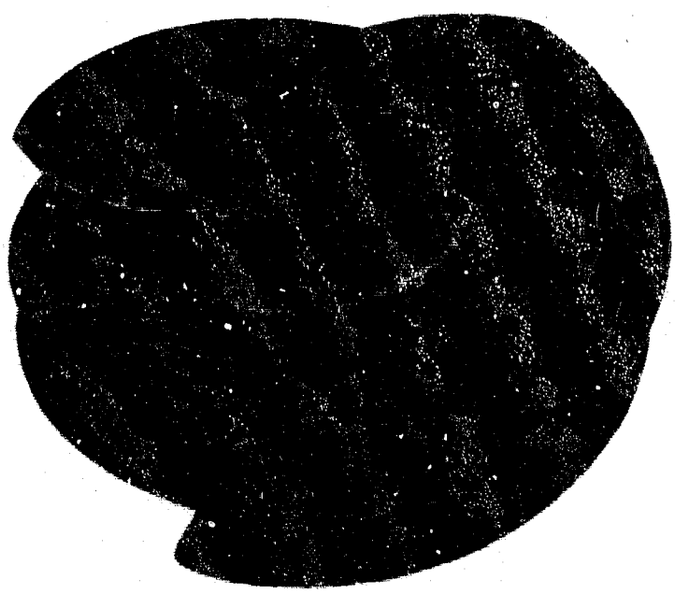

Figure 975. Disassembly View of Fuel Pump Inducer Showing Good Condition FE 100920

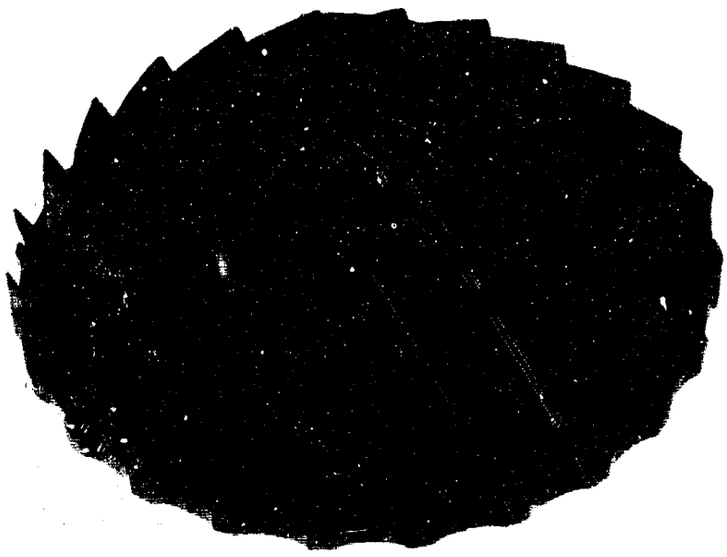

Figure 976. Disassembly View of Fuel Pump 1st-Stage Impeller Showing Good Condition FE 100919

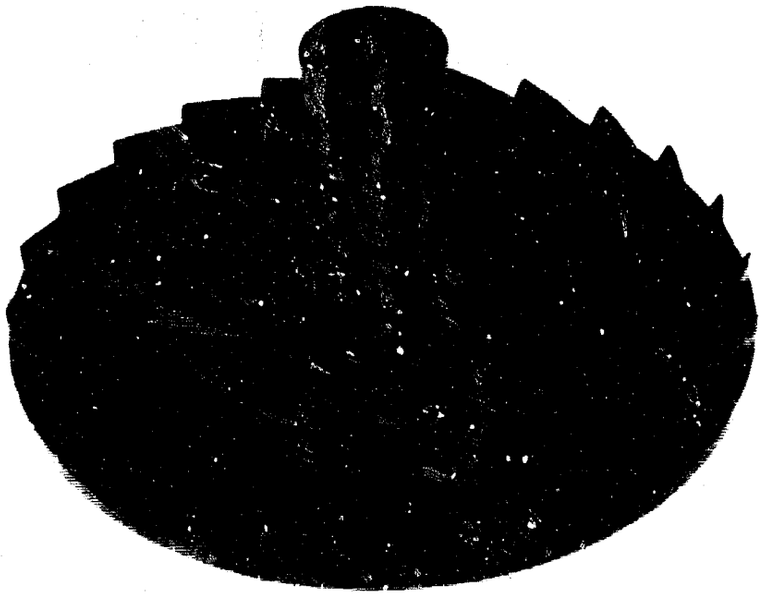

Figure 977. Disassembly View of Fuel Pump 2nd-Stage Impeller Showing Good Condition FE 100918

The transition case inspection showed no damage, except for the centerball distortion described previously and shown in figure 966. The preburner injector condition was unchanged from the pre-hot turbine test condition as shown in figure 978. The transpiration cooled preburner liner was in excellent condition as shown in figure 979. The oxidizer pump simulator showed no major discrepancy except for a circumferential crack in the inside diameter turnaround duct. Preliminary inspection revealed that the crack apparently was initiated at an instrumentation hole. Subsequent dimensional inspection of the cracked duct revealed the wall thickness averaged 0.045 in. or 0.010 in. under the minimum requirement.

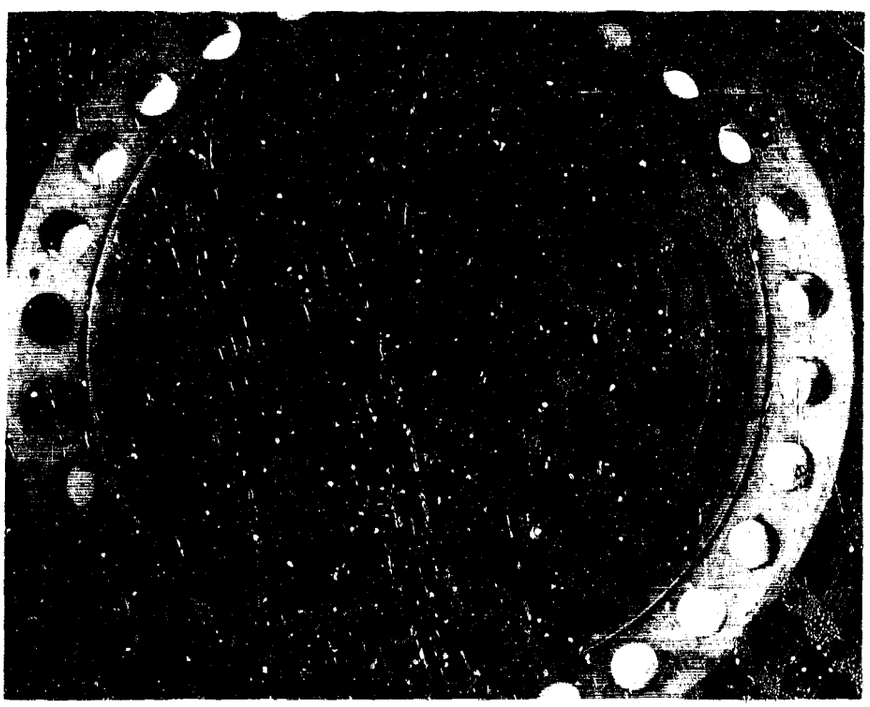

Figure 978. Disassembly View of Preburner Injector Showing Good Condition FE 100697

Data analysis of the hot turbine fuel pump tests has demonstrated that the preburner operated as predicted and that the temperature profile was better than the cycle requirement. At an average combustion temperature of 2325°R (100%, r = 7) the preburner profile requirement was 150°R, and during test No. 5.02 with an average combustion temperature 2405°R the temperature profile was 126°R as measured at the oxidizer turbine simulator. The recorded temperature profile at 100%, r = 5 and 6 was 65°R and 94°R, respectively. At the 50%, r = 5 level the measured temperature profile was 44°R. These profiles are based on temperatures recorded on four temperature rakes with three thermocouples on each rake that were installed in the oxidizer turbine simulator. No temperature rakes were used on the fuel turbine because of the potential damage to the turbine in the event of structural failure of a temperature rake. Performance analysis of the fuel turbopump test data shows that the overall pump performance exceeds the design goals and agrees closely with the B-6 test results on this fuel turbopump assembly, F35147. Figure 980 shows the predicted pump pressure rise vs inlet flow map and the test data from the

turbopump rig tests and hot turbine tests. Figure 981 is a plot of overall pump efficiency vs inlet flow showing the design point and the test data from these tests. Figure 982 shows the overall unit head vs inlet unit flow with the design point and the engine cycle requirements and the test data from these three tests. Figure 983 shows the turbine efficiency vs velocity ratio recorded on these tests. The axial thrust balance was satisfactory at all speeds and flowrates, and the thrust unbalance was toward the pump inlet at all speeds and flowrates. The greatest unbalance condition utilized approximately 45% of the thrust balance piston capability as shown in figure 984. Vibration data analysis showed that the maximum vibration levels recorded on the hot turbine test rig were of the same order of magnitude (less than 10 g) as was recorded on the fuel turbopump rig tests on the B-6 test facility. Table CIX is a summary of the six hot firing tests conducted on the hot turbine test rig.

Figure 979. Disassembly View of the Preburner Combustion Chamber Showing the Good Condition of the Transpiration Cooled and Uncooled Liners FE 100700

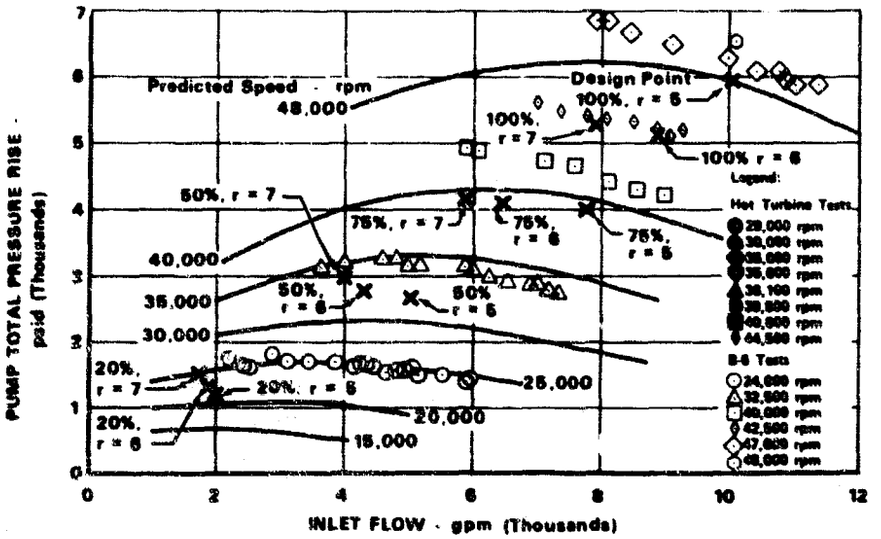

Figure 980. Pump Pressure Rise vs Inlet Flow, Rig F35155 FD 41270B

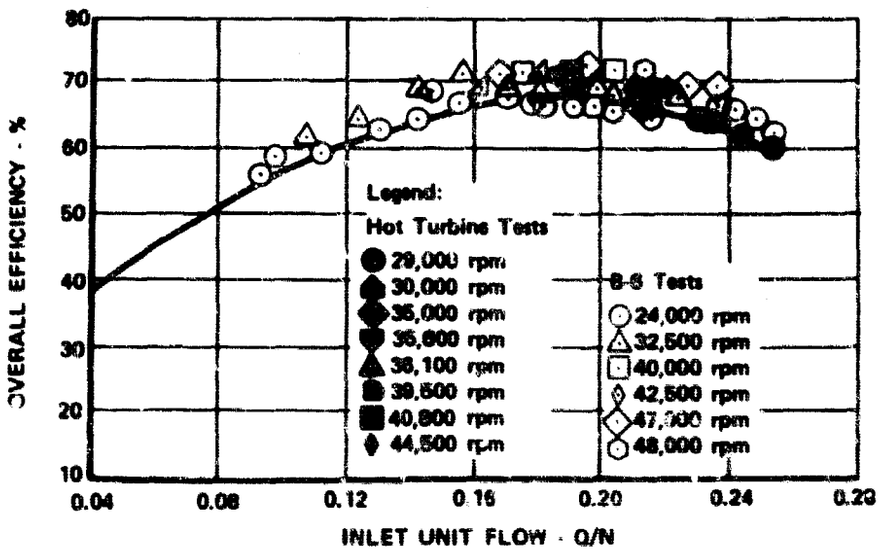

Figure 981. Overall Pump Efficiency vs Inlet Flow, Rig F35155 FD 42267C

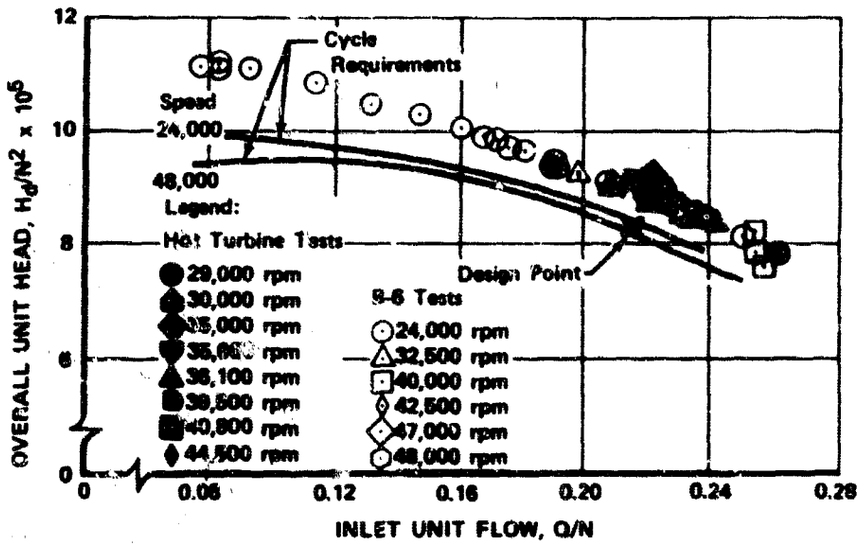

Figure 982. Overall Unit Head vs Inlet Unit Flow, Rig F35155 FD 34745C

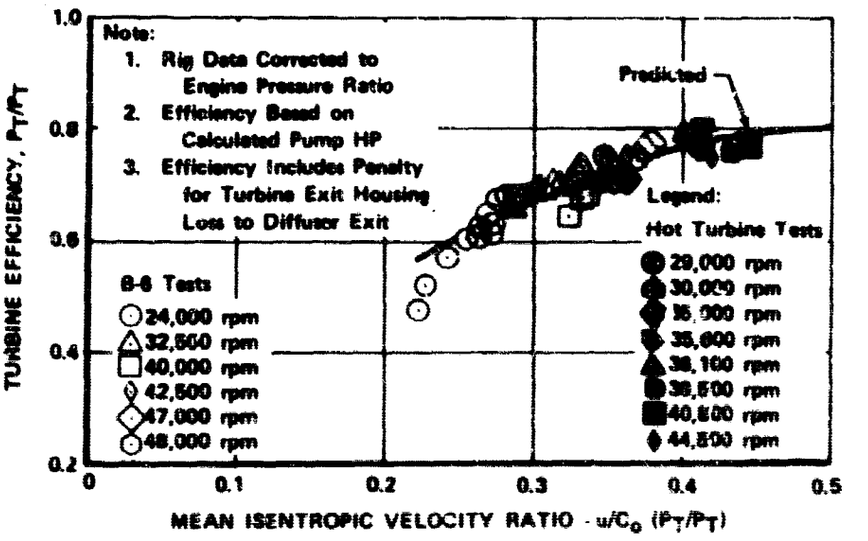

Figure 983. Turbine Efficiency vs Velocity Ratio, Rig F35155 FD 34753C

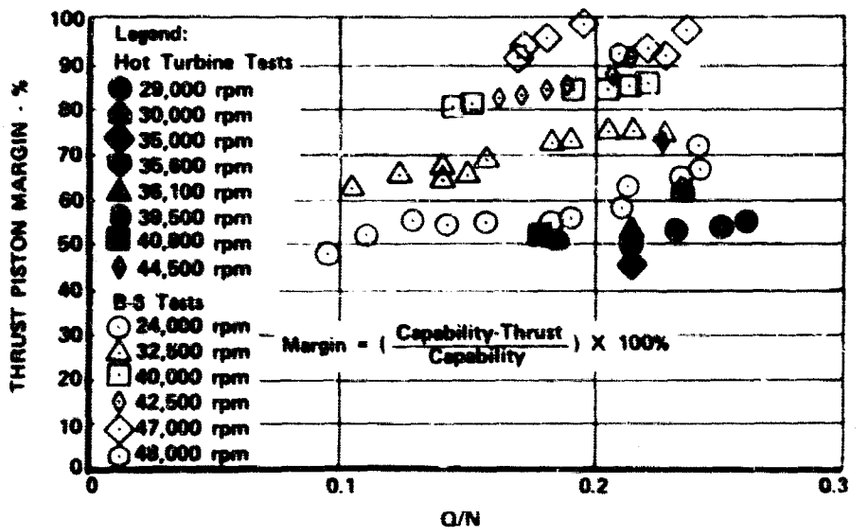

Figure 984. Thrust Balance Margin vs Inlet Unit Flow, Rig F35155 FD 42862C

Table CIX. Summary of Hot Turbine Test Rig Data

Run	Thrust Level Percent	Engine Mixture Ratio	Average Combustion Temperature Based on Average Mixture Ratio (°R)	Preburner Chamber Pressure (psia)	Pump Discharge Pressure (psia)	Pump Speed (rpm)	Pump Inlet Flow (gpm)	Comments
1.02	50	5	1,450	1,868	2,340	29,360	7,400	Full duration test of 13.7 seconds. Rig in good condition.
2.01								False high main case liner differential pressure advance at 6.4 seconds.
3.01	75	5	1,605	2,970	3,610	35,630	7,530	False high main case skin temperature advance at 14.5 seconds.
4.01	75	5	1,615	2,965	3,560	35,330	7,460	False high main case skin temperature advance at 17.2 seconds.
	75	6	1,985	2 882	3,369	34,610	7,310	
5.02	75	5	1,610	3,045	3,737	36,500	7,540	Full duration test of 22 seconds. Rig in good condition.
	100	6	2,070	4,086	4,981	40,900	7,651	
	100	7	2,395	3,889	4,623	39,500	7,422	
6.01	50	7	2,115	1.612	2,423	30,000	7,076	False loss of pump speed advance at 20 seconds. Rig in good condition.
	100	5	1,912	4,200	5,554	44,500	9,956	

SECTION VIII
ENGINE INTEGRATION

A. INTRODUCTION

The staged combustion, high pressure deomonstrator engine with a two-position bell nozzle is a 250,000-lb thrust (class), throtteable, high-performance rocket propulsion system.

Integra ion of the system is accomplished by the interconnection of the major engine components for the transfer of fuel and oxidizer by use of plumbin and seals designed for high pressure application.

B. PLUMBING

1. Introduction

Reusable high-pressure rocket engine plumbing must incorporate many features not common to previous plumbing designs. Specifically, the XLR129 high-pressure plumbing must be:

1. Flexible - To allow for dimensional changes as a result of pressure, temperature thrust, and tolerance stack up of components. All rocket engines are subjected to the same dimensional changes; however, when operating pressures reach 6000 psia, these changes are magnified.

2. High Strength and Lightweight - Operating pressures of the XLR129 require use of high-strength Inconel 718 and others rather than aluminum used extensively on previous state-of-the art rocket engines.

3. Capable of Being Assembled in the Field with Ease - Engine life and reusability requirements coupled with philosophy for component replacement and engine maintainability demand field assembly type plumbing.

4. Capable of Snap Fit for Flange Assembly - Flow mismatch must be held to a minimum; therefore, requiring some foolproof positive centering feature for all mating parts.

Previous state-of-the-art plumbing design criteria fell short of the XLR129 requirements; therefore, requiring the necessary ground work to be accomplished before design could proceed with confidence. Through vendor coordination and in-house fabrication studies, the design approach and guide lines were verified.

High-Pressure (up to 6000 psi) plumbing was designed by: (1) avoiding the use of hot (turbine gas temperature) external lines; and (2) selecting Inconel 718 (AMS 5663) high-strength tube material, not only for lowest weight, but to ensure tube walls thin enough to realize a useful amount of tube flexibility with reasonable tube lengths. The engine transition case houses the only hot line on the engine, and consists of an unrestrained Y-duct connecting the preburner outlet with the main turbine inlets. Gas leakage at these slip joints is internal and the adverse thermal and pressure growth effects normally associated with external plumbing are completely avoided.

The clean sheet design approach proved unsatisfactory for the XLR129 high-pressure plumbing. Plumbing design became an irrelative process where (1) requirements were established (pressure, flow and temperature), (2) inlet and exit diameters compatible with mating components were selected, (3) preliminary line was routed on the engineering mockup, (4) interference with other lines or components was resolved, (5) preliminary layout was completed, (6) preliminary end point moments were established using computer program, (7) if moment values were excessive (beyond capability of mating component, the line or flange) configuration changes were made and evaluated as described in (3) through (7) above, (8) after obtaining satisfactory results from preliminary layout, a detail design was completed and evaluated. Figures 985, 986 and 987 shows the engineering mockup used during the process described above.

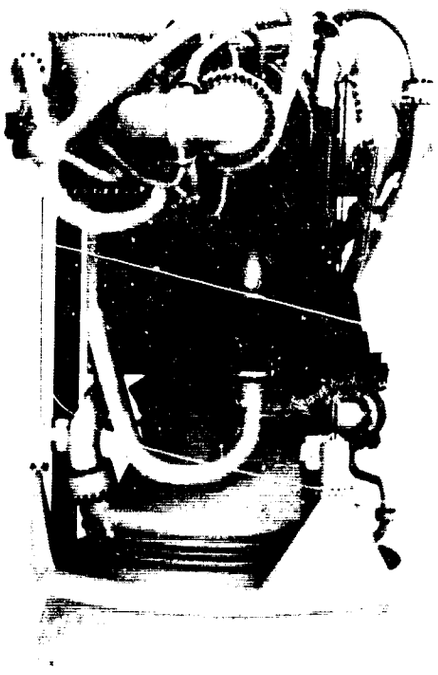

Figure 985. XLR129 Engine Plumbing, View 1 FE 92413

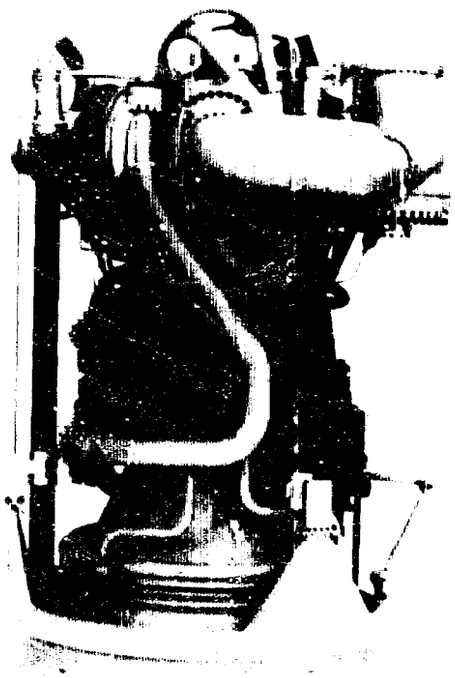

Figure 986. XLR129 Engine Plumbing, View 2 FE 92410

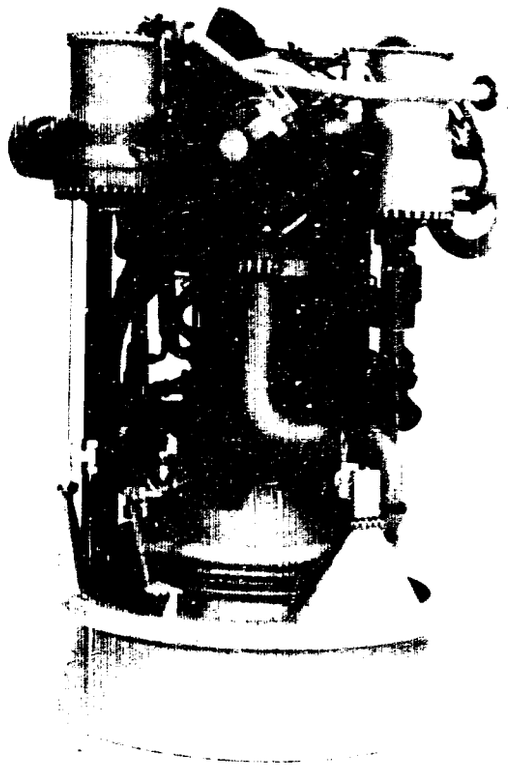

Figure 987. XLR129 Engine Plumbing, View 3 FE 92415

2. Summary, Conclusions and Recommendations

Layout design was completed on all plumbing lines; detail design was completed on the preburner fuel line, fuel pump discharge lines and small line connectors and boss connector.

Fabrication, inspection, and hydrostatic pressure testing was completed for the preburner fuel line. Detail design and fabrication of remaining lines was terminated because of program redirection.

Engine plumbing can be fabricated so that all engine requirements are met within the 290 lb allowable weight assigned to the plumbing. Flange design and tube stress analysis requires particular care to ensure the deflections do not exceed 0.002 in. (total) at the flange seal. Tube routings were chosen to accomplish this feature. Selective redesign of engine component flanges will provide more attractive and lighter weight (overall) plumbing. Allowable moment capacity of flanges must include considerations for plumbing lines during the initial designs. Also flange location on components should be adjusted to provide the minimum plumbing length and maximum accessibility for installation and maintenance.

3. Hardware Description and Fabrication

a. Preburner Fuel Line

The preburner fuel line supplies high-pressure hydrogen from the exit of the regeneratively cooled section of the primary nozzle to the preburner injector. Figure 988 shows the line configuration. Features of the line are:

1.	Maximum operating pressure	5123 psia
2.	Design point flowrate	76.5 lb/sec
3.	Design point temperature	177°R
4.	Nominal inside diameter	3.8 in.
5.	Minimum allowable wall thickness	0.1 in.
6.	Nominal wall thickness (straight section)	0.14 in.
7.	Bend radius/diameter	1.62
8.	Calculated maximum pressure loss	21 psid
9.	Fluid velocity	
	Large End	280 ft/sec
	Small End	450 ft/sec
10.	Maximum tube stress	90% of 0.2% yield at 1.5 times maximum design pressure

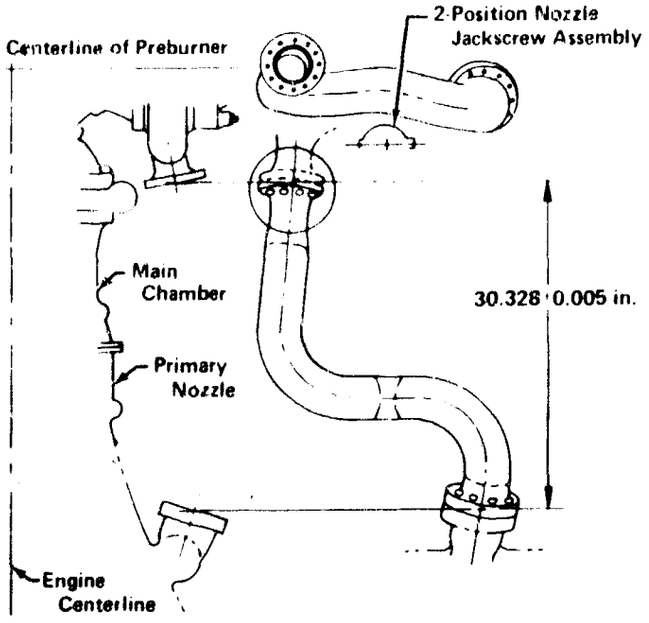

Figure 988. Preburner Fuel Line FD 46877

The preburner fuel line was fabricated from welded and drawn Inconel 718 (AMS 5663) tubing. Prior to the final stages of fabrication, material testing was conducted to confirm properties of the welded and drawn tubing. Routine acceptance tests were performed on the tubing to ensure all P&WA specifications had been fulfilled, and to verify the exceptions taken to the P&WA specification did not cause larger-than-predicted reductions in material properties. Specifically, the P&WA specification calls for 50% reduction in cross sectional area during the drawing process and the tube fabrication vendor could guarantee only 20% reduction. P&WA's materials personnel estimated a 10% reduction in material properties (in the weld) due to the decrease in percentage of cross sectional area during drawing.

Microstructure analysis was performed and the grain structure was fully recrystallized with only very slight evidence of cold work. No ETA phase was present. ETA phase appears as a needle-like phase in the microstructure and is an orthorhombic Ni_3 Cb structure. It is not coherent with the matrix as is the gamma prime Ni_3 (Al, Cb) structure and can cause loss of strength and ductility if present in excessive amounts. ETA phase can be caused by too low solution heat treat temperature or overaging.

Tensile tests were conducted to compare the tensile strength across the weld with that of the parent material. Circular rings were cut from the tubing as shown in figure 989a and b. The rings were cut so the welds would be centered.

The samples were flattened, as shown in figure 989d solution heat treated for 1 hour at 1900°F, precipitation heat treated as follows:

1. Heat to 1785°R ± 15°
2. Hold at heat for 8 hours
3. Furnace cool at a rate of 100° ± 15°/hr. to 1610°R ± 15°
4. Hold at 1610°R ± 15° for 8 hours
5. Air cool to room temperature.

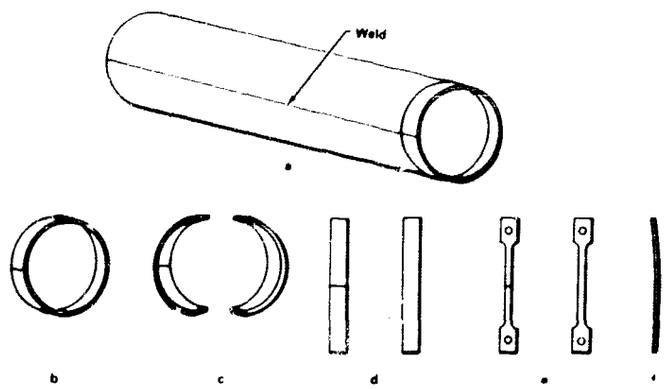

Figure 989. Tensile Test Rings Cut From Tubing FD 38222

Test samples were cut as shown in figure 989c. The specimens retained a slight curvature after flattening as illustrated in figure 996f.

The results of the tensile test shown in table CX indicated the weld was equal to the yield and ultimate tensile strength of the parent material, yet both were below the minimum acceptable strength of 160,000 psi.

Table CX. Tensile Strength Comparison

	Yield Strength (ksi)	Ultimate Tens. Strength (ksi)	Elongation (%)
Welded Material	138.3	171.5	13.5
	135.2	165.2	12.0
	139.6	162.8	7.0
	137.7	170.3	13.5
Parent Material	133.2	173.3	21.5
	129.0	168.9	24.5
	132.7	172.6	23.0
	126.6	168.5	22.5

To ensure the yield and ultimate tensile strength of the tubing is above the minimum requirements of P&WA specification, samples were taken parallel to the tube axis as shown in figure 990. Two of the samples were solution heat treated for one hour at 2210°R, and the other one at 2360°R. They were then precipitation heat treated as previously described in this section. One of the 2210°R samples was through the weld. Tests indicated that the material was within specification. The results were as shown in table CXI.

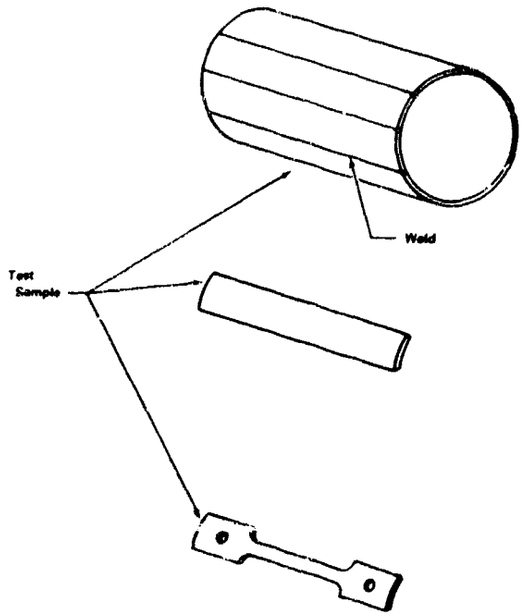

Figure 990. Tensile Test Samples Cut From Tubing FD 38223

Table CXI. Tubing Tensile Strength

	Yield Strength (ksi)	Ultimate Ten. Strength (ksi)	Elongation (%)
2360°R	161.3	189.3	24
2210°R	161.5	190.5	23.5
Weld (2210°R)	162.7	190.8	7.0

Comparing the results of circular rings (flattened as shown in figure 989) table CX with axial samples (figure 990) table CXI, the axial strength appears much higher. However, the material properties shown in table CXI were throught to be degraded due to the flattening process. At the time of these tests, this was just an assumption and required verification.

To ensure the material had the required strength in both directions, samples were taken from the sheet stock in two directions perpendicular to each other. These samples were heat treated and tested in a manner similar to the other samples. The results of these tests indicated the material exceeded the minimum requirements in both directions.

These tests do not rule out the possibility of reduced properties occurring during the drawing or bending operation, and hydrostatic testing is the only way to verify the final tube properties.

The final test performed to verify the material properties was hydrostatic testing of the final tube assembly to 7500 psi. This pressure is 1.5 x maximum cycle pressure at 100% thrust when adjusted for temperature (test was performed at room temperature as opposed to the operating temperature of 177°R). During hydrostatic testing, the tube end points were restrained and circumferential plastic strain was measured and found to be less than 0.2% (0.002 in./in.) as required.

The test was successful; therefore, verifying all material properties and minimum wall thickness requirements were within specification. The final tube assembly was inspected by P&WA and found to be completely withing specification tolerances. The actual tube wall thickness (minimum) in the bends was of particular interest. The minimum allowable was 0.100 in. and the minimum measured was 0.114 in. The wall thickness reduction (in the bends) was 18.5% maximum as compared to the estimated reduction of 28.5%. The completed tube assembly is shown in figure 991.

Figure 991. Preburner Fuel Line, Curved Section FE 10592

b. Fuel Pump Discharge Lines

The main fuel pump discharge plumbing features two 2nd-stage diffuser outlets merged together at a Y-section downstream. The combined flowpath curves around the downstream end of the main burner chamber, passes through the preburner fuel valve, and enters the primary nozzle inlet manifold. The routing most suitable to the engine creates unequal geometry pipe segments upstream of the Y-fitting. It is, therefore, expedient to introduce an orifice plate within the shorter segment to balance the individual diffuser flows. Features of these lines are:

1.	Maximum operating pressure	5610 psia
2.	Design point flowrate	99.5 lb/sec
3.	Design point temperature	139°R

Line inside diameters are shown in figure VIII-8.

4.	Minimum allowable wall thickness	
	Small lines	0.073 in.
	Large lines	0.107 in.
5.	Nominal wall thickness	
	Small lines	0.100 in.
	Large lines	0.152 in.
6.	Bend radius/diameter	
	Small lines	1.5 minimum
	Large lines	1.5 minimum
7.	Calculated maximum pressure loss	55 psid
8.	Maximum tube stress	90% of 0.2% yield at 1.5 times maximum design pressure

The general arrangement of this assembly is shown in figure 992. The material selected for the tubes was Inconel 718 (AMS 5663) welded and drawn. Detail design was completed on this assembly; however, due to program redirection, it was not fabricated.

c. Oxidizer Pump Discharge Lines

The oxidizer pump discharge lines are part of a welded assembly consisting of the oxidizer pump volute housing, two diffuser sections and both discharge lines, which are joined at a spherical housing referred to as the collector. The collector is located at the turbine inlet of the oxidizer low-speed inducer and serves as a manifold to receive the flow of oxidizer from the pump and to direct a portion of the pump discharge flow to the preburner injector and the supply for the oxidizer pump thrust piston. Welded joints were used rather than bolted

flanges (where possible) to provide minimum weight design. This procedure afforded a weight saving of approximately 20 lb. Two flanged joints are required, however, these being at the collector/inducer interface and near the collector to connect with the preburner oxidizer supply line.

Features of the line are:

1.	Maximum operating pressure	6000 psia
2.	Design point flowrate	408 lb/sec
3.	Design point temperature	244°R
4.	Line inside diameters - as shown in figure VIII-9	
5.	Minimum allowable wall thickness	0.095 in.
6.	Nominal wall thickness	0.135-0.145 in.
7.	Bend radius/diameter	1.5 minimum
8.	Calculated maximum pressure loss	25.4 psid
9.	Maximum tube stress	90% of 0.2% yield at 150% maximum design point

These lines are shown in figure 993. Inconel 718 (AMS 5663) welded and drawn tubing was selected as material to be used for the tubing. Program redirection stopped work on this assembly prior to completion of detail design.

d. Preburner Oxidizer Supply Line

The preburner oxidizer supply line directs liquid oxygen from the oxidizer pump discharge to the preburner oxidizer control valve. The tube size was selected to match the inside diameter of the mating components. Inconel 718 (AMS 5663) welded and drawn tubing was again chosen for the line material. Features of the line are:

1.	Maximum operating pressure	5919 psia
2.	Design point flowrate	82 lb/sec
3.	Design point temperature	244°R
4.	Nominal inside diameter	1.925 in.
5.	Minimum allowable wall thickness	0.065 in.
6.	Nominal wall thickness (straight section)	0.100 in.
7.	Bend radius/diameter	1.5 minimum

8.	Calculated pressure loss	6.2 psid
9.	Maximum tube stress	90% of 0.2% yield at 150% design pressure

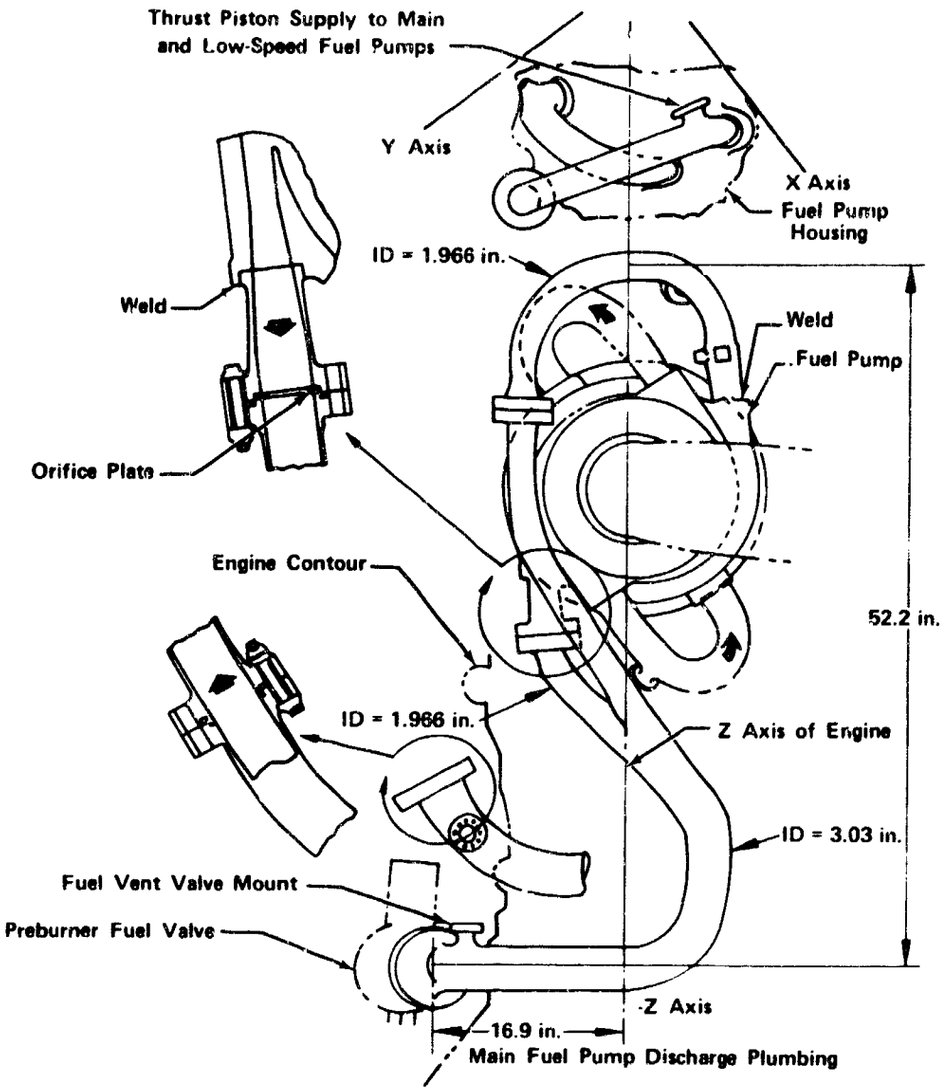

Figure 992. Main Fuel Pump Discharge Plumbing FD 46880

The line configuration is shown in figure 994. Detail design and fabrication were prevented by program redirection.

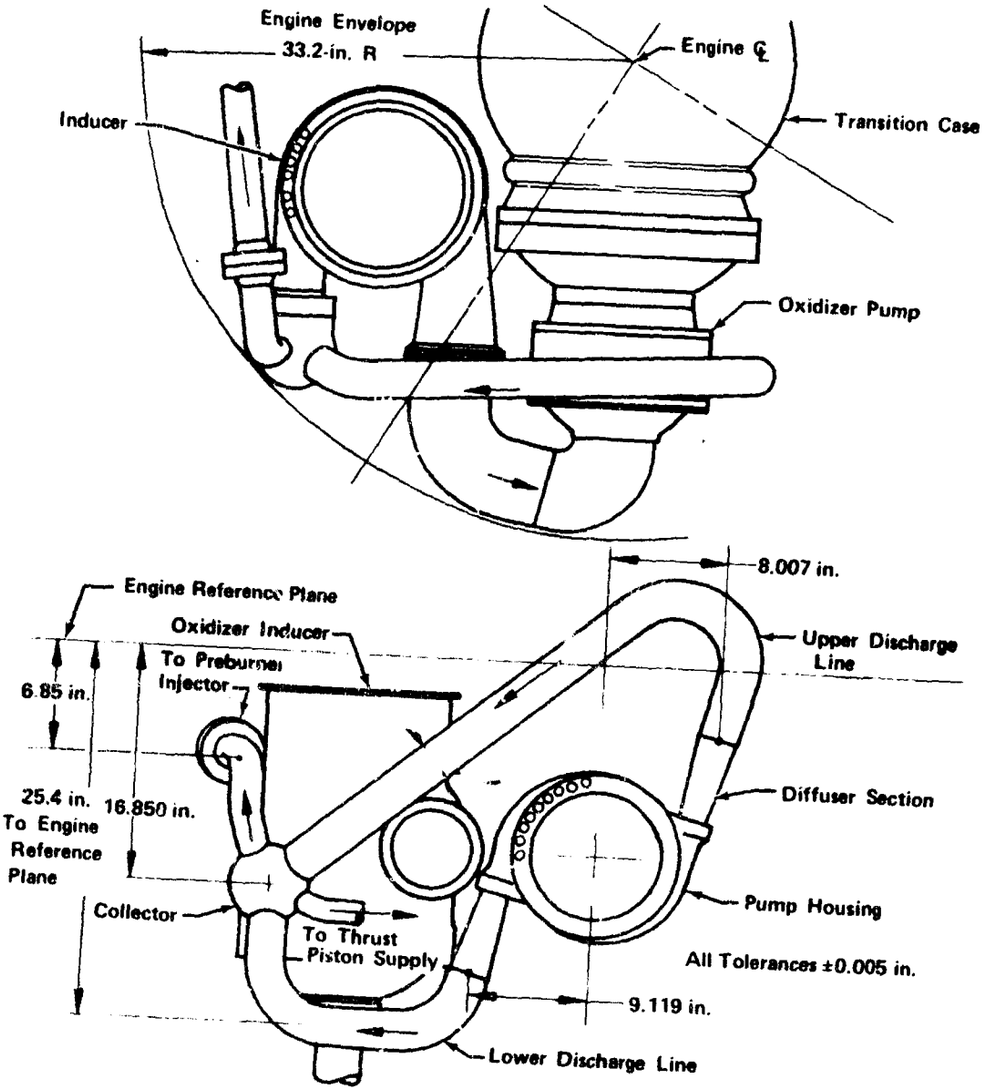

Figure 993. General Arrangement of Oxidizer Pump Discharge Lines With Oxidizer Low-Speed Inducer FD 46881

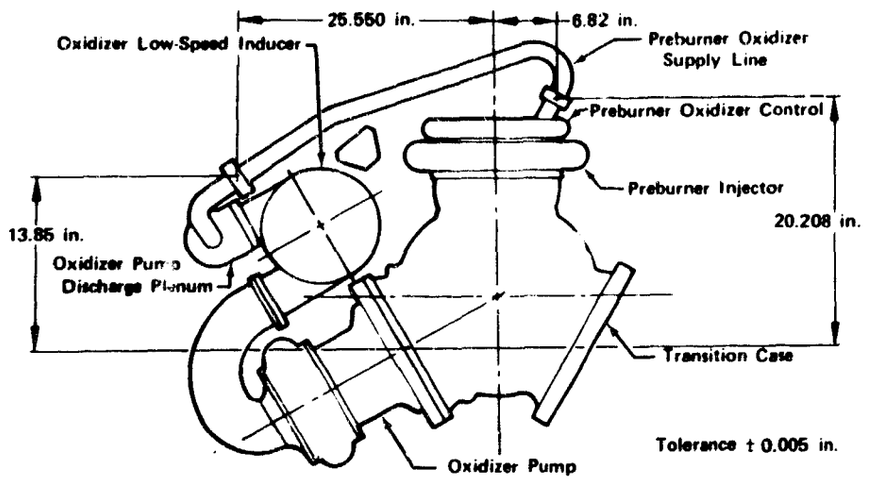

Figure 994. Preburner Oxidizer Supply Line FD 37046

e. Main Burner Oxidizer Line

The main burner oxidizer line conducts high-pressure liquid oxygen from the oxidizer low-speed inducer turbine discharge to the main burner control valve. The material selected for the tube design was Inconel 718 (AMS 5663) welded and drawn. Features of the line are:

1.	Maximum operating pressure	4800 psia
2.	Design point flowrate	370 lb/sec
3.	Design point temperature	244°R
4.	Line inside diameter	2.850 in.
5.	Minimum allowable wall thickness	0.082 in.
6.	Nominal wall thickness	0.117 in.
7.	Bend radius/diameter	1.5 minimum
8.	Calculated maximum pressure loss	26 psid
9.	Maximum tube stress	90% of 0.2% yield at 1.5 maximum design pressure

The line configuration is shown in figure 995. Detail design and fabrication were prevented by program redirection.

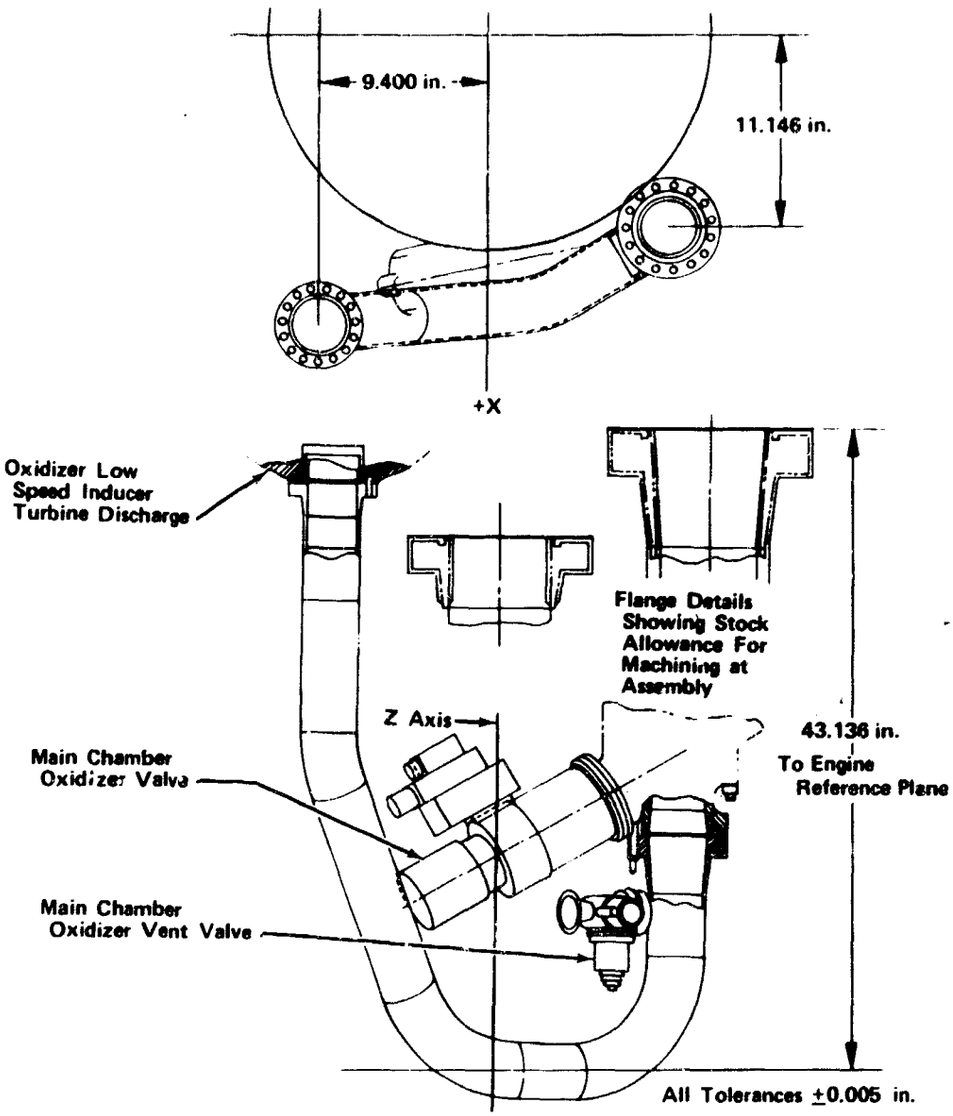

Figure 995. Main Burner Oxidizer Supply FD 46883

f. Fuel Turbopump Inlet Line

The fuel turbopump inlet line design consists of a flanged circular straight section that attaches to the fuel low-speed inducer flange, a circular-to-elliptical section contoured to match the 66.4 in. diameter engine power head envelope, and a final curved elbow of complex shape.

The exit portion of this line contains a series of splitter vanes to achieve a uniform velocity profile with low flow loss, and avoid possible cavitation.

These vanes are designed per the SAE Aerospace Applied Thermodynamics Manual and the method adapted to liquid flow in circular pipes. The elbow and turning vane concept has been evaluated in testing performed by Pratt & Whitney Aircraft and reported in Section IV, Paragraph C of this report.

The pipe section was designed in two half-sections with a vertical web in the center. The web thickness was determined by the internal pressure tending to deform the ellipse into a circular section and using a 1.5 safety factor throughout. Inconel 718 (AMS 5663) was chosen for the material. The features of the line are:

1.	Maximum operating pressure	140 psia
2.	Design point flowrate	90.31 lb/sec
3.	Design point temperature	47°R
4.	Inside diameter at low speed inducer discharge	5.988 in.
5.	Inside diameter at fuel pump inlet	6.676 in.

The line configuration is shown in figure 996. Detail design and fabrication were prevented by program redirection.

g. Oxidizer Turbopump Inlet Line

The inlet pipe to the oxidizer turbopump shown in figure 997 conducts low-speed inducer discharge flow to the inlet of the main pumps with minimum velocity distortion, low pressure loss, and without cavitation. This line incorporates the special feature of a curcular manifold for injecting various recirculation or return flows back into the main pump inlet with minimum flow disturbance.

The design incorporates vanes over a large portion of the total length, primarily because of the inherent requirement to turn the flow through a total angle of 180 deg. This design condition is dictated by engine envelope restraints.

The distinctive mechanical feature of the oxidizer inlet duct is that it is made integral with the oxidizer turbopump inlet housing.

The material used is Inconel 625. The design temperature, pressure and flowrate is 204°R, 267 psia and 619 lb/sec, respectively. Further description is contained in Section V, paragraph G, Oxidizer Turbopumps.

h. Fuel Low-Speed Inducer, Turbine Supply Line

The fuel low-speed inducer turbine supply line conducts hydrogen from the transpiration coolant heat exchanger section of the primary nozzle forward to the turbine inlet on the fuel low-speed inducer as shown on figure 998.

Two tapoff T-fittings are incorporated into this line to supply fuel coolant to the engine transition case and provide a turbine bypass flowpath connection. The features of this line are:

1.	Maximum operating pressure	5121 psia
2.	Design point flowrate	5.5 lb/sec
3.	Design point temperature	408°R
4.	Line inside diameter	1.08 in.
5.	Minimum allowable wall thickness	0.041 in.
6.	Nominal wall thickness	0.072 in.
7.	Bend radius/diameter	1.5 minimum
8.	Calculated maximum pressure loss	34.8 psid
9.	Maximum tube stress	90% of 0.2% yield at 1.5 times maximum design pressure

Inconel 718 (AMS 5663) welded and drawn tubing was used for the design. Detail design and fabrication was prevented by program redirection.

i. Primary Nozzle Fuel Supply Line

The transpiration coolant section of the primary nozzle receives its supply by opening the preburner fuel valve and uncovering a port in the side of the valve. Hydrogen then passes through the subject tube to the transpiration coolant heat exchanger section of the primary nozzle. A special orifice is incorporated at the nozzle interface to balance the fuel flow system with no external power accessory installed on the fuel low-speed inducer. Near the valve end there is an integral T-fitting to supply coolant flow to the oxidizer pump rear bearing and fuel to each of the igniter assemblies. Feature of this line are:

1.	Maximum operating pressure	5446 psia
2.	Design point flowrate	7.75 lb/sec
3.	Design point temperature	139.3°R
4.	Nominal inside diameter	1.152 in.
5.	Minimum allowable wall thickness	0.034 in.
6.	Nominal wall thickness (straight section)	0.049 in.
7.	Bend radius/diameter	1.5 minimum

8.	Predicted maximum pressure loss (including orifice)	167 psid
9.	Maximum tube stress	90% of 0.2% yield at 1.5 times maximum design pressure

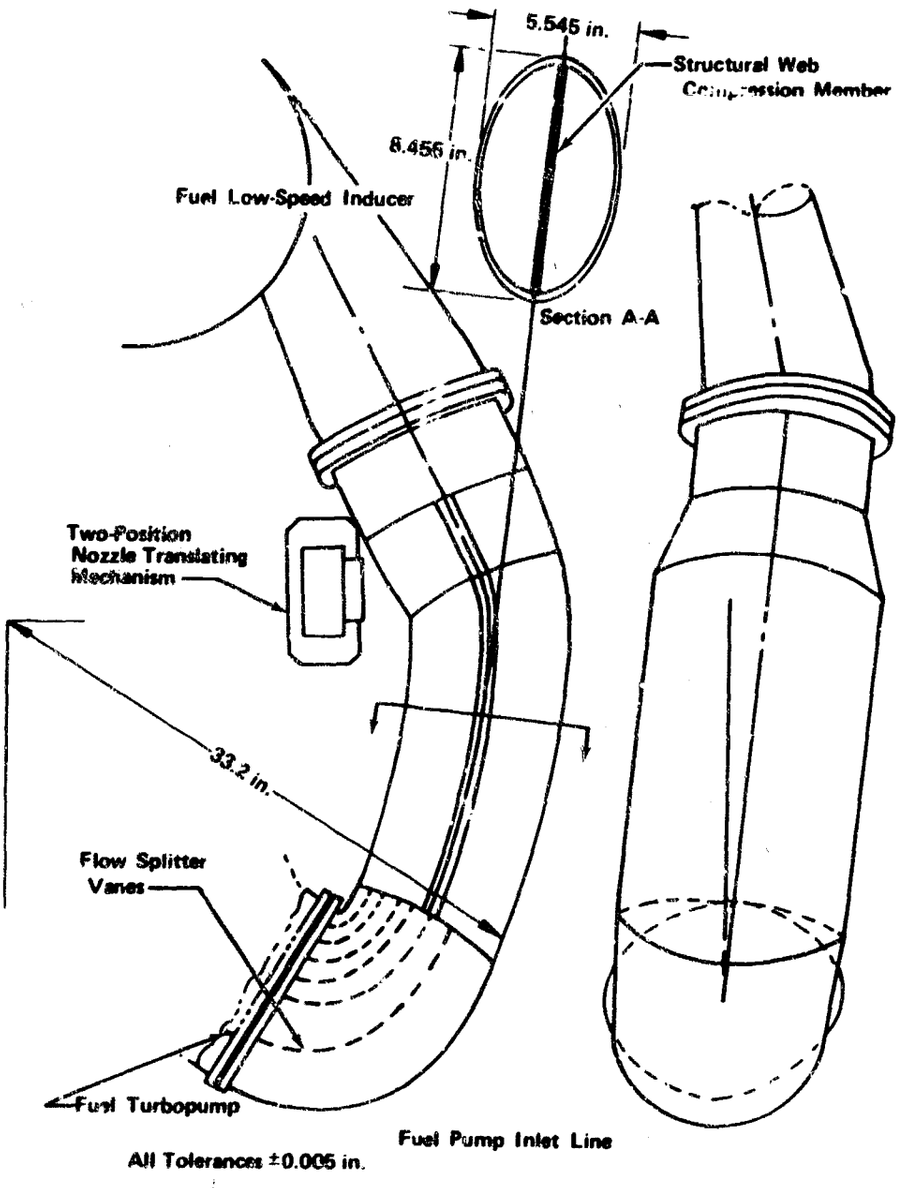

Figure 996. Fuel Pump Inlet Line FD 46884

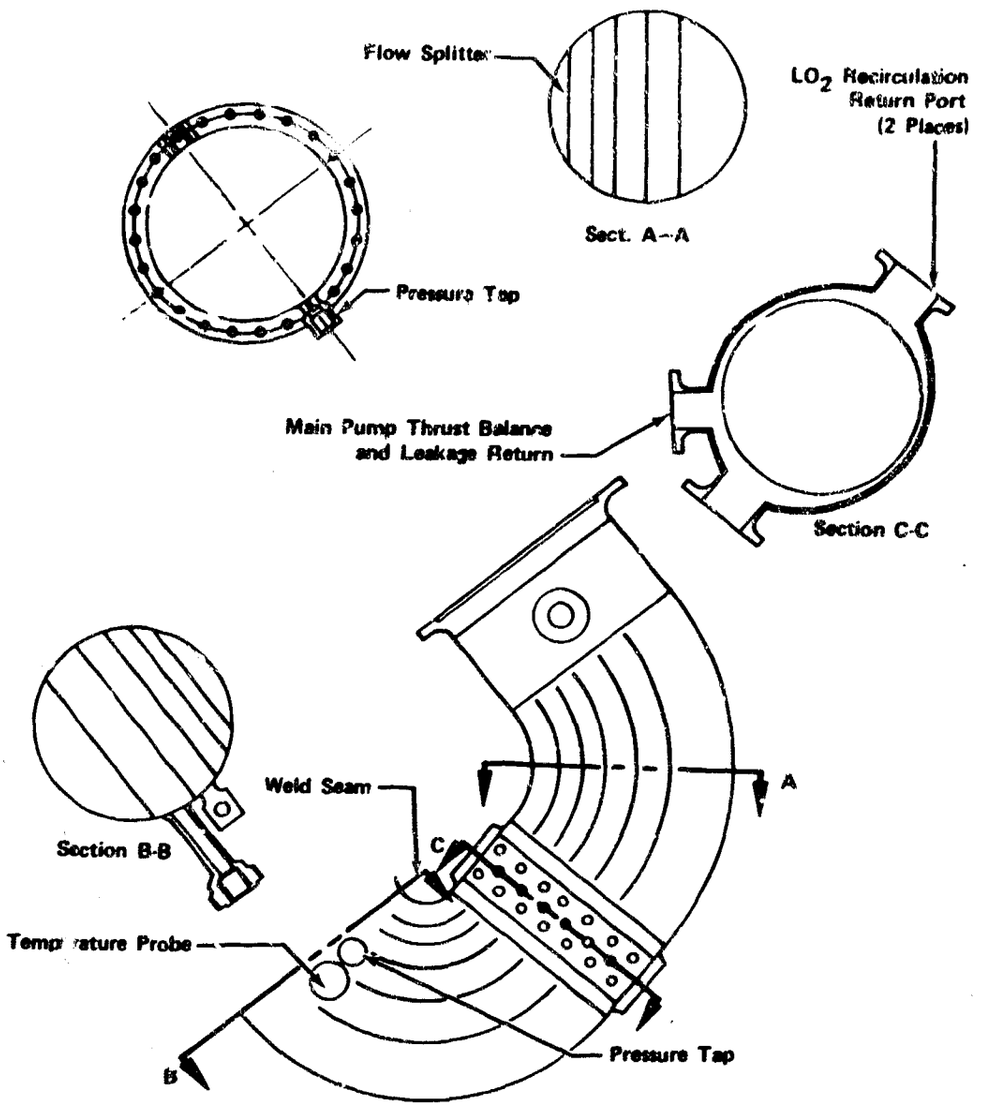

Figure 997. Oxidizer Low-Speed Inducer-to-Oxidizer Turbopump FD 34601

The line configuration is shown in figure 999. Tube outside diameter being less than 1.5 in. allows the use of seamless or welded and drawn Inconel 718 (AMS 5663) tubing for the design. Detail design and fabrication were prevented by program redirection.

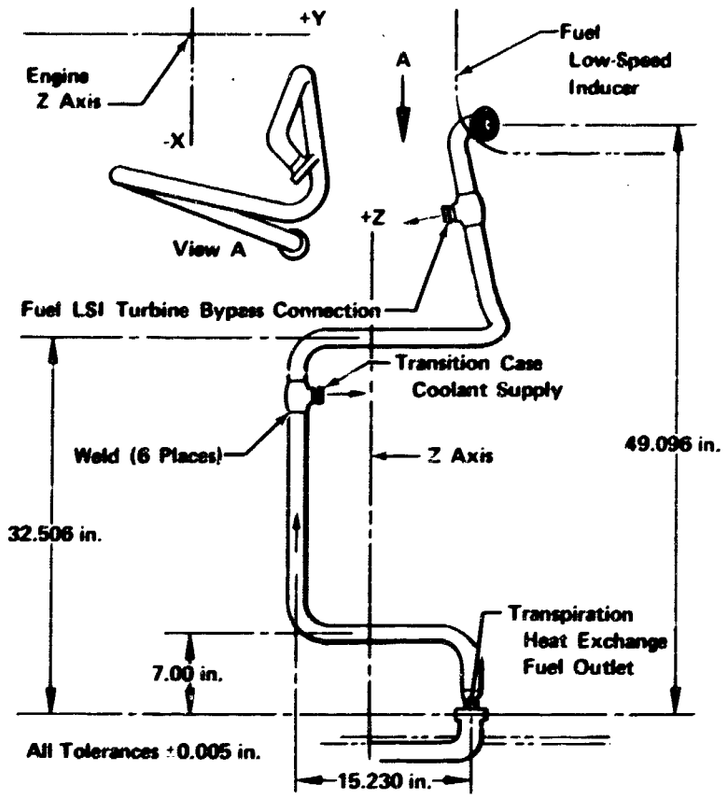

Figure 998. Fuel Low-Speed Inducer Turbine Drive Fuel Supply FD 46886

j. Main Chamber Coolant Supply Line

Fuel coolant to the main chamber is supplied from the discharge of the fuel low-speed inducer turbine. As shown in figure 1000, the upper flange incorporates a 90 deg outlet tee for a 0.750 in. drive turbine bypass tube. Features of the line are:

1.	Maximum operating pressure	3528 psia
2.	Design point flowrate	5.55 lb/sec
3.	Design point temperature	386°R
4.	Nominal inside diameter	1.412 in.
5.	Minimum allowable wall thickness	0.028 in.
6.	Nominal wall thickness (straight section)	0.044 in.
7.	Bend radius/diameter	1.5 minimum

8.	Calculated maximum pressure loss	23 psid
9.	Maximum tube stress	90% of 0.2% yield at 1.5 times maximum design pressure

Detail design and fabrication were prevented by program redirection.

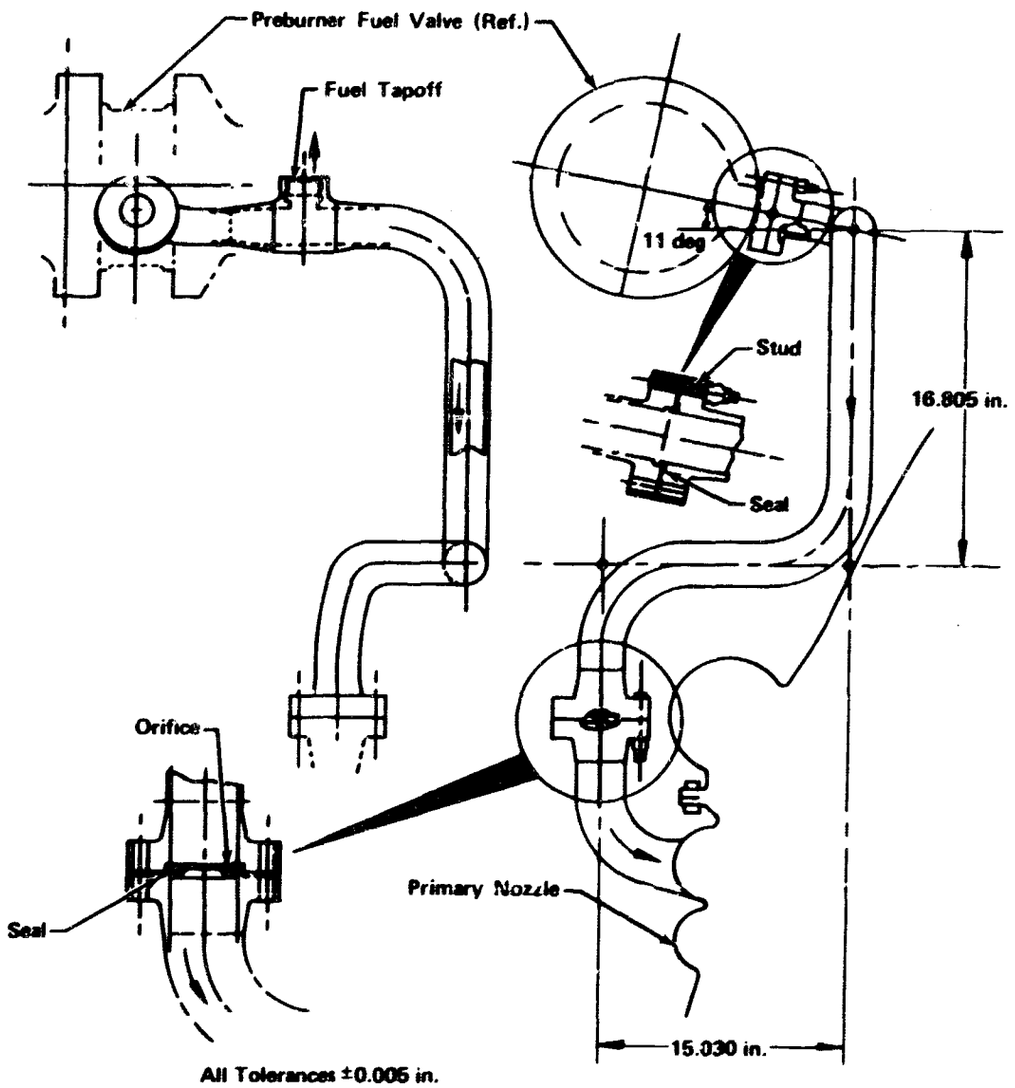

Figure 999. Primary Nozzle Fuel Supply Line FD 46887

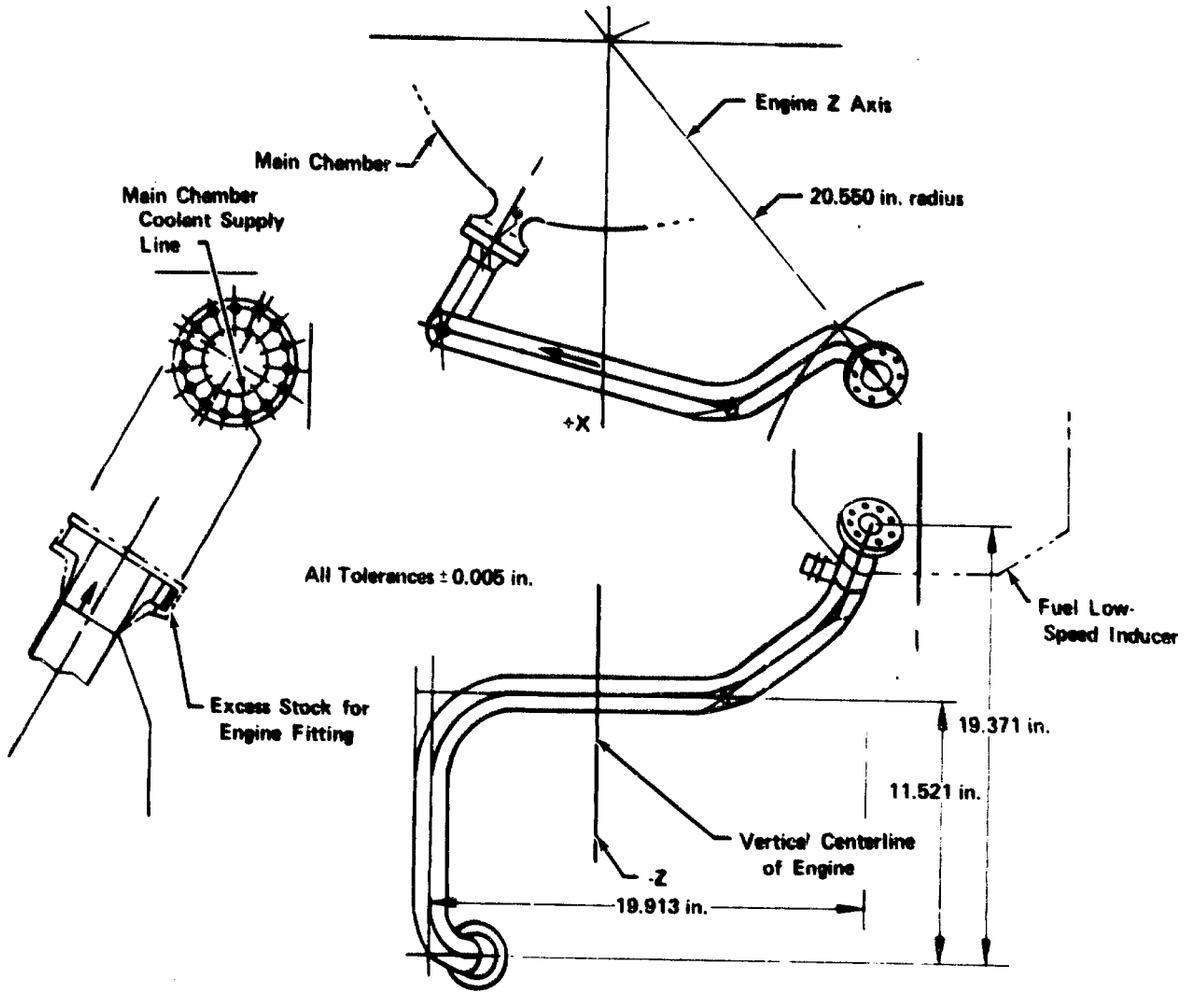

Figure 1000. Main Chamber Coolant Supply Line

FD 46888

k. Small Line Connector

The initial selection effort consisted of a literature search to determine the availability of flightweight commercial connectors rated for XLR129 requirements (up to 6900 psi operating pressure). This investigation resulted in the selection of the AFRPL Threaded Connectors developed by Battelle Memorial Institute.

The existing AFRPL Threaded Connectors were type 347 SST (MS 27850 through 27855) rated for 4000 psi working pressure and 6000 psi proof pressure. The demonstrated leakage rate for these connectors is well below the 10^{-4} sccs required.

Battelle Memorial Institute was contracted to uprate their 347 SST connector design to the program requirements. Operating conditions and structural limits were supplied by Pratt & Whitney Aircraft. These specifications included the nominal tube outside diameter, wall thickness, tube material, operating temperature and pressure, externally applied moments and fatigue limits.

Because the connectors are joined to the tubes by a butt weld, material selection was the first requirement. Inconel 718 (AMS 5663) was selected for both the tubing and fittings because of its high strength and weldability. See figure 1001 for illustration of connector and seal.

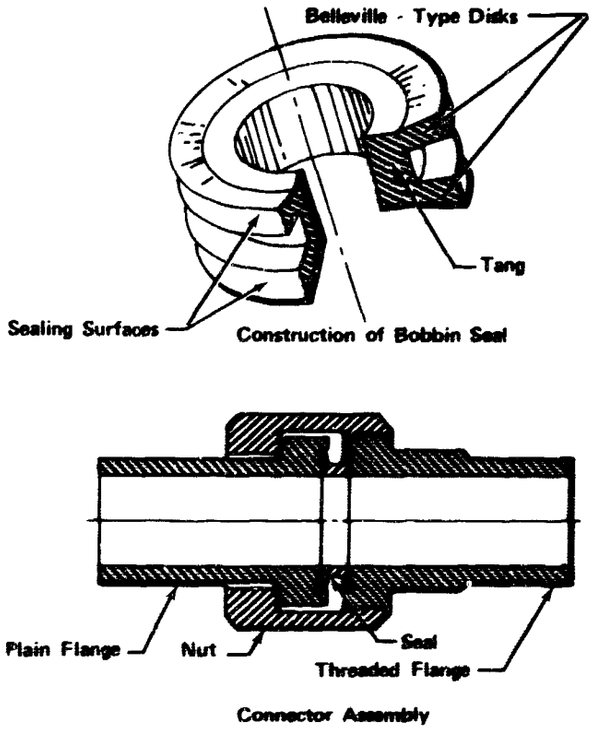

Figure 1001. Connector and Seal FD 34605A

1. Boss Connectors

The need for a 6000 psi tube-to-housing boss connector capable of meeting leakage requirements resulted in the adaptation of the Bobbin Seal and portions of the tube connector to fulfill this requirement. Two designs have evolved; one consists of a semipermanently installed connector which adapts the boss to the line (figure 1002), and the other design in which the flange on the end of the tube is mated directly with the boss (figure 1003). Both designs use the same boss and also the same Bobbin Seal as the high pressure line connector. The boss connector shown on figure 1002 was selected for initial engine design. This selection was made to eliminate the requirement for welded (male) connectors on housings, etc., since repair of these connectors would require reheat treating the Inconel 718 (AMS 5663) material and to make assembly of small lines a simple job rather than one requiring the insertion of a tube into a recessed cavity not visibly accessible. As engine development progresses, a weight reduction and the elimination of one leakage path (seal) can be accomplished by incorporating the design shown on figure 1003.

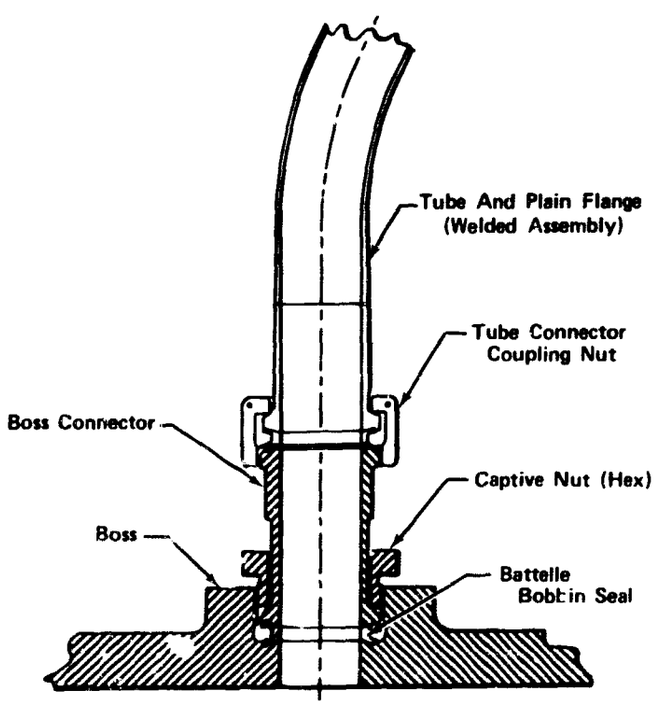

Figure 1002. Inconel 718 High-Pressure Boss Connector FD 34707

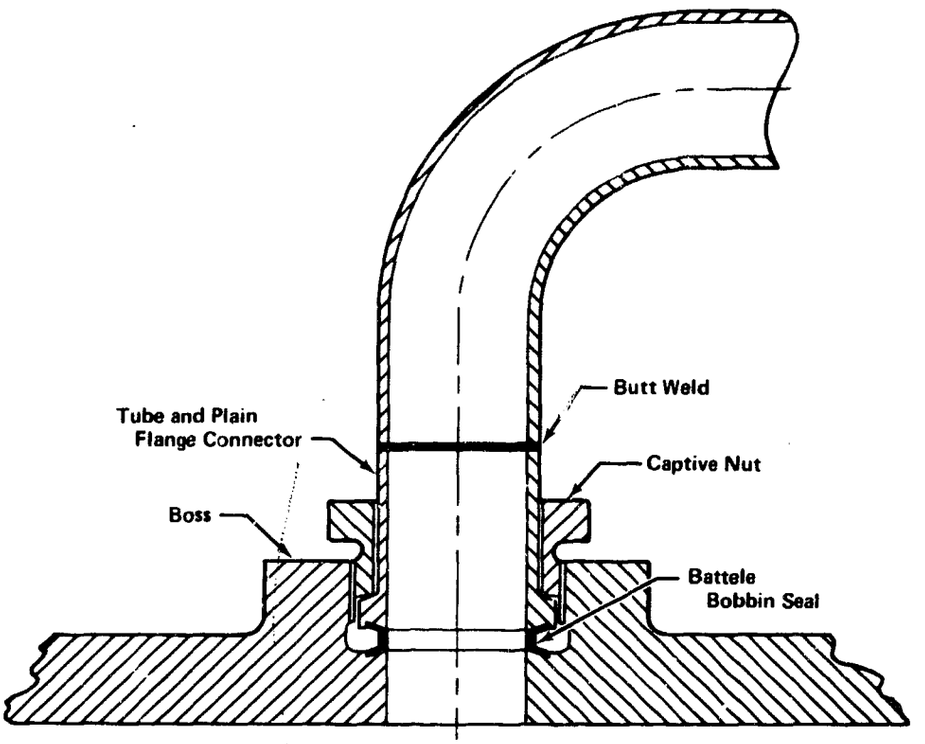

Figure 1003. Alternate Boss Connector FD 46891

C. STATIC SEALS

1. Introduction

During seal rig, component, and stages combustion rig testing conducted in Phase I (Contract AF04(611)11401), excessive overboard static seal leakage was experienced. Dual static seals were incorporated in the rig couplings. The measured primary static seal leakage at maximum thrust during the staged combustion rig test firings was equivalent to an impulse loss of approximately 2 sec, and additional uncontrolled overboard leakage was visible. Static pressure tests with the main chamber oxidizer valve indicated the leakage problem was aggravated by excessive flange separation and inadequate static seals.

Under the demonstrator engine program, extensive high pressure coupling analysis was conducted to establish a lightweight, minimum deflection coupling design. Minimizing flange deflection was necessary to meet the XLR129 leakage goal of 10^{-4} standard cubic centimeters per second (sccs) per inch of seal circumference at pressures up to 7000 psig for 500 pressure cycles. Conventional analysis methods proved inadequate for lightweight high-pressure coupling deflection and weight optimization predictions, so computer analysis programs were developed to assist the designer. A 6 in. aluminum hydrostatic coupling rig was designed and tested for stress and deflection at XLR129 operating pressures. A finite element disk analysis computer program was

then modified to provide satisfactory deflection prediction correlation with the test results. Continued analysis indicated that zero-deflection coupling flanges would not meet the lightweight engine requirement; however, allowing a total deflection of 0.002 in. at the sealing diameter would significantly reduce coupling weight, especially if the raised face configuration was utilized. The 0.002 in. deflection allowance and raised face configuration were adopted for the seal test rig design and specified for the demonstrator engine coupling designs. A simplified finite element computer program was written and utilized for the engine flange designs.

2. Summary, Conclusions and Recommendations

A 5 in. ID, Inconel 718 seal test rig was designed, using the finite element computer program. It was to have 0.002 in. total deflection at the sealing diameter at 7000 psig internal pressure at LN_2 temperature. Six commercially available cryogenic seals with zero-leakage and a 0.002 in. claimed deflection capability were selected for test in the rig. Details of the seal test rig design and seal selection considerations are presented in the Demonstrator Engine Design Report, AFPRL-TR-70-6.

Thirty-four cryogenic pressure-cycle endurance and seal leakage tests were conducted with eight basic seal designs. The toroidal-segment seal was the only configuration that consistently met the 10^{-4} sccs/in. allowable leakage limit. A toroidal segment seal design-standard was established for seal diameters from 1 in. to approximately 35 in.

Deflection tests conducted during the seal pressure cycle endurance and leakage test program confirmed the validity of the finite element computer analysis technique The computer program model was kept current during the tests to provide a good stress and deflection analysis capability for the demonstrator engine flanges.

Based on the seal leakage and deflection tests, it was concluded that lightweight (approximately 15 lb for a 5 in. ID) flanged joints capable of restricting leakage to 10^{-4} sccs/in. at pressures to 7000 psig are feasible. It is recommended that high-pressure flanges be designed to allow 0.002 in. total deflection at the seal point, and that the toroidal segment seal be used to minimize leakage.

3. Hardware Description

a. Seal Test Rig

The seal test rig, as shown in figure 1004, consists of a cylindrical pressure vessel, made in halves, approximately 20 in. long with a 5 in. ID and is joined together centrally by 15 tie bolts. The pressure vessel, flanges and tie bolts are made of Inconel 718. Ports are provided to attach the vessel to a nitrogen pressure source and to allow access for internal instrumentation. The pressure vessel is surrounded by a cylinder that is sealed at both ends and acts as a collector for seal leakage. Schemes for reworking the seal gland to provide the proper gland configuration for each seal to be tested were included in the design.

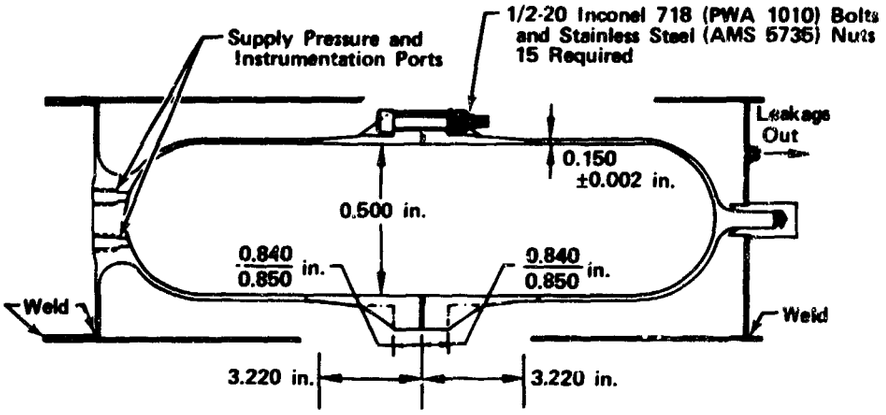

Figure 1004. Static Seal Rig FD 25707B

b. Toroidal Segment Seal

The toroidal segment seal was the only configuration that consistently met the 10^{-4} sccs/in. allowable leakage limit. The initial samples of this configuration tended to leak excessively at intermediate pressures so the seal was redesigned to improve low and intermediate pressure performance. The redesigned seals consist of a toroidal segment ring constructed of Inco X-750 with a 0.0005-0.001 lead plating. At sealing diameters greater than 19 in., seals backed by the pilot are required. Seal and groove configurations and dimensions are shown in figures 1005 through 1007.

To effect a seal, forces are developed along two surfaces of each seal leg as shown in figure 1008. Primary sealing is accomplished by the radial sealing force, H, developed at installation. As the seal is installed, it is axially compressed by an amount ΔV which causes a radial growth, ΔR_O, see figure 1009. If ΔR_O is greater than the radial clearance between the seal OD and the groove OD, then the seal is subjected to hoop compression by the groove wall, thus developing the radial force. The addition of pressure increases force H, thus maintaining a sealing pressure greater than the internal pressure.

Seals with diameters up to 19 in. are designed so the minimum radial force developed at installation for the maximum sealing diameter of each seal configuration is 33 lbs/in. of circumference. By machining the seal legs so the maximum radial contact area per seal leg is 0.010 in.^{2}/in. of circumference, then the minimum contact pressure becomes 3300 psi which is approximately twice the yield stress of the lead plating.

Seals with diameters greater than 19 in. are designed so the total radial deformation, consisting of ΔR_O and ΔR_{ID}, (figure 1005) caused by ΔV results in a seal cross-sectional depth greater than the groove depth, causing the seal to be squeezed between the pilot and groove OD. Thus, by limiting the seal deformation the radial forces at installation for large sealing diameters is greatly increased. Analyses of this configuration indicates that plastic moments are formed at two points on the seal cross section. The uncertainty of seal action after this occurs requires that installation forces be experimentally determined.

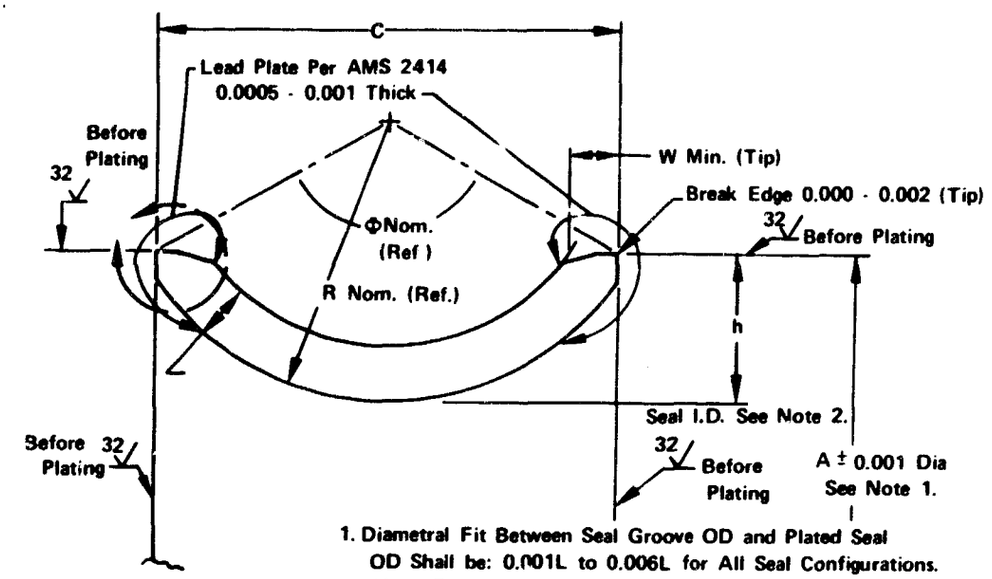

1. Diametral Fit Between Seal Groove OD and Plated Seal OD Shall be: 0.001L to 0.006L for All Seal Configurations. These Fits Are Prior to Ass'y.
2. Fits Between Pilot OD and Seal ID for Seal Configuration 9 Shall be 0.002L to 0.014L Prior to Ass'y.
3. Seal Dim. Given are Prior to Plating Unless Otherwise Noted.

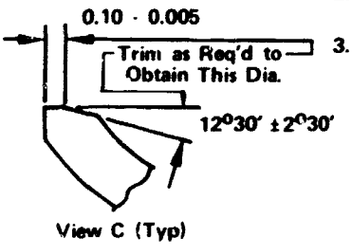

View C (Typ)

Seal Dimensions							
Seal Config. No.	A Dia Min. and Max	C	h	t	ΦNom (Ref.)	R Nom (Ref.)	W Min.
1	1000 to 2000	0.107 0.109	0.036 0.034	0.011 0.013	124°	0.064	0.010
2	2000 to 3000	0.107 0.109	0.036 0.034	0.018 0.021	120°12'	0.067	0.019
3	3000 to 4250	0.160 0.164	0.056 0.052	0.023 0.026	126°30'	0.095	0.083
4	4250 to 8500	0.211 0.217	0.074 0.070	0.023 0.026	130°36'	0.122	0.023
5	8500 to 14500	0.265 0.265	0.090 0.090	0.033 0.039	125°12'	0.158	0.033
6	14500 to 16500	0.265 0.271	0.090 0.084	0.039 0.044	123°	0.162	0.039
7	16500 to 18000	0.265 0.271	0.090 0.084	0.046 0.051	120°36'	0.166	0.046
8	18000 to 18000	0.267 0.271	0.090 0.084	0.046 0.051	120°12'	0.166	0.046
9	719000	0.211 0.217	0.074 0.070	0.016 0.019	131°48'	0.120	0.016

Figure 1005. Seal Configurations Dimensions FD 49146

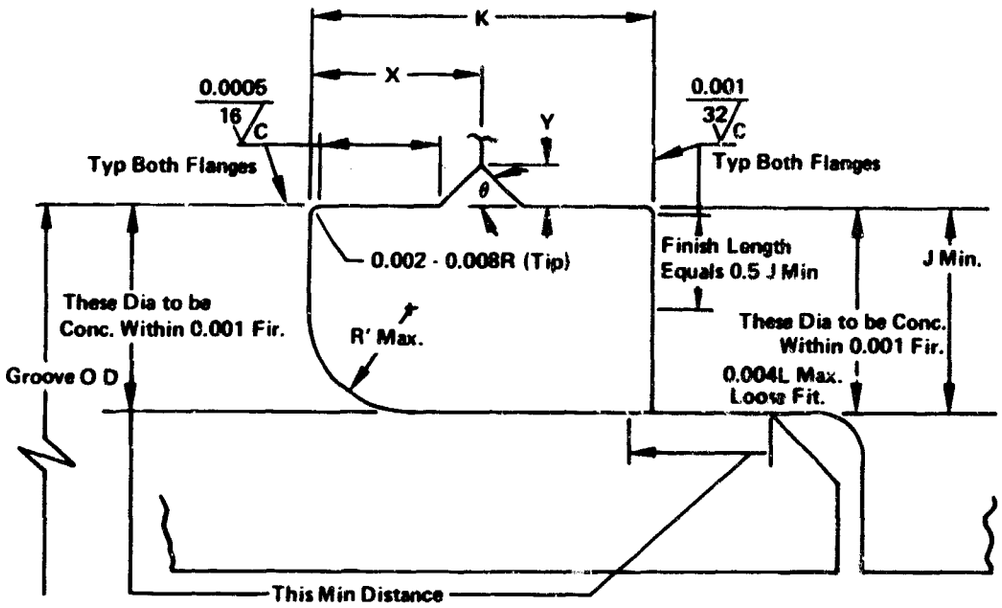

Seal Config. No.	Groove Dimensions					
	J	K	R'	θ	X	Y
1	0.056	0.088 0.092	0.028	45° ± 12°	0.044 0.046	0.010 0.020
2	0.056	0.088 0.092	0.028	45° ± 12°	0.044 0.046	0.010 0.020
3	0.073	0.144 0.140	0.040	45° ± 12°	0.070 0.072	0.012 0.032
4	0.108	0.181 0.177	0.054	45° ± 12°	0.088 0.090	0.012 0.032
5	0.130	0.223 0.219	0.066	30° ± 12°	0.109 0.111	0.012 0.032
6	0.130	0.223 0.219	0.066	30° ± 12°	0.109 0.111	0.012 0.032
7	0.130	0.223 0.219	0.066	30° ± 12°	0.109 0.111	0.012 0.032
8	0.130	0.223 0.219	0.066	30° ± 12°	0.109 0.111	0.012 0.032
9						

Figure 1006. Groove Dimensions for Seal Configurations 1 Through 8 FD 49147

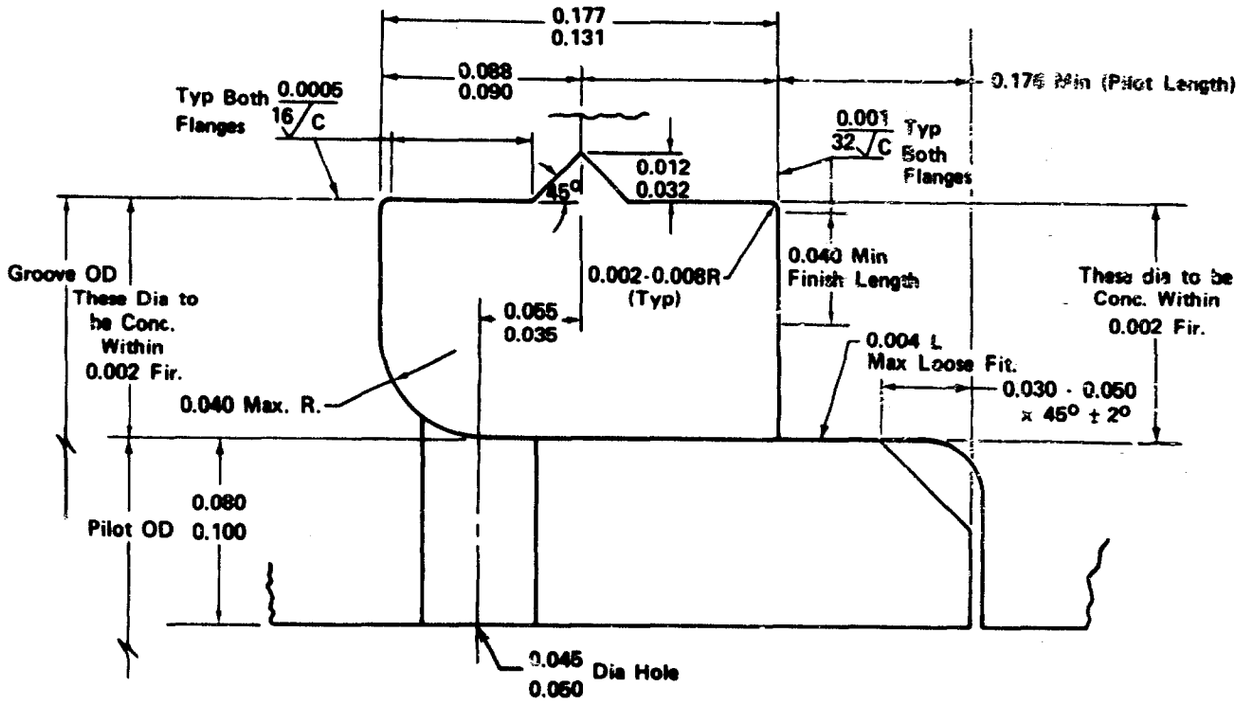

Figure 1007. Groove Dimensions for Seal Configuration 9

FD 49148

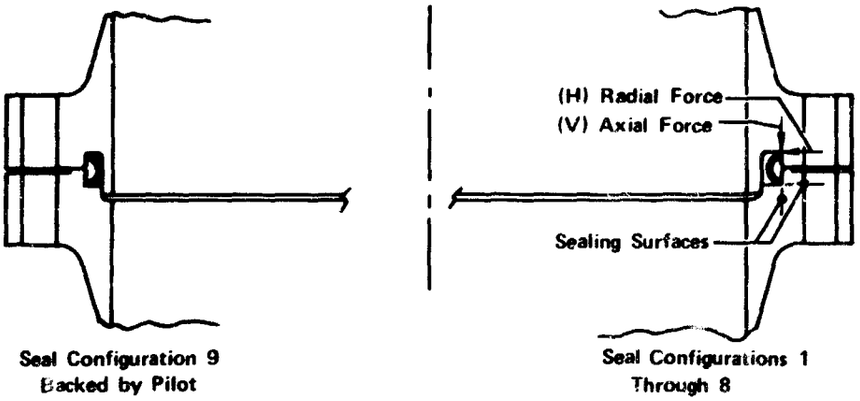

Figure 1008. Typical Seal Installations FD 49150

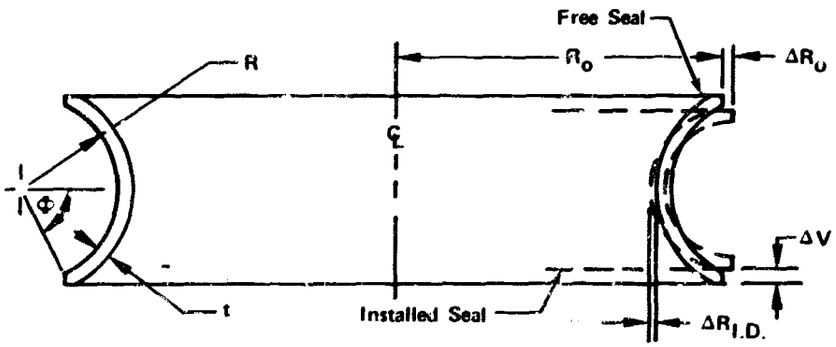

Figure 1009. Seal Nomenclature FD 49149

4. Testing

a. Test Rig 35120 - Builds 1 Through 4

Builds 1 through 4 of test rig 35120 were conducted during the Supporting Data and Analysis Task to evaluate deflections of a 6 in. ID aluminum coupling and the Phase I main chamber oxidizer valve. These tests, described in this report, provided data used to design the 5 in. ID Inconel 718 test rig used during static seal testing.

b. Test Rig 35120 - Builds 5 Through 8

Builds 5 through 8 of test rig 35120 were conducted to evaluate Teflon coated, vented metal O-ring static seals during pressure cycles and leakage

tests to the maximum rig design pressure of 7000 psig at cryogenic temperatures. An additional objective was to measure the coupling stress and deflection at ambient temperature caused by assembly and maximum design pressure loads. The test rig is shown in figure 1010.

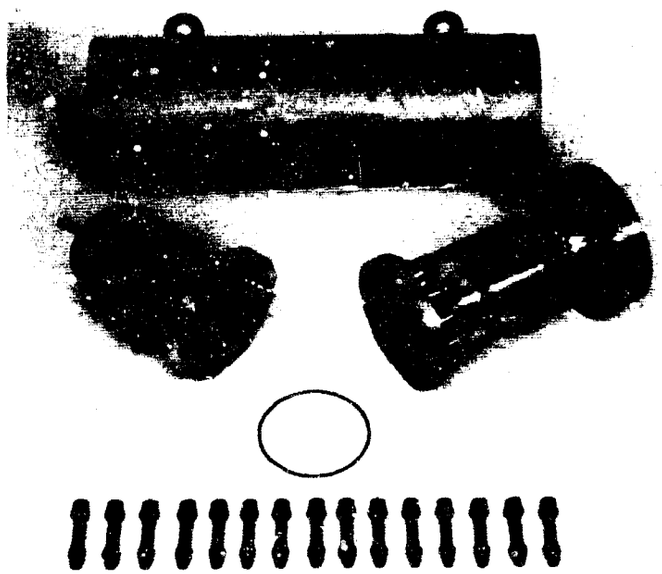

Figure 1010. Seal Test Rig FE 83175

For builds 5 and 6, the cylinder half at the right in figure 1010 had not been fully heat-treated. The hardness of this cylinder half was R-22 compared to the mating flange hardness of R-45. The housing was fully heat-treated to a hardness of R-43 and refinished prior to build 7.

Prior to build 7, two 0.015 in. deep grooves, 180 deg apart, were machined radially across the raised face bearing surface of the cylinder half at the left in figure 1010. The rig was then instrumented to measure hoop and axial stress, bolt stress and flange deflection. Figure 1011 shows the location of the strain gages and proximity probes, and figure 1012 shows the installation of proximity probes No. 1 and 2.

Build 8 was assembled with the measured bolt stretch increased 0.001 in. to 0.0008 in. total. A wooden filler plug was also installed in the high pressure cavity to reduce the internal pressure volume. The O-ring seal vent holes were deburred, and the O-ring ID was vacuumed to remove the chips.

Builds 5, 6, and 8 were mounted and tested in the B-22 test stand. The vacuum leak-check pressure rise was limited to 20 microns in 2 hr for builds 5 and 6. This limit was raised to 500 microns in 1 hr for build 8 to compensate for wooden filler plug outgassing at vacuum test conditions.

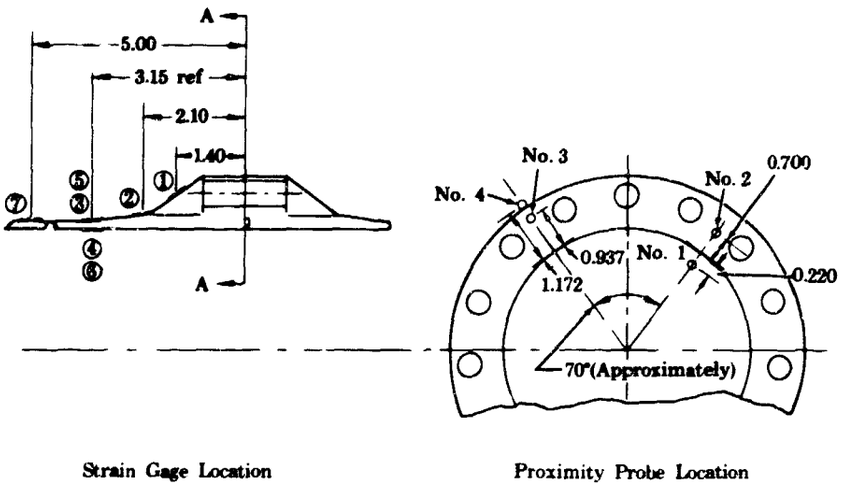

Figure 1011. Strain Gage and Proximity Probe Locations FD 29211

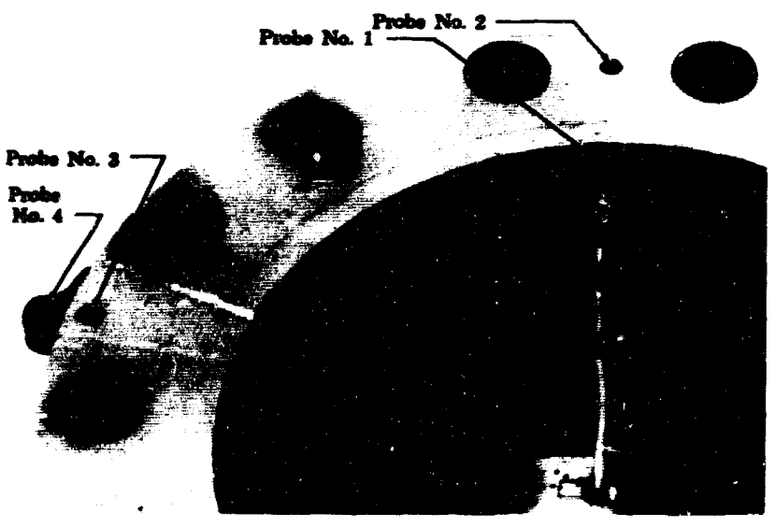

Figure 1012. Proximity Probe Installation Pressure Cycle FD 29212

Build 7 was tested for deflection measurements in the Instrument Laboratory at ambient temperature. Hydraulic oil was used as the pressurizing fluid.

The results of build 5 cycle test are shown in figure 1013. The maximum acceptable leakage limit for this seal is 16.6×10^{-4} sccs. This limit was exceeded at pressure levels greater than 2000 psig before the pressure cycle test and at pressures greater than 1000 psig after 500 pressure cycles were completed. Seal leakage exceeded 10 sccs at 5000 psig throughout testing and

exceeded the stand flowmeter limit of 472 sccs at 6000 psig, which was the maximum test pressure. Pressure during cycling was limited to 5000 psig because of excessive leakage at higher pressures.

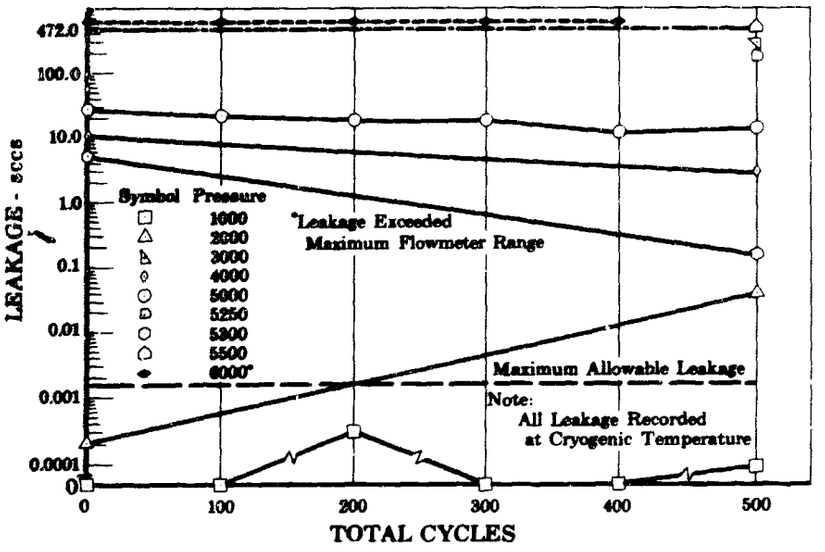

Figure 1013. Vented O-Ring, Build 5, Leakage vs Total Cycles FD 29213

Post-test inspection of the seal revealed the seal was in good condition (figure 1014) and there was good seal contact with the flange surface.

The flat flange showed a slight pivot point deformation as indicated in figure 1015. Although this photograph was taken after build 6, some deformation had been noted during the build 5 post-test inspection.

The results of build 6 pressure cycle test are shown in figure 1016. The seal leakage results for this build were similar to the build 5 results. The allowable leakage limit was exceeded at pressures greater than 3000 psig prior to test and 2000 psig after the 500 pressure cycles were completed. Leakage at 5000 psig exceeded 10 sccs throughout the test, and leakage at the maximum test pressure of 5800 psig exceeded the stand flowmeter limit. The pressure during cycling was limited to 5000 psig because of excessive leakage at higher pressures.

Post-test inspection revealed iron-base chrome alloy particles imbedded in the Teflon coating of the O-ring. Figure 1017 shows the contamination on the seal and figures 1015 and 1018 show flange face surface damage caused by the contamination. The particle sizes were larger than would be expected to pass through the nominal 10 micron filter in the test stand nitrogen supply line just upstream of the rig inlet. X-rays of two unused O-rings from the same shipment revealed chips inside the O-ring and burrs around the vent holes. X-rays of the used O-rings from builds 5 and 6 showed no internal chips or burrs.

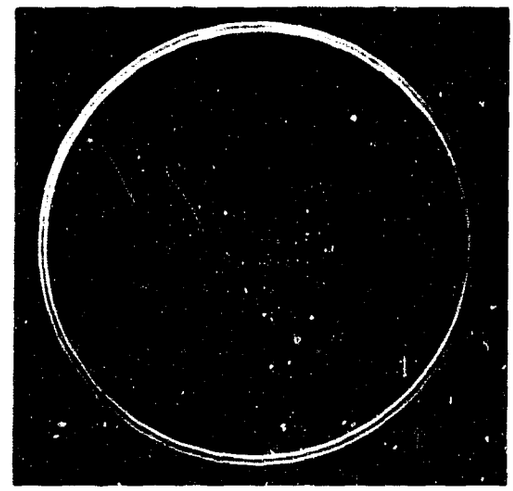

Figure 1014. Post-Test Seal Condition, Build 5 FD 29214

Figure 1015. Flat Flange Pivot Point Deformation FD 29215

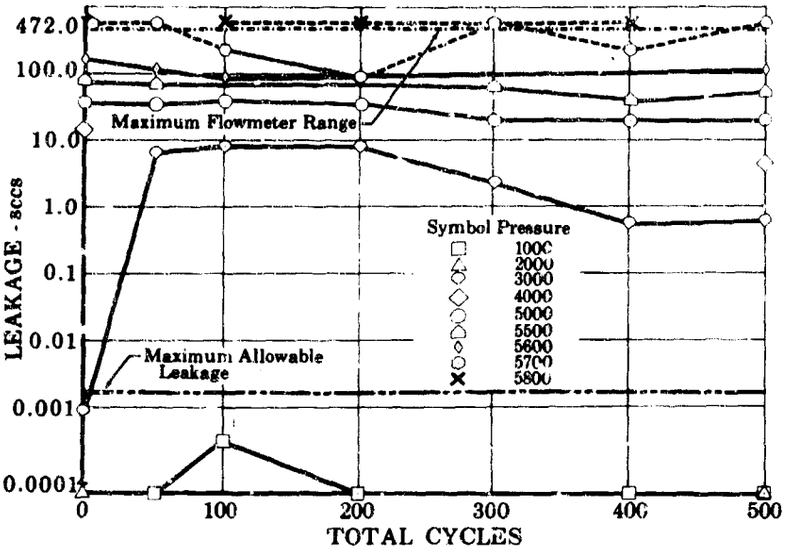

Figure 1016. Vented O-Ring, Build 6, Leakage vs Total Cycles FD 29104

Figure 1017. Post-Test Seal Condition, Build 6 FD 29216

Figure 1018. Flange Face Surface Damage FD 28217

The flat flange also showed additional pivot point deformation as shown in figure 1015.

The flange deflection obtained during assembly and hydrostatic test of build 7 is shown in figure 1019. The measurements were made with the proximity probes shown in figure 1012. A zero bolt-load reference measurement with the seal removed was not taken prior to the test, so a thickness gage measurement of the flange OD gap taken at 200 in.-lb bolt torque was selected for the reference. It was assumed that negligible bearing area compression had occurred at that point, and the ID probe deflection was assumed to be approximately 30% of the final value based on an approximate average final bolt torque of 600 in.-lb. When the data points were connected as shown, the data indicated that there was a slight separation at the raised face OD at 7000 psig. The No. 2 proximity probe indicated movement between 6000 and 7000 psig, as did the average indicated bolt load. It was concluded that the total deflection at the No. 1 probe may have been in error, based on the 200 in.-lb torque point assumption. The deflections measured thereafter are considered valid and indicated a maximum seal point deflection of approximately 0.0033 in.

Bolt pull test calibrations prior to assembly indicated that the required design load per bolt of 16,500 lb would result from the measured 0.007 in. bolt stretch obtained during assembly. The degree of bolt bending and average bolt load reduction indicated by the strain gage measurements were greater than was anticipated.

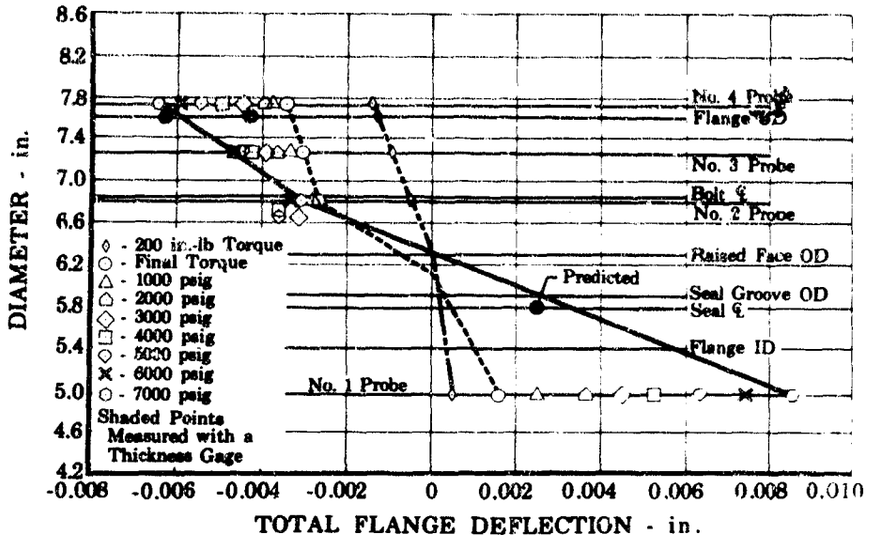

Figure 1019. Flange Deflection, Build 7 FD 29143

The results of build 8 pressure cycle test are shown in figure 1020. Seal leakage exceeded the allowable limit at pressures greater than 2000 psig. Leakage at 5000 psig was 160 sccs prior to the pressure cycles and 30 sccs after the 500 cycles were completed. Leakage at 7000 psig was 100 sccs before the cycles and 22 sccs after the cycle test. The maximum seal leakage after the 500 pressure cycles were completed was 40 sccs and occurred at 4000 psig internal pressure. The minimum leakage at 7000 psig was 11 sccs and occurred after approximately 50% of the cycles were completed. Pressure cycles were performed to 7000 psig.

Post-test inspection showed the seal and flange surfaces to be in good condition and free of mars or scratches as shown in figure 1021.

c. Test Rig 35120 - Builds 9 and 10

Builds No. 9 and 10 of test rig 35120 were conducted to evaluate Teflon-coated C-shaped seals during pressure cycles and leakage tests to the maximum rig design pressure of 7000 psig at cryogenic temperatures.

Builds 9 and 10 used measured bolt stretch of 0.006-0.0062 in. The average bolt stretch obtained was approximately 0.0047 in. and the average load per bolt was 11,000 lb.

Build 9 was mounted and tested in the B-22 test stand. Build 10 was tested in the assembly area at ambient temperature.

Built 9 and 10 seal configurations including pretest sealing conditions and post-test seal dimensions are shown in figures 1022 and 1023.

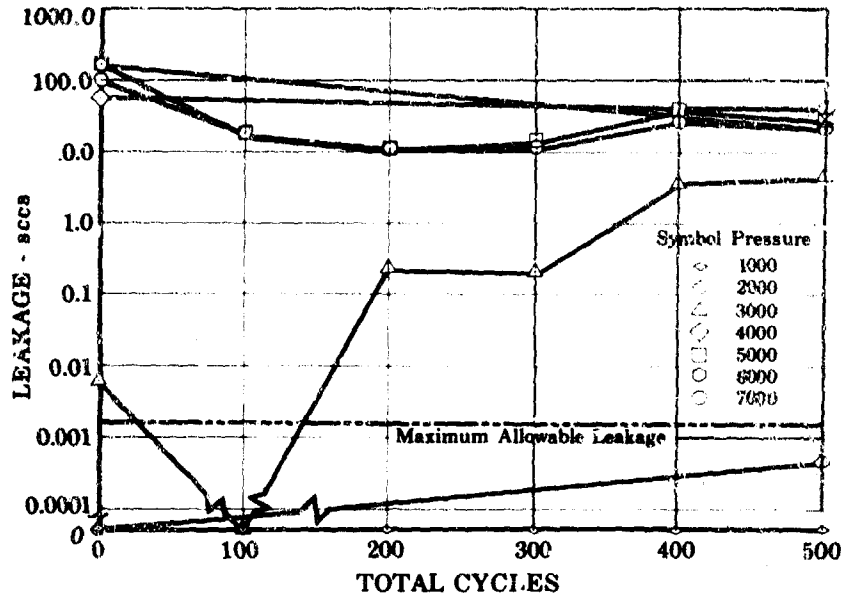

Figure 1020. Vented O-Ring, Build 8, Leakage vs Total Cycles FD 29106

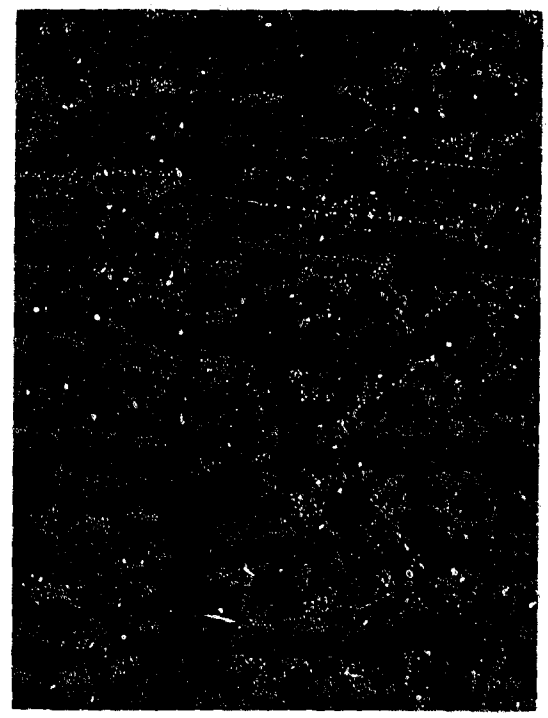

Figure 1021. Post-Test Seal Condition, Build 8 FD 29218

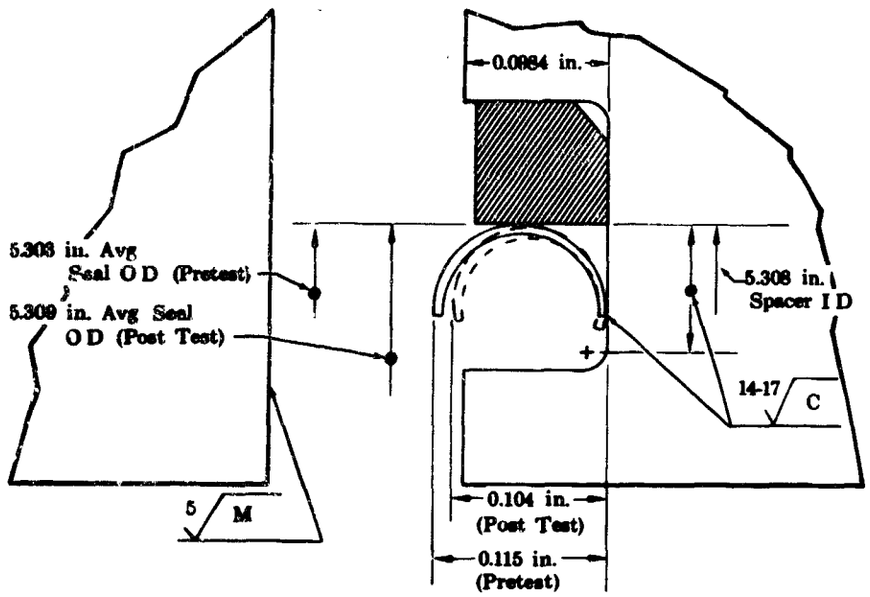

Figure 1022. Del C-Seal and Sealing Surface Conditions, Build 9 FD 31832

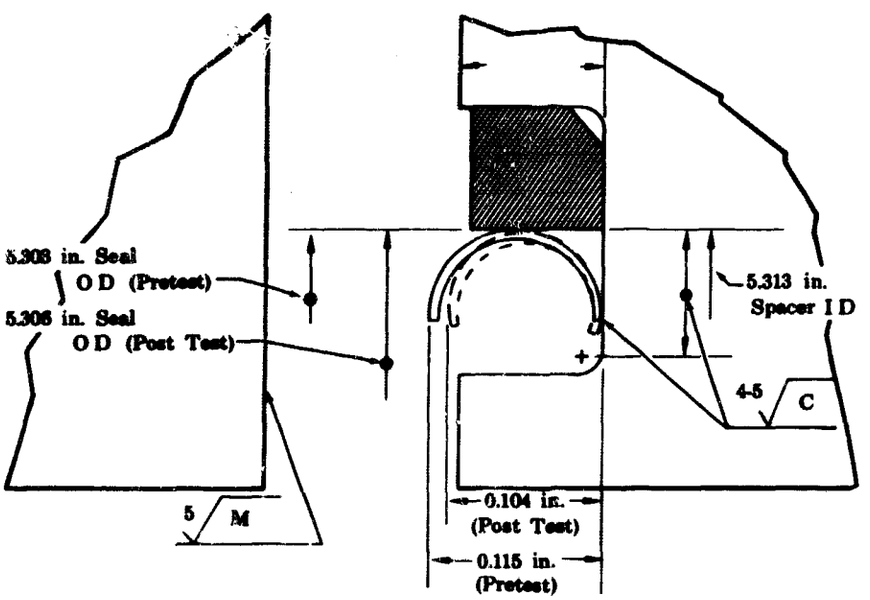

Figure 1023. Del C-Seal and Sealing Conditions, Build 10 FD 31833

The results of build 9 pressure cycle test are shown in figure 1024. Leakage throughout the test was in excess of the 16 x 10^{-4} sccs maximum allowable limit. Leakage at 3000 psig internal pressure was greater than 100 sccs and leakage at 7000 psig exceeded the stand flowmeter limit of 470 sccs. The pressure cycles were performed to 6000 psig because of the excessive leakage at higher pressures after 10% of the cycles were completed to 7000 psig.

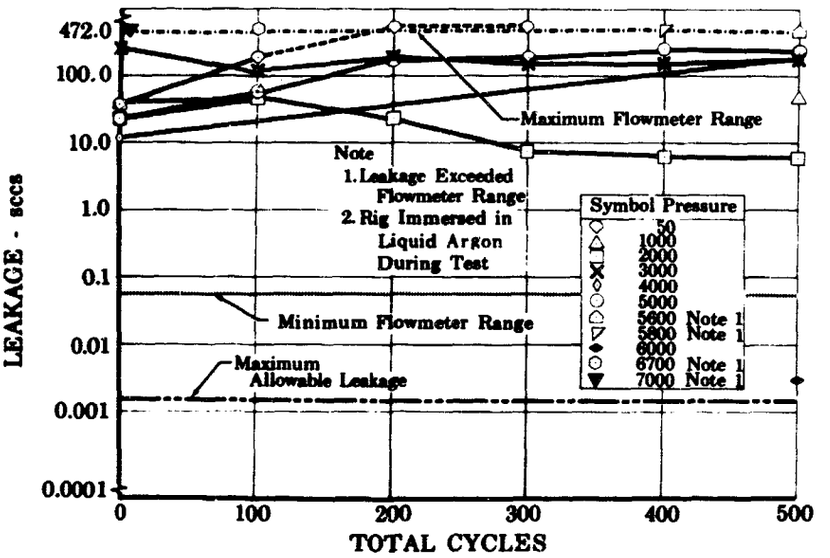

Figure 1024. Del C-Seal, Build 9, Leakage vs Total Cycles FD 29108A

Build 9 post-test seal inspection showed the seal twisted in the spacer as shown in figure 1025. The seal coating was worn through as shown in figure 1026 and the flange surface was severely scored as shown in figure 1027. Build 9 post-test seal dimensions are shown in figure 1022.

A comparison of build 10 ambient test results with those obtained in build 9 is shown in figure 1028. Because of the excessive leakage at ambient temperature, the cryogenic pressure cycle test for build 10 was not performed.

Build 10 post-test inspection showed the same type seal twisting as shown in figure 1029. Build 10 post-test seal dimensions are shown in figure 1023.

d. Test Rig 35120 - Builds 11 and 12

Builds 11 and 12 of test rig 35120 were conducted to evaluate a silver-plated Servotronics omega seal during pressure cycles and leakage tests to the maximum rig design pressure of 7000 psig at cryogenic temperatures.

The seal rig was assembled as shown in figure 1030. The spacer shown was not used with this seal. The omega seal sealing conditions for builds 11 and 12 are also shown in figure 1030.

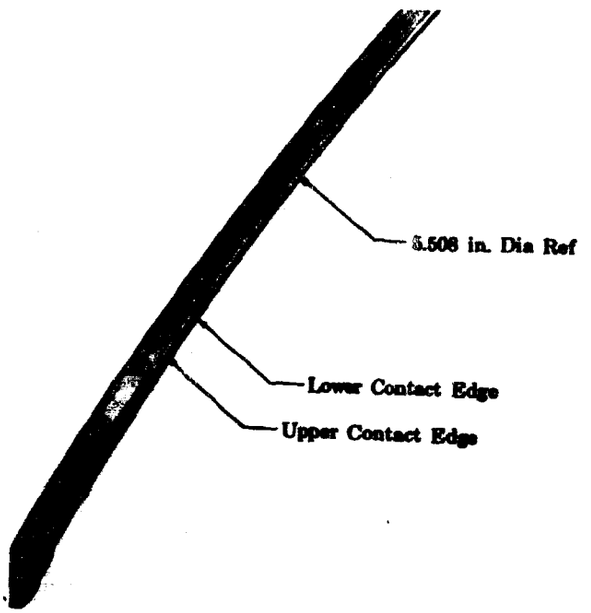

Figure 1025. Del C-Seal Deformation, Build 9 FD 31834

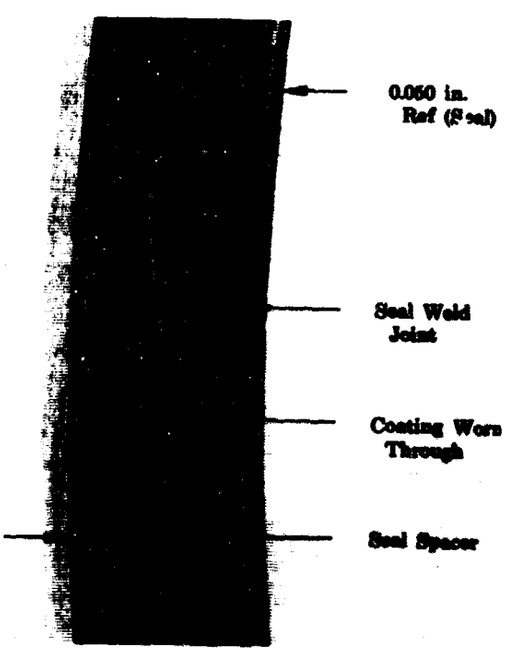

Figure 1026. Del C-Seal and Spacer Post Test Condition, Build 9 FD 31835

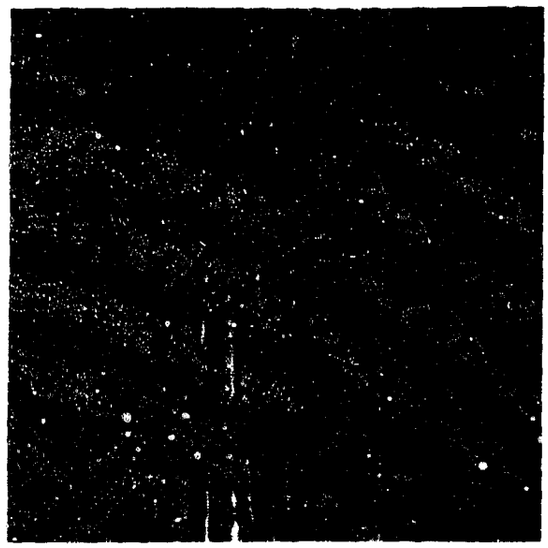

Figure 1027. Flat Face Flange Surface, Build 9 FD 31836

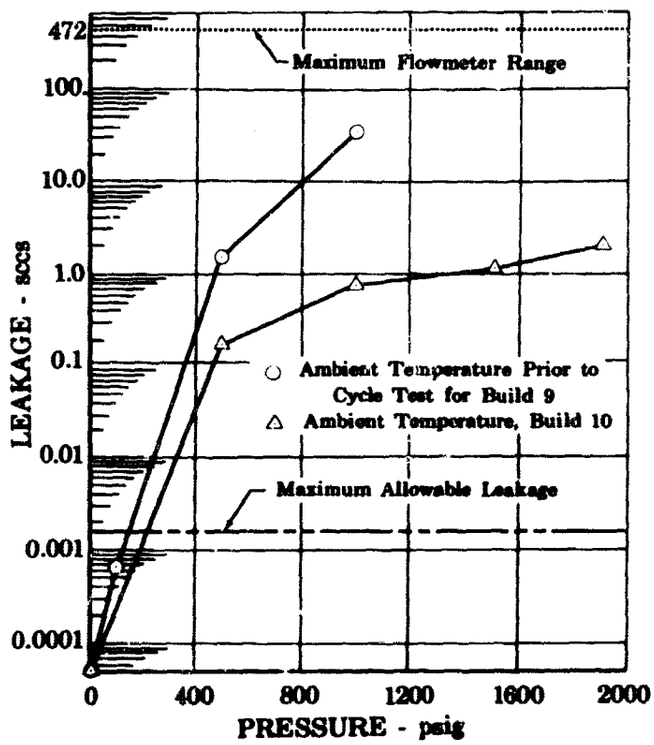

Figure 1028. Del C-Seal, Builds 9 and 10, Leakage vs Pressure FD 31876

Figure 1029. Del C-Seal in Groove, Build 9 FD 31838

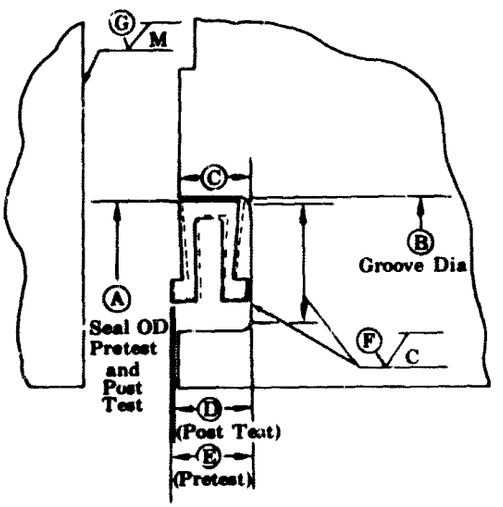

	Build 11	Build 12
A	5.496	5.496
B	5.5131	5.5131
C	0.103	0.103
D	0.1045	0.1044
E	0.1113	0.1113
F	6-16	4
G	4	6-10

Figure 1030. Servotronics Omega Seal and Sealing Conditions, Builds 11 and 12 FD 31037

The bolts were stretched to an indicated 0.006 to 0.0062 in. The average bolt stretch, due to bending, was 0.0047 in. and the average load per bolt was 11,000 lb.

Builds 11 and 12 were mounted and tested in the B-22 test stand. The stand collection system was vacuum leak checked prior to the rig mount and the collection cavity rig connections were pressure checked at 15 psig after the mount was completed.

The results of build 11 and build 12 pressure cycle tests are presented in figures 1031 and 1032. The leakages prior to test, with the rig immersed in liquid argon, were measured with a positive displacement meter at all test pressures. For build 11, the leakage after each 100 cycle interval was highest at 1000 psig rig internal pressure and the maximum was 34 sccs after 300 cycles had been completed. The maximum leakage at 7000 psig was 10 sccs after 300 cycles were completed and was less than 3 sccs after 500 cycles were completed. Leakage at 100 psig was between 5 and 10 sccs after each 100 cycles. For build 12, the maximum leakage of 17 sccs occurred at 1000 psig rig pressure after 400 pressure cycles had been completed. Maximum leakage at 7000 psig was 1.2 sccs at 7000 psig after the total 500 cycles were completed. Leakage at 100 psig was 5 to 10 sccs throughout the test after the first 200 cycles.

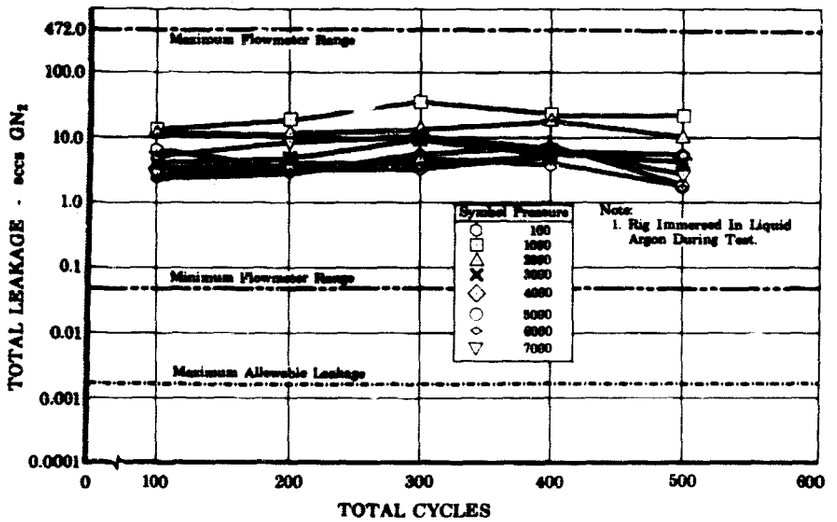

Figure 1031. Servotronics Omega Seal, Build 11, Leakage vs Total Cycles FD 31038

Build 11 post-test inspection showed the seal and flange surfaces in excellent condition. The seal wear is shown in figure 1033, for the groove side and is typical for both builds. The flange and groove surfaces were unmarred with only a light seal contact line apparent as shown in figure 1034.

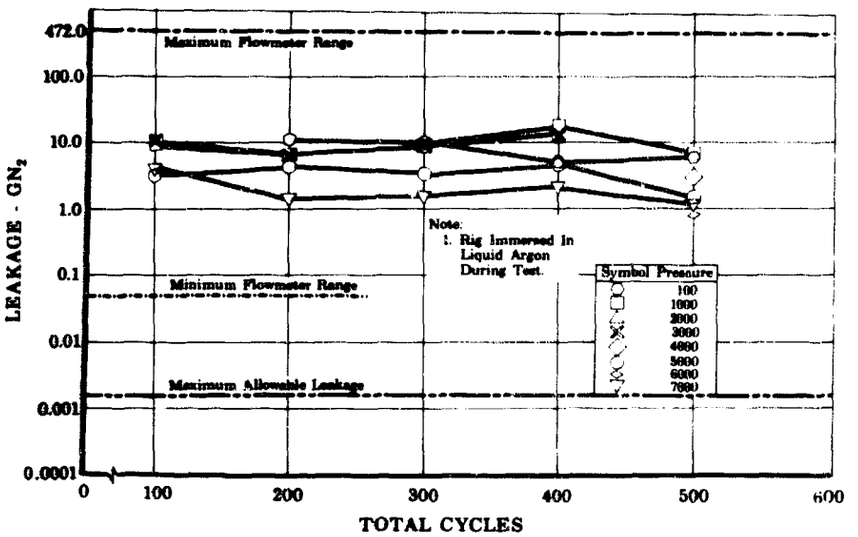

Figure 1032. Servotronics Omega Seal, Build 12, Leakage vs Total Cycles FD 31039

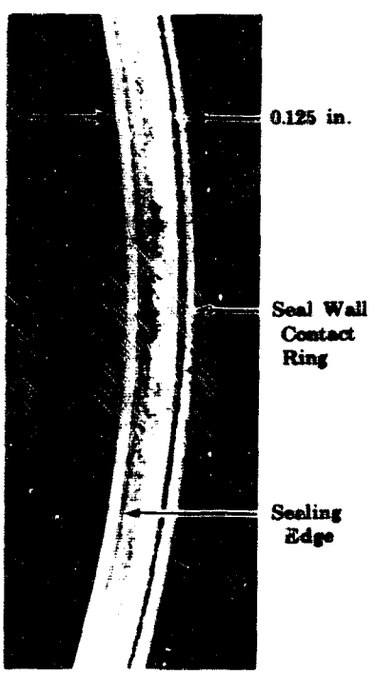

Figure 1033. Typical Groove Side of Omega Seal FD 31040

Figure 1034. Flat Face Flange FD 31041

Build 12 post-test inspection showed the flange surfaces to be in excellent condition. The seal wear was similar to that of build 11 and is shown in figure 1035. Some cracks in the side of the seal were noted. Figure 1036 shows a cross section of a cracked area.

e. Test Rig 35120 - Builds 13 and 14

Builds 13 and 14 of test rig 35120 were conducted to evaluate the silver-plated Servotronics apex seal during pressure cycles and leakage tests to the maximum rig design pressure of 7000 psig at cryogenic temperatures.

The seal rig was assembled as shown in figure 1037. The sealing conditions for builds 13 and 14 are shown in figure 1037.

The bolts were stretched to an indicated 0.006 to 0.0062 in. Because of bolt bending, the average bolt stretch was approximately 0.0047 in., and the average load per bolt was 11,000 lb.

Builds 13 and 14 were mounted and tested in the B-22 test stand. The stand was vacuum leak checked prior to rig mount and the rig collection system connections were pressure checked at 15 psig after the mount was completed.

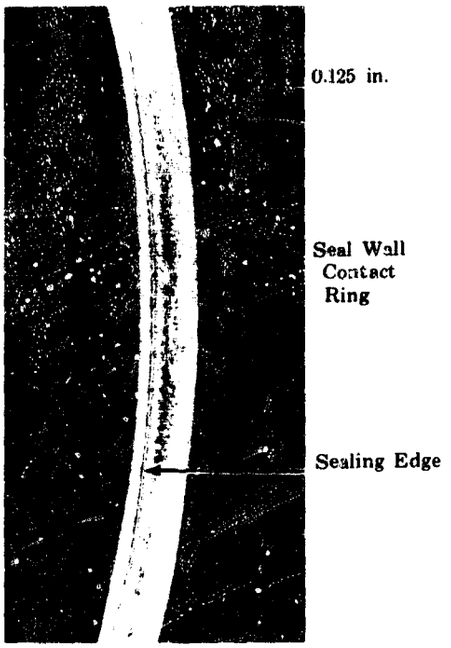

Figure 1035. Typical Flat Face Flange Side of Omega Seal FD 31042

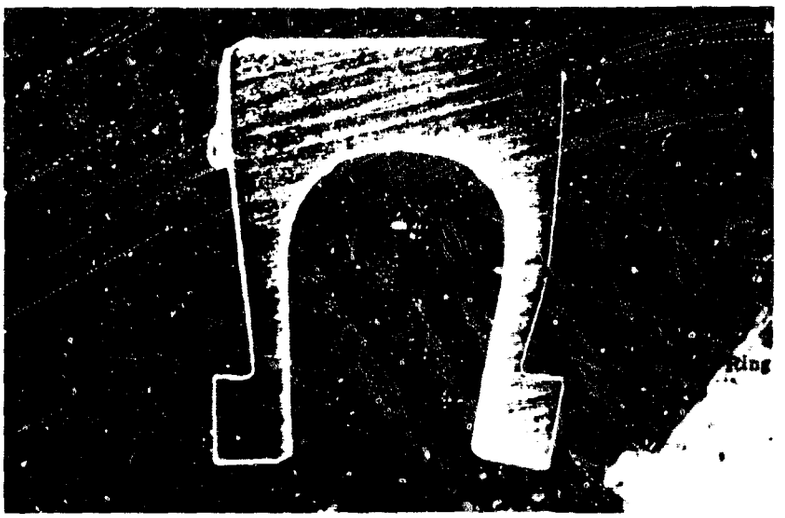

Figure 1036. Cross Section of Omega Seal Through Cracked Area 35 Times Size FD 31043

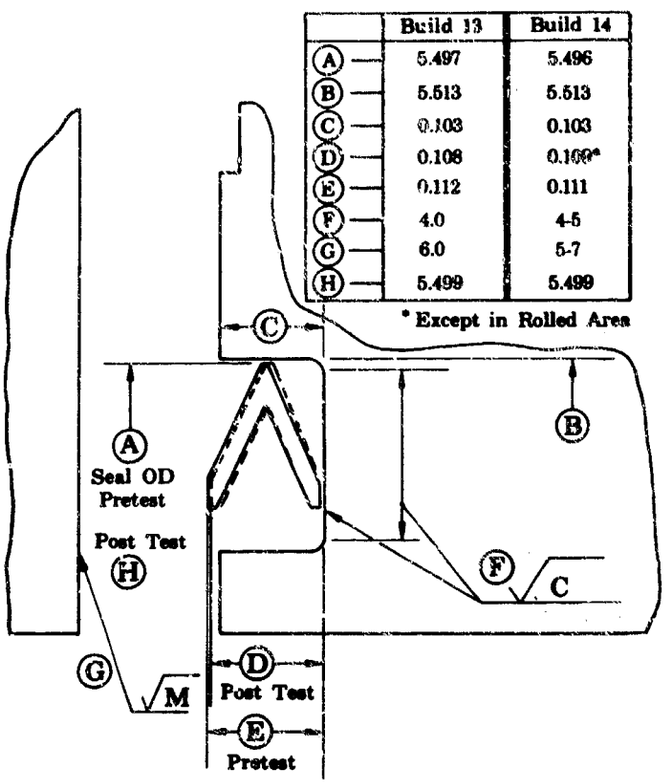

Figure 1037. Servotronics Apex Seal and Sealing Conditions, Builds 13 and 14 FD 31402

The results of builds 13 and 14 are presented in figures 1038 and 1039. Leakage prior to the cycle test with the rig at cryogenic temperature for both seals was approximately 5 sccs at 7000 psig. The maximum leakage prior to test was 25 to 30 sccs at 7000 psig. The maximum leakage prior to test was 25 to 30 sccs for both builds and occurred at 5000 psig rig internal pressure. For build 13, leakage indication after the first 100 cycles dropped considerably from the pretest indication. Measurements after completing 100 cycles were taken using displacement type meters. Subsequent investigation has proved the installation of these meters introduced a leakage indication error proportional to the volume between the leak and the meter. The erroneous data from these meters are not included. Leakage after the total 500 pressure cycles was 2.8 sccs at 7000 psig and 7.6 sccs maximum at 5000 psig. For build 14, leakage after the first 100 pressure cycles at 7000 psig was 2.8 sccs. While this datum point was being recorded the leakage indication went off scale. The internal pressure was reduced until the leakage could be measured with the available flow meters. Leakage at 3000 psig was greater than 470 sccs and the leakage at 2800 psig was 330 sccs. An additional 100 pressure cycles to 3000 psig were performed in an attempt to reseat the seal. After these 100 cycles were completed, the leakage at 4000 psig was 225 sccs and was greater than 470 sccs at 4300 psig. An additional 100 cycles to 4000 psig were completed. Leakage was still excessive and the test was terminated after 300 pressure cycles.

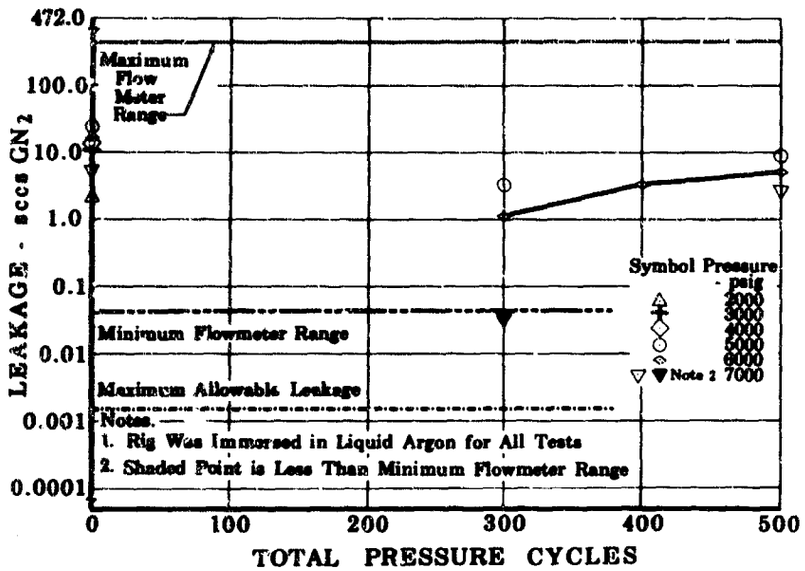

Figure 1038. Servotronics Apex Seal, Build 13, Leakage vs Total Cycles FD 31638A

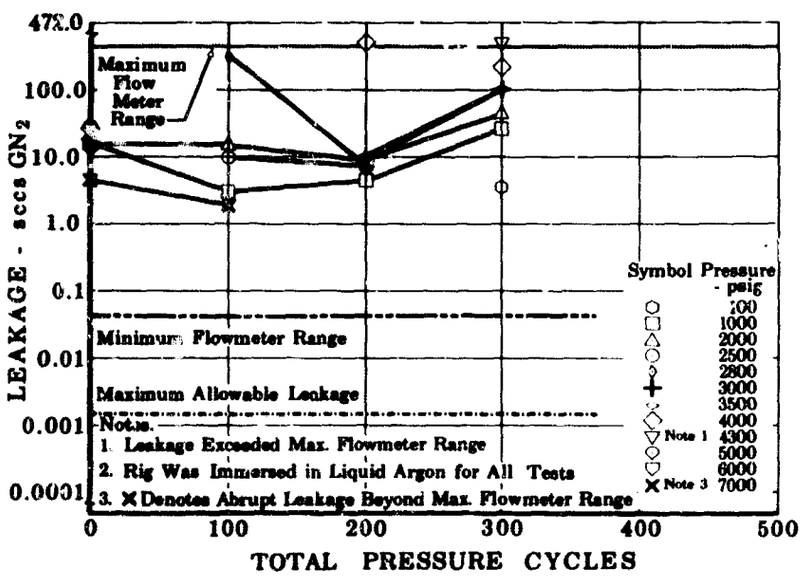

Figure 1039. Servotronics Apex Seal, Build 14, Leakage vs Total Cycles FD 31639A

Build 13 seal was in good condition at teardown. Figure 1040 shows the seal contact area for the groove side and figure 1041 shows the contact area for the flat face flange side. The mating surfaces were in excellent condition.

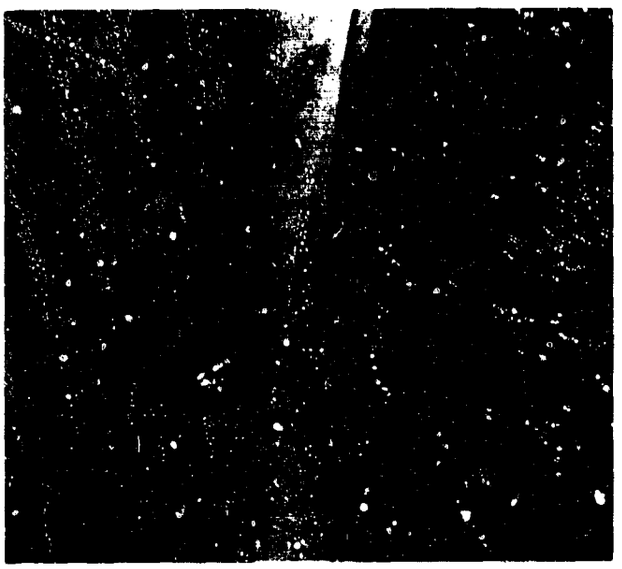

Figure 1040. Apex Seal Groove Side FD 31403

Figure 1041. Apex Seal Flat Face Side FD 31404

Build 14 seal was collapsed in an area as shown in figure 1042. Zyglo inspection of the seal indicated a crack in the seal OD. Subsequent sectioning of the seal showed the crack to be only in the plating and no cracks in the base material were found. The seal apparently rolled in the groove as shown schematically in figure 1043.

Figure 1042. Build 14 Seal Collapse Area FD 31405

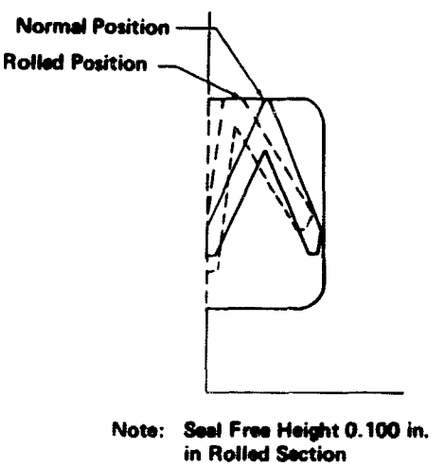

Figure 1043. Apex Seal Rolled Position FD 31406

f. Test Rig 35120 - Builds 15, 16, 17, 18, and 21

Builds 15, 16, 17, 18, and 21 of Test rig 35120 were conducted to evaluate the Pressure Science, Inc. C-ring seal by performing pressure cycles to 7000 psig at cryogenic temperature. The seal rig was assembled as shown in figure 1044.

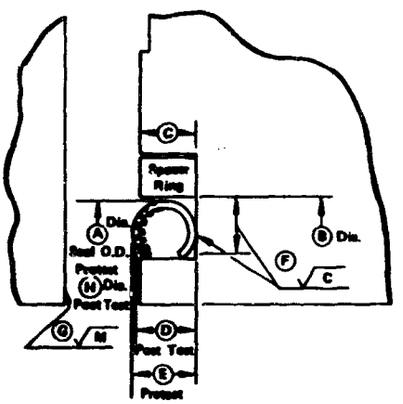

	Build 15	Build 16	Build 17	Build 18	Build 21
A	5.395	5.395	5.397 5.390	5.395	5.3845
B	5.379	5.379	5.379	5.379	5.437
C	0.103	0.1018	0.1022	0.106	0.106
D	0.106	0.106	0.106	0.106	0.1065
E	0.128	0.1275 0.1285	0.129 0.128	0.132 0.135	0.126
F	8C	4-8C	8C	12C	0-8C
G	8M	5-8M	8M	8M	5-8M
H	5.377	5.375	5.376	5.373	5.387
I	Indium From Vendor	0.001 A_g and 0.0005 Teflon	0.001 Silver Plate	0.001 Lead Plate	0.001 Lead Indium per PWA 42

Figure 1044. Pressure Science, Inc. C-Ring Seal and Sealing Conditions for Builds 15, 16, 17, 18, 21 FD 33106

The bolts were stretched to an indicated 0.006 to 0.0062 in. Because of bolt bending the average bolt stretch was approximately 0.0047 in. and the average load per bolt was 11,000 lb.

Builds 15 through 18 were mounted and tested in the B-22 test stand. The stand was vacuum leak checked prior to rig mount and the rig collection system connections were pressure checked at 15 psig after rig was mounted.

Build 21 was tested at the assembly pressure test area at ambient temperature using GN_2 pressurizing gas.

The test results of builds 15 through 18 are shown in figures 1045 through 1048. The results indicate that the greatest leakage occurred between 1000 and 4000 psig rig internal presssure. The maximum leakage for builds 15 through 18 was 42 sccs and occurred at 3000 psig during build 17 (silver plated seal) after 400 pressure cycles had been completed. Build 21 leakage was excessive at ambient conditions and the cryogenic cycle test was not performed.

The build 15 indium coated seal indicated low leakage prior to and after the first 100 cycles. Measurements for this leakage were taken using displacement meters, which have subsequently been found to introduce a leakage indication error proportional to the volume between the leak and the meter. The erroneous data from these meters are not included. The maximum leakage after 200 cycles were completed was 0.4 sccs and occurred at 3000 psig

internal pressure. The maximum leakage for the test was 3.7 sccs and occurred at 1000 psig rig internal pressure after the total 500 cycles had been completed.

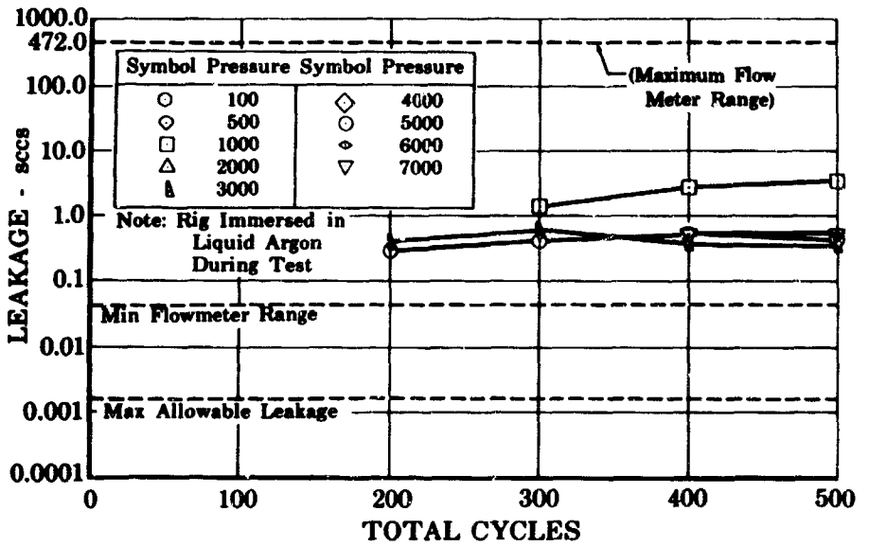

Figure 1045. Indium Coated C-Ring Build 15, Leakage vs Total Cycles — FD 33107

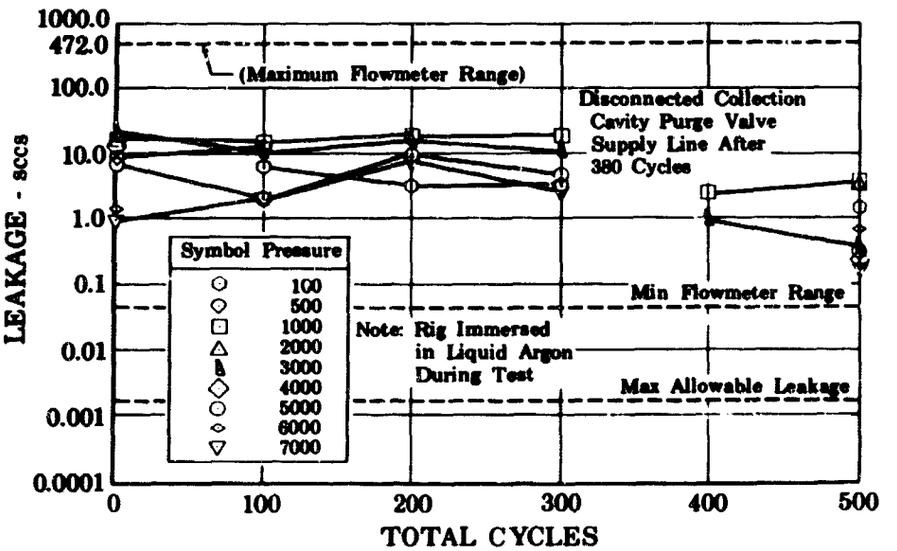

Figure 1046. Silver Plated Teflon Primer Coated C-Ring, Build 16, Leakage vs Total Cycles — FD 33108

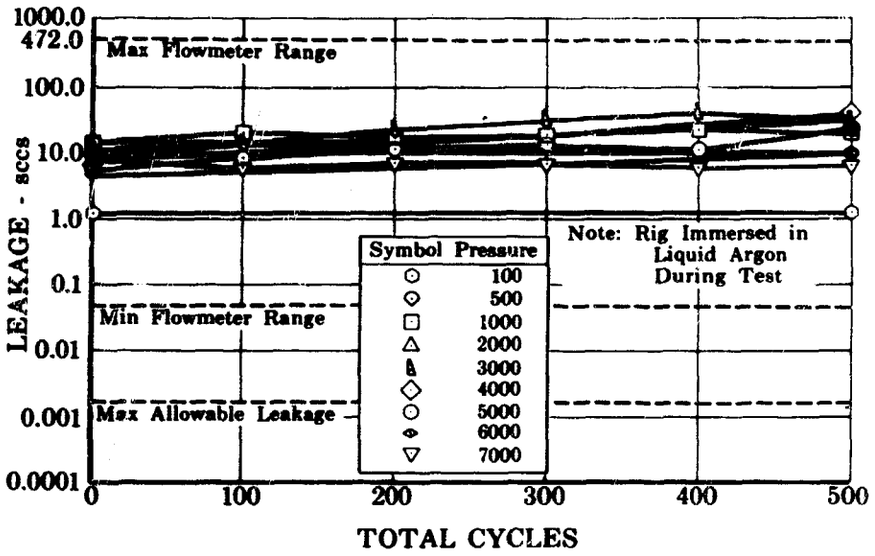

Figure 1047. Silver Plated C-Ring, Build 17, Leakage vs Total Cycles FD 33119

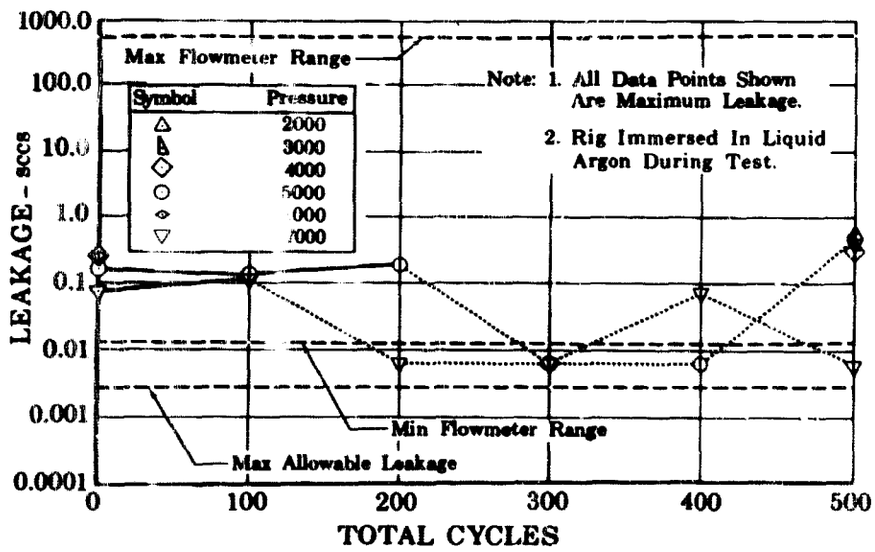

Figure 1048. Lead Plated C-Ring, Build 18, Leakage vs Total Cycles FD 33120

Post-test inspection indicated that the indium plated seal had worn through the indium coating as shown in figure 1049. Seal wear on the flange surface is shown in figure 1050 and is typical for both flanges.

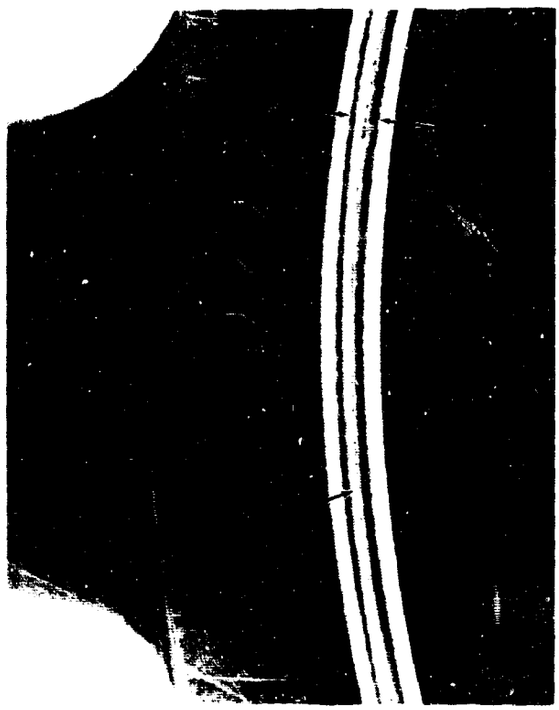

Figure 1049. Indium Coated C-Ring Static Seal FD 33121

The build 16 silver plated teflon primer coated seal showed approximately 18 sccs leakage at 1000 psig rig internal pressure for the first 300 cycles. The collection cavity purge valve was found to be leaking after 380 cycles. The line was disconnected and capped prior to leakage measurements after 400 cycles and the leakage generally decreased (less than 4 sccs at 1000 psig) indicating that purge valve leakage had contributed to the previous seal leakage measurements. The maximum leakage after 500 cycles were completed was 3.7 sccs and occurred at 1000 psig rig internal pressure.

Post-test inspection of the silver plated teflon primer coated seal showed that the seal coating did not conform completely to the mating surface as shown in figure 1051. The mating surfaces were in excellent condition.

The build 17 silver plated seal leakage was generally higher than the other C-rings tested. The minimum leakage occurred at 100 psig rig internal pressure and was greater than 1.0 sccs. The maximum seal leakage was 42 sccs and occurred at 3000 psig after 400 pressure cycles were completed.

Figure 1050. Flange Face of Indium Coated Seal FD 33122

Figure 1051. Silver Plated Teflon Primer Coated C-Ring Static Seal FD 33123

Post-test inspection of the silver plated seal indicated that the seal contact load was not satisfactory, as shown in figure 1052. The seal wear on the opposite side (groove side) was also very low as shown in figure 1053. The mating surfaces were in excellent condition.

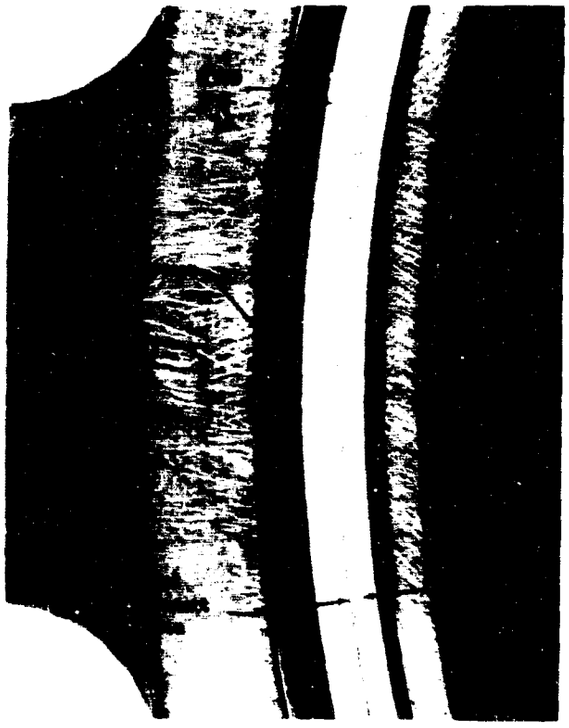

Figure 1052. Silver Plated C-Ring Static Seal FD 33124

The build 18 lead plated seal leakage was consistently lower than the other C-rings tested. The maximum leakage was 0.7 sccs and occurred at 2000 psi after the 500 cycles were completed. The installation of the displacement meter, which previously gave erroneous data, was corrected prior to this test and the data from this meter are included in figure 1048. The leakage that is indicated as being below the minimum flowmeter range caused a slight rise in collection cavity pressure as measured with a water manometer. A collection cavity pressure of 0.5 to 0.7 in. of water was required prior to leakage indication on the displacement meter. The time required to build up this pressure at those data points was excessively long and the actual leakage indication was not measured.

The post-test condition of the lead plated seal is shown in figure 1054. A closeup of the uniform seal contact area is shown in figure 1055.

The build 21 lead-indium plated seal was tested only at ambient temperature. Leakage was 2.0 sccs at the 1000-psig rig internal pressure and 1.0 sccs at 500 psig. The rig was cycled to 1000 psig 10 times in an attempt to seat the seal. Leakage after these cycles was 4.0 sccs at 1000 psig. This leakage was approximately 100 times greater than the ambient leakage of build 18.

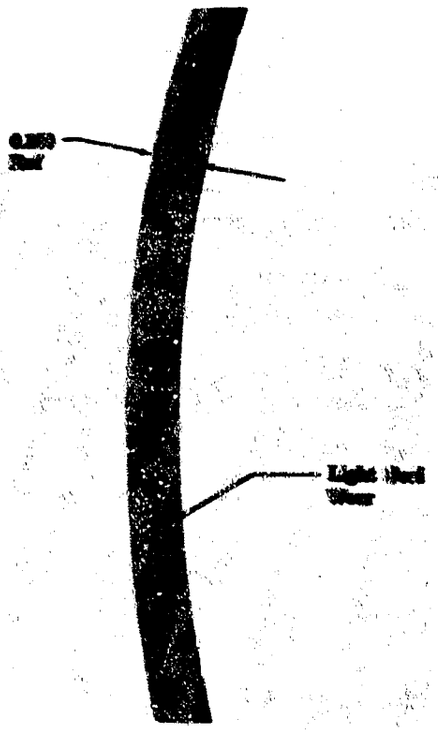

Figure 1053. Silver Plated C-Ring Static Seal FD 33125

Post-test inspection of the lead-indium plated seal indicated good condition, as shown in figure 1056. The seal contact deformation was marginal on the groove side as shown in figure 1057. Subsequent investigation has shown that the groove OD (spacer ID) was oversize for this seal. The ambient temperature 1000 psig pressure check was sufficient to exceed the material tensile strength with the seal unsupported on the seal OD. The mating surfaces were in excellent condition.

The Pressure Science C-ring did not meet the required 10^{-4} sccs maximum seal leakage per inch of seal circumference.

The lead plate seal coating was the best of the coatings tested. The indium coating was apparently too soft. The seal unit load was not sufficient to uniformly deform the silver plate or the teflon primer coat.

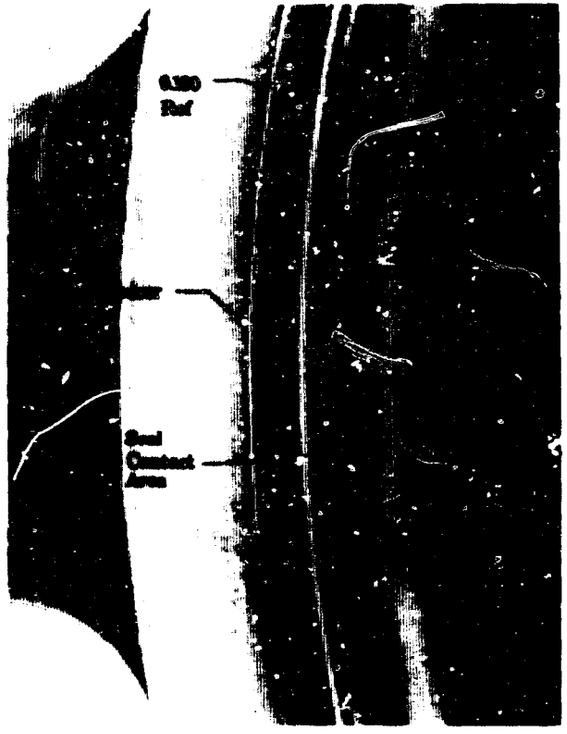

Figure 1054. Lead Plated C-Ring Static Seal FD 33126

Figure 1055. Flange Face FD 33127

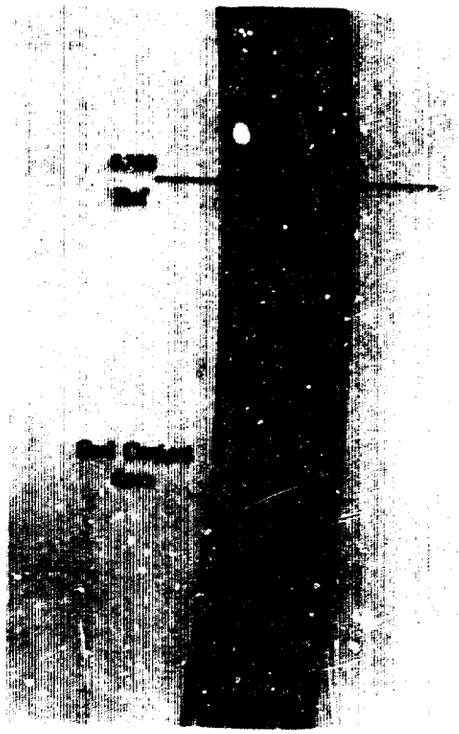

Figure 1056. Lead-Indium Plated C-Ring Static Seal

FD 33128

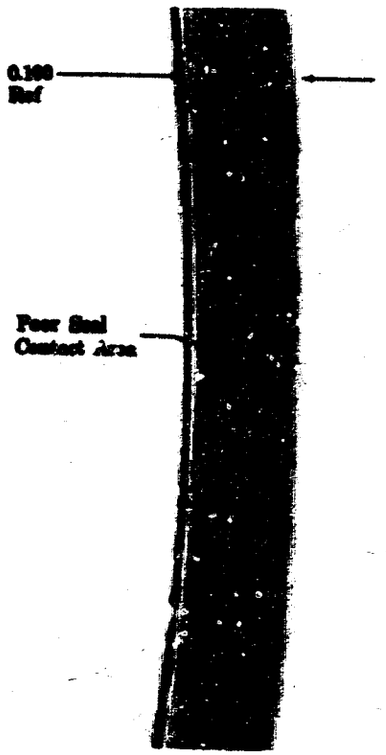

Figure 1057. Lead-Indium Plated C-Ring (Groove Side)

FD 33129

g. Test Rig 35120 - Builds 19, 20, 22, 23, 24, and 25

Builds 19, 20, 22, 23, 24, and 25 of test rig 35120 were conducted to evaluate the teflon coated Parker V-Seal by performing pressure cycles and leakage tests to the maximum design pressure of 7000 psig at cryogenic temperature. An additional objective was to measure the flange deflection due to bolt load and pressure. The test rig was assembled for each build as shown in figure 1058.

	Build 19	Build 20	Build 22	*Build 24	*Build 25
(A)	5.436	5.4355	5.431	—	5.436
(B)	5.513	5.513	5.513	5.513	5.513
(C)	0.106	0.106	0.1095	0.1095	0.1095
(D)	0.113	0.114	—	0.114	0.114
(E)	0.123	0.124	0.124	—	—
(F)	12C	4-5C	16-21C	—	5C
(G)	5M	5-6M	12-16C	—	8-10C
(H)	5.444	5.444	—	5.441	5.443
(I)	5.4371	5.4371	5.4371	5.4371	5.4371
(J)	Not Used	Not Used	Not Used	0.040	0.032

*Build 24 Seal Recoated After Use in Build 23E
*Build 25 Seal Recoated After Use in Build 23A and 23F

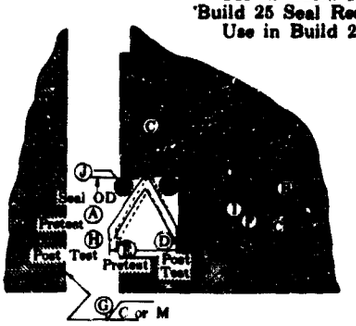

Figure 1058. Parker V-Seal and Sealing Conditions, Builds 19, 20, 22, 23, 24, and 25 FD 33417

The bolts for builds 19, 20, and 22 were stretched to an indicated 0.006-0.0062 in. Due to bolt bending, the average load per bolt was approximately 11,000 lb. The bolts for builds 24 and 25 incorporated spherical washers to reduce bolt bending. The bolts were stretched an indicated 0.006-0.0062 in. to obtain an average load per bolt of 14,500 lb.

The housings were reoperated prior to build 22 to increase the groove dimensions to maximum design condition of 0.106 in. groove depth.

Build 23 was instrumented with proximity probes and strain gages as shown in figure 1059 to measure the coupling deflection and bolt loads. Builds 23 and 23A were assembled with Parker V-Seals. Builds 23B and 23C were assembled using a 0.010 in. wall O-ring. Builds 23D, 23E and 23F were assembled using two 0.040 in. diameter Inconel 600 support rings with the Parker V-Seals as shown in figure 1058.

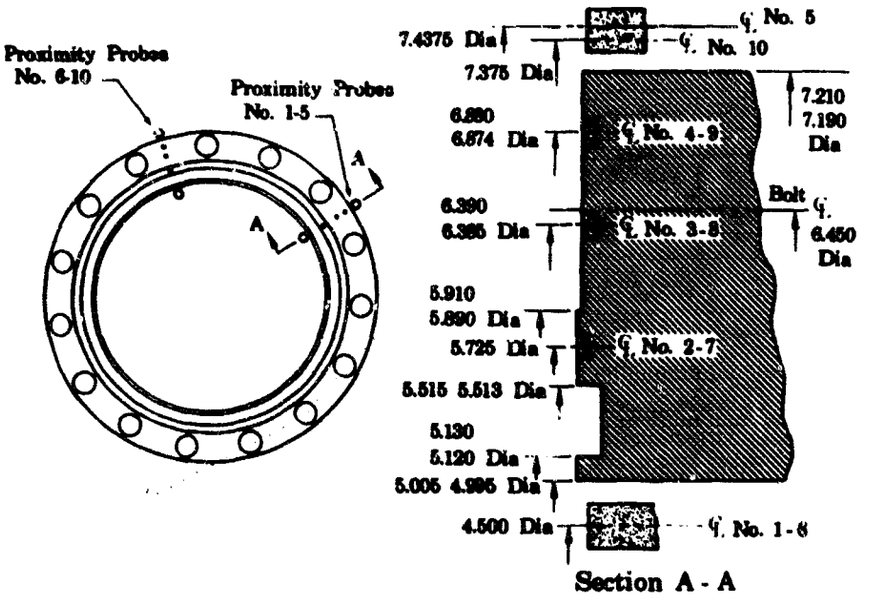

Figure 1059. Proximity Probe Locations, Build 23 FD 33416

Build 24 incorporated two 0.040 in. Inconel 600 wire support rings as shown in figure 1058. The seal used in this build was recoated with Teflon after previous use in build 23E.

Build 25 incorporated two 0.032 in. Hasteloy W wire support rings as shown in figure 1058. The seal used in this build was previously used in build 23A and build 23F, and was recoated with Teflon.

Sealing conditions for the endurance test builds are shown in figure 1058.

Builds 19 and 20 were mounted incorporating rotameter and positive displacement meters to measure leakage. Builds 22, 24 and 25 were mounted in installations incorporating rotameters and the gas chromatograph method of leakage measurement. Build 23 was tested at ambient conditions in the strain gage laboratory using hydraulic oil as the pressurizing media.

The cryogenic test results of builds 19, 20, 22, 24 and 25 are presented in figures 1060, 1061, 1062, 1063 and 1064, respectively. The Parker V-Seal leakage was generally lower than previous seals tested during this seal evaluation program except during build 22 when the seal rolled similar to the Apex Seal illustrated in figure 1043.

For build 19 (Reference figure 1060), the maximum leakage measured was 2.7 sccs at 5000 psig and zero cycles. After 300 cycles were completed, the indicated leakage was less than the available flowmeter range at all pressure levels tested and remained below the measurable limit.

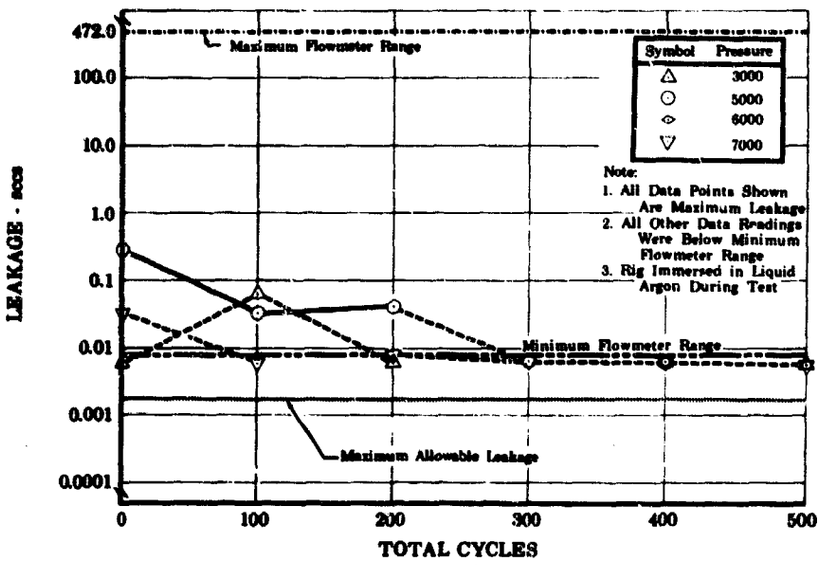

Figure 1060. Parker V-Seal, Build 19, Leakage vs Total Cycles FD 33418

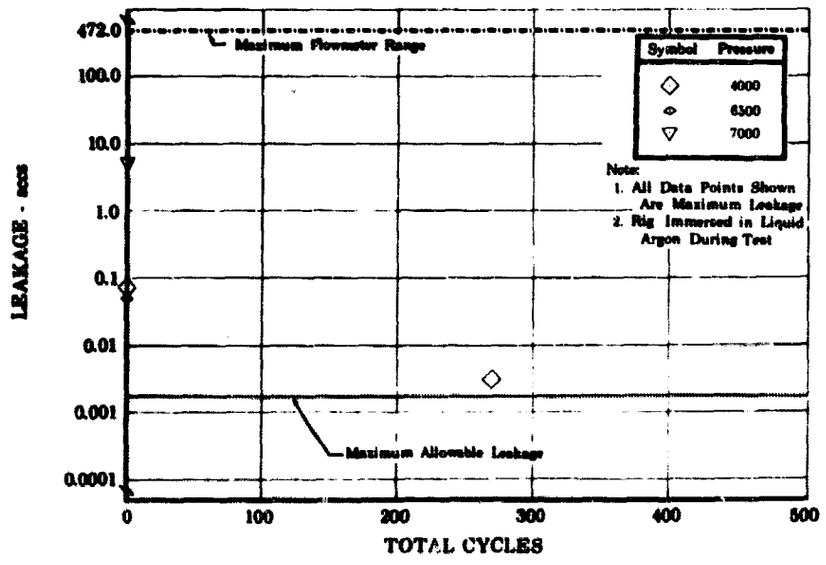

Figure 1061. Parker V-Seal, Build 20, Leakage vs Total Cycles FD 33419

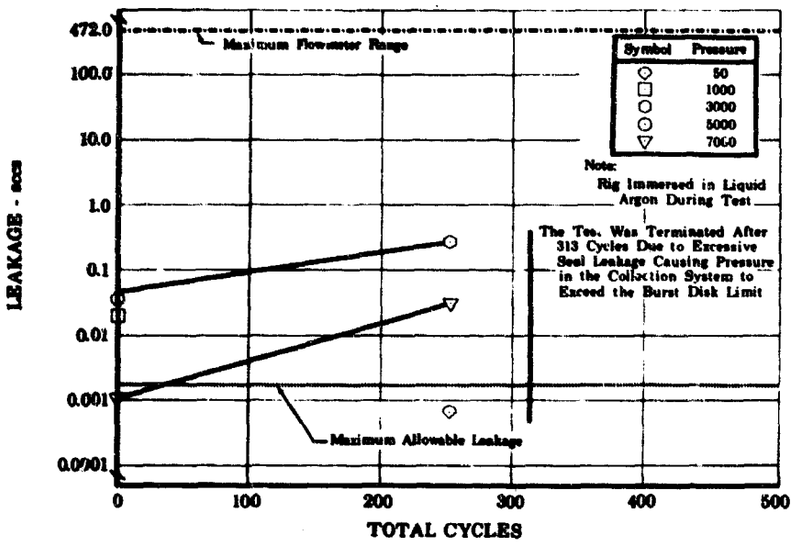

Figure 1062. Parker V-Seal, Build 22, Leakage vs Total Cycles FD 33420

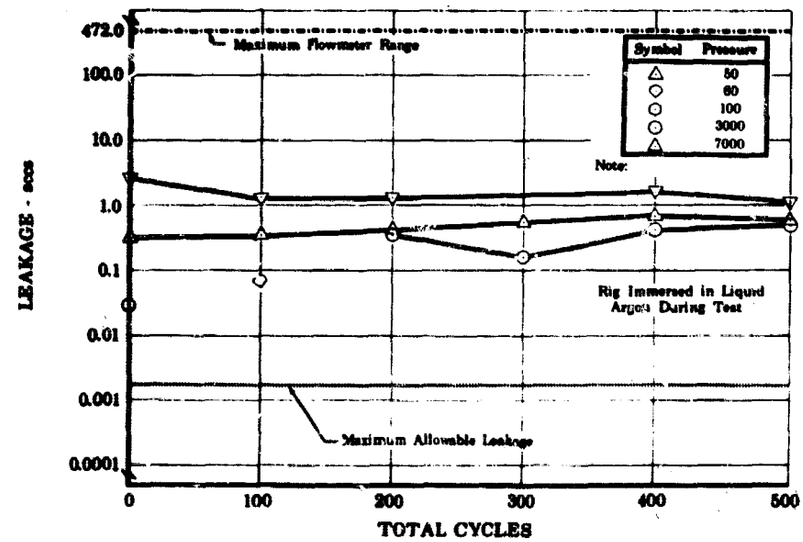

Figure 1063. Parker V-Seal, Build 24, Leakage vs Total Cycles FD 33421

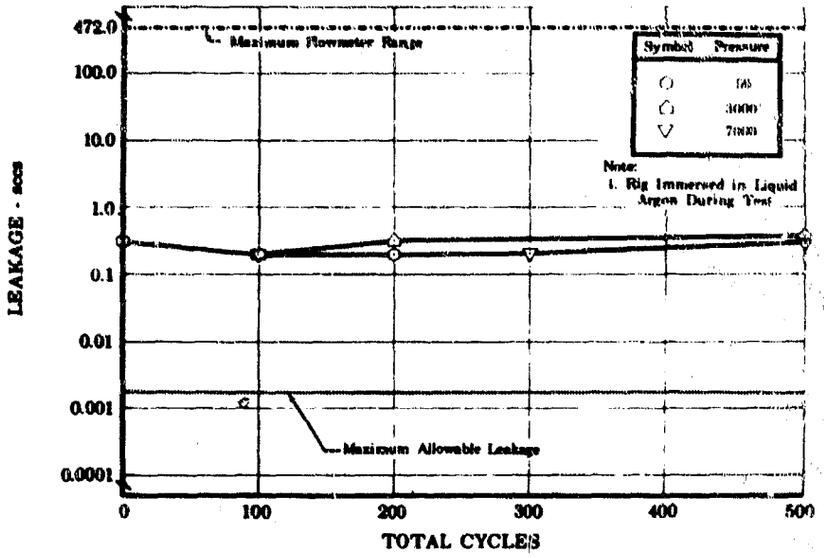

Figure 1064. Parker V-Seal, Build 25, Leakage vs Total Cycles FD 33432

For build 20 (Reference figure 1061), the maximum leakage measured was 4.6 sccs at 7000 psig and zero cycles. At 500 cycles, the indicated leakage was less than the available flowmeter range at all pressure levels tested. Several methods of leakage measurement were attempted during this build.

For build 22 (Reference figure 1062), the maximum leakage measured was 0.268 sccs at 3000 psig and 250 cycles. At 313 cycles excessive seal leakage occurred. This lack of sealing was attributed to the Parker V-Seal rolling in the seal groove similar to the Apex Seal shown in figure 1043. Several pressure cycles to 5000 psig did not reseat the seal and the cycle test was terminated.

For build 24 (Reference figure 1063), the maximum leakage for the test occurred at 7000 psig prior to cycling and was 2.8 sccs. Leakage at 7000 psig was approximately 1.5 sccs throughout the cycle test.

For build 25 (Reference figure 1064), the maximum leakage was 1.95 sccs at 7000 psig and 100 cycles. The leakage at this point was measured using a rotameter.

The ambient test results of the coupling deflection tests of build 23 are shown in figure 1065. Builds 23 and 23A were terminated when excessive hydraulic fluid leakage occurred at approximately 2500 psig. Build 23B was disassembled to repair strain gages. Build 23C deflection test results are presented in figure 1065. The strain gage data from builds 23, 23A and 23C are shown in figure 1066. Builds 23D, 23E and 23F were assembled to substantiate the use of support rings to prevent seal rolling.

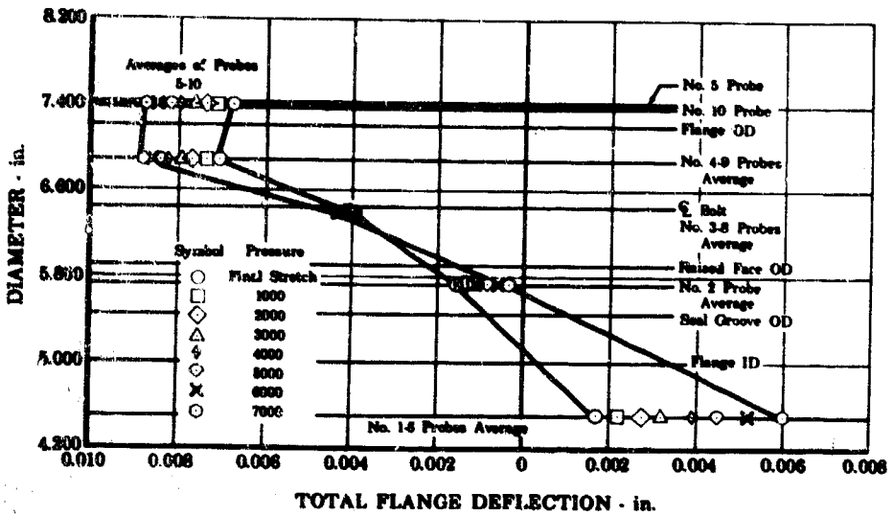

Figure 1065. Flange Deflection, Build 23C FD 33422

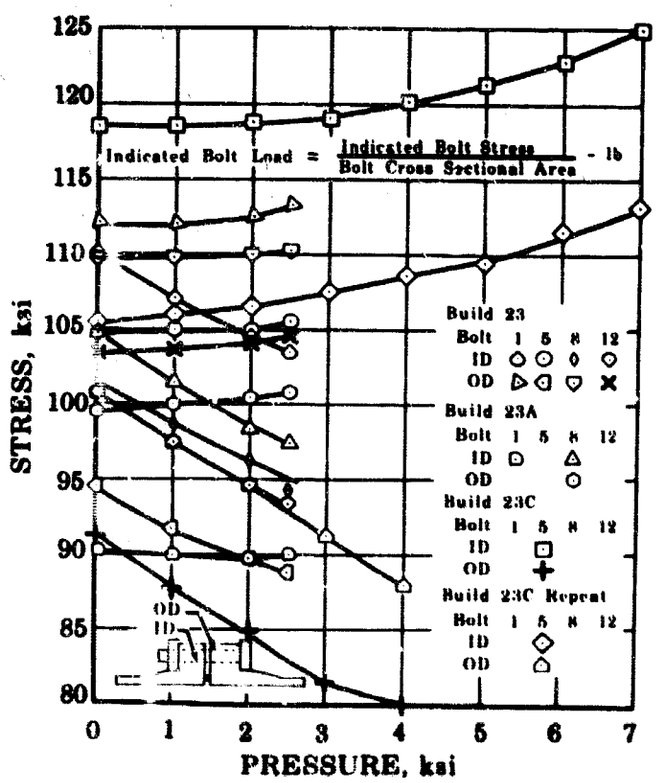

Figure 1066. Bolt Stress vs Pressure, Build 23 FD 33423

The maximum allowable leakage requirement of 10^{-4} sccs of GN_2 per inch of seal circumference necessitated development of a leakage measurement device to reliably measure leakage in this range. During the Parker V-Seal testing, several methods of leakage methods were used. Rotameters were used to measure leakages of 0.05 sccs to 470 sccs during seal testing. Unstable indication at the low leakage points near 0.05 sccs were attributed to slight temperature changes in the collection cavity. A typical leakage plot showing decay with time, was recorded during build 20 and is shown in figure 1067. Positive displacement meters, one using water and one using alcohol as the displaced fluid, were used during the early seal tests. The leakage source was connected above the column of liquid creating a slight vacuum on the collection system. The error induced by this installation is proportional to the volume of the collection system and had resulted in a rather large error due to the large leakage cavity volume. The installation was corrected and the water displacement meter was used for leakages down to 0.001 sccs. Changes in the collection cavity temperature and the pressure required to eject a bubble into the column caused erratic indications. The small diameter (0.125 in.) of the alcohol displacement meter tube made injection of the bubble into the column difficult and the meter was not used. During build 20, several means of measuring the leakage were attempted. The horizontal displacement of an air bubble injected in a tube between two water vessels and the displacement of a mercury bubble across a horizontal tube were two methods used. Both required a stable positive pressure which was not attainable due to the unstable temperature. The gas chromatograph means of measuring leakage, shown schematically in figure 1068, was used with consistent results on build 21 and was refined during builds 22, 24 and 25. The collection cavity was pressurized to 10 psig with helium and the cavity was monitored for increase in nitrogen content. The chromatograph was calibrated using known gas mixtures.

The chromatograph used consisted of:

1. Tungsten filament Glomac gas detector, S/N TR2B illustrated in figure 1069.

2. A 6 ft long, 1/4 in. diameter column filled with a molecular sieve compound.

3. A 300 milliampere Glomac power supply, S/N 178G.

4. A Sargent recording strip chart, S/N 1697024. The generally used set up to date results in a 200 part per million per millivolt indication on the recording chart. (2 parts per million per 0.1 in. chart deflection.)

Post-test inspection of build 19 revealed portions of the Teflon coating were blistered and frayed along the sealing edge and the seal OD. The primer coat was intact as shown in figure 1070. The seal groove was in good condition and unmarked by the seal as shown in figure 1071.

Post-test inspection of build 20 seal condition showed the Teflon frayed similar to build 19 as shown in figure 1072. The flange sealing surfaces were in good condition.

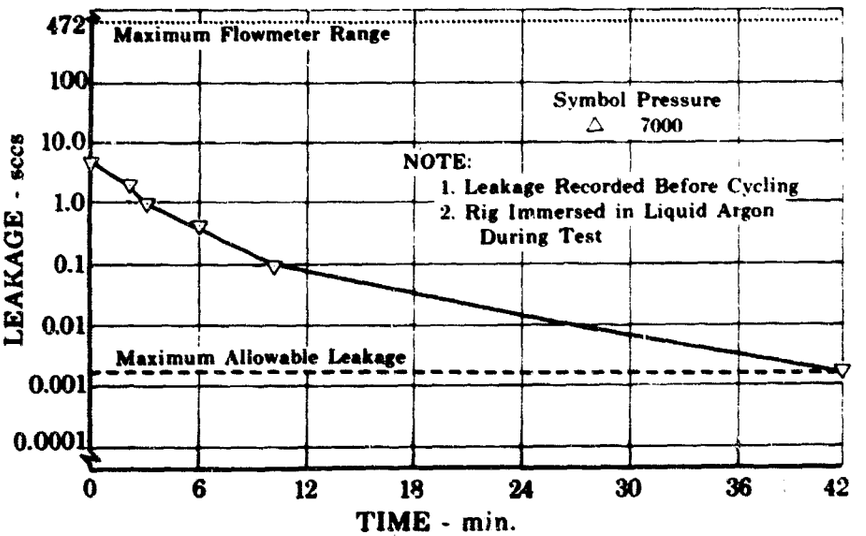

Figure 1067. Parker V-Seal, Build 20 Leakage vs Time FD 33424

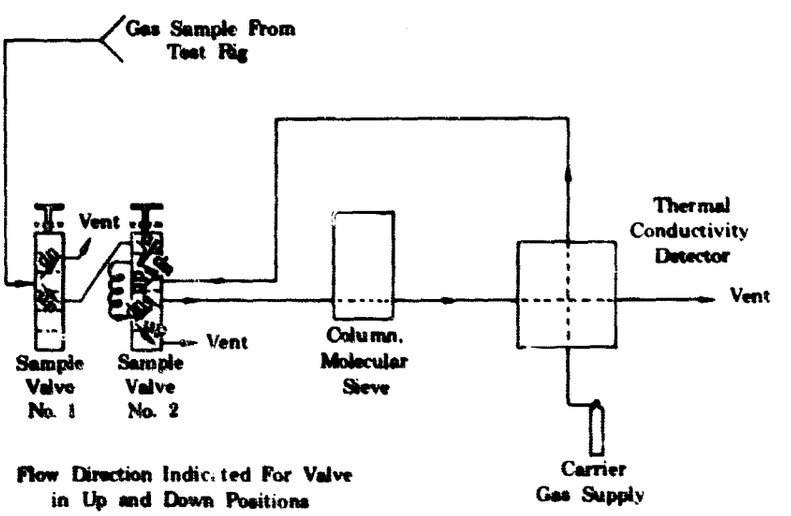

Figure 1068. Chromatograph, Gas Flow Schematic, Builds 22, 24, and 25 FD 33425

Post-test inspection of build 22 seal and groove appearances showed conditions similar to build 19 except that the seal had rolled in the groove as illustrated in figure 1073.

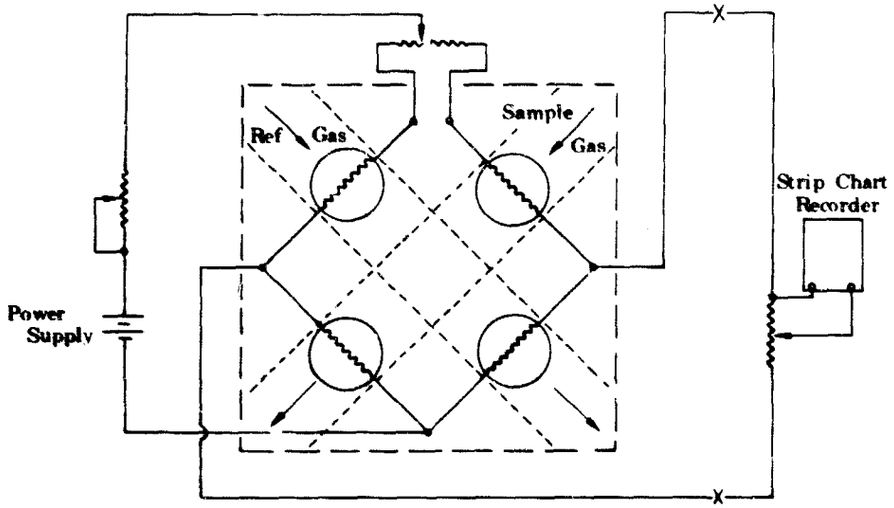

Figure 1069. Thermal Conductivity Detector, Balanced Bridge Circuit — **FD 33426**

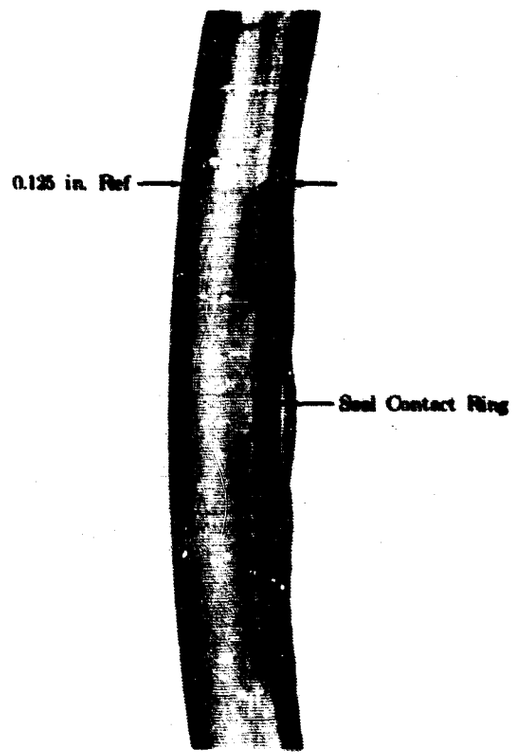

Figure 1070. Parker V-Seal, Build 19 — **FD 33427**

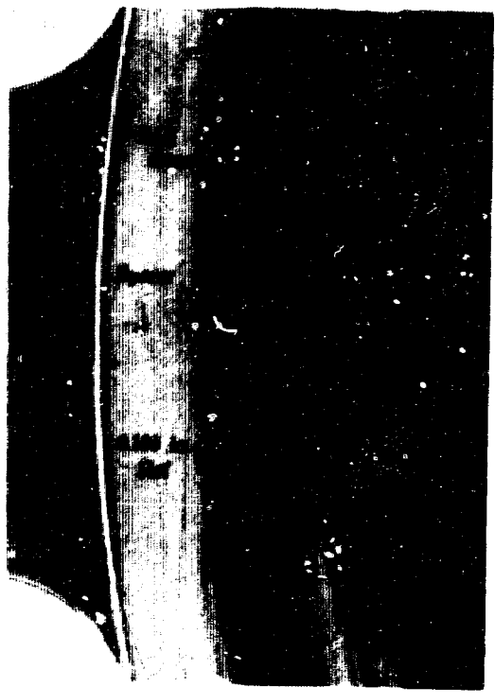

Figure 1071. Seal Groove, Build 19 FD 33429

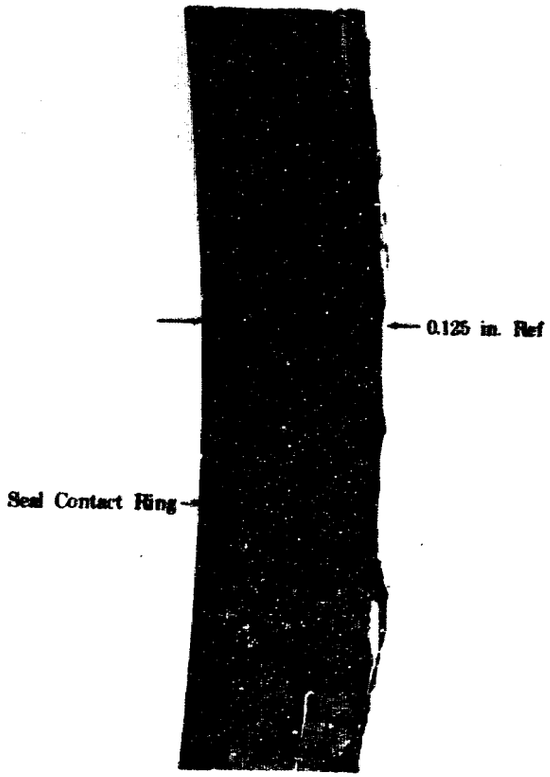

Figure 1072. Parker V-Seal, Build 20 FD 33430

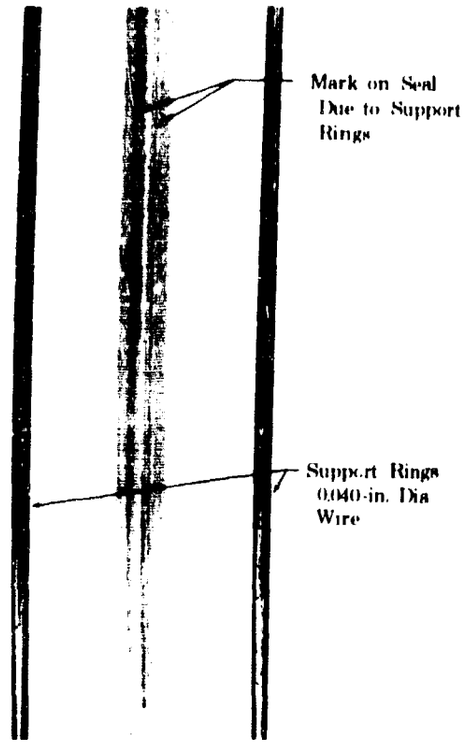

Figure 1073. Seal and Support Rings, Build 24 FD 33431

Post-test inspection of builds 24 and 25 showed the seal and groove in excellent shape. No tearing or blistering of the sealing surface was evident and only minor fraying on the seal OD occurred. The 0.040 in. diameter wire support rings of build 24 showed light contact with the seal as shown in figure 1073.

h. Test Rig 35120 - Builds 26 Through 30

Builds 26 through 30 of test rig 35120 were conducted to evaluate the inverted C-Seal by performing pressure cycles and leakage tests to the maximum design pressure of 7000 psig at cryogenic temperature.

The seal test rig housings were modified to incorporate a 0.050 in. deep seal groove, in both flange faces as shown in figure 1074. Two 0.020 in. deep grooves were machined across the bearing surface after build 26 to assure sealing did occur at the seal and not at the pivot point.

The sealing conditions for each build are shown in figure 1074. The inverted C-Seals were fabricated by reoperating Pressure Science external pressure seals. The seal OD for builds 26 and 27 was ground to give 180° seal cross sectional circumference in the free state. Seals for builds 28, 29 and 30 were stretched to increase the seal ID and the OD was ground to give 150° seal cross sectional circumference in the free state. This provided approximately 180° seal circumference in the compressed condition.

	Build 26	Build 27	Build 28	Build 29	Build 30
(A)	5.454	5.4539	5.458 5.448	5.4493	5.452
(B)		5.475 5.429	5.460	5.451	5.460
(C)	5.312	5.203	5.348 5.338	5.348	5.335
(D)		5.340 5.290	5.339	5.337	5.343
(E)	0.143	0.1342	0.124		0.123
(F)	0.104	0.105 0.090*	0.015	0.106 0.104	0.106
Seal Coating	0.0015 0.002 Lead	0.0015 0.002 Lead	0.0005 0.001 Lead	0.0005 0.001 Lead	0.0005 Primer and One Coat Teflon

*In Collapsed Area

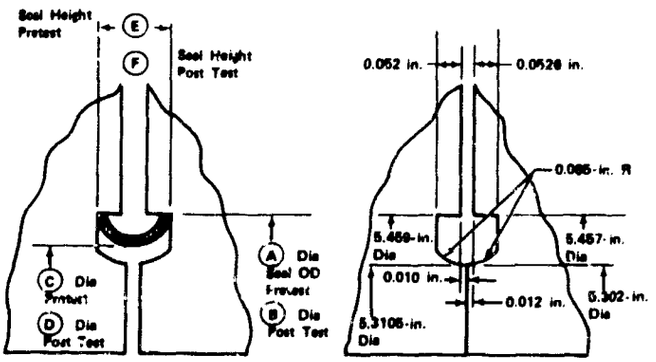

Figure 1074. Inverted C-Seal and Sealing Conditions FD 33748

The bolts were stretched to an indicated 0.0060 to 0.0065 in. Spherical washers were used under the bolt head and the nuts to minimize bolt bending. Bolt load for this stretch is 14,500 lb per bolt.

The rig was installed for each build on B-22 test stand and the gas chromatograph method of leakage measured used.

The test results for the inverted C-Seal are shown in figures 1076 through 1078. The test results showed generally lower leakages at all pressures than previous seals tested. The maximum leakage recorded was 8.7 sccs and occurred during build 30 (the Teflon coated seal) at 5000 psig rig internal pressure after 500 cycles had been completed. The seal of build 27 collapsed and the leakage was greater than the available measurement capabilities after one cycle and is not shown.

For build 26, all leakage measurements taken at 50 psig through 7000 psig rig internal pressure after 300 pressure cycles were completed indicated less than the allowable leakage of 10^{-4} per inch of seal circumference. The maximum total leakage during the test occurred at 3000 psig after 50 cycles were completed and was 0.027 sccs. The maximum total leakage after 500 cycles were completed was 0.00067 sccs (0.4×10^{-4} sccs per inch of seal circumference) and occurred at 3000 psig.

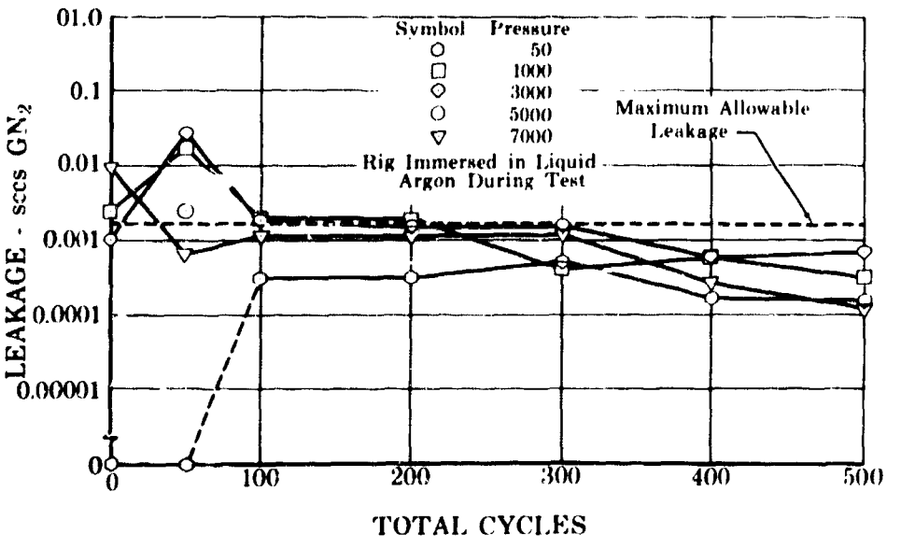

Figure 1075. Inverted C-Seal, Build 26, Leakage vs Total Cycles

FD 33087

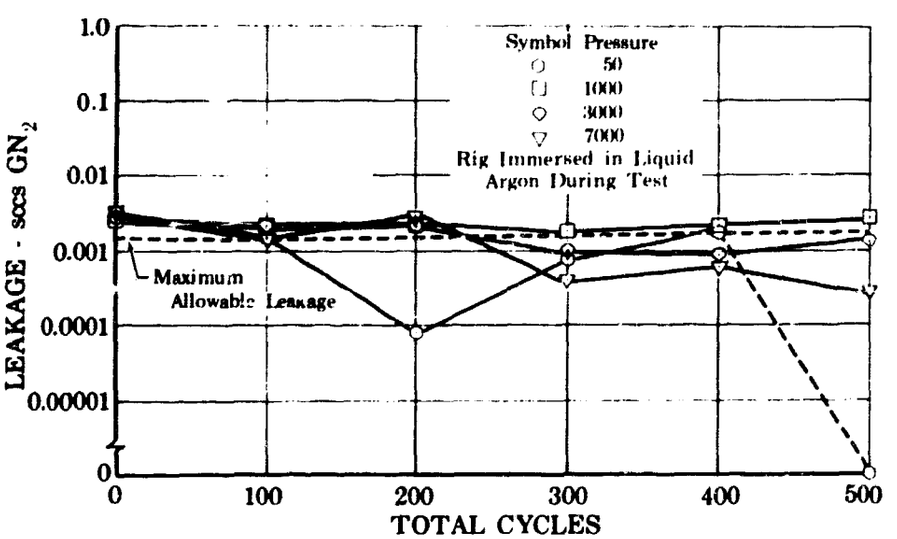

Figure 1076. Inverted C-Seal, Build 28, Leakage vs Total Cycles

FD 33089

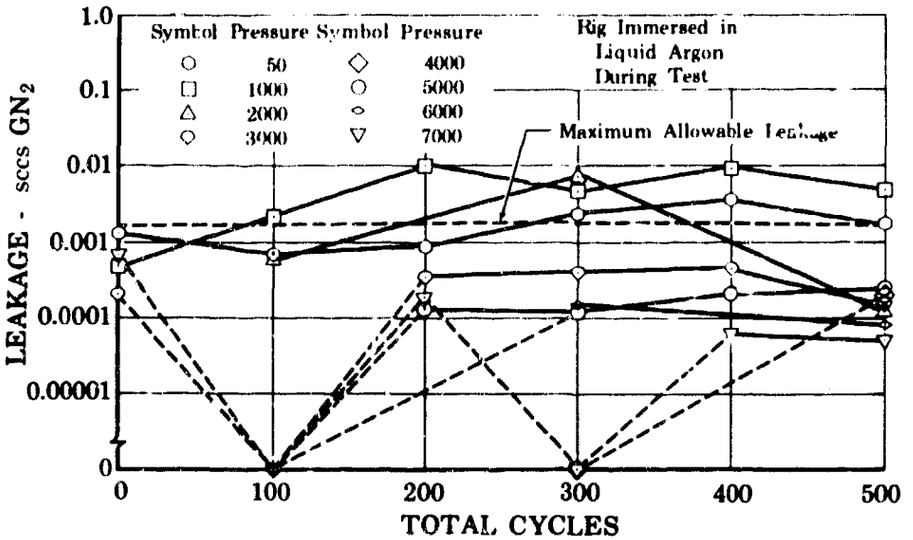

Figure 1077. Inverted C-Seal, Build 29, Leakage vs Total Cycles

FD 33090

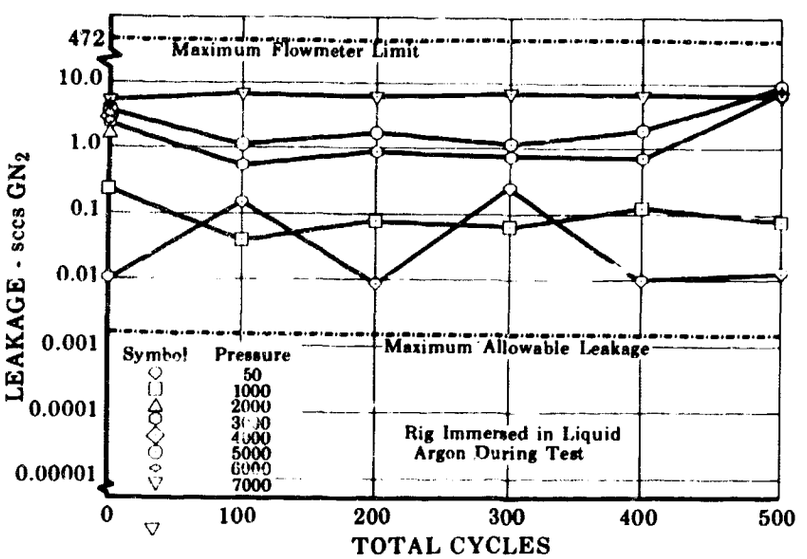

Figure 1078. Inverted C-Seal, Build 30, Leakage vs Total Cycles

FD 33392

For build 27, the leakage prior to cycling was within the allowable leakage limit at 50, 1000, and 7000 psig, and was 0.115 sccs at 3000 psig. After one cycle, the collection cavity pressure rise indicated excessive leakage and measurements showed approximately 45 sccs at 1000, 3000, and 5000 psig, and 470 sccs at 7000 psig. A second attempt to measure leakage indicated 216 sccs at 1000 psig and over 470 sccs at 3000 psig. The cycle test was terminated.

For build 28, the maximum total leakage occurred prior to cycling at 7000 psig and was 0.0033 sccs. The total leakage at 5000 psig was approximately a constant 0.0025 sccs throughout the test. Total leakage at 7000 psig after 500 cycles were completed was 0.00029 sccs.

For build 29, the maximum total leakage for build 29 was 0.01 sccs and occurred at 1000 psig after 200 cycles had been completed. The maximum total leakage at 50 psig was 0.0033 sccs and occurred after completing two pressure cycles. Total leakage at 7000 psig was within the allowable leakage limit throughout the test and was 0.00045 sccs after 500 cycles were completed.

For build 30, leakage at all test pressure levels was greater than the maximum allowable leakage. The total leakage at 7000 psig varied from 5 to 7 sccs throughout the test. The minimum total leakage was 0.009 sccs and occurred at 50 psig.

Build 26 seal inspection showed the seal had rolled past the groove corner when compressed as shown in figure 1079. Sealing apparently took place on the seal side and not in the groove corner as intended. The seal was marred on the inside diameter indicating contact with the groove inside land on the seal. The flanges were in excellent condition. Build 27 seal was collapsed between bolts No. 4 and No. 5 as shown in figure 1080. Figure 1081 shows the cross sections of the collapsed area and the adjacent area. The adjacent area shows excessive seal material as in build 26. The collapsed area shows seal contacted the groove prior to collapse. Build 28 seal was in excellent condition. The cross sectional view, figure 1082, indicated sealing took place in the groove corner. All parts were in excellent condition. Build 29 seal was in the same good condition as shown in figure 1083. No discrepancies were noted during this build. Build 30 seal showed some metal particle contamination in the Teflon coating. The Teflon was frayed as shown in figure 1084. The seal cross section is shown in figure 1085.

1. Test Rig 35120 - Builds 31 through 35

Tests for builds 31, 32, 32A, 33, 34, 34A and 35 were completed using rig 35120 on stand B-22. Build and test objectives were as follows:

1. The primary objective of this test series was to evaluate the pivot ring seal by performing pressure cycles to 7000 psig at cryogenic temperature.

2. The secondary objective was to evaluate methods of performing temperature cycles between 140° R and 620° R, and determine the minimum time required for one cycle.

3. An additional objective was to evaluate the effectiveness of the F-46159 air ratchet wrench, as a means of providing uniform bolt stretch during assembly. See figure 1086.

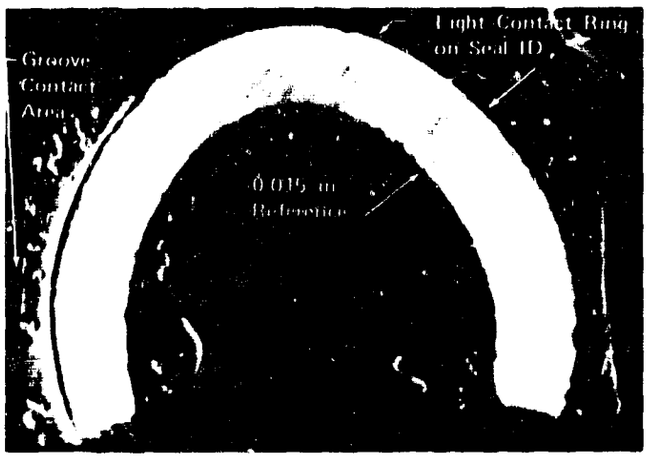

Figure 1079. Build 26 Seal Condition FD 33741

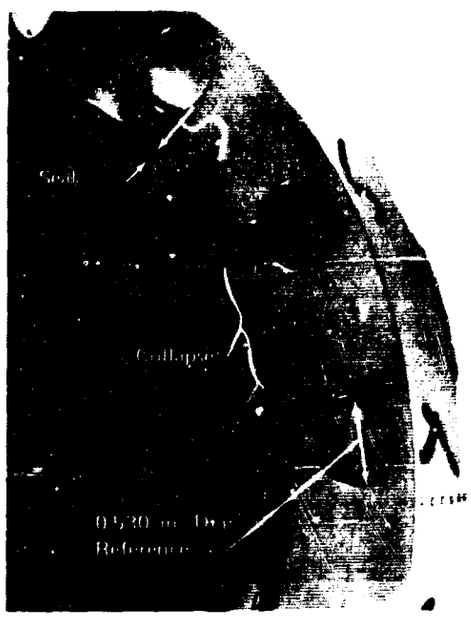

Figure 1080. Build 27 Seal Condition FD 33742

Figure 1081. Build 27 Seal Condition, Cross Sectional View FD 33743

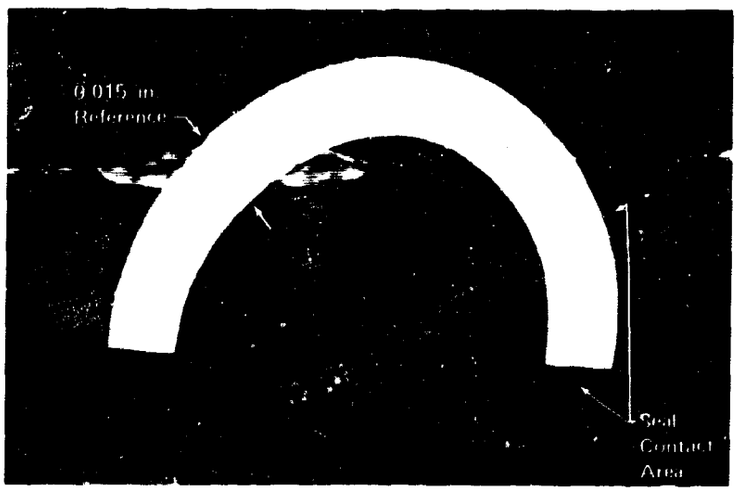

Figure 1082. Build 28 Seal Condition FD 33744

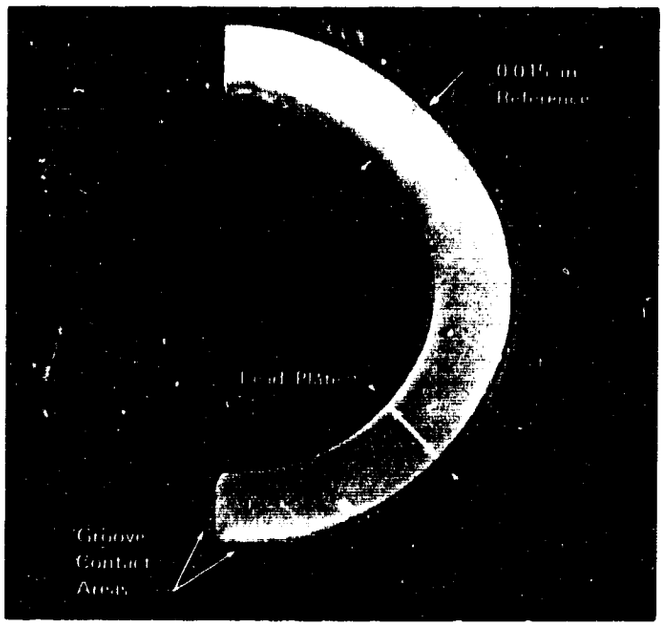

Figure 1083. Build 29 Seal Condition FD 33745

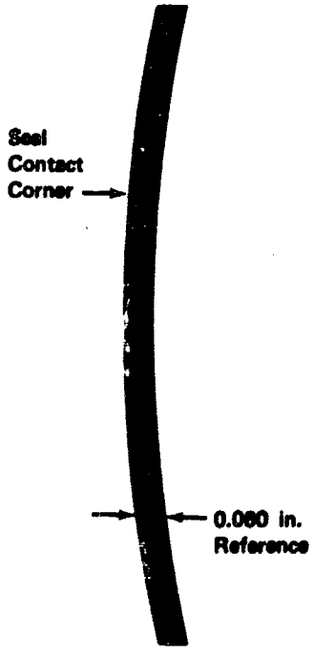

Figure 1084. Build 30 Seal Condition FD 33746

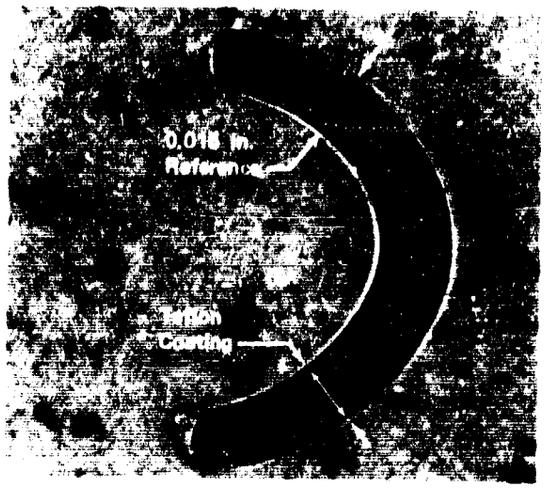

Figure 1085. Build 30 Seal Condition, Cross Section View FD 33747

Figure 1086. Air Ratchet Wrench, F-46159 FD 38705

The seal test rig housings were modified to incorporate a 0.075-in. radius groove in both housings, and the seals were machined as shown in figure 1087. The seal height was sufficient to make the seal become the bearing surface and pivot point. The seal bearing surface area was reduced after build 32 to increase maximum sealing bearing load from 55,000 lb/in.^{2} to 136,000 lb/in.^{2} of sealing surface for builds 33 and 34, and to 150,000 lb/in.^{2} of sealing surface for build 35. On builds 31 through 34A, an indicated 0.006 to 0.0065 in. final stretch was performed using standard torquing methods to comply with tolerance requirements. On all builds the bolts and spherical washers were cleaned and coated with three coats of slipspray. On build 35, the initial 100 in.-lb torque was applied by standard torquing methods. The F-46159 air ratchet wrench was then used to attempt final stretch. A 250 in. torque (minimum wrench torque) and 30 deg and 60 deg angles of turn (90 deg total) as shown in figure 1088 were performed. Figure 1089 shows the bolt stretch as a result of this procedure. Final stretch of 0.006 to 0.0065 in. was attained using standard torquing methods.

Ref	31	32A	33	34	34A	35
(A)	5.607	5.5999	5.5907	5.588	5.581	5.581
(B)	5.307	5.2925	5.290	5.287	5.303	5.303
(C)	0.1824	0.1831	0.1832	0.186*	0.180	0.180
(D)	0.075 0.070	0.075 0.070	0.075 0.070	0.075 0.070	0.082 0.080	0.082 0.080
(E)	0.150	0.146	0.090 0.088	0.090 0.088	0.089	0.079
Seal Plate	0.001 0.002 Lead	0.002 0.003 Lead	0.002 0.003 Lead	0.0015 0.002 Lead	0.0015 0.002 Lead	0.0015 0.002 Lead

*Plated

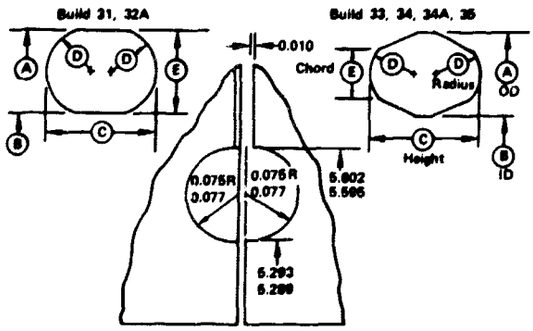

Figure 1087. Pivot Ring Seal and Sealing Conditions for Builds 31, 32A, 33, 34A and 35. FD 38487

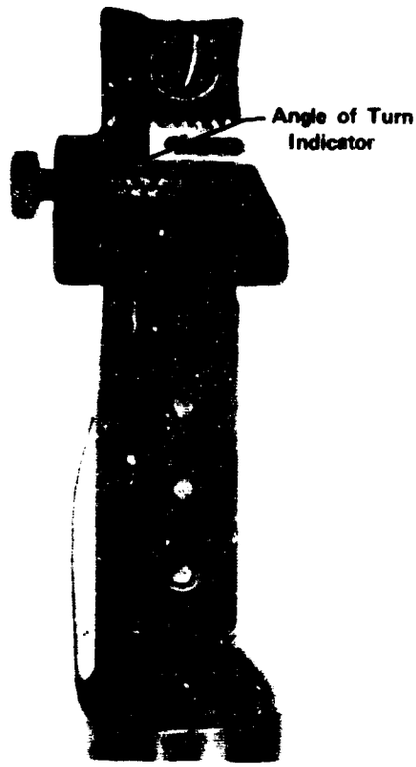

Figure 1088. Air Wrench Angle of Turn Indicator FD 38706

Pressure cycle test results of builds 31 through 35 are represented below. Highest leakage occurred at 7000 psig rig internal pressure during build 32A at a total leakage rate of 20 sccs.

Build 31 total leakage measurements before and after cycle test completion were above the maximum allowable limit. The total leakage at 7000 psig was from 0.0017 sccs after 200 cycles to 0.06 sccs after the 500 cycles were completed. Figure 1090 shows the relationship of leakage vs total cycles for build 31.

Build 32 ambient pressure check at assembly showed 50 sccs leakage at 1000 psig. The cryogenic pressure cycle test was omitted for this build.

Build 32A leakage rates, as shown in figure 1091, indicate that leakage at 5000 and 7000 psig was above the allowable limit throughout the pressure cycle test with 1000 psig leakages of 13 to 20 sccs. The run was terminated after 200 cycles due to excessive leakage.

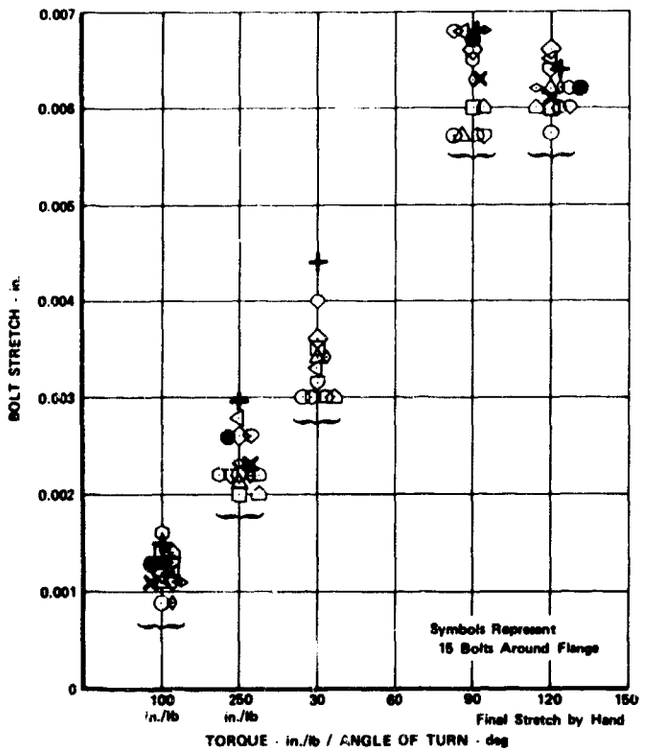

Figure 1089. Bolt Stretch vs Torque/Angle of Turn, Build 35 FD 38497

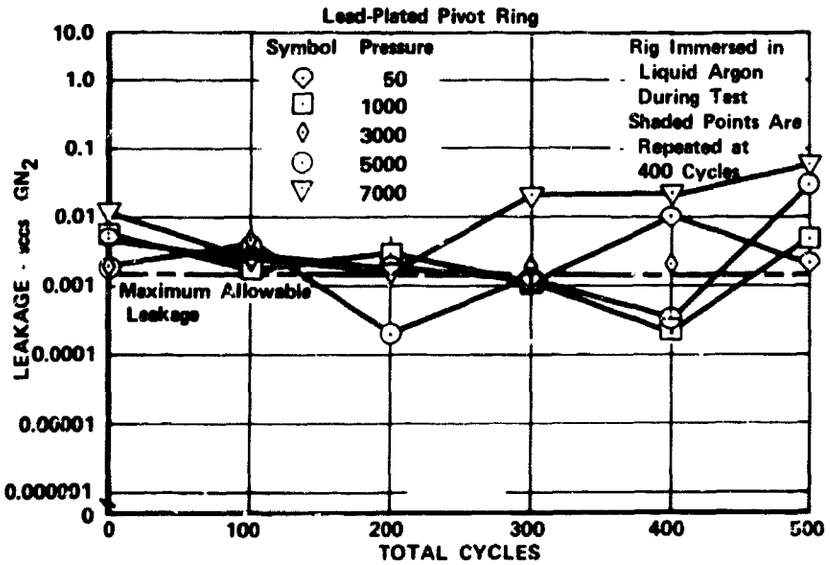

Figure 1090. Lead-Plated Pivot Ring, Build 31 Leakage vs Total Cycles FD 38378

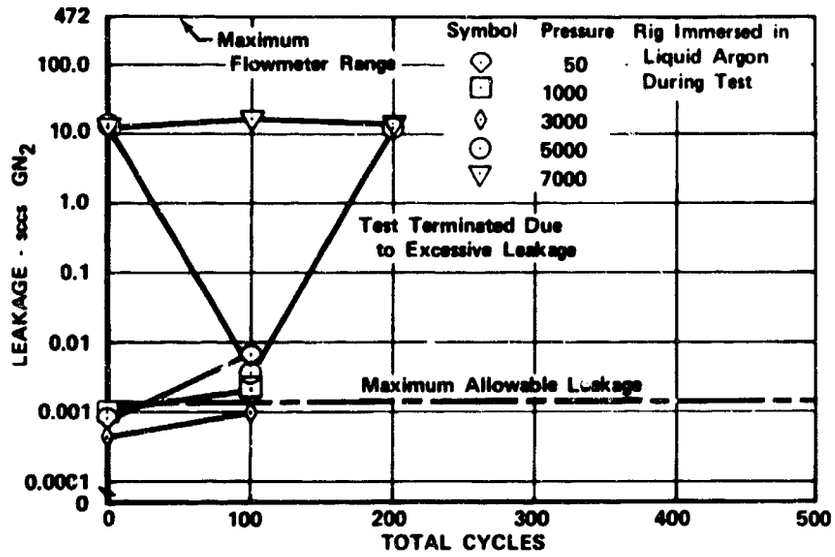

Figure 1091. Lead-Plated Pivot Ring, Build 32A, Leakage vs Total Cycles FD 38500

Build 33 leakage rates, as indicated in figure 1092, revealed that leakage throughout the test was less than the minimum allowable leakage except for a 0.009 sccs total leakage at 7000 psig (after 400 pressure cycles had been completed). A repeat of this point indicated 0.0012 sccs total leakage, which is less than the 0.0016 sccs maximum allowable leakage.

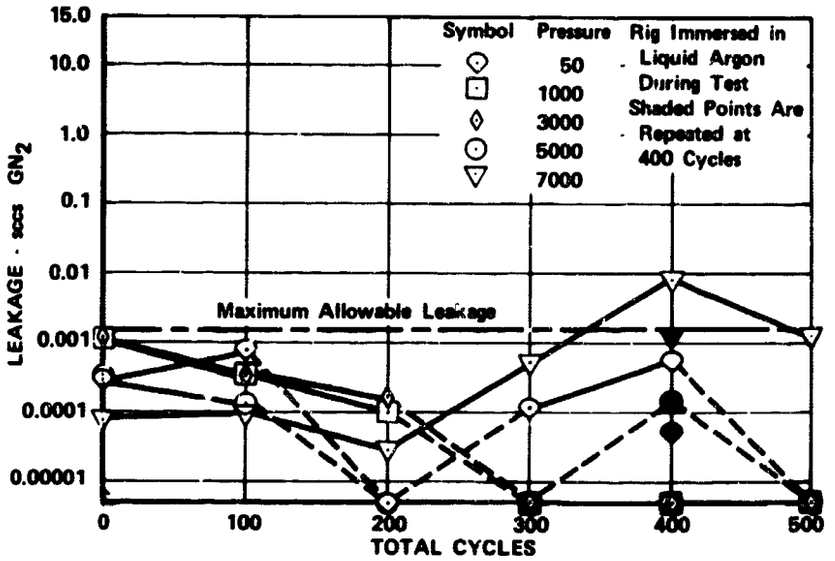

Figure 1092. Lead-Plated Pivot Ring, Build 33, Leakage vs Total Cycles FD 38651

Build 34 cryogenic test was canceled when the flanges cocked approximately 0.010 in. during assembly. The rig was disassembled for inspection and the cryogenic test omitted for this build.

Build 34A leakage rate curves shown in figure 1093 reveal that the total leakage at 7000 psig during the pressure cycle test was 0.0035 sccs before cycling, decreasing to within the allowable limit after 100 cycles. As cycling continued, the leakage at 7000 psig increased to 0.4 sccs after the 500 pressure cycles were completed. The test stand was modified for performing thermal cycles after the pressure cycle tests of build 34A. Thirteen thermal cycles were completed during this build. Warmup to 600° R was accomplished by several combinations of immersing the rig in hot water (650° R) and bubbling steam into an ambient water bath. Typical warmup transients are shown in figure 1094. Cold shock was accomplished by immersing the rig in LN_2. The maximum leakage after 13 thermal cycles was 0.124 sccs and occurred at 7000 psig. Six pressure cycles at 7000 psig were performed and the maximum leakage decreased to 0.009 sccs at 7000 psig rig internal pressure. Figure 1095 compares the thermal cycle cooldown rates of build 34A (LN_2 bath) with build 35 (LN_2 flow). Flange OD and ID temperature probes were used in this build.

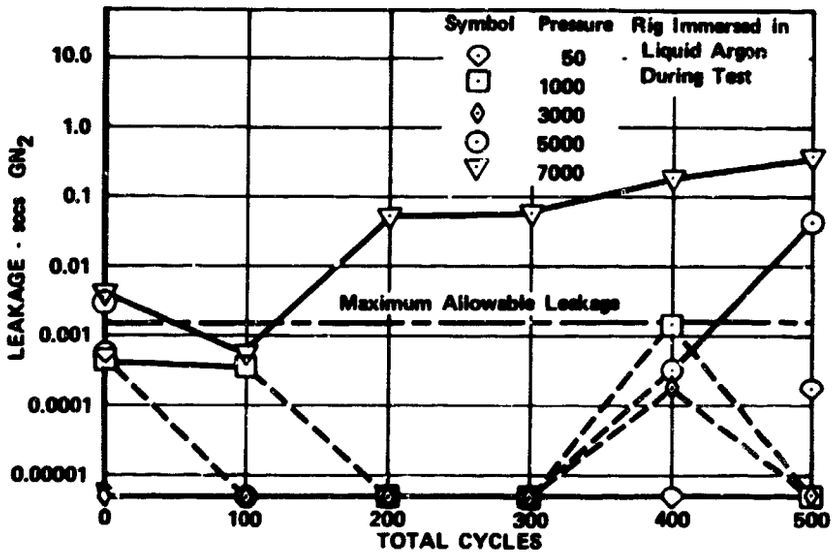

Figure 1093. Lead-Plated Pivot Ring, Build 34A, Leakage vs Total Cycles FD 38652

Build 35 cycle test was run with results as shown in figure 1096. The only leakage noted during the test occurred at 7000 psig and the maximum total leakage was 0.193 sccs after 100 pressure cycles. Leakage had reduced to 0.052 sccs at 7000 psig after 500 pressure cycles were completed. As shown in figure 1095, thermal cooldown was accomplished by LN_2 flow.

Seven thermal shock cycles were performed by flowing LN_2 through the pressure cavity of the rig. Leakage remained constant during the thermal cycle test as shown in figure 1097. Cold shock by this method produced a 375°R differential temperature across the flange as shown in figure 1095 (note thermocouples are 90 deg apart). Warmup was accomplished by submerging the rig in steam heated water and flowing ambient GN_2 through the rig. Flange OD and ID temperature probes were provided on build 35.

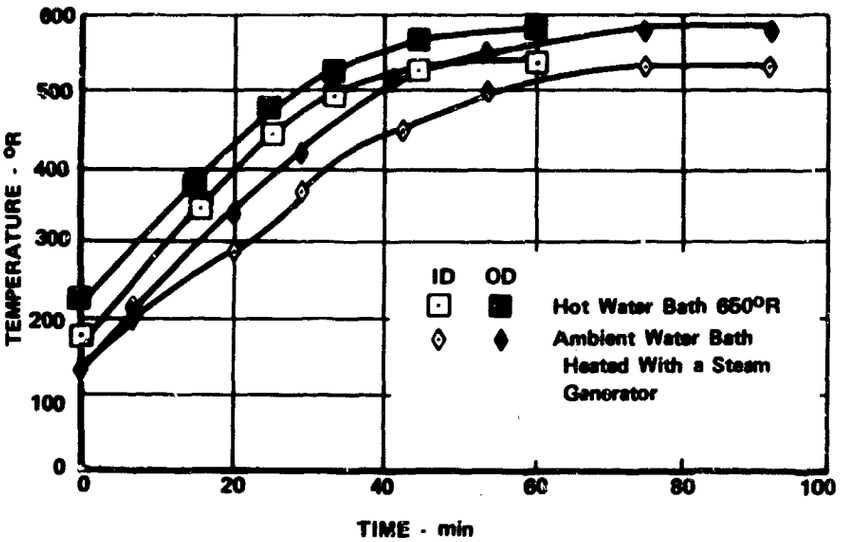

Figure 1094. Warmup Temperature vs Time, Build 34A During Thermal Cycling FD 38499

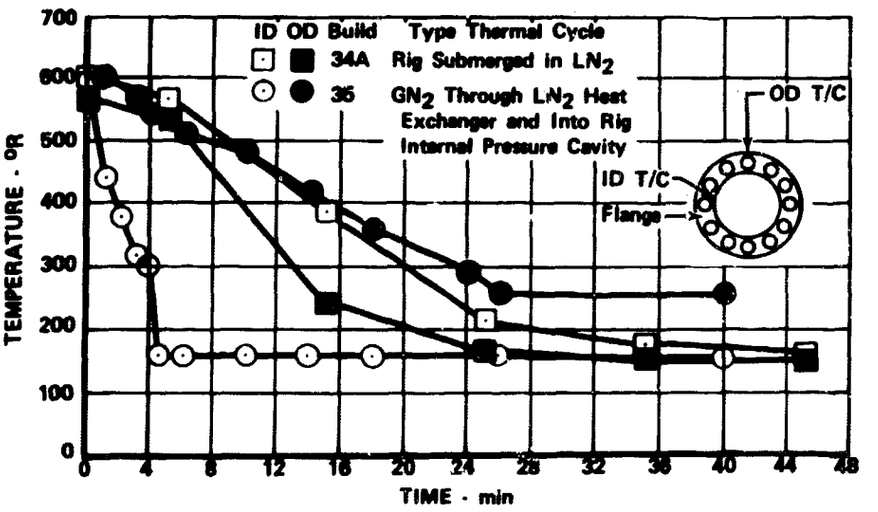

Figure 1095. Flange Temperature vs Time, Builds 34A and 35 FD 38496

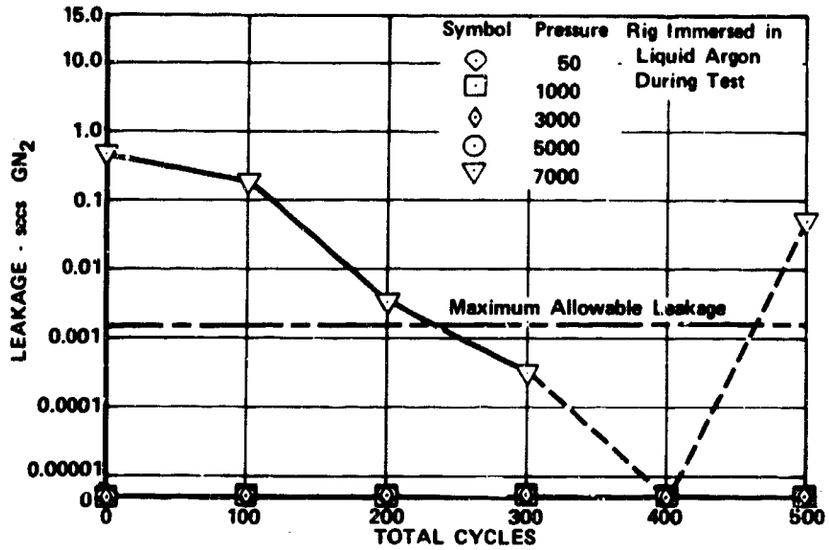

Figure 1096. Silver-Plated Pivot Ring, Build 35, Leakage vs Total Cycles FD 38653

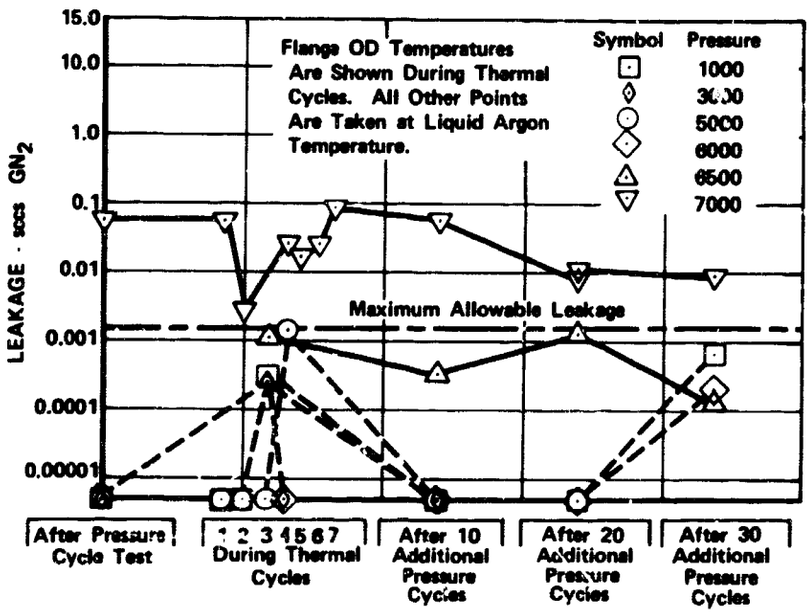

Figure 1097. Thermal Cycle Test With Silver-Plated Pivot Ring, Build 35 FD 38654

Post-test inspection of build 31 revealed that the pivot ring seal had moved radially on the bearing surface, as shown in figure 1098. A plating defect was evident but flange grooves were in excellent condition.

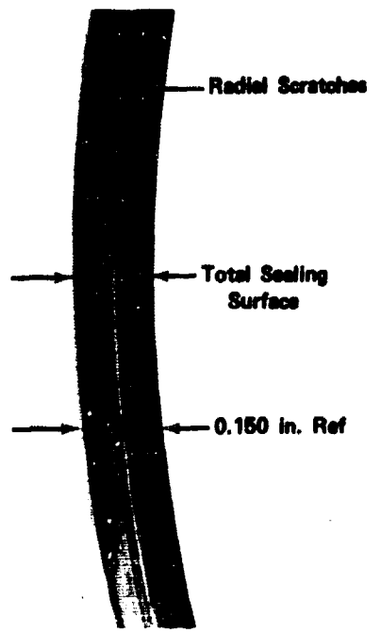

Figure 1098. Lead-Plated Pivot Ring Seal Showing Radial Scratches FD 38488

Post-test inspection of build 32 revealed a lack of plating in the electrode contact area as shown in figure 1099.

Post-test inspection of build 32A indicated a lack of plating uniformity and an irregular sealing surface. This build was plated by rotating the seal on the contracts. Figure 1100 shows areas of light plating.

Post-test inspection of build 33 revealed that the pivot ring was in good condition as shown in figure 1101 with some minute dark spots in the plating. The bearing area was on the outer diameter of the intended bearing area as shown in figures 1101 and 1102.

Post-pressure-test inspection of build 34 revealed that the seal was 0.030 in. out of round and 0.034 in. out of flat. The seal was apparently cocked during flange boltup, and further tests were suspended when this condition was discovered.

Post-test inspection of build 34A revealed that the housing seal grooves had radial scratches, as shown in figure 1103. The pivot ring had plating voids and imperfections and tangential machining marks imprinted on the seal from the housing groove as shown in figure 1104.

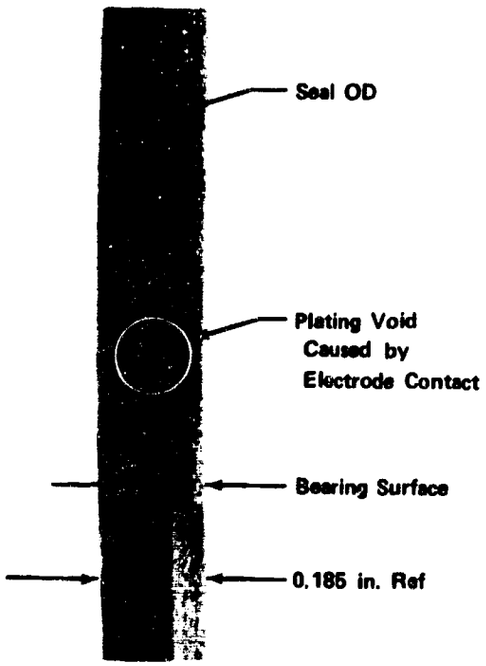

Figure 1099. Plating Void In Lead-Plated Pivot Ring Seal FD 38489

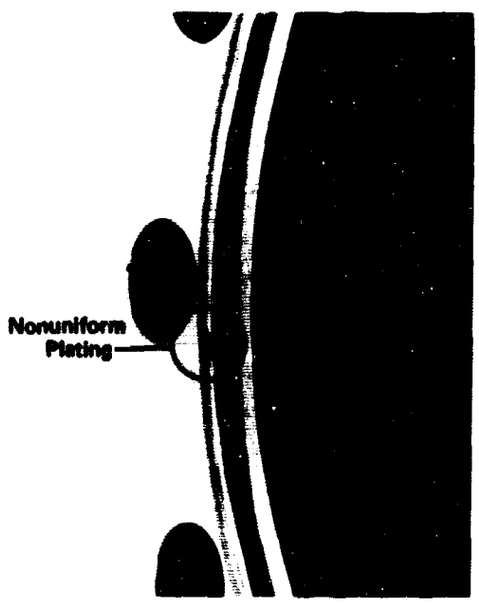

Figure 1100. Lead-Plated Pivot Ring Seal In Flange Showing Nonuniform Plating FD 38490

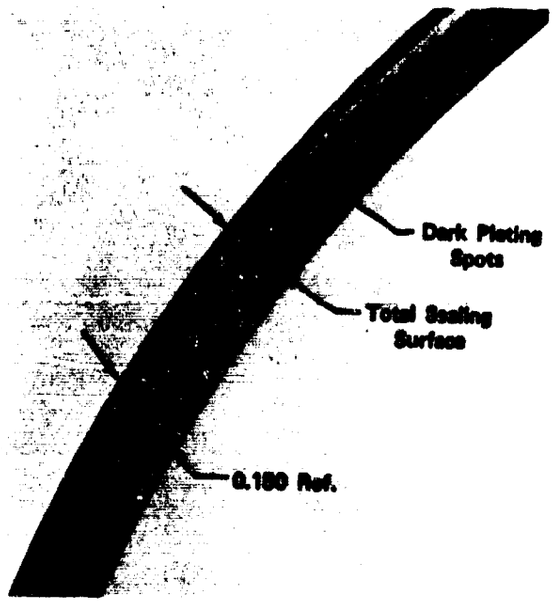

Figure 1101. Lead-Plated Pivot Ring Seal Showing Darkened Spots FD 38491

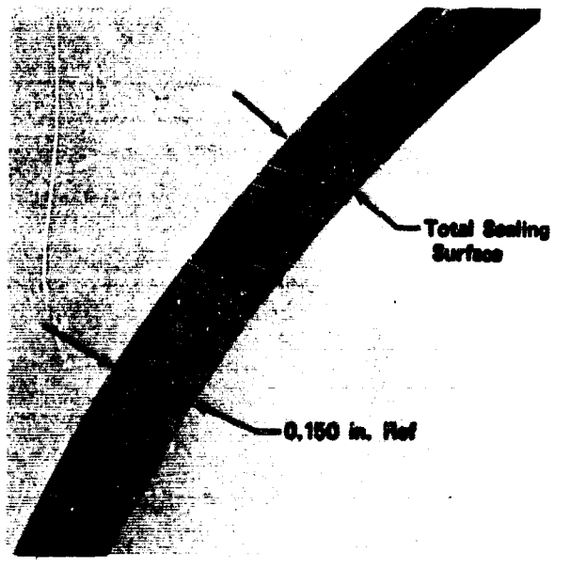

Figure 1102. Lead-Plated Pivot Ring Seal FD 38492

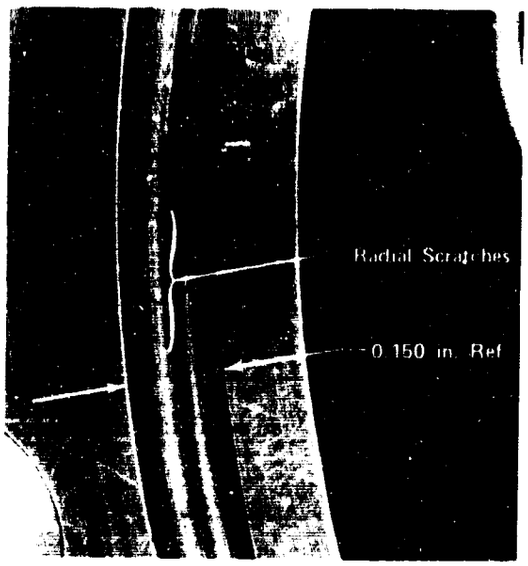

Figure 1103. Flange Seal Groove Showing Radial Scratches

FD 38493

Figure 1104. Lead-Plated Pivot Ring Seal In Flange Showing Voids and Imprinted Marks

FD 38494

Post-test inspection of build 35 indicated that the silver-plated pivot ring was in good condition after the pressure-thermal cycle test. Seal contact area on each side of the seal was uniform as shown in figures 1105 and 1106.

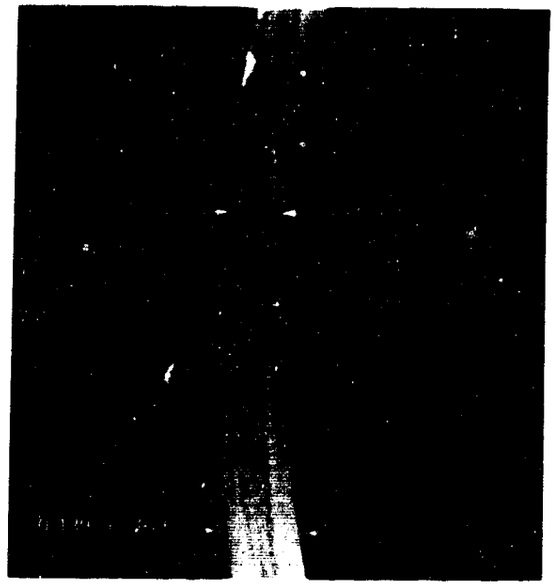

Figure 1105. Silver-Plated Pivot Ring Seal FD 38495

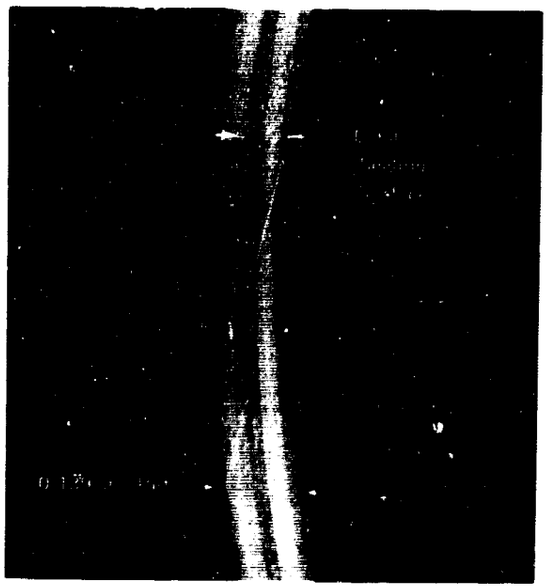

Figure 1106. Silver-Plated Pivot Ring Seal, Reverse Side FD 38498

Test results revealed that the pivot ring seal approached the allowable leakage limit of less than 10^{-4} sccs/in. of seal circumference at rig internal pressures of less than 5000 psig. The leakage was generally greater than the allowable limit at 7000 psig rig internal pressure after the 500 pressure cycles of each build, except for build 33 which was slightly less than the maximum allowable leakage. Build 33 test results indicated the increased seal unit load significantly improved the sealing characteristics. Test results of builds 34 and 35 indicated the increased seal unit load is still insufficient at 7000 psig. Reduction in seal load due to flange separation with the increase in internal pressure is an undesirable characteristic of this type seal design. This seal design is not recommended for continued development.

j. Test Rig 35120 - Builds 36 Through 40

Builds 36 through 40 of test rig 35120 were conducted on Stand B-22 to evaluate the toroidal segment seal by performing pressure cycles to 7000 psig at cryogenic temperatures, and thermal cycling from 150° R to 600° R.

The F-46159 air ratchet wrench was used during rig assembly to evaluate bolt stretch uniformity.

The seal test rig housings were modified to incorporate a 0.100 in. deep groove near the flange ID to accept the toroidal segment seal as shown in figure 1107. A minimum amount of material was removed from the flange cross section to allow reasonable flange stiffness comparison with previous seals tested. The seal configurations and sealing conditions are also shown in figure 1107. The seals were fabricated by reoperating Pressure Science Inc. Inconel X750 external pressure seals. A spacer was installed for build 38 to support the seal and increase the assembly preload. Seals for builds 39 and 40 were fully heat treated for increased strength.

The bolts were stretched at assembly to obtain a minimum total bolt load of 177,000 lb (1.2 times the blow-off load at 7000 psi). The bolt stretch required to obtain this load was 0.0045 in. and was obtained by torquing the nuts with the air ratchet wrench F-46159, as shown in figure 1086. The bolts were first tightened to a minimum torque setting. The nuts were then rotated through the required angle of turn using the air wrench angle of turn indicator.

Before stretching, all bolts and spherical washers were cleaned and sprayed with three coats of Slipspray dry lubricant. All builds were torqued to 100 in.-lb (using a hand wrench) to seat the seal. Torquing was done on the bolts in sets of two 180 deg apart at 90 deg intervals until all bolts were torqued as required. Minimum wrench torque of approximately 250 in.-lb was performed in the same manner. Angle-of-turn stretch was then performed in order on the bolts around the flange. Flange ID and bolt shank temperature probes were provided on all builds.

The B22 test stand was modified to allow performing thermal cycles after the pressure cycle tests. A combination of ambient water and a steam generator were used to heat the rig to approximately 600° R. Flowing GN_2 through a LN_2 heat exchanger and through the pressure cavity was used to cold-shock the rig to 160° R.

Ref	Build 36	Build 37	Build 38	Build 39	Build 40
Ⓐ	0.215 0.217	0.215 0.217	0.2162	0.2165	0.2165
Ⓑ	5.0005	5.000	5.007	5.008	5.005
Ⓒ	5.163 5.165	5.163 5.165	5.1645	5.164	5.1647
Ⓓ	0.005 0.010	0.005 0.010	0.008	0.008	0.008
Ⓔ	0.015	0.015	0.015	0.025	0.025
Seal Coating	0.0005 0.001 Lead	0.0005 0.001 Lead	0.0005 0.001 Lead	0.0005 0.001 Lead	0.0005 0.001 Lead

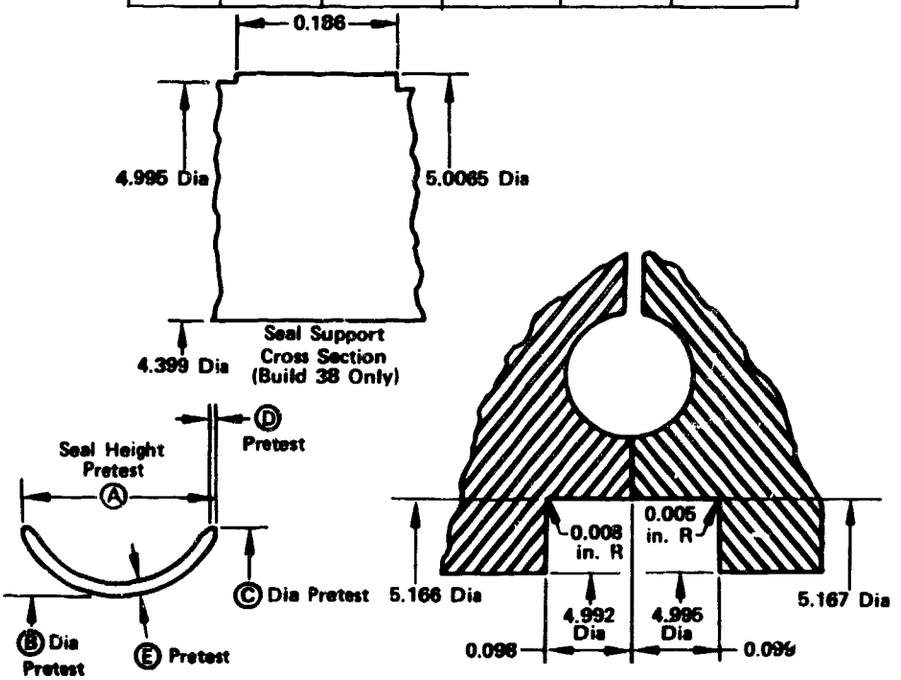

Figure 1107. Toroidal Segment Seal and Sealing Conditions for Builds -36, -37, -38, -39 and -40 FD 38704

Build 36 seal test rig bolts were torqued to 100 in.-lb and two angles of turn of 25 deg each were performed, with results shown in figure 1108. Stretch scatter after the first 25 deg was 0.0018 in. and 0.0027 in. after the second 25 deg with all but one of the bolts being stretched between 0.003 in. and 0.045 in. Due to excessive play in the angle-of-turn indicator, the final angle of turn was not considered valid and only the final stretch is presented. Bolt stretch scatter at teardown was 0.0016 in. and the average bolt stretch had decreased approximately 0.0007 in.

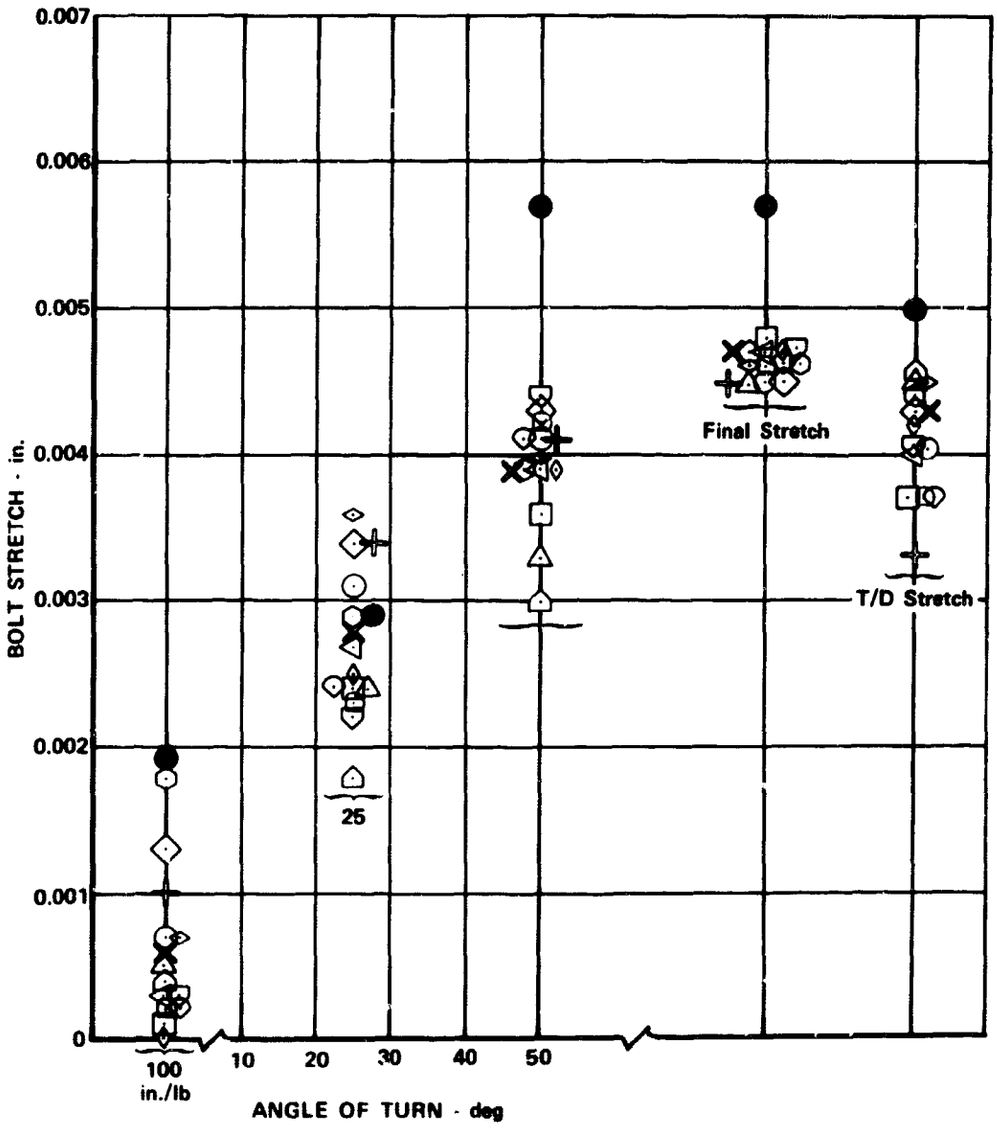

Figure 1108. Bolt Stretch vs Torque/Angle of Turn, Build 36 FD 38707

Build 36 leakage rates shown in figure 1109 indicate that leakage prior to pressure cycling at internal pressures from 50 to 7000 psig was below the maximum allowable total leakage limit of 0.0016 sccs. Leakage at 50 and 100 psig after 100 cycles was above the allowable limit and remained above throughout the test. Leakage after the 500 pressure cycles were completed was above the maximum allowable limit at all pressure levels between 50 and 7000 psig with the maximum of 2.3 sccs occurring at 1000 psig. Five thermal cycles were completed during this build to develop a procedure for cold shocking the coupling. The maximum differential temperature between the flange ID and the bolt head was 230 deg. Leakage during the thermal cycles was as shown in figure 1110.

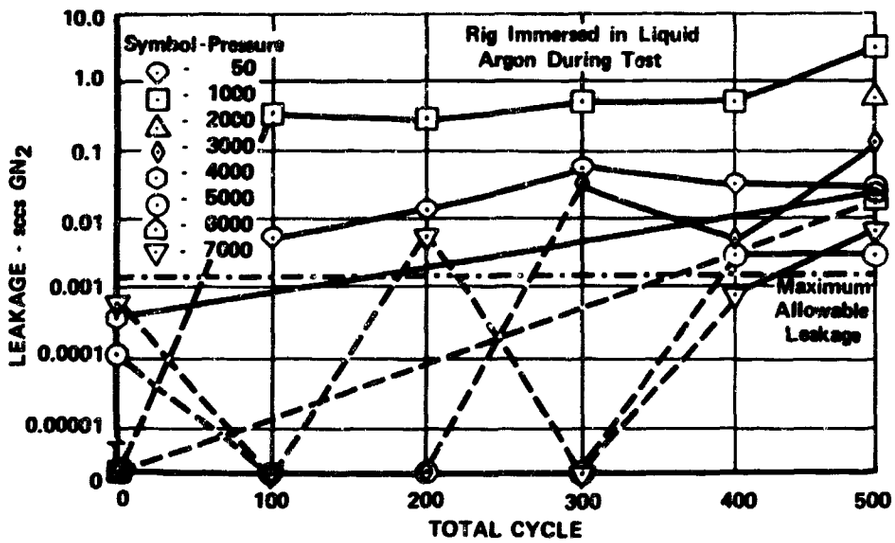

Figure 1109. Toroidal Segment Seal, Build 36, Leakage vs Total Cycles FD 38713

Build 37 setup bolt torque stretch results were as shown in figure 1111. The nuts were torqued to 100 in. lb and then rotated through a 50 deg angle. Bolt stretch scatter was 0.0022. The nuts were then selectively rotated 10 to 20 deg to obtain a 0.001 in. bolt stretch tolerance. Bolt stretch at teardown was 0.0016 in. and the average bolt stretch had decreased approximately 0.001 in.

Total leakage at 50 and 1000 psig rig internal pressure prior to the pressure cycle test was greater than 0.01 sccs and was greater than 0.1 sccs at 50, 1000 and 2000 psig through the remainder of the test as shown in figure 1112. Total leakage at 3000 and 5000 psig was undetectable for the first 200 cycles and was approximately 0.01 sccs for the remainder of the test. Total leakage at 7000 psig after the 500 pressure cycles were completed was less than the maximum allowable total leakage of 0.0016 sccs. Three thermal cycles were artempted during this build. The results were erratic. Post-test inspection revealed the lead wire of the thermocouple on the bolt shank was broken inside the collection cavity. Total leakage at 7000 psig after one thermal cycle was 0.0007 sccs.

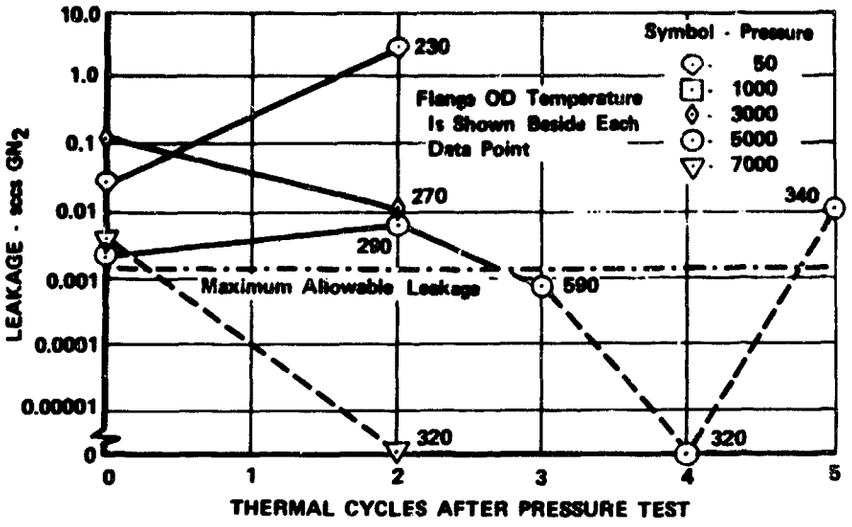

Figure 1110. Toroidal Segment Seal, Build 36, Leakage vs Thermal Cycles FD 38715

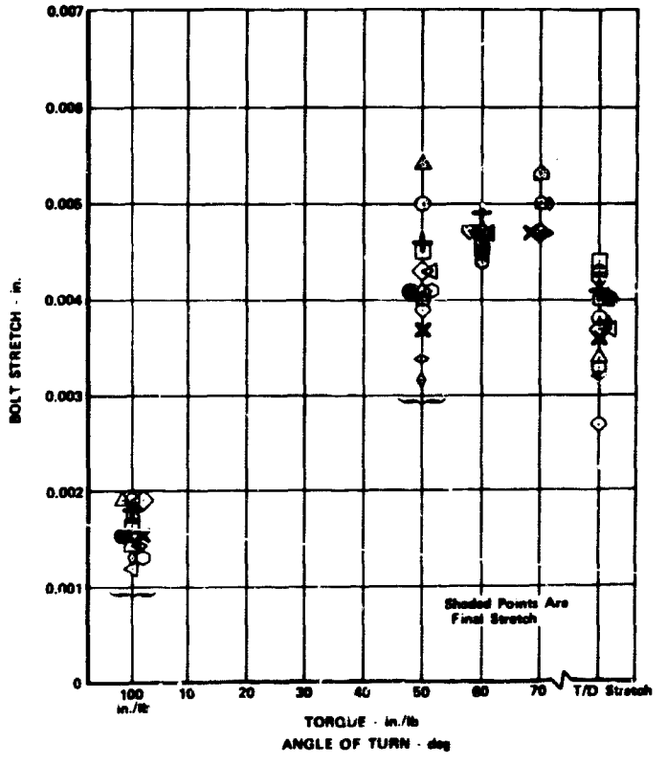

Figure 1111. Bolt Stretch vs Torque/Angle of Turn, Build 37 FD 38708

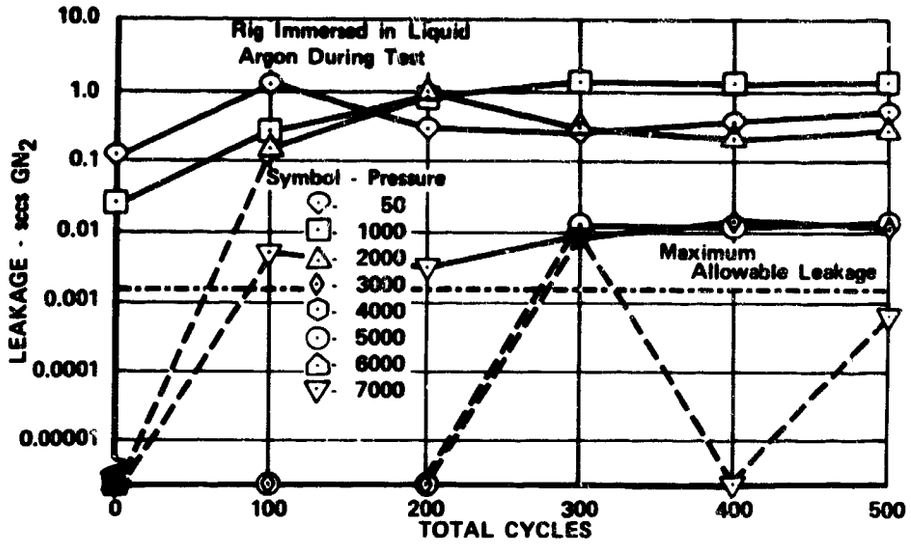

Figure 1112. Toroidal Segment Seal, Build 37, Leakage vs Total Cycles FD 38716

Build 38 setup bolt torque stretch results were as shown in figure 1113. The nuts were torqued to 100 in.-lb and then rotated through a 60 deg angle. The average stretch was less than had been previously obtained and the stretch scatter was 0.0033 in. An additional 20 deg angle of turn did not provide the desired bolt stretch. The bolts were individually loosened to 100 in.-lb torque and again rotated through a 60 deg angle of turn. The average stretch was approximately 0.001 in. more than the first time and the stretch scatter was 0.0024 in. Selected nuts were rotated through 5 to 20 deg angles to obtain the 0.001 in. bolt stretch tolerance. Bolt stretch scatter at teardown was 0.0015 in. and the average stretch was approximately the same as pretest stretch.

Build 38 leakage rates shown in figure 1114 indicate that no seal leakage was detectable at any test pressure after 100 pressure cycles had been completed. Before cycling the maximum leakage was 0.0065 sccs at 1000 psig. Leakage at 7000 psig prior to cycling was 0.00065 sccs. Six thermal cycles were performed after the pressure cycle test was completed. Total leakage recorded during these thermal cycles is shown in figure 1115. All leakage indications during the thermal cycles were below the maximum allowable leakage limit of 0.0016 sccs. A typical temperature transient is shown in figure 1116. The maximum differential temperature between the flange ID and the bolt was 260 deg.

Build 39 seal rig nuts were torqued to 100 in.-lb, as shown in figure 1117, then to the minimum wrench torque, and then the nuts were rotated through a 30 deg angle. Final stretch was attained at 60 to 90 deg with one bolt requiring 110 deg. Post-test bolt stretch scatter was 0.0016 in. and the average stretch had decreased approximately 0.0005 in.

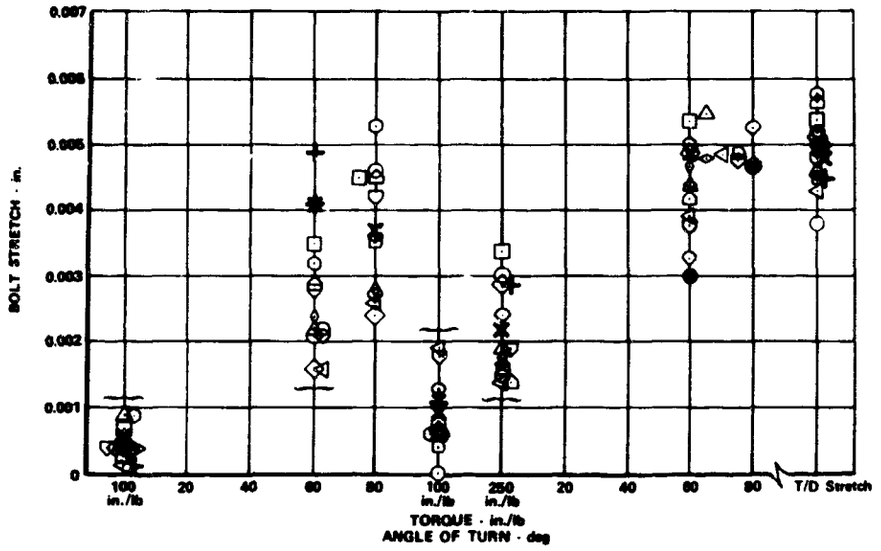

Figure 1113. Bolt Stretch vs Torque/Angle of Turn, Build 38 FD 38709

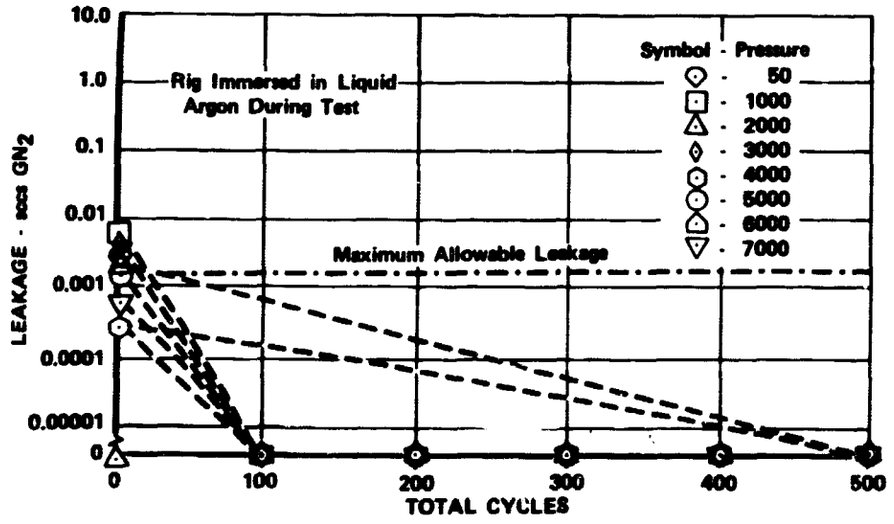

Figure 1114. Toroidal Segment Seal, Build 38, Leakage vs Total Cycles FD 38717

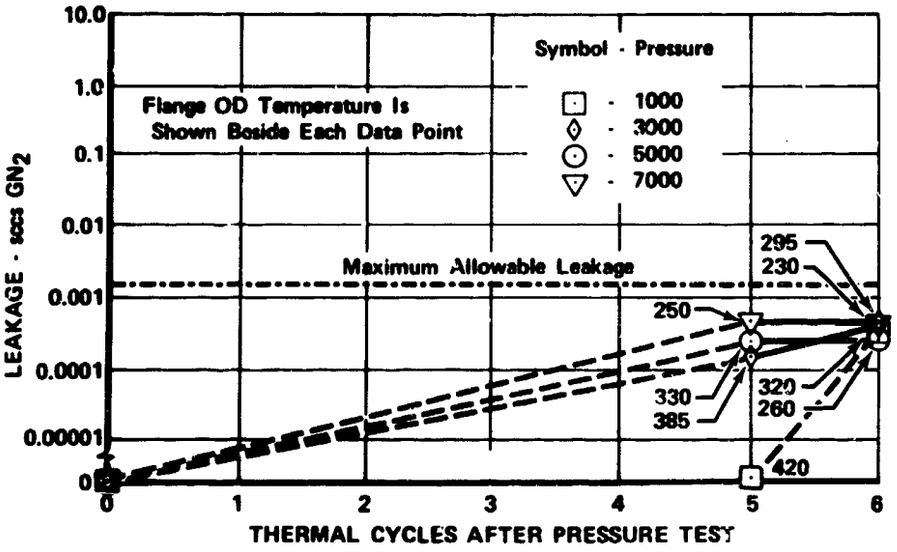

Figure 1115. Toroidal Segment Seal, Build 38, Leakage vs Thermal Cycles FD 38718

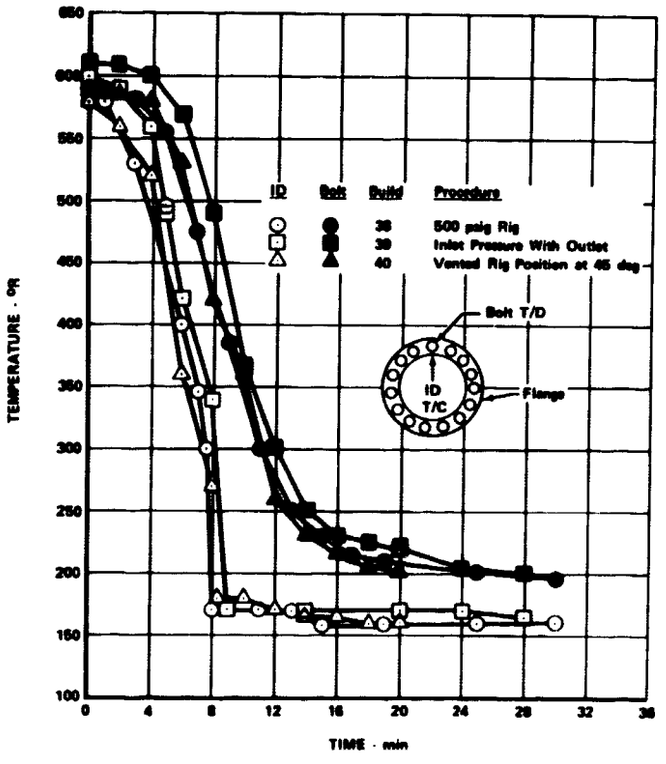

Figure 1116. Thermal Cycles of Builds 38, 39, and 40 Using GN_2 Through LN_2 Heat Exchanger and Into Rig With Atmospheric Surroundings FD 38719

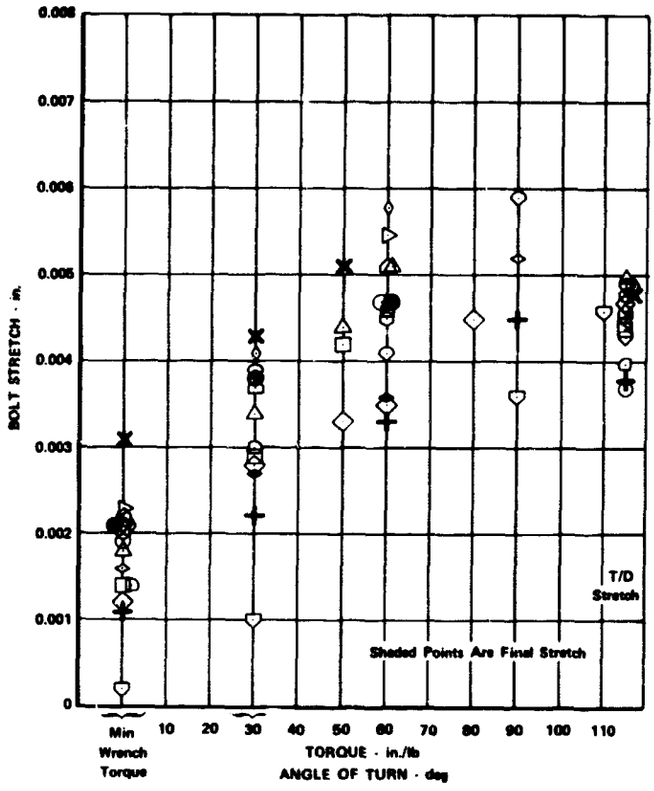

Figure 1117. Bolt Stretch vs Torque/Angle of Turn, Build 39 FD 38710

Leakage rates shown in figure 1118 for build 39 indicates that the total seal leakage after one pressure cycle to 7000 psig was less than the maximum allowable leakage of 0.0016 sccs at 50 through 7000 psig. During the first pressure cycle the maximum total leakage of 0.4 sccs occurred at 1000 psig. Six thermal cycles were performed during this build. The maximum differential temperature between the flange ID and the bolt shank was 260 deg as shown in figure 1116. Maximum leakage recorded was 0.0011 sccs and occurred at 1000 psig after three cycles as shown in figure 1119.

Build 40 rig bolts were stretched as shown in figure 1120. The nuts were torqued to 100 in.-lb, then the minimum wrench torque setting and rotated through a 30 deg angle of turn. The nuts were then rotated an additional 40 to 60 deg angle of turn and the stretch scatter was 0.0015 in. Four bolts were backed off and retightened to obtain the desired 0.001 in. tolerance. Post-test bolt stretch scatter was 0.0017 in. and the average stretch had decreased by 0.0015 in.

Build 40 leakage rates are shown in figure 1121. The maximum total leakage prior to cycling occurred at 50 and 1000 psig and was 0.002 sccs. Points were repeated after one cycle and maximum leakage was at 2000 psig and was 0.03 sccs. After 100 cycles the only detectable leakage was at

1000 psig and that leakage was below the maximum allowable leakage limit of 0.0016 sccs. Throughout the remainder of the test, no leakage could be detected. Six thermal shock cycles similar to the one shown in figure 1117 were performed. No leakage was detectable at 50, 1000, and 5000 psig the pressure levels tested after the third and sixth thermal cycles had been completed.

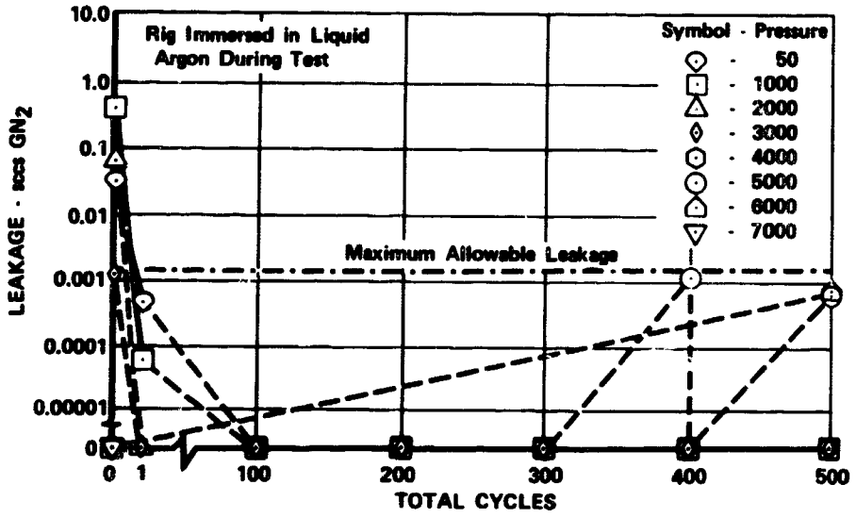

Figure 1118. Toroidal Segment Seal, Build 39, Leakage vs Total Cycles FD 38720

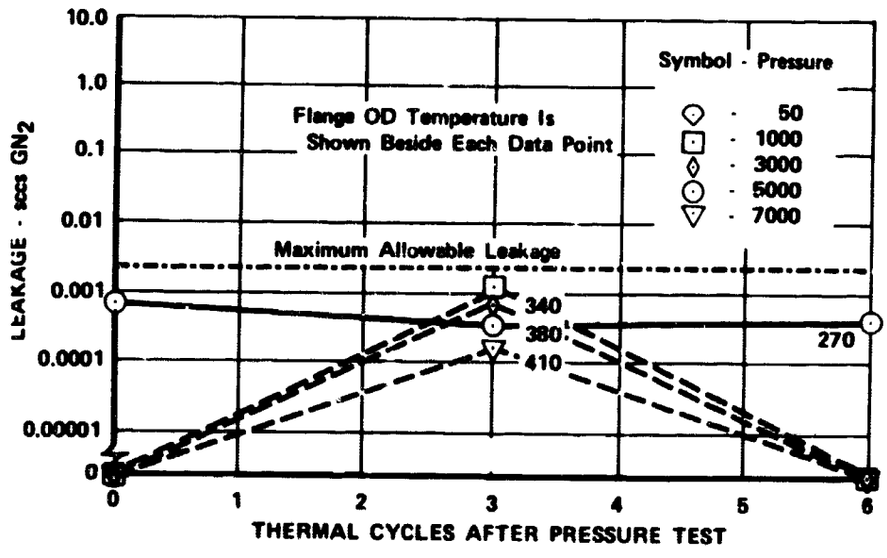

Figure 1119. Toroidal Segment Seal, Build 39, Leakage vs Thermal Cycles FD 38714

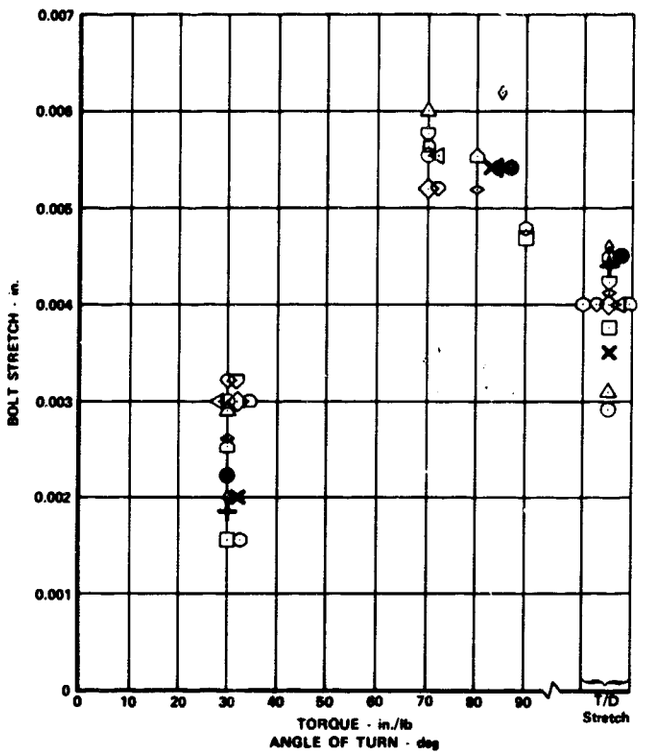

Figure 1120. Bolt Stretch vs Torque/Angle of Turn, Build 40 FD 38711

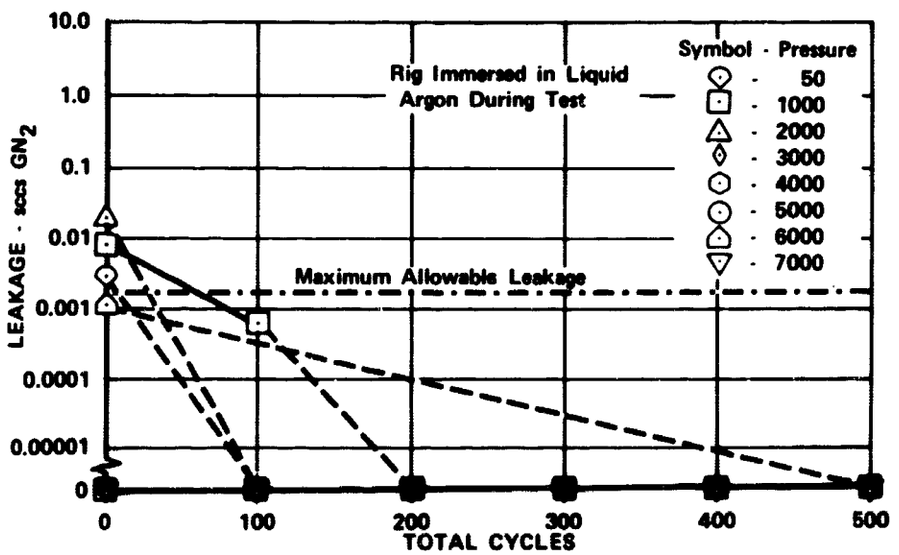

Figure 1121. Toroidal Segment Seal, Build 40, Leakage vs Total Cycles FD 38721

Post-test inspection on build 36 seal indicated that the seal was in good condition except for imperfections on the sealing edge and side, as shown in figures 1122 and 1123.

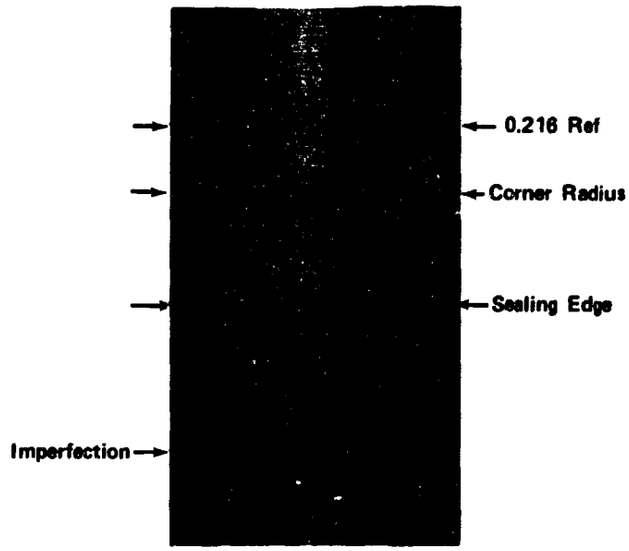

Figure 1122. Build 36 Seal Showing Post-Test Minor Edge Imperfections FD 38722

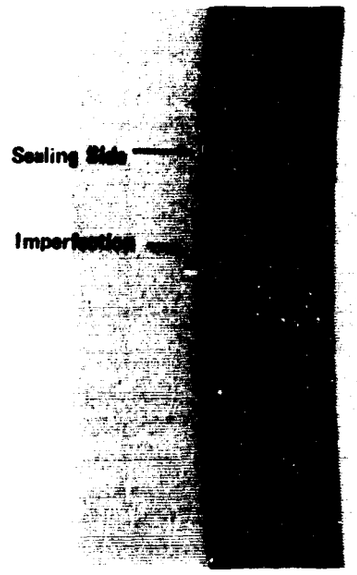

Figure 1123. Build 36 Seal Showing Post-Test, Minor Side Imperfections FD 38723

Build 37 post-test inspection revealed some contamination of nickel-base particles as shown in figures 1124. The sealing side had some plating indentations as shown in figure 1125 probably caused by the contamination. The seal cross section is shown in figure 1126. The seal hardness was Rockwell C20. Examination revealed that the seal grooves were in excellent condition.

Figure 1124. Build 37 Seal Showing Post-Test Metallic Contamination FD 38724

Figure 1125. Build 37 Seal Showing Post-Test Contamination Voids FD 38725

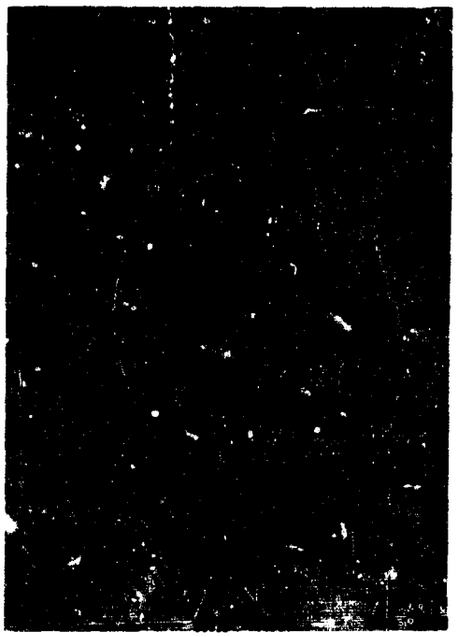

Figure 1126. Build 37 Toroidal Segment Seal Cross Section FD 38726

Post-test inspection revealed that the build 38 seal was tight on the seal support at teardown. The seal edge was clear of imperfections as shown in figure 1127. The sealing area on the side of the seal was also in good condition as shown in figure 1128. The seal hardness was Rockwell C24. Examination revealed that the flange grooves were in excellent condition.

Figure 1127. Build 38 Seal Edge at Post-Test Inspection FD 38759

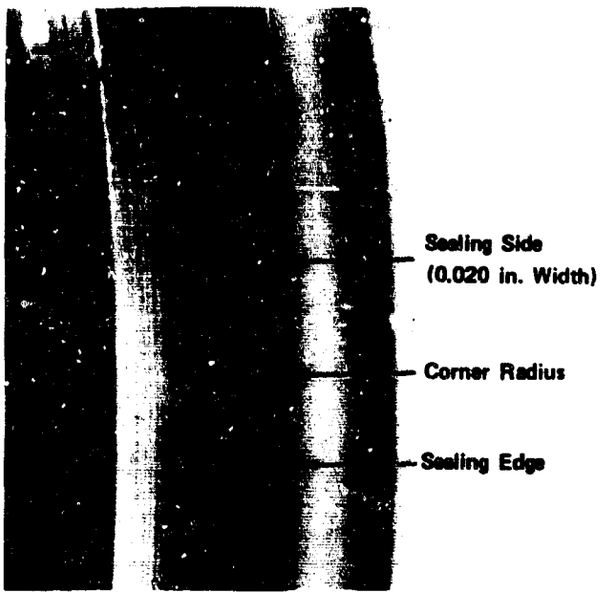

Figure 1128. Build 38 Seal Side at Post-Test Inspection FD 38760

Post-test inspection of build 39 seal revealed that the seal was in good condition as indicated in figures 1129 and 1130. The seal cross section, as shown in figure 1131, showed some small cracks in the seal ID. Inspection revealed lead plating in the cracks, indicating that cracks were present before cycle test. Seal hardness was Rockwell C41. Examination revealed that seal grooves had minute radial surface scratches in the flange grooves.

Post-test inspection of the build 40 seal revealed that the seal was in excellent condition as shown in figures 1132 and 1133. The sealing edge was not as pronounced as the previous seals tested. The seal cross section is shown in figure 1134. The post-test seal hardness was Rockwell C35. Examination revealed that the flange grooves were in excellent condition.

Leakage during builds 38, 39, and 40 remained below the maximum allowable leakage limit after the first 100 cycles were completed. Leakage during builds 36 and 37 was generally higher at low rig internal pressures. The maximum leakage recorded during this test series was 2.3 sccs and occurred at 1000 psig rig internal pressure after 500 pressure cycles of build 36 had been completed. Thermal shock cycles from 600° R to 160° R were performed on each build. Leakage measurements calculations during the thermal cycles are based on an average temperature of the flange OD temperature and ambient temperature. Flange deflection due to pressure for builds 36, 37, and 40 is shown in figure 1135.

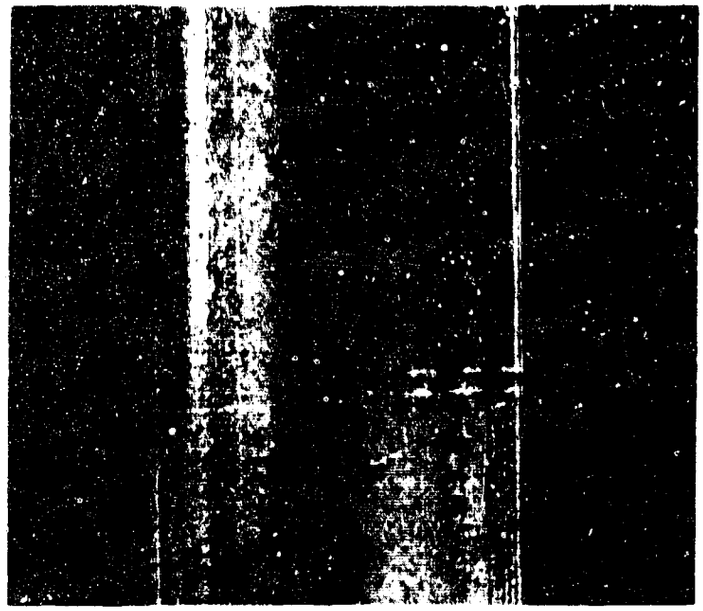

Figure 1129. Build 39 Seal Side at Post-Test Inspection FD 96526

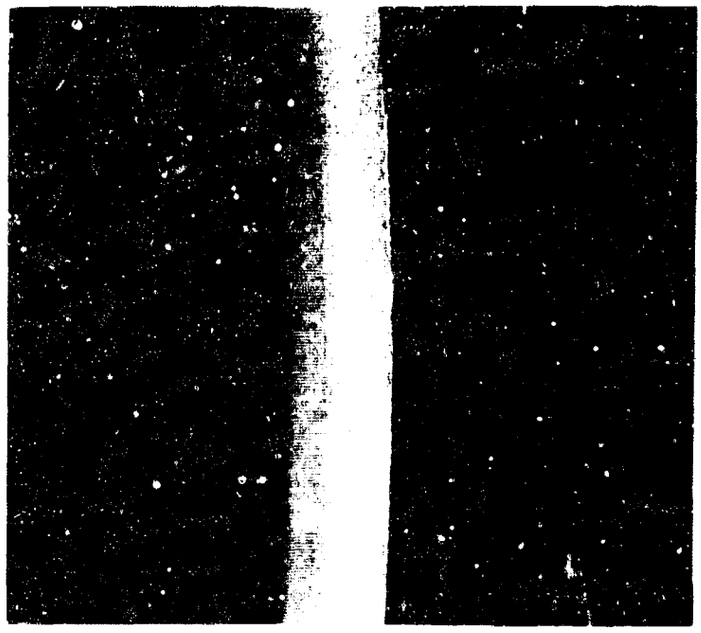

Figure 1130. Build 39 Seal Edge at Post-Test Inspection FE 96527

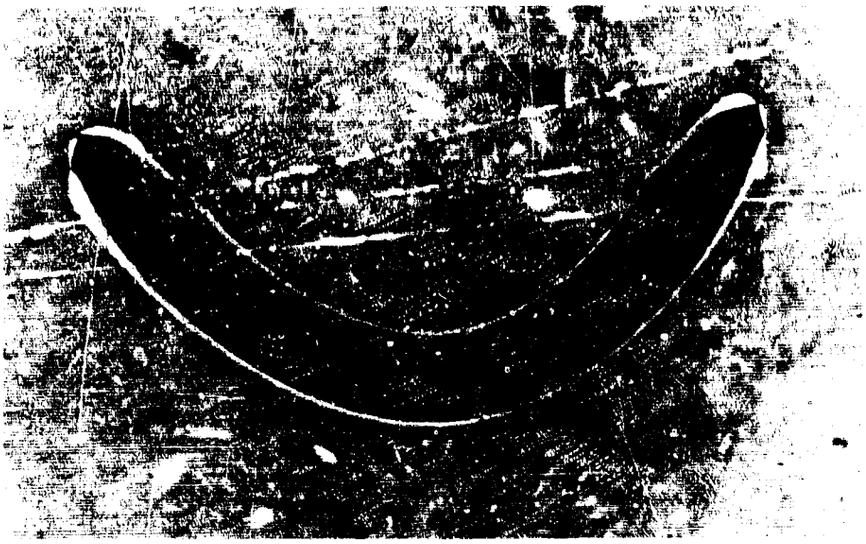

Figure 1131. Build 39 Seal Cross Section Showing Minute, Radial ID Scratches — FAL 17829

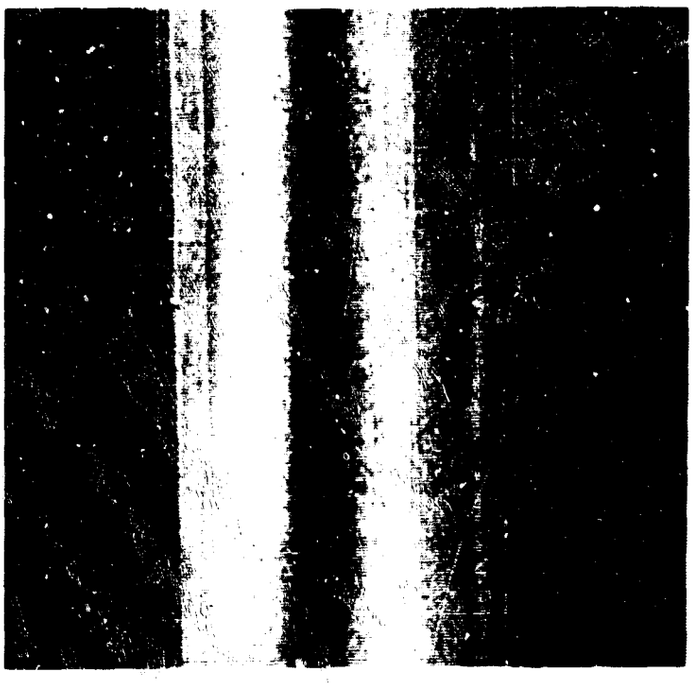

Figure 1132. Build 40 Seal Side at Post-Test Inspection — FE 96528

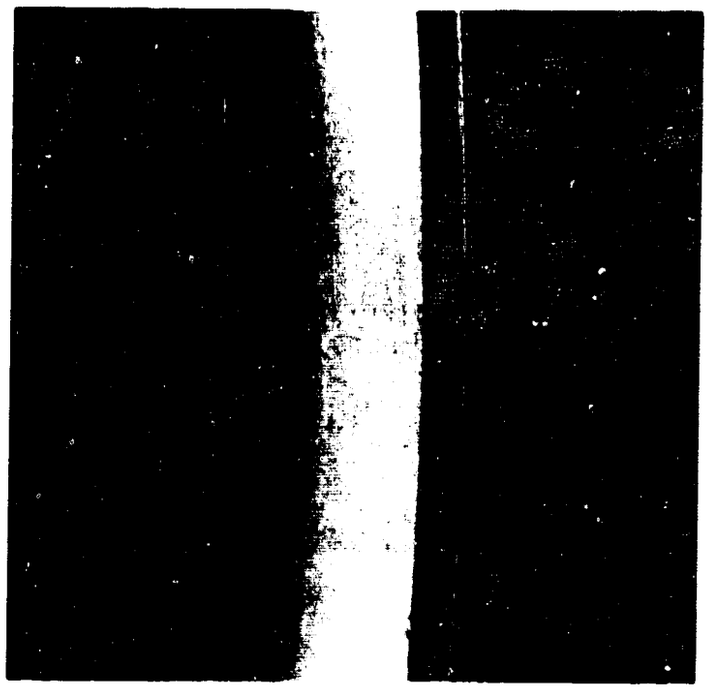

Figure 1133. Build 40 Seal Edge at Post-Test Inspection FE 96529

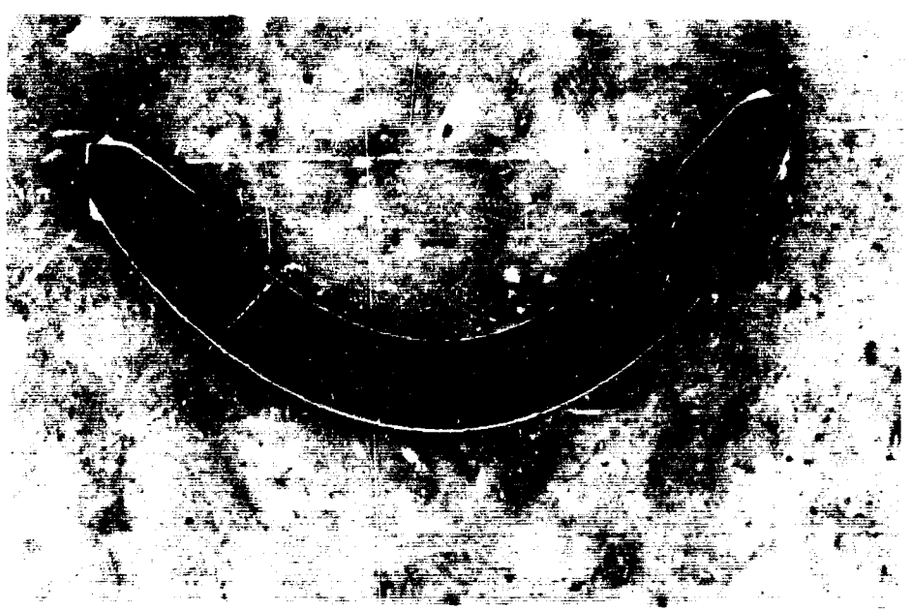

Figure 1134. Build 40 Seal Cross Section at Post-Test Inspection FAL 17830

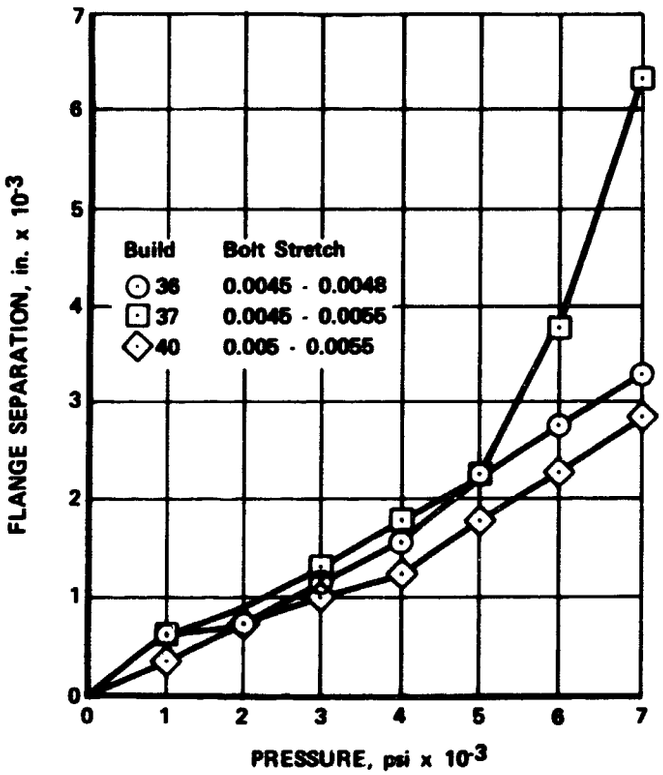

Figure 1135. Flange Deflection vs Pressure for Builds 36, 37 and 40 FD 38712

The fully heat-treated, lead plated, 0.025 in. thick toroidal segment seal met the requirement of less than 10^{-4} sccs leakage per inch of seal circumference under all tested conditions at pressures of 3000- to 7000-psig rig internal pressure. After several pressure cycles to 7000 psig, this seal leakage was below and remained below the required limit at pressures of 50 through 7000 psig throughout the 500-cycle pressure test and the six thermal cycle tests. The annealed and supported 0.015-in.-thick, lead-plated seal of build 38 produced approximately the same results as the 0.025 in. thick seals. The air ratchet wrench F-46159 produced a 0.0025 in. bolt stretch scatter when all the bolts were rotated through the same angle of turn. The bolt stretch scatter after the 500 pressure cycles was between 0.0016 in. and 0.0017 in. on all five tests. Tolerance prior to test was 0.001 in. or better.

APPENDIX
ENGINE CONTROL SYSTEM

This report constitutes a summary of significant results generated by Bendix Corp. study teams relative to the design of a Control System for the Pratt and Whitney Aircraft XLR129 engine. The major conclusions resulting from this program are as follows:

1. The recommended engine control logic consists of a time-based gross mode which positions four primary control valves for basic steady-state and transient operation, three limited authority feedback loops to perform accurate trim and six limiter loops for absolute engine protection.

2. A specially designed engine-mounted digital computer with a one megahertz computation rate and 8192 word memory capacity will handle all of the control system's dynamic processes and monitoring chores. Furthermore, such a computer could be readily implemented for the XLR129 engine using state-of-the-art components.

3. Actual experience with a dynamic digital model of the engine and controller confirmed that this system will indeed operate with safety and stability throughout the required thrust and mixture ratio envelope.

4. The force screen type propellent flow sensor with its fast response capability and inherent accuracy is an essential element of the system. This device can be successfully developed into flightworthy hardware most efficiently by handling its density compensation with computer software programing.

5. Both pneumatic and electromechanical valve actuator systems were studied. Each has adequate performance capability for successful use in the XLR129 engine. A comparison of the two systems is shown in table CXII. However, Bendix has selected the pneumatic valve actuator system primarily because of that comparison which highlights one particular advantage. Specifically, the small electric power requirement of the pneumatic transfer valve will permit the unique design of four of the engine computer's input-output channels giving them sufficient power handling capability to drive the transfer valves directly. Failure monitoring and self-test would then be a free software service, involving no extra electrical components whatsoever. It will be noted that this arrangement completely eliminates the four high-risk, complicated servo power amplifiers which would be required for an electromechanical system.

6. Suitable state-of-the-art sensing devices exist which, with repackaging, can be used to monitor the rotating speed, temperature and pressure parameters of the XLR129 engine that are required by the Control System. In may cases, optimum component usage can be achieved by a hybrid arrangement in which the responsibility for signal conditioning and monitoring is shared between sensor hardware and computer software programming. A summary of the selected sensor types is contained in table CXIII.

The resulting control system for the XLR129 engine will be fully capable of providing automatic starts and shutdowns together with precision steady-state operation at, or optimum transients between, any selected points within the thrust-mixture envelope without danger of ever exceeding a critical parameter. However, the effectiveness of the transpiration cooling and fuel NPSP control channels would be greatly improved by a change in engine configuration to add a control valve for the fuel LSI turbine similar to that used on the LOX side. Bendix recommends that such a control be incorporated. In addition, the sensitivity of the engine system to variations in rotating component tolerances would be greatly reduced by a change in engine configuration to add a method of independently controlling the shaft speed of the main oxidizer turbopump.

Table CXII. Actuator Selection Rationale

	Electro-Mech.	Pneumatic
Satisfy Performance Requirement?	Acceptable	Acceptable
Reliability and Flight Safety	Acceptable, but Downgraded by Additional Servo Amplifier Electronic Components Used	Acceptable
Weight and Volume	Equivalent	Equivalent
Overall Efficiency	Power Source Is Vehicle Dependent	Power Source Is Directly Available From Engine Cycle (Except for Start and Shutdown)
Redundancy Complexity	Requires Multiple Servo Amplifiers	Satisfied With Multiple Transfer Valve Windings Only
Maintainability	Acceptable, but Rendered More Difficult by Necessity of Servicing Servo Amplifiers	Acceptable
Ease Of Solving the Environmental Problem	Servo Amplifiers Require Thermal Conditioning	Relatively Immune to Environmental Problems
Development Risks	Servo Amplifiers Are High Risk Components	Minor

Table CXII. (Continued)

	Electro-Mech.	Pneumatic
Cost	Equivalent	Equivalent
Radio Frequency Noise Problem	Servo Amplifier Switching Transients Require Careful Isolation	None

Table CXIII. Summary of Selected Sensor Types

Application	Sensor
Inducer and Main Pump Speeds	Proximity Probe, Eddy Current Type
Turbine Exhaust Temperatures	Chromel Alumel Thermocouple, Dual Junction Type
Propellent Temperatures	Immersion Probe, Platinum Resistance Type
Propellent Pressures	Thin Film Strain Gauge Pressure Transducer, Specially Packaged for Quick Thermal Equilibrium

SECTION I
CONTROL SYSTEM ANALYSIS

A. INTRODUCTION

This section describes the results of the study effort conducted by the Bendix Corporation concerning Phase I System Analysis and Block Diagrams for Pratt & Whitney's XLR129 Rocket Engine.

Analysis indicates that the XLR129 Rocket Engine (cycle 8B) may be controlled by four valves using:

- Three full time principal closed-loops
- Unique acceleration schedules
- Six protective closed-loops
- Basic open-loop gross mode

Digital computer simulation studies conducted at the Bendix Corporation have verified the feasibility of the suggested control approach.

The study effort has demonstrated the importance of controlling the turbopumps for safe transient and steady-state engine operation. With the insight gained into the XLR129 engine cycle, a unique acceleration mode was conceived which permits rapid accelerations by keeping the turbopumps dynamically balanced during the transient. The fuel pump speed loop emerged as the primary closed-loop because it contributes to turbopump matching by modifying the acceleration mode with feedback information on the state of the fuel turbopump.

Further systems work is needed in the following general areas and categories to solidify, strengthen and develop the fundamental control concept of the XLR129 engine cycle:

- Additional control points for critical engine functions
- Parameter selection and sizing of limiter loops
- Hierarchy of closed-loop controls for engine protection and reliability

Although a four control point system is possible, the practical advantages of additional, independent control points for cooling flow, fuel NPSP and LOX pump speed need to be investigated in depth.

More analysis, study and simulation are needed to refine the engine flow control loops and limiter control loops. Also, a hierarchy of the principal control loops needs to be established to provide the safest and most reliable engine operating modes in the event of control loop failure.

B. Control System Description

1. Basic Control Philosophy
2. Gross Mode Control System
3. Fuel Pump Speed Loop
4. Oxidizer Flow Trim Loop
5. Fuel Flow Trim Loop
6. LOX NPSP Protection
7. Preburner Temperature Limiter Loop
8. Cavitation Protection For The Main Fuel Pump
9. Transpiration Cooling Flow Protection
10. Main Turbopump Overspeed Protection
11. Start and Shutdown Operation
12. Prestart Logic
13. Start and Shutdown Schedule Selection Logic

B. CONTROL SYSTEM DESCRIPTION

The full time control system is composed of basic gross mode open-loop scheduling plus three closed loops. Six protective loops are added to the system, and are active only if the engine parameter they protect is approaching a limit. The engine control philosophy behind the control design is to utilize known engine characteristics to maintain the steady-state main turbopump matching throughout any transient the engine is requested to make. By maintaining turbopump balance, the control, in response to thrust or O/F ratio in the engine, accelerate, decelerate and accurately trim the engine for steady-state operation.

This section describes the control system block diagram. Each loop and the gross mode are isolated from the overall block diagram for individual discussion. The topics covered in this section include:

- Basic Control System Philosophy
- Gross Mode Control
- Full Time Closed Loops
- Protective Closed Loops
- Start and Shutdown Operation

1. Basic Control System Philosophy

Computer simulations at Bendix Corporation demonstrate that a single open-loop controller can safely decelerate and change O/F ratio of the Pratt & Whitney XLR129 rocket engine. This open-loop controller, or gross mode control, responds to a requested change by moving the four engine control valves simultaneously along their steady-state schedules on a timed basis.

Accelerations are a special problem and cannot be made rapidly using only a timed sequencing of events along steady-state schedules. It was desirable to retain the gross mode because of its simplicity and reliability so additional compensation, active only during accelerations, was added to the gross mode to permit open-loop accelerations. The compensation consists of differently biasing the O/F ratio of each control valve's steady-state schedule so that the engine will accelerate along a known, safe path between any thrust levels. This unique acceleration path is traveled for every acceleration and is not dependent on the initial state of the engine when the acceleration was started. Individual bias values were chosen to keep the main turbopumps matched and close to their steady-state speed schedules throughout the transient by loading the LOX pump and unloading the slower fuel pump so they accelerate together. The net effect of the O/F biasing on an acceleration is that the engine is put in the mid O/F range with the turbopumps balanced and close to a mid O/F schedule, thus avoiding the problems peculiar to the extreme O/F values. The actual mechanics of the compensation are discussed in the discussion on the gross mode.

Closed-loops are added to the control system to aid the gross mode with current feedback information. To support the gross mode in controlling the engine the closed-loops provide:

- Additional control of turbopumps
- Accurate and stable steady-state operation
- Maintenance of engine parameter safety margins

A block diagram of the complete control system is given in figure 1136. This diagram shows the full time control system, protective closed-loops, and start and shutdown logic.

The full time control system consists of the gross mode plus three continuously acting closed-loops which monitor the following parameters:

- Main fuel pump speed
- Total LOX flow
- Total fuel flow

The speed closed-loop aids the gross mode in regulating power available to the turbines and insures that the fuel pump speed is held to its steady-state schedule. The flow closed-loops assist in maintaining the proper loads on the pumps during transients, and at steady-state they accurately trim thrust and O/F ratio to requested values.

In addition to the three full time control loops, six protective loops are added to the gross mode. These protective loops are active only when an engine parameter approaches a limit. The parameters protected or limited by these loops are:

- Main LOX pump NPSP
- Preburner temperature
- Main fuel pump NPSP
- Transpiration cooling
- Maximum LOX pump speed
- Maximum fuel pump speed

The protective loops act to protect the engine by restoring the critical parameter to a safe condition either directly if there is a control point which directly affects the parameter or indirectly by slowing the transient to allow the engine to go toward steady-state equilibrium.

A

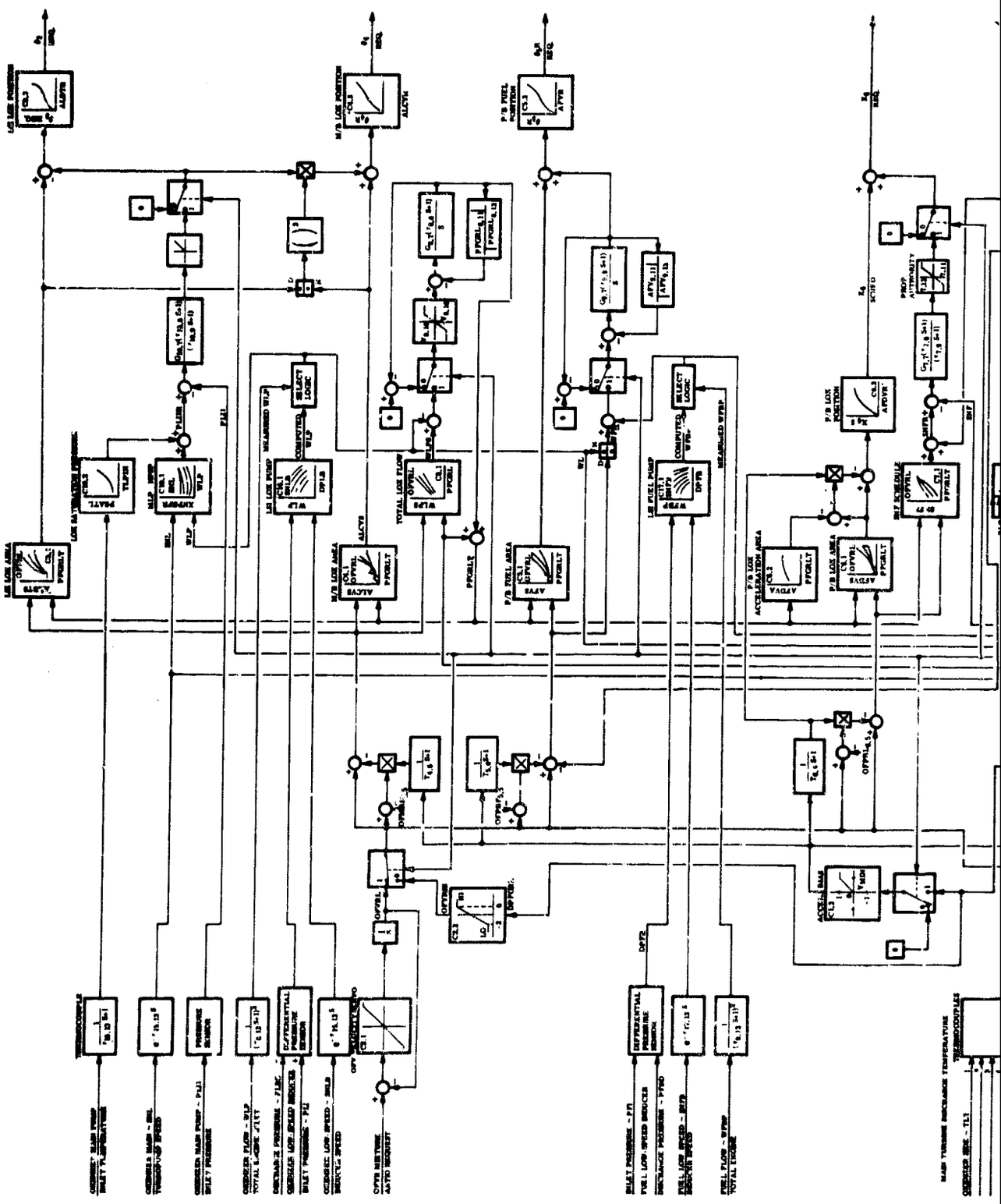

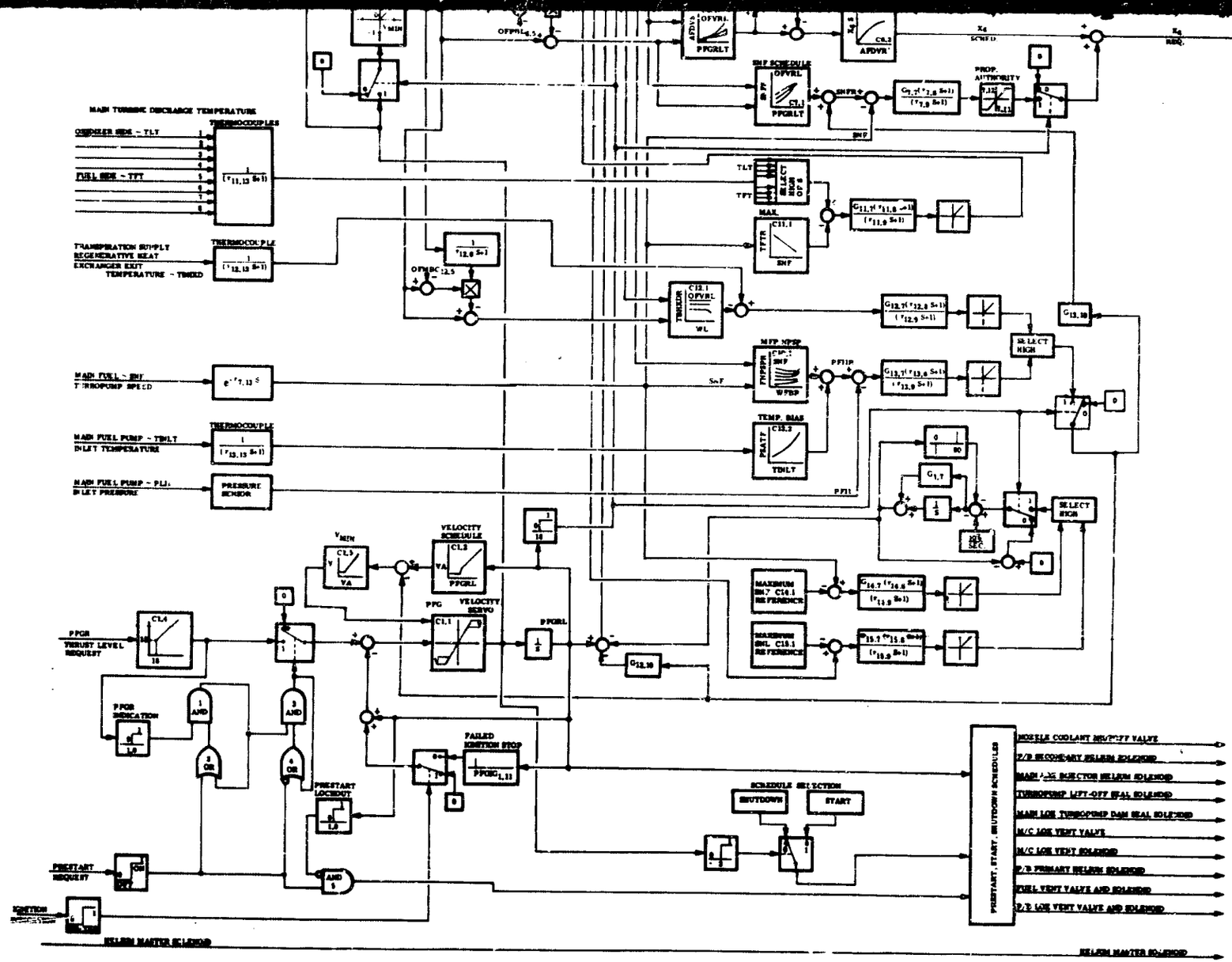

Figure 1136. Complete Control System

During prestart, start, and shutdown the closed loops are opened, the trim integrators are zeroed and the gross mode is given complete authority. The gross mode's velocity limited thrust servo incorporates the logic necessary for start or shutdown and provides a time base for sequencing all the control valves and solenoids. The four control valves are scheduled using an extension of their normal steady-state schedules into thrust levels below idle.

2. Gross Mode Control System

The gross mode control provides open-loop, time-based scheduling of the four engine control valve positions in response to thrust and O/F ratio requests.

As shown in figure 1137, the gross mode consists of:

- Steady-state control valve schedules
- Acceleration compensation
- Velocity controlled input servos

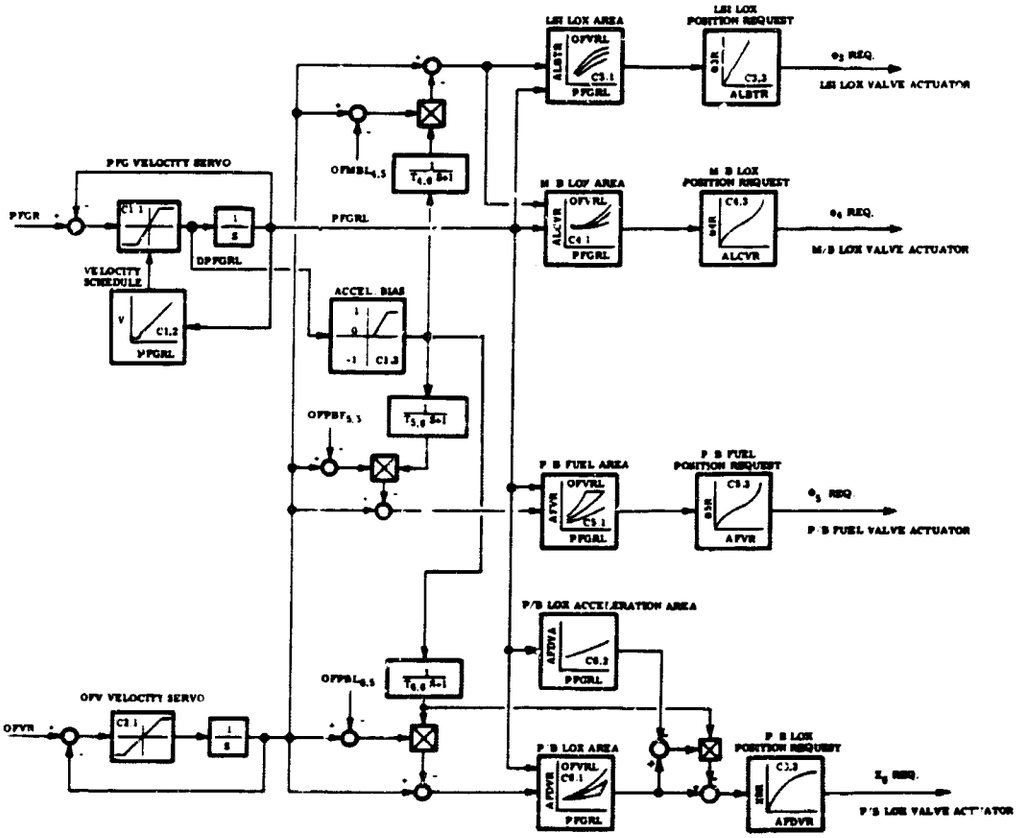

Figure 1137. Gross Control Mode

Thrust and O/F request inputs change the scheduled steady-state control valve positions by means of velocity limited servos. The scheduled positions are the inputs to the control valve actuators. Additional compensation, used only during accelerations, is incorporated in the gross mode to overcome engine dynamics in order to rapidly accelerate the engine.

The key to safe accelerations without sensor information is the compensation which is activated only during engine accelerations. This acceleration biasing modifies the O/F signal sent to each control valve schedule so that the engine is moved into a "safe" O/F region during accelerations and then returned to the requested O/F level at the end of the transient. Computer studies show that the path the engine takes during an acceleration is not dependent on the starting point and does provide safe margins on all critical parameters.

The biasing values were chosen to keep engine balance during an acceleration by:

- Loading the LOX pump
- Unloading the fuel pump
- Minimizing the disturbance on the system

During a requested acceleration the positive velocity of the thrust servo acts through an acceleration bias schedule to produce a signal to switch the control valves from the requested O/F ratio schedules to their acceleration schedules. The switching is accomplished by a lagged zero-to-one multiplication signal which produces a smooth transition between the acceleration path and steady-state schedule without causing an upset of the balance present at steady-state.

The value of $OFMBL_{4.5}$ (refer to part C for nomenclature definitions) is below the average O/F acceleration value in order to maintain a load on the main LOX pump to prevent LOX pump speed far in excess of steady-state values with the resultant LOX flow unbalance. $OFPBF_{5.5}$ is high relative to $OFMBL_{4.5}$, causing the requested load on the fuel pump to be light compared with the LOX pump steady-state load. Thus, because of relative loading, the slower fuel pump can stay matched with the LOX pump during an acceleration transient. The preburner LOX valve acceleration schedule is chosen to keep additional power available to the turbines, but not enough power to cause NPSP problems or overtemperature in the preburner.

The thrust and O/F ratio command signals to the control are filtered through servos to limit the maximum velocity with which the control will respond to a requested change. The thrust servo has the additional feature of a variable maximum velocity as a function of its output, to take advantage of the faster turbopump response at the higher thrust levels.

3. Fuel Pump Speed Loop

The normal tendency during a transient is for fuel pump speed, and therefore fuel pressure, to lag behind the rest of the system due to slower pump dynamics. This is beneficial on a deceleration but harmful during an

acceleration when lagged fuel pressures mean inadequate cooling flow and lower fuel flow into the engine. Acceleration biasing of the gross mode control compensates roughly for this effect. Adding the closed fuel pump speed loop to the gross mode further reduces the fuel pump lag during a transient, resulting in additional improvement in engine acceleration performance.

As shown in figure 1138, the speed loop is closed on the preburner LOX valve position scheduled by the gross mode. A reference steady-state fuel pump speed value is computed as a function of requested thrust and O/F ratio and compared with the actual speed to form a speed error signal. The speed error signal, acting through dynamic compensation, proportionally changes the scheduled preburner LOX valve position, resulting in a change of power available to the fuel pump. The power change to the turbopumps changes fuel pump speed to hold it within the droop of the proportional closed-loop. To maintain compatibility with the gross mode during an acceleration, the reference speed schedule is also switched onto a constant O/F biasing value, $OFPBL_{6.5}$, which has a value that results in the engine being driven into the mid O/F range.

Extensive computer studies at Bendix Navigation and Control Division show that the fuel pump speed closed-loop is extremely effective in producing safe accelerations. With the closed-loop maintaining proper power to the fuel turbopump at every transient condition, ample transpiration cooling flow exists and proper fuel flow is delivered for every scheduled area. Also with suitable gross mode load balancing, the LOX pump is driven near its scheduled path at the same time.

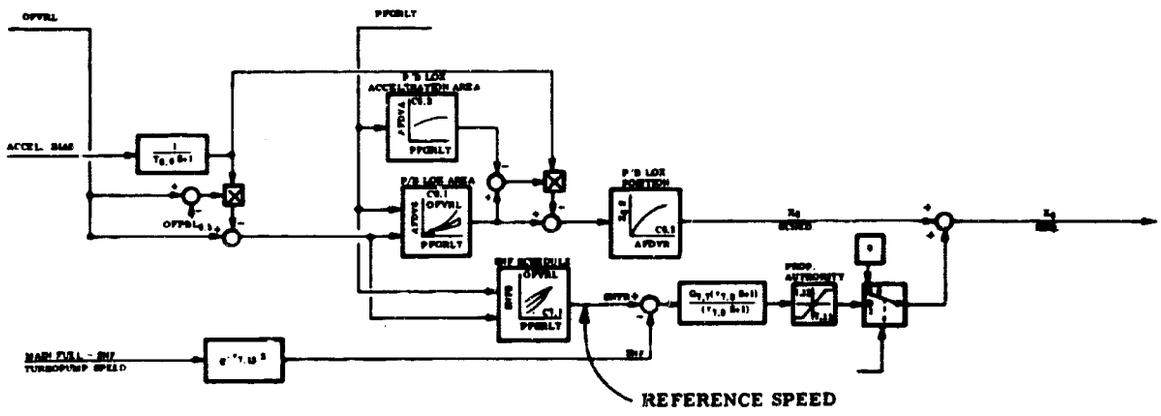

Figure 1138. Fuel Pump Speed Loop

4. Oxidizer Flow Trim Loop

Controlled thrust level is a basic requirement for engine operation. Precise thrust level is provided by accurately trimming total engine oxidizer flow to the scheduled value.

A reference total oxidizer flow is scheduled as a function of velocity limited vehicle O/F ratio and velocity limited thrust level requests. The actual total oxidizer flow is either a direct measurement or, in the event of a flow sensor failure, a synthesized signal computed as a function of the oxidizer LSI turbopump speed, inlet and exit pressures. The referenced oxidizer flow is compared with the actual total oxidizer flow to generate an error signal. The error signal acts through a proportional plus integral controller to trim the thrust level request to all control valve schedules. Note that the thrust level request to the total LOX flow schedule (figure 1139) is taken directly from the thrust servo and does not contain the LOX flow trim value.

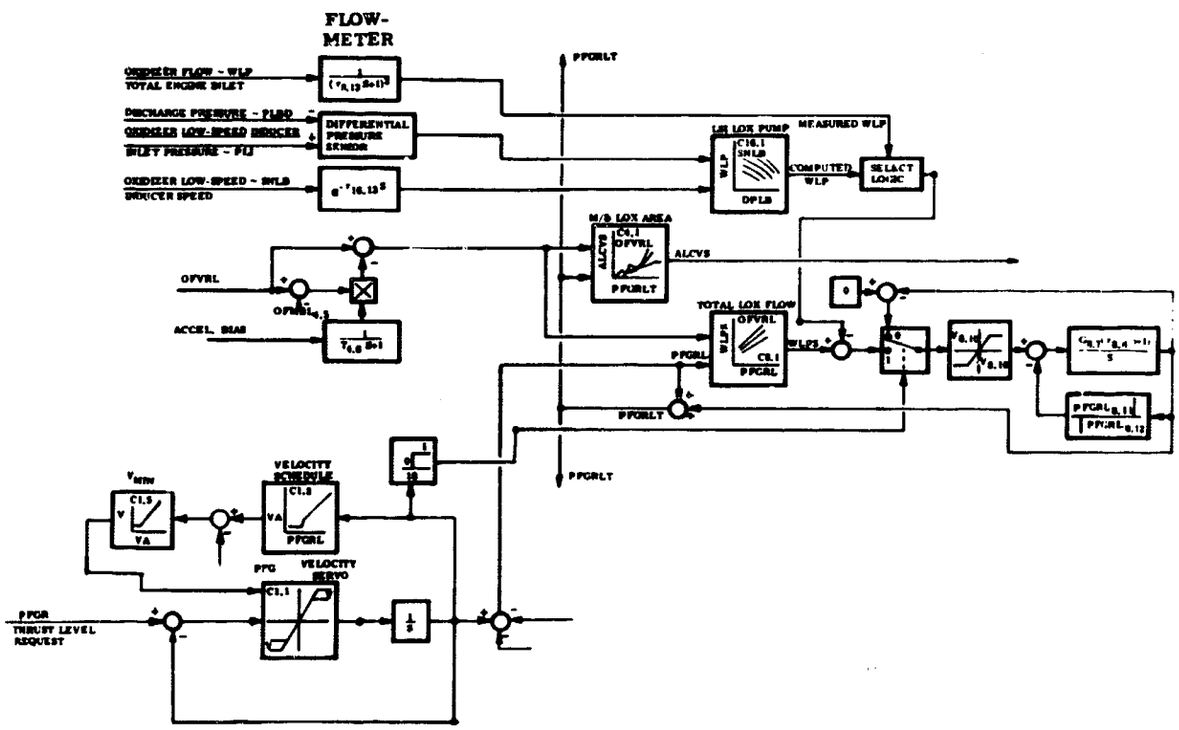

Figure 1139. LOX Flow Trim Loop

The authority limits around the integrator fix the amount of thrust trim available at all engine thrust levels by zeroing the input to the integrator. The error to the LOX flow trimmer is also limited to restrict the rate of thrust level correction. The resultant rate of thrust request to the schedules is the rate of the velocity servo plus the trimmed rate. During start and shutdown cycles the thrust trim loop is opened and the integrator zeroed.

5. Fuel Flow Trim Loop

Accurate mixture ratio balance must be maintained at steady-state for proper propellant management. During a transient it is important that a coordination of LOX and fuel pump loads be made to keep the pumps balanced and moving along known schedules.

A fuel flow reference value is calculated by dividing the measured total oxidizer flow by either the velocity limited O/F ratio or, during an acceleration, the constant acceleration bias value, $OFPBF_{5.5}$ (see figure 1140). The actual total fuel flow is measured directly or, in the case of flow sensor failure, computed as a function of fuel LSI turbopump speed, inlet and exit pressures. The reference fuel flow is compared with the actual total fuel flow to generate an error signal. This error signal acts through a dynamically compensated integrator to trim the gross mode scheduled preburner fuel valve position. The trimming of the fuel valve drives the actual fuel flow, and therefore the pump load and engine O/F ratio, to the desired value.

Integrator authority limits are provided in the trim loop to prevent excessive fuel valve excursions. During start and shutdown cycles, the fuel trim is opened and the integrator zeroed.

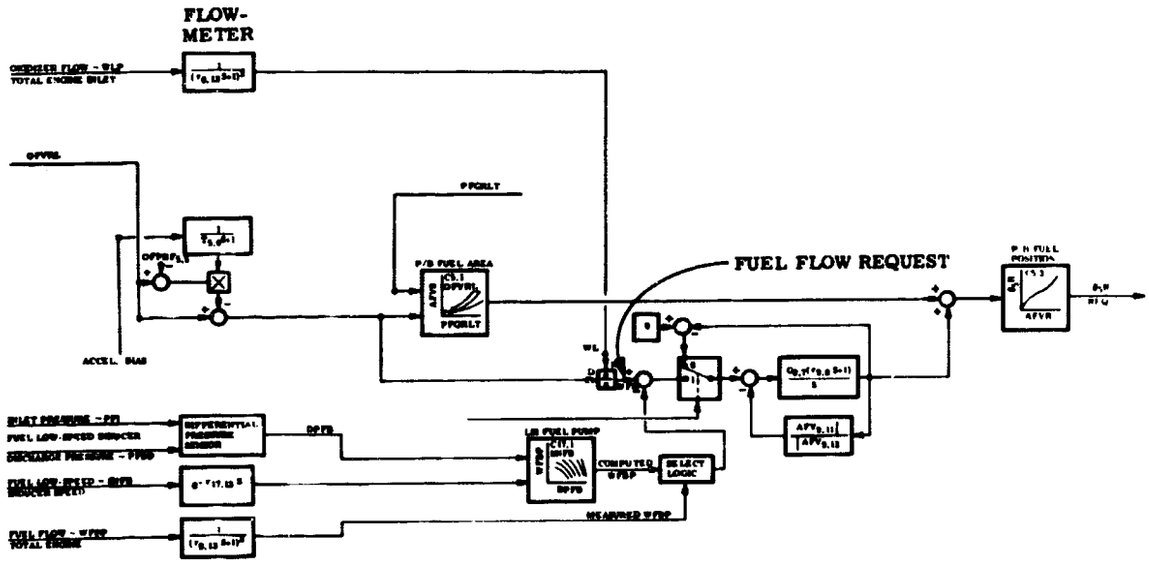

Figure 1140. Fuel Flow Trim Loop

6. LOX NPSP Protection

LOX flow cavitation occurring in the main turbopump causes a sudden reduction in the total oxidizer flow delivered to the engine. This disturbance in oxidizer flow will change the engine thrust and unbalance the oxidizer-to-fuel ratio. The LOX low speed inducer (LSI) valve provides direct control of the main LOX pump inlet pressure and can be trimmed by a closed loop to prevent cavitation in the main pump.

A minimum, safe main LOX turbopump inlet pressure is calculated as the sum of actual main LOX pump net positive suction pressure (NPSP) plus the vaporization pressure of the LOX at the inlet to the main pump (see figure 1141). The main pump NPSP is computed as a function of the turbopump speed and the acutal total oxidizer flow. The vaporization pressure is calculated as a

function of the main turbopump LOX inlet temperature plus an additional safety margin. This minimum inlet pressure is compared with the actual pressure to generate an error signal. When the actual pressure drops below the minimum operating pressure, the error signal acts through a dynamically compensated network to close the LSI area and open the main chamber area in proportion to the cubic ratio of valve areas. This double area reset results in a larger pressure drop existing across the LSI turbine without disturbing the scheduled LOX flow into the main chamber. As a result, more power is supplied to the LSI pump, raising the inlet pressure of the main pump above the value at which cavitation occurs.

When a positive or safe pressure margin is experienced during normal engine operation, no correction is made in the scheduled areas.

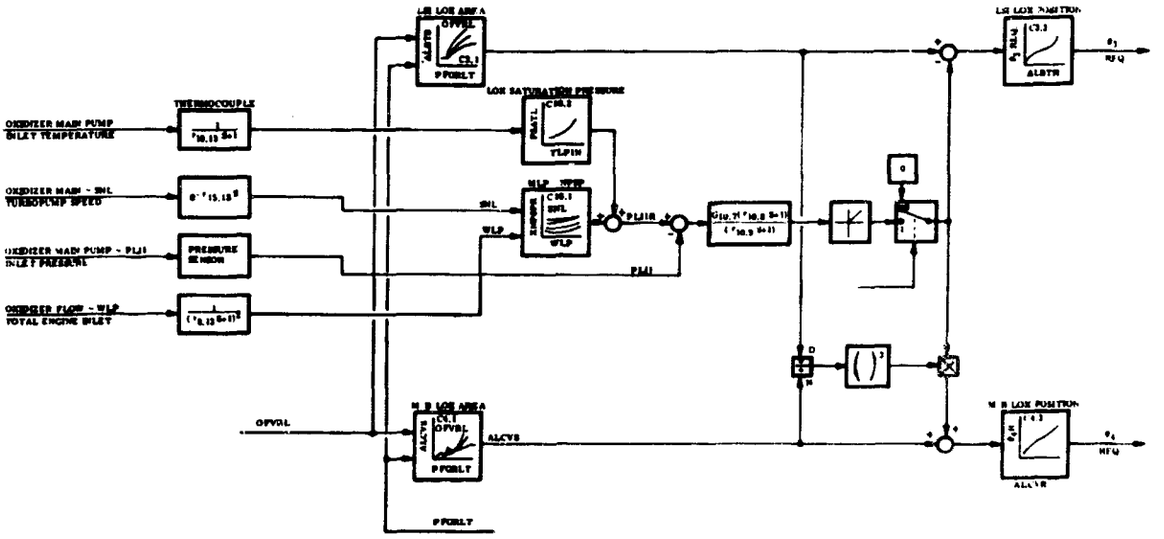

Figure 1141. LOX NPSP Protection Loop

7. Preburner Temperature Limiter Loop

The preburner temperature or turbine inlet temperature is influenced directly by the preburner O/F ratio. If an abnormal condition occurs to cause a high preburner temperature at any time, the preburner temperature limiter loop (figure 1142) will act to reduce the preburner O/F ratio and consequently the preburner temperature by increasing the fuel flow into the preburner.

When a temperature correction is necessary, the preburner temperature loop acts to lower the O/F ratio reference value to the preburner fuel valve schedule and the O/F reference to the fuel flow trim loop. With a lower O/F ratio reference value the schedule and the loop increase the fuel flow to the engine and the preburner temperature is lowered to a safe value.

The maximum reference temperature limit is scheduled as a function of the main fuel pump speed to allow maximum operating temperatures. The

preburner temperature is indirectly sensed by four probes located at the exit of each turbine. Trim occurs only if the highest temperature sensed exceeds the scheduled limit. Compensation is provided in the loop to overcome the effects of thermocouple dynamics.

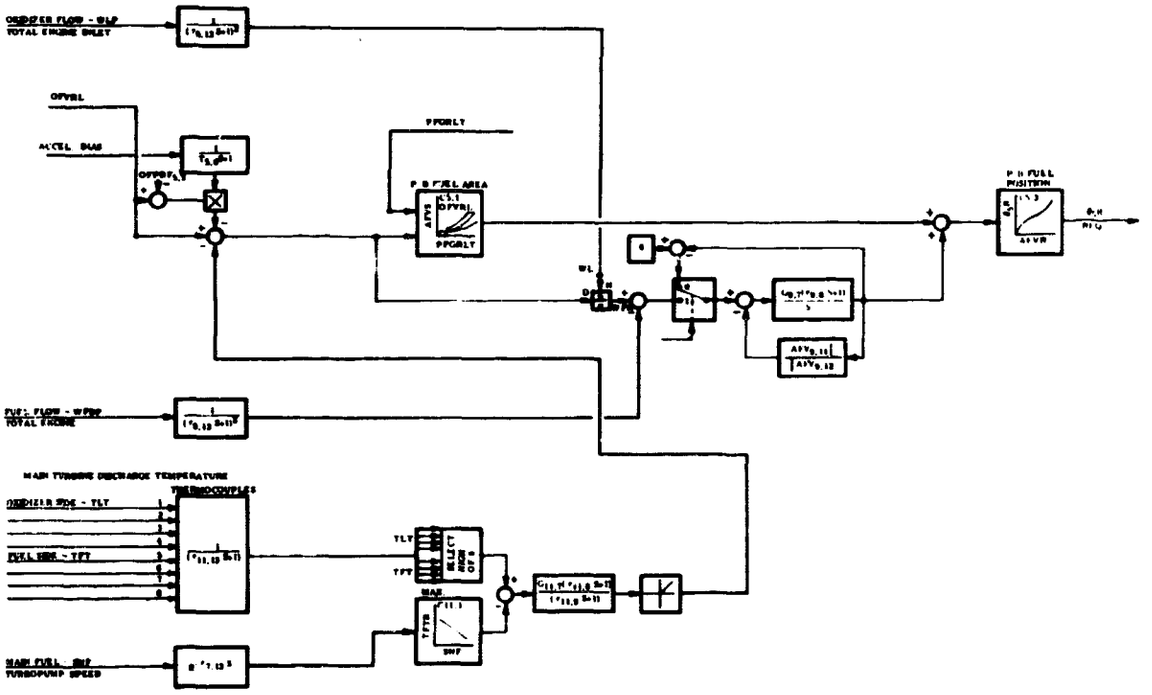

Figure 1142. Preburner Temperature Protection Loop

8. Cavitation Protection For The Main Fuel Pump

Cavitation at the main fuel pump inlet can be the cause of a sudden reduction in fuel flow through the pump to the engine. This disturbance in fuel flow will unbalance the oxidizer to fuel ratio and cause serious overtemperature in the engine.

The pressure supplied by the fuel boost pump gives the net positive suction pressure (NPSP) margin needed by the main fuel pump to prevent cavitation. The power to drive the inducer pump is delivered by the low speed inducer turbine placed in the transpiration cooling flow circuit. As further described in the section on transpiration cooling flow protection, the high pressure delivered by the main fuel pump provides the pressure drop across the circuit to maintain cooling flow and also power to the boost pump.

During an acceleration transient, the lagged response of the fuel boost pump causes the pressure delivered to the main pump to be lowered. The lowered pressure reduces the NPSP margin. The NPSP margin is improved in two ways: first, by decreasing thrust and acceleration rate,

and second, by augmenting the speed schedule to maintain pump speed, i.e., fuel pressure (figure 1143). The total action improves the NPSP margin by:

- Increasing the power to the low speed inducer by increasing the pressure drop across the cooling flow circuit
- Increasing boost pump output pressure by unloading the boost pump with a reduction in total fuel flow
- Preventing the required NPSP from increasing and allowing the slower boost pump to catch up by holding the main fuel pump speed constant

The NPSP of the main fuel pump is given by a map (or by an equation if desirable) which has inputs of main fuel pump speed (SNF) and total fuel flow (WF) passing through the pump. The saturation pressure is a function of the fuel temperature entering the main pump. The sum of NPSP and the saturation pressure is the required minimum main pump inlet pressure needed to prevent cavitation. Comparing the required pressure with the measured pressure forms an error signal which is dynamically conditioned and acts to improve the cavitation margin as described above.

9. Transpiration Cooling Flow Protection

The walls of the main chamber must be cooled to prevent overheating by the hot combustion gases. A portion of total fuel flow is supplied to the main chamber through the transpiration cooling circuit which contains a fixed area restriction in parallel with the fuel low speed inducer turbine. Since the flow path effectively consists of a constant area restriction, the proper transpiration cooling flow must be supplied by the pressure drop maintained from the output pressure of the fuel pump to the pressure in the main chamber. The proper pressure drop is assumed to exist normally at steady-state by controlling the main fuel pump speed with a closed-loop.

The required transpiration cooling flow is strongly affected by and increases nearly linearly with the thrust level of the engine. Also, if the fuel pump speed is held to its scheduled value with thrust level, adequate cooling flow will be supplied for the reasons mentioned above. If, during an acceleration transient, cooling flow becomes marginal due to a lagged response by the fuel pump, the cooling flow limiter will slow the request thrust rate to allow the SNF pump to catch up to its scheduled value (figure 1144). In addition the limiter will improve the cooling flow margin by reducing the required cooling flow with respect to the actual cooling flow. This improvement in margin is accomplished by reducing thrust without changing fuel pump speed. The limiter proportionally reduces the requested thrust level to all the schedules and simultaneously biases the scheduled fuel pump speed so that there is no change in requested speed.

The transpiration supply regenerative heat exchanger exit temperature (TBHXD) provides a good indication of the cooling conditions in the main chamber. By sensing this exit temperature and comparing it to a scheduled value, a temperature error is formed which indicates the cooling flow margin. Correction will be made only if the actual temperature rises above the scheduled value. Dynamic compensation is provided to allow optimization of the response of the transpiration cooling protection loop.

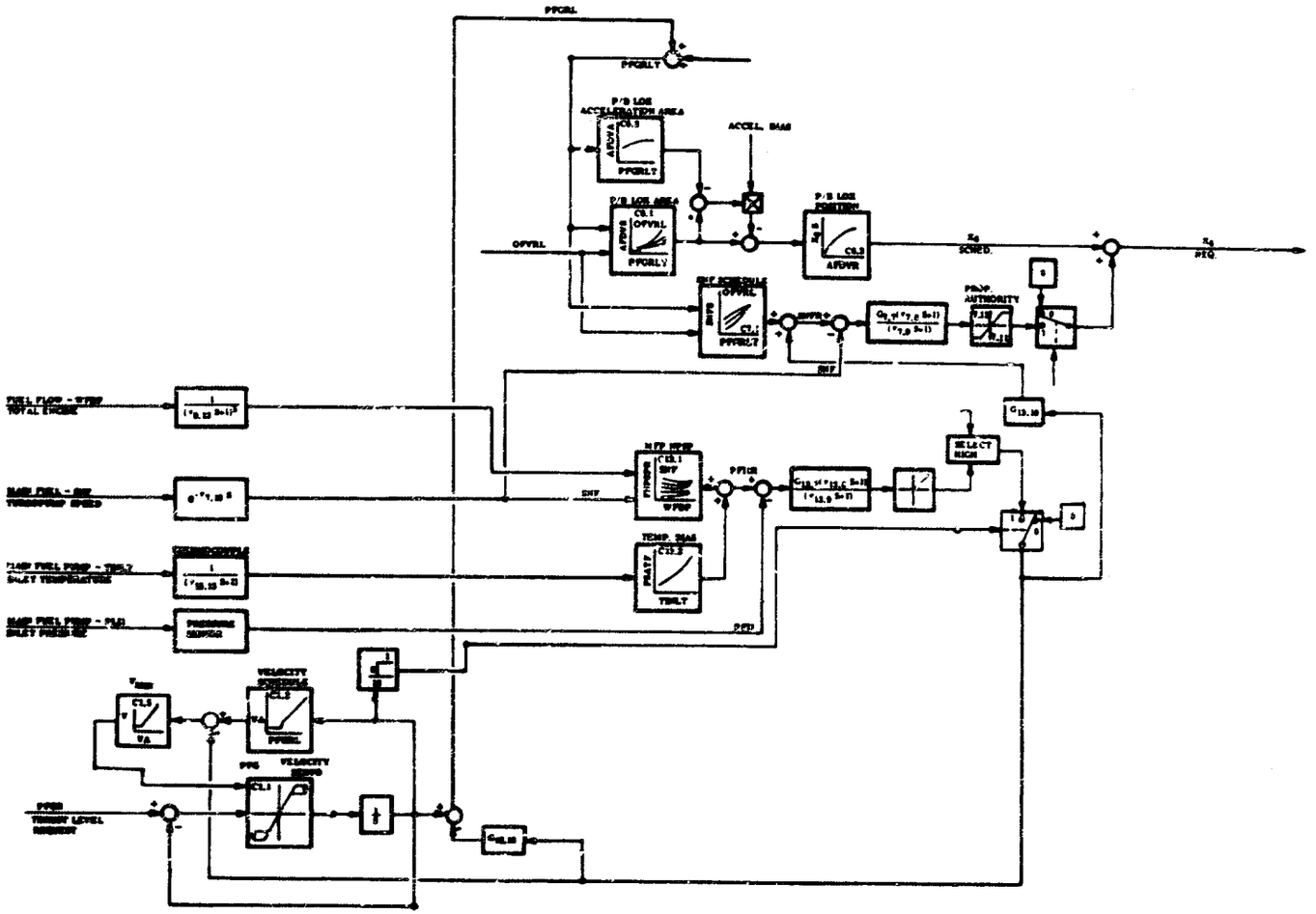

Figure 1143. Fuel NPSP Protection Loop

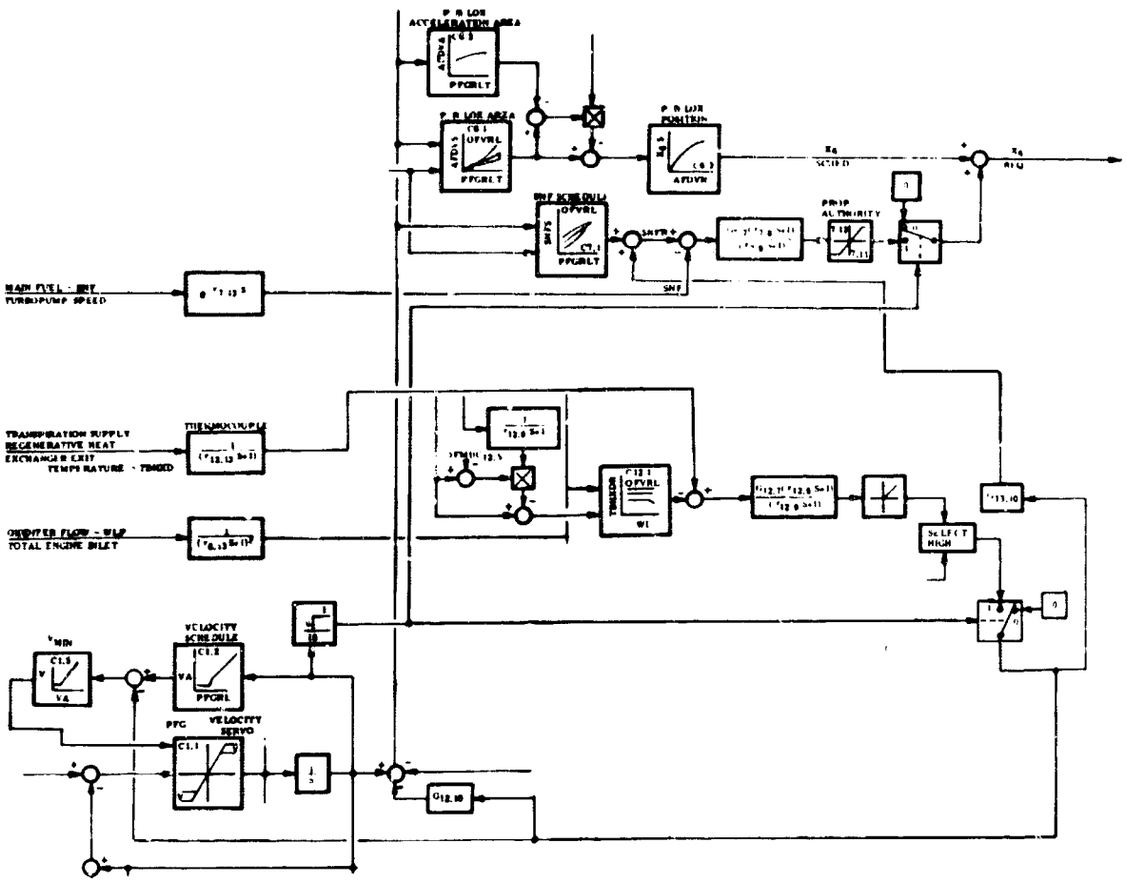

Figure 1144. Transpiration Cooling Protection Loop

10. Main Turbopump Overspeed Protection

The overspeed protection for both main fuel and main oxidizer turbopumps gives positive corrective action without upsetting the power and flow balance within the engine. By trimming the thrust request during overspeed conditions, corrective action will be taken while keeping all of the system schedules coordinated.

Both main pump speeds are compared to their maximum limits to form two speed errors (figure 1145). Each error is conditioned to remove the dynamic characteristics of each pump speed loop. Thrust level trim occurs only when an overspeed condition exists. If an overspeed condition exists simultaneously for both pumps, the largest error is selected for corrective action by a select high function.

The error from the select high function acts to slow or to reduce the thrust level set by the thrust request servo. A speed error will act in a proportional plus integral manner to reduce thrust level to correct for the turbopump overspeed problem.

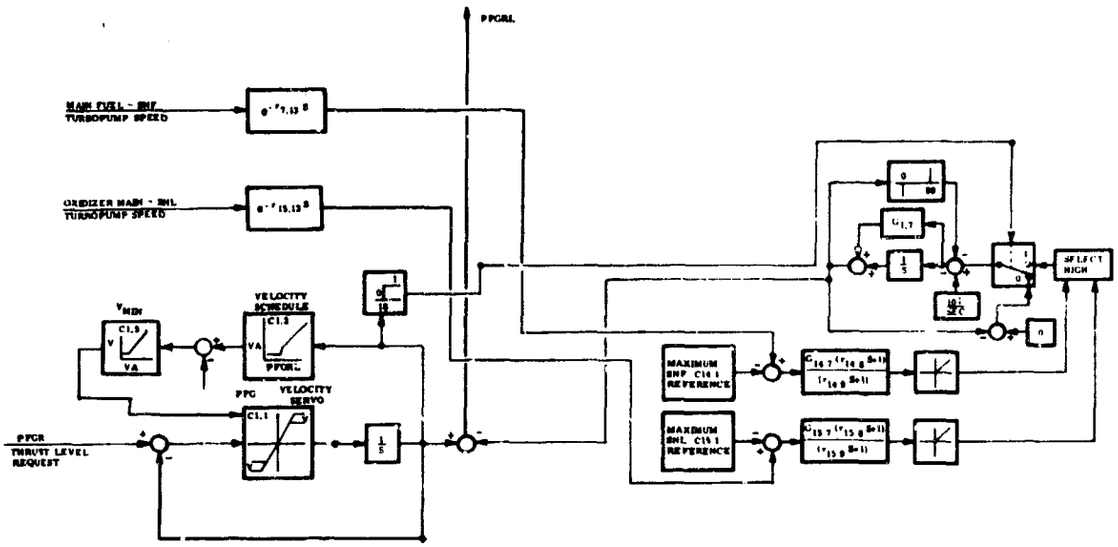

Figure 1145. Main Pump Overspeed Protection Loop

11. Start and Shutdown Operation

Safe engine start and shutdown prescribe three functional requirements for the control system:

- Indicate start procedure immediately after cycling the prestart functions (on-off)
- Provide time-based sequence control of valves and solenoids
- Hold system at a selected, safe start level in the event of a failed ignition

Figure 1146 represents the control functions for start and shutdown operation.

A rate controlled signal from the thrust level actuator delivered simultaneously to both the start and shutdown schedules provides a time-base for the schedules. As a function of the input signal level, each start and shutdown operation can be separately sequenced and controlled at a definite rate.

The number of separate start and shutdown schedules is minimized by extending and utilizing the gross schedules of the four control valves needed in the gross control system. These are:

- Preburner LOX valve
- Main chamber LOX valve
- LOX low speed inducer valve
- Preburner fuel valve

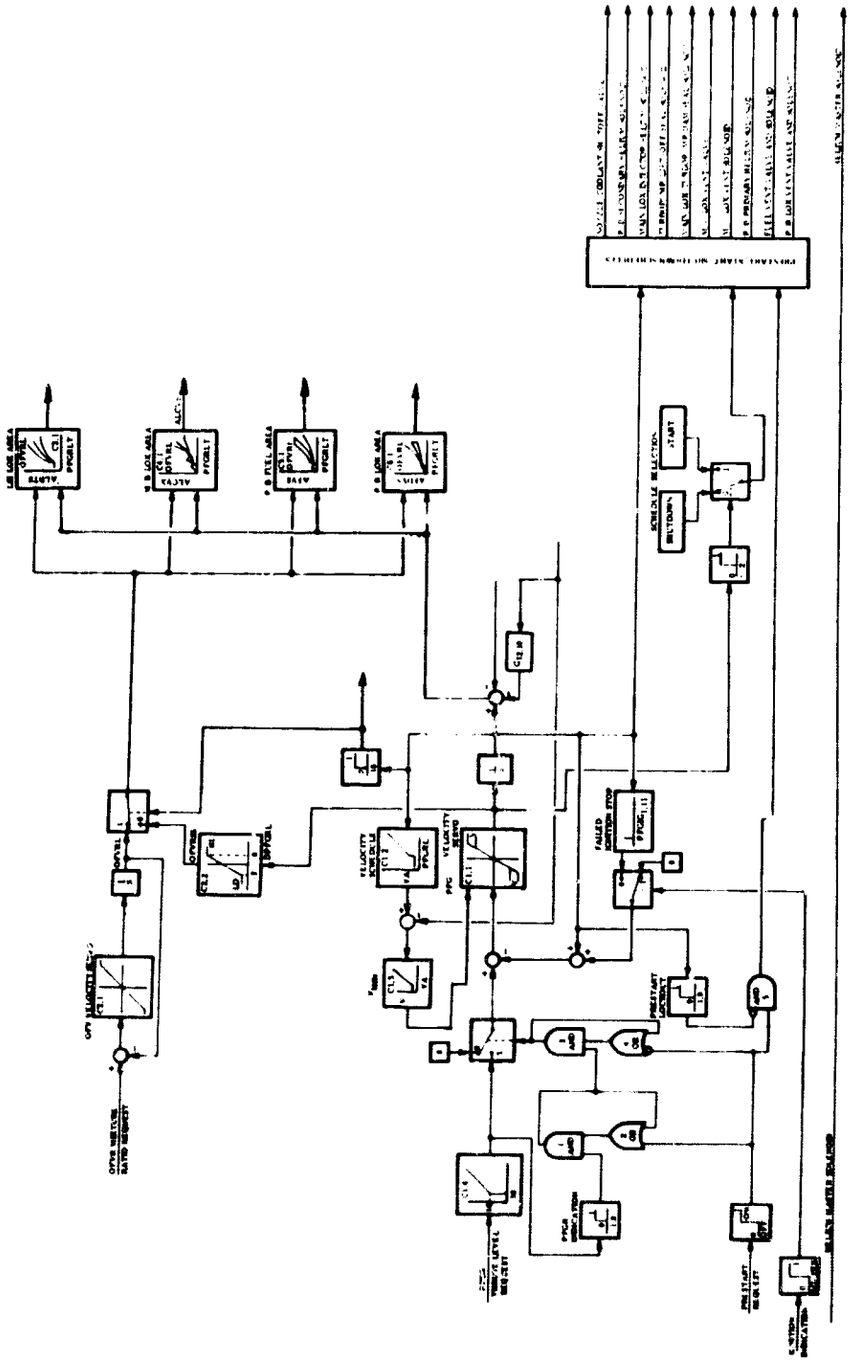

Figure 1146. Prestart, Start and Shutdown Schedules and Logic

A positive velocity servo error drives the four valves to the start schedule and a negative error drives the valves to the shutdown schedule by changing the O/F ratio used in computing the valve schedules.

12. Prestart Logic

The prestart logic prevents engine startup without first cycling (on-off) the prestart request. Completion of the prestart cycle immediately begins engine start procedure if requested by the thrust level. Note that the thrust lever must be advanced at least to idle to initiate start. Function C1.4 prevents a thrust lever request in the start of shutdown region where timed valve sequences are critical. Figure 1147 shows the prestart logic and schedules.

If the thrust lever request (PFGR) is advanced for starting, application of prestart requests, in sequence:

- Actuates the prestart schedules through AND gate 5
- Energizes logic gates 1 and 2 and sends the energized signal to AND gate 3
- Keeps switch 6 referenced to zero thrust request preventing any start sequence

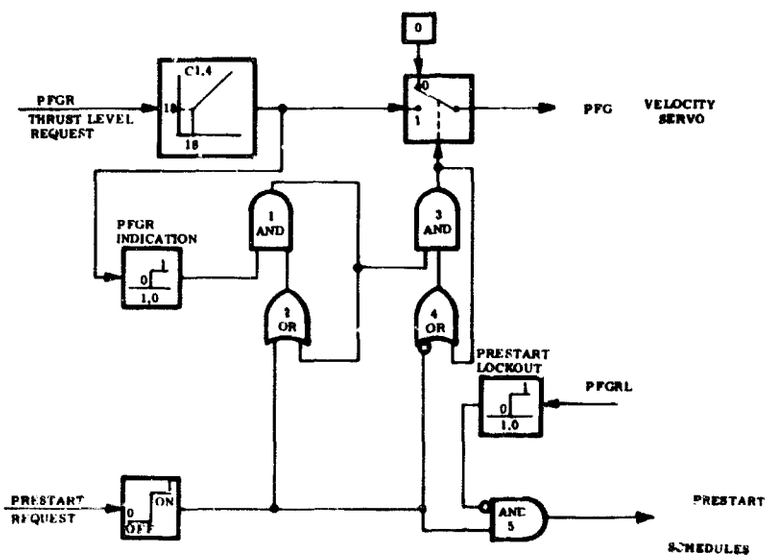

Figure 1147. Prestart Logic

Note, a thrust request la[illegible] logic gates 1 and 2 energized. Removal of the prestart request:

- Turns off the prestart schedules
- Energizes logic gates 3 and 4 which closes switch 6 and passes the thrust request signal to the PFG velocity servo to start engine

When the actuated thrust level advances for starting, the prestart functions are locked out (prestart lockout signal to AND gate 5) to prevent accidental cycling during engine operation.

Note, the master solenoid is turned on with electrical startup and turned off with electrical shutdown.

13. Start and Shutdown Schedule Selection Logic

The thrust level servo, after receiving the thrust request signal from the prestart logic, moves at a controlled rate through the start and shutdown region to provide a time-base on which to schedule the start and shutdown functions. In addition to position, the direction of the thrust velocity servo is sent to the schedules to indicate whether a start or shutdown request has been made. Figure 1148 shows the start and shutdown schedule selection logic.

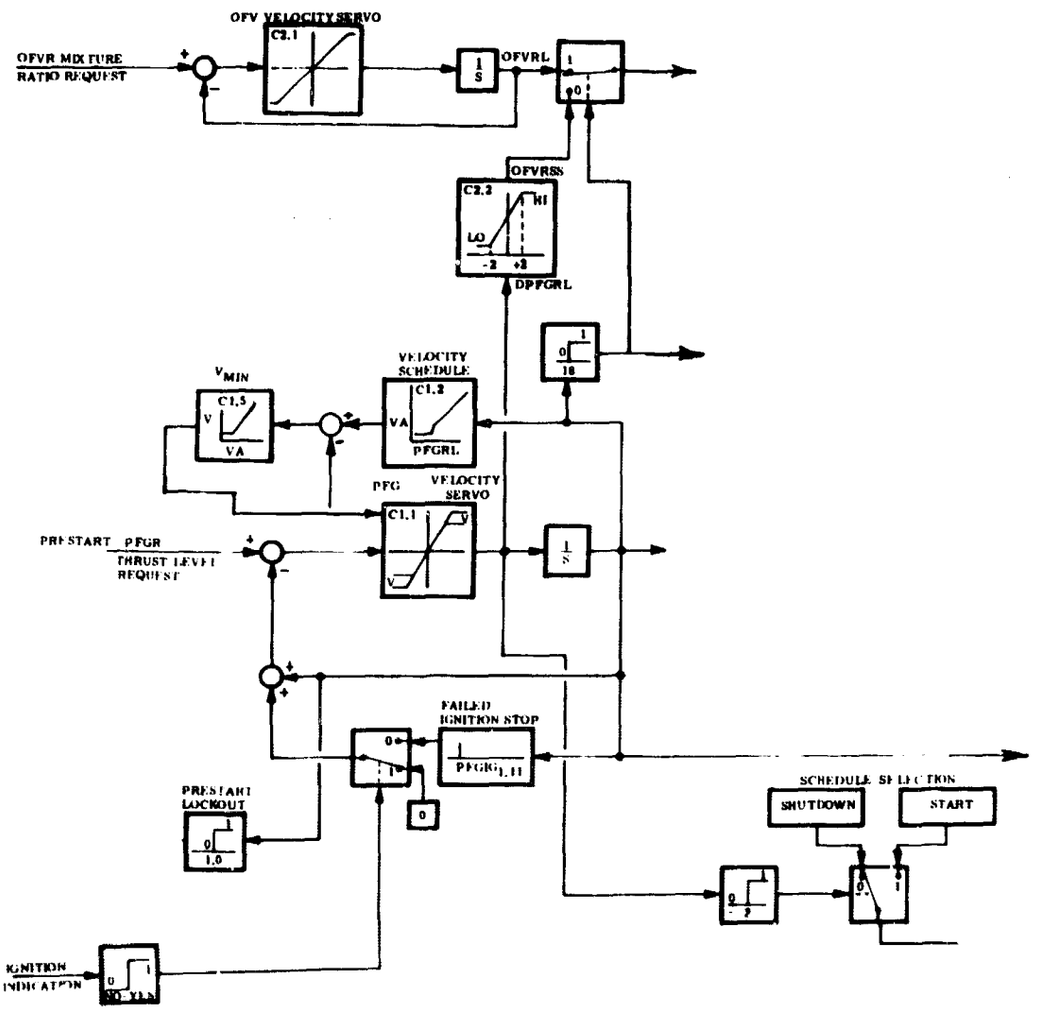

Figure 1148. Start and Shutdown Schedule Selection Logic

Ignition indication is determined by monitoring a start sensitive engine parameter and comparing it to a known value in the start region. If failed ignition occurs, a servo stop holds the servo output to a safe level on the start schedules until ignition does occur or the system is requested to shut-down. Note, because the failed ignition stop drives the servo velocity to zero, the start and shutdown schedules are selected with velocities of 0.0 percent/second or above for start and -2.0 percent/second or below for shutdown.

All closed loops are zeroed and deactivated during start and shutdown by opening a switch placed in each of the closed-loops. Each switch is opened and closed as a function of thrust level output of the servo (switch closes when PFGRL becomes greater than some prescribed level, say 18 percent).

C. BLOCK DIAGRAM NOMENCLATURE

The following table defines the curves and gains for the XLR129 control system. Note for the block diagram curves, the output variable and its units are given in the last two columns. In the subscript, the first number refers to the control section and the second number identifies the variable.

Name	Description	Value	Units
	1.0-PFG Velocity Servo Section		
C1.1	PFG thrust level servo velocity gain with variable velocity limits (gain = 20% sec/% error).	DPFGRL	%/sec
C1.2	Schedule of maximum thrust level request velocity (VA = 0.67 x PFGRL in normal thrust level range)	VA	%/sec
C1.3	Acceleration bias function for unique acceleration schedules (Vmin = 13%/sec)		unitless
C1.5	Minimum thrust velocity limits (minimum absolute value = 5%/sec)	V	%/sec
G1.4	Thrust level request schedule (prevents a thrust level request in the start and shutdown region)	PFGR	%
G1.7	Thrust level proportional reset gain used by engine protection loops	0.08	$\frac{\%}{\%/sec}$
PFGIG1.11	Failed ignition thrust level stop		%
	2.0-OFV Velocity Servo Section		
C2.1	OFV (Vehicle oxidizer to fuel flow ratio) servo velocity gain and maximum limits (1.0 unit/sec) (5.0 units/sec/unit error)	DOFVRL	$\frac{1}{sec}$

Name	Description	Value	Units
C2.2	Start and shutdown schedule of OFVRL	OFVRSS	unitless
	3.0-LOX Low Speed Inducer (LSI) Valve		
C3.1	Steady-state area schedule	ALBTS	$in.^2$
C3.3	Position schedule	$\theta_3 R$	degrees
	4.0-Main Burner (M/B) LOX Valve		
C4.1	Steady-state area schedule	ALCVS	$in.^2$
C4.3	Position schedule	$\theta_4 R$	degrees
OFMBL4.5	Acceleration OFV reset to LSI and M/B valve and total LOX flow		unitless
T4.6	Acceleration OFV reset lag time constant	0.20	sec
	5.0-Preburner (P/B) Fuel Valve		
C5.1	Steady-state area schedule	AFVS	$in.^2$
C5.3	Position schedule	$\theta_5 R$	degrees
OFPBF5.5	Acceleration OFV reset to P/B fuel valve and fuel flow		unitless
T5.6	Acceleration OFV reset lag time constant	0.20	sec
	6.0-Preburner (P/B) LOX Valve		
C6.1	Steady-state area schedule	AFDVS	$in.^2$
C6.2	Acceleration area schedule	AFDVA	$in.^2$
C6.3	Position schedule	$X_6 R$	in.
OFPBL6.5	Acceleration OFV reset to P/B LOX valve and SNF schedule		unitless
T6.6	Acceleration OFV reset lag time constant	0.20	sec
	7.0-Main Fuel Turbopump Speed (SNF) Closed-Loop		
C7.1	SNF schedule	SNFS	rpm
G7.7	SNF loop proportional gain	2.0×10^{-5}	in./rpm

Name	Description	Value	Units
T7.8	SNF loop lead compensation	0.10	sec
T7.9	SNF loop lag compensation	0.20	sec
7.11	Lower authority limit on P/B LOX valve travel		in.
7.12	Upper authority limit on P/B LOX valve travel		in.
T7.13	SNF sensor effective time delay	0.0005	sec
	8.0-Total Engine Oxidizer Flow Trim Loop		
C8.1	Total engine LOX flow schedule	WL	$\frac{\text{lbs}}{\text{sec}}$
G8.7	LOX flow trim integrator gain	2.0	$\frac{\%/\text{sec}}{\text{lbs/sec}}$
T8.8	Lead compensation	0.16	sec
V8.10	Maximum and minimum trim rate limits	5.0	lbs/sec
PFGRL8.11	Lower authority limit on thrust request		%
PFGRL8.12	Upper authority limit on thrust request		%
T8.13	LOX flow sensor effective lag dynamics	0.02	sec
	9.0-Total Engine Oxidizer to Fuel Flow Ratio (OFV) Trim Loop		
G9.7	OFV trim integrator gain	0.388	$\frac{\text{in.}^2/\text{sec}}{\text{lbs/sec}}$
T9.8	Lead compensation	0.05	sec
AFV9.11	Lower authority limit on P/B fuel valve area		in.^2
AFV9.12	Upper authority limit on P/B fuel valve area		in.^2
T9.13	Fuel flow sensor effective lag dynamics	0.02	sec
	10.0-Main Oxidizer Pump Cavitation Protection Loop		
C10.1	Main LOX pump equired net positive suction pressure NPSP)	XNPSPR	psi

Name	Description	Value	Units
C10.2	LOX saturation pressure at the main pump inlet	PSATL	psia
G10.7	Proportional gain to the LSI valve area	0.02	$in.^2/psi$
T10.8	Lead compensation dynamics	0	sec
T10.9	Lag compensation dynamics	0	sec
T10.13	Temperature sensor (thermocouple) effective lag dynamics		sec
	11.0-Maximum Preburner Temperature Limiter Loop		
C11.1	Schedule of main fuel pump turbine maximum exit temperature	TFTR	°R
G11.7	Proportional gain to requested engine OFV ratio	0.02	$\frac{1}{°R}$
T11.8	Lead compensation dynamics	0.05	sec
T11.9	Lag compensation dynamics	0.02	sec
T11.13	Effective lag dynamics for each of the eight turbine exit temperature sensors (thermocouple)	0.05	sec
	12.0-Transpiration Cooling Protection Loop		
C12.1	Schedule of maximum transpiration supply regenerative heat exchanger exit temperature.	TBHXDR	°R
OFMBC12.5	Acceleration OFV reset to the maximum TBHXDR schedule for main burner cooling protection		unitless
T12.6	Acceleration OFV reset lag time constant	0.20	sec
G12.7	Integrator gain to rate of thrust request correction on PFGRL	0.25	$\frac{\%/sec}{°R}$
T12.8	Lead compensation dynamics	0.50	sec
T12.9	Lag compensation dynamics	0	sec
G12.10	Thrust proportional reset gain	0.16	$\frac{\%}{\%/sec}$

Name	Description	Value	Units
T12.13	Temperature sensor (thermocouple) effective lag dynamics	0.50	sec
	13.0-Main Fuel Pump Cavitation Protection Loop		
C13.1	Main fuel pump required net positive suction pressure (NPSP)	FNPSPR	psi
C13.2	Fuel (hydrogen) saturation pressure at the main pump inlet	PSATF	psia
G13.7	Integrator gain to rate of thrust request correction on PFGRL	5.0	%/sec
T13.8	Lead compensation dynamics		sec
T13.9	Lag compensation dynamics		sec
G13.10	Speed proportional reset gain (G13.10 = G1.7 x ΔSNF/ ΔPFG)	26.50	rpm / %/sec
T13.13	Fuel inlet temperature sensor effective lag dynamics		sec
	14.0-Main Fuel Turbopump Overspeed Limiter		
C14.1	Maximum SNF speed reference		rpm
G14.7	Integrator gain to rate of thrust request correction on PFGRL	0.05	%/sec / rpm
T14.8	Lead compensation dynamics	0.10	sec
T14.9	Lag compensation dynamics	0.02	sec
	15.0-Main LOX Turbopump Overspeed Limiter		
C15.1	Maximum SNL speed reference		rpm
G15.7	Integrator gain to rate of thrust request correction on PFGRL	0.10	%/sec / rpm
T15.8	Lead compensation dynamics	0.10	sec
T15.9	Lag compensation dynamics	0.02	sec
T15.13	SNL sensor effective time delay	0.005	sec

Name	Description	Value	Units
	16.0-Circuit for Computing Oxidizer Flow From LOX Boost Pump Characteristics		
C16.1	LOX boost pump flow, pressure and speed characteristics	WLP	lbs/sec
T16.13	SNLP sensor effective time delay	0.005	sec
	17.0-Circuit for Computing Fuel Flow From Fuel Boost Pump Characteristics		
C17.1	Fuel pump flow, pressure and speed characteristics	WFPB	lbs/sec
T17.13	SNFB sensor effective time delay	0.005	sec

SECTION II
CONTROL COMPUTER

A. SUMMARY

This section represents a summary of the study effort conducted by Bendix Corporation as part of Pratt & Whitney Aircraft Contract Number F04611-68-C-0002 concerning the feasibility of applying hybrid analog-digital control techniques to high performance rocket engines. Specifically, primary importance was assigned to the development of suitable techniques which could be implemented without dependence upon new state-of-the-art development work or radical departures from current control computer technology.

At the beginning of this study, the direction given to the investigation led to running an engine with "off the shelf" computing hardware. The effort was then redirected towards an "on engine" mounted device which could be implemented within the near future. It is towards this concept that this report is responsive.

Based on conducted studies, it has been proven that the control requirements of the XLR129 High Pressure Engine can be met with currently known electronic technology. Within the currently specified control requirements, the rate of computation as well as the extent of data storage of the proposed control computer is adequate to accommodate all the necessary computations required for safe control of the XLR129 engine. Furthermore, while running the engine under full supervisory control it is capable of monitoring vital performance parameters and can safely shut down the engine in the case of "out-of-tolerance" malfunction.

The control computer described employs some concepts which have been successfully proven in similar engine control applications and therefore represents no real departure from realizable goals. Reference is made to conventional existing circuits where such information was available and where it was deemed beneficial to the understanding of the function involved. It is necessary to realize that in no way is this identification of circuits to be limiting in any sense to a particular device, since this study concerned itself with conceptual approaches only.

The Bendix BDX-800 specialized control repertoire was deemed a satisfactory vehicle by means of which the control requirements could be related to suitable up-to-date electronic computing technology. Programming of the control functions was similarly guided by the system block diagrams which in turn were derived from the Engine Performance Data Deck furnished by Pratt and Whitney Engineering. This programming function was attempted to define the magnitude of the control program and its demands upon the computer memory size and iteration cycle time. Further refinements in the programming area may be required to compress the many divergent computing and monitoring requirements into the real time period available.

B. GENERAL

1. Introduction

The specific objectives of this study program with respect to the Input/Output (I/O) section have been the investigation, evaluation, and recommendation of various design factors with a view toward an overall integrated system approach, and greater insight into the solution of interfacing problems associated with a rocket engine control computer.

Basically, the I/O section will accept various preconditioned sensor signals (temperature, pressure, flow rate, etc.) and multiplex them by means of an analog multiplexer (Junction Isolated Field Effect Transistor switches) in accordance with central computer control signals utilizing I/O control gating logic. The output of the multiplexer is then converted to 12-bit digital words by an analog-to-digital (A/D) converter (successive-approximation type). These digital words are then processed by the Control Processing Unit (CPU) in accordance with a predetermined program. The output of the CPU is then addressed to one of four digital-to-analog (D/A) converters (parallel resistor ladder type) which provides a DC analog to one of four actuator servos (brushless DC torquer type).

In addition, the input section will convert speed sensor signals (variable time method) to digital signals for processing by the CPU. The output section of the CPU will also provide 11 discrete signals for solenoids and actuator switches. Also, a redundant I/O section will be provided for the redundant central computer.

Both the fixed time interval and variable time interval measurement methods are discussed and compared. The variable time interval approach is selected and applied to the four speed inputs. In addition, monitoring circuits are provided and described for the two redundant speed sensors, and a test program to detect speed input circuit failures is presented.

The sensor failure input circuits, which provide interfacing between the sensor failure signals and device controller, are also described.

2. Computer

The computer receives data from the pressure, temperature, speed, and flowmeter sensors; monitors the positions of the actuators; and supplies output commands to the actuators and solenoids. In addition, the computer is given operational commands by the ship's central computer, provides test signals to the computer subsystems, observes the effect of the test signals, and outputs data to the ship's central computer, which judges the validity of the computer's performance.

The computer is divided into four sections:

1 Input Subsystem

2. Output Subsystem

3. CPU Interface

4. Central Processing Unit

The input subsystem includes the analog multiplexer, analog to digital converter, speed measurement circuits, and sensor failure input circuits. The output subsystem is composed of the digital to analog converters, the actuator servo amplifiers, and the solenoid drivers. The CPU interface permits communication between the central processing unit and the input subsystem, output subsystem, and ship's central computer. The central processing unit executes all required computations, and stores the XLR129 operational and test programs.

3. Input Circuits

a. Multiplexer and A/D Converter

The preconditioned input sensor signals (up to 40 channels) will be multiplexed by means of an analog multiplexer (J-FET type) in accordance with central computer control signals. The J-FET switch was selected because of its low ON resistance, zero offset voltage, good temperature stability, and adequate speed.

The output of the multiplexer is then converted to 12-bit digital words by means of a A/D converter. The successive-approximation converter is recommended because it has a faster data access time and requires less hardware than the range-comparison method.

b. Speed Circuits

The speed equation is formulated for the fixed time interval measurement method. The implications of this equation are examined, and a block diagram is presented, which indicates the hardware implementation for this method. These items are also discussed for the variable time interval measurement method. The features of these two approaches are compared, and a logic diagram implementation is given for the approach utilized by the XLR129. In addition, fault detection is considered for both sensors and measurement circuits. The inputs from the sensors are checked for a constant high voltage level, a constant low voltage level, and an input frequency, which exceeds the input's limit. The measurement circuits are exercised by inserting a simulated input and observing the measurement circuit output.

c. Sensor Failure Input Circuits

A logic implementation is described, which orders the sensor failure data into a form acceptable to the computer.

4. Output Subsystem

a. D/A Circuit

The digital output of the CPU is converted to an analog signal by means of parallel resistor ladder type of D/A converter. This converter method is recommended because of its high accuracy, fast operation, and good temperature stability.

b. Actuator Servos

The servos controlling the actuator valves will utilize brushless DC torque motors. The major advantages of these servos are the elimination of gear trains, a wide servo bandwidth, and low power dissipation at null.

The servo electronics will utilize op-amp microcircuits, DC lead-lag compensation, and miniature components throughout. This approach will result in efficient servo compensation, minimum heat generation, and a small packaging size.

c. Solenoid Drivers

The implementation and characteristics of two driver circuits are presented and discussed. The first circuit requires the most hardware, but minimizes power consumption. The alternate driver is simplest and costs the least, but the power requirement increases.

5. Central Processing Unit Interface

Communications between the BDX 800 central processing unit (CPU) and the input/output subsystem are analyzed and defined in terms of computer instruction repertoire, instruction timing and logical implementation. An exchange of information is initiated by a BDX 800 input/output instruction in the computer program. Each instruction triggers the start of a series of steps subdivided to function in the computer timing intervals. In addition, the CPU and input/output units generate, initiate and acknowledge signals to control the flow of the data transmitted and received. In addition, individual discussions are included for the CPU interface with the analog to digital converter, speed measurement circuits, failure input circuits, digital to analog converter, discrete output circuits and ship central computer.

6. Central Processing Unit

The central processing unit is a conventional general purpose digital computer. The memory stores the system operational and test programs. The CPU accepts and supplies data from and to the device controllers (CPU interface) and performs computations as directed by the system programs.

7. Recommendations

The overall conclusion reached by this study effort indicates that a high reliability system can be achieved, meeting all essential requirements, by utilizing the recommended techniques and circuits in this report. The specific recommendations are briefly outlined below:

1. Central Processing Unit (CPU) - use available Bendix type (BDX-800) because of tested reliability and relatively low cost.

2. Input Multiplexer - use junction FET switch type for high accuracy and temperature stability reasons.

3. Analog-to-Digital Converter - use successive approximation technique for faster data access time, high accuracy, and reduced hardware reasons.

4. Output Section - use digital multiplexer in conjunction with four digital-to-analog converters for higher accuracy, faster conversion, and better temperature stability reasons.

5. Actuator Servos - use brushless DC torquer servo with DC compensation circuits for high reliability and reduced cost.

6. I/O Controllers - use minimization techniques and high noise immunity MSI logic for reduced hardware and high reliability.

7. Solenoid Drivers - use prescribed technique resulting in less hardware, and higher reliability.

8. Speed Signal Converter - use variable time method in order to reduce hardware, decrease cost, and improve reliability.

8. Preliminary Requirements for Input/Output Processor

a. Input Isolation

The input signal lines shall be buffered to prevent a failure in one channel from propagating into another channel.

b. Updating Rate

The I/O section shall be capable of processing a minimum of 40 channels within each computer cycle time of 10 milliseconds.

c. Shielded Wires

When required, signal lines may be shielded to prevent EMI pickup.

d. A/D Converter

Data Input: 0 to +10 volts DC

Conversion Time: less than 100 μs

Data Access Time: less than 120 μs

Source Resistance: less than 500 ohms

Output Code: 12 bit resolution, natural binary code

Output Register: parallel output, 0 to +5 volts TTL compatible

Accuracy: ± 1-1/2 LSB (Common Reference Supply Voltage for A/D Converter and input sensors)

e. Input Analog Multiplexer

Number of input channels = 40

Input voltage range = 0 to +10 volts

Address logic levels = 0 and +5 volts

On Resistance = less than 250 ohms

Off Resistance = greater than 100 megohms

Switching time = less than 2 μs

f. D/A Converter

Data Input: 12 bit natural binary, parallel

Conversion Time: less than 5 μs

Input Logic Levels: 0 and +5 volts, TTL Compatible

Output Signals = 0 to +10 volts DC

Accuracy = ± 1 LSB (Common reference supply voltage for D/A Converters and servo feedback device)

g. Speed Sensor Converter

Range of input pulses per revolution = 4095 to 20,475

Clock Frequency: 3MHz

Output Code: 15 bit resolution, natural binary

Output Buffer Register: parallel output, 0 to +5 volts TTL Compatible

h. Controllers

Input Address: 4 bits

Control Inputs: 5 channels

Output Control: 2 channels

Transfer Gating: Bidirectional Control for 16 lines

Storage Register: 16 bits

Clock Frequency: 1 MHz

I/O Instruction Time: 6 μs

i. Discrete Outputs

Solenoid Drivers: Seven drivers for 0.5 to 1.0 amp capacity

Gating Control for Drivers: 0 or +5 volts logic

Actuator Changeover Switches: Four Switches with 0 or +5 volts gating logic control

j. Discrete Inputs

Sensor Faults: Detect 35 sensor inputs

Selector Control: Divide inputs into 3 groups of 12 each

k. Operational Temperature Range

-55°C to +125°C

l. Warm-Up Time

The time required for the equipment to warm-up prior to operation shall not exceed five (5) minutes.

m. Power Consumption

The total power consumption of the I/O Section shall be less than 45 VA.

9. Interface Description

Table CXIV lists information about the signals which enter or leave the computer (CPU plus I/O). These include sensors, valves, control signals, from the ships central computer, and solenoids.

Table CXIV. Computer Signal Interfaces

Input Output Signals		Signal Source	Signal Destination	Type of Signals	Range	Sensor Accuracy	Conversion Accuracy	Number Of Bits	Resolution Available
Origin	Signal Name								
Control Room	Prestart Check Out	Control Panel	Input Output Unit	(Voltage TBD) Digital	On-Off	--	-	1	--
Control Room	Initiate Start Seq	Control Panel	Input Output Unit	(Voltage TBD) Digital	On-Off	--	--	1	-
Control Room	Initiate Auto Pwr Mode	Control Panel	Input Output Unit	(Voltage TBD) Digital	On-Off	--	--	1	--
Control Room	Shutdown	Control Panel	Input Output Unit	(Voltage TBD) Digital	On-Off	--	--	1	--
Control Room	Thrust Level	Control Panel	Input Output Unit	(Voltage TBD) Digital	20 -110	--	--	10	10
Control Room	Mixture Ratio	Control Panel	Input Output Unit	(Voltage TBD) Digital	5.0-7.0	--	--	5	0.5
Safe Room	Time T-x	Input Output Unit	Recorder	(Voltage TBD) Digital	TBD	--	--	1	--
Safe Room	Thrust Command	Input Output Unit	Recorder	(Voltage TBD) Digital	TBD	--	--	10	10
Safe Room	Mixture Ratio Command	Input Output Unit	Recorder	(Voltage TBD) Digital	TBD	--	--	5	0.5
Safe Room	Fuel Valve Position	Input Output Unit	Recorder	(Voltage TBD) Digital	TBD	--	--	12	1 [illegible]
Safe Room	Preburner LOX Valve Position	Input/Output Unit	Recorder	(Voltage TBD) Digital	TBD	--	--	12	1 [illegible]
Safe Room	Main Chamber LOX Valve Position	Input Output Unit	Recorder	(Voltage TBD) Digital	TBD	--	--	12	1 [illegible]
Safe Room	Inducer Turbine Valve Position	Input Output Unit	Recorder	(Voltage TBD) Digital	TBD	--	--	12	1 [illegible]
Safe Room	Fuel Valve Trim Mag.	Input Output Unit	Recorder	(Voltage TBD) Digital	TBD	--	--	12	1 [illegible]
Safe Room	Main Chamber LOX Valve Trim Mag.	Input Output Unit	Recorder	(Voltage TBD) Digital	TBD	--	--	12	1 [illegible]
Safe Room	Inducer Turbine Valve Trim Mag.	Input Output Unit	Recorder	(Voltage TBD) Digital	TBD	--	--	12	1 [illegible]
Safe Room	Fuel Pump Speed Error	Input/Output Unit	Recorder	(Voltage TBD) Digital	TBD	--	--	12	1 [illegible]
Safe Room	Fuel Pump Cavitation Margin	Input/Output Unit	Recorder	(Voltage TBD) Digital	TBD	--	--	12	1 [illegible]
Safe Room	Lox Pump Cavitation Margin	Input Output Unit	Recorder	(Voltage TBD) Digital	TBD	--	--	12	1 [illegible]
Safe Room	Unsatisfied Thrust Cmd Margin	Input/Output Unit	Recorder	(Voltage TBD) Digital	TBD	--	--	12	1 [illegible]
Safe Room	Unsatisfied Mixture Ratio Cmd Margin	Input/Output Unit	Recorder	(Voltage TBD) Digital	TBD	--	--	12	1 [illegible]
Safe Room	Fuel Pump Overspeed Margin	Input/Output Unit	Recorder	(Voltage TBD) Digital	TBD	--	--	12	1 [illegible]
Safe Room	LOX Pump Overspeed Margin	Input Output Unit	Recorder	(Voltage TBD) Digital	TBD	--	--	12	1 [illegible]
Safe Room	Preburner Temp	Input/Output Unit	Recorder	(Voltage TBD) Digital	TBD	--	--	12	1 [illegible]
Safe Room	Cooling Margin	Input Output Unit	Recorder	(Voltage TBD) Digital	TBD	--	--	12	1 [illegible]
Safe Room	Preburner LOX Valve Trim Mag.	Input Output Unit	Recorder	(Voltage TBD) Digital	TBD	--	--	12	1 [illegible]
Engine Test Stand	Main LOX Turbopump Speed	Capacitive Pick-up Sensor	Input/Output Unit	(0 vdc - 5 vdc) Pulse	6,000 30,000 rpm	10 rpm	5 rpm	12	1 [illegible]
Engine Test Stand	LOX LSI Speed	Capacitive Pick-up Sensor	Input Output Unit	(0 vdc - 5 vdc) Pulse	1,800 5,800 rpm	10 rpm	5 rpm	12	1 [illegible]
Engine Test Stand	Fuel LSI Speed	Capacitive Pick-up Sensor	Input Output Unit	(0 vdc - 5 vdc) Pulse	5,000 24,000 rpm	10 rpm	5 rpm	12	1 [illegible]
Engine Test Stand	Main Fuel Turbopump Speed	Capacitive Pick-up Sensor	Input/Output Unit	(0 vdc - 5 vdc) Pulse	10,000 48,000 rpm	10 rpm	5 rpm	12	1 [illegible]
Engine Test Stand	Main Pump Inlet LOX Temp	Resistance Probe Sensor	Input/Output Unit	(0 vdc - 10 vdc) DC	175-225 R	2 F	0.2 F	12	1 [illegible]
Engine Test Stand	Preburner Temp	Thermocouple Sensor	Input Output Unit	(0 vdc - 10 vdc) DC	1,000 2,400°R	10 F	1 F	12	1 [illegible]
Engine Test Stand	Main Pump Inlet Fuel Temp	Resistance Probe Sensor	Input Output Unit	(0 vdc - 10 vdc) DC	25 - 50°R	1 F	0.1 F	12	1 [illegible]

Table CXIV. Computer Signal Interfaces (Concluded)

Input Output Signals		Signal Source	Signal Destination	Type of Signals	Range	Sensor Accuracy	Conversion Accuracy	Number Of Bits	Resolution Available
Origin	Signal Name								
Engine Test Stand	Transpiration Temp		Input/Output Unit	(0 vdc - 10 vdc) DC	350 - 500°R	±4°F	0.4°F	12	1 40%
Engine Test Stand	Total Engine LOX Flow	Flowmeter	Input/Output Unit	(0 vdc - 10 vdc) DC	91-482 lb sec	1 lb sec	0.1 lb sec	12	1 40%
Engine Test Stand	Total Engine LOX Flow	Flowmeter	Input/Output Unit	(0 vdc - 10 vdc) DC	14-91 lb sec	±.2 lb sec	0.02 lb sec	12	1 40%
Engine Test Stand	ΔP LOX LSI Pressure	Strain Gage Sensor	Input/Output Unit	(0 vdc - 10 vdc) DC	45-270 psia	±4 psia	0.4 psia	12	1 40%
Engine Test Stand	ΔP Fuel LSI Pressure	Strain Gage Sensor	Input/Output Unit	(0 vdc - 10 vdc) DC	20-120 psia	±4 psia	0.4 psia	12	1 40%
Engine Test Stand	Main Chamber Pressure	Strain Gage Sensor	Input/Output Unit	(0 vdc - 10 vdc) DC	400-5,000 psia	±25 psia	2.5 psia	12	1 40%
Engine Test Stand	ΔP Transpiration Pressure	Strain Gage Sensor	Input/Output Unit	(0 vdc - 10 vdc) DC	200-700 psia	±5 psia	0.5 psia	12	1 40%
Engine Test Stand	LOX LSI Exit Pressure	Strain Gage Sensor	Input/Output Unit	(0 vdc - 10 vdc) DC	90-310 psia	±4 psia	0.4 psia	12	1 40%
Engine Test Stand	Fuel LSI Exit Pressure	Strain Gage Sensor	Input/Output Unit	(0 vdc - 10 vdc) DC	85-155 psia	±4 psia	0.4 psia	12	1 40%
Engine Test Stand	Preburner Oxidizer Valve Secondary FB	Servo Amp	Input/Output Unit	(0 vdc - 10 vdc) DC	0-90 deg	TBD		12	1 40%
Engine Test Stand	Preburner Oxidizer Valve Primary FB	Servo Amp	Input/Output Unit	(0 vdc - 10 vdc) DC	0-90 deg	TBD		12	1 40%
Engine Test Stand	Main Chamber Oxidizer Valve FB	Servo Amp	Input/Output Unit	(0 vdc - 10 vdc) DC	0-90 deg	TBD		12	1 40%
Engine Test Stand	Preburner Fuel Valve (Preburner Flow) FB	Servo Amp	Input/Output Unit	(0 vdc - 10 vdc) DC	0-90 deg	TBD		12	1 40%
Safe Room	Preburner Oxidizer Valve Secondary Cmd	Input/Output Unit	Servo Amp	(0 vdc - 10 vdc) DC	0-90 deg	TBD	TBD	12	1 40%
Safe Room	Preburner Oxidizer Valve Primary Cmd	Input/Output Unit	Servo Amp	(0 vdc - 10 vdc) DC	0-90 deg	TBD	TBD	12	1 40%
Safe Room	Main Chamber Oxidizer Valve Cmd	Input/Output Unit	Servo Amp	(0 vdc - 10 vdc) DC	0-90 deg	TBD	TBD	12	1 40%
Safe Room	Preburner Fuel Valve (Preburner Flow) Cmd	Input/Output Unit	Servo Amp	(0 vdc - 10 vdc) DC	0-90 deg	TBD	TBD	12	1 40%
Safe Room	Preburner Fuel Valve	Input/Output Unit	Solenoid	(0 vdc - 5 vdc) Digital	On-Off	--	--	1	--
Safe Room	Nozzle Coolant Valve	Input/Output Unit	Solenoid	(0 vdc - 5 vdc) Digital	On-Off	--	--	1	--
Safe Room	Turbopump Lift-Off Seals	Input/Output Unit	Solenoid	(0 vdc - 5 vdc) Digital	On-Off	--	--	1	--
Safe Room	Preburner Secondary Purge	Input/Output Unit	Solenoid	(0 vdc - 5 vdc) Digital	On-Off	--	--	1	--
Safe Room	Main Burner LOX Injector Purge	Input/Output Unit	Solenoid	(0 vdc - 5 vdc) Digital	On-Off	--	--	1	--
Safe Room	Preburner Primary Purge	Input/Output Unit	Solenoid	(0 vdc - 5 vdc) Digital	On-Off	--	--	1	--

C. Input Interface

1. Multiplexer
2. A/D Converter
3. Speed Circuits
4. Failure Input Circuits

10. Power Estimate for I/O Section

Multiplexer	0.40
A/D Converter	1.50
Reference Supply (I/O + Sensors)	4.00
Speed Circuits	3.00
4 D/A Converters	2.40
11 Solenoid Drivers	2.20
4 Servo Amplifiers	8.00
Logic Gating	3.60
5 Volt Power Supply	7.00
Misc. Power Supplies	6.00
	38.10 Watts

11. Accuracy Estimate of I/O Section

Multiplexer	±.012%
A/D Converter	±.034%
D/A Converter	±.025%
	±.071%

(Approx. = ±3 LSB)

C. INPUT INTERFACE

The input subsystem contains the following components:

1. ANALOG MULTIPLEXER
2. ANALOG TO DIGITAL CONVERTER
3. SPEED MEASUREMENT CIRCUITS
4. SENSOR FAILURE INPUT CIRCUITS

The analog multiplexer (J-FET Switches) will accept various pre-conditioned sensor signals and actuator feedback signals and multiplex them in accordance with central computer control signals utilizing I/O control gating logic. The output of the multiplexer is then converted to 12 bit digital words by means of an A/D converter (successive-approximation type). These digital words are then processed by the CPU in accordance with a predetermined program. Both the fixed time interval and variable time interval measurement methods are discussed and compared. The variable time interval approach is selected and applied to the measurement of the four pump speeds. In addition, monitoring circuits are provided and described for the two redundant speed sensors, and a test program to detect speed input circuit failures is presented.

A logic implementation is shown and described, which orders the sensor failure data into a form acceptable to the computer.

1. Multiplexer

In order to process the various input sensor signals by a single A/D converter, a multiplexer will be required in the I/O Section. The basic theory of analog multiplexing is relatively simple. A multiplexer merely accepts several signal sources and switches them sequentially, or as required, to a single output line. Thus, an analog multiplexer performs the same function as a rotary switch in which the wiper arm is rotated electrically instead of mechanically. However, a solid-state multiplexer can switch channels much faster than its mechanical counterpart. In this application, the sampling frequency will be 10 to 50 times the signal bandwidth so that any sampling rate errors will be insignificant and can be neglected.

Switching of the input data may be accomplished by bipolar transistors, diode transmission gates, junction field-effect transistors (J-FET's) or metal oxide semiconductor devices (MOSFET's).

Bipolar transistors and diode gates have several shortcomings as multiplexer switches. They exhibit a built-in offset voltage between the data input and the output line and require relatively elaborate schemes to drive them. They do, however, have the advantage of high speed and low on resistance.

The J-FET switch has moderate speed and a low ON resistance and, unlike transistor and diode switches, has zero offset voltage. At present, J-FET's do not lend themselves to monolithic integration that would facilitate the construction of integrated multiplexers. However, hybrid circuits are available with built-in driving circuitry.

The MOSFET switch has the same basic advantages as the J-FET switch and furthermore can be readily integrated with its associated drive circuitry. However, these switches have a higher ON resistance than J-FET's and suffer from temperature sensitivity.

The major requirements for the multiplexer in this application are; low ON resistance, zero offset voltage, temperature stability, and moderate speed. Based upon these considerations, the recommended type of multiplexer is the hybrid J-FET device. A typical J-FET multiplexer is illustrated in figure 1149.

2. A/D Converter

An analysis of the various sensor input signals (temperature, pressure, and flowmeter) indicates that the maximum sensor accuracy required will be about 1 part in 400 (8 bits). In order to allow for conversion and interface in accuracies the A/D converter should have a 12 bit resolution (1 part in 4096). Although several methods exist for A/D conversion, the two most practical approaches that have been considered for this application are the successive approximation type and the multichannel ramp-comparison type. Important features of both types are shown in table CXV. The recommended type is the successive-approximation type (figure 1150 since it has a faster data access time and requires less hardware. Basically, the successive approximation A/D Converter compares the input analog voltage to a series of digitally

generated voltages. The generated voltages are made to converge on the input voltage until the two are equal. Then, the binary number representing the generated voltage is read out of the converter.

3. Speed Circuits

To provide a maximum number of samples, the speed inputs will be measured continuously. This feature is particularly important for low speeds, which consume the most time for each measurement. At 1800 RPM each revolution and measurement requires 33-1/3 milliseconds, and 30 measurements per second are possible.

The circuits for each input will be designed for a specific speed range. However, the speed input may lie outside this range. This condition may arise during engine start-up or shutdown, and from engine, sensor or circuit failures. The computer program can detect such occurrences.

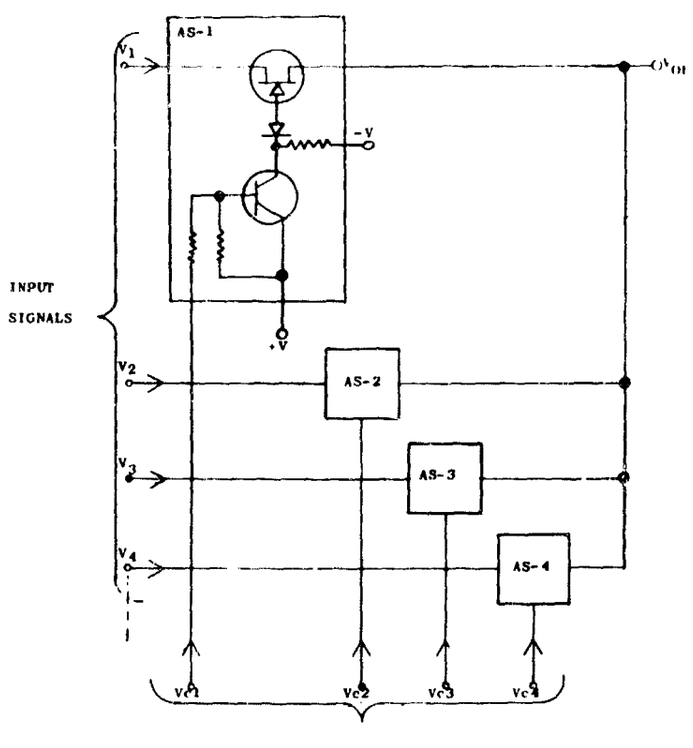

Figure 1149. J-FET Multiplexer

Table CXV. Comparison of A/D Converters

SUCCESSIVE APPROXIMATION TYPE	
Advantages	**Disadvantages**
1. Fast Conversion (40 ms)	1. Temp. stable components requir as in all A/D Conv
2. High Accuracy	
3. Less Hardware	
4. High MTBF	

MULTICHANNEL RAMP COMPARISON	
Advantages	**Disadvantages**
1. Simplifies median selection	1. Excessive Hardware
2. High Accuracy	2. Updating lag time is 4 ms
	3. Lower MTBF

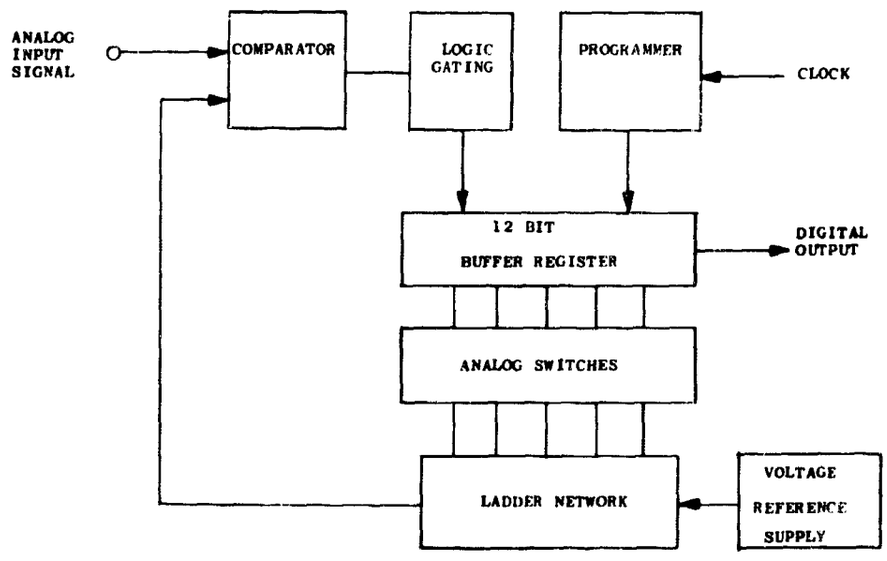

Figure 1150. Preferred A/D Converter, Successive Approximation Type

a. Fixed Time Interval Measurement Method

The general equation for average speed is $s = \frac{\Delta D}{\Delta T}$, where ΔD is the distance traveled and ΔT is the time required to move this distance. The fixed time interval measurement method is based upon holding ΔT at a fixed value and measuring ΔD to determine the speed. For pump speed, ΔD is measured by counting the pulses generated by the pump blades, and ΔT appears as a specific number of clock pulses from a fixed frequency oscillator. A block diagram for the fixed time interval method is presented in figure 1151.

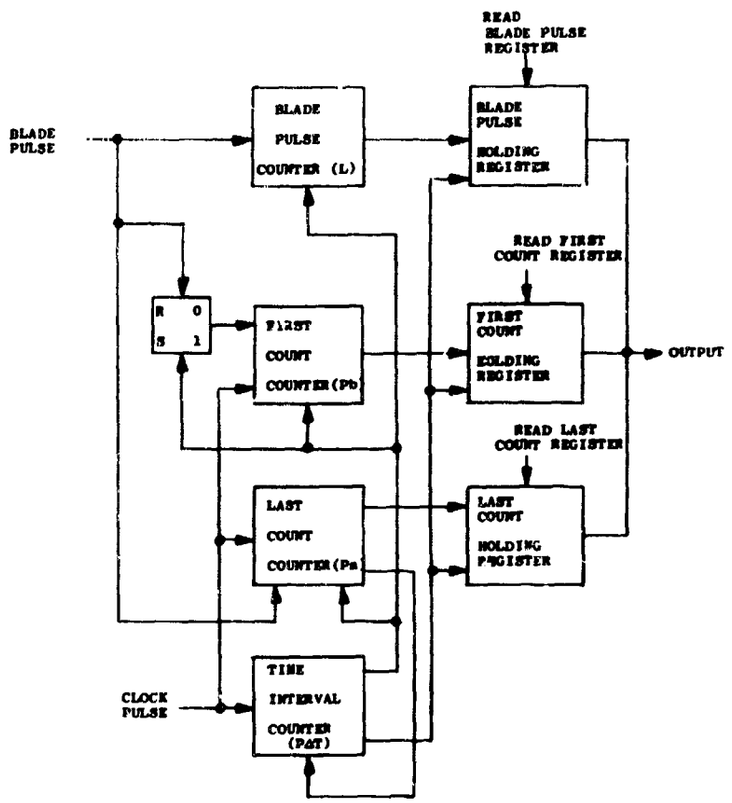

Figure 1151. Fixed Time Interval Block Diagram

b. Variable Time Interval Measurement Method

Returning to the general equation for average speed, $S = \frac{\Delta D}{\Delta T}$, the variable time interval measurement method holds ΔD at a fixed value and measures ΔT to determine the speed. Figures 1152 and 1153 show the variable time interval method.

c. Comparison

(1) Fixed Time Interval Features

The fixed time interval approach features uniform timing, which is independent of speed, for each measurement, and exhibits a constant

resolution (1/10,000), independent of the speed, which depends upon the time interval and clock frequency. However, three counters and holding registers, with control circuitry, are required for each speed range, and three program instructions are needed to input the data for each speed range. Also, the solution rate begins to fall below the 100 solutions per second baseline for speeds less than 10,000 RPM (assuming a measurement based upon 1 RPM minimum).

(2) Variable Time Interval Features

The variable time interval approach features a sele. able resolution, which has been chosen as 12 bits minimum (1 part in 4096). However, at high speeds, a clock frequency holding register, with control circuitry, is required for each speed range, and a single program instruction is needed to input the data for each speed range. Also, the solution rate does not fall below the 100 solutions per second baseline until the speed is less than 6,000 RPM (assuming a measurement based upon 1 RPM minimum).

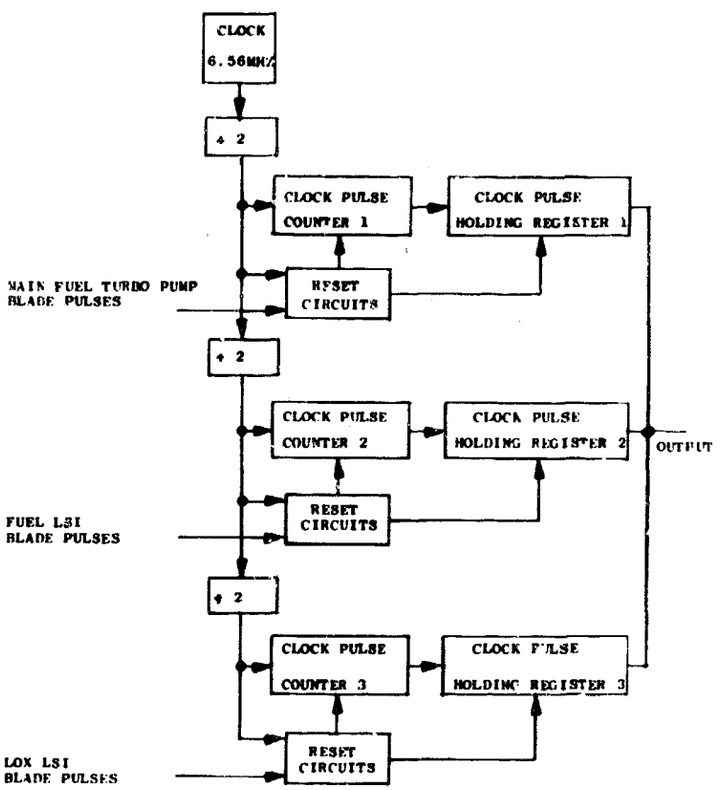

Figure 1152. Variable Time Interval Block Diagram, Part A

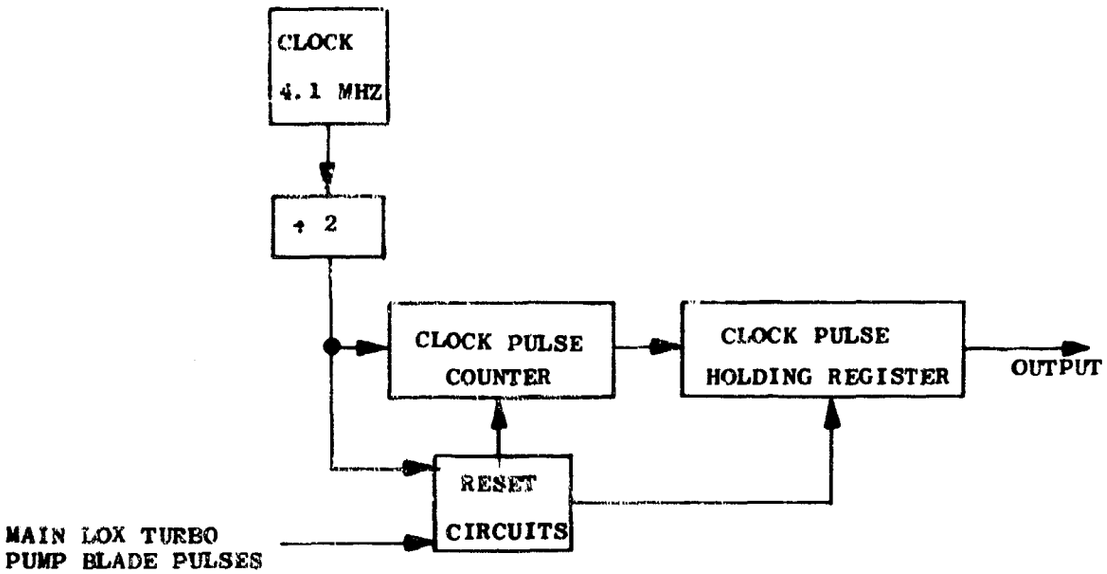

Figure 1153. Variable Time Interval Block Diagram, Part B

(3) Selection

Comparison of the two . proaches indicates that the variable time interval technique is smaller, lighter and less costly to implement with hardware, and requires fewer program instructions to input data. Also, higher solution rates are possible for low speeds with this approach. This technique employs a higher operating speed (3.28 MHz versus 1 MHz) than the fixed time interval measurement method, but this increase does not appear to be significant. Consequently, the variable time interval measurement method will be applied to all the speed inputs.

d. Fault Detection

The fault detection task is divided into two areas -- sensor fault detection and circuit fault detection. The sensor fault detection plan employs constant sensor monitoring. When a sensor malfunction is observed, this information is sent to the computer, which uses this data to select the good sensor (if one exists) as a source of blade pulses. The computer will also be able to clear a sensor fault either when the system begins operation or later if desired, provided the sensor is operable. Of course, the monitoring and measurement circuits may also fail. The detection of these faults depends upon the computer test program, which is executed periodically. This program will involve blocking the sensor inputs, inserting simulated sensor faults into the sensor monitoring circuits, and observing the monitor circuits' outputs. In addition, if these circuits pass these tests, a simulated sensor signal will be inserted, and the measuring circuits will process this input. The computer may then observe the measuring circuits' output, and determine the validity of the measurement circuits.

Figure 1154 shows the sensor fault detection and selection circuits for dual redundant speed sensors. This configuration would be used for each speed input. The circuits for each sensor are identical. Three types of faults are detected:

1. Input Frequency High
2. Constant Low Level
3. Constant High Level
4. Failure Input Circuits

The failure input circuits collects the sensor failure signals to be sent to the computer. Since there are some 30 failure signals and only 16 I/O lines to the computer, the input signals must be divided into two groups, and each group will be sent to the computer separately. The computer will first select a group, and then input the group data.

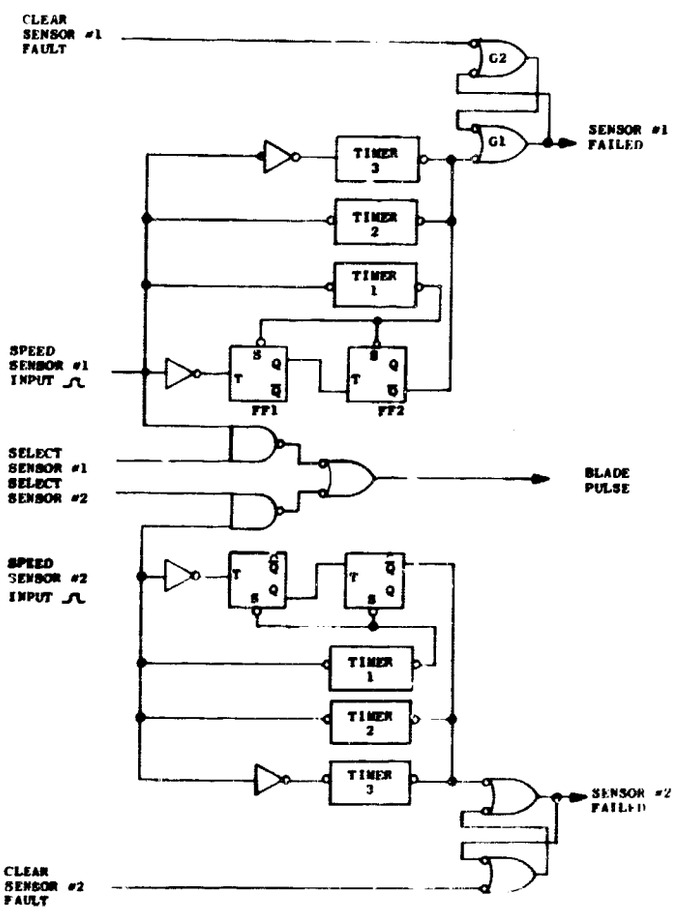

Figure 1154. Sensor Fault Detection and Selection

D. OUTPUT INTERFACE

The output subsystem is composed of the following elements:

1. Digital to Analog Converters
2. Servo Amplifiers
3. Solenoid Drivers

The output of the CPU is addressed to one of the four D/A converters (parallel resistor ladder type) which provides a DC analog signal to one of four actuator servos (brushless DC torquer type). The implementation and characteristics of two solenoid driver circuits are presented and discussed. The first circuit requires the most hardware, but minimizes power consumption. The alternate driver is simplest and costs the least, but the power requirement increases. The two alternate output interfacing schemes that have been considered for this application are depicted in figures 1155 and 1156.

1. Recommended Output Section

The recommended scheme, figure 1155, utilizes a digital demultiplexer and four D/A converters which, in turn, provide the analog signals for the four actuator servos. Each D/A converter consists of a buffer register, analog switches, and a ladder network which can all be obtained in convenient microcircuit packages.

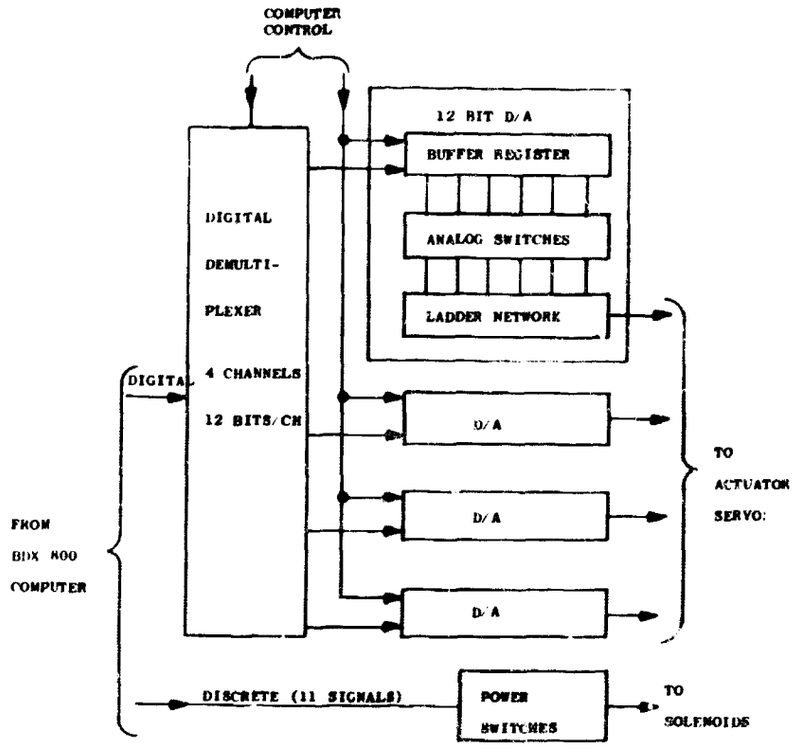

Figure 1155. Recommended Output Section

The major advantages of this approach are the higher accuracy obtainable (±1 LSB error for 12 bits), faster settling time and therefore, faster conversion, and better temperature stability. It should be noted that the function of the demultiplexer can be incorporated into the buffer register of each D/A converter by utilizing clocked D type flip-flops (e.g., SN5474).

2. Alternate Output Section

An alternate scheme, figure 1156, utilizes one D/A converter which feeds an analog demultiplexer which, in turn, feeds four analog sample and hold circuits. The sample and hold circuit consists of two precision analog switches, a precision RC circuit, and a buffer operational amplifier.

Although a sample and hold circuit may appear to have some advantages over a D/A converter in terms of hardware, there are several disadvantages to this approach. Due to the additional analog circuitry the accuracy is reduced (±2 LSB error for 12 bits). In addition, the RC circuit in the sample and hold section is temperature sensitive and a longer settling time is required.

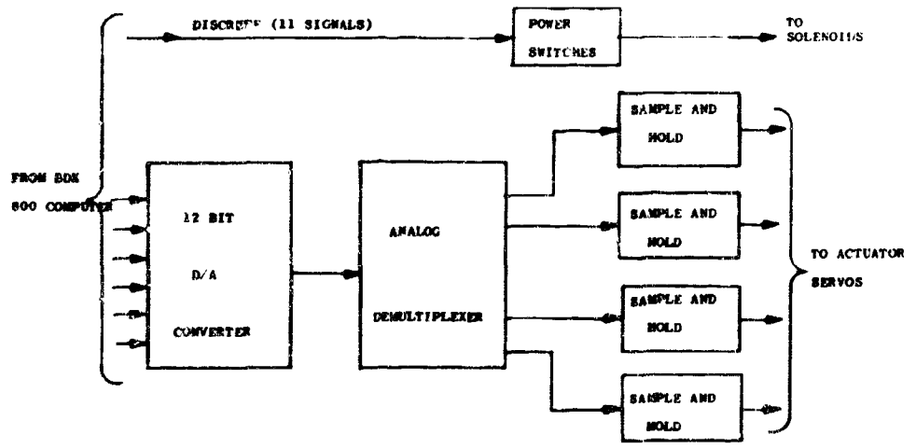

Figure 1156. Alternate Output Section

3. Actuator Servos

The servos controlling the actuator valves will utilize DC torque motors. torque motors. The major advantages of these servos are the elimination of gear trains, a wide servo bandwidth, and low power dissipation at null.

The simplicity of the brushless DC torquer motor depends upon the high energy permanent magnet rotor, which has either two or four poles, depending on the desired rotation angle. The rotor turns within a toroidal coil assembly of copper wire wound around an iron ring and encapsulated in tough plastic. Such motors produce smooth, step-free torque because commutators and brushes have been eliminated. Since there is no electrical or mechanical contact between the rotor and stator, radio noise and mechanical wear are also eliminated. Power is consumed only when torque is delivered which results in high electrical efficiency.

The electronic circuitry for controlling a DC servo utilizes microcircuits and miniature components throughout, which results in a small packaging size. In addition, it possesses high efficiency and minimized heat generation.

4. Solenoid Drivers

a. Pull-Hold Solenoid Drive Circuit

A quantity of eleven solenoids are actuated by the computer. Figure 1157 shows one possible drive circuit. The main feature of this circuit is its ability to supply a hold current to the solenoid, which is different from the pull-in current drawn by the solenoid. This circuit has been designed to produce the required pull-in and holding circuits to the solenoids under digital control. Typical pull-in currents are 0.5 amperes and holding currents are 0.2 amperes. For different solenoid requirements, suitable changes in the circuit design can be made.

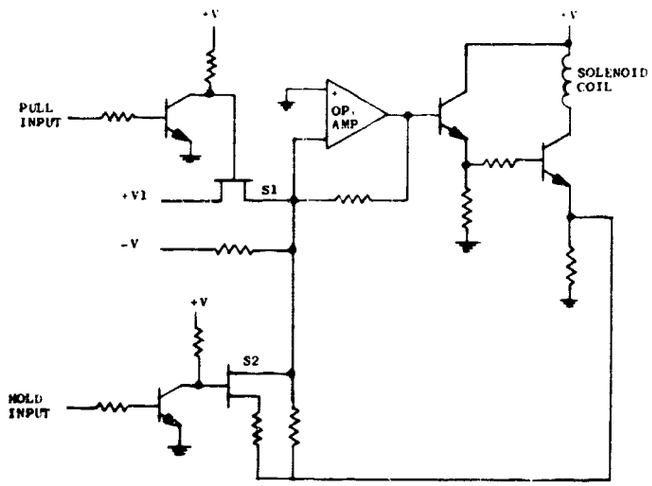

	S1	S2
PULL	OFF	OFF
HOLD	OFF	ON
OFF	ON	DON'T CARE

Figure 1157. Pull-Hold Solenoid Drive Circuit

b. Solenoid Driver

Figure 1157 shows an alternate driver circuit design. The solenoid coil is energized or de-energized by the digital input signal. A high input signal activates the solenoid, and a low input signal keeps the solenoid inactive. The driver will handle a typical drive current of 0.5 amperes. If other current ratings are desired, the circuit can be modified accordingly.

c. Conclusions

The pull-hold drive circuit conserves system power, which can be an important asset for this application. The solenoid driver of figure 1158 wastes power, but is simple and inexpensive. Either circuit can be used. However, until the additional cost of the pull-hold drive circuit is justified, the solenoid driver of figure 1158 will be used for this application.

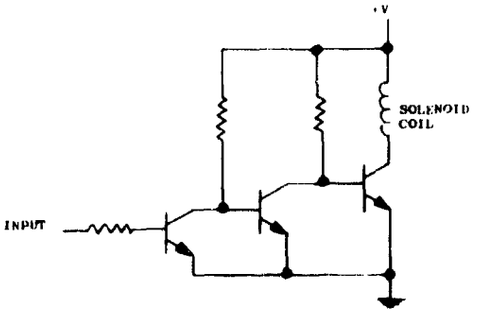

Figure 1158. Solenoid Driver

E. COMPUTER INTERFACE

Communications between the CPU and the Input/Output subsystem are based upon a cooperative action-reaction principle. The CPU input/output instruction initiates an input/output action with certain control signals, and waits for a reaction from the designated input/output unit through various return control signals. The CPU compensates for all signal transmission delays. The decoding and sequencing logic performing the acceptance, control and transmittal of signals from and to the CPU is called the unit controller. These controllers execute the format transformations and operation sequencing required at this interface. Figure 1159 illustrates the general form of the computer interface.

1. Controller Organization

Figure 1160 shows the individual lines, which carry signals between the CPU and each input/output controller. The I/O bus is a 16-bit bi-directional bus reserved for address and data information. At power turn-on the system clear line delivers a signal to the input/output subsystem, which causes all the memory elements to reset to states suitable for starting input/output subsystem operation. The computer clock (uninhibited) line transmits an uninterrupted pulse train, originated by the CPU clock, to the input/output subsystem. The clock timing is determined by the CPU memory speed limit, which presently is one megahertz. The remaining lines are for control purposes.

2. Applications

a. A/D Converter Controller

The A/D converter to computer interface, via the A/D converter controller, is shown in figure 1161. In order to convert analog data to digital form and transfer this information into the CPU, the program is required to specify the channel to be converted, issue a start conversion command, and input the converted data.

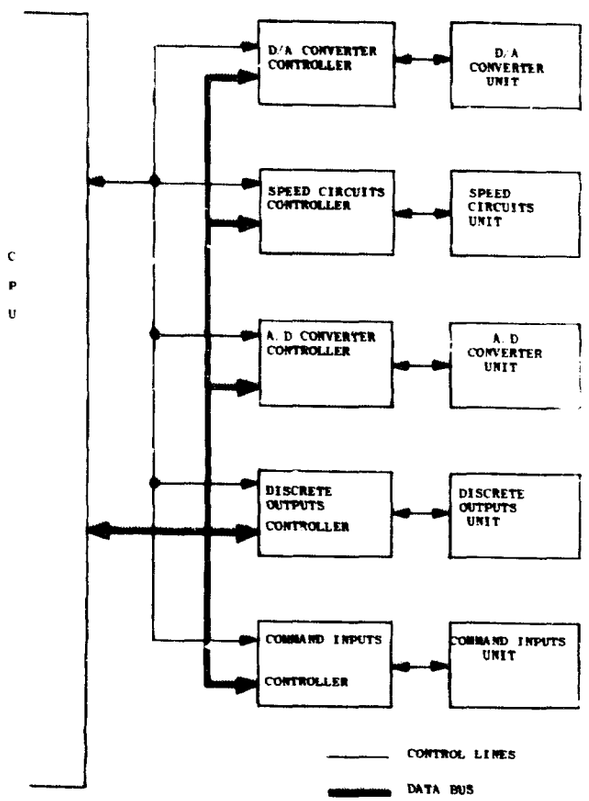

Figure 1159. Computer Interface Block Diagram

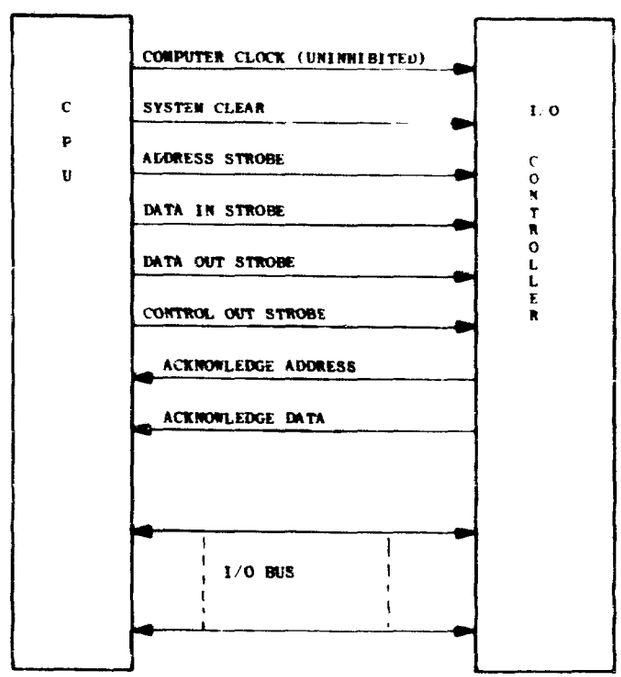

Figure 1160. Signals Between the CPU and Each Controller

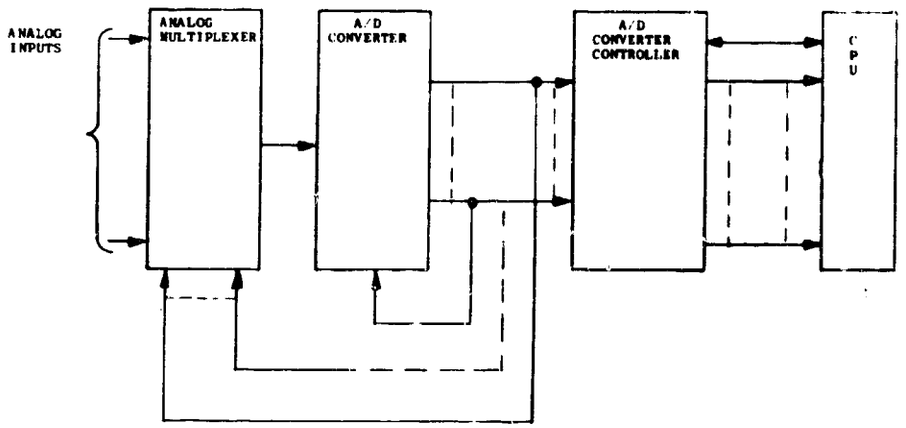

Figure 1161. A/D Converter to Computer Interface

b. Speed Input Controller

The speed inputs to computer interface, via speed input controllers, is shown in figure 1162. One controller is provided for each speed input, and only a single program instruction is needed to obtain data from a controller. Since speed measurement is a continuous operation with periodic updatings of the device data, the CPU may request data during an updating. Consequently, an input data and skip instruction is required. The test instruction is used to supply control signals during the computer controlled system test.

c. D/A Converter Controller

The computer to D/A converter interfaces, via D/A converter contollers, are shown in figure 1163. One controller is provided for each D/A converter, and only a single program instruction is needed to supply data to a controller.

d. Discrete Output Controller

The computer to discrete output interface, via the discrete output controller, is shown in figure 1164. One controller is provided for the discrete outputs, and only one program instruction is needed to supply data to the controller.

e. Ship Central Computer Controller

The CPU will receive thrust level and mixture ratio data, and prestart, start and shutdown commands from the ship central computer. One program instruction will cause data transfer from the controller to the CPU. In addition, the CPU must output data to the ship central computer, which judges the validity of the CPU's performance by monitoring specific data. One program instruction will cause data to transfer from the CPU to the controller.

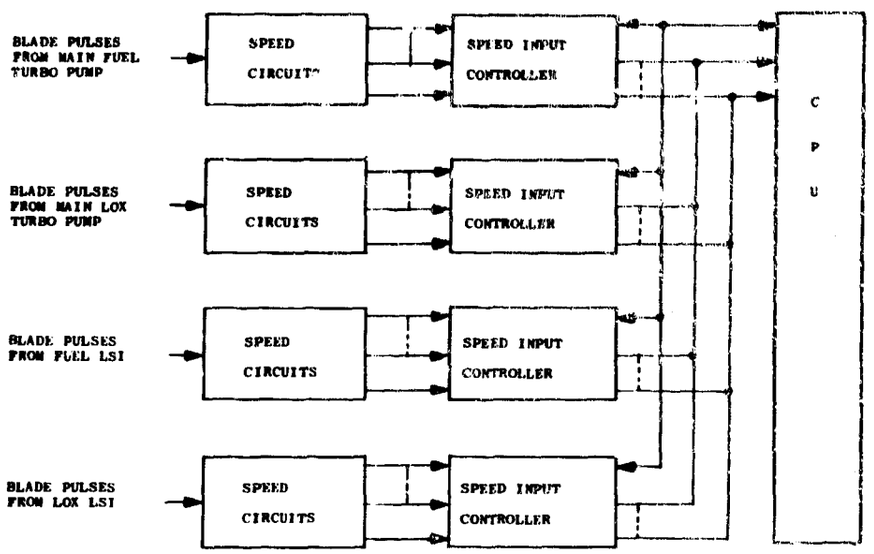

Figure 1162. Speed Inputs to Computer Interface

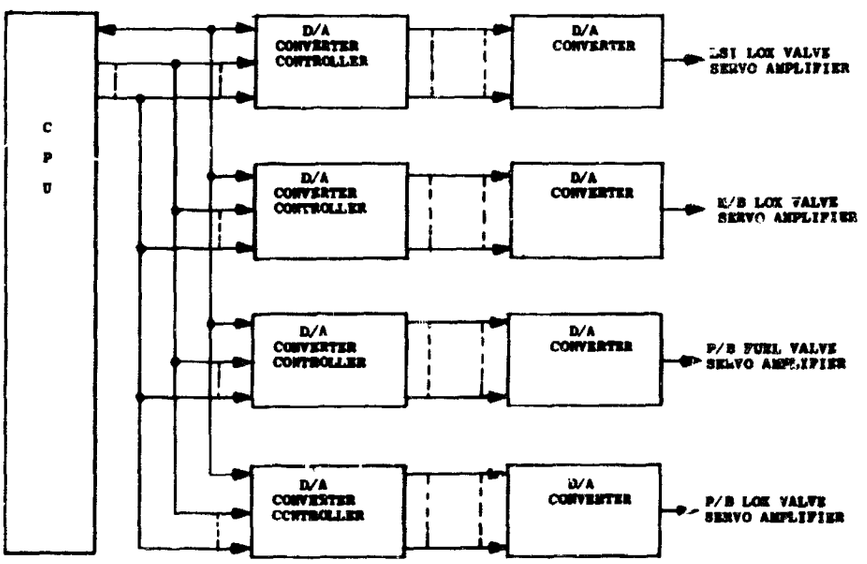

Figure 1163. Computer to D/A Converter Interface

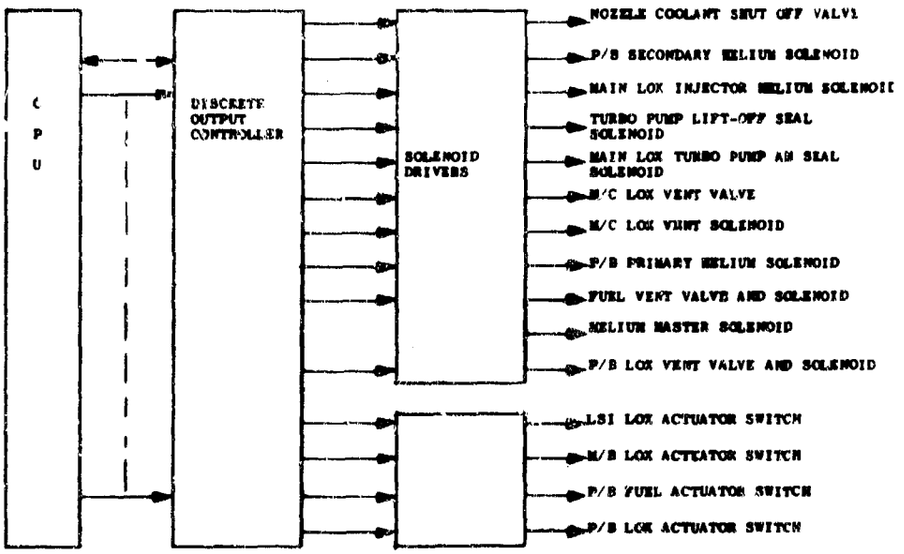

Figure 1164. Computer to Discrete Output Interface

f. Failure Input Controller

The failure input to computer interface, via the failure input controller, is shown in figure 1165. Since there are approximately 30 failure inputs and only 16 I/O bus lines, the failure inputs are divided into groups. Consequently, two program commands are required to transfer data from the controller to the CPU.

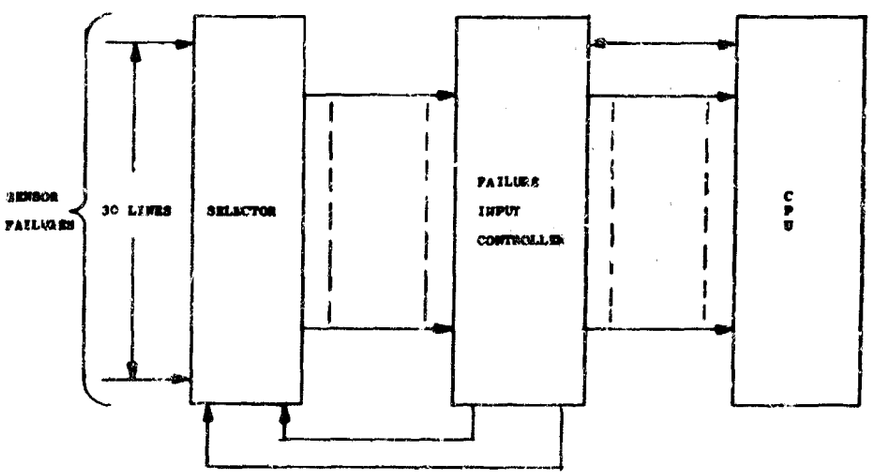

Figure 1165. Failure Inputs to Computer Interface

F. CENTRAL PROCESSING UNIT

1. General Organization of BDX 800

The BDX 800 digital computer consists of the basic units shown in figure 1166. A brief functional description of the various units depicted in the diagram is presented in the following paragraphs:

a. Central Processor Unit (CPU)

The central processor unit of the BDX 800 is a programmable digital processor which executes sequences of instructions stored in memory. The CPU performs arithmetic and logical operations on data; it decides what and how operations are to be performed, where the necessary information is to be obtained, and where the results are to be stored.

b. Memory

The memory unit provides storage capabilities for both instructions and data. The storage requirements will be met with a 8192 word Metal Oxide Semiconductor memory, and these words are each 16 bits in length. The DRO Core Memory will permit computer program modifications and changes in system constants to be made rapidly and conveniently via software during the development phase of the program. Production units will use a MOS read only memory to provide the program, and a MOS random access memory to store data and command information. Each storage location has a unique address used to specify that location. The memory unit interfaces with the CPU via 2 buses: a data bus and an address bus. The 16-bit bi-directional data bus is used for the transmission of a data word to and from the memory unit, while the 16-bit unidirectional address bus is used for selecting a unique location in memory.

c. Input/Output (I/O)

The input/output unit provides the means of transferring information between the CPU and the I/O devices. The I/O section of the BDX 800 provides the required conditioning, multiplexing, and conversion of analog input signals to digital form; and the conversion of digital output signals to analog form. It accommodates the reading, in and out, of discrete signals, and monitoring and speed circuit data. This section also provides the indicators, masks, priority logic, and address encoding for the interrupts.

2. Central Processor

The BDX 800 CPU is a 16-bit, parallel, general purpose processor designed for aerospace application. The salient features of the computer are summarized briefly below:

Type:	General purpose, full parallel organization, single address
Arithmetic:	Binary, fixed point, negative numbers in 2's complement form 16-bit data word

Operation Registers:	A register - most significant half of accumulator - 16 bits
	Q register - least significant half of accumulator - 16 bits
	X register - Index register
	P register - Program counter
	Status Register - 3 bit condition register 5 bit N register
Instruction Repertoire:	Arithmetic: add, subtract, multiply, divide, load, store, shifts, rotations, and normalize.
	Jumps: unconditional jump, variable skips, 2 subroutine jumps.
	Logical: And
	I/O: Input, Output, Output Control
Miscellaneous:	Clock Rate: 1 MHz
	Logic: T^2L Microcircuits

Instruction Execution Time:	
Add	- 4 usec
Subtract	- 4 usec
Multiply	- 19 usec
Divide	- 19 usec
Load Memory	- 4 usec
Store	- 4 usec
Compare	- 4 usec
And	- 4 usec
Unconditional Jump	- 4 usec

3. Interrupts

A priority interrupt system is incorporated within the BDX 800 central processor, allowing the computer program to be interrupted to service conditions in both the central processor and I/O section. The BDX 800 has 16 computer program interrupts. Four of these interrupts, called internal interrupts, are generated internal to the control processor, and are controlled completely by the CPU. The remaining 12 interrupts, called external interrupts, are generated externally to the CPU, and are under control of the interrupt controller in the I/O section.

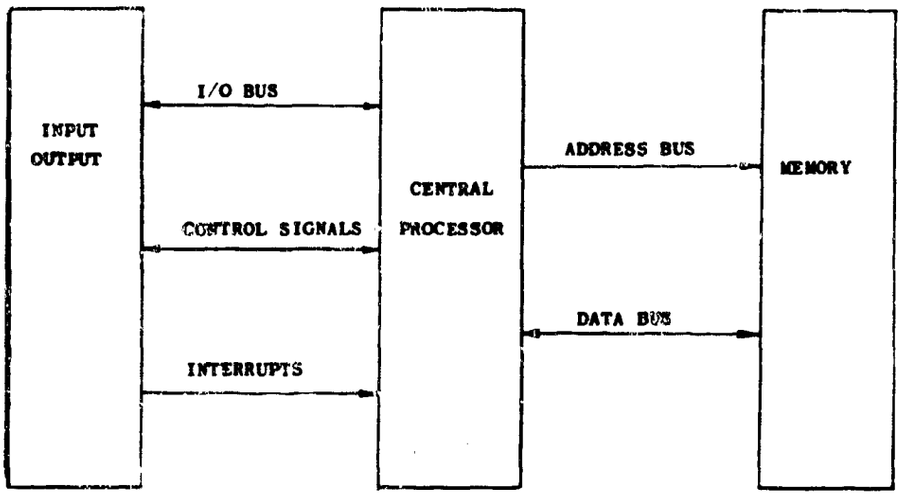

Figure 1166. BDX 800 Computer Organization

4. Input/Output Communication

To properly implement the I/O instructions, the I/O devices must respond to certain signals from the CPU, and conversely, the CPU must react to signals from these devices. The design of the BDX 800 is such that the central processor waits for acknowledgement from the I/O unit of the receipt of all signals from the CPU. The logic associated with each I/O device to accept, control, and transmit signals from and to the CPU in order to properly control the device is referred to as the device controller. The BDX 800 CPU interfaces with the I/O unit through the device controllers; it is these controllers that must obey certain formatting and sequencing rules in order to function properly with respect to the processor.

The data and control lines between the CPU and I/O unit are shown in figure 1167. The basic channel of communication for address and data information between the CPU and I/O is the I/O bus. The I/O bus is a 16-bit bi-directional bus. The System Clear line is used to send a signal from the power supply at power turn-on to enable the I/O to initialize the proper registers and flip-flops. The Oscillator line is used to supply a continuous oscillator signal by the I/O to the CPU for general timing purposes, allowing asynchronous operation of the I/O and CPU.

The BDX 800 CPU communicates with the following I/O devices:

1. A/D Converter
2. Speed Input Circuits
3. D/A Converter
4. Discrete Outputs

5. Ship Central Computer

6. Sensor Failure Circuits

In addition, it is capable of exchanging information with the following peripheral equipment:

1. Teletype

2. Tape Reader

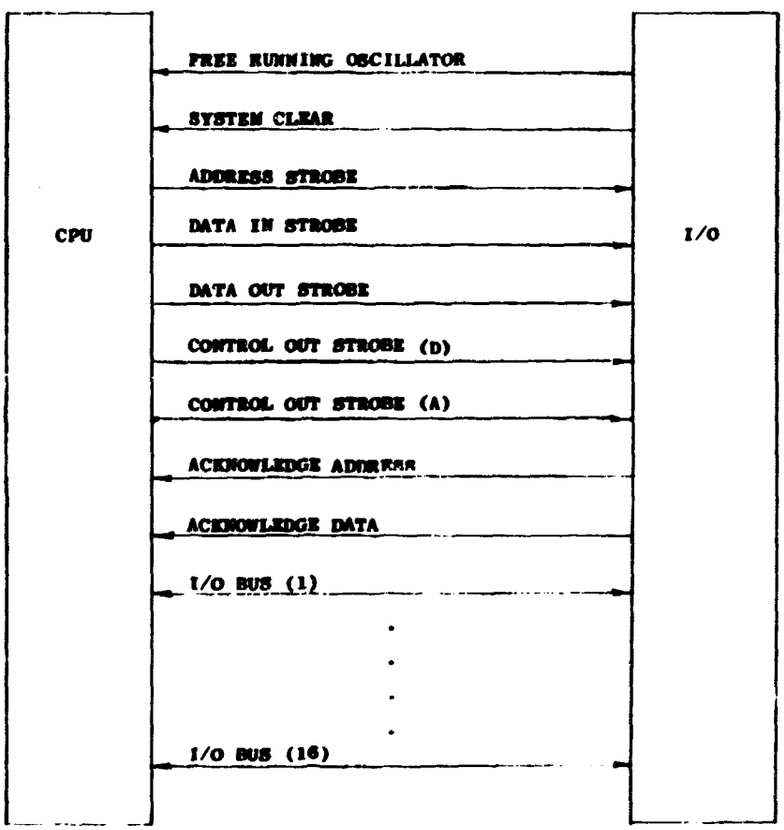

Figure 1167. CPU-I/O Interface Lines

5. Peripheral Equipment

The BDX 800 is capable of communicating with the following peripheral equipment: teletype and tape reader. These units are not part of the XLR-129 operating system.

a. Teletype

The CPU communication with the teletype is through the teletype controller. The function of the teletype controller is to provide translation of the BDX 800

G. Block Diagram Discussion

1. General
2. Scaling
3. Self-Test and Monitoring
4. Min/Max Limits Subroutine
5. Computer Self-Test Routines
6. Conclusions

I/O interface signals to a set of signals suitable for communication with a conventional teletype machine which, typically, consists of a keyboard, a printer, a paper tape reader, and a paper tape punch. The controller is designed to interface with any teletype machine having the standard teletype interface consisting of one serial input terminal and one serial output terminal transmitting (or receiving) 8 bit words (7 bit characters and 1 even parity bit) at a maximum rate of 10 characters per second.

b. Tape Reader

The function of the tape reader controller is to provide a translation of the BDX 800 I/O interface signals to a set of signals usable to control a high speed photoelectric tape reader. The controller is designed to drive a Digitronics Type 2540 reader and Type 4566A spooler, although it is easily adaptable to any tape reader which provides a microcircuit interface.

G. BLOCK DIAGRAM DISCUSSION

1. General

The fuel control program for the XLR129 rocket engine was designed, using the block diagram shown in figure 1168. Figure 1168 reflects all design changes made in the system, particularly in the Schedule Selection and Control Rate Logic. These changes were adapted for efficient memory and computation time utilization, and, in the case of the Schedule Selection and Control Rate Logic, ensure that the engine is either in start-up mode, shut-down mode, or gross control mode. The computer is programmed for each of these modes as required rather than for all of them simultaneously as proposed originally. This results in a more efficient use of the computation cycle time.

2. Scaling

The modification of input data for acceptance by the digital computer is accomplished by appropriate scaling of that data. Scaling is the process of expressing the range of a parameter in terms of available bits in the word corresponding to that parameter.

Scaling is expressed in the following format:

$$(A)' = K_1 A + K_2$$

Where: (A)' is the decimal equivalent of the binary number for the parameter A, expressed in counts; A is the absolute value of the parameter in its particular units, i.e., deg R, RPM, etc.; and K_1 is a parameter expressed in COUNTS/UNIT. K_2 is the parameter offset from binary to zero.

For example, the quantity TLR = PFGR has a range from 0% to 110%. If this is made to correspond to the range in bits from 0 to 32768, then:

$$(TLR)' = \frac{32768}{110} \quad (TLR)$$

$$\sim 297.6 \ (TLR)$$

A

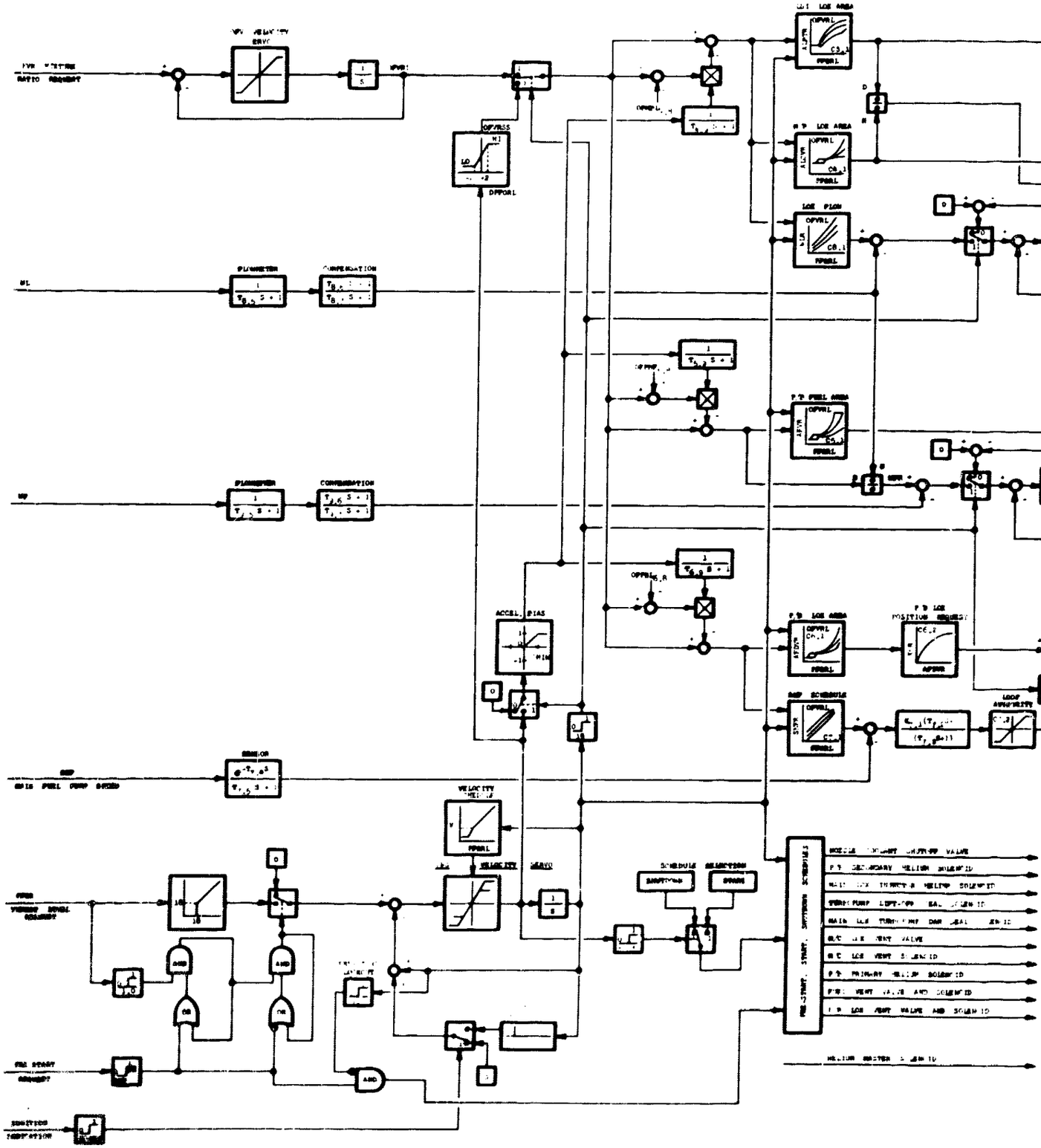

Figure 1168. Control System With Start, Shutdown and Pre-Start Logic

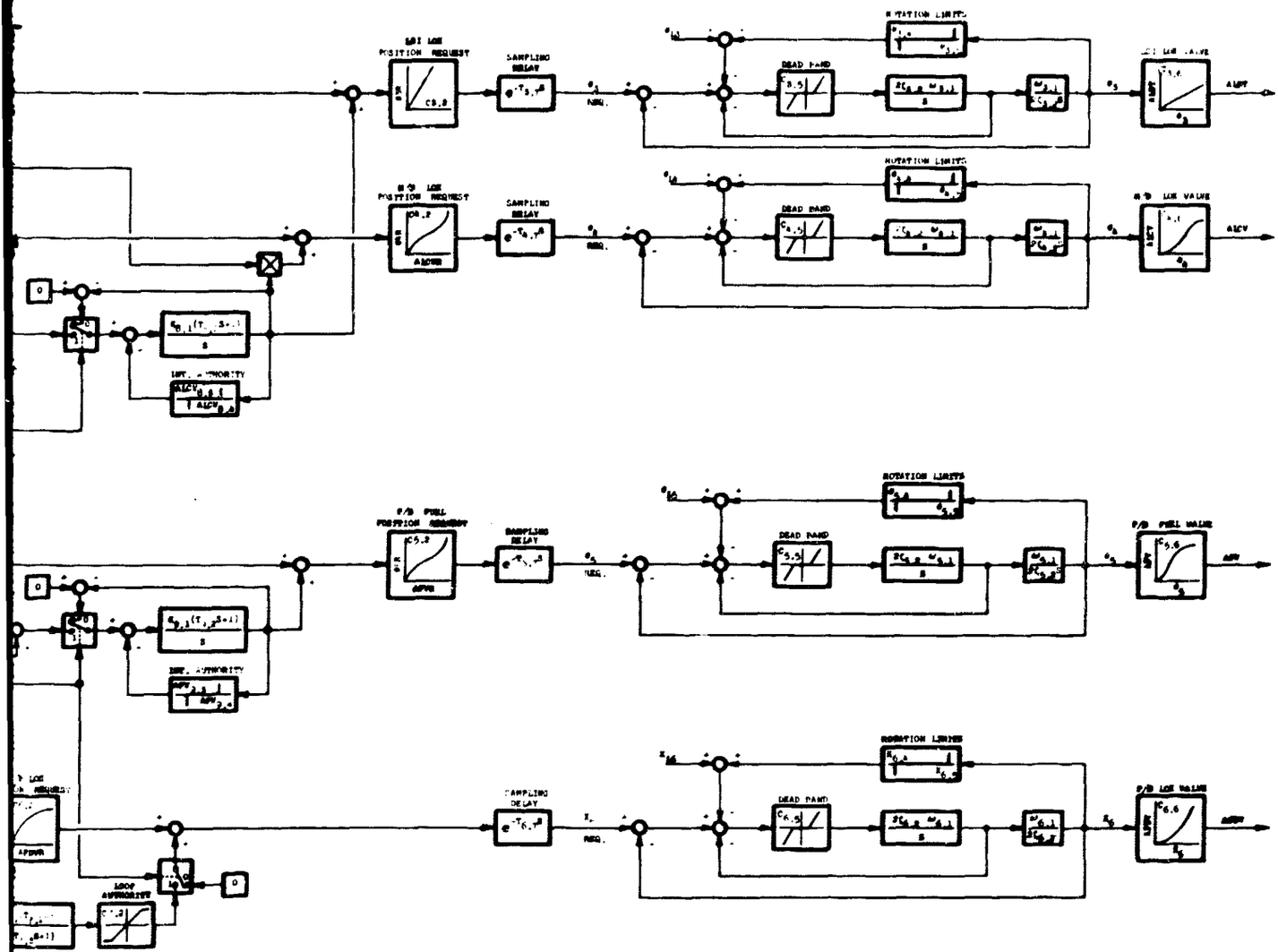
SAMPLING DELAY
DEAD BAND
ROTATION LIMITS
SAMPLING DELAY
DEAD BAND
ROTATION LIMITS
SAMPLING DELAY
DEAD BAND
ROTATION LIMITS

The scaling factor has been reduced slightly to avoid the effects of noise at saturation values.

The scaling factors for the inputs to the control system are as follows:

1. Prestart Request - This is a discrete quantity being 0 for Off and 1 for On.

2. Thrust Level Request - The quantity TLR is scaled at 297.6 counts per unit thrust.

3. Main Fuel Pump Speed - The quantity SNF is scaled at 0.63 counts per fuel pump speed.

4. Mixture Ratio Request - The quantity OFVR is scaled at 4059 counts per mixture ratio.

The scaling factors for the outputs of the control system are as follows:

1. LSI Lox Valve - The quantity 3R is scaled at 40.43885289 counts per degree.

2. M/B Lox Valve - The quantity 4R is scaled at 45.5 counts per degree.

3. P/B Lox Valve - The quantity X6R is scaled at 23,405 counts per inch.

4. P/B Fuel Valve - The quantity 5R is scaled at 71.8421 counts per degree.

In addition, the following valves and solenoids are scheduled as discrete quantities being either zero when closed, or scaled for 4095 when open:

- Nozzle Coolant Shutoff Valve
- P/B Secondary Helium Solenoid
- Main Lox Injector Helium Solenoid
- Turbopump Lift-Off Seal Solenoid
- Main Lox Turbopump Dam Seal Solenoid
- M/C Lox Vent Solenoid
- P/B Primary Helium Solenoid
- Fuel Vent Valve and Solenoid
- P/B Lox Vent Valve and Solenoid
- M/C Lox Vent Valve

Table CXVI. Number of Steps Used in Program

Subroutines			
LKUP 20		Univarient Function Generator	
LKUP3 35		Bivarient Function Generator	
LDLG 66		Digital Filtering	
Total 121			121
Tables	1417		
Constants	74		
Warmup	30		
Program	620	Initialization	
Total	2141		2141
		GRAND TOTAL	2262
I/O	-	To be determined	
Monitoring	-	To be determined	
CPU Check	-	To be determined	

Table CXVII. Estimates of Size of the Final Program

Memory Size Estimate	
Present Program	2262 Words
Projected Requirements	8192 Words
Estimates for Final Program	
Program, Data, Constants	4096
CPU Check	2048
I/O Check (Prestart)	1024
Initialization	128
I/O Instructions	256

Table CXVII. Estimates of Size of the Final Program (Concluded)

Monitoring	128
Growth	512
	8192 Words

H. FLIGHT SAFETY

1. Mission Reliability

Because the original XLR129 Engine Control study was not flight hardware-oriented, the area of redundancy and its probable impact on mission reliability was not fully explored. It was apparent that for supervised engine hardware testing, the additional financial burden that redundancy of any kind represents could not be tolerated. As the intent of the investigation changed, a new look at control redundancy needs was initiated. The following paragraphs are a brief review of how much redundancy is desirable, based on the preliminary outline of need in terms of mission reliability.

a. Mission Task Definitions

As related to the Bendix Engine Control System, the mission is defined as optimum control of the engine so as to avoid engine degradation and to achieve desired mixture ratio and thrust commands. Figure 116 shows a hybrid block diagram illustrating the proposed system for accomplishing these objectives. No reference is made on this diagram to any redundancy concepts. The use of a number of sensors and sophisticated trim loops has been proposed as the means of meeting these objectives. Successful operation of all of these sensors and trim loops to obtain the objectives is hereafter referred to as FULL CAPABILITY MODE. Implied in this concept is the ability of such a system to perform optimally even in the case of a slightly non-standard engine or in the case of minor deterioration or modification of some engine parameters during the mission. In the absence of such anomalies, it is considered that the engine may be controlled optimally by means of a less sophisticated system, requiring no sensors or trim control loops, such a system being defined as the GROSS CONTROL MODE. Since the combination of possible failures may not require complete reversion to this mode, there is also the possibility of various types of SEMI-GROSS CONTROL MODE.

Any failure, or combination thereof, which allows continuance of the engine mission is defined as FAIL OPERATE. Failures which require and allow successful shut-down of the engine are defined as FAIL SAFE. Combinations of failures which do not allow either control or shut-down of the engine are necessarily defined as CATASTROPHIC.

b. Use of Redundancy to Improve Reliability

Redundancy of the various system components has been proposed as a method of improving mission reliability. The degree of redundancy proposed differs for various components, based upon special characteristics of each situation. The following discussion covers the degree of redundancy, criteria

for selection, and gives an estimate of failure rate per hour (based upon detailed analysis of each component). However, to facilitate subsequent analysis, an attempt is made to standardize failure rates, adopting for each group a round-number approximation, always chosen on the conservative side.

(1) Pressure Sensors

The following pressure sensors are used:

Los LSI ΔP

Fuel LSI ΔP

Lox pump inlet P

Fuel pump inlet P

Transpiration ΔP

Main chamber P

Each of the pressure sensors is triply redundant. Median selection is used as the criterion determining which signal is to be used. A failure rate of 8×10^{-6} ($= \gamma A$) is estimated for each of the 18 individual sensors.

(2) Temperature Sensors

The following temperature sensors are used:

Preburner Chamber temperature

Fuel pump inlet temperature

Lox pump inlet temperature

Transpiration temperature

Preburner Chamber temperature has eightfold redundancy; using four dual junction liquid oxygen turbine exit probes and four dual junction fuel turbine exit probes. The redundancy is mandated not for reliability, but in order to select the highest temperature. The selection criterion is thus to select the highest valid signal; validity to be determined by the permissible deviation from the average of the eight sensors.

Complete loss of these signals will automatically result in loss of overtemperature transient compensation, whereas acceptance of a non-valid overtemperature signal will result in excessive cooling. In the following analysis, this signal is neglected, only in order to simplify the analysis.

The remaining three temperature sensors are each triply redundant. Median selection is the criterion. A failure rate of 4×10^{-6} ($= \lambda_B$) is estimated for each of the six individual sensors.

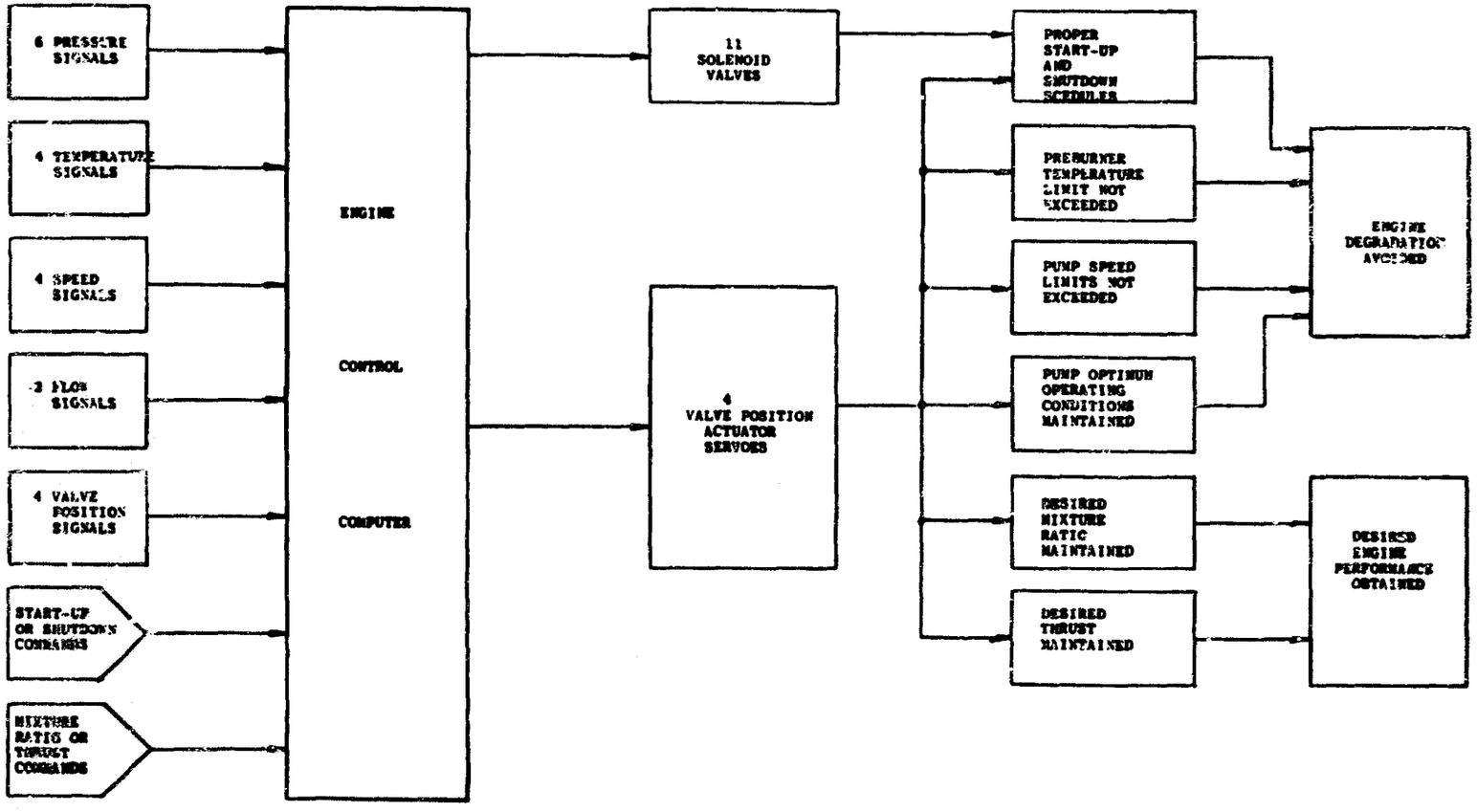

Figure 1169. Hybrid Block Diagram Defining Engine Control Task

(3) Speed Sensors

The following speed sensors are used:

Fuel LSI speed

LOX LSI speed

Main fuel pump speed

Main LOX pump speed

Each of the speed sensors is dual redundant. Due to the nature of the speed pulse signal, it is possible to determine with a high degree of reliability whether a speed signal is valid. The criterion would thus be to use the arbitrary primary sensor, when valid, and to use the arbitrary standby sensor when the primary is not valid. Reversion to a cured primary would be available in case of a failed standby signal. A failure rate of 4×10^{-6} ($= \lambda_C$) is estimated for each of the eight individual sensors.

(4) Flow Sensors

The following flow sensors are used:

Main fuel flow sensor

Main LOX flow sensor

Each flow sensor is dual redundant. A computed flow signal is also available. Selection criterion would be to use that sensor signal which is closest to the computed signal. There is thus a possibility of using a median selection criterion; however, the following analysis will be based upon the assumption of dual redundant sensors. A failure rate of 48×10^{-6} ($= \lambda_D$) is estimated for each of the four individual sensors.

(5) Main Computers

The main computer is dual redundant, there being two identical units, the primary and the standby. Each contains: input circuitry, output circuitry, arithmetic unit, program memory, function memory, solenoid drive circuitry, power supply section, and the major part of what is normally classified as signal conditioning circuitry.

A computer will have an extensive self-test capability, discussed elsewhere. There is a temptation to consider dividing the computer self-test into a large number of areas of the computer function, in order to allow complete usage of whatever areas are acceptable. However, self-test procedures will allow for a reasonable tolerance from ideal performance, and it can be seen that a failure to pass such tests will in most cases be a rather extensive type of failure mode. Hence, it is felt that the computer should only be divided into two self-test areas: the capability of performing Full Capability Mode functions acceptable, and the ability to perform Gross Control Mode functions. Gross Control Mode, of course, includes the ability to decelerate and shutdown the engine according to the most sophisticated detailed requirements.

The criteria for computer usage would be:

1. To transfer full control to the standby unit in event of any failure of the primary unit; and

2. To use Gross Control Mode of the standby unit in event of any failure of its Full Capability Mode.

3. The possibility has not been ruled out that there may be several Semi-Gross Control Modes. The intent here would be to retain as long as possible the overtemperature control trim loop and the speed control trim loops. In most cases, these modes would result automatically, not from failure within the computer but from failure of some of the less important input signals.

The failure rate of a full computer unit is estimated as 800×10^{-6} ($= \lambda_{\epsilon}$) and the failure rate of its gross control section as 280×10^{-6} ($= \lambda_{\epsilon_2}$).

c. Requirement for Emergency Shutdown Computer

The principal computers, primary and standby, are identical and are defined to include I/O circuitry, solenoid drive circuitry, and power supplies. Failure rates for a 15-minute mission are assumed to be 200×10^{-6} for the primary computer and 70×10^{-6} for the gross capability of the standby computer. Failure of both of these items, not necessarily simultaneously, would result in a catastrophic failure since there would be 14×10^{-9}, which is considered excessive. Thus the need is indicated for a third computer unit, separately housed and power supplied, defined as the Emergency Shutdown Computer (ESDC). Such computer would have the defined capability of taking control of the engine, at any thrust level, and generating acceptable valve commands and solenoid drive signals to decelerate the engine from the existing thrust level to idle, and then to shutdown.

Such a computer would obviously be simpler and more reliable than the two basic computers, and indeed must be, if its use is to be relied on in the event of failure of both of the basic computers. Based upon the hypothetical design discussed below, it is felt that this unit could have a mission failure rate of less than 20×10^{-6} ($= \lambda_{\epsilon}$).

Study of the failure mode effect chart will show that, under the circumstances mentioned, all four valve servos are operable. If this were not the case, a fail-safe shutdown would have already been called for by means of one of the two basic computers. Also, it is seen that the ESDC must have automatic self-test ability, either within itself or performed with the help of the standby computer. Otherwise, the above mentioned catastrophic failure rate of 14×10^{-9} would be applicable in the event that the ESDC had failed before being needed.

d. Design of Emergency Shutdown Computer

Since the concept of an ESDC is a new one, not previously discussed during this program, it is appropriate to include at this point a brief discussion of its design.

Figure 1170 shows the hypothetical design of the ESDC. The heart of the computer is an up-down 8-bit counter, which during normal mission tracks the position of one of the servo valves. The mainburner LOX valve is suggested as being most closely related to thrust level. The median signal of the valve position is automatically selected, as described previously.

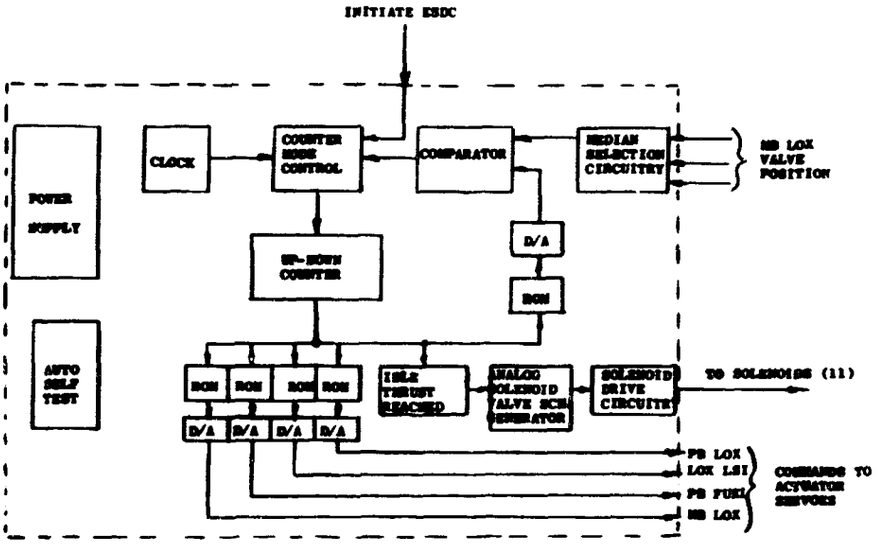

Figure 1170. Block Diagram: Emergency Shutdown Computer

At the time that the standby computer fails, the counter contains a number corresponding to the mainburner LOX valve position. The counter is then switched to a countdown mode of operation which reduces this signal at a constant rate versus time. By means of MOSFET ROM modules, each count calls for a predetermined command for each of the four servos. These schedules are based upon an assumed nominal mixture ratio.

When the thrust commanded has decayed to the idle level, this condition is detected and energizes an analog circuit which generates the proper solenoid valve control signals for the final 2.0 seconds.

e. Another Aspect of Primary-Standby Computer Transfer Philosophy

It has been estimated previously that the probability of any failure in the Primary Computer will be 200×10^{-6} during the mission. Complete transfer of all functions to the Standby Computer has then been postulated, leading to a probability of 34×10^{-9} that the trim capability will also fail in the Standby Computer and that a fail-operate Gross Mode will be reverted to, and a probability of 14×10^{-9} that fail-safe shutdown will be called for using the ESDC.

There is one school of thought which says that failures within the Standby Computer should not be allowed to call for these reversions, since there is a possibility that the Primary Computer would possibly still have the capability of handling the necessary functions, having been abandoned because of some minor failure. This philosophy would ideally advocate re-transfer of the four

computer output commands, taking each from whichever computer had the capability. It is not felt that this philosophy is the best one, because experience indicates that computer failures causing one output command to be erroneous will almost inevitably cause the others also to be erroneous. Therefore, the possibility of using this philosophy is extremely slight.

f. Actuator Servos

Figure 1171 shows the configuration of an actuator servo. There is, of necessity, a small section of mechanical components not susceptible to redundancy. This section is highly reliable, having an estimated failure rate of 6×10^{-6} ($= \lambda_J$). Other than this, the actuator is fully dual redundant. The basic electromechanical component is dual redundant, with an estimated failure rate of 20×10^{-6} ($= \lambda_\mu$). This may represent, in the case of an electrical motor, a dual control winding. The servo-amplifier and associated electronics is also considered dual redundant. However, since it is recognized that a minimal capability servo-amplifier would have a relatively high failure rate, estimated at 96×10^{-6} ($= \lambda_G$), it is decided that each of the dual sections will really be dual redundant itself. This is accomplished by use of a push-push design with completely independent gain channels, such that either half alone is capable of providing adequate drive power to the load. This is a hard-wired redundancy feature, requiring no failure detection or switching to implement. It must be recognized that there is the assumption of premission verification of the full availability of this section.

Present thinking is that each actuator shall have at least a triple redundant (possibly quadruple redundant) valve position feedback signal (by whatever means generated). Each of the two channels is hard-wired to a feedback signal, which is thus considered analytically as a part of that channel's failure rate. The reason for the triple redundant valve position information is based upon system monitoring needs, and upon the consideration that even in the event of failure of both channels of an actuator, there is still a need to know its valve position.

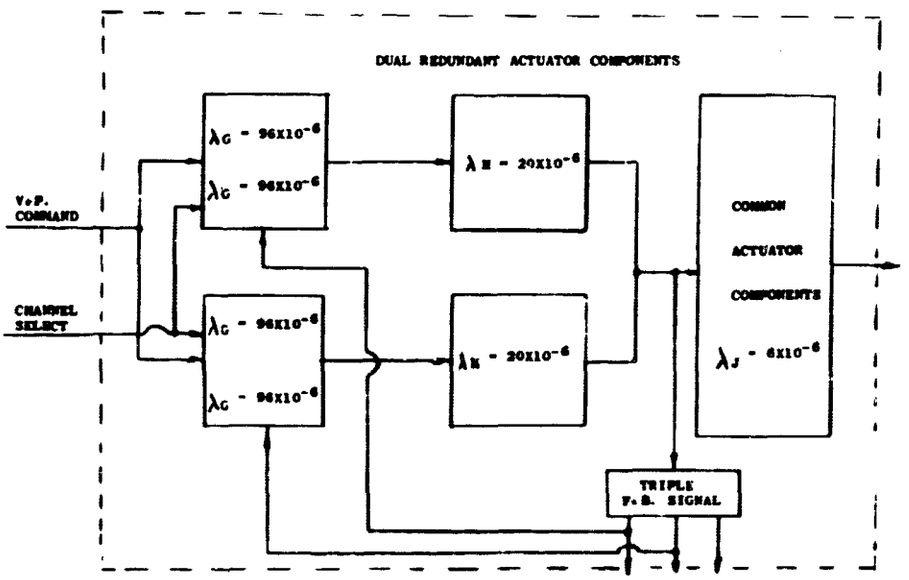

Figure 1171. Actuator Servo Configuration

In further analysis, it will be useful to have some consolidated failure figures for an actuator servo. It can be seen that the failure rate of a single channel is $\lambda^2_G + \lambda_H$, or approximately $\lambda_H = P_{K1}$. The rate for a second channel failure is calculated as $(\lambda^2_G + \lambda_H)^2 + \lambda_J = P_{K2}$, to include the rate of the nonredundant components, thus defining second channel failure as a failure which removes all actuator control capability.

2. A First Approach to Mission Reliability

Based upon the preceding discussion, figure 1172 shows the mission reliability configuration. Failure probabilities during the mission (assumed 15 minutes) are calculated according to the relation $P = \lambda_t = 0.25\lambda$.

Figure 1173 is a logic flow diagram of the failure mode. An attempt has been made to arrange the diagram from left to right, in the most likely time sequence, although this is, of course, not actually correct, since there is the possibility of an unlikely sequence of events occurring before a more likely sequence of events. Nevertheless, the numerical values shown are correct, based on the foregoing assumptions.

At this stage, some simplifications have been made, as follows:

1. Treatment of the flowmeter signals as dual redundant, even though there is a third computed signal.

2. The various possibilities of Semi-Gross Control Modes have not been considered individually.

3. The drawings shows equations for the combined failure rates, e.g., the probability of failure of two out of three pressure signals in a redundant group is $3P_A^2$. While the AND and OR logic symbols are shown to clarify the sequence relations, the correct combined probabilities are not calculated in all cases according to this logic. For example, various diamonds showing second failures show the actual calculation of the second failure probability is shown to include the first failure. Thus, the correct numerical values are shown at the various final effect blocks.

   Based on the P values generated and a consideration of the failure modes inherent in the Control Configuration, figure 1173 has been developed to pictorially illustrate the logical relations between some of the basic system failure mechanisms.

4. Finally, the most important simplication involved in figure 1173 is that all failure detection and mode transfer is assumed to be performed with a 100% confidence level. The relatively minor effect of this assumption will be discussed in the following section.

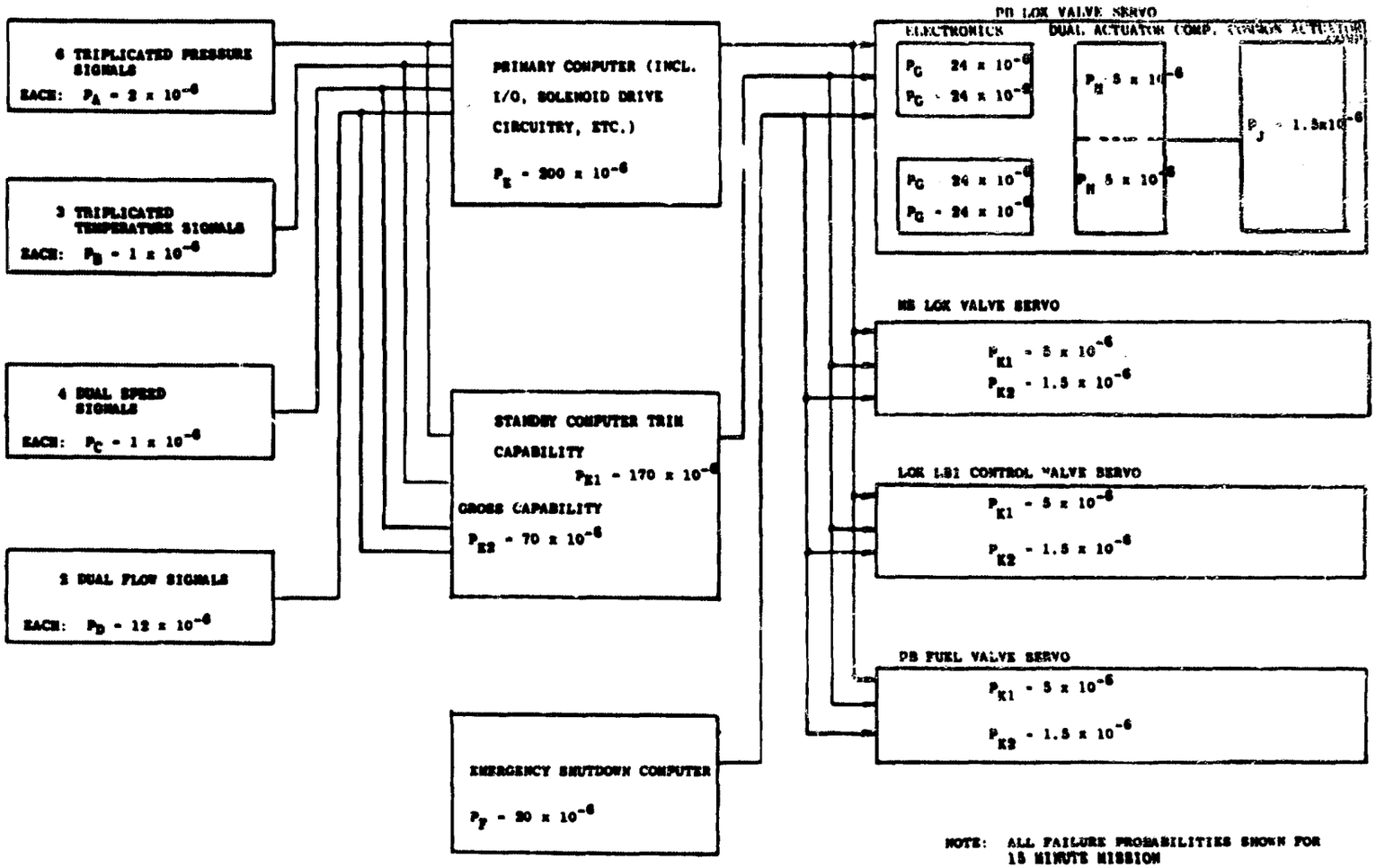

Figure 1172. Mission Reliability Configuration

A

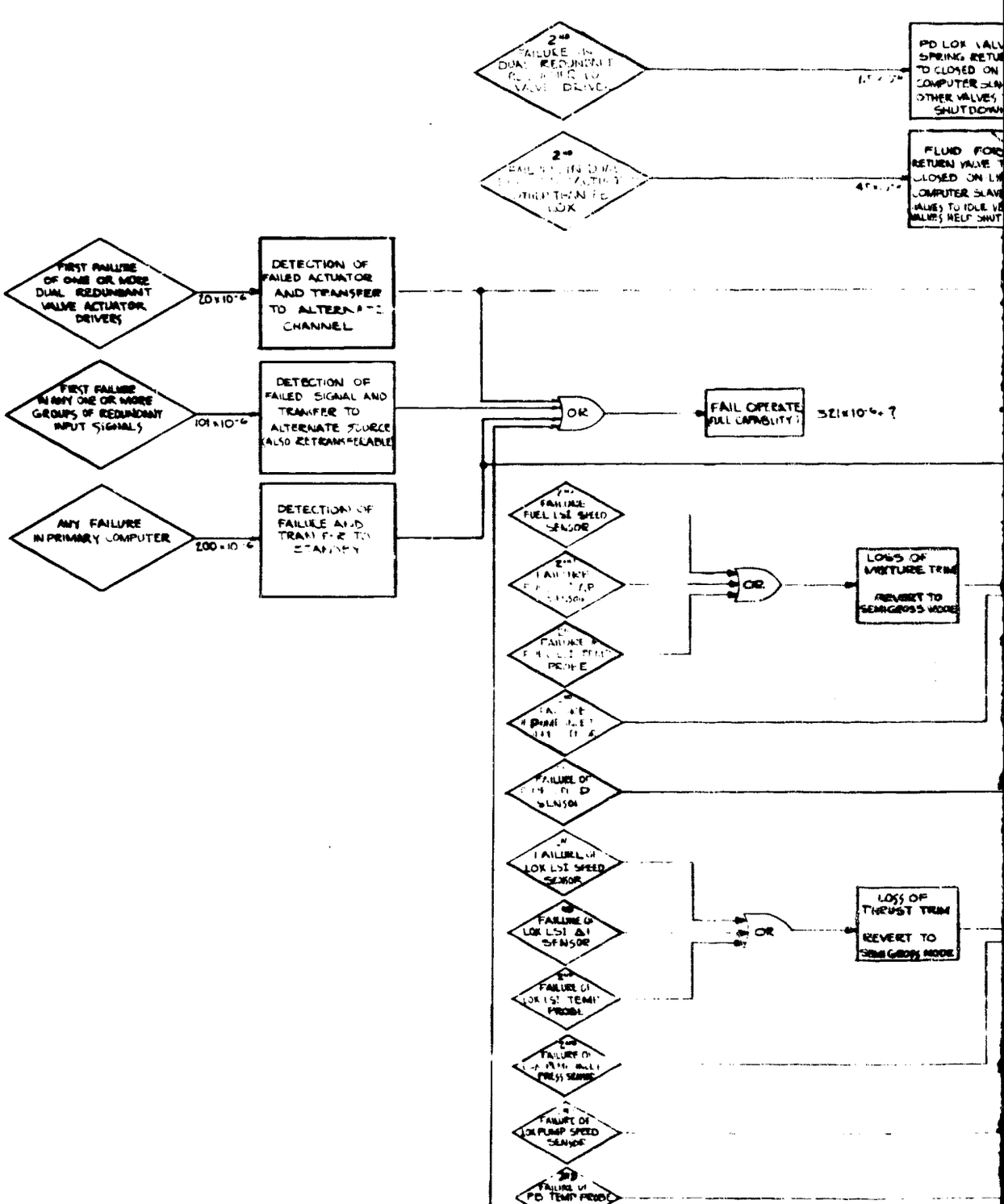

Figure 1173. Failure Mode Logic Flow Diagram

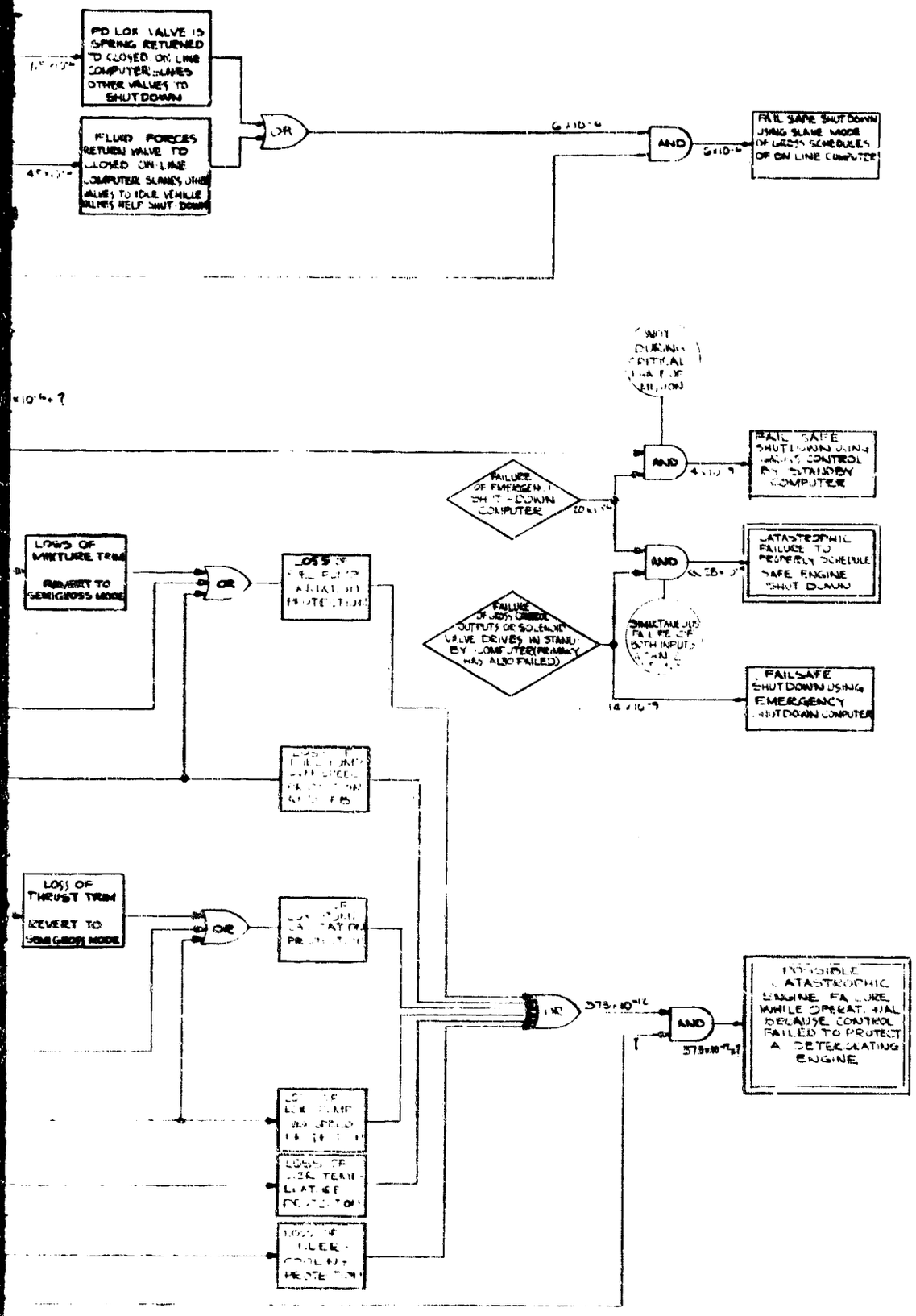
FD LOX VALVE IS SPRING RETURNED TO CLOSED ON LINE COMPUTER SLAVES OTHER VALVES TO SHUT DOWN
FLUID FORCES RETURN VALVE TO CLOSED ON LINE COMPUTER SLAVES OTHER VALVES TO IDLE VEHICLE VALVES SELF SHUT DOWN
OR
6 x 10⁻⁶
AND
6 x 10⁻⁶
FAIL SAFE SHUT DOWN USING SLAVE MODE OF LOX'S SCHEDULES OF ON LINE COMPUTER
AND
FAILURE OF EMERGENCY SHUT-DOWN COMPUTER
AND
FAIL SAFE SHUT DOWN USING CONTROL BY STAND BY COMPUTER
CATASTROPHIC FAILURE TO PROPERLY SCHEDULE SAFE ENGINE SHUT DOWN
FAILURE OF LOX'S OUTPUTS OR SOLENOID VALVE DRIVES IN STAND BY COMPUTER (PRIMARY HAS ALSO FAILED)
FAILSAFE SHUTDOWN USING EMERGENCY SHUTDOWN COMPUTER
14 x 10⁻⁹
LOSS OF MIXTURE TRIM REVERT TO SEMI GROSS MODE
OR
LOSS OF THRUST TRIM REVERT TO SEMI GROSS MODE
OR
AND
AND
POSSIBLE CATASTROPHIC ENGINE FAILURE WHILE OPERATIONAL BECAUSE CONTROL FAILED TO PROTECT A DETERIORATING ENGINE

I. Vehicle Interface

1. Signal Format
2. Data Word Transmission
3. Transmission System

For a 15-minute mission, the probabilities of the various modes of shutdown are shown in figure 1173 as follows:

1. Fail-safe shutdown using modified gross schedules of on-line computer;

   Mission probability = 6×10^{-6}

2. Fail-safe shutdown using ESDC;

   Mission probability = 14×10^{-9}

3. Catastrophic failure to control or shutdown engine;

   Mission probability = $<< 28 \times 10^{-14}$

4. Fail-safe shutdown using gross control by Standby Computer;

   Mission probability = 4×10^{-9}

It should be noted that the probability shown for case (1) may be extremely pessimistic, since it is entirely based upon the assumed failure rate of the non-redundant components of an actuator servo. Even the general type of actuator, whether electromechanical or pneumatic, is not firmly decided at this point. This analysis points up the extreme importance which must be given to the design of the critical area represented by λ_J.

It should also be noted that the probability listed for case (3) as $<< 28 \times 10^{-14}$ may probably be multiplied by a factor of 2.2×10^{-3} (= 2/15 x 60) to reflect the restriction of simultaneous failure within the same two seconds of the 15-minute mission. Therefore this catastrophic failure probability may be as low as 62.5×10^{-17}.

I. VEHICLE INTERFACE

As part of the investigations for the XLR129 Control Computer, a basic vehicle communication concept was developed to permit access to the Control System by an external supervisory device which can command discrete engine performance conditions. This supervisory device can be either an on-board central programming computer or a separate, self-contained control device.

The command language should be compatible with the normal instruction pattern residing within the Control Computer. Thereby, insertion of discrete commands will be accomplished without additional circuitry or excessive programming changes or memory storage requirements.

The Command Module, the external command generator, accesses the engine control whenever it is to be operated independently of the vehicle and is also capable of displaying the status of the control's internally active Command Conditions.

1. Signal Format

The word structure (figure 1174) consists of 12 data bits, 1 parity bit and 3 bits for identification coding. The bits of the word are presented to the input/output section of the engine control computer in parallel format.

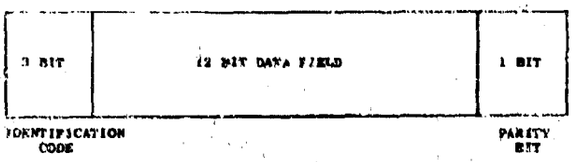

Figure 1174. Signal Format

The identification code is utilized to differentiate between percent thrust, mixture ratio, discrete signals, and monitor data. The discrete signals are prestart, start and shutdown. The monitor data is a series of words which reveal the internal state of the engine control computer. The external supervisory device uses the monitor data to judge if the engine control computer is operating properly. Specific codes may be assigned to identify each command as follows:

Discrete Signals	011
Mixture Ratio	001
Percent Thrust	010
Monitor Word	100

The data field contains the data values in natural binary for percent thrust, mixture ratio and monitor words. For discrete signals the data field contains a binary code which identifies the specific discrete command requested. The binary signal code identifying the discrete commands are as follows:

	Code	Data	Parity
Prestart	011	000000000001	0
Start	011	000000000100	0
Shutdown	011	000000010000	0

2. Data Word Transmission

Figure 1175 shows the lines carrying signals between the external supervisory device and the engine control computer.

a. Output Control Operation

The output control operation transfers a control field to the engine control computer when the external supervisory device addresses this unit. The control field is the content of a register in the external supervisory device and is 16 bits long.

b. Input Data Operation

The input data operation transfers data from the engine control computer to the external supervisory device, when the engine control computer is addressed. Each data word is 16 bits long.

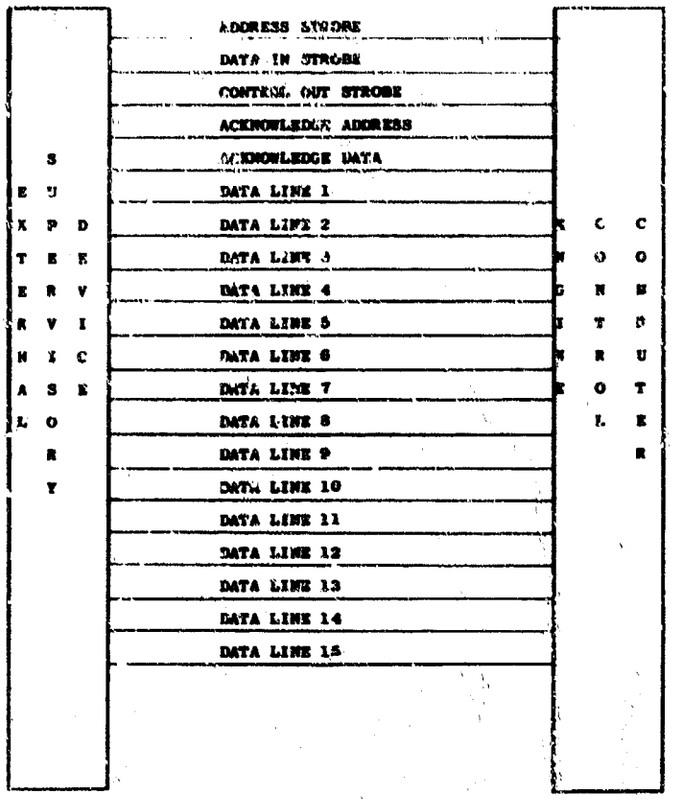

Figure 1175. Vehicle Interface

3. Transmission System

Integrated circuits with 0 to +5 vdc levels have in inadequate noise margin for use as drivers and receivers in a digital data transmission system. The transmission of data over lines greater than a few inches in the presence of noise requires special drivers and receivers to prevent corruption of the data. A two wire system (figure 1176) allows rejection of common-mode system noise through the use of differential drivers and receivers. Receivers commonly reject common-mode noise of +3 volts to -3 volts, but higher noise rejection (+7.5 volts to -7.5 volts) is possible. The driver inhibit input effectively disconnects the driver from the transmission line, which allows the connection of more than one driver to the same transmission line without interference. Normal line impedances of 50 to 200 ohms are acceptable. This transmission system will be duplicated for each of the 20 signals exchanged between the external supervisory device and the engine control computer.

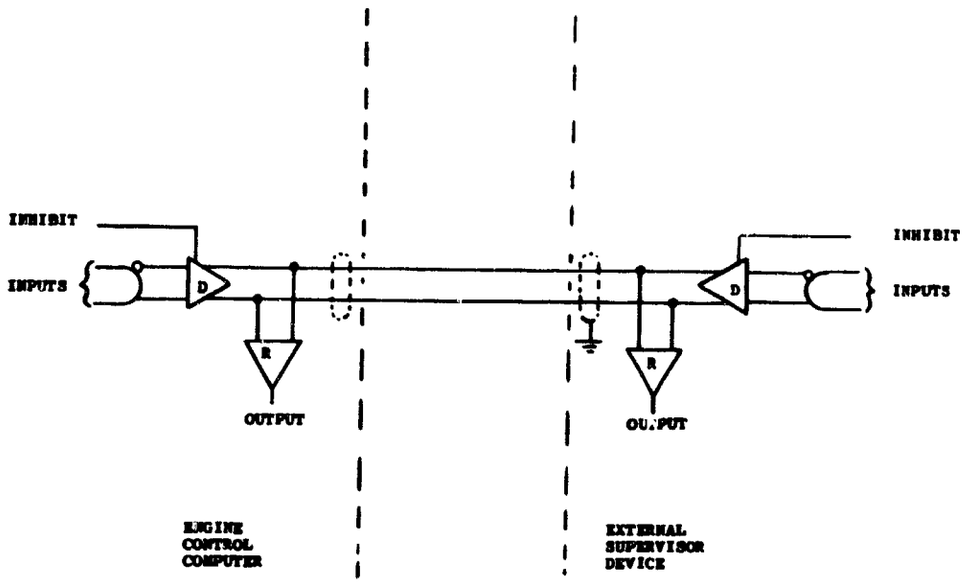

Figure 1176. Differential Transmission System

SECTION III
DYNAMIC MODEL RESEARCH STUDY

A. GENERAL

This report describes the results of that portion of Pratt & Whitney's Engine Control Development Program (Contract F04611-67-C-0002) which concerned itself with the creation of a Dynamic Digital Model of an XLR129 Engine operating in combination with a Bendix Control System. The Model was planned for general use as required throughout the program to assist in the resolution of complex control problems and the possible highlighting of borderline engine cycle deficiencies.

The dynamic model emerged as a powerful engineering tool. Except for relatively slow solution rates, which necessitated more than one hour of residence in the Bendix IBM 360/50 to produce a three second acceleration history, the XLR129 Dynamic Model proved to be a virtually indispensable engineering tool with which to predict and correct areas of probably dynamic instability and/or limiting parameter violations.

Excellent control performance was consistently demonstrated. After a fruitful preliminary period of trial-and error modifications to Control System in an effort to eliminate any possibility of encountering dynamic instability, it became feasible to demonstrate a wide assortment of optimum accelerations, all well within the boundaries of engine cycle restraints. Furthermore, by taking advantage of a unique fail-operating design concept, equally fine performance could also be achieved after total sensor failure simulation when the Control System could automatically revert to its simple open-loop gross mode.

The engine protective loops were shown to have good responsiveness. These loops too, required trial-and-error modifications before all channels were correctly compensated and unexpected interactions eliminated. Only then was the Model able to demonstrate its full protective potential in those most important parameters which include pump speeds, transpiration cooling, preburner overtemperature, and cavitation margin.

The modification of the engine cycle to incorporate a fuel inducer turbine valve is strongly recommended to enhance power plant integrity. Although transpiration flow augmentation was obtainable by the expedient of fuel pump speed and fuel valve area biasing, no technique could be devised which showed any promise of providing improved fuel pump cavitation margin on demand. A fuel LSI turbine valve, similar to the lox LSI design, is strongly recommended to solve this problem.

Valve sensitivity factors were established. Use of the Model provided a particularly easy method of establishing the open-loop engine cycle response to small valve position perturbations. Even the associated dynamic response data proved useful in predicting required constants for new compensation networks.

The early identification, within the engine, of marginal inducer performance and inadequate cooling proved to be valuable task spin-offs. Dynamic Model

acceleration studies early in the program clearly indicated that engine component sizing could be advantageously adjusted to improve throat cooling and cavitation margin. The necessary changes were incorporated and the resulting cycle improvements are reflected in all of the data presented in this report.

B. SUMMARY OF STUDY RESULTS

Dynamic Model operation confirms that the Engine Control System created by the Bendix (South Bend) System Team is both functionally and dynamically compatible to Pratt & Whitney's XLR129. The complete system includes the following basic elements:

1. A Primary Control consisting of a simple system for the open loop command of discrete valve positions but featuring a program of time-based logic for automatic safe acceleration bias. Limited authority trims are utilized to improve the accuracy of achieved thrust, mixture-ratio and fuel pump speed.

2. An Engine Protection System featuring stable override loops for fuel pump overspeed, lox pump overspeed, fuel pump cavitation, lox pump cavitation, transpiration cooling deficiency, and preburner overtemperature.

The engine will respond to a step command between any two points within its operational envelope in less than 2.5 seconds with conservatively low level of all potentially critical parameters.

Simulated flowmeter or speed sensor failure, even during maximum acceleration, was shown to have only minor impact on performance inasmuch as the Control System simply reverted to Gross Mode and continued functioning as usual. Only steady-state accuracy might suffer by the Control System being non-responsive to a possible deteriorating engine cycle.

A series of tests were devised to simulate engine malfunction of such a nature that each critical parameter in turn would be forced into that type of dangerous operating condition which would automatically trigger a corresponding protective loop. These circuits were shown to react with sufficient responsiveness and authority to effectively counteract the unwanted conditions. However, as previously recommended, the studies do clearly indicate that a fuel LSI turbine control valve, similar to the existing oxidizer LSI turbine valve, would greatly improve the fuel pump cavitation margin confidence level.

Although the prediction of engine response to small valve area perturbations resists direct calculation, simple steady-state Model operation can provide this essential data with relative ease. Surprisingly, this work provided the unexpected information spin-off that cooperative valve area trim far exceeds the performance available for a loop which operates on only a single valve. For example, it was found that the main burner oxidizer valve, when used alone, exhibited a reversed direction logic from that which might be inferred from its flow map.

The Dynamic Engine Model offered a convenient method of predicting the lowest useable cycle rate for the Flight Computer Program. To obtain this information, the Model computation frequency was arbitrarily reduced until control accuracy suffered.

C. OVERALL SYSTEM

The overall XLR129 Control System consists of the following parts:

- Start and Shutdown Logic
- Primary Control -

  Gross Mode

  Propellent Trim

  Fuel Pump Speed Feedback

- Protective Override System

D. START AND SHUTDOWN LOGIC

Although the scope of this task does not include the implementation of a Dynamic Model for the study of start-up and shutdown processes, the Bendix Primary Control System for the XLR129 Engine does contain applicable logic based on related model testing conducted at Pratt and Whitney's West Palm Beach facility.

E. PRIMARY CONTROL

The Dynamic Model of the Primary Control used to record the acceleration time histories consisted on the following essential elements:

- Gross Control
- Thrust Trim
- Mixture Trim
- Fuel Pump Speed Feedback

First the complete Primary Control is implemented. Following this, flowmeter failure is simulated, thus reverting the system to Gross Control plus speed feedback. Finally all sensors are assumed to be failed, leaving only the Gross Control operative. Figure 1177 shows the control characteristics with all sensors failed.

Acceleration runs with and without fuel pump speed trim are shown in figures 1178 and 1179 respectively. Figure 1180 illustrates the final control system acceleration characteristics.

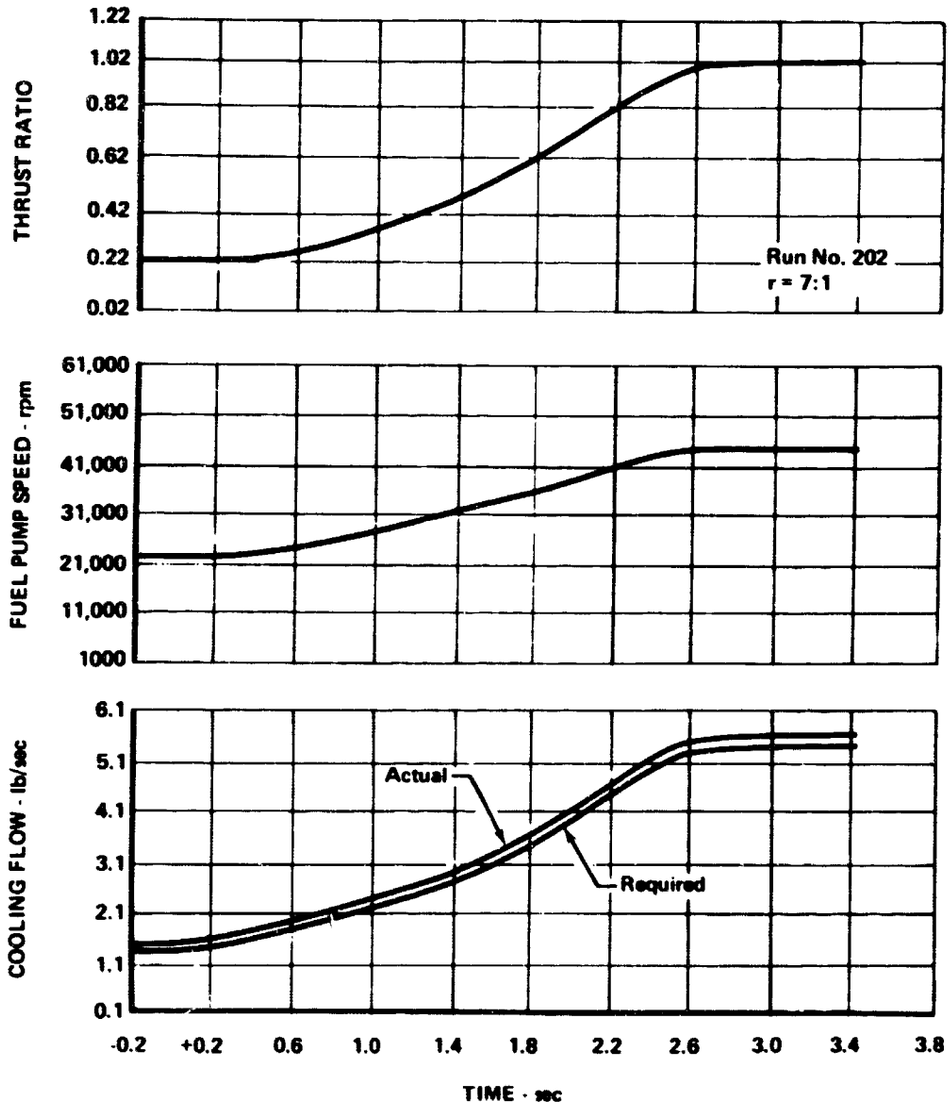

Figure 1177. Engine Control Simulated Failure of All Sensors

FD 47714

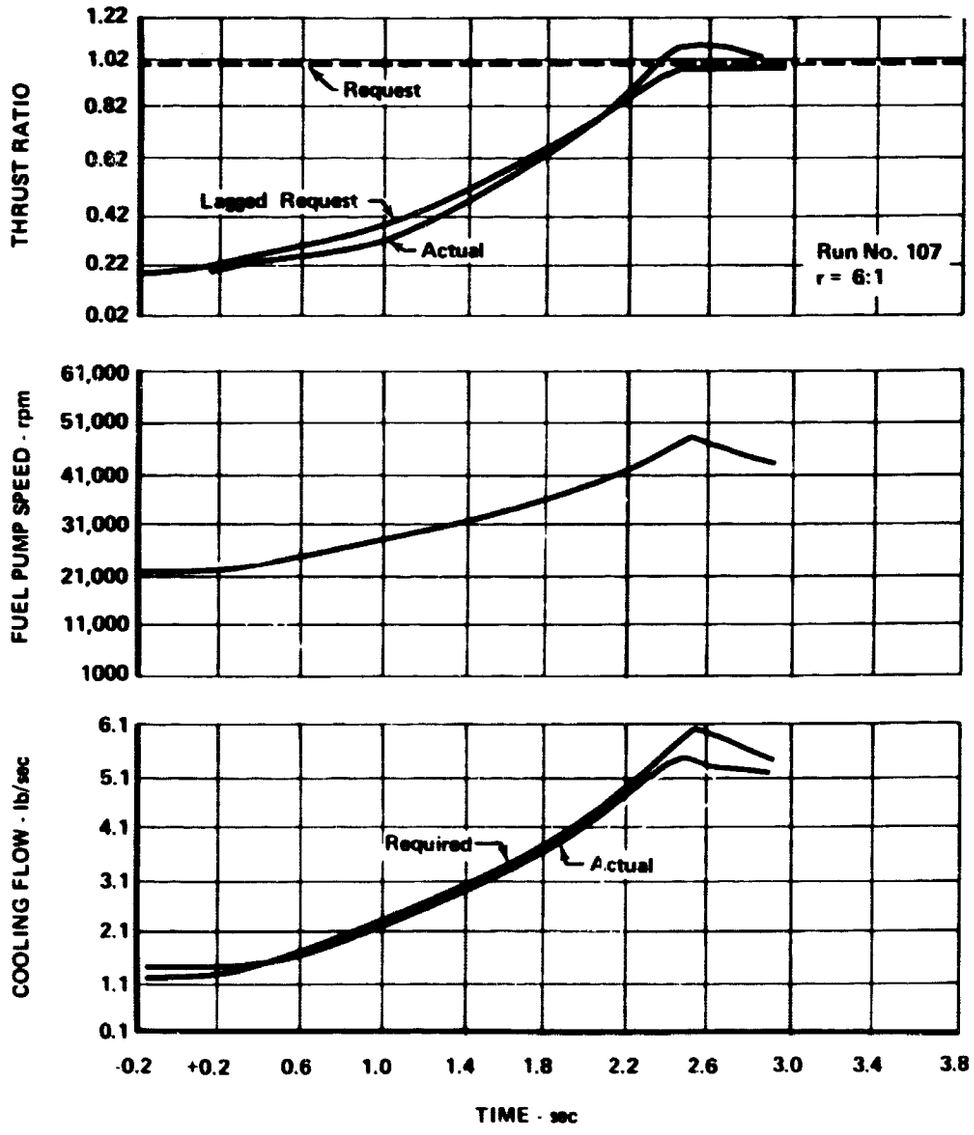

Figure 1178. Acceleration Without Fuel Pump Speed Trim FD 47715

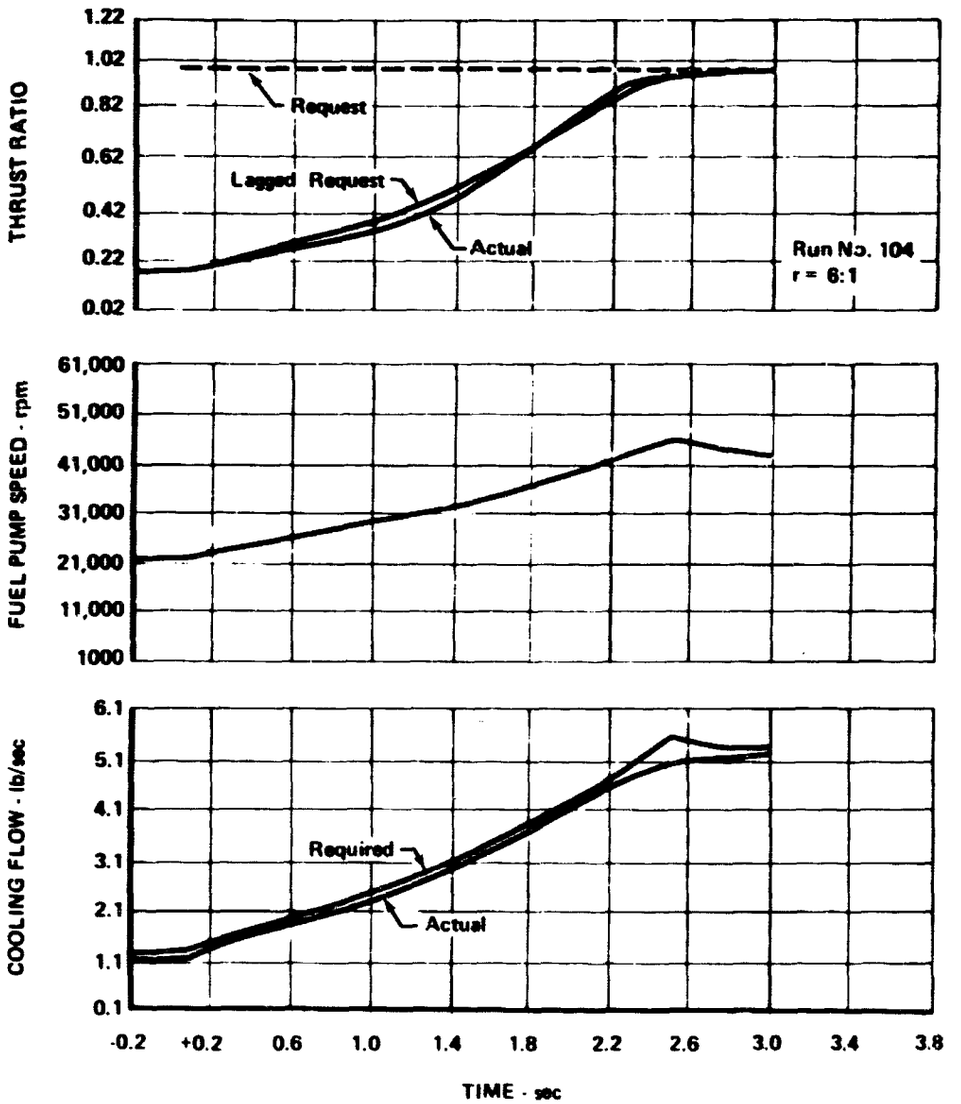

Figure 1179. Acceleration With Fuel Pump Speed Trim

FD 47716

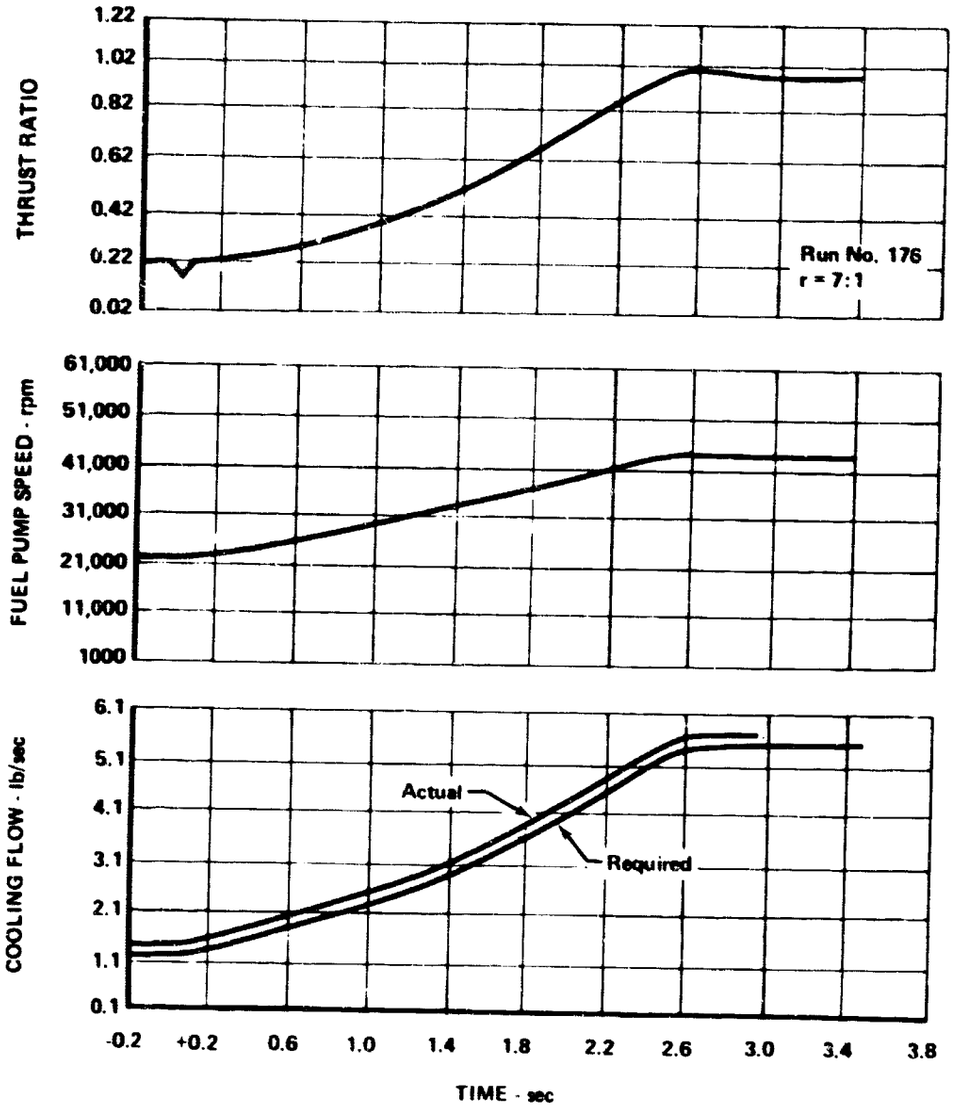

Figure 1180. Final Control System Acceleration FD 47717

F. ENGINE PROTECTION LOOPS

Under all normal conditions, the Primary Control will indeed regulate the XLR129 throughout its entire operating envelope and maintain and adequate margin of safety for all critical parameters, even during periods of intense dynamic change. However, with progressive engine deterioration, parameters other than those required for normal control might very well exceed safe limits. It was the object of this phase to identify these critical parameters and, by Model techniques, demonstrate an override system which has the capability of sharply limiting any tendency for the cycle to exceed a prescribed set of maximum values. Figure 1181 illustrates the operation of the fuel pump over-speed protection system.

The parameters which have been selected for safety protection are listed below:

- Fuel Pump and Lox Pump Overspeed
- Transpiration Cooling and Fuel Pump NPSP
- Oxidizer Pump NPSP
- Preburner Overtemperature

G. VALVE SENSITIVITY

Special open-loop runs were made to establish the open-loop engine response to small valve area perturbations. Typical test data are presented in table CXVIII. The following essential information was obtained:

- Sensitivity factors for each valve at both high and low power settings.
- Realistic time-constants for all rotating components and combustion processes at both high and low power settings.

Table CXVIII. Valve Sensitivity Tests, Runs 112A Through 119A, Cycle 8A

	Ref	Fuel Area Δ	LSI Area Δ	Main LOX Area Δ	PBLOX Area Δ
1. Idle - Median Mixture (Response Time Constant = 0.2 Seconds)					
AFV	.4240	.4155(Δ)	.4240	.4240	.4240
ALBT	.6400	.6400	.6272(Δ)	.6400	.6400
ALCV	1.0520	1.0520	1.0520	1.0310(Δ)	1.0520
AFDV	.0390	.0390	.0390	.0390	.0382(Δ)
PFG	.2007	.2004	.2027	.2017	.1983
OFE	6.0146	6.0903	5.9645	5.9918	5.9867
OFC	6.6670	6.7511	6.6048	6.6333	6.6292
TP	1862.1	1889.5	1871.4	1863.8	1837.8
SNF	22455	22544	22745	22588	22251
SNL	10715	10714	10884	10788	10607

Table CXVIII. Valve Sensitivity Tests, Runs 112A Through 119A, Cycle 8A (Concluded)

2. Full Power - Median Mixture (Response Time Constant = 0.1 Seconds)					
AFV	3.4730	3.4035(Δ)	3.4730	3.4730	3.4730
ALVT	3.1800	3.1800	3.1167(Δ)	3.1800	3.1800
ALCV	2.1170	2.1170	2.1170	2.0747(Δ)	2.1170
AFDV	.5000	.5000	.5000	.5000	.4900 (Δ)
PFG	1.0001	1.0002	1.0084	1.0140	.9864
OFE	6.0390	6.0467	6.0266	6.0030	6.0428
OFC	6.2835	6.2923	6.2696	6.2447	6.2883
TB	2090.0	2093.7	2098.0	2102.5	2075.4
SNF	44439	44462	44734	44980	44003
SNL	23349	23352	23517	23666	23105

H. MINIMUM ACCEPTABLE COMPUTATION RATE FOR REAL-TIME HARDWARE

The Dynamic Digital Model proved to be an efficient engineering tool with which to investigate the possibility of using decreased computer cycle timing as a method of programming earlier failure information.

The engine simulator, as provided by Pratt and Whitney, operates at a step size of 0.001 seconds. Pratt and Whitney determined that the system models the prototype quite well at that rate.

Early in the study, it was estimated that the control computer would require about 10 milliseconds to perform a complete control computation cycle plus some self-test functions. The bulk of the digital simulation work was therefore performed modelling this granularity. Comparisons made early in the study showed no discernible difference between 10 millisecond and 1 millisecond control rate, and throughout the work the 10 millisecond cycle performed in a very satisfactory manner.

More recent work has shown that the prototype control computer could be successfully programmed to operate at a 10 millisecond rate, if the self-test functions were spread over a relatively large number of cycles. It would be convenient, therefore, to have more time per cycle available for these functions.

Simulation with the digital model was carried out decreasing the control rate to 15 milliseconds. These were performed with the complete control system on a nominal engine acceleration. No degradation in performance or stability was noted.

No simulations were made at rates lower than 15 milliseconds because certain routines are sensitive to the time increment. These could either be rewritten to iterate for a solution, or the interval could be divided for these routines, but it was not deemed urgent to investigate further. Based on the highest natural frequency encountered in the engine system, it is felt that, with suitable precaution, a computer rate corresponding to 20 milliseconds per cycle would result in satisfactory performance.

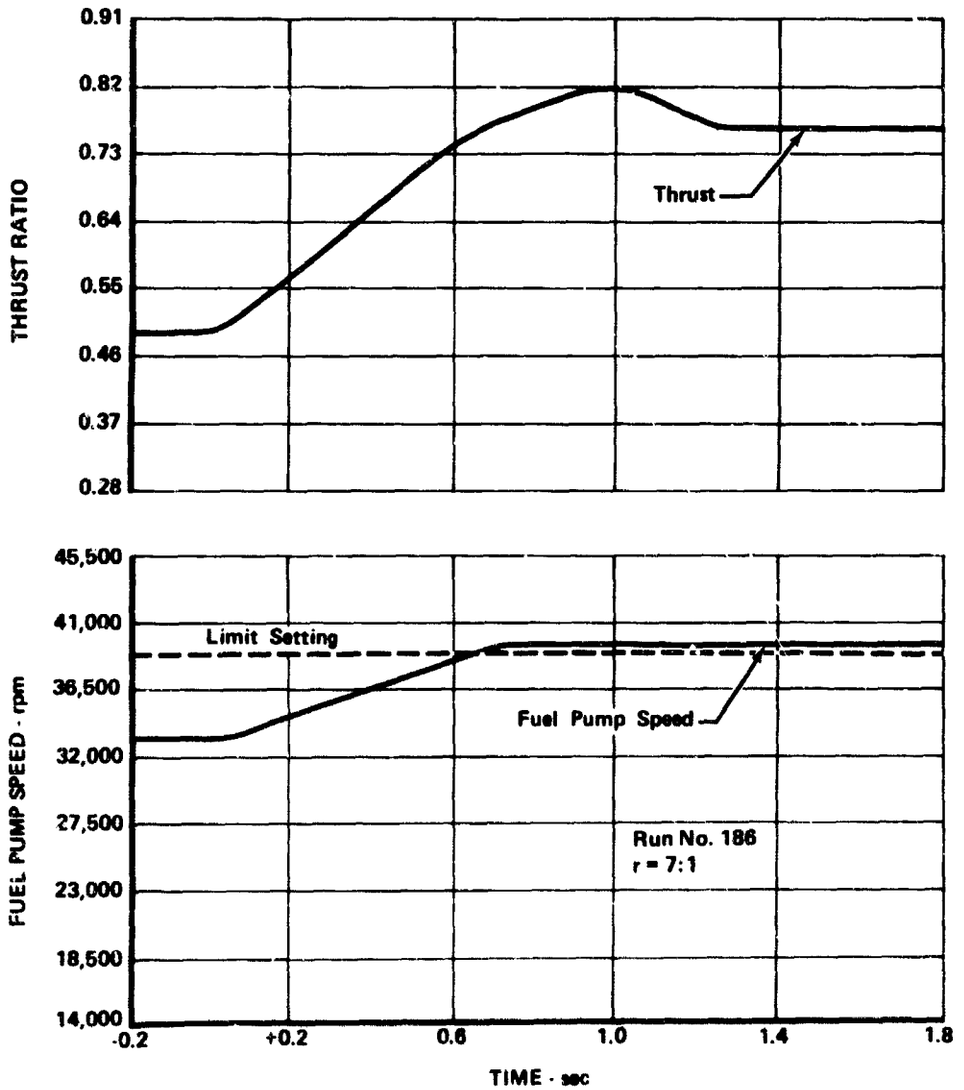

Figure 1181. Engine Control Fuel Pump Overspeed Protection FD 47718

SECTION IV
FLOWMETER STUDY PROGRAM

A. INTRODUCTION

Fuel and oxidizer flowmeters are required as primary, active feedback elements for XLR129 engine control system. Accurate flowrate information is required by the engine control system to prevent fluid cavitation during transients such as accelerations. Unique requirements for the flowmeter systems for the XLR129 engine include high flowrates, fast response, and installation in short, curved flowlines.

This study program described in this report provides evaluation of the selection of the design concept and preliminary design of the force screen flow sensor for the flowmeter system.

B. REQUIREMENTS

The study program for the flowmeters on the XLR129 engine was outlined as follows: The primary objective was to give Bendix the opportunity to conduct an in-depth tradeoff study of available flowmeter types. The documentation from the study would permit P&WA to monitor the steps leading to the flowmeter type selection.

As a secondary objective, the study was to support the Digital Model computer research by providing a continuously updated estimate of flowmeter dynamics. The availability of such information would minimize possible lost research time which could result from creating a model with overly optimistic component performance.

1. Flowmeter Design Requirements

The flowmeter design requirements for the study program were as follows:

1. Propellants: Hydrogen and oxygen in liquid states
2. Minimum and Maximum Mass Flowrates for Each Propellant: 1616 to 10,087 gpm fuel; 607 to 3185 gpm LOX
3. Maximum Pressure Drop: 20 psi total for 2 series redundant flowmeters
4. Size and Configuration: Fuel meter 6-in. dia, LOX meter 5-in. dia, suitable for short piping runs
5. Type of Flow: Turbulent because of short piping runs and high velocities
6. Accuracy: 1% of reading
7. Response: Minimum 5 cps breakpoint
8. Reliability: Dual redundant flowmeters for duplicate standby

9. Weight: Minimum, but not specified

10. Electronic Component Temperature Environment: Mounted on oxidizer heat sinked body

11. Cryogen Compatibility: Hydrogen and oxygen

12. Two Phase Flow: Without damage or performance degradation after exposure. (Operation per specification not required.)

13. Environments Such as Vibration, Acceleration, Noise, etc.: Launch and Spaceflight environments not specifically defined.

C. RESULTS OF STUDY PROGRAM

1. Flowmeter Survey

The initial phase of the study program consisted of a survey of existing flowmeter designs for application on the XLR129 engine control system. One of the methods used for the survey involved mailing questionnaires and cover letters, containing general XLR129 flowmeter requirements, to 38 major suppliers of flowmeters. The type and number of responses are summarized as follows:

1. Responsive with a proposed design: 17

2. Non-responsive because of no applicable design: 5

3. Non-responsive because of proprietary considerations: 1

4. Non-responsive for unknown reasons: 15

The format for the responses included the questionnaire forms and/or other appropriate technical flowmeter literature.

A literature survey of pertinent articles and reports was conducted to provide the basic principles and concepts for evaluation of the various types of proposed flowmeters for the XLR129 engine control system.

A third type of survey for the flowmeter study consisted of visits to the Pratt and Whitney West Palm Beach facility, the NASA Marshall Space Flight Center and Eastech, Inc. The visits to P&WA and MSFC were made to obtain information accumulated from extensive experience and testing in the flowmeter field. The P&WA flowmeter evaluation personnel conceded that the XLR129 flowmeter requirements were extremely difficult, and different from previous flowmeter applications. P&WA suggested consideration of volumetric turbine flowmeters based on the extensive history of this type in cryogenic applications. Also P&WA suggested that pressure drop devices be considered since this type of flowmeter is readily adaptable to flight hardware and is capable of providing the required response time. The purpose of the survey visit to Eastech, Inc. was to investigate a relatively new potentially promising vortex shedding type of flowmeter for application on the XLR129 engine control system. The vortex shedding flowmeter, which was demonstrated in both air and water, provides a volumetric flow output signal, has a 100 to 1 range and has no moving parts.

Further description of the vortex shedding flowmeter is provided in the sections of this report covering design evaluation and trade-off studies.

2. General Design Evaluation

A preliminary general design evaluation was made for the flowmeter designs proposed in the responses for the mail survey. The pertinent data for the proposed designs from each of the responses is included in the Summary Chart shown in table CXIX. The background and experience with volumetric turbine flowmeters are demonstrated in the Summary Chart which shows the volumetric turbine principle utilized in eight of the proposed designs. Two additional proposed designs consist of angular momentum turbines which provide a direct indicated true mass output. The vortex shedding type and the hydrodynamic oscillatory types are similar to each other in principle but different in the method of mechanization. Thermal heat transfer between an externally heated element and the fluid is related to mass flow and is determined by temperature measurements in two of the proposed designs shown in the Summary Chart. Another proposed design utilizes a venturi and measured pressure drops. The remaining design on the Summary Chart is the force screen flow sensor. Two additional designs were proposed which do not appear on the Summary Chart because of being received too late in the program. One of these consists of a pressure drop device designed for laminar flow and, therefore is not suitable for the XLR129 flowmeter application. The other proposed design not included in the Summary Chart is a thermal heat transfer type which is similar to the two thermal flowmeters indicated in the Summary Chart. In conclusion, the Summary Chart shows the following 6 basic types of flowmeters:

1. Angular Momentum (direct true mass) Turbine
2. Volumetric Turbine
3. Force Screen
4. Vortex Shedding, Hydrodynamic Oscillatory
5. Thermal Heat Transfer
6. Pressure Drop

The preliminary design evaluation resulted in a reduction of the 6 proposed design types to the 3 types most suitable for the XLR129 flowmeter application. The angular momentum turbine type of flowmeter was eliminated from consideration because of the following:

1. General lack of durability -- in some designs, overspeed problems occur as a result of high velocity gaseous flow. Also some designs have an excessive number of moving parts.
2. Installation requirements
3. Configuration compatability.

Table CXIX. Summary of Flowmeter

	Operating Principle	Indicated Output	Cryogenics Compatibility	Configuration Compatibility (3 inch total length for 2 flowmeters in series)	Response Time, msec	Accuracy, %	Maximum Pressure Drop Per Flowmeter
1. Black Sivals & Bryson, Inc.	Angular Momentum	True Mass	Present models are not suitable. Min. low temp. is -50° F.	Poor Excessive length	600	0.25 - 1.00	Low
2. Porter Aeronautical Corp.	Angular Momentum	True Mass	Yes	Poor. Excessive length	2 - 5	0.1	Low
3. Daniel Industries, Inc.	Volumetric Turbine	Volumetric Rate	Some models are designed for cryogenic applications.	Poor. Excessive length	Data Unavailable.	Data Unavailable.	Low
4. Flow Technology, Inc.	Volumetric Turbine	Volumetric Rate	Yes	Poor. Excessive length	3	0.1 to 0.5	4 psi Low
5. IT&T Corp.	Volumetric Turbine	Volumetric Rate	Yes	Poor. Excessive length	Low	0.1	Low
6. Rockwell Mfg., Inc.	Volumetric Turbine	Volumetric Rate	Not Standard	Poor. Excessive length	Low	0.15	<5 psi
7. Foxboro	Volumetric Turbine	Volumetric Rate	Yes	Poor. Excessive length	6 - 25	0.2 to 0.5	<6 psi
8. Sentry Equipment Co.	Paddle Wheel Volumetric Turbine	Volumetric Rate	No	Length average but unacceptable	Low	1% of full-scale	Acceptable
9. Rotron Controls	Squirrel Cage Volumetric Turbine	Volumetric Rate	Not applied to date. Modifications are required	Length average but unacceptable	100 - 300	0.5% of reading	Data unavailable
10. Quantam Dynamics, Inc.	Volumetric Turbine with Density Compensation	Either True Mass or Volumetric Flow Rate	Yes	Poor Excessive length	3 - 15	0.1% (Volmetric)	Low
11. Bendix	Force Screen With or Without Density Compensation	Either True Mass or Volumetric Flow Rate	Yes	Good Configuration provides minimum length design	2	1%	5 psi
12. Eastech	Vortex Shedding	Volumetric Rate	Not stated in literature, but method should be compatible with cryogenics	Poor Excessive length	4500	0.5%	19 psi
13. CGS Scientific Corp.	Thermal	True Mass	Present design not compatible	Poor Excessive length	<1	2% of reading	Low
14. Thermal Instr. Co.	Thermal	True Mass	Yes, but not developed	Data unavailable	1000 - 2000	0.5%	Data unavailable
15. Fischer & Porter Co.	Hydrodynamic Oscillatory	Volumetric Rate	Yes	Data unavailable	About 50	0.5% of rate	Data unavailable
16. Flow-Dyne Engineering	Venturi-Pressure Measurement	Pressure Differential or Velocity Squared	Yes	Poor Excessive length	Data unavailable	3% Full Scale	Low

*The data provided in this table was taken from letters, data sheets and brochures from flowmeter manufacture
In response to Bendix inquires for information concerning flowmeters for the XLR129 engine.

ry of Flowmeter Survey Results

	Maximum Pressure Drop Per Flowmeter	Rangeability	Ability to Withstand Two Phase Flow	Weight	Development Status	Tolerance For Vibration and Noise
00	Low	13:1	OK within density limits of model. 53,300 lb/hr of 1.3 lb/ft^3 gas. Acceptable.	Present models are heavy for industrial use.	Models on market since January 1969. However, development is required.	1 g Vibration
	Low	15:1 to 30:1	Gas velocities up to 350 ft/sec Acceptable	Average	Essentially production	Data unavailable
ble.	Low	3:1 to 10:1	Will not tolerate two phase flow. Would require bypass venting of high velocity gases.	Models were designed for minimum weight. Average	Commerically available	Poor for vibration and noise
5	4 psi Low	20:1	High overspeed capability	Data unavailable	Data unavailable	Data unavailable
	Low	20:1	Acceptable	Average	Production	Acceptable
	<5 psi	70:1	Undetermined	Heavy	Production	Undetermined
5	<6 psi	24:1	Overrange flow of 150% of maximum rated flow	Average	Development required	Data unavailable
-	Acceptable	Data unavailable	Leakage problem	Average	Stock Item	Probably acceptable
	Data unavailable	10:1	Acceptable	Average	Production	Acceptable
-	Low	200:1	Acceptable	Average	Production	Acceptable
	5 psi	10:1	Acceptable	Lightweight	Development required	Acceptable
	19 psi	100:1	Acceptable	Lightweight	Development required	Acceptable
	Low	100:1	Present design not compatible	Average	R & D required	Acceptable
	Data unavailable	10:1 t 500:1	Acceptable	Lightweight	Development required	Acceptable
ate	Data unavailable	20:1	Acceptable up to some unspecified momentum limit	Average	Feasibility models under test. Early development stage	Within limits
ale	Low	Data unavailable	Acceptable	High Industrial application	Production	Acceptable

eter manufacturers

The volumetric turbine design was retained for further consideration because of previous experience and testing of this type of design in cryogenic applications. In general, the volumetric turbine designs are more durable and have fewer moving parts than angular momentum turbine designs. The thermal heat transfer designs were eliminated from further consideration because the thermal design concept involves sampling in a flow line with non-uniform velocity distribution. Furthermore, the thermal type has not been developed for cryogenic applications and has probable inadequacies in response time and accuracy. Pressure drop devices such as venturi's were also eliminated from further consideration for reasons similar to those given for the thermal heat transfer designs. Therefore, the volumetric turbine, vortex shedding and force screen concepts were retained for further detailed consideration for the XLR129 flowmeter application.

3. Evaluation of Design Concepts

The three flowmeter concepts selected for detailed evaluation are as follows:

1. Volumetric turbine
2. Vortex shedding
3. Force screen.

Since none of the three flowmeter concepts provides a direct mass flowrate output, the fluid density must be either measured or computed and combined appropriately with the flow sensor output for inferential mass flowrate measurement. The three methods selected for determining fluid density are as follows:

1. Vibrating vane densitometer
2. Honeycomb capacitance densitometer
3. Computation of density from pressure and temperature measurements.

Therefore, detailed evaluations were required for both the flow sensor and the method of determining density.

4. Recommended Flowmeter Design

The recommended flowmeter design for the XLR129 engine control application consists of a force screen flow sensor and a densitometer which computes fluid density from temperature and pressure measurements. Figure 1182 shows a schematic representation of the recommended flowmeter system which utilizes an open loop force screen flow sensor with mechanical spring restraint for the force screen. The three inputs to the flowmeter system from the fluid are drag force on the force screen, temperature and pressure. The fluid drag force F, is proportional to the produce of density times volumetric flowrate (or velocity) squared ρV^2, for a given flow area and force screen. The force, F, on the force screen is restrained by square law springs which provide a deflection proportional to the square root of density times volumetric flowrate, $(\sqrt{\rho})$ (V) (figure 1179). A linear pick-up is used to provide a flow sensor output proportional to the square root of density times volumetric flowrate, $(\sqrt{\rho})$ ( ).

The volumetric turbine, vortex shedding and force screen concepts were evaluated, and the advantages and disadvantages for each concept were listed as trade-off considerations shown in table CXX.

Engine mount considerations are included in the trade-off list as installation and flow conditioning requirements and size and configuration. Installation and flow conditioning requirements refer to straight lengths of flow line in front of the flow sensor. Location of the flowmeter in the short, curved flow lines between the low speed inducer and the turbopump is a major consideration in the selection of a flow sensor concept. The velocity distribution in the short, curved flow lines will not be uniform even if straightening vanes are incorporated in the flow lines, and therefore, the vortex shedding concept which samples around the bluff body will be subject to errors related to velocity distribution. In contrast the force screen concept senses flow over the entire flow area, and if the force screen concept is properly mechanized, an average flow is measured in a flow with a non-uniform velocity distribution.

Other important considerations for selection of the flowmeter concept include response time and pressure drop. The engine control system requires a flowmeter with a fast response to provide system stability during rapid accelerations and decelerations of the engine. Furthermore, the pressure drops in the flowlines caused by the flowmeters must be minimized for maximum operating efficiency. The vortex shedding meter requires a sampling of 100 pulses to average out random variations in the vortex oscillation phenomenon. Using LOX as an example with a 6-inch diameter flow line, the time for 100 pulses is 0.857 seconds at rated thrust and 4.47 seconds at idle. The estimated pressure drop for the LOX flow at rated thrust is 23 psi per flowmeter. Improvement in response time can be achieved with an increase in pressure drop. For comparison, the force screen flow sensor has a response time in the range of 0.002 to 0.005 seconds and an estimated pressure drop in LOX at rated thrust of 2 to 4 psi. The volumetric turbine concept was unacceptable because of non-uniform fluid velocity distributions in the short, curved flow line and the general size and configuration of the turbine flow sensor.

In summary, the main trade-off considerations for the evaluation of the flow sensor were:

(1) Engine mount considerations - included as "installation and flow conditioning requirements" involving sampling vs sensing over the entire flow area. Also "size and configuration."

(2) Response time

(3) Pressure drop

Therefore, based on these trade-off considerations, the force screen flow sensor is the recommended design concept for the XLR129 engine control system application.

Table CXX. Flow Sensor Trade-Off Considerations

	Advantages	Disadvantages
Flow Sensor Type		
Free Turbine (Volumetric)	Availability Experience Low Pressure Drop Volumetric Rate Output	Installation and Flow Conditioning Requirements Size and Configuration Rotating Turbine With Bearings Overspeed From High Velocity Gases
Vortex Shedding	No Moving Parts Rugged Design Volumetric Rate Output	Slow Response Large Pressure Drop Installation and Flow Conditioning Requirements Lack of Experience and Test Data Samples Flow Around Bluff Body Development Required Modification Required for Cryogenics
Force Screen	Installation and Flow Conditioning Requirements Size and Configuration Fast Response No Moving Parts Low Pressure Drop Senses Flow Over Entire Area	Development Required Primary Sensor Output $\propto \rho V^2$ Vibration Susceptibility (Open Loop Only)

The densitometer for the recommended flowmeter design utilizes a temperature sensor, a pressure sensor and the on-board computer as shown in figure 1182. Temperature and pressure values are sent to the computer for analog to digital conversion. The computer utilizes appropriate thermodynamic property equations for computation of density. The square root of density, $\sqrt{\rho}$, is computed and multiplied by the flow sensor output (proportional to $\sqrt{\rho}\,V$) to provide the desired mass flowrate output from the flow system.

Mass flow rate $= \sqrt{\rho} \cdot \sqrt{\rho}\ V = \rho V$

ρ = density

V = volumetric flow rate

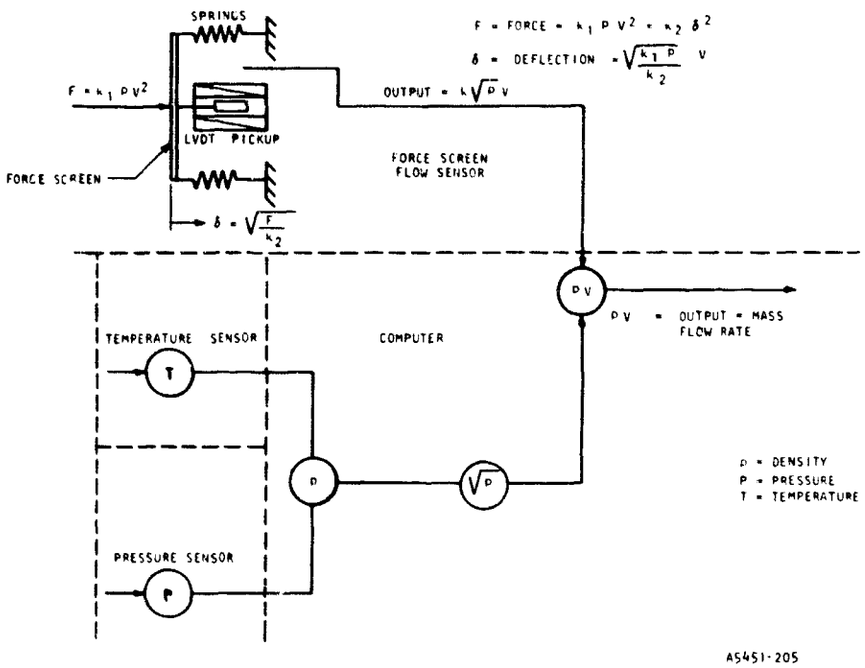

Figure 1182. Flowmeter Schematic

5. Force Screen Flow Sensor Mechanization

Various methods of mechanization were considered for the force screen flow sensor. Considerations included the following:

1. Open loop versus closed loop design.

2. Use of either linear or square law springs for open loop design.

3. Support of the force screen on either the circumference or a center position.

4. Type of spring design such as cantilever springs, circular diaphragm springs, helical tension and compression springs, etc.

5. Use of springs for screen support and also restraint for open loop design.

6. Type of displacement transducer including linear variable differential transformer, strain gage, and capacitance types.

7. Flowmeter requirements for XLR129 engine including short curved lines and non-uniform velocity distributions.

The proposed mechanization for the force screen flow sensor is shown in the sketch in figure 1183. The design is a basic open loop system with the force screen supported and restrained at a center location by two circular, corrugated support diaphragms. The support diaphragms have a square law force-deflection characteristic to provide screen deflections proportional to the square root of density times volumetric flowrate. The support at the center of the screen is accomplished by mounting the support and restraint diaphragms inside a center support structure which is suspended from the flowline by four radial support and straightening vanes. A linear variable differential transformer is used as the displacement transducer and is located on the flow centerline. A damping coil is mounted near the outside of the force screen and located in a magnetic field provided by the permanent magnet to provide system damping if required. An electrical signal which is suitably phased with the LVDT output is sent to the damping coil to stabilize the system for sinusoidal input accelerations.

The design mechanization shown in figure 1183 allows non-uniform velocity distributions since the total fluid drag force on the screen is indicated as an average measured deflection at the center of the screen. The two support diaphragms provide the desired square law longitudinal restraint along with an extremely rigid lateral restraint. In addition the LVDT transducer is relatively insensitive to lateral deflection of the LVDT core.

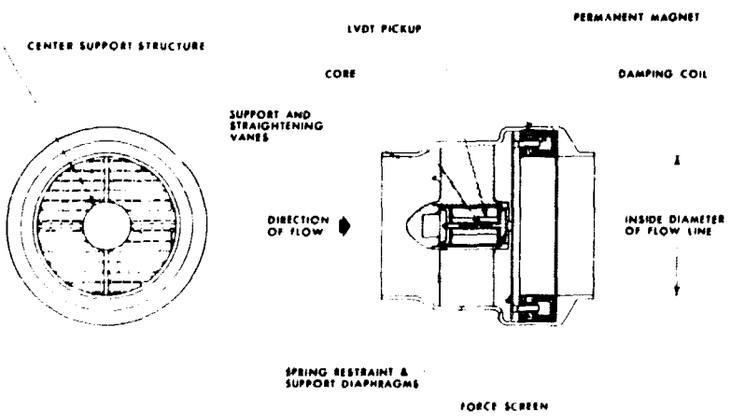

Figure 1183. Force Screen Flow Sensor

D. SUMMARY, RECOMMENDATIONS AND CONCLUSIONS

The flowmeter study program has provided a survey of flowmeter concepts and available flowmeter designs for application on the XLR129 engine control system. The advantages and disadvantages of the most relevant flow sensors and densitometers were listed and used in a trade-off study for selection of a recommended flowmeter system design. The recommended design consists of a force screen flow sensor and computation of density from measured values of temperature and pressure, although the use of pressure may not be required for the oxidizer system.

Preliminary design of the flow sensor and an error analysis for the flowmeter system were also included in the study program. The essential design features of the recommended flow sensor include the following:

1. Basic open loop system.

2. Force screen supported and restrained by two circular corrugated diaphragms having square law deflection characteristics.

3. LVDT deflection pickup on the flow centerline.

4. Provisions for electromagnetic dampling, if required.

5. Acceptable for wide range of non-uniform flow velocity distributions.

The following recommendations are suggested for further study of the flowmeter system for specific applications on engine control systems:

1. The flow sensor configuration should be firmly established and included in a design layout of the flowlines for the XLR129 engine or its successor.

2. Flowmeter performance requirements, including accuracy and dynamics, should be studied using the digital computer model program for the anticipated engine control system.

3. A design and development program phase is recommended for the force screen flow sensor described in this report. Design layouts would be prepared, and further study of potential problem areas would be included in this phase.

In conclusion the recommended flowmeter system, consisting of the force screen flow sensor and density computation from temperatures and pressures, is suitable for supplying the mass flowrate information for the engine control system which provides the required control and protection for the engine.

SECTION V
ELECTROMECHANICAL VALVE
CONTROL SYSTEM

A. INTRODUCTION

This report presents the results of a feasibility study of electromechanical valve control systems for the Pratt & Whitney XLR129 Rocket Engine.

Trade studies were conducted on the basic components of the system such as servomotors, transducers, transmissions and electronics as well as on the system approach to be utilized for the fail operational system requirement. The major development areas of electromechanical valve control systems are outlined in this report.

The major conclusion of this report is that electromechanical valve control systems are feasible for applications such as the XLR129 Rocket Engine.

B. SYSTEM SELECTION

Both AC and DC electromechanical systems were studied for feasibility for the XLR129 rocket engine. Both approaches have been determined to be feasible for this application.

The preferred approach utilizes brushless DC servomotors and is shown in figure 1184. The servomotor, transmission and position sensor would be close-coupled to the cryogenic valve and would therefore be designed for operation at cryogenic temperatures. The electronics associated with the servo loop would be designed for operation at temperatures no less than -65° F. The electronics would be packaged so that logic functions would be in the computer and the remaining electronics would be in a separate temperature controlled environment.

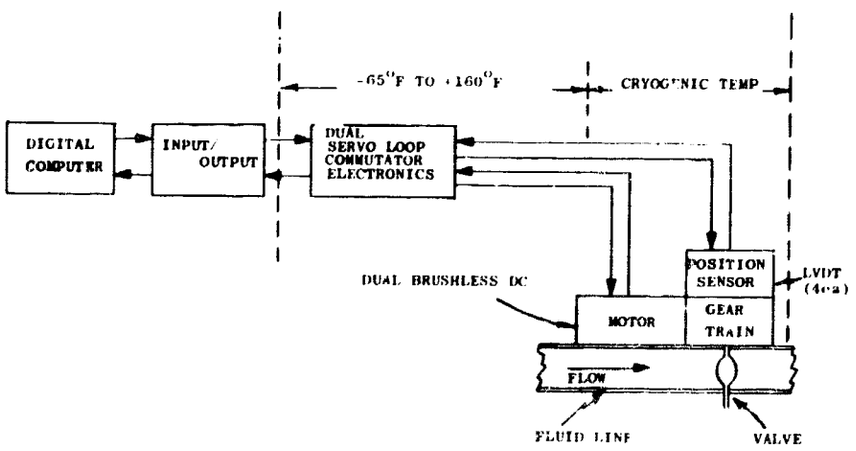

Figure 1184. Electromechanical System Selection

Both AC and DC approaches can be designed to meet the performance requirements for the XLR129 rocket engine. The major reason for the preference of DC over AC for this application is because of the reduced input power required by the brushless DC servomotors with respect to the AC servomotor.

C. SUMMARY AND COMPARISON OF AC AND DC SYSTEMS

Table CXXI shows a weight breakdown for fail operational AC and DC system approaches. As can be seen, the total system weight does not vary significantly for AC or DC approaches.

Table CXXI. System Weight Breakdown for Complete Engine Control System

Component	AC (lb) AC (lb)	DC (lb)
Servomotors	12.2	8.4
Position Sensors	5.0	5.0
Transmissions	90.0	82.0
Fail Operative Electronics	3.0	6.0
Total System Weight*	110.2	101.4

*This estimate does not reflect connectors and cabling due to unknown installation requirements.

The major difference between the AC and DC system approaches is shown in table CXXII, which summarizes the peak power conditions for the four valves. The peak power was determined for each valve by multiplying the maximum load torque by the maximum dynamic velocity of the valve. The peak dynamic velocity was established by applying a ±2% thrust amplitude at the servo loop bandpass. As can be seen from the table, the efficiency of the DC approach is approximately 50 per cent higher than the AC approach. If not for the assumption that the primary source of available power is AC, the comparison would be still more favorable for the DC system approach.

Table CXXIII summarizes the peak start-up power requirements for AC and DC approaches. Again, the assumption is that the primary source of power is AC. The total peak start-up power is 539 watts for a DC system approach and 821 watts for an AC system approach. The peak start-up power was calculated for each valve by multiplying the peak load torque in the start-up regime by the average slow velocity during start-up. Also contained in table CXXIII are the start-up times associated with the three valves having a start-up requirement. Deviations from the 200 ms original requirement will be required for the P/B fuel valve and the main ox valve to minimize the electric power required for start-up and also to keep the dynamic operating point far enough away from the stall point on the torque-speed curve of the servomotor. The critical P/B ox valve has been designed to have a 100 ms start-up capability.

Table CXXII. Peak Power Summary

	Plo (Watts)		Pmo (Watts)		Pmi (Watts)		Ps (Watts)		PL (Watts)		OVERALL EFF. (PLo/PL x 100)	
	BDCM	ACM	BDCM	ACM	BDCM	ACM	BDCM	ACM	BDCM	ACM	BDC	AC
P B OX	157	157	212	212	231	565	290	569	362	569	43.4	27.6
P B FUEL	50	50	76	76	83	181	104	203	130	203	38.5	24.6
MAIN OX	254	254	358	358	389	854	487	902	610	902	41.6	28.6
LSI	137	137	193	193	210	460	262	517	326	517	42.0	26.5

745.7 WATTS = 1HP
BDCM BRUSHLESS DC MOTOR
ACM 2 PHASE AC MOTOR
* 1.2 Pmi + 1/2 Pmi (.8 - Fφ + Vφ

Plo Load Power
Pmo Motor Output Power
Pmi Motor Input Power
Ps Supply Power
PL Line Power (AC)

Table CXXIII. Peak Start-Up Power Summary Table

	Plo (Watts)		Pmo (Watts)		Pmi (Watts)		Ps (Watts)		PL (Watts)	
	BDCM	AC	BDCM	AC	BDCM	AC	BDCM	AC	BDCM	AC
P/B OX VALVE START-UP 100 MS	78	78	105	105	114	250	143	281	178	281
P B FUEL VALVE START-UP 400 MS	24	24	36	36	40	86	50	96	62	96
MAIN OX VALVE START-UP 500 MS	125	125	176	176	191	420	239	444	299	444

Total Peak Start Up Power { -DC 535 Watts; -AC 821 Watts }

Figure 1185 shows the power distribution of the system with the efficiencies associated with the electrical supply processing.

D. Description of Electromechanical System

1. Reliability
2. Simplicity
3. Partitioning
4. Redundancy
5. Redundant Operational Philosophy
6. Motor Electronics Combinations
7. Monitoring
8. Maintainability
9. Repairability

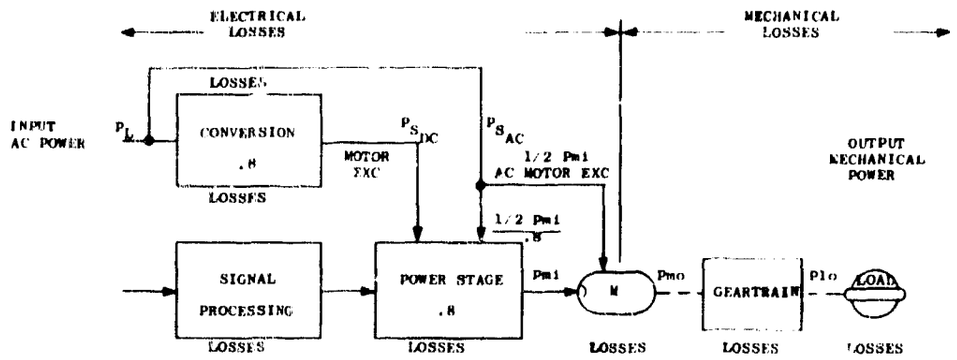

Figure 1185. Power Distribution

D. DESCRIPTION OF ELECTROMECHANICAL SYSTEM

This section of the report discusses the overall electromechanical system features and philosophy. The basic system chosen (see figure 1184) controls valve position by closing a loop around a brushless DC servomotor-gear train combination. This basic approach is feasible for controlling the valves. The required dynamic performance is feasible for the electromechanical valve control system. The system described in this section is a fail operative system. Thus two failures are required in a given servo loop in order to lose control of the valve.

The major features and concepts of the valve control system are presented and discussed below.

1. Reliability

The system reliability objectives would be built in from the ground up by considering each piece part, derating, materials selection and processing to optimize individual MTBF's for the application. Going beyond parts selection, the electromechanical mechanization enhances system reliability by limiting the marriage to electrical and mechanical interfaces in conjunction with the redundancy and test concepts which provides for alternatives after 1st and 2nd failure occurance.

2. Simplicity

A determined effort has been made to attain the simplest basic system motor-electronics drive consistent with minimum weight objectives. In addition, the ground rules and redundancy concepts which are subsequently explained are predicated on simplicity rather than complexity or sophistication. Other approaches to attaining a fail-operative system imposed increased weight, lower MTBF, and test complications.

3. Partitioning

Independence of subsystems from other systems can be very advantageous. In this case considering the Electromechanical System as a subsystem, and recognizing that the four valve schedules are interrelated, the subsystem accuracy and failure survival are dependent on all variable parameters.

The failure analysis of the engine actuating systems and variations in performance are subject to both internal and external influence.

From the performance point of view, direct coupling of the electronically controlled motor to the valve via a gear train provides a transfer path independent of pneumatic pressure changes either steady state or dynamic.

From a failure point of view, the redundancy philosophy is dependent on the ability of the fluid forces to load and back drive the valve and gear train and motor shaft until the valve reaches a closed position. In addition, switching provisions can be provided to suit the application in order to guarantee an automatic or manual capability of disconnecting a motor hardover.

4. Redundancy

The following statements reflect a conglomeration of ground rules, assumptions, conditions and limitations which serve as a rationale for the redundancy mechanization.

1. Each engine has four valves.

2. Engine performance is critical (time and magnitude relative to all valve positions).

3. Each valve actuator shall remain operative after a first failure.

4. Each valve actuator shall be operative or provide intelligence reflecting valve position after a second failure.

5. Any combination of 1st and 2nd failures shall not result in a condition which precludes a programmed slaved or controlled engine shutdown.

6. The valve has prime reliability.

7. The gear train has prime reliability.

8. The motor shaft and bearings have prime reliability.

9. The on time is relatively short thereby allowing a concept of testing the "off line" Servo Amplifier and switch over capability prior to final system usage.

10. The "off line" Servo Amplifier is unmonitored after initial test. A subsequent failure although improbable is allowed since failure of the "on line" Servo Amplifier is detected by the monitoring system which initiates a switch over the standby channel. The undetected failure would appear to be a 2nd failure which when sensed would revert the particular actuator to an automatic back drive shutdown profile.

11. Only DC voltage command signals are provided.

12. Only DC voltage position information will be accepted for monitoring.

13. All monitoring and decisions will be accomplished by the main computer.

14. Appropriate "engage-disengage" switch over logic will be provided pending application.

5. Redundant Operational Philosophy

Figure 1186 reflects the redundant provisions for the actuator. It includes an "on line" servo amplifier, an "off line" servo amplifier and four position indicators. Two of the position indicators are used as feedback paths for the servo amplifier while the other used as feedback paths for the servo amplifier while the other two (#3 and #4) are used as backup position indicators for slaving of the other three servo loop electronics associated with the other three valves should both the "on line" and "off line" servo loops fail.

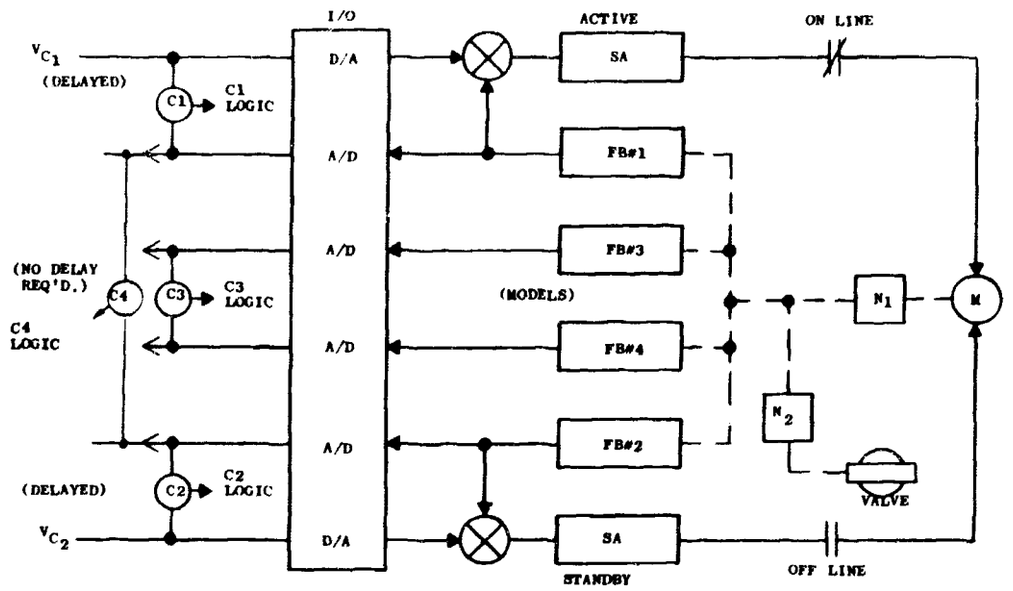

Figure 1186. Fail Operative Mechanization Including Quad Feedback Provisions

Monitoring of the servo loop and feedback electronics is accomplished with comparators which detect an error and provide the appropriate logi which is operated on by the computer, in turn, executing the command to automatically compensate for the failure.

The "Fail Operative" intent is satisfied as follows:

A test routine is executed which demonstrates that the entire mechanization is operational including the ability to switch over from the "on line" to "off line" and return to "on line" servo. The purpose of this test is to provide a

confidence that the "off line" Servo Amplifier forward loop and the switch over capability are functioning properly. Since the mission time is relatively short, the probability of two failures occurring within that time span is unlikely but should they occur, the backup slaving technique precludes damage to an engine. As a result, a motor model and associated transients with switching are eliminated which increases MTBF, decreases weight and allows the standby loop to be in a ready state with little power dissipation in the output stage since no load exists.

6. Motor Electronics Combinations

The Brushless DC Motor was chosen for its efficiency which facilitates small size and weight by allowing the excess heat to be thermally conducted into the cryogenic sources.

An additional advantage is related to the complete subsystem partitioning between the electro-mechanical actuator and the mechanical valve. The union of the two systems is accomplished with compatible mechanical interfaces of the gearbox and valve.

The "AC Induction Motor" requires that cryogenic fluid be ported through the motor for cooling to limit the maximum temperature rise. All other single motor comparisons are relatively equal.

Another important aspect of the study is brought out when considering the electronics associated with the power stages. For the AC motor, a low noise (RFI) - high efficiency power stage is available featuring Silicon Control Rectifiers which are switched "on" and "off" at relatively low current levels. For the DC motor, a high noise (RFI) - high efficiency power stage is available featuring bi-polar switching transistors which form a bridge network for each of two commutator control windings.

The net result is that of trading off "RFI and weight" against "system partitioning."

7. Monitoring

The monitoring functions have been allocated to the digital computer. This not only minimizes the hardware and test requirements (to demonstrate a fail safe status) but, allows flexibility in setting thresholds and interpretation of information provided by the Actuator Electronics.

Figure 1186 reflects the comparator locations intended. This concept would be applicable to any dual command-quadruple feedback mechanization.

The total engine control is represented in figure 1187. Each of the valves will have a complement of redundant electronics, dual motor, gear loop, and quad transducers. A variety of packaging options can be provided as required to satisfy installation integrity.

The location and packaging of power conditioning units may be treated as necessary, again consistent with the particular application.

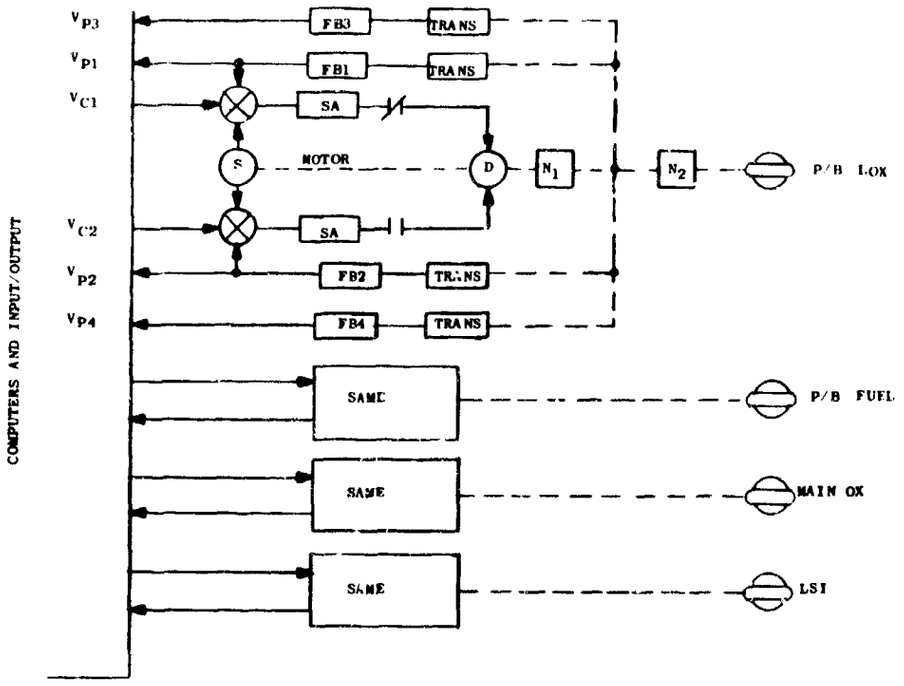

Figure 1187. Engine Control System

8. Maintainability

The Electromechanical Actuator System will be packaged in four separate units. The Electronics Assembly will house all of the servo loop and conditioning electronics, the Transducer Assembly will house the four transducers, the Motor Assembly and Gear Box Assembly will be separate assemblies but they may be treated as a pair in order to maintain a control on useful and reliability since a prime reliability factor has been assigned. A prime reliability factor would be enhanced by a well defined and controlled preventative maintenance and overhaul procedure.

A computer programmed test routine serves the purpose of establishing confidence prior to use and facilitates fault detection and isolation.

Each of the valves therefore has a complement of electromechanical hardware which enhances maintainability by considering packaging, functional grouping, channel separation, and test to demonstrate operational capability.

9. Repairability

Each assembly is repairable as separate units and to lower levels as follows:

1. Electronics Assembly - Functionally related groups of circuits will be located on subassemblies which are suited to direct replacement consistent with the packaging and weigh reduction optimization. Each

of the subassemblies will contain components which are removable and replaceable. A component may be a two or more lead discrete part or multiple lead operational amplifier, or hybrid package. The cost of the damaged component being replaced will vary but the design will ultimately reflect trade offs of structural integrity, weight, cost agreements pending future commitments.

2. Transducer Assembly - In the case of RVDT's (Rotational Variable Differential Transformers) matched sets of high reliability and long MTBF are being considered. At the moment, it is anticipated that repair of this unit would not be practical considering useful life expectancies.

3. Gear Box - Since this unit must have high reliability, and that its useful life can be established, only the housing should be considered as a reuseable item assuming that bearing or gear deterioration should preclude any subsequent use of those parts.

4. Motor - The Brushless DC Motor will be a repairable item. The bearings would be the only part which we would anticipate replacing automatically since prime reliability has been assigned to them and the shaft. With nominal use, all other parts of the motor should have a long MTBF but the mechanics would allow replacement when necessary. The AC Motor can also be repairable, again with bearings being the most frequently replaced item.

E. DEVELOPMENT RISKS

The major development risks associated with an electro-mechanical valve control system for the XLR129 rocket engine are presented below.

1. Electronics

The major development associated with the electronics described in this report is that which would be required to extend the operating range of the electronics below the present temperature range of -65° F to +160° F. Many suppliers of semi-conductors were contacted during the early phases of the program. They indicated that the development of electronic circuits to operate at cryogenic environments would require extensive in-house experimentation and development as well as overall industry backing.

2. Lubrication

Dry film lubricants are the only feasible type of lubricant that can be considered for this application. Some development will be required to obtain lubricants capable of handling the contact stresses in the transmission gearing without generating high friction with subsequent loss of efficiency.

3. Position Sensor

Some development is anticipated relative to materials and temperature compensation of the rotary variable differential transducer.

SECTION VI
PNEUMATIC VALVE CONTROL SYSTEM

A. INTRODUCTION

This section describes the results of the study effort conducted by the Bendix Corp. concerning the feasibility of pneumatic controllers to actuate and control four principal propellant valves on the Pratt & Whitney Aircraft XLR129 Rocket Engine. It is concluded that pneumatic controller systems are indeed feasible for applications such as the XLR129 rocket engine.

The actuation problem is considered from an overall system point of view. An attempt is made to take into account the total system requirements with respect to vehicle-engine-control interfaces as they affect and influence:

- Energy and power requirements.
- Engine mounting and interconnections.
- Energy regulation and conditioning.
- Startup and shutdown provisions.

As an overall feasibility investigation, this report aims to identify and pinpoint major and pertinent system features, both favorable and unfavorable. Further studies aimed directly at selected problem areas are identified and recommended.

B. SYSTEM SELECTION

A pneumatic valve controller system is recommended for the XLR129 engine because:

- It satisfies all current performance requirements.
- It integrates with the engine cycle naturally and easily.
- It requires minimal external power for flight, startup and shutdown.
- It possesses growth potential to accommodate improved performance, orbital restart capability and additional actuation functions including those with very high power requirements such as gimbal actuation.
- It utilizes proven concepts and requires no major development risks.
- It compares favorably with other motive concepts with respect to cost, weight and reliability.

Analysis shows that the high speed pneumatic motor is capable of meeting all of the current performance goals established for the XLR129 engine actuators including the start and shutdown speeds and the stringent frequency response requirements.

C. Summary

1. Total System Weight
2. System Power Requirements
3. Reliability of Components
4. Cost Considerations

By utilizing the gas energy available in the engine cycle, the total integration of the pneumatic system is relatively straightforward and natural. For the XLR129, it is suggested that some of the energy is an existing igniter cooling circuit be utilized. This scheme taps available energy and requires no separate or extra supply. The abundance of high pressure gas in the engine cycle also suggests that pneumatic actuation is a natural choice.

Minimal external gas and electrical power is needed for startup and shutdown. For a typical start, the pneumatic system will require approximately 1/3 pound of helium gas and 30 watts of electrical power. Shutdown and/or prestart requirements are essentially the same. Flight operation requires about 15 watts of electrical power on the average and a maximum requirement of approximately 30 watts, with all of the gas power coming directly from and returning to the engine cycle.

C. SUMMARY

Pneumatic actuators meet all known operational requirements for the XLR129 engine application, with sufficient growth potential to meet increased requirements.

1. Total System Weight

Four motor-valve assemblies		15.4 lb
Filters		0.3
Pneumatic lines and manifolds		3.4
Regulator and check valves		5.6
Helium cutoff valve		1.0
Supervisory electronics		1.0
Electrical cabling and connectors		2.3
	Subtotal	29.0 lb
Four transmissions		97.0 lb (37)

2. System Power Requirements

At steady-state, holding against 30 percent maximum load.

Hydrogen flow 0.2 lb_m/sec
Electrical power 15 watts

At steady-state, no load.

Hydrogen flow 0.12 lb_m/sec, ΔP = 300 psid
Electrical power 9 watts

Maximum running requirements.

Hydrogen flow 0.7 lb_m/sec, ΔP = 300 psid
Electrical power 30 watts

Start and shutdown requirements.

Helium	0.3 lb_m, ΔP = 300 psid
Electrical power	15 watts
	25 watts maximum for 250 msec

Prestart requirement

Helium flow (fill plus leakage) 0.044 lb_m + 0.057 lb_m/sec
Electrical power 15 watts

3. Reliability of Components

Motors and valves

Prime reliable
Gas filtration for contamination protection

Transmissions

Prime reliable

Electronics

Triple redundancy of supervisory electronics.
Failure detection by monitoring position error and feedback conditioning circuits

Torque motors

Dual windings - prime reliable
Contamination protection provided

Pneumatic distribution system

Manifold and piping - prime reliable
Regulator - double redundancy
Check valves - double redundancy

Electrical cabling and connectors

Prime reliable
Shielded, protective conduits provided

4. Cost Considerations

Two motor sizes satisfy all actuators.

No major advancement is state-of-art required.

Development of proven cryogenic environment concepts suggested.

Materials
Lubrication
Seals

Hardware, piece part, costs are reasonable.

D. DESCRIPTION OF PNEUMATIC CONTROLLER SYSTEM

The pneumatic controller system for the XLR129 engine utilizes a system pressure regulator and four pneumatic motor-transmission assemblies powered by a portion of the engine ignition case liner cooling flow, and providing:

- Closed-loop positioning of each engine control valve.
- Sequencing for start, in-flight and shutdown operations.

This section describes the complete pneumatic controller system from several points of view:

- General System
- Pneumatic Interface with Engine
- Electrical Interface with Control Computer
- Pneumatic Actuator Assembly

1. General System

The pneumatic controller system described herein consists of the following major functional elements:

- Four Actuator Assemblies

  Torque motor-valve
  Motor
  Transmission
  Feedback transducer
  Filter

- Energy Regulation and Distribution System

  Pressure regulator
  Helium solenoid valve and check valve
  Fuel check valve
  Inlet and exhaust manifolds

- Electronic Control and Power Supply

  Error computation and dynamic compensation
  Current amplifier
  Feedback conditioning
  Cabling and connectors

Four independent valve controller assemblies were designed to meet the steady-state and dynamic requirements of each of the engine fuel and LOX valves (see figure 1188).

Main burner LOX valve
Low speed inducer LOX valve
Preburner LOX valve
Preburner fuel valve

One electrical connector and two pneumatic connections interface each controller with the engine and the electronic control unit.

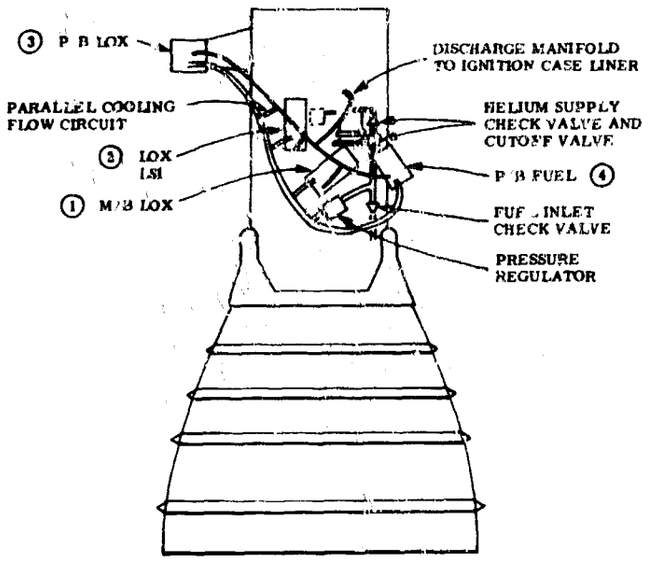

Figure 1188. XLR129 Pneumatic Valve Controller System

2. Pneumatic System Interface With Engine

The pneumatic system of four valve controllers (figure 1189) uses a portion of the available fuel flow of the ignition case cooling circuit and returns the flow to the engine after use. As shown in the sketch on the facing page, hydrogen is taken from the transpiration cooling flow heat exchanger exit and regulated to a constant pressure level above the exhaust pressure of the engine transition case for use by the parallel arrangement of the pneumatic motors. For all the motors to produce 30 percent of their maximum design torque, 1/5 lb_m/sec hydrogen flow would be required. A bleed is supplied across the regulated pressure drop to make up the additional cooling flow required by the balanced engine cycle.

For either prestart, start or shutdown, a signal from the control computer opens a solenoid operated cutoff valve in the helium supply line to the pneumatic motor circuit. By an arrangement of check valves, the higher pressure gas, either helium or hydrogen, is admitted to the pneumatic system for running the motors and the lower pressure gas line is kept closed. In this manner, the opening and closing of the solenoid cutoff valve need not be critically timed.

For an engine start, the system requires approximately 1/3 lb_m of helium gas. Shutdown and/or prestart requirements are essentially the same.

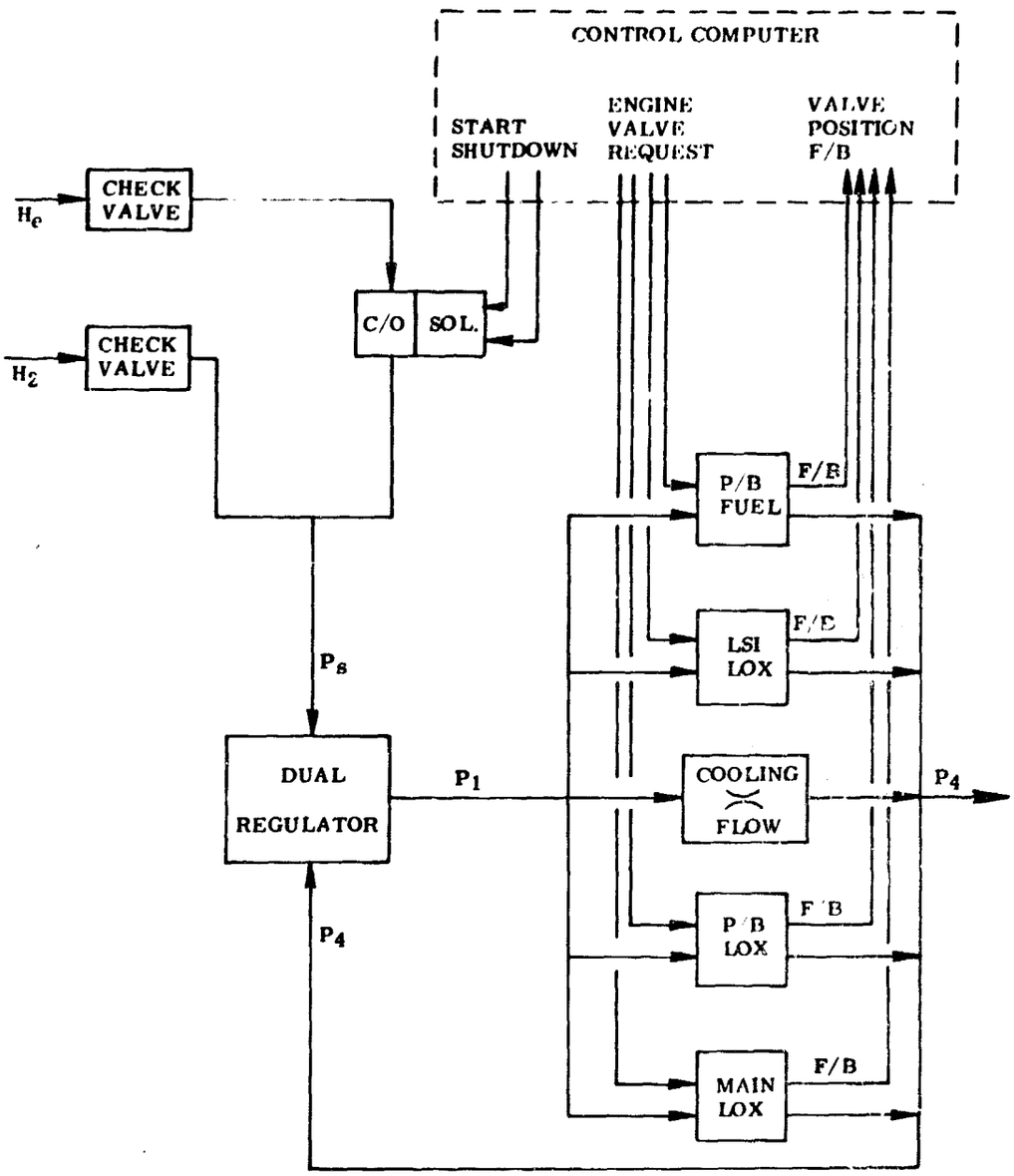

Figure 1189. Pneumatic Flow Diagram

3. Electrical Interface With Control Computer

The supervisory electronics are a part of the control system computer package and provide:

- Error computation.
- Dynamic compensation.
- Feedback conditioning.

The supervisory electronics for each actuator (figure 1190) compares the position commanded by the engine control unit with the actual position of the actuator output, sensed through a feedback transducer, to generate an error signal. It dynamically compensates, amplifies, and conditions the error signal to command a new position output of the torque motor located in the pneumatic actuator assembly. This torque motor movement displaces a followup type slide valve supplying penumatic power to the motor. The motor runs until the electrically sensed actuator output nulls out the commanded position. In addition, the state of the error signal is sent back to the engine control computer as an indicator of actuator health.

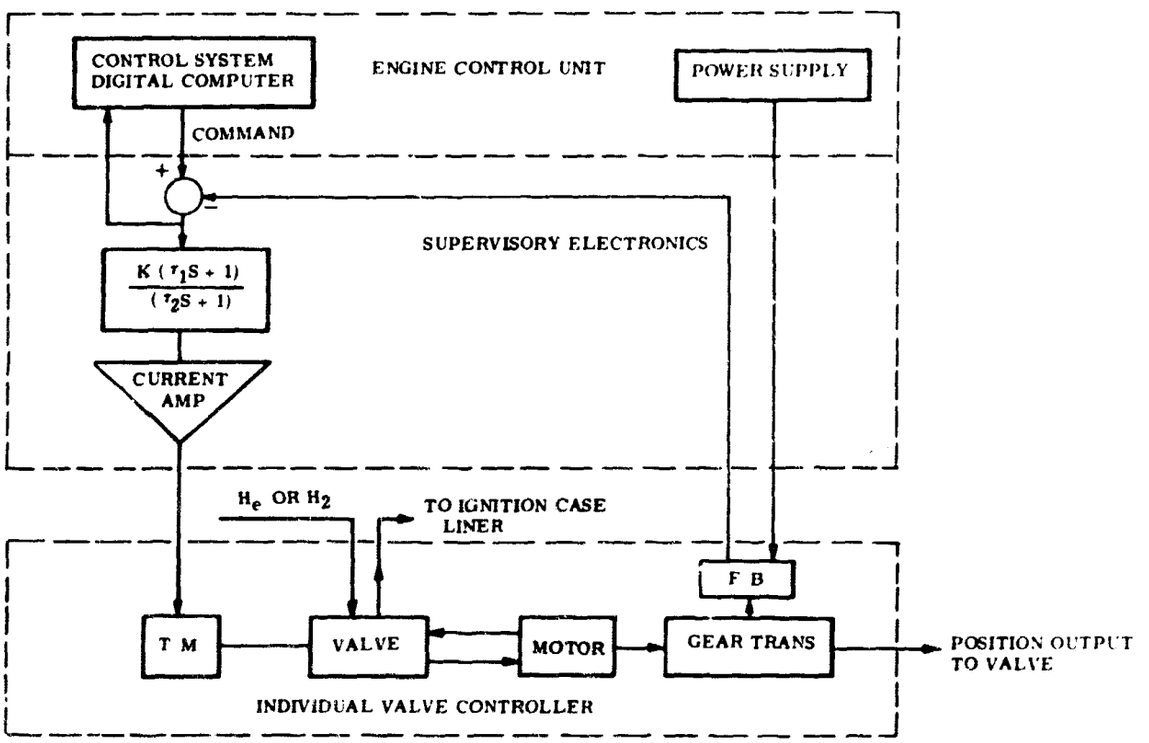

Figure 1190. Functional Block Diagram Electronic Interface of Pneumatic Controller

The electronic supervisory package will be an integral part of the engine control computer package. It is estimated that the supervisory electronics for four actuators will add one pound and 13.5 cubic inches to the engine control unit. The power required by the supervisory electronics to operate the torque motor, feedback transducer, and error conditioning circuits will be supplied from the engine control unit. Engine prestart, start and shutdown requires a maximum of approximately 30 watts of electrical power. For normal engine operation the estimated power requirement is 15 watts.

4. Pneumatic Actuator Assembly

Each of the four engine valves is controlled and actuated by a specifically designed modular assembly consisting of:

- Torque motor.
- Slide valve.
- Gear motor.
- Speed reducer.
- Feedback element.

Three of the valve controllers provide a rotational output, and the fourth provides a linear output to match the requirements of the engine valves. A sketch showing the modular package effect of a valve controller assembly is shown in figure 1191.

Each valve controller assembly will have a single electrical connector to provide power to the torque motor and feedback transducer. It is estimated that the electrical harness and connectors required for the four valve controller system will weigh 2.3 pounds.

Each valve controller will have two pneumatic connections, a supply and a return line to the motor-slide valve combination. A third pneumatic line, venting of leakage, is shown on the assembly sketch, but is not included in the overall weight due to the questionable size and length required. The supply line to each valve controller is either 0.250 or 0.375 inch diameter tubing, according to the motor size, and originates from a 0.625 inch diameter supply manifold. The return line from each valve controller is either 0.375 or 0.500 inch diameter tubing leading to an 0.875 inch diameter discharge manifold.

Using a steel tube wall thickness based on a maximum tensile stress of 50,000 psi and a maximum line pressure of 5000 psi, the estimated tubing length and weight of the system are:

Helium Line	24 inches	0.4 pounds
Supply Manifold	110	0.7
Discharge Manifold	88	1.1
Fittings	(12)	1.2
TOTAL		3.4 pounds

E. Development Areas and Further Considerations

1. Lubrication
2. Materials
3. Seals
4. Transmission Protection
5. Weight Trade-Off Studies

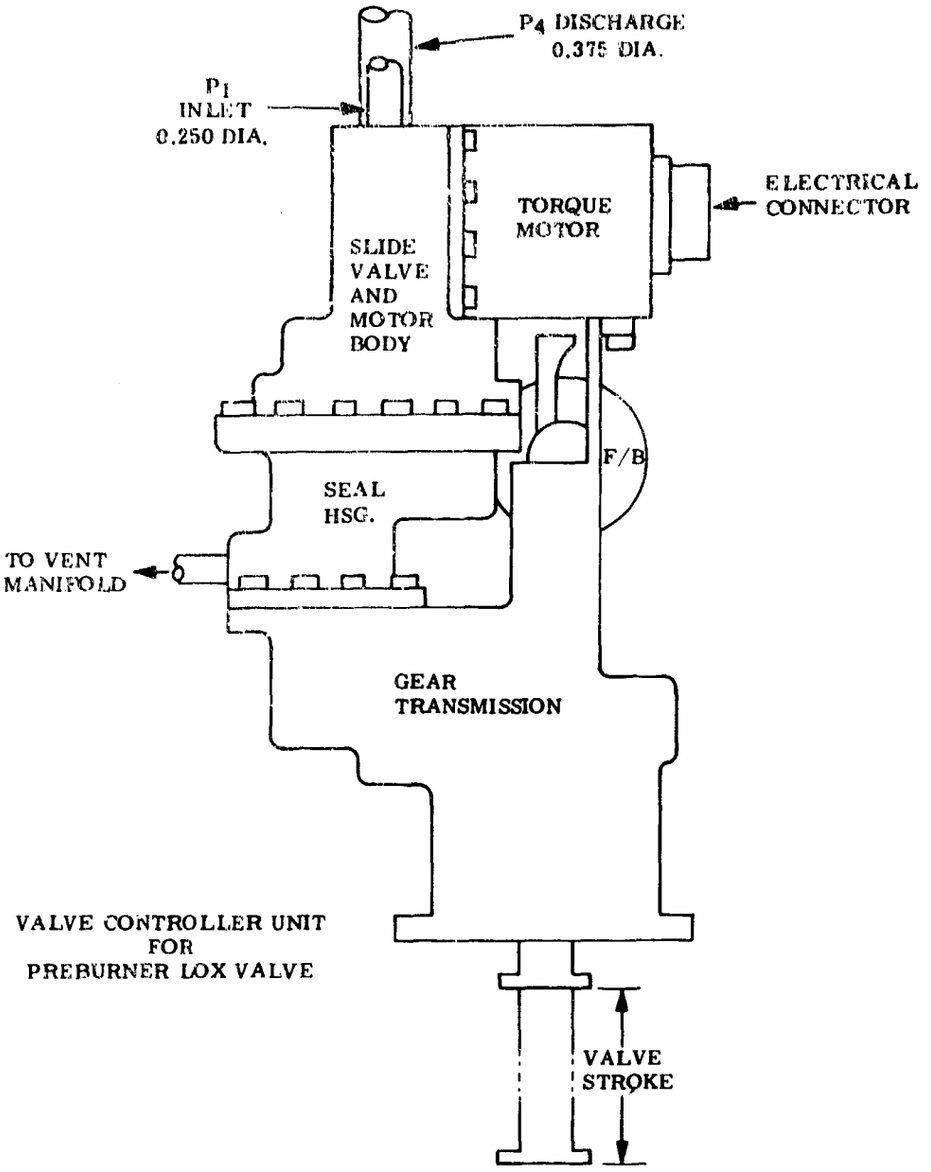

Figure 1191. Valve Controller Unit for Preburner LOX Valve

E. DEVELOPMENT AREAS AND FURTHER CONSIDERATIONS

During the course of this study, the following problem areas were noted. These may be resolved by modifying system design criteria, or may be answered by a more thorough search and analysis, or may require development effort for solution. Most of the problem areas relate in one way or another with the cryogenic environment.

1. Lubrication

Dry film lubricants appear to be most suitable for the cryogenic environment. Motor and transmission gears may be coated with either Everlube 812, Inlox 44, or other dry film lubricant. Bearing lubrication may be provided by special polyimide retainers or equivalent.

2. Materials

Study of materials other than A-286 stainless steel suitable for valves, sleeves, and housing is recommended. Possible use of ceramics for slide valves should be considered.

3. Seals

Seals will be an important problem area. The output seals can be similar to the types used for the engine control valves. High speed motor seals represent a definite development area. Double seals on motor shaft with venting between seals may be a solution for the dynamic seal. The static sealing problem may be lessened or alleviated by a vented dome cover over the complete motor-valve assembly.

4. Transmission Protection

Consideration must be given to protect the transmission if the engine control valve strikes a physical stop, as, for example, at shutdown. This may be accomplished in a number of ways:

- Design valve for overtravel in the shutoff position.
- Modify shutdown schedule to prevent damage.
- Incorporate a clutch or other limiting means.

5. Weight Trade-Off Studies

Investigation of other transmission types is indicated to achieve a balance between system weight, performance and cost.

SECTION VII
SENSOR STUDY

A. GENERAL

This section describes the results of the Bendix Corporation effort on that portion of P & WA's Engine Control Development Program (Contract FO 4611-68C-0002) which concerns itself with a trade study between select individual sensor types from the broad family groupings of rotational speed, liquid or gaseous pressure, combustion temperature, and cryogenic temperature. Each candidate design was examined in detail and relative performance factors identified to build a secure foundation upon which to base final selections for the sensing requirements of the XLR129 Engine Control System.

1. Rationale of Judgement

Factors of prime importance that were used to help guide the final choice of sensor types included accuracy, reliability, repeatability, and environmental restraints. In addition, particular attention was given to interfacing sensors with the system as a whole for ease of conditioning, selecting and monitoring individual signals. This approach enhances the probability that the final selection of components will indeed optimize the system.

2. Recommendations

As a result of the trade studies contained herein, the following sensor types have been chosen for use in the XLR129 Engine Control System to measure essential parameters:

a. Rotational Speed of Main Pumps and Inducers

Eddy-current sensors are recommended for the measurement of rotational speed in combination with associated circuitry which provides the necessary logic to select between dual redundant master and standby signal sources at each pump.

b. Combustion Temperature Associated With the Main Turbines

Dual Chromel-Alumel thermocouples, positioned in groups of four downstream from both main pump turbines, are recommended to protect the hot section rotating components, with associated analog-to-digital conversion circuitry, providing not only the highest temperature selection logic but also supporting data of such a nature that the main computer can be programmed to reject "unreasonable" readings and favor an alternate probe.

c. Propellent Inlet Temperatures

Platinum resistance sensors are recommended to monitor the temperature levels of both cryogenic propellents, with associated analog circuitry, providing not only signal conditioning but also the necessary logic to select the middle value of three redundant probes at each measurement station.

d. Liquid and Gaseous Pressures

Thin film strain elements, vacuum deposited on a metallic diaphragm with ceramic film insulation, are recommended to monitor all liquid and gaseous pressures, with associated analog circuitry, providing not only signal conditioning but also the necessary logic to select the middle value of three redundant probes at each measurement station.

B. ROTATIONAL SPEED SENSING

1. General

When interfacing with digital software, as is the case with the XLR129 Engine Control System, rotational speed sensing can be readily implemented by simply measuring the length of time required for a single shaft revolution. Thus, the proposed system will count the number of master clock pulses which occur between consecutive passages of a given pump blade. The speed probe will sense the arrival of the blade and instruct a counter to receive clock pulses. The next arrival of the blade will cause the counter to empty its data into temporary storage ready for processing and simultaneously initiate a new counting cycle.

Three such types of blade-proximity-detecting devices were examined for this study, including the eddy-current device which was ultimately selected to be best suited for this application:

a. Capacitive

b. Electromagnetic

c. Eddy Current

2. Speed Sensor

The pump speed sensing arrangement is shown in figure 1192. Each of the four pumps has a master sensor and a standby sensor which provide redundant pickups. Every speed sensor has separate and individual signal conditioning circuitry, which is processed and checked by the signal failure rejection logic. The selected sensor signal is sent to computer, which determines the pump speed.

3. Comparison of Speed Sensors

The advantages and disadvantages of the three sensor types are presented in table CXXIV.

a. Capacitive Sensor

The principle advantage of the capacitive sensor is its uniform performance, which is independent of whatever metal is used to form the pump blade. The blade is a capacitor plate, and as the distance between the blade and sensor changes the sensor capacitance ($C < 0.7pf$) is

altered ($\Delta C < 0.07$pf). However, the disadvantages associated with this type sensor are considerable. The sensor output will vary if the sensor moves so that its distance from the blade is changed, or if the dielectric constant of the insulating material is modified by impurities or temperature fluctuations. In addition, the cabling from the sensor to the electronic circuits introduces a capacitance (10-50pf/ft) which can change with temperature and cable motion. In this case, the cable can be a noise generator, which may distort or nullify the sensor data. This type has been eliminated from contention because of the unreliability of the output. Also, commercial units are not available for the XLR129 temperature range ($\approx 20^{\circ}$K).

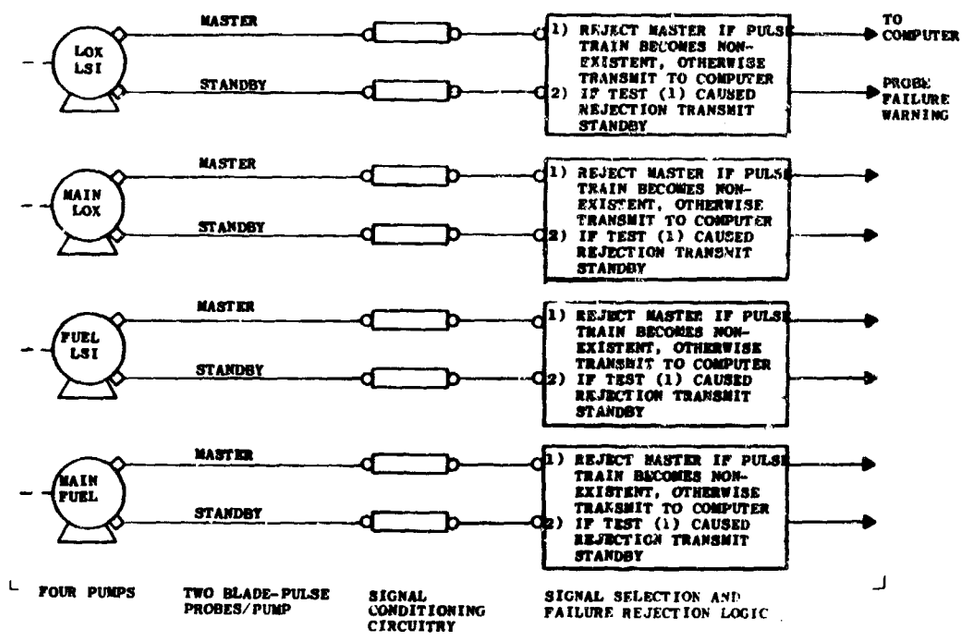

Figure 1192. Pump Speed Sensing Arrangement

Table CXXIV. Pump Speed Sensing Arrangement

	Advantages	Restrictions
Capacitive Sensor	Performance does not depend on what metal the blade is composed of.	1. The cabling to the sensor introduces capacitance variations. 2. Holding the distance between plates is difficult. 3. The insulation resistance may change. 4. Commercial unit temperature range unsatisfactory.

Table CXXIV. Pump Speed Sensing Arrangement (Concluded)

Electro-Magnetic Sensor	1. Self-generating output. 2. Low impedance output. 3. Sensor can be remote from electronics.	1. The metal blade must have magnetic properties. 2. Commercial unit temperature range unsatisfactory.
Eddy Current Sensor	1. Wide range of blade conductivities permit satisfactory performance. 2. Insensitive to lateral shifts between sensor and blade. 3. Sensor can be remote from electronics.	1. Sensor and associated electronics are costly. 2. Temperature range restricts number of commercial units available.

b. Electromagnetic Sensor

The main advantage of this sensor is that it requires no electronic circuits (except pulse shaping if necessary). The sensor may be remote from the unit receiving the data, and the distance between the two is governed only by how much degradation, caused by the cable capacitance, of the sensor signal is acceptable. The great disadvantage associated with this sensor type is the requirement that the blade material have magnetic properties. Present blades are composed of titanium, and a piece of iron would have to be inserted in each blade. The magnetic material of the blade modifies the magnetic field of the sensor, and this change generates a voltage in the sensor coil. This material requirement is considered too restricting and also unnecessary. Consequently, this type was eliminated from the competition. Also, small units, operable at cryogenic temperatures, are not commercially available.

c. Eddy Current Sensor

This sensor will operate with any metal blade, and sensor movement produces only small variations in the sensor output. These variations can be compensated for by the sensor's electronic circuits. In addition, the cabling from the sensor to the electronics does not affect the sensor signal. Consequently, the sensor may be placed at a distance from the sensor's electronic circuits. A standard pigtail length of 5 feet is normal. Microdot 275-3802 cable pairs with BNC connectors and may be used to connect the sensor to the conditioning circuits. A sensor with a 0.375-inch diameter and a 1-inch length is functional for a range of 0 to 0.05 inches. This type sensor and the associated interfacing circuits are expensive, but the system is versatile and practical. The temperature range limits the choice of a unit, but satisfactory commercial units are available.

C. Temperature Sensors

1. High Temperature Sensors
2. Low Temperature Sensors

C. TEMPERATURE SENSORS

1. High Temperature Sensors

The location of the preburner sensors has been moved downstream of the turbines. This location now sees a maximum temperature of 1800°F, which is well within the range of chromel-alumel thermocouples. Chromel-alumel thermocouples have been selected because of their proven reliability and high signal level (25mv/°F) and accuracy (±0.75%). The maximum operating temperature of chromel-alumel is 2500°F, which is adequate for the maximum temperature of the turbine exit (1727.6°F). A listing of various temperature sensors is shown in table CXXV for comparison and reference purposes.

Various processing techniques of the eight temperature sensors have been considered and a ramp comparison A/D technique has been selected for use in this system. Several schemes for converting temperature data to computer data were considered and the ramp conversion, which is more direct, will meet the speed and accuracy requirements.

The A/D configuration, as shown in figure 1193, consists of three basic parts; namely, the ramp generator, comparators and the digital circuits. Analog outputs from the temperature sensors, ranging from 0 to 10 volts, are connected to 8 input comparators. The comparator outputs, in turn, are connected by a summing circuit to 3 amplifiers. Each amplifier compares a threshold voltage with the summing junction to control a counter. Data presented by the counters to the computer represent the median temperature of the sensors, second highest temperature reading and the highest temperature sensor.

The A/D operation begins with a clock signal from the CPU to start a 10-volt ramp generator and counters. When the input comparator detects that the sweep voltage is larger than the sensor input the comparator output switches from a low to a high state. As the fourth sensor is detected, the summing junction voltage exceeds the threshold voltage (E4) of the amplifier. The amplifier output switches from a high state to a low state and stops the counter. The conversion from an analog voltage input to a digital word is similar for the other counters.

Table CXXV. Temperature Sensor Data

Sensors	Full Range, °F	Accuracy, °F or percent, Over Range, °F	
		ISA Standard Limits	ISA Special Limits
Thermocouples			
Chromel/Alumel	-300 to +2500	4°F 0 to +530 3/4% +530 to +2500	--
Iron/Constantan	-310 to +1400	4°F 0 to +530 3/4% +530 to +1400	2°F 0 to +530 3/8% +530 to +1400
Copper/Constantan	-310 to +750	2% -150 to -75 1-1/2°F -75 to +200 3/4% +200 to +700	1% -300 to -75 3/4°F -75 to +200 3/8% +200 to +700
Platinum 10% Rhodium/Platinum	+32 to +3200	5°F +32 to +1000 1/2% +1000 to +2700	--
Tungsten/Tungsten 26% Rhenium Tungsten 5% Rhenium/Tungsten 26% Rhenium	+32 to +5200	8°F +32 to +800 1% +800 to +4200	
Resistance Thermometers			
Platinum (high purity strain-free)	-435 to +900	±0.01°F, limited range; ±0.05%, full range	
Platinum (commercial purity)	-320 to +2000	0.2%, full range	
Nickel	-320 to +800	0.4%, full range	
Balco	-320 to +500	0.4%, full range	
Semiconductor (germanium)	-458 to -400	0.01°F, full range	
Semiconductor (thermistors)	-40 to +300	0.05°F, limited range; 1°F, full range	
Bimetallic Thermometers	0 to 1000	2°F, limited range; 10°F, full range	
Liquid Filled Thermometer (glass stem)	-328 to +800	0.05°F, limited range; 1°F, full range	
Liquid Filled Thermometer (metal bulb)	-150 to +700	2°F, limited range; 5°F, full range	
Quartz Thermometer	-80 to +482	0.00005°F, 10 sec sample period 0.05% linear	

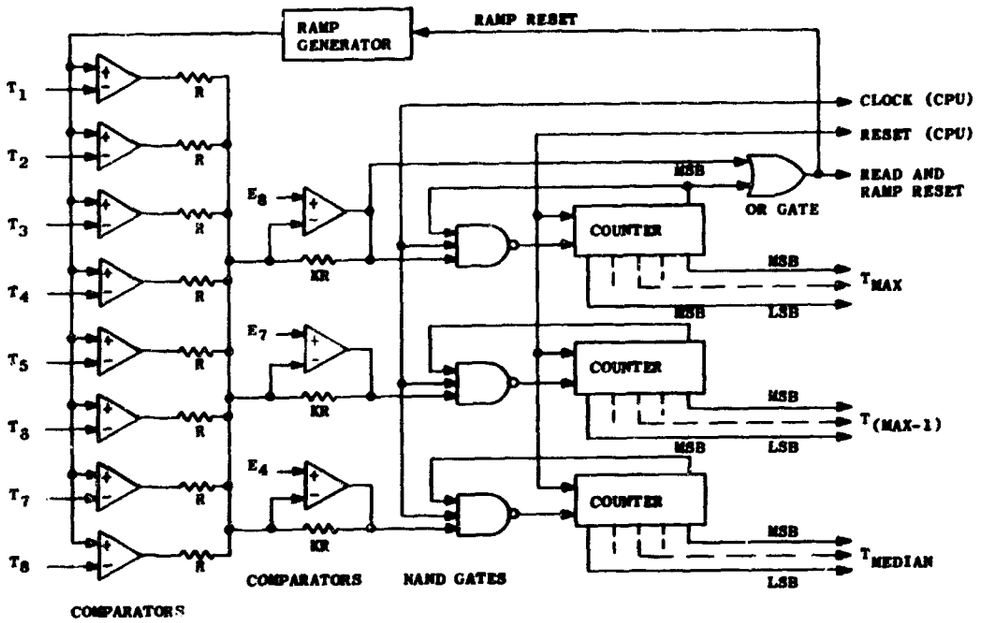

Figure 1193. Preburner Selection, Conversion, and Monitoring

A block diagram of signal selection and failure rejection modes is shown in figure 1194.

2. Low Temperature Sensors

Platinum resistance sensors are recommended for all the low temperature applications. Platinum exhibits an extremely predictable change in resistance with temperature in accordance with the Callendar-Van Dusen equation.

$$P_T/R_O = 1 + \alpha\left[T - \sigma\left(\frac{T}{100} - 1\right)\left(\frac{T}{100}1 - \beta\right)\left(\frac{T}{100} - 1\right)\left(\frac{T}{100}\right)^3\right] \quad (1)$$

Where: R_T = Resistance at T °C

R_O = Resistance at 0°C

α, σ, β = Constants for each platinum element

The Callendar-Van Dusen equation is applicable down to the boiling point of oxygen (-182.97°C). Below this temperature, the equation is replaced by a table of Resistance vs. Temperature.

Below a temperature of -260°C, the sensitivity of the platinum resistance sensor devreases rapidly, however, the lowest temperature that will be measured will not be below -254°C. The boiling point of H_2 is -252.7°C at one atmospheric pressure and, in order to prevent cavitation of the pumps, some pressure greater than one atmosphere will be present at the point of temperature measurement.

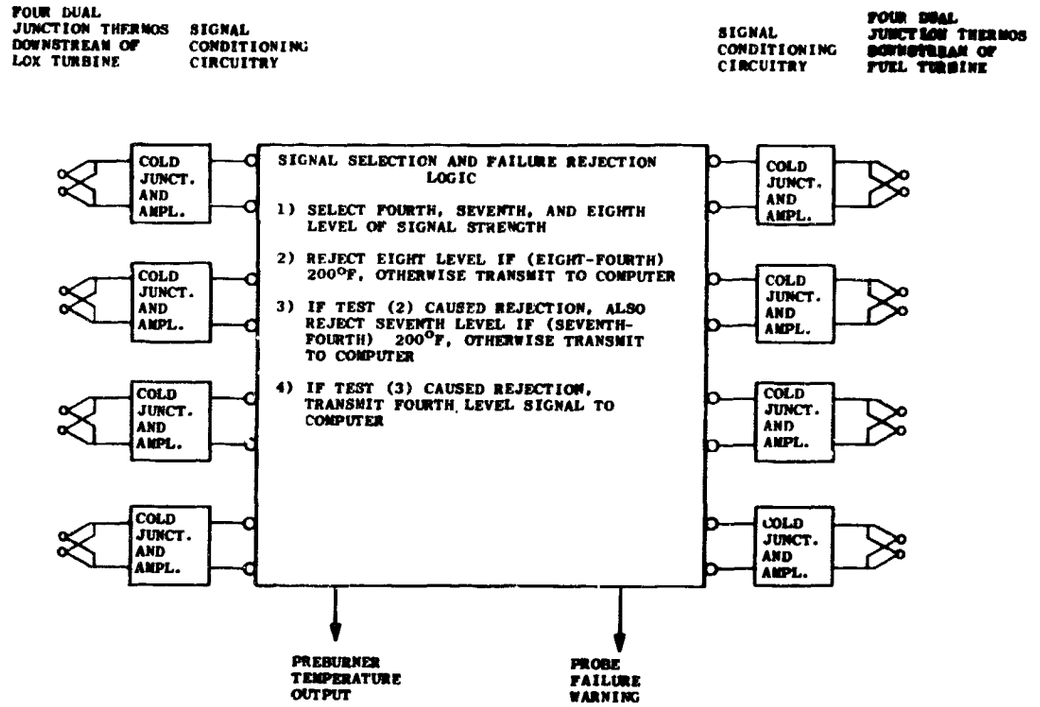

Figure 1194. Preburner Temperature Probes

Rather than require several sensor types for each temperature range, platinum was selected for all the temperatures except the highest (e.g. preburner temperature). This choice was based on several important factors which are listed below:

1. platinum resistance range (13.51°K to 755.77°K)
2. range of temperature sensing (19.62°K to 277.61°K)
3. high accuracy (±.01°F over limited range)
4. ease of signal conditioning
5. proven reliability

D. PRESSURE SENSORS

After evaluating the various types of pressure sensors currently available, the recommended type is the thin film strain gage (Statham Model PA822). Its major advantages are: high accuracy, low sensitivity to temperature effects, good static and dynamic response, may be excited with AC or DC, low sensitivity to shock and vibration, and continuous resolution.

Strain gage transducers can be categorized into two general classes; the unbonded strain gage and the bonded strain gage. The unbonded strain gage is a strain sensitive wire which is attached between a fixed reference point

and a movable force collector. The parameter to be measured causes the force collector to move, thereby changing the length of the strain wire. This produces a change is resistance through the gage factor of the strain wire. The bonded strain gage is similar in principle, except it is entirely attached by an adhesive to a member whose strain is to be measured. The force collector generates strain in the metal member by operating it is a tension, compression, or bending mode.

The force requirement of the unbonded strain gage is very low since it is only necessary to displace the small strain gage filament. This permits the design of small size and low range, as well as high range transducers. The force requirements for the bonded strain gage are higher, since it is necessary to displace the metal member to which the strain gage is bonded. Therefore, design limitations are encountered in small size and low range applications. Since the bonding adhesive and backing material are in the force path, the accuracy of the measurement is affected by these materials. The commonly used adhesives and backing materials are of the epoxy type, which restrict the use of the bonded strain gage in radiation and high-temperature environments.

Conventional strain gages are made from metal and metal alloys in wire or foil form. The strain gage may be a single straight section or a grid pattern of the desired configuration. For the commonly used strain gage materials, the gage factor is from 2.0 to 5.0. The higher gage factor materials tend to be more sensitive to temperature and less stable than the lower gage factor materials.

A new development in the strain gage field was made with the introduction of the semiconductor strain gage. This device is basically a bonded strain gage using doped silicon as the material. By controlling the dopant in the silicon, the strain gage properties can be optimized for a specific application The silicon strain gage generally provides a higher gage factor than the metal strain gage, but with higher temperature coefficients. Gage factors from 50 to 200 are typical, either positive or negative.

In unbonded strain gage transducers, a metal substrate is used to provide the desired mechanical properties, and a ceramic film is vacuum deposited on the metal to provide the required electrical insulation. The four strain gages are then vacuum deposited on the insulator. They are electrically connected into a bridge circuit by vacuum deposited interconnecting leads. These multiple evaporations are made during a single pumpdown by using multiple sources and appropriate substrate mask patterns.

Lead wire is attached to the film by microcircuit techniques such as welding and thermo-compression bonding of small noble metal wire. With the attachment of lead wire, the thin film sensor is complete. Its construction is entirely inorganic because only metal and ceramic materials are used. The lead wire attachment is made directly to the film and does not use an intermediate solder or brazing compound. Then the sensor is packaged into a finished transducer using conventional transducer assembly techniques.

The sensing element may have any configuration, but in this application, the pressure transducer element will be a flat diaphragm.

A typical bonded strain gage weighing 1 1/2 ounces is made by the Kistler Instrument Corporation, useable within a temperature range of -320°F to +300°F. Full scale output is 30 millivolts with a source impedance of 350 ohms. Their model 402 is a bonded strain gage in a four active arm Wheatstone bridge in a one cubic inch configuration.

The recommended unbonded type is the Statham Instruments Corporation Model PA822, designed for use between -320 and +80°F and for pressures between 0-15 to 0-5000 psia, while the Kistler bonded unit is restricted to 0-300 to 0-2000 psia. The Statham Unit weighs 4-1/2 ounces and occupies about two cubic inches.

A special problem that exists in using this pressure sensor is the time required for thermal equilibrium at cryogenic temperatures. Discussions with the manufacturer, Statham Instruments, have yielded a proposed solution for this problem, however. Normally, an isolated sensor may take up to 3 hours to reach thermal equilibrium when taken from a room temperature environment and subjected to oxidizer temperature. However, by grouping all redundant sensors in close proximity, and mounting them on a substantial heat sink, which in turn is mounted on the oxidizer line, the thermal equilibrium time factor should be drastically reduced. Preliminary estimates indicate that this time factor can be made in order of 3 to 5 minutes by utilizing this technique.

The bridge resistances in the unbonded type can be made in the range of 350 ohms to 5000 ohms which permits optimizing the transducer bridge design. Each leg has the maximum area consistent with other design factors in order to permit internally generated heat to be dissipated over a substantial area. The strain gage bridge is separated from the metal sensing element by a thin film of ceramic insulation which has a high thermal conductivity. Thus, the strain gages are effectively heatsinked to the sensing element. High resistance bridges permit higher excitation voltages at the same power input. This increases the output voltage level and provides a higher signal-to-noise ratio. A typical circuit utilizing a thin film strain gage is depicted in figure 1195. Table CXXVII compares various electrical displacement transducers.

Block diagrams of signal selection and failure rejection modes for both Pump Pressure and Cooling Pressure are illustrated in figures 1196 and 1197 respectively.

E. MEDIAN SELECTION CIRCUIT

Since most of the input sensor signals will be triply redundant, a median selection circuit will be utilized. The philosophy of the median selection approach is based upon the fact that if one sensor fails in either a high or low condition, the correctly operating median signal is still selected.

The median selection circuit that is recommended for this application is shown in figure 59. Since there are three inputs (E_1, E_2, E_3) it is possible to have eight combinations at the output of the comparators. Of these eight, two are "don't care" conditions and therefore aids in reducing circuitry. By means of NAND logic, the median control signal (E_{C1}, E_{C2}, or E_{C3}) selects the median sensor signal E_M as shown in figure 1198.

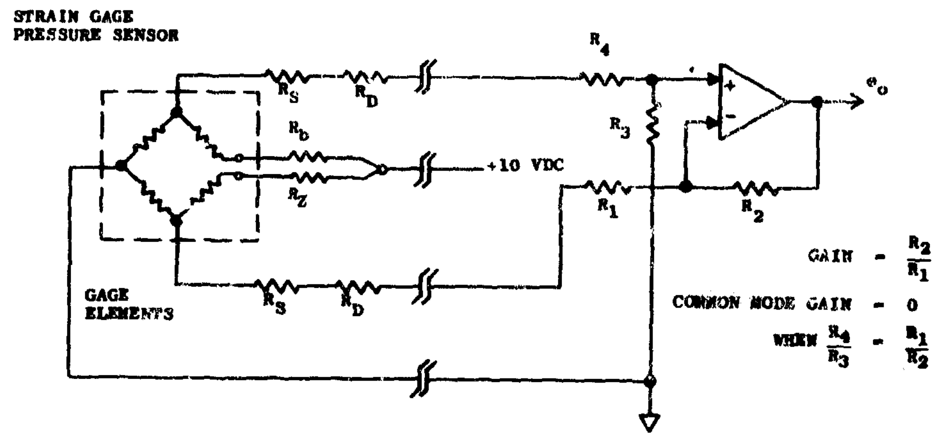

R_b - Zero Balance

R_Z - Zero Temp. Compensation

R_d - Output Control

R_s - Span Resistor

R_p - Input Impedance Control

Figure 1195. Pressure Sensor

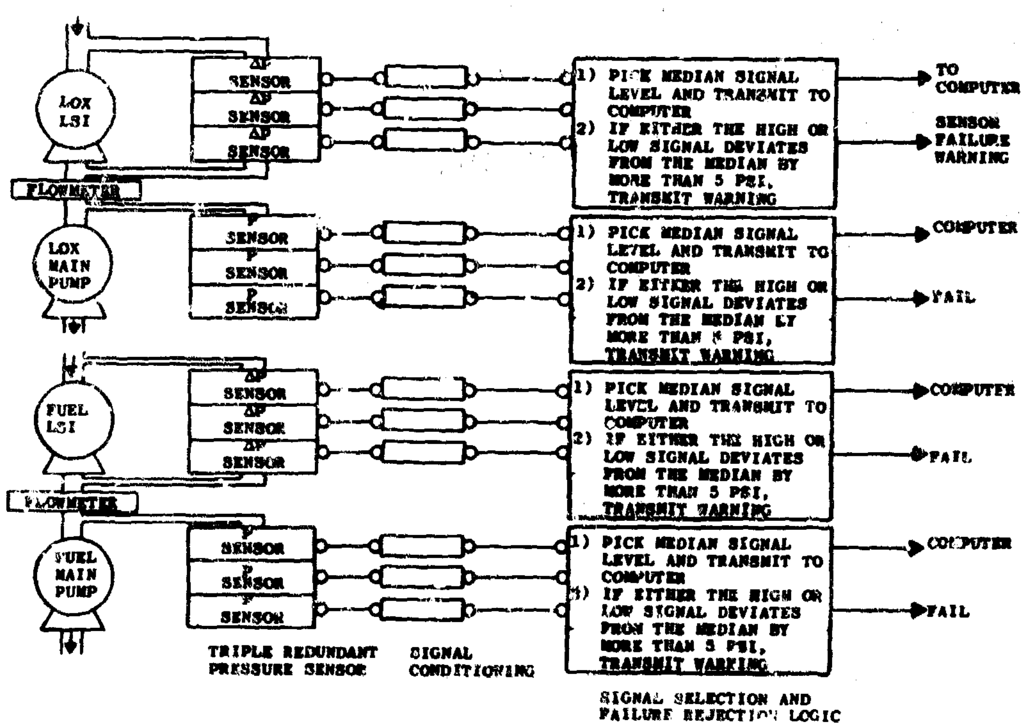

Figure 1196. Pump Pressure Sensing

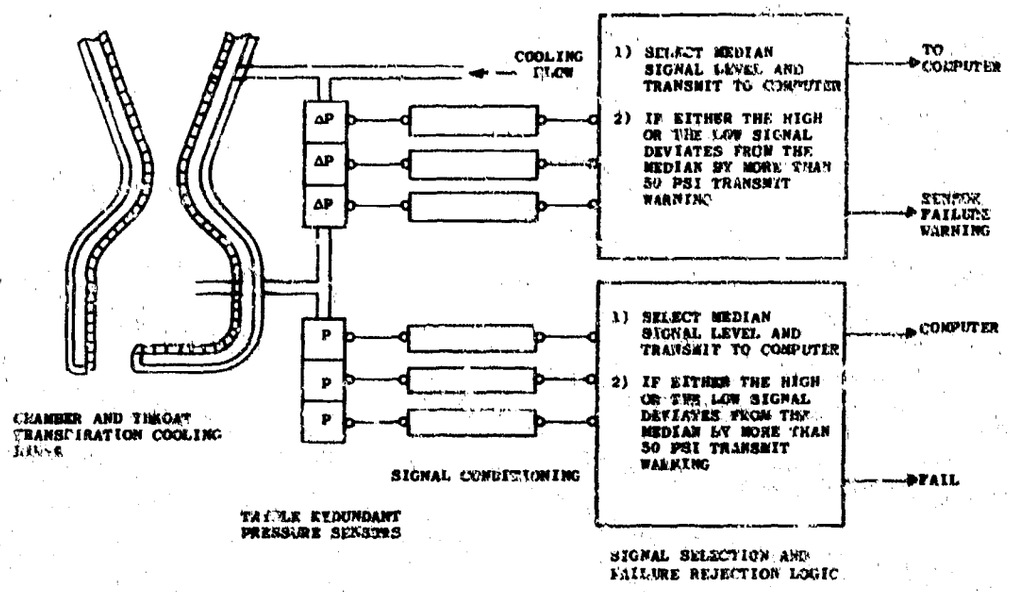

Figure 1197. Cooling Pressure Sensing

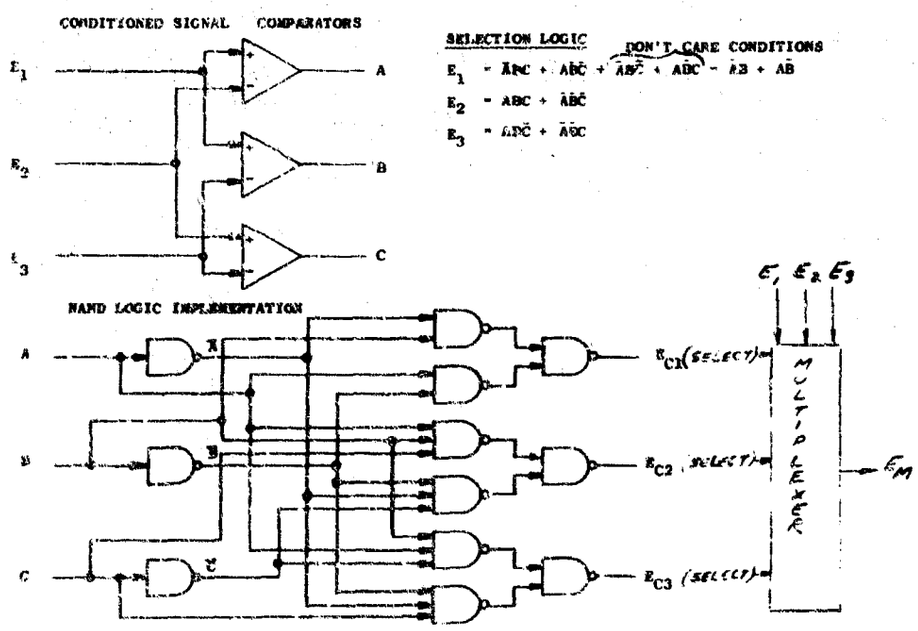

Figure 1198. Typical Signal Selection and Failure Rejection Process

Table CXXVI. Comparison of Various Electrical Displacement Transducers

		Principle Advantages	Disadvantages
1.	Capacitive	a. Excellent frequency response b. Simple to construct and inexpensive to produce c. Low "g" response (advantage in pressure transducers) d. Measures either static or dynamic phenomena e. Minimum diaphragm mass f. Small volumetric displacement g. Continuous resolution	a. Motion of connecting cable, or long lead length, will cause distortion and/or erratic signals b. High impedance output c. Must be reactively and resistively balanced d. Very sensitive to temperature variations e. Receiving instrument is usually large and complex
2.	Differential Transformer	a. Continuous resolution b. High output c. Low hysteresis	a. Must be excited with AC only b. Receiving instrument must be selected to operate on AC signals, or demodulator network must be used for DC output c. Low natural frequency d. Large displacement required e. Sensitive to vibration
3.	Inductive	a. Responds to static or dynamic measurements b. Continuous resolution c. High output (40 mv/v) d. Direct FM in telemetry e. High signal-to-noise ratio	a. Must be excited with AC only b. Must be reactively and resistively balanced c. Frequency response normally limited by force-summing construction d. Large volumetric displacement and low frequency response e. Proximity to magnetic objects, or fields, causes erratic performance
4.	Ionization	a. High output - with suitable RF source ,60 v may be provided b. High sensitivity up to 5v/$\mu\mu$f change. It can detect capacitance changes of 0.001 $\mu\mu$f c. Measures static or dynamic conditions d. Free of friction e. Minimum coercive force f. High frequency response	a. Must be excited with RF only b. It is mainly a transfer device; displacement must be produced by other mechanical members c. Complex accessory equipment is mandatory
5.	Force Balance	a. High output b. Static or dynamic measurements can be made c. High accuracy d. High stability e. High resolution	a. Low frequency response b. Expensive c. Bulky and heavy d. Very sensitive to acceleration or shock e. May be very complex electronically
6.	Chmstrictive	a. High output b. Good frequency response c. Easy to manufacture d. Rugged e. High reliability due to simplicity f. Inexpensive g. Static or dynamic response	a. Questionable thermal behavior b. Probably noisy c. Probably affected by vibration d. Questionable repeatability
7.	Oscillating	a. Small size b. Measures dynamic or static phenomena c. Convenient for telemetering purposes d. Output may be shown as actual decimal unit counts representing applied stimulus e. High output level	a. Limited temperature range b. Low accuracy c. Requires special equipment to provide analog information d. Expensive e. Poor thermal coefficient of sensitivity f. Poor thermal zero shift
8.	Photoelectric	a. High output b. Possible efficiencies of 80% c. Simple to construct d. Static or dynamic conditions may be measured	a. Large displacement required b. Low frequency response c. Possible poor long-term stability d. Limited temperature range
9.	Potentiometric	a. High output b. Inexpensive c. Easily serviced d. Easy to excite and install e. May be excited with AC or DC f. Wide range of functions g. No amplification or impedance matching is necessary	a. Usually large size b. The resolution is finite in most cases c. High mechanical friction d. Limited life e. Sensitive to vibration f. Develops high noise levels with wear g. Requires large force-summing member h. Low frequency response i. Large displacement required
10.	Vibrating Wire	a. Output frequency may be transmitted over long distance with no loss in accuracy b. Frequency-modulated output c. Eliminates carrier oscillator in FR/FM telemetering d. High output e. Receiving instrument may be extremely accurate	a. Very sensitive to thermal changes b. Very sensitive to shock and vibration c. Relatively large nonlinearity and hysteresis errors d. Questionable stability
11.	Strain Gauge	a. High accuracy b. Low sensitivity to temperature effects c. Static and dynamic response d. May be excited with AC or DC e. Low sensitivity to shock and vibration f. Continuous resolution	a. Low output (higher output available with silicon strain gages with some compromise of thermal and stability characteristics) b. Low range limitation for bonded type

UNCLASSIFIED
Security Classification

DOCUMENT CONTROL DATA - R & D

(Security classification of title, body of abstract and indexing annotation must be entered when the overall report is classified)

1. ORIGINATING ACTIVITY (Corporate author)
Pratt & Whitney Aircraft
Division of United Aircraft Corporation
Florida Research and Development Center, W. P. Bch., Fla.

2a. REPORT SECURITY CLASSIFICATION
UNCLASSIFIED

2b. GROUP
N/A

3. REPORT TITLE
XLR129-P-1 Air Force Reusable Rocket Engine Program

4. DESCRIPTIVE NOTES (Type of report and inclusive dates)
Final Report

5. AUTHOR(S) (First name, middle initial, last name)
Mr. Robert R. Atherton, Program Manager
Pratt & Whitney Aircraft, Mail Location B-50
Florida Research and Development Center, West Palm Beach, Florida

6. REPORT DATE	7a. TOTAL NO. OF PAGES	7b. NO. OF REFS
30 November 1970	1306	1

8a. CONTRACT OR GRANT NO.	9a. ORIGINATOR'S REPORT NUMBER(S)
F0 4611-68-C-0002	PWA FR-3832
b. PROJECT NO. 57X3600	
c. P63681C 63408F	9b. OTHER REPORT NO(S) (Any other numbers that may be assigned this report)
d. S669800 2894703	AFRPL-TR-71-1

10. DISTRIBUTION STATEMENT
This document is subject to special export controls and each transmittal to foreign governments or foreign nationals may be made only with prior approval of AFRPL (RPOR/STINFO) Edwards AFB, California 93523.

11. SUPPLEMENTARY NOTES	12. SPONSORING MILITARY ACTIVITY
None	AFFTC, Procurement Division (FTMKR-2) Edwards Air Force Base, California 93523

13. ABSTRACT

The objective of this program was to demonstrate the performance and mechanical integrity of a 250,000 lb thrust reusable rocket engine designated the XLR129-P-1. The program, sponsored by the Air Force Rocket Propulsion Laboratory, was accomplished by Pratt & Whitney Aircraft at the Florida Research and Development Center and consisted of design and analysis of all engine components and the demonstrator engine. Fabrication and testing of the critical major components was also accomplished. This effort was the second phase of the Air Force Cryogenic Rocket Engine Advanced Development Program, Project 2 of Program Element 63048F. During the first year, experimental evaluation was conducted in the areas of a fixed fuel area preburner injector, hydrogen cooled roller bearings, compact pump inlets, lightweight nozzle fabrication techniques and selected control valves. These tests provided the background needed for the design of these particular components. During the second year, the design of all components and the demonstrator engine was completed. The engine was designed to operate with liquid oxygen and liquid hydrogen propellants, uses the staged combustion cycle, includes a variable thrust, and a variable mixture ratio capability. During the third year, fabrication and testing of certain components such as the preburner injector, transition case, and fuel turbopump was accomplished. Critical control system components such as the preburner oxidizer valve, the preburner fuel valve and static seals were also tested and evaluated. These tests demonstrated the feasibility of these components. The program commenced 6 November 1967, and ended on 15 August 1970.

DD FORM 1 NOV 68 1473

UNCLASSIFIED
Security Classification

14. KEY WORDS	LINK A		LINK B		LINK C	
	ROLE	WT	ROLE	WT	ROLE	WT
Air Force						
Pratt & Whitney Aircraft, FRDC						
XLR129-P-1 Reusable Rocket Engine Program						
Supporting Data and Analysis						
Fixed Fuel Area Preburner Injector						
Roller Bearing Durability Tests						
250K Oxygen/Hydrogen Demonstrator Engine						
Pump Inlet Evaluation						
Nozzle Fabrication						
Controls Components						
Component Development						
Engine Integration and Demonstration						
Flight Engine						
Engineering Support						